

RÉPUBLIQUE FRANÇAISE
*Liberté*
*Égalité*
*Fraternité*

# Coastal hazards assessment in Mauritius and Rodrigues (phase 2 report, vol.1)

Final report

**BRGM/RC-73987-FR**

16 June 2025

GARCIN Manuel, PEDREROS Rodrigo, DESMAZES Franck, LOUISOR Jessie, LE ROY Sylvestre, BONNARDOT François, THIEBLEMONT Rémi, CAPDERREY Cécile, BAILLS Audrey, ROHMER Jeremy, FILIPPINI Andrea

| **Verified by :** | | **Approved by :** | |
|---|---|---|---|
| Nom : | Remi BELON | Nom : | Cyril MALLET |
| Function : | Coastal Engineer | Function : | Head of DRIS/R3C |
| Date : | 23/04/2025 | Date : | 05/05/2025 |
| Signature : | | Signature : | |

**BRGM's quality and environmental management system is certified to ISO 9001 and ISO 14001 standards.**

**Contact:** qualite@brgm.fr

# Warning

This report is sent exclusively to the beneficiary of the study (Ministry of Environment, Solid Waste Management and Climate Change of the Republic of Mauritius) and to the *Agence Française de Développement*.

The beneficiary shall be responsible for distributing copies of this initial print run.

The disclosure and re-use of this report are governed by the terms of the agreement (CMU1091 01D).

BRGM cannot be held responsible for any disclosure of the contents of this report to a third party for which it is not responsible and for any consequences that may result.

# Your opinion is important to us

As part of our quality approach and the continuous improvement of our practices, we want to measure the effectiveness of our work.

We would therefore be grateful if you could give us your opinion on this report by completing the form available at this address https://forms.office.com/r/yMgFcU6Ctq or by scanning this QR code:

**Key words:** Coastal hazards, Risks, Erosion, Flooding, Cyclone, Sea level, Climate change, Mauritius, Rodrigues, Indian Ocean.

In reference lists, this report shall be cited as follows:

GARCIN Manuel, PEDREROS Rodrigo, DESMAZES Franck, LOUISOR Jessie, LE ROY Sylvestre, BONNARDOT François, THIEBLEMONT Rémi, CAPDERREY Cécile, BAILLS Audrey, ROHMER Jeremy, FILIPPINI Andrea (2025) – Coastal hazards assessment in Mauritius and Rodrigues (phase 2 report, vol.1). Final report. BRGM/RC-73987-FR, 264 p., 226 fig., 40 tab., 3 app.

Other volumes:

BERNARDIE-TAHIR Nathalie, CERBELAUD Fabien, CHERCHELAY Marie, BOODOO Zyaad (2025) – Coastal risks assessment in Mauritius and Rodrigues (phase2 report, Vol. 2). Final report. BRGM/RC-73988-FR, 134p., 74 fig., 15 tab., 1 app.

BAILLS Audrey, CAPDERREY Cécile, GARCIN Manuel (2025) – Adaptation measures and nature-based solutions in Mauritius and Rodrigues (phase 2 report, vol. 3). (final report). BRGM/RC-73989-FR, 144 p., 56 fig., 36 tab., 2 app.

© BRGM, 2025, this document may not be reproduced, either wholly or partially, without the express permission of BRGM and the Beneficiary.
IM003-MT008-P2-20/01/2022

# Abstract

The coastline of the islands of the Republic of Mauritius is regularly exposed to the hazards of coastal erosion and marine flooding. The coasts of Mauritius and Rodrigues are home to a large population with many social and economic issues at stake (infrastructure, buildings, tourism, etc.). In the context of climate change and rising sea level, it is important to anticipate their effects on coastal hazards and risks.

AFD (*Agence Française de Développement*) has therefore financed the "Operational study of coastal risks (coastal flooding and coastal erosion) on the islands of Mauritius (Mauritius and Rodrigues) in the context of climate change" project (Agreement: n° CMU 1091 01D) ) whose beneficiary is the Ministry of Environment, Solid Waste Management and Climate Change. The project is coordinated by BRGM and involves the Indian Ocean Regional Office of Météo France and the universities of Limoges (Géolab) and Mascareignes.

The aim of the project is to provide maps of coastal erosion and marine flooding hazards for three timeframes (current, 2050 and 2100) and to assess the associated risks. These maps are produced for a scale of 1:20,000 and cover the islands of Mauritius and Rodrigues. Three "hotspots" (Flic-en-Flac, Anse la Raie and Port Mathurin), where the stakes are high for the Republic but also representative of the problems encountered, have been chosen in agreement with the Steering Committee. In these "hotspots", hazards and risks have been assessed on a more precise spatial scale (of the order of 1:5,000).

The phase 2 report is the third deliverable defined in the project specifications. It consists of three main volumes:

- The first volume (this report) deals with the forcing factors (cyclone, sea level rise, southern swell) and the methods and tools used to assess and map current and future (2050, 2100) coastal hazards.

- The second volume describes the vulnerabilities and perceptions of different populations and stakeholders to coastal hazards and climate change. It also deals with the assessment of the risks induced by coastal hazards over the three timeframes covered by the project on the coasts of the two islands and on the hotspots.

- The third volume examines possible adaptation measures to coastal hazards in Mauritius and Rodrigues in the context of climate change, and more specifically nature-based solutions.

This volume includes 3 appendices, each dealing with a specific topic and providing elements of understanding and details of the results obtained. The first appendix deals with the assessment of recent coastal erosion in Rodrigues, for which no data were available, the second deals with the assessment of current and future (2050-2100) southern swells, and the third presents the coastal land cover database created for the purposes of the project (coastal flooding modelling).

In this report, the project and the general method used to assess coastal hazards in Mauritius and Rodrigues are presented. Next, a critical analysis of the basic data such as bathymetry and topography is provided, followed by a characterisation of the various forcing factors in the present and future. Lastly, the hazards of submersion, erosion and coastline retreat are assessed at the scale of the two islands and then at that of the hotspots.

The work carried out on cyclonic risks (both current and future) has allowed the characterisation of cyclones with a return period of 100 years. A comparative analysis of the changes in atmospheric pressure (relative value w.r.t. 1011 hPa) and wind speed induced by future cyclones (2050 and 2100) in relation to the current climate reveals a decrease of pressure and an intensification of wind speed in Mauritius and Rodrigues, particularly evident in the 2100 climate scenario. The analysis of extreme values indicates an augmentation of wind speed ranging from

5% to 10% and a decline in atmospheric pressure of up to 20%. This intensification appears to be more pronounced in Rodrigues than in Mauritius. The increased intensity of future cyclones will increase the intensity of meteorological and oceanic parameters (swells, storm surges, etc.) that generate coastal hazards for both Mauritius and Rodrigues. This increase is particularly important for major events with a long return period (100-year events), which are used to assess coastal hazards. Given our current state of knowledge, there will be no significant change in the intensity or frequency of southern swells in the future in this sector of Indian Ocean including Mauritius and Rodrigues. It is therefore evident that cyclones represent the primary factor responsible for the generation of waves and surges on both islands, a phenomenon that is anticipated to persist into the future.

Sea level rise (induced by climate change) will be significant for both islands, especially after 2050 (e.g. 0,87 m for Mauritius in 2100 for RCP8.5). It has been shown that Rodrigues is affected by a subsidence movement of -2 mm/yr, which increases the rate of relative sea level rise for this island and will lead to a rise of 1,08 m for Rodrigues (again for 2100 and for the RCP8.5 scenario).

It is highly likely that rising sea levels, combined with an increase in the intensity of cyclones and the meteorological and oceanic factors they induce, will lead to an increase in the hazard of coastal flooding, erosion and shoreline retreat.

Significant erosion and coastline retreat have been identified in certain areas of Mauritius. The causes of this retreat are multifaceted, including both natural and anthropogenic factors, as well as natural phenomena exacerbated by anthropogenic activities. The results of the conducted scenarios demonstrate that in specific regions already vulnerable to erosion, considerable retreats could occur, reaching several tens of metres to a hundred metres by the year 2100.

Although some of Rodrigues' sandy beaches are actually able to recover after a phase of erosion, an assessment of the potential retreat of the coastline shows that retreats could be greater in certain sectors of Rodrigues than in Mauritius. However, the estimated potential retreat values should be treated with caution due to the lack of data on the historical evolution of the Rodrigues coastline.

Coastal flood hazard maps were produced for the whole coasts of Mauritius and Rodrigues at 1:20,000 scale. Specific sites (hotspots of Flic-en-Flac, Anse la Raie and Port Mathurin) have been assessed and mapped at a higher resolution (1:5,000). Some stretches of coastline are already highly exposed to coastal flooding, whether in Mauritius or Rodrigues. The areas potentially impacted are sometimes extended. In some sectors the stakes are relatively low (e.g. Anse La Raie in Mauritius). In others, however, there are numerous urban and/or industrial stakes, some of them strategic (e.g. Port Louis, Mahebourg in Mauritius, Port Mathurin and Pointe Monnier in Rodrigues). In other areas, especially Mauritius, numerous tourist assets are at risk, while in Rodrigues, agricultural areas and coastal aquifers crucial to the island are also at risk. In the future, as conditions evolve (intensification of cyclones, sea level rise), our works show that the hazard levels and the surface areas concerned will increase sharply.

# Synthèse

Le littoral des îles de la République de Maurice est régulièrement exposé aux risques d'érosion côtière et de submersion marine. Les côtes de Maurice et de Rodrigues abritent une population importante avec de nombreux enjeux sociaux et économiques (infrastructures, bâtiments, tourisme, etc.). Dans le contexte du changement climatique et de l'élévation du niveau de la mer, il est important d'anticiper leurs effets sur les aléas et les risques côtiers.

L'AFD a donc financé le projet « Etude opérationnelle des risques côtiers (inondation et érosion côtière) sur les îles de Maurice (Maurice et Rodrigues) dans le contexte du changement climatique » (Convention : n° CMU 1091 01D) ) dont le bénéficiaire est le Ministère de l'environnement, de la gestion des déchets solides et du changement climatique. Le projet est coordonné par le BRGM et associe la Direction Régionale de l'océan Indien de Météo France et les universités de Limoges (Géolab) et des Mascareignes.

L'objectif du projet est de fournir des cartes des aléas d'érosion côtière et de submersion marine à trois échéances (actuelle, 2050 et 2100) et d'évaluer les risques associés. Ces cartes sont produites pour être utilisées à une échelle de 1/20 000$^{ème}$ et couvrent l'ensemble des littoraux des îles Maurice et Rodrigues. Trois « *hotspots* » (Flic-en-Flac, Anse la Raie et Port Mathurin), où les enjeux sont importants pour la République mais aussi représentatifs des problèmes rencontrés, ont été choisis par le Comité de Pilotage du projet. Dans ces « hotspots », les aléas et les risques sont évalués à une échelle spatiale plus précise (de l'ordre du 1/5 000$^{ème}$).

Ce rapport de phase 2 est le troisième livrable défini dans les spécifications du projet. Il est composé de trois volumes principaux.

- Le premier volume (ce rapport) traite des facteurs de forçage (cyclone, élévation du niveau de la mer, houle australe) générateurs des aléas côtiers et des modalités qui ont été mises en œuvre pour évaluer et cartographier les aléas côtiers actuels et futurs (2050, 2100).
- Le second décrit les vulnérabilités et les perceptions des différentes populations et parties prenantes face aux aléas côtiers et au changement climatique. Il traite également de l'évaluation des risques induits par les aléas côtiers aux trois échéances couvertes par le projet.
- Le troisième volume examine les mesures d'adaptation possibles aux risques côtiers à Maurice et à Rodrigues dans le contexte du changement climatique. Parmi ces mesures d'adaptation, les solutions basées sur la nature semblent prometteuses. Elles sont donc discutées plus en détail pour les deux îles.

Ce volume comporte trois annexes détaillant des thèmes spécifiques, donnant les éléments de compréhension et les détails des résultats obtenus. La première annexe traite de l'évaluation de l'érosion côtière récente à Rodrigues, pour laquelle aucune donnée n'existait, la deuxième traite de l'évaluation des houles australes actuelles et futures (2050-2100), et la troisième présente la base de données de l'occupation du sol de la zone littorale qui a été créée pour les besoins du projet (modélisation de l'inondation côtière).

Dans ce rapport, le projet et la méthode générale utilisée pour évaluer les aléas côtiers à Maurice et Rodrigues sont présentés. Ensuite, une analyse critique des données de base comme la bathymétrie et la topographie est fournie puis une caractérisation des différents facteurs de forçage dans l'actuel et dans le futur est produite. Enfin, l'évaluation des aléas de submersion et d'érosion et de recul du trait de côte à l'échelle des deux îles puis à celle des hotspots est produite.

Les travaux menés sur les risques cycloniques (actuels et futurs) ont permis de caractériser les cyclones de période de retour 100 ans. Une analyse comparative des changements de la pression atmosphérique (valeur relative par rapport à 1011hPa) et de la vitesse du vent induits par les cyclones futurs (2050 et 2100) par rapport au climat actuel révèle une diminution de la

pression et une intensification de la vitesse du vent à Maurice et à Rodrigues, particulièrement évidente dans le scénario climatique 2100. L'analyse des valeurs extrêmes indique une augmentation de la vitesse du vent allant de 5% à 10% et une baisse de la pression atmosphérique allant jusqu'à 20%. Cette intensification semble être plus prononcée à Rodrigues qu'à Maurice. L'intensité accrue des futurs cyclones augmentera l'intensité des paramètres météorologiques et océaniques (houles, surcotes, etc.) qui génèrent des risques côtiers à la fois pour Maurice et Rodrigues. Cette augmentation est particulièrement importante pour les événements majeurs à longue période de retour (événements centennaux), qui sont utilisés pour évaluer les risques côtiers. Dans l'état actuel de nos connaissances, il n'y aura pas de changement significatif de l'intensité ou de la fréquence des houles australes dans le futur dans ce secteur de l'océan Indien incluant l'île Maurice et l'île Rodrigues. Il est donc évident que les cyclones représentent le principal facteur responsable des aléas côtiers notamment futurs.

L'élévation du niveau de la mer (induite par le changement climatique) sera significative pour les deux îles, surtout après 2050 (par exemple 0,87 m pour l'île Maurice en 2100 pour RCP8.5). Il a été démontré que l'île de Rodrigues est affectée par un mouvement de subsidence de -2 mm/an, ce qui augmente le taux d'élévation relative du niveau de la mer pour cette île et conduira à une élévation de 1,08 m pour Rodrigues (toujours pour 2100 et pour le scénario RCP8.5).

Il est très probable que l'élévation du niveau de la mer, combinée à une augmentation de l'intensité des cyclones et des facteurs météorologiques et océaniques qu'ils induisent, conduira à une augmentation des aléas d'inondation côtière, d'érosion et de recul du trait de côte.

Une érosion importante et un recul du trait de côte ont été identifiés dans certaines zones de l'île Maurice. Les causes de ce recul sont multiples, incluant à la fois des facteurs naturels et anthropiques, ainsi que des phénomènes naturels exacerbés par des activités anthropiques. Les résultats des scénarios réalisés démontrent que dans des régions spécifiques déjà vulnérables à l'érosion, des reculs importants pourraient se produire, atteignant plusieurs dizaines de mètres à une centaine de mètres d'ici 2100. En revanche, l'île de Rodrigues est en général moins touchée par l'érosion et présente une plus grande résilience face au recul de la côte. Une partie importante de son littoral sableux peut en effet se rétablir après un recul. Cependant, certains secteurs présentent déjà une érosion chronique, et il est probable que d'autres, qui semblent actuellement non critiques, seront affectés dans le futur, en partie à cause de l'élévation du niveau de la mer et en partie à cause du changement des paramètres météo-océaniques.

Des cartes des risques d'inondation côtière ont été produites pour l'ensemble des côtes de l'île Maurice et de Rodrigues à l'échelle 1/20 000. Des sites spécifiques (points chauds de Flic-en-Flac, Anse la Raie et Port Mathurin) ont été évalués et cartographiés à une résolution plus élevée (1/5 000). Certaines parties du littoral sont déjà fortement exposées aux inondations côtières, que ce soit à Maurice ou à Rodrigues. Les zones potentiellement impactées sont parfois étendues. Dans certains secteurs, les enjeux sont relativement faibles (ex. Anse La Raie à Maurice). Dans d'autres, en revanche, les enjeux urbains et/ou industriels sont nombreux et parfois stratégiques (Port Louis, Mahébourg à Maurice, Port Mathurin et Pointe Monnier à Rodrigues). Dans d'autres régions, en particulier à Maurice, de nombreux enjeux touristiques sont menacés, tandis qu'à Rodrigues, des zones agricoles et des aquifères côtiers cruciaux pour l'île le sont également. Dans le futur, avec l'évolution des conditions climatiques (intensification des cyclones, élévation du niveau de la mer, etc.), nos travaux montrent que les surfaces exposées aux aléas et que leurs niveaux augmenteront fortement.

# Content


**1. INTRODUCTION ..... 21**

**2. BACKGROUND INPUT DATA ..... 25**

2.1 TOPOGRAPHIC AND BATHYMETRIC DATA ..... 25
*2.1.1 Sources of altimetric and bathymetric data ..... 25*
*2.1.2 Limits of topographic and bathymetric data ..... 28*

**3. FORCING FACTORS ..... 31**

3.1 INTRODUCTION ..... 31
3.2 CLIMATE CHANGE ..... 31
*3.2.1 Selection of climate scenarios ..... 31*
3.3 PRESENT AND FUTURE CYCLONES ..... 31
*3.3.1 Introduction ..... 31*
*3.3.2 Method ..... 32*
3.3.2.1 Intensity bias correction for the three data sets ..... 32
3.3.2.2 Selection of trajectory scenarios ..... 33
3.3.2.3 Wind and pressure fields generation ..... 35
3.3.2.4 "*Future projection*" of the climate 2000 scenarios ..... 36
*3.3.3 Statistical analysis for present day cyclones, and in future (2050 and 2100) ..... 37*
3.3.3.1 Method ..... 37
3.3.3.2 Results ..... 38
3.3.3.2.1 Analysis at Mauritius ..... 38
3.3.3.2.2 Analysis at Rodrigues ..... 41
3.3.3.3 In summary ..... 45
3.4 ANALYSIS OF THE CYCLONE-INDUCED EXTREME METEOCEANIC FORCING CONDITIONS (PRESENT DAY AND FUTURE) ..... 45
*3.4.1 Data ..... 45*
*3.4.2 Methods ..... 49*
*3.4.3 Results at Mauritius forcing point ..... 50*
3.4.3.1 Marginals ..... 50
3.4.3.2 Multivariate extreme value analysis ..... 53
3.4.3.3 Covariate estimates ..... 54
*3.4.4 Results at Rodrigues forcing point ..... 56*
3.4.4.1 Marginals ..... 56
3.4.4.2 Multivariate extreme value analysis ..... 59
3.4.4.3 Covariate estimates ..... 60
3.5 ANALYSIS OF SEA LEVELS IN MAURITIUS AND RODRIGUES ..... 63
*3.5.1 Introduction ..... 63*
*3.5.2 Analysis of recent sea levels in Mauritius and Rodrigues ..... 63*
3.5.2.1 Data ..... 63
3.5.2.1.1 Tide gauges ..... 63
3.5.2.1.2 Satellite altimetry ..... 64
3.5.2.1.3 GPS stations ..... 64
3.5.2.1.4 Climate modelling ..... 64
3.5.2.2 Results ..... 65
**3.5.2.2.1** Observations ..... 65
3.5.2.2.2 Comparison between observations and models ..... 68
3.5.2.3 Summary ..... 69
*3.5.3 Future relative sea levels in Mauritius and Rodrigues ..... 70*
3.5.3.1 Method ..... 70
3.5.3.1.1 The sterodynamic component ($\boldsymbol{\Delta Z}$) ..... 70
3.5.3.1.2 The barystatic (mass) component ($\boldsymbol{\Delta Rbarystatic - GRD}$) ..... 70
3.5.3.1.3 Vertical land motions ($\boldsymbol{\Delta VLM}$) ..... 71
3.5.3.2 Data ..... 72

3.5.3.2.1 The contribution of land and groundwater, Greenland icesheet, and continental glaciers to sea-level changes. ....72
3.5.3.2.2 The sterodynamic component ....72
3.5.3.2.3 The contribution of Antarctica ....72
3.5.3.2.4 Subsidence ....73
3.5.3.3 Design of a "*high-end*" scenario ....73
3.5.3.4 Results ....73
3.5.3.4.1 Mauritius ....73
3.5.3.4.2 Rodrigues ....75
3.6 SOUTHERN SWELLS .... 77

**4. ASSESSMENT AND MAPPING OF THE SHORELINE RETREAT AND COASTAL FLOODING HAZARDS IN THE MAURITIUS AND RODRIGUES ISLANDS ....79**

4.1 INTRODUCTION .... 79
*4.1.1 Coastal erosion and coastal retreat hazard .... 79*
4.1.1.1 Concepts ....79
4.1.1.2 Coastline mobility factor ....79
4.1.1.3 Definition of the coastal retreat hazard ....81
*4.1.2 Coastal flooding .... 81*
4.1.2.1 Physical processes causing coastal flooding ....81
4.1.2.2 Coastal flooding types ....82
4.2 THE WHOLE COAST OF MAURITIUS AND RODRIGUES (1:20,000 SCALE) .... 84
*4.2.1 Methods .... 84*
4.2.1.1 Method for assessment of coastal erosion and coastal retreat hazard at 1:20,000 ....84
4.2.1.1.1 Introduction ....84
4.2.1.1.2 Method ....84
4.2.1.1.2.1 Segmentation of the territory into homogeneous coastal zones (HCZ) ....84
4.2.1.1.2.2 Analysis of sandy coastline change data ....85
4.2.1.1.2.3 Estimated impact of extreme events (Lmax) ....88
4.2.1.1.2.4 Estimating the effect of climate change ....90
4.2.1.1.2.5 Description of Shoreline Retreat Projection Scenarios ....95
4.2.1.2 Method for assessment of coastal flooding hazard at 1:20 000 ....101
4.2.1.2.1 Description of numerical modelling tools ....102
4.2.1.2.2 Production of the topo-bathymetric DTMs ....103
4.2.1.2.3 Identification of hydraulic features ....106
4.2.1.2.4 Meshing ....111
4.2.1.2.5 Land use and bottom friction ....112
*4.2.2 Results .... 114*
4.2.2.1 Mauritius ....114
4.2.2.1.1 Coastal retreat hazard ....114
4.2.2.1.1.1 Current timeframe ....115
4.2.2.1.1.2 Timeframe 2050 ....117
4.2.2.1.1.1 Timeframe 2100 ....119
4.2.2.1.2 Coastal flooding hazard ....122
4.2.2.1.2.1 Model Validation on historical event ....122
4.2.2.1.2.2 Determining actual, 2050 and 2100 climate reference scenarios ....126
4.2.2.1.2.3 Simulation results ....134
4.2.2.2 Rodrigues ....147
4.2.2.2.1 Coastal retreat hazard ....147
4.2.2.2.1.1 Current timeframe ....147
4.2.2.2.1.2 Timeframe 2050 ....150
4.2.2.2.1.3 Timeframe 2100 ....152
4.2.2.2.2 Coastal flooding hazard ....155
4.2.2.2.2.1 Model Validation on historical event ....155
4.2.2.2.2.2 Determining actual climate, 2050 and 2100 climate reference scenarios ....157
4.2.2.2.2.3 Simulation results ....165
4.3 FLIC-EN-FLAC, ANSE LA RAIE (MAURITIUS) AND PORT-MATHURIN (RODRIGUES) SITES AT 1:5,000 SCALE .... 177
*4.3.1 Introduction .... 177*
*4.3.2 Sites presentation (hotspots) .... 177*

4.3.2.1 Flic-en-Flac (Mauritius) ..... 177
4.3.2.2 Anse la Raie (Mauritius) ..... 181
4.3.2.3 Port-Mathurin (Rodrigues) ..... 184
*4.3.3 Methods ..... 187*
4.3.3.1 Assessment method of the coastal erosion and coastline retreat at local scale (1:5,000) ..... 187
4.3.3.2 Assessment method of the coastal flooding hazard at local scale (1:5,000) ..... 187
4.3.3.2.1 Elaboration of the high-resolution topo-bathymetric DTMs ..... 187
4.3.3.2.2 Culverts identification ..... 189
4.3.3.2.3 Meshing ..... 191
4.3.3.2.4 Land use and bottom friction ..... 193
*4.3.4 Results ..... 194*
4.3.4.1 Flic-en-Flac (Mauritius) ..... 194
4.3.4.1.1 Coastal retreat hazard ..... 194
4.3.4.1.1.1 Coastal homogeneous zones and sedimentary sub-cells ..... 194
4.3.4.1.1.2 Analysis of coastline evolution ..... 194
4.3.4.1.1.3 Additional erosion caused by sea level rise (SLR-R) ..... 196
4.3.4.1.1.4 Coastline retreat hazard at the sub-cells scale ..... 197
4.3.4.1.1.5 Maps of coastline retreat hazard at local scale ..... 201
4.3.4.1.2 Coastal flooding hazard ..... 209
4.3.4.1.2.1 Model Validation on historical event ..... 210
4.3.4.1.2.2 Simulation results ..... 212
4.3.4.2 Anse la Raie (Mauritius) ..... 215
4.3.4.2.1 Coastal retreat hazard ..... 215
4.3.4.2.1.1 Coastal homogeneous zones and sedimentary sub-cells ..... 215
4.3.4.2.1.2 Analysis of coastline evolution ..... 215
4.3.4.2.1.3 Additional erosion caused by sea level rise (SLR-R) ..... 219
4.3.4.2.1.4 Coastline retreat hazard at the sub-cells scale ..... 220
4.3.4.2.1.5 Maps of coastline retreat hazard at local scale ..... 222
4.3.4.2.2 Coastal flooding hazard ..... 227
4.3.4.2.2.1 Model Validation on historical event ..... 227
4.3.4.2.2.2 Simulation results ..... 228
4.3.4.3 Port Mathurin (Rodrigues) ..... 236
4.3.4.3.1 Coastal retreat hazard ..... 236
4.3.4.3.1.1 Coastal homogeneous zones and sedimentary sub-cells ..... 236
4.3.4.3.1.2 Analysis of coastline evolution ..... 237
4.3.4.3.1.3 Additional erosion caused by sea level rise (SLR-R) ..... 240
4.3.4.3.1.4 Coastline retreat hazard at the sub-cells scale ..... 240
4.3.4.3.1.5 Maps of coastline retreat hazard at local scale ..... 243
4.3.4.3.2 Coastal flooding hazard ..... 249

**5. CONCLUSION ..... 255**

**6. REFERENCES ..... 256**

**7. APPENDIX ..... 261**

# List of figures

*Figure 1 : Relationship between the tasks involved in the project* 23
*Figure 2 : Overview of the LiDAR DTM of Mauritius Island* 26
*Figure 3 : Overview of the DTM of Rodrigues Island* 26
*Figure 4 : Overview of the distribution of bathymetric soundings on Mauritius, supplied by the MHL* 27
*Figure 5: Overview of the distribution of bathymetric soundings on Mauritius, supplied by the MOI* 27
*Figure 6 : Localisation of analysed coastal geodesic points and differences between their altitudes and the corresponding value of the LiDAR DTM (from Garcin et al., 2023)* 29
*Figure 7 : Distribution of altitude (in the LiDAR DTM of Mauritius) along a digitalized « wet-dry » interface on aerial photographs in the sector of Flic-en-Flac* 30
*Figure 8 : Example of the inconsistencies of soundings data near Port-Mathurin* 30
*Figure 9 : Left: raw maximum mean wind distribution curves: ARPEGE50-ClimatConstant 2000 simulation in blue, BT-CMRS 1985-2022 data in black; right: the same data after correction for intensity bias* 33
*Figure 10 : Representation of the 2,500 trajectories detected in the ARPEGE50-ClimatConstant 2000 simulation* 34
*Figure 11 : Representation of the 220 trajectories selected for the study of current climate coastal risk in Mauritius* 35
*Figure 12 : Representation of the 164 trajectories selected for Rodrigues (current climate)* 35
*Figure 13 : Example of a wind field for one of the cyclone systems approaching Mauritius* 36
*Figure 14 : Proposed evolution of the cyclone intensity distribution curve for the two timeframes considered* 37
*Figure 15: Example of the evolution of the wind speed field (left), expressed in km/h, and relative atmospheric pressure (right) expressed in hPa (compared with the reference pressure 1011 hPa) for the 18th cyclone in 2000, 2050, 2080-2100 in Mauritius.* 39
*Figure 16 : Evolution of statistical quantities (represented in the form of a boxplot and a violin diagram) of the maximum values reached in the zone defined at +/- 2° around Mauritius. Left: wind speed noted U; right: relative atmospheric pressure noted SLP (compared with the reference pressure 1011hPa) for different climates (2000, 2050 and 2080-2100).* 40
*Figure 17 : Evolution of return level plot for maximum wind speed values U reached in the zone defined at +/- 2° around Mauritius for different climates 2000 and 2050 (left) and 2000 and 2080-2100 (right).* 41
*Figure 18 : Evolution of return level plot for maximum relative atmospheric pressure values SLP reached in the zone defined at +/- 2° around Mauritius for different climates 2000 and 2050 (left) and 2000 and 2080-2100 (right).* 41
*Figure 19 : Example of the evolution of the wind speed field (left), expressed in km/h, and relative atmospheric pressure (right) expressed in hPa (compared with the reference pressure 1011 hPa) for the 18th cyclone in 2000, 2050, 2080-2100 in Rodrigues.* 42
*Figure 20 : Evolution of statistical quantities (represented in the form of a boxplot and a violin diagram) of the maximum values reached in the zone defined at +/- 2° around Rodrigues. Left: wind speed noted U; right: relative atmospheric pressure noted SLP (compared with the reference pressure 1011hPa) for different climates (2000, 2050 and 2080-2100).* 43
*Figure 21 : Evolution of return level plot for maximum wind speed values U reached in the zone defined at +/- 2° around Rodrigues for different climates 2000 and 2050 (left) and 2000 and 2080-2100 (right).* 44
*Figure 22 : Evolution of return level plot for maximum relative atmospheric pressure values SLP reached in the zone defined at +/- 2° around Rodrigues for different climates 2000 and 2050 (left) and 2000 and 2080-2100 (right).* 44
*Figure 23 : Meshes used to calculate waves on Mauritius (A) and Rodrigues (B).* 46
*Figure 24 : Comparison of waves from WW3 and satellites for ITC DINA on 20/01/2002 at 19:30 UTC.* 47
*Figure 25 : Comparison of waves from WW3 and satellites for ITC DINA on 22/01/2002 at 06:30 UTC.* 47
*Figure 26 : Comparison of waves from WW3 and satellites for ITC DINA on 23/01/2002 at 06:30 UTC.* 48
*Figure 27: Localisation of the points where the local high resolution hydrodynamic models are forced for both sites of interest (left: Mauritius, right: Rodrigues).* 48
*Figure 28: Return level plot for significant wave height Hs at Mauritius forcing point for present day (top) and future (bottom) climate scenario.* 51
*Figure 29: Return level plot for wind speed U at Mauritius forcing point for present day (top) and future climate scenario (bottom). The points represent the return levels calculated empirically from the data.* 52
*Figure 30: Return level plot for sea surface height SSH at Mauritius forcing point for present day (top) and future climate scenario (bottom). The points represent the return levels calculated empirically from the data.* 52

*Figure 31: Observations (black) and Monte-Carlo-based randomly generated (blue) combinations (Hs; U; SSH) in Mauritius for present day climate conditions depicted in 2D diagrams Hs versus U; Hs versus SSH and U versus SSH at Mauritius forcing point (present day climate scenario). 53*
*Figure 32: Joint exceedance iso-contours for return period of 100 years within the space (SSH ; Hs) with the colour indicating the U values in Mauritius forcing point for present day (top) and future (bottom) climate scenario. 54*
*Figure 33: Relation between peak period Tp and significant wave height Hs at Mauritius forcing point for present day (top) and future (bottom) climate scenario. 55*
*Figure 34: Wave rose in Mauritius forcing point for present day (left) and future climate scenario (right). 55*
*Figure 35 : Wind rose in Mauritius forcing point for present day (left) and future climate scenario (right). 56*
*Figure 36: Return level plot for significant wave height Hs at Rodrigues forcing point for present day (top) and future (bottom) climate scenario. 57*
*Figure 37: Return level plot for wind speed U at Rodrigues forcing point for present day (top) and future climate scenario (bottom). 58*
*Figure 38: Return level plot for sea surface height SSH at Rodrigues forcing point for present day (top) and future climate scenario (bottom). 59*
*Figure 39: Joint exceedance iso-contours for return period of 100 years within the space (SSH ; Hs) with the colour indicating the U values at Rodrigues forcing point for present day (top) and future (bottom) climate scenario. 60*
*Figure 40: Relation between peak period Tp and significant wave height Hs at Rodrigues forcing point for present day (top) and future (bottom) climate scenario. 61*
*Figure 41: Wave rose at Rodrigues forcing point for present day (left) and future climate scenario (right). 61*
*Figure 42: Wind rose at Rodrigues forcing point for present day (left) and future climate scenario (right) 62*
*Figure 43: Annual relative sea level measured by tide gauges in (a) Mauritius and (b) Rodrigues between 1987 and 2016-2017. The sea level trend and its uncertainty, derived from a linear regression, is calculated either over the entire observed period (black dashed line) or over the period 1995-2017 (red dashed line). 65*
*Figure 44: Superposition of annual time series of relative sea level (black) and absolute sea level (red) in Mauritius (a) and Rodrigues (c) compared with the reference period 1995-2016. Differences between absolute and relative sea levels in (b) Mauritius and (d) Rodrigues. 66*
*Figure 45: Trends in sea level rise in the Indian Ocean calculated from altimetry data over the periods (a) 1993-2000, (b) 1999-2010 and (c) 2009-2018. Mauritius and Rodrigues are in the black circle. 67*
*Figure 46: Comparison between the annual mean relative sea level observed at the Mauritius tide gauge (pink curve) and the regional level simulated by the historical simulations (black curve, before 2006) and the projections (tinted curves, after 2007) of the CMIP5 climate models. 69*
*Figure 47 : Example of the average sterodynamic component (in m) simulated by the CMIP5 models ensemble in 2100 (relative to the 1986-2005 reference period) according to the RCP4.5 climate scenario. This map is produced with the climate service https://sealevelrise.brgm.fr. The spatial resolution is 1° x 1° longitude x latitude. 70*
*Figure 48 : Spatial fingerprint of relative sea level associated with mass balances of (a) the Greenland ice sheet and (b) continental glaciers. Values are unitless coefficients corresponding to the ratio between local and global elevation. From Kopp et al. (2015). 71*
*Figure 49 : Results of sea-level projections for Mauritius relative to the reference period (1990-2000) for historical reconstruction (black), RCPs 2.6 (green), 4.5 (blue), 8.5 (red) and the high-end scenario (dark red dash). The envelope indicates the likely range (66%-100% probability in IPCC terminology). The pink curve shows the annual average of tide gauge observations. 74*
*Figure 50 : Results of sea-level projections for Rodrigues relative to the reference period (1990-2000) for historical reconstruction (black), RCPs 2.6 (green), 4.5 (blue), 8.5 (red) and the high-end scenario (dark red dash). The envelope indicates the likely range (66%-100% probability in IPCC terminology). The pink curve shows the annual average of tide gauge observations. 75*
*Figure 51 : As Figure 50 but considering an additional land subsidence of 2 mm/year 76*
*Figure 52 : Impact of morphology and topography of the backshore on the coastal retreat linked to the sea level rise (SL: sea level; Coast.: coastline) 80*
*Figure 53 : Effect on the coastal retreat of A) sea level rise, B) coastal erosion, C) both (SL: sea level, Coast: coastline) 81*
*Figure 54 : Diagram of the different contributions to the water level during a storm (surges) as far as the shore (source BRGM) 82*
*Figure 55 : Example of possible chronologies in the event of marine submersion (overtopping / overflow / failure, ©BRGM) 83*

*Figure 56 : Matrix for determining coastal flooding hazard.* 84
*Figure 57 : Homogeneous coastal zones of Flic-en-Flac* 85
*Figure 58 : Calculation of the sedimentary dune reservoir used to assess the extreme retreat of an open sandy coastline (FEMA)* 89
*Figure 59 : Bruun erosion rule. Assumed evolution of the beach profile and main descriptive parameters: a, rise in sea level; L, length of beach profile subject to wave influence; h, height between the coastline and the bottom of the pre-littoral domain. From Bruun 1983.* 92
*Figure 60 : Modified Bruun rule used within the project* 93
*Figure 61 : Overview of the DTM at the regional DTM (note that the inland part of Mauritius is not integrated)* 104
*Figure 62 : Overview of the coastal DTM of Mauritius Island (note that the inland part is not integrated and the corresponding DTM corresponds to an interpolation of the coastal data)* 105
*Figure 63 : Overview of the coastal DTM of Rodrigues Island* 106
*Figure 64 : Examples of « high constraint lines » (obstacles to the flow): dike in Trou d'Eau Douce (left) and raised seafront in Grand-Baie (right)* 107
*Figure 65 : Examples of « low constraint lines » (preferential passage for the flow): stream outlet in Rivière du Rempart (left) and channel between the mainland and an island near Rivière des Galets (right)* 107
*Figure 66 : Use of constraint lines in the Maurice island model (DTM in the background). Black line represents the coastline.* 108
*Figure 67 : Use of constraint lines in the Rodrigues Island model (DTM in the background). Black line represents the coastline.* 109
*Figure 68 : Examples of hydraulic connections in Port-Louis (left) and Trou d'Eau Douce (right)* 109
*Figure 69 : zoom on some culverts in the Calodyne and Butte à l'herbe beach area that are taken into account in the Anse la Raie model (DTM in the background). Black line represents the coastline.* 110
*Figure 70 : zoom on some culverts in the Anse Grande Var area that are taken into account in the Rodrigues model (DTM in the background). Black line represents the coastline.* 110
*Figure 71 : Extension of the computational mesh on the Mauritius Island, including the location of the forcing points; grid overview with two zooms on the Port Louis (bottom left) and Trou d'Eau Douce (bottom right) areas.* 111
*Figure 72 : Extension of the computational mesh on the Rodrigues Island, including the location of the forcing points; grid overview with two subsequent zooms on the lagoon (bottom right) and on the Port Mathurin (bottom left) area.* 112
*Figure 73 : Land cover in Mauritius; close-up views on the Flic-en-Flac (top-right) and Maurice-north areas.* 113
*Figure 74 : Land cover in Rodrigues and close-up view on the Port Mathurin area (right).* 114
*Figure 75 : Map of potential coastline retreat (CLR) by sediment cell and homogeneous coastal zone in Mauritius for the current period and intermediate scenario.* 115
*Figure 76 : Maps of potential coastline retreat (CLR) by sediment cell and homogeneous coastal zones in Mauritius for the current period and the three studied scenarios.* 116
*Figure 77 : Assessment of potential coastline retreats (CLR) assessed by sedimentary cells and homogeneous zones for the current period in Mauritius. Frequency histogram and cumulative percentage graph.* 116
*Figure 78 : Map of potential coastline retreat (CLR) by sediment cell and homogeneous coastal zone in Mauritius for the 2050 period and intermediate scenario.* 117
*Figure 79 : Maps of potential coastline retreat (CLR) by sediment cell and homogeneous coastal zones in Mauritius for the 2050 period and the three studied scenarios* 118
*Figure 80 : Assessment of potential coastline retreats (CLR) assessed by sedimentary cells and homogeneous zones for the 2050 period in Mauritius. Frequency histogram and cumulative percentage graph.* 118
*Figure 81 : Map of potential shoreline retreat (CLR) by sediment cell and homogeneous coastal zone in Mauritius for the 2100 period and intermediate scenario.* 120
*Figure 82 : Maps of potential coastline retreat (CLR) by sediment cell and homogeneous coastal zones in Mauritius in 2100 (Mauritius) and the three studied scenarios* 121
*Figure 83 : Assessment of potential coastline retreats (CLR) assessed by sedimentary cells and homogeneous coastal zones in 2100 (Mauritius). Frequency histogram and cumulative percentage graph.* 121
*Figure 84 : Cyclone Berguitta 2018 best track form the IBTrACS database.* 122
*Figure 85 : Comparison of waves from WW3 and satellites for TC Berguitta on 16/01/2018 at 14:00 UTC* 123
*Figure 86 : Simulation of maximum Hs and wave peak directions generated by Berguitta (2018) in Mauritius.* 124
*Figure 87 : Simulation of maximum water levels generated by Berguitta (2018) in Mauritius.* 124

*Figure 88 : Validation of the computed water level against tidal gauge data at Port-Louis.* 125
*Figure 89 : Extract from the video showing the coastal flooding on the public beach at Poste Lafayette during Berguitta (source, https://www.facebook.com/www.defimedia.info/videos/cyclone-berguitta-le-niveau-de-la-mer-monte-%C3%A0-poste-lafayette-dans-lest-de-l%C3%AEle/1717829278280088/).* 125
*Figure 90 : Simulated water heights on Poste Lafayette beach during Berguitta.* 125
*Figure 91 : Positioning of scenarios 1498 and 357 in the joint exceedance iso-contours for return period of 100 years within the space (NM ; Hs) with the colour indicating the U values in Mauritius forcing point for actual and 2050 climate scenario.* 126
*Figure 92 : Positioning of scenarios 1498 and 2423 in the joint exceedance iso-contours for return period of 100 years within the space (SSH ; Hs) with the colour indicating the U values in Mauritius forcing point for 2100 climate scenario.* 126
*Figure 93 : Cyclones' tracks for the three chosen scenarios 357, 1498, and 2423 of the Météo-France database.* 127
*Figure 94 : De-trended monthly MSL (mean sea level) plotted for each month of the year for the length of the respective tide gauge record of Port-Louis (1986-2024).* 128
*Figure 95 : Time evolution of the pressure field over the Mauritius computational domain during the 357 scenario on actual and 2050 climate.* 129
*Figure 96 : Time evolution of the wind field over the Mauritius computational domain during the 357 scenario on actual and 2050 climate.* 129
*Figure 97 : Tidal signal during the 357 scenarios, provided by the FES2014 database on the seven forcing locations of the Mauritius model.* 130
*Figure 98 : Time evolution of the pressure field over the Mauritius computational domain during the 1498 scenario on actual and 2050 climate.* 130
*Figure 99 : Time evolution of the wind field over the Mauritius computational domain during the 1498 scenario on actual and 2050 climate.* 131
*Figure 100 : Time evolution of the pressure field over the Mauritius computational domain during the 1498 scenario on 2080-2100 climate.* 131
*Figure 101 : Time evolution of the wind field over the Mauritius computational domain during the 1498 scenario on 2080-2100 climate.* 132
*Figure 102: Tidal signal during the 1498 scenario, provided by the FES2014 database on the seven forcing locations of the Mauritius model.* 132
*Figure 103 : Time evolution of the pressure field over the Mauritius computational domain during the 2423 scenario on 2100 climate.* 133
*Figure 104 : Time evolution of the wind field over the Mauritius computational domain during the 2423 scenario on 2100 climate.* 133
*Figure 105 : Tidal signal during the 2423 scenario, provided by the FES2014 database on the seven forcing locations of the Mauritius model.* 134
*Figure 106 : Overall map of the computed maximum significant wave height with actual climate on scenarios 1498 (left) and 357 (right).* 135
*Figure 107 : Overall map of the computed maximum significant wave height with 2050 climate on scenarios 1498 (left) and 357 (right).* 135
*Figure 108 : Overall map of the computed maximum significant wave height with 2080-2100 climate on scenarios 1498 (left) and 2423 (right).* 136
*Figure 109 : Overall map of the computed maximum sea currents velocity with actual climate on scenarios 1498 (left) and 357 (right).* 137
*Figure 110 : Overall map of the computed maximum sea currents velocity with 2050 climate on scenarios 1498 (left) and 357 (right).* 137
*Figure 111 : Overall map of the computed maximum sea currents velocity with 2080-2100 climate on scenarios 1498 (left) and 2423 (right).* 138
*Figure 112 : Overall map of the computed maximum sea surface height with actual climate on scenarios 1498 (left) and 357 (right).* 139
*Figure 113 : Overall map of the computed maximum sea surface height with 2050 climate on scenarios 1498 (left) and 357 (right).* 139
*Figure 114 : Overall map of the computed maximum sea surface height with 2080-2100 climate on scenarios 1498 (left) and 2423 (right).* 140

*Figure 115 : A close-up comparison of the computed maximum sea surface height on the Grand Baie area for the most impactful scenarios.* 141
*Figure 116 : A close-up comparison of the computed maximum sea surface height on the Mahébourg area for the most impactful scenarios.* 142
*Figure 117 : A close-up comparison of the computed maximum sea surface height on the Port Louis area for the most impactful scenarios.* 143
*Figure 118 : Flooding hazard maps on the Grand Baie area for present-day climate conditions (top), 2050 climate (centre) and 2080-2100 climate (bottom).* 144
*Figure 119 : Flooding hazard maps on the Mahébourg area for present-day climate conditions (top), 2050 climate (centre) and 2080-2100 climate (bottom).* 145
*Figure 120 : Flooding hazard maps on the Port Louis area for present-day climate conditions (top), 2050 climate (centre) and 2080-2100 climate (bottom).* 146
*Figure 121 : Coastal zones of Rodrigues and geology. Six rocky areas with small sedimentary areas whose potential retreat has been assessed.* 147
*Figure 122 : Map of potential shoreline retreat (CLR) by sediment cell and homogeneous coastal zone in Rodrigues for the current period and intermediate scenario.* 148
*Figure 123 : Maps of potential coastline retreat (CLR) by sediment cell and homogeneous zones in Rodrigues for the current period and the three studied scenarios* 149
*Figure 124 : Assessment of potential coastline retreats (CLR) assessed by sedimentary cells and homogeneous coastal zones for the current period in Rodrigues. Frequency histogram (%) and cumulative percentage graph.* 149
*Figure 125 : Map of potential coastline retreat (CLR) by sediment cell and homogeneous coastal zone in Rodrigues for the 2050 period and intermediate scenario.* 150
*Figure 126 : Maps of potential coastline retreat (CLR) by sediment cell and homogeneous coastal zones in Rodrigues for the 2050 period and the three studied scenarios* 151
*Figure 127 : Assessment of potential coastline retreats (CLR) assessed by sedimentary cells and homogeneous coastal zones for the 2050 period in Rodrigues. Frequency histogram (%) and cumulative percentage graph.* 151
*Figure 128 : Map of potential shoreline retreat (CLR) by sediment cell and homogeneous coastal zone in Rodrigues for the 2100 period and intermediate scenario.* 153
*Figure 129 : Maps of potential coastline retreat (CLR) by sediment cell and homogeneous coastal zones in Rodrigues for the 2100 period and the three studied scenarios* 154
*Figure 130 : Assessment of potential coastline retreats (CLR) assessed by sedimentary cells and homogeneous coastal zones for the 2100 period in Rodrigues. Frequency histogram (%) and cumulative percentage graph.* 154
*Figure 131 : Cyclone Bella 1991 best track from the IBTrACS database.* 155
*Figure 132 : Computed maximum significant wave height and the wave propagation peak direction generated by Bella (1991) on the whole computational domain.* 156
*Figure 133 : Computed maximum water levels (SSH_max) on the cyclone Bella (1991).* 156
*Figure 134 : Validation of the computed water level against tidal gauge data at Port-Mathurin.* 157
*Figure 135 : Computed and water height on the cyclone Bella (1991)– zoom on the Port Mathurin area.* 157
*Figure 136 : Positioning of scenarios 63 and 591 in the joint exceedance iso-contours for return period of 100 years within the space (NM; Hs) with the colour indicating the U values at Rodrigues forcing point for actual and 2050 climate scenario.* 158
*Figure 137 : Positioning of scenarios 63 and 591 in the joint exceedance iso-contours for return period of 100 years within the space (NM; Hs) with the colour indicating the U values at Rodrigues forcing point for 2100 climate scenario.* 158
*Figure 138 : Cyclones' tracks for the scenario ITC 63 and ITC 591of the Météo-France database.* 159
*Figure 139 : De-trended monthly MSL (mean sea level) plotted for each month of the year for the length of the respective tide gauge record of Port-Mathurin (1986-2024).* 160
*Figure 140 : Time evolution of the pressure field over the Rodrigues computational domain during the 63 scenario on actual and 2050 climate.* 161
*Figure 141 : Time evolution of the wind field over the Rodrigues computational domain during the 63 scenario on actual and 2050 climate.* 162
*Figure 142 : Time evolution of the pressure field over the Rodrigues computational domain during the 63 scenario on 2080-2100 climate.* 163
*Figure 143 : Time evolution of the wind field over the Rodrigues computational domain during the 63 scenario on 2100 climate.* 164

*Figure 144 : Tidal signal during the 63 scenario, provided by the FES2014 database on the four forcing locations of the Rodrigues model.* 165
*Figure 145 : Overall map of the computed maximum sea currents velocity on the scenario 63 with actual climate (left) and with 2080-2100 climate and island subsidence (right).* 166
*Figure 146 : Overall map of the computed maximum significant wave height on the scenario 63 with actual climate (left) and with 2080-2100 climate and island subsidence (right).* 166
*Figure 147 : Close-up view on the north (right) and south lagoon channels for the computed maximum significant wave height on the scenario 63 with actual climate.* 167
*Figure 148 : Overall map of the computed maximum sea surface height (SSH_max) on the scenario 63 with present-day climate conditions (top), 2050 climate (centre) and 2100 climate (bottom).* 168
*Figure 149 : A close-up comparison on the Anse Mourouk area of the computed maximum sea surface height (SSH_max) on the scenario 63 with present-day climate conditions (top), 2050 climate (centre) and 2100 climate (bottom).* 169
*Figure 150 : A close-up comparison on the Anse Mourouk area of the computed maximum water height (H_max) on the scenario 63 with present-day climate conditions (top), 2050 climate (centre) and 2100 climate (bottom).* 170
*Figure 151 : Flooding hazard maps on the Anse Mourouk area for present-day climate conditions (top), 2050 climate (centre) and 2100 climate (bottom).* 171
*Figure 152 : A close-up comparison on the Grand Baie area of the computed maximum sea surface height (SSH_max) on the scenario 63 with present-day climate conditions (top), 2050 climate (centre) and 2100 climate (bottom).* 172
*Figure 153 : A close-up comparison on the Grand Baie area of the computed maximum water height (H_max) on the scenario 63 with present-day climate conditions (top), 2050 climate (centre) and 2100 climate (bottom).* 173
*Figure 154 : Flooding hazard maps on the Grand Baie area for present-day climate conditions (top), 2050 climate (centre) and 2100 climate (bottom).* 174
*Figure 155 : Time series of the sea surface level on different locations around the island for the actual climate scenario.* 175
*Figure 156 : Wave setup time history for some locations of the Rodrigues island on the scenario 63 with actual climate conditions.* 176
*Figure 157 : Left: topography and location of profiles at the Flic-en-Flac site; centre: lithology of the coastline; right: potential hazards and flow of sediments.* 179
*Figure 158 : Erosion scarp of the upper beach (Flic-en-Flac, northern third of the beach, 2022)* 180
*Figure 159 : Variability of the topographic sections of the dune (Flic-en-Flac, profiles location in the Figure 157)* 181
*Figure 160 : Left: lithology of the coastline at Anse la Raie, right: topography behind Anse la Raie* 182
*Figure 161 : The relationship between Anse la Raie and the reef complex and the input of bioclastic sand* 183
*Figure 162 : Very low-lying area of Anse la Raie - Note the high vulnerability of the road to coastal flooding* 184
*Figure 163 : The Port-Mathurin site* 185
*Figure 164 : Lithology and topography of the Port-Mathurin site* 186
*Figure 165 : Left: concrete quay at the Port-Mathurin harbour; right: low-lying urban area immediately behind the Port-Mathurin coastline* 186
*Figure 166 : low-lying urban area on either side of a river mouth (Port-Mathurin); right: low-lying area on the seafront made up of embankments and protected by revetments (Port-Mathurin)* 187
*Figure 167 : Overview of the local DTM of the Flic-en-Flac site on the Mauritius Island (2m resolution)* 188
*Figure 168 : Overview of the local DTM of the Anse la Raie site on the Mauritius Island (2m resolution).* 189
*Figure 169 : Use of constraint lines in the Flic-en-Flac model (DTM in the background).* 190
*Figure 170 : Use of constraint lines in the Anse la Raie model (DTM in the background).* 191
*Figure 171 : Extension of the computational mesh and grid overview on the Flic-en-Flac area, including the location of the forcing point.* 192
*Figure 172 : Extension of the computational mesh and grid overview on the Anse la Raie area, including the location of the forcing points.* 193
*Figure 173 : Homogeneous coastal zones, sub-cells (JICA, 2015) and coastal geology of Flic-en-Flac.* 194
*Figure 174 : Map of coastline retreat estimations (CLR) for 2025 timeframe, at the scale of homogeneous coastal zones and sub-cells of Flic-en-Flac.* 199
*Figure 175 : Map of coastline retreat estimations (CLR) for 2050 timeframe, at the scale of homogeneous coastal zones and sub-cells of Flic-en-Flac.* 200

*Figure 176 : Map of coastline retreat estimations (CLR) for 2100 timeframe, at the scale of homogeneous coastal zones and sub-cells of Flic-en-Flac.* 201
*Figure 177 : Maps of coastline retreat hazard for 2025, 2050 and 2100, median scenario. Zoom of 4 hazard-sensitive areas for Flic-en-Flac.* 202
*Figure 178 : Maps of coastline retreat hazard for 2025, 2050 and 2100, intermediate scenario. Zoom of 4 hazard-sensitive areas for Flic-en-Flac* 203
*Figure 179 : Maps of coastline retreat hazard for 2025, 2050 and 2100, safe scenario. Zoom of 4 hazard-sensitive areas for Flic-en-Flac.* 204
*Figure 180 : Maps of coastline retreat hazard for 2025, median, intermediate and safe scenarios. Zoom of 4 hazard-sensitive areas for Flic-en-Flac.* 206
*Figure 181 : Maps of coastline retreat hazard for 2050, median, intermediate and safe scenarios. Zoom of 4 hazard-sensitive areas for Flic-en-Flac* 207
*Figure 182 : Maps of coastline retreat hazard and sea level rise impacts for 2100, median, intermediate and safe scenarios. Zoom of 4 hazard-sensitive areas for Flic-en-Flac.* 208
*Figure 183 : Layout of SWASH profiles on Flic-en-Flac and Uhaina injection points (red crosses). Right panel: zoom between the profiles 22 and 29.* 210
*Figure 184 : Cyclone Belal 2024 best track from the IBTrACS database.* 211
*Figure 185 : Simulation of maximum Hs and wave peak directions generated by Belal (2024) on Flic-en-Flac.* 211
*Figure 186 : Simulated overtopping for Belal at Flic-en-Flac between profiles 20 and 24.* 212
*Figure 187 : Extract from the video showing the coastal flooding on Flic-en-Flac during Belal (source: https://www.tiktok.com/@radiomoris/video/7324249532991032608).* 212
*Figure 188 : Simulation of maximum Hs and wave peak directions generated by the scenario 1498 on the three climate horizons at Flic-en-Flac.* 213
*Figure 189 : Main stages of the coastal flooding at Flic-en-Flac (actual climate scenario; T0: beginning of the simulation).* 214
*Figure 190 : Coastal flooding hazard generated by the scenario 1498 on the three climate horizons at Flic-en-Flac.* 214
*Figure 191 : Homogeneous coastal zones and coastal geology of Anse la Raie, Cap Malheureux.* 215
*Figure 192 : Coastline change at Anse la Raie from 2009 to 2023 (appendix 1)* 216
*Figure 193 : Position and condition of the coral reefs in front of Anse la Raie (according to ESA, 2009)* 219
*Figure 194 : Map of coastline retreat estimations (CLR) for 2025 timeframe, at the scale of Anse la Raie and neighbouring sub-cells of Cap Malheureux.* 221
*Figure 195 : Map of coastline retreat estimations (CLR) for 2050 timeframe, at the scale of Anse la Raie and neighbouring sub-cells of Cap Malheureux.* 221
*Figure 196 : Map of coastline retreat estimations (CLR) for 2100 timeframe, at the scale of Anse la Raie and neighbouring sub-cells of Cap Malheureux.* 222
*Figure 197 : Coastline retreat hazard for 2025, median, intermediate and safe scenarios for Anse la Raie.* 223
*Figure 198 : Coastline retreat hazard for 2050, median, intermediate and safe scenarios for Anse la Raie.* 224
*Figure 199 : Coastline retreat hazard and sea-level rise impacts for 2100, median, intermediate and safe scenarios for Anse la Raie.* 224
*Figure 200 : Maps of coastline retreat hazard for 2025, 2050 and 2100, median scenario for Anse la Raie.* 225
*Figure 201 : Maps of coastline retreat hazard for 2025, 2050 and 2100, intermediate scenario for Anse la Raie.* 226
*Figure 202 : Maps of coastline retreat hazard for 2025, 2050 and 2100, safe scenario for Anse la Raie.* 226
*Figure 203 : Extract from the video showing the coastal flooding in Anse La Raie during Berguitta (source:https://www.facebook.com/www.defimedia.info/videos/cyclone-berguitta-en-direct-danse-la-raie-dans-le-nord-de-l%C3%AEle/1717750718287944/)* 227
*Figure 204 : Simulated water heights at Anse La Raie beach during Berguitta.* 227
*Figure 205 : Computed maximum significant wave height (top) and sea current velocities (bottom) for the scenario 1498 with present-day climate conditions.* 229
*Figure 206 : Time series of the total sea level (SSH) and wave setup contribution on Anse la Raie for actual climate (top), 2050 climate (centre) and 2080-2100 climate (bottom).* 230
*Figure 207 : Computed maximum sea surface height (SSH_max) on the scenario 1498 with present-day climate conditions (top-left), 2050 climate (top-right) and 2100 climate (bottom).* 231
*Figure 208 : Close-up view of the computed maximum sea surface height (SSH_max) on the Anse la Raie area for the three climate scenarios.* 232

*Figure 209 : Close-up view of the computed maximum water height (H_max) on the Anse la Raie area for the three climate scenarios.* 233
*Figure 210 : Close-up view of the computed maximum current velocities (U_max) on the Anse la Raie area for the three climate scenarios.* 234
*Figure 211 : Computed hazard on the Anse la Raie area for the three climate scenarios.* 235
*Figure 212 : Computed hazard map on the Roches Noires area for the three climate scenarios.* 236
*Figure 213 : Homogeneous coastal zones and coastal geology of Port Mathurin, Rodrigues.* 237
*Figure 214 : Damages observed on the Port Mathurin riprap structures (December 2024).* 238
*Figure 215 : Map of coastline retreat estimations for 2025 timeframe, at the scale of Port Mathurin and neighbouring sub-cells in Rodrigues.* 241
*Figure 216 : Map of coastline retreat estimations for 2050 timeframe, at the scale of Port Mathurin and neighbouring sub-cells in Rodrigues.* 242
*Figure 217 : Map of coastline retreat estimations for 2100 timeframe, at the scale of Port Mathurin and neighbouring sub-cells in Rodrigues.* 243
*Figure 218 : Coastline retreat hazard in Port Mathurin for 2025 under median, intermediate, and safe scenarios.* 244
*Figure 219 : Coastline retreat hazard in Port Mathurin for 2050 under median, intermediate, and safe scenarios.* 245
*Figure 220 : Coastline retreat hazard in Port Mathurin for 2100 under median, intermediate, and safe scenarios.* 246
*Figure 221 : Coastline retreat hazard in Port Mathurin by 2025, 2050, and 2100 under the median (a), intermediate (b), and safe (c) scenarios.* 248
*Figure 222 : Time series of the total sea level (SSH) and wave setup contribution at the tide gauge position on Port Mathurin for the actual climate scenario (top), 2050 climate (centre) and 2100 climate (bottom).* 250
*Figure 223 : A close-up comparison on the Port Mathurin area of the computed maximum sea surface height (SSH_max) on the scenario 63 with present-day climate conditions (top), 2050 climate (centre) and 2100 climate (bottom).* 251
*Figure 224 : A close-up comparison on the Port Mathurin area of the computed maximum water height (H_max) on the scenario 63 with present-day climate conditions (top), 2050 climate (centre) and 2100 climate (bottom).* 252
*Figure 225 : A close-up comparison on the Port Mathurin area of the computed maximum sea currents velocity (U_max) on the scenario 63 with present-day climate conditions (top), 2050 climate (centre) and 2100 climate (bottom).* 253
*Figure 226 : Flooding hazard maps on the Port Mathurin for present-day climate conditions (top), 2050 climate (centre) and 2100 climate (bottom).* 254

# List of tables

*Table1 : 100-year return levels for each driver using the marginal for Mauritius (present day and future climate scenario). Numbers in brackets correspond to the 95% confidence interval.* 51
*Table 2. 100-year return levels for each driver using the marginal for Rodrigues (present day and future climate scenario). Numbers in brackets correspond to the 95% confidence interval.* 56
*Table 3: Characteristics of tide gauge observations* 64
*Table 4: Ground movement vertical velocity (in mm/year) estimated by different solutions at the permanent GPS stations available in Mauritius and Rodrigues.* 67
*Table 5 : Data sources and estimates for the Glaciers, Greenland and Antarctica components in 2050 and 2100 use to design the high-end scenario.* 73
*Table 6: Values of relative sea level projections corresponding to Figure 49 for Mauritius in 2050 and 2100 with respect to the reference period. The median is shown in bold and the likely range is in brackets.* 75
*Table 7 : Values of relative sea level projections corresponding to Figure 50 for Rodrigues in 2050 and 2100 with respect to the reference period. The median is shown in bold and the likely range is in brackets.* 76
*Table 8 : Coastline change rates for Flic-en-Flac coastal sub-cells, according to JICA (2015)* 86
*Table 9 : Sandy coastline retreat settings for Flic-en-Flac coastal sub-cells* 86
*Table 10 : Instantaneous retreat values (Lmax) for present, 2050 and 2100* 88
*Table 11 : Comparison of Lmax values from different sources* 90
*Table 12 : Instantaneous retreat values (Lmax) using FEMA 540SF approach for present, 2050 and 2100* 90
*Table 13 : Different closure depths in relation with wave characteristics and the type of coast* 94
*Table 14: Coastline retreat rate parameters for the 3 variants of scenario and different study timeframes* 98

*Table 15: Lmax parameters for coral lagoons of the west coast of Mauritius, based on Baird study (2003) for Flic-en-Flac.* 98
*Table 16 : Lmax parameters for coral lagoons of the Est coast of Mauritius, based on Baird study (2003) for Bellemare.* 98
*Table 17 : Lmax parameters for Mauritius (open sandy coast) and Rodrigues. Adaptation of the Fema 540SF method.* 98
*Table 18: Sea-level rise parameters for coastline retreat study, Mauritius.* 99
*Table 19: Sea-level rise parameters for coastline retreat study, Rodrigues.* 99
*Table 20: Assumptions used to reduce the estimate of coral sediment production ($E_m$)* 99
*Table 21: Coastline retreat scenarios (m) for basaltic rocky coast* 100
*Table 22: Coastline retreat scenarios (m) for limestone coast of Rodrigues* 100
*Table 23: Simplified scenario for additional retreat of the rocky coastline, in the event of erosion of the barrier beach* 101
*Table 24 : Scenarios for estimating the SLR-R parameter, this altitude corresponds to the possible rise in sea level over low-lying areas of Mauritius.* 101
*Table 25: Scenarios for estimating the SLR-R parameter, This altitude corresponds to the possible rise in sea level over low-lying areas of Rodrigues.* 101
*Table 26 : Coastline retreat parameters for each sub-cell, HCZ and coastal cell of Flic-en-Flac territory* 195
*Table 27 : Estimated impact of extreme events (Lmax) -Flic-en-Flac* 196
*Table 28 : Estimated values of additional coastal retreat for Flic-en-Flac coastline* 197
*Table 29 : Coastline retreat estimations for homogeneous zones and sub-cells of Flic-en-Flac, 2025, 2050 and 2100 timeframes* 198
*Table 30 : Coastline retreat parameters for neighbouring or similar coastal cells to Cap Malheureux, whose evolution is dealt with by JICA (2015).* 217
*Table 31 : Coastline retreat parameters for each homogeneous zone of Cap Malheureux territory, on the basis of expert opinion. The Anse la Raie site corresponds to the CaM_CHZ04 zone.* 217
*Table 32 : Estimated impact of extreme events (Lmax) for Anse La Raie, based on Baird model (2003) for Bellemare* 218
*Table 33 : Estimated values of additional coastal retreat for Anse la Raie coastline* 220
*Table 34 : Coastline retreat estimations (m) for homogeneous zone of Anse la Raie (Cap Malheureux), 2025, 2050 and 2100 timeframes* 220
*Table 35 : Estimated impact of extreme events (Lmax) -Port Mathurin, downtown (RPoM_02).* 237
*Table 36 : Coastline retreat parameters for shoreline change sectors of Rodrigues based on satellite image analysis.* 239
*Table 37 : Coastline retreat parameters for Pointe Monnier homogeneous zone (RPoM_01), Port Mathurin, Rodrigues.* 239
*Table 38 : Estimated impact of extreme events (Lmax) -Pointe Monnier, Port Mathurin, (RPoM_01).* 240
*Table 39 : Estimated values of additional coastal retreat for Pointe Monnier coastline (Port Mathurin)* 240
*Table 40 : Coastline retreat estimations (m) for homogeneous zone of Port Mathurin (Rodrigues), 2025, 2050 and 2100 timeframes.* 241

# List of abbreviations

| Symbol | Definition |
|---|---|
| AR | Assessment Report |
| C3S | Copernicus Climate Change Service |
| CLR | Coastline Retreat hazard |
| CMEMS | Copernicus Marine Environmental Monitoring Service |
| CMIP5 | Coupled Model Intercomparison Project Phase 5 |
| Dc | Depth of Closure |
| DEM | Digital Elevation Model |
| Di | Internal depth of closure |
| Dp | Peak wave diection |
| DTM | Digital Terrain Model |
| Du | Wind direction |
| ESA | Environmentally Sensitive Area of Mauritius |
| FEMA | Federal Emergency Management Agency (USA) |
| FES2014 | Finite Element Solution - 2014 |
| GESLA | Global Extreme Sea Level Analysis |
| GFZ | Deutsches GeoForschungsZentrum |
| GHC | Greenhouse Gas Protocol |
| GIS | Geographic Information System |
| GPD | Generalised Pareto distribution |
| GPS | Global Positioning System |
| GRD | Gravitational Rotational solid-Earth Deformation |
| GrIS | Greenland Ice-Sheet |
| H_max | Maximum water height |
| HAT | Highest Astronomical Tide |
| HCZ | Homogeneous Coastal Zone (for CLR study) |
| Hs | Significant wave height |
| Hs_max | Maximum significant wave height |
| IBTrACS | International Best Track Archive for Climate Stewardship |
| ICDC | Integrated Climate Data Center |
| IPCC | Intergovernmental Panel on Climate Change |
| JICA | Japan International Cooperation Agency |
| JPL | Jet Propulsion Laboratory |
| LAT | Lowest Astronomical Tide |
| Lmax | Estimated impact of extrem event for CLR |
| MICI | Marine Ice Cliff Instability |

| | |
|---|---|
| MISI | Marine Ice Sheet Instability |
| MSL | Mean Sea Level |
| NGL | Nevada Geodetic Laboratory |
| PSMSL | Permanent Service for Mean Sea Level |
| RCP | Representative Concentration Pathway |
| RSL | Relative Sea Level |
| SC | Sub-cell (for CLR Study) |
| SLP | Relative atmospheric pressure |
| SLR | Sea Level Rise |
| SLR-R | Coastline Retreat due to SLR |
| SONEL | Système d'Observation du Niveau des Eaux Littorales |
| SROCC | Special Report on the Ocean and Cryosphere in a Changing Climate |
| SSH | Sea Surface Height |
| SSH_max | Maximum sea surface height |
| SSP | Shared Socioeconomic Pathways |
| $S_t$ | Wave steepness |
| Tp | Peak wave period |
| Tx | Rate of coastline retreat |
| $U$ | Wind speed |
| U_max | Maximum sea currents velocity |
| ULR | University of La Rochelle |
| VLM | Vertical Land Motion |
| WW3 | WAVEWATCH-3 model |
| v | Dependence model threshold |
| $u$, $\sigma$ and $\xi$ | GPD parameters |

# 1. INTRODUCTION

For several years now, the Mauritian government has been resolutely tackling the problem of climate change. In 2010, the Republic of Mauritius' national communication to the United Nations Framework Convention on Climate Change (UNFCCC) stated that the most significant impact of climate change in the coming years would be the increasing exposure of its islands to natural disasters. According to the World Risk Reports 2017 and 2022, Mauritius is ranked as the 13th country with the highest disaster risk and the 7th country most exposed to natural hazards. The expected effects of climate change are manifold. For example, in coastal areas, tropical cyclones may intensify, heavy rainfall (flash floods) may increase, and the environment may deteriorate (e.g. coral reefs). These changes are linked to a number of parameters induced by climate change, such as the sea level rise, the increase in sea surface temperature (SST), and the increase in the salinity and acidity of ocean waters. Changes in these factors will increase the exposure of coastal populations and coastal infrastructures to coastal hazards. The impacts on the tourism industry, which is a crucial economic sector for the GDP[1] of the Republic of Mauritius, are potentially very strong. It is therefore necessary to anticipate the effects of climate change, with the aim of ensuring that society adapts in a reasoned manner.

Consequently, the implementation of a disaster risk reduction strategy in the Republic of Mauritius is a key priority for actions to adapt to climate change. The main adaptation measures recommended by the "Nationally Determined Contributions" (NDC) for the period 2016-2030 are as follows:

- strengthening the protection of essential public infrastructures and coastal ecosystems;

- strengthening the protection of coastal zones;

- strengthening water supply security.

As part of the long-term assistance provided by AFD to support the Mauritian authorities, and following Mauritius' INDC and COP 21 commitments on Climate Change, Memoranda of Understanding have been signed between the Mauritian government and AFD to operationalize the Paris Agreement.

BRGM (the French Geological Survey) recently (2019) conducted a study on the vulnerability of the Republic of Mauritius to seismic and tsunami hazards under a UNDP call for tenders. The results of this study were presented by BRGM in Port-Louis on 19 September 2019 at a validation workshop attended by Mauritian stakeholders. Numerous recommendations were made at the end of the study. These included the need for the Republic of Mauritius to conduct an in-depth study of coastal risks. The Mauritian coastline is regularly exposed to the hazards of coastal erosion, retreat of the coastline and coastal flooding. It is also home to a large population and many social and economic issues (particularly tourism). This is the background to the MauRisCot project (2022-2025): "Operational study of coastal risks (coastal flooding and coastal erosion) on the islands of the Republic of Mauritius in the context of climate change" financed by AFD (Agreement: n° CMU 1091 01D). In addition to the multi-disciplinary expertise of BRGM, which is coordinating the project, the skills of the Indian Ocean Regional Office of Météo-France and the Universities of Limoges (GéoLab) and Mascareignes are being involved.

The aim of this project is to provide coastal erosion and coastal flooding hazard maps for three timeframes (present, 2050 and 2100) and to assess the associated risks. These maps will be produced on a scale of 1:20,000 and will cover the islands of Mauritius and Rodrigues. Three "hotspots", where the stakes are high for the Republic but also representative of the problems

[1] *Gross domestic product*

encountered, will be chosen in agreement with the Steering Committee. In these "hotspots", hazards and risks will be assessed on a more precise spatial scale (of the order of 1:5,000).

The project involved 17 tasks, the structure of which is shown in Figure 1.

These tasks are grouped into 6 main actions:

- Physical and environmental characterisation of the environments. This task was based on an analysis of the knowledge, data and bibliography dealing with these themes, and was enriched by field observations carried out on the coastline of the two islands.
- Definition and assessment of current and future forcings taking into account climate change (sea levels, cyclones, austral swells).
- Assessment and mapping of coastal retreat and coastal flooding hazards. This task was initially carried out on all the coastlines of the two islands, then for three sites of interest on a more precise scale.
- Socio-economic characterisation and coastal issues at the scale of the two islands and the three sites selected.
- Mapping of coastal risks by cross-referencing the mapping of hazards and issues.
- Assessment of the socio-economic impact of coastal risks, and evaluation of adaptation measures to deal with coastal risks in the context of climate change. A particular effort has been made to assess existing ecosystem services and the possibility of implementing nature-based solutions to make the coasts of Mauritius and Rodrigues more resilient.

It should be remembered that certain tasks not originally planned were carried out in this project in order to compensate for the absence of certain fundamental data for hazard assessment. These included, for example, the creation of a geo-referenced database of coastal structures and facilities on the two islands. The method used to carry out this work was presented in the phase 1 report (Rapport BRGM/RC-72793-FR, 2023) and the cartographic data produced will form part of the project deliverables. Another initially unplanned project involved characterising the erosion and mobility of the coastline on Rodrigues Island. This work was necessary because no data existed on this subject, but it was absolutely necessary to carry out this work. It is presented in appendix 1.

This phase 2 report is the third deliverable defined in the project specifications. It is composed of three main volumes and several appendices.

The first volume (this report BRGM/RC-73987-FR) deals with forcing factors (cyclone, sea-level rise, austral swells) and the modalities implemented to assess and map current and future (2050, 2100) coastal hazards.

The second (report BRGM/RC-73988-FR) describes the vulnerabilities and perceptions of different populations and stakeholders of coastal hazards and climate change. It also deals with the assessment of risks induced by coastal hazards at the three timeframes covered by the project.

The third volume (report BRGM/RC-73989-FR) looks at possible adaptation measures to coastal hazards in Mauritius and Rodrigues in the context of climate change and treat more in-depth nature-based solutions which appear promising.

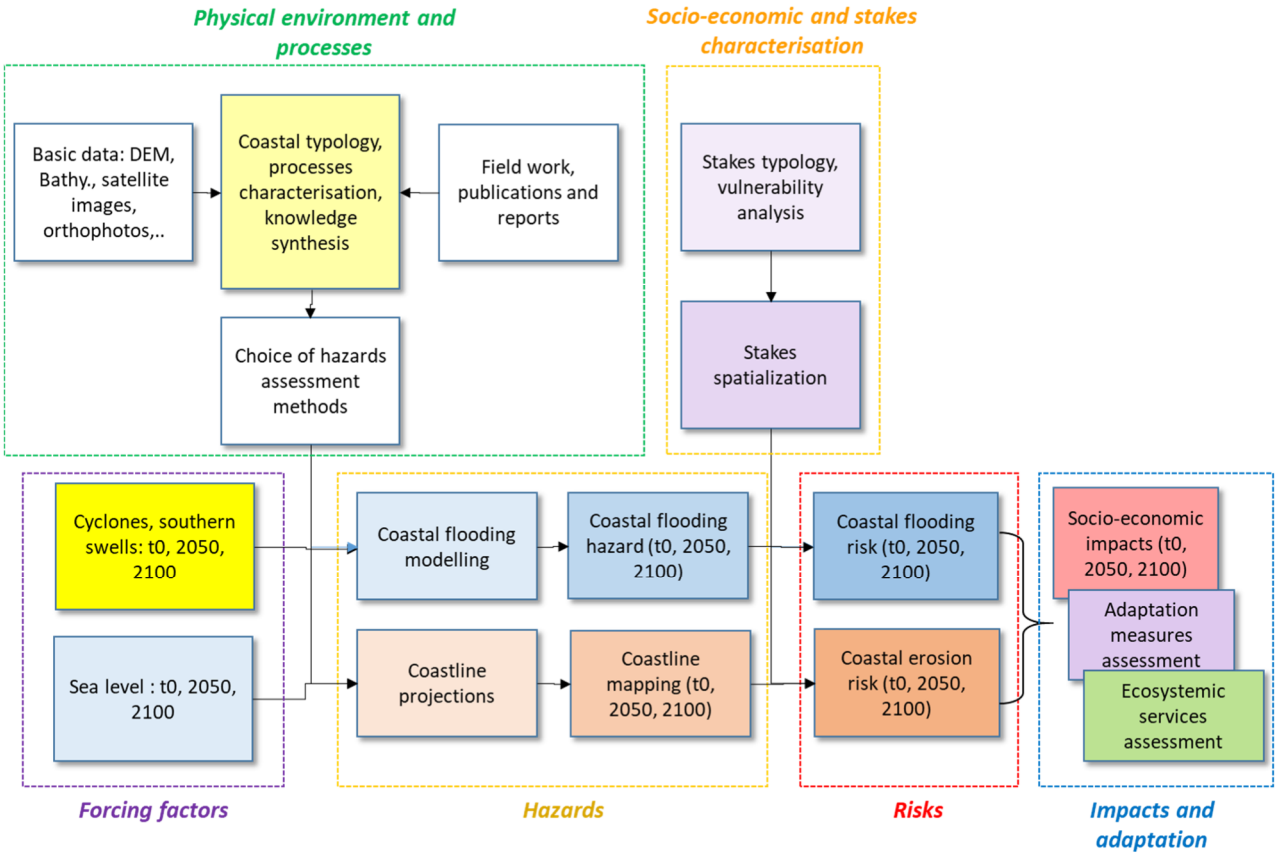


*Figure 1 : Relationship between the tasks involved in the project*

# 2. BACKGROUND INPUT DATA

Assessing and mapping the coastal hazards (coastal flooding, coastal erosion and coastline retreat) requires the collection of a topographic and bathymetric data set adapted (spatial resolution, quality and accuracy) to the methods and models used, and to the resolution and accuracy of the results targeted. An analysis of their quality, accuracy and reliability has been carried out and is presented in the following chapter.

## 2.1 TOPOGRAPHIC AND BATHYMETRIC DATA

### 2.1.1 Sources of altimetric and bathymetric data

Most of topo-bathymetric data were provided by Mauritian authorities. The main sources of topographic data are:

- The LiDAR DTM (Digital Terrain Model) of Mauritius island, at a 1m-resolution (Figure 2);
- A quite coarse DTM (Digital Terrain Model, about 20 m resolution) of Rodrigues Island (Figure 3);
- Other global topographic data (SRTM[2] and DeltaDTM[3]) have been used as a complement, especially for the centre of the islands and to represent other islands of Indian Ocean in large scale simulations.

Bathymetric data comes from a number of sources whose acquisition dates, resolution and accuracy vary greatly:

- Quite coarse bathymetric data, mainly offshore Mauritius and Rodrigues islands, provided by the Ministry of Housing and Lands (MHL) (Figure 4 : blue and red soundings, only outside the lagoon for Mauritius);
- Locally, quite dense coastal bathymetric data in Mauritius lagoon, provided by the Ministry of Housing and Lands (MHL) (Figure 4 : orange, blue and red soundings in Mauritius lagoon);
- Locally, very dense coastal bathymetric data in Mauritius and Rodrigues lagoon, provided by MOI (Figure 5);
- Other global bathymetric data have been used as a complement, especially to represent the Indian Ocean in large scale simulations (Gebco[4]).

Due to the lack of data in some sectors, some data have been digitalized from nautical charts and integrated in the bathymetric database.

[2] https://portal.opentopography.org/raster?opentopoID=OTSRTM.082015.4326.1
[3] https://data.4tu.nl/datasets/1da2e70f-6c4d-4b03-86bd-b53e789cc629
[4] https://www.gebco.net/

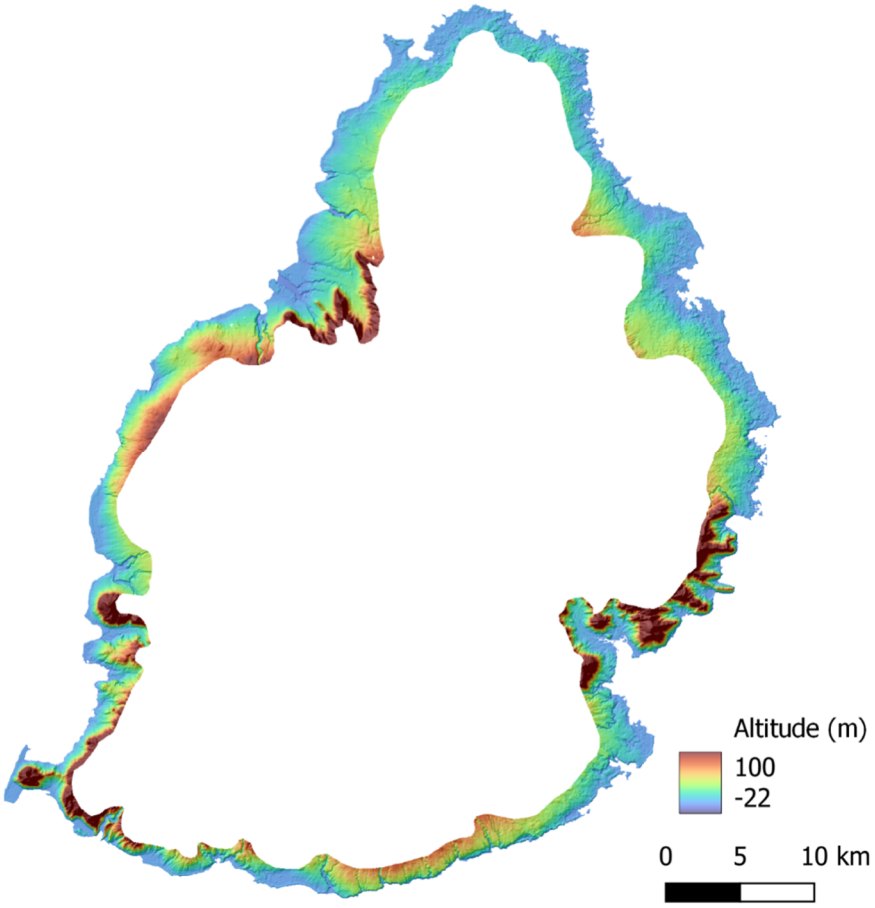


*Figure 2 : Overview of the LiDAR DTM of Mauritius Island*

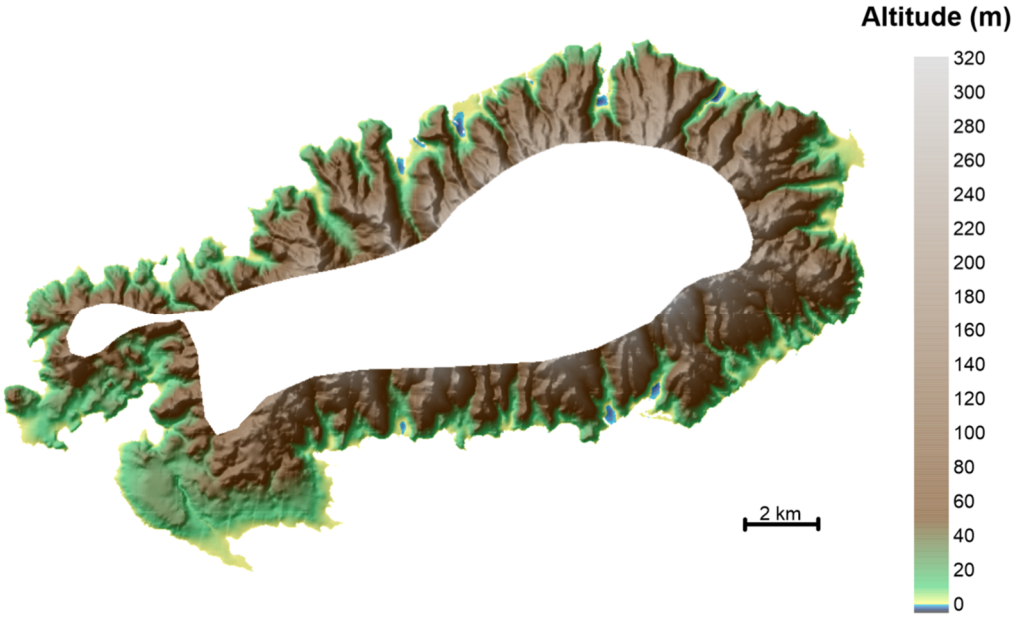


*Figure 3 : Overview of the DTM of Rodrigues Island*

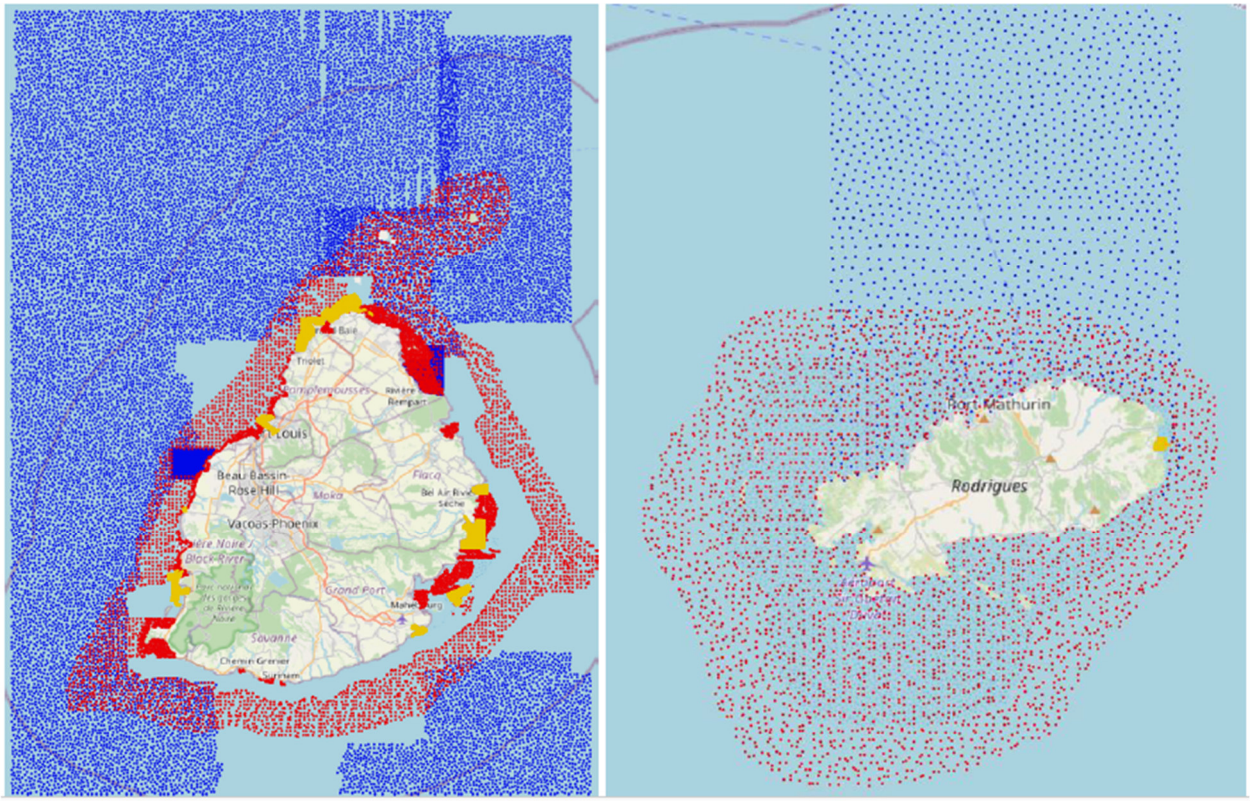


*Figure 4 : Overview of the distribution of bathymetric soundings on Mauritius, supplied by the MHL*

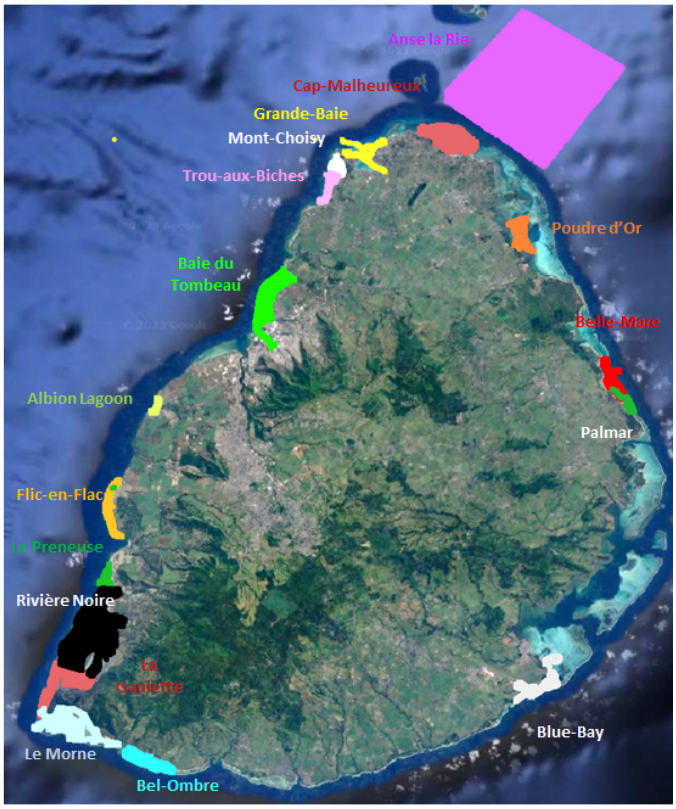


*Figure 5: Overview of the distribution of bathymetric soundings on Mauritius, supplied by the MOI*

### 2.1.2 Limits of topographic and bathymetric data

As evoked in the Phase 1 report (Garcin et al., 2023), the data have been provided without any metadata, and some defaults have been identified.

The comparison of the LiDAR DTM of Mauritius with the well-known altitude of geodesic points shows some differences that can reach several tens of centimetres up to more than 1m (Figure 6); no logical explanation or geographical distribution have been identified to understand this bias. At the July 2023 project meeting, stakeholders indicated that this product (Mauritius LiDAR DTM) had never been finalised by the supplier, which would explain these inconsistencies.

Moreover, the uncertainty on topography is confirmed by local analysis of beaches configurations and morphologies (several beaches tend to present an unrealistic “longshore slope”).

This is illustrated for Flic-en-Flac in the Figure 7 where the “*wet-dry*” interface has been digitalized on aerial photographs. This limit is supposed to correspond to the same time of the tide and the altitude of this interface from the LiDAR DTM should be the same. The analysis of the altitude of this limit has been realized at a spacing of 20m and reveals that the elevation values are strongly variable.

These biases can have very important consequences on the coastal flooding map. In areas where the actual elevation is lower than that of the DTM, the models will underestimate the extent of the flooding and the height of water. Conversely, in sectors where the actual altitude is higher than that of the DTM, the model will overestimate the extent of the flooding and the height of water.

Concerning the bathymetric soundings, we can note that some marine areas are not surveyed. This is for example the case of the south lagoon of Mauritius, or the lagoon around Pointe Coton in Rodrigues.

A few ‘imaginary soundings’ have been added in these zones to avoid aberrant interpolations between the topographic data and the offshore data and to avoid an unrealistic representation of the topo-bathymetry.

Moreover, some sounding data sets appear to be inconsistent with each other (Figure 8). This is particularly the case for soundings supplied by the MOI where the vertical referencing is not specified. We also observed inconsistencies in bathymetric values when the boat's tracks passed over the same sector several times.

Insofar as possible, these inconsistent data have been corrected (vertical offsets) or deleted to assure a realistic representation of the bathymetry.

These biases are not as critical as the previous ones on the LiDAR DTM, but they can have influences on the estimation of the wave behaviour in shallow waters, leading to potential errors in the estimation of wave breaking and resulting wave-setup. In consequence, these biases have an effect on the coastal flooding mapping.

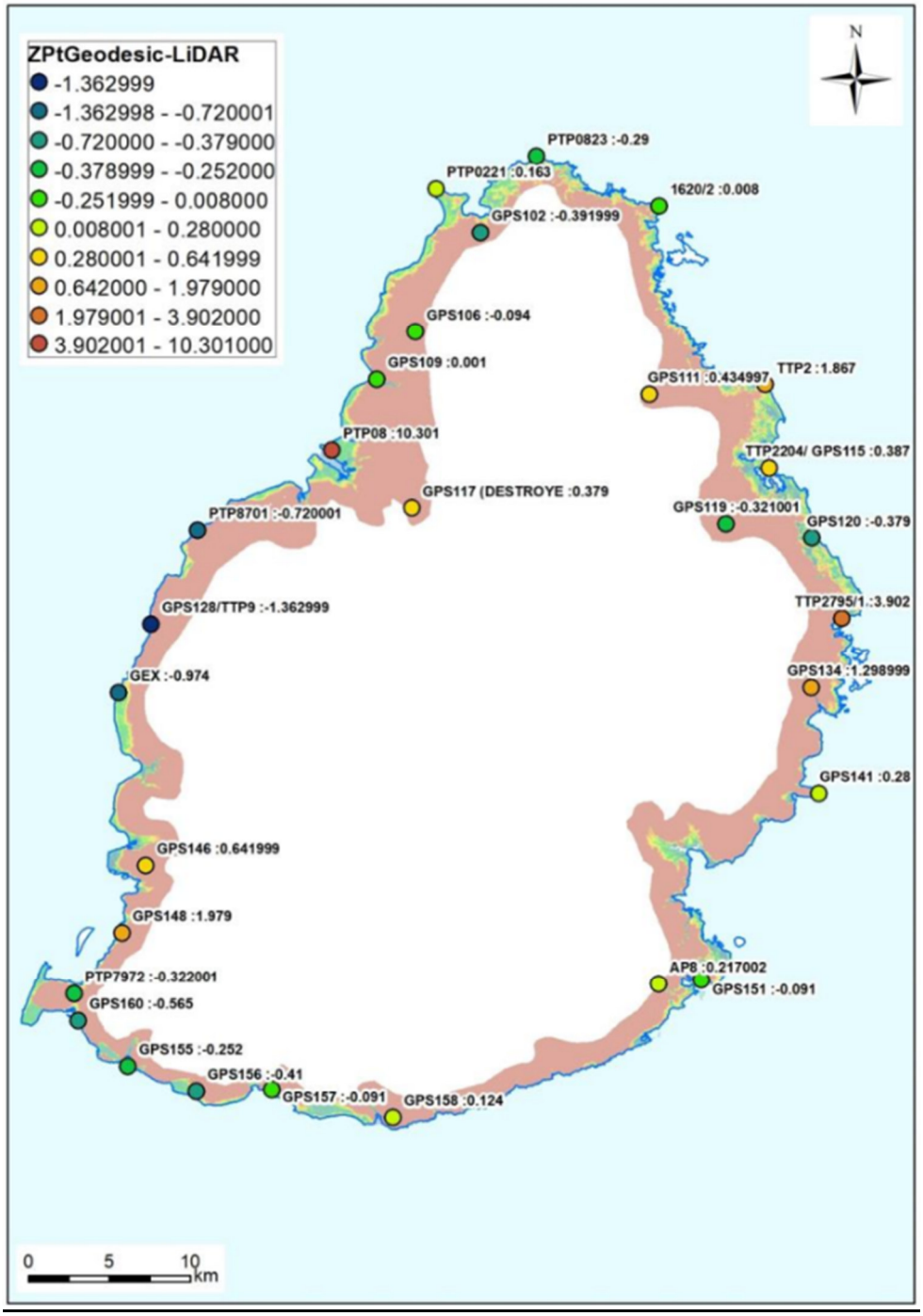


*Figure 6 : Localisation of analysed coastal geodesic points and differences between their altitudes and the corresponding value of the LiDAR DTM (from Garcin et al., 2023)*

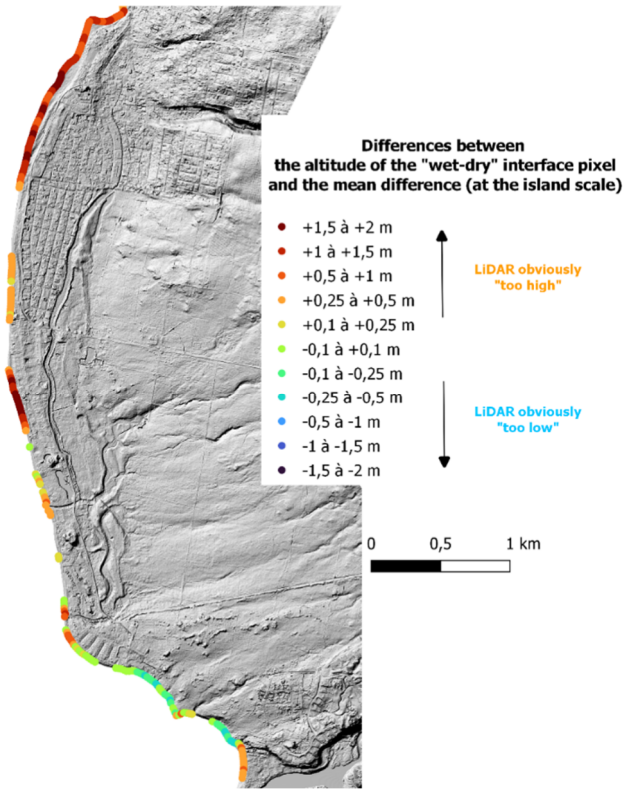


*Figure 7 : Distribution of altitude (in the LiDAR DTM of Mauritius) along a digitalized « wet-dry » interface on aerial photographs in the sector of Flic-en-Flac*

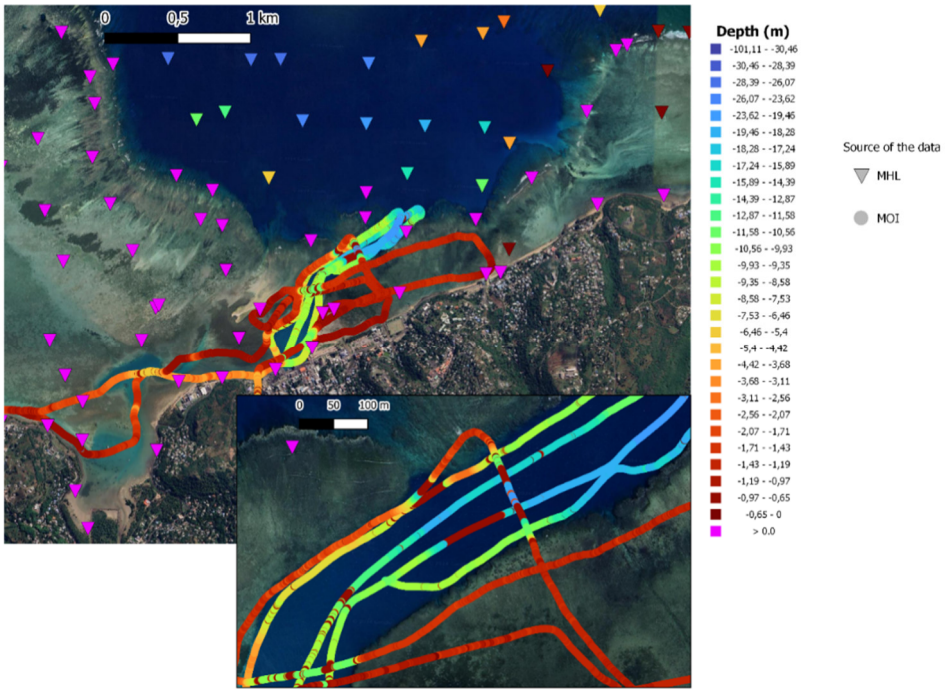


*Figure 8 : Example of the inconsistencies of soundings data near Port-Mathurin*

*The main map in the top shows that coarse data provided by MHL and dense data provided by MOI are not in the same vertical referencing; the zoomed-in map below shows potential inconsistencies between different tracks of the boat in dense data.*

# 3. FORCING FACTORS

## 3.1 INTRODUCTION

The coastal flooding, coastal erosion and shoreline retreat are primarily determined by meteorological and marine parameters, particularly cyclonic waves, austral swells, regional sea level, storm surges, and so forth. These parameters are collectively referred to as 'forcing factors' and are dependent on the climate and its projected future evolution. This chapter presents the forcing factors that currently influence the hazards affecting Mauritius and Rodrigues. It then presents the probable evolution of these forcing factors, based on the latest scientific knowledge. These forcing factors are then used to assess and map the coastal hazards and risks for the two islands over three timeframes (present, 2050, 2100).

## 3.2 CLIMATE CHANGE

### 3.2.1 Selection of climate scenarios

The choice of climate scenarios used to assess future hazards allows us to take into account the uncertainties associated with anthropogenic Greenhouse Gas (GHG) emissions in the future. They depend on world socioeconomic development and the level to which States follow GHG reduction international protocols. The future scenarios are called "Representative Concentration Pathways" (RCP) (Meinshausen *et al*. 2011). Climate parameters and induced effects that will affect coastal evolution (mean sea level, wind regimes, wave climates, cyclogenesis, etc.) change with climate scenarios.

Three scenarios are considered:

- RCP2.6, which is aligned with COP21 (Paris agreement of 2015) and means a drastic reduction of greenhouse gas emissions.
- RCP4.5, which corresponds to a middle-of-the-road climate change trajectory, with an efficient mitigation of greenhouse gases emissions.
- RCP8.5, which corresponds to a high-emission scenario, where greenhouse gases emissions continue increasing.

Our choice is based on the analyses presented in chapter 3.5. Our two scenarios (chapter 3.5) are based on a moderate to optimistic climate trajectory (RCP 4.5) and a pessimistic one (RCP 8.5). These scenarios will enable us to generate coastline retreat hazard maps for three-time horizons: present, 2050 and 2100. By mapping the position of the coastline for each timeframe and for the two scenarios, we can generate envelopes of uncertainty for the position of the coastline in the future. These envelopes will form the coastline retreat hazard map.

## 3.3 PRESENT AND FUTURE CYCLONES

### 3.3.1 Introduction

As part of the "Mauritius coastal risk" project, we need a representation of cyclone activity around Mauritius and Rodrigues in the present climate (recent historical period, i.e. the last 40 years), referred to as climate 2000 in the following, but also in the future climate for two time horizons:

one corresponding to the climate expected towards the middle of the century (climate 2050) and the other expected towards the end of the century (climate 2100).
A number of datasets from climate simulations carried out in recent years at Météo-France, specifically to represent cyclone activity, among other things, can be used for the purposes of this project.

The three simulation scenarios used are:

- constant climate simulation (400 years) based on the ARPEGE model from Météo-France at a horizontal resolution of 50km covering the entire globe.
- simulation carried out as part of the RenovRisk Cyclone project (scientific coordination LACy) using a stretched version of the ARPEGE model. In the Indian Ocean, and more specifically in the area of interest, the model's grid spacing is between 10 and 15 km.
- simulation carried out as part of the BRIO project (coordinated by Météo-France) using the ALADIN regional climate model with a 12 km grid.

In the remainder of this chapter, these three datasets will be referred to as **ARPEGE50-ClimatConstant**, **ARPEGEstr-RenovRisk** and **ALADIN12-BRIO** respectively.

For this study, the reference dataset is the best-track database of the CMRS-cyclone for La Réunion **(BT-CMRS**).

## 3.3.2 Method

From a methodological point of view, the study consists of:

- for climate 2000: defining a large number of scenarios with a potential impact on Mauritius and Rodrigues, covering the range of possibilities as far as possible in terms of cyclone trajectory and intensity.
- projecting this set of scenarios for the two future time horizons (mid- and end-of-century climate) by using information from climate modelling on expected changes in the intensity of tropical low-pressure systems in the south-west Indian Ocean.
- for all scenarios (present and future), generating of 2D wind and pressure fields to be used in wave and storm surge models to assess the risk of coastal flooding.

Although the climate models used in this study reproduce relatively realistic cyclone activity, there are biases that are sometimes significant, particularly in the intensity of the cyclones modelled. The existence of these biases requires, prior to the steps described above, the implementation of statistical corrections to enable the different data sets to be recalibrated to a realistic intensity distribution (use of a reference data set for the past climate).

### 3.3.2.1 Intensity bias correction for the three data sets

Each simulation set has its own specific intensity bias. These biases are due to a sometimes-inaccurate representation of cyclone activity in the climate model used. While this poor representation is often attributed to the horizontal resolution of the model being insufficient to realistically represent the internal processes of tropical cyclones, it may also be due to inappropriate physical parameterisations in some cases, and the lack of coupling with the ocean in others. There may be many causes and these are often difficult to identify. The ARPEGE50-ClimatConstant simulation overestimates maximum cyclone intensities, while the ALADIN12-BRIO simulation tends to underestimate them.

On the basis of this observation, it is necessary to recalibrate the intensities of tropical cyclones simulated by climate models. To do this, we apply bias correction methods with a quantile-

mapping method commonly used to correct precipitation biases in climate models. This is the CDFT-BRIO method (documented in the BRIO project report).

First, the maximum intensity of each cyclone during its lifetime was corrected. Each cyclone event is described by a succession of points in latitude-longitude, and an intensity defined by the maximum 10-minute mean wind estimated near the centre of the system. This information is delivered by the tracking algorithm (F. Chauvin) at 6-hour intervals.

To apply this correction, we used the BT-CMRS dataset covering the recent period of 1985-2022 as a reference set. This dataset provides information on the actual distribution of cyclones in the south-west Indian Ocean. The maximum intensities of the cyclones derived from the various models are plotted on this distribution curve. The graphs in Figure 9 show the results of the bias correction on the distribution of maximum winds.

Once the distribution of maximum intensities has been rectified, a linear regression is performed on all the winds at the various points along the trajectory in order to recalibrate each scenario in relation to its new maximum wind value and the initial minimum wind value, which most often corresponds to the first point along each trajectory.

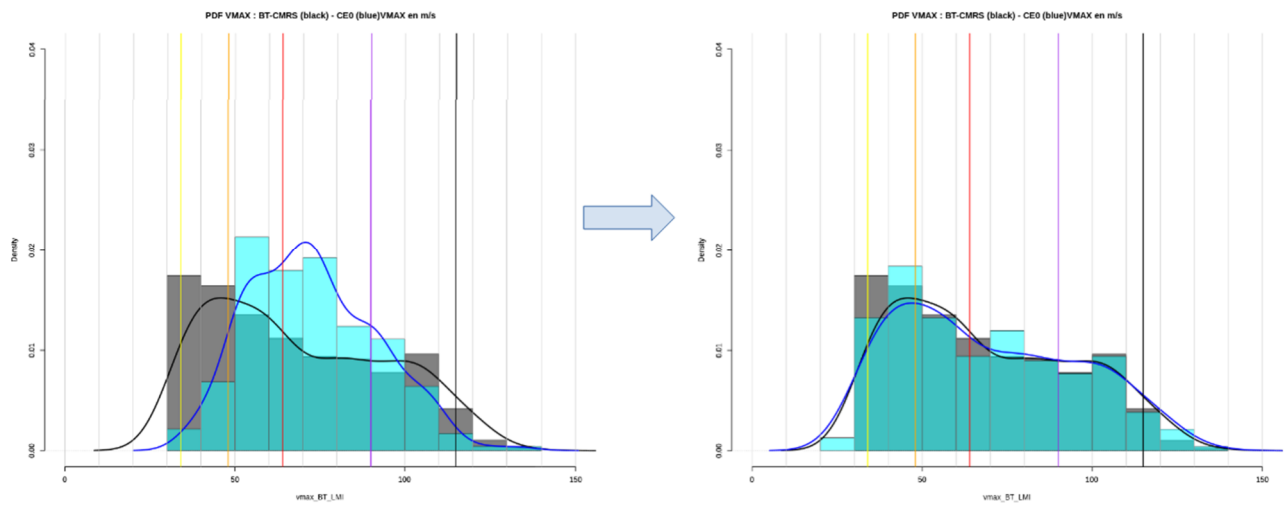


*Figure 9 : Left: raw maximum mean wind distribution curves: ARPEGE50-ClimatConstant 2000 simulation in blue, BT-CMRS 1985-2022 data in black; right: the same data after correction for intensity bias*

### 3.3.2.2 Selection of trajectory scenarios

The ARPEGE50-ClimatConstant simulations were largely motivated by the need to gain a better understanding of the evolution and variability of cyclone activity in the various ocean basins affected by these extreme phenomena. They involve running long simulations (400 years), fixing global warming at a given level, in order to simulate a sufficiently large sample of cyclone events to enable robust statistical analyses. Two simulations of this type are available: one on the recent climate ("year 2000") and the other on a future climate ("year 2050") corresponding to warming forced by the RCP8.5 scenario of the 5th IPCC assessment report. The simulations were carried out at a resolution of 50 km across the globe. It has already been verified that these simulations do indeed produce cyclone activity in the various tropical basins concerned, including the South-West Indian Ocean basin. Using tracking methods, we can reconstruct the trajectories and intensities of the cyclones simulated by the model. Over 400 years, the model produces around

2,500 tropical depression systems, ranging from tropical storms to intense systems with significant trajectory variability.

In the end, therefore, it was the set of trajectories from the constant climate simulation for the year 2000 that was used to define a set of cyclone scenarios. All the trajectories resulting from the "climate 2000" simulation are shown in Figure 10.

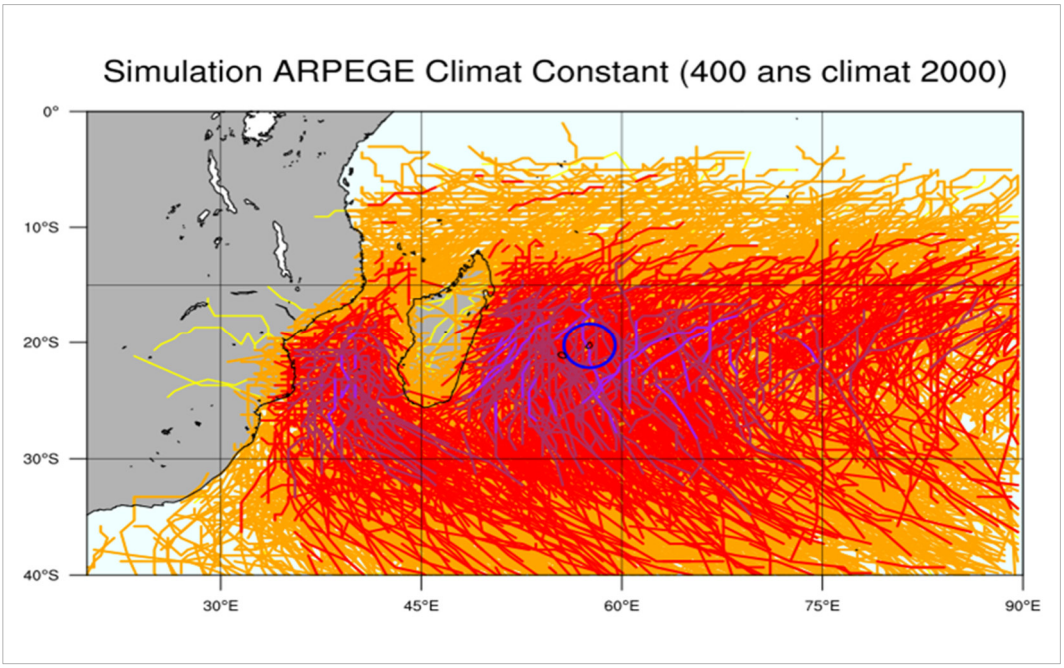


*Figure 10 : Representation of the 2,500 trajectories detected in the ARPEGE50-ClimatConstant 2000 simulation*

*Orange for storms, red for cyclones, brick red for intense cyclones and violet for very intense cyclones*

For a trajectory to have a significant impact on the coastline, only trajectories passing within a 200 km radius of Mauritius were considered, at least at the tropical storm stage (average wind speed greater than 64 knots). In the end, 220 scenarios were considered, 104 of them reaching the tropical cyclone stage within the 200 km radius (Figure 11).

A selection based on the same criteria was made for Rodrigues. The number of scenarios considered for Rodrigues was 164, about half of which reached the cyclone stage within a 200 km radius of Rodrigues (Figure 12).

For the rest of the study, the scenario treatments for Rodrigues are strictly identical to those carried out for Mauritius.

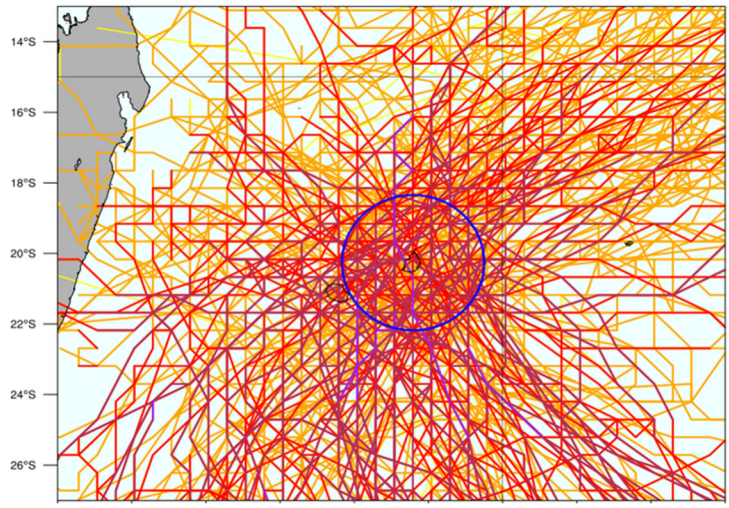


*Figure 11 : Representation of the 220 trajectories selected for the study of current climate coastal risk in Mauritius*

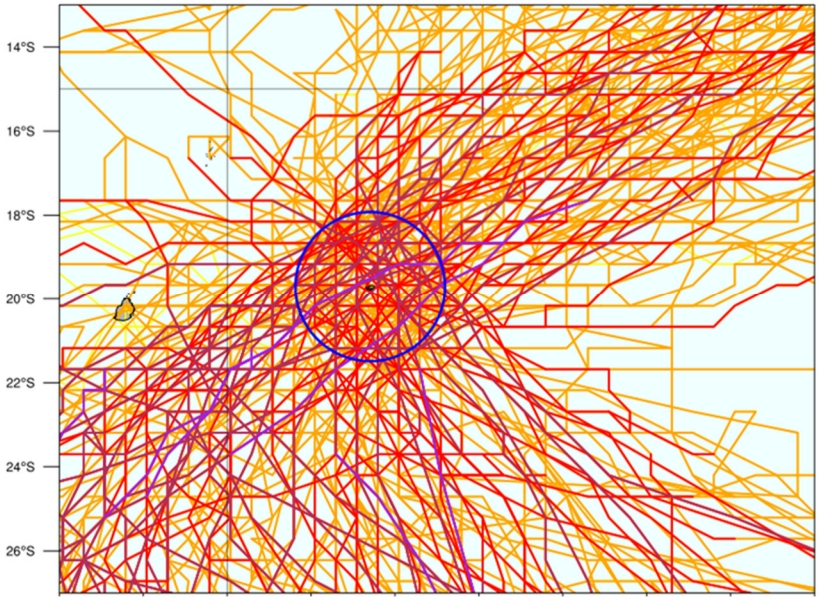


*Figure 12 : Representation of the 164 trajectories selected for Rodrigues (current climate)*

### 3.3.2.3 Wind and pressure fields generation

Wind-pressure fields consistent with each scenario are generated in several stages:

a) Estimation at each point of a trajectory of wind extensions greater than 28 knots along 4 dials to describe the size of the phenomenon,

b) Calculation of winds and pressure using Holland's parametric model (2010 version), taking into account the wind extensions estimated in the previous step,

c) Filtering of the cyclonic vortex in the wind fields of the ARPEGE50-ClimatConstant model by thresholding winds above 14m/s,

d) Merge of the wind fields from Holland's model (representing the core of the cyclonic system) and the filtered wind field from the ARPE50-ClimatConstant simulation (representing the cyclonic system's environment).

A file in netcdf format is generated for each scenario. This file contains the wind and pressure parameters at three-hourly intervals over the lifetime of the event in the domain shown in Figure 13. This data is used to feed the wave, surge and flooding models.

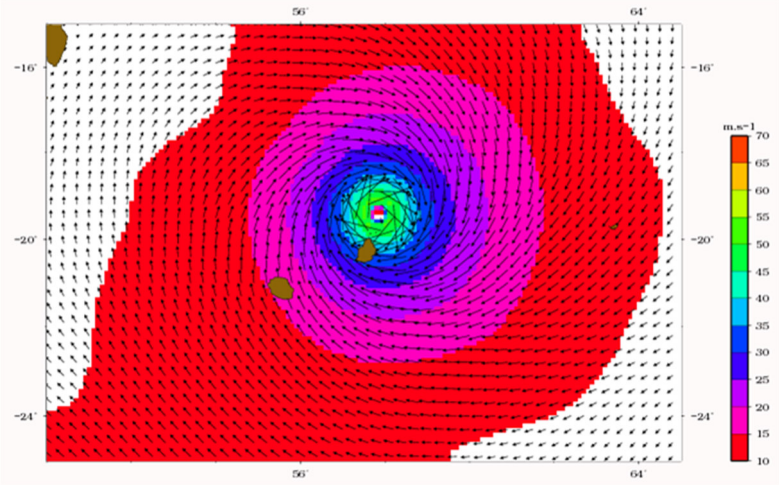


*Figure 13 : Example of a wind field for one of the cyclone systems approaching Mauritius*

### 3.3.2.4 "*Future projection*" of the climate 2000 scenarios

Assessing the impact of climate change on cyclone activity in the South-West Basin is no simple matter. On a global scale or that of the various cyclone basins, there is not necessarily a scientific consensus on many questions, because of the difficulty climate models have had in accurately representing cyclone activity over the recent period. As mentioned previously, biases in the intensity or frequency of phenomena, as well as in the location of areas with a high density of cyclones in the different basins, are sources of uncertainty as to the evolution of this activity in the decades to come and should therefore be interpreted cautiously.

Nonetheless there now seems to be a consensus on a number of signals. Among these, the increase in the average intensity of cyclones (associated with an increase in the proportion of the most intense systems) is one of the expected effects of global warming. This future trend is clearly shown in the two high-resolution simulations used for the project (ALADIN12-BRIO and ARPEGEstr-RenovRisk) for the middle and end of the 21st century.

The graph in Figure 14 shows the projected evolution of the intensity distribution curve for the two time horizons considered.

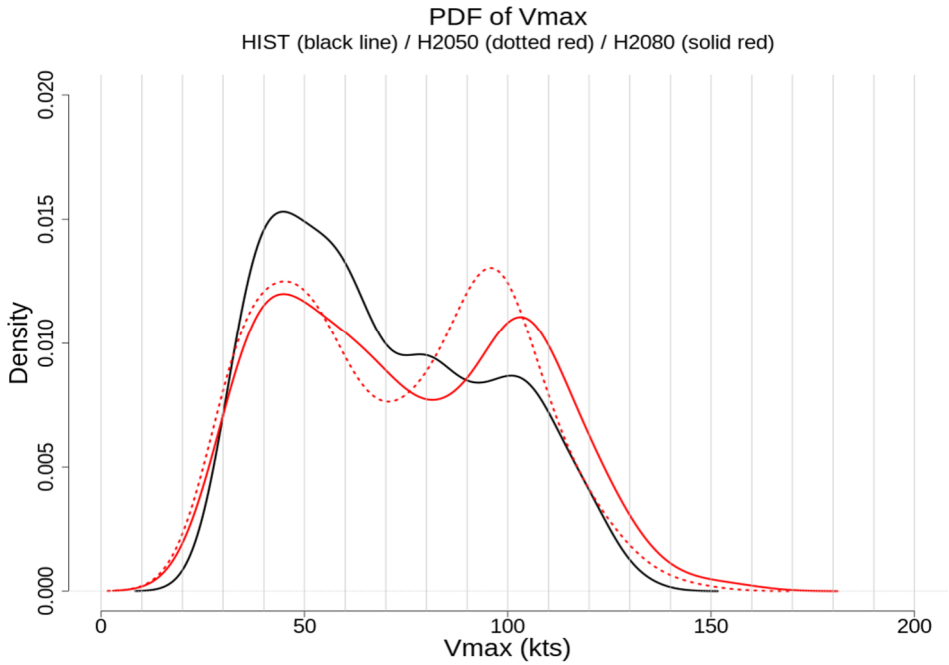


*Figure 14 : Proposed evolution of the cyclone intensity distribution curve for the two timeframes considered*

The project into the future of the scenarios in this study consists in redistributing the maximum intensities of each climate 2000 scenario (black curve in Figure 14) according to the distribution of maximum intensities in the future (dotted red curve for the mid-century time horizon and solid red curve for the end-of-century time horizon). The number of scenarios and the trajectories therefore remain unchanged in the future climate. Only the intensities change.

The wind and pressure fields will then be calculated in the same way as for climate 2000.

### 3.3.3 Statistical analysis for present day cyclones, and in future (2050 and 2100)

In this section, we analyse the changes in wind speed as well in atmospheric pressure that are induced by present day cyclones (climate 2000 scenario) as well as for future conditions (climate 2050 and 2100 scenario). Please note that, for simplicity of terminology, the term “climate 2080” actually corresponds to climate conditions over the period 2080-2100.

The following analysis is based on the datasets comprising respectively 220 and 164 systems (cyclones and tropical storms) provided by Météo-France La Reunion over an area defined by a 200km radius around Mauritius and Rodrigues (see the previous sections for further details).

#### 3.3.3.1 Method

The objective is to analyse the changes in extreme values between the climate scenarios of the following variables:

- wind speed denoted *U* (expressed in km/h),

- drop in atmospheric pressure denoted *SLP* and named in the following relative pressure. The latter is defined as the difference between the reference atmospheric pressure of 1013.25 hPa and that during the cyclone's passage.

For both sites, the following procedure is applied:

(1) At each pixel of the mesh grid provided by Météo-France La Reunion (spatial resolution of 0.1°), we estimate the maximum value taken over time during the passage of each cyclone. This provides a set of maps for both variables *U* and *SLP* (total number of 220 and 164 for Mauritius and Rodrigues).

(2) We analyse the evolution of the percentiles (computed empirically) of the maximum values (calculated over time) for both variables over an area at +/- 2° around each site. In the following, a 75% percentile is interpreted as the value exceeded by 25% of the most intense cyclones.

(3) The extreme values are analysed using the tools of the theory of extreme value statistics (Coles et al. 2001); the advantage being to extrapolate beyond the empirically observed percentiles. This consists in fitting a statistical model based on the Generalised Pareto distribution (denoted GPD). This fitting (i.e. the estimation of the GPD parameters) requires to choose the thresholds above which the values are considered "extreme". This is carried out using a series of techniques (Coles et al. 2001), e.g. analysis of quantile-quantile plot, « *mean residual life plots* ». The uncertainty in this fitting is accounted for by computing confidence interval (at the level of 95 %) using the bootstrap sampling method (Efron, 1992) with a thousand of random replicates. Once estimated, the extreme values are translated into return levels, i.e. level value associated to a certain return period (for instance 100 years).

### 3.3.3.2 Results

#### *3.3.3.2.1 Analysis at Mauritius*

Figure 15 illustrates the evolution of the two variables at different date over the whole area around both sites for a particular cyclone (here the 18th) which has been "futurized" on the basis of Meteo-France La Reunion's approach. For this example, we note an intensification for *U* of the order of 10 to 20% between 2000 and 2080-2100, and of <10% for *SLP*. A similar tendency is notice more or less for each of the other 220 cyclones.

To give a more global view, Figure 15: Example of the evolution of the wind speed field (left), expressed in km/h, and relative atmospheric pressure (right) expressed in hPa (compared with the reference pressure 1011 hPa) for the 18th cyclone in 2000, 2050, 2080-2100 in Mauritius.

The Figure 16 shows the evolution of the statistical magnitudes of the maximum values reached in the zone defined at +/- 2° around Mauritius in the form of a boxplot combined with a violin diagram. On the boxplot, the central line shows the position of the median (the value exceeded by 50% of cyclones, i.e. 110 in this case), while the limits of the box show the quartiles (percentiles at 25 and 75%, i.e. the value exceeded by 75% and 25% of cyclones, i.e. 165 and 55 in this case). The violin diagram shows the full density and, in this case, its strong asymmetry in relation to the median.

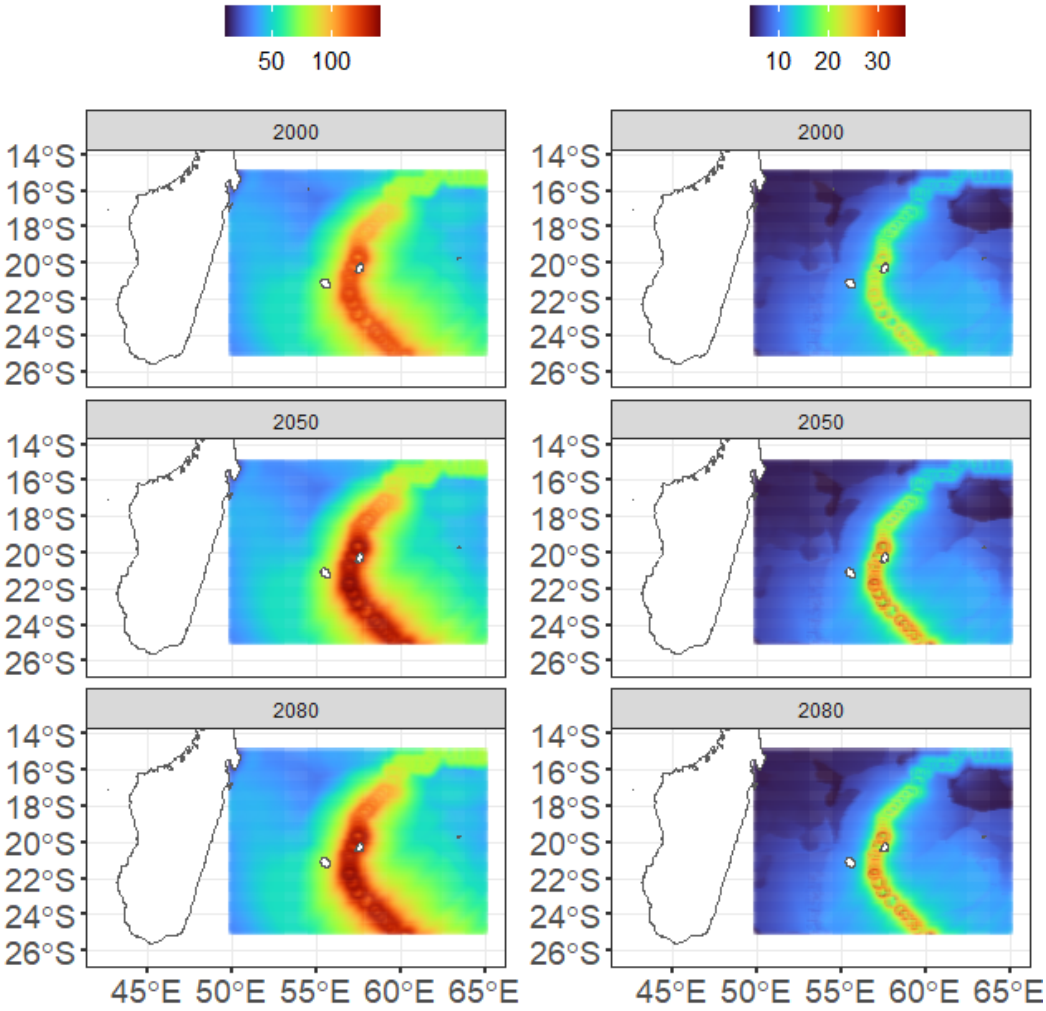


*Figure 15: Example of the evolution of the wind speed field (left), expressed in km/h, and relative atmospheric pressure (right) expressed in hPa (compared with the reference pressure 1011 hPa) for the 18th cyclone in 2000, 2050, 2080-2100 in Mauritius.*

We note here the relatively small effect of intensification of statistical magnitudes between the "2000" and "2050" climates. Application of the Durbin-Conover test (Conover, 1999) allows us to test the hypothesis that the distributions of each of the two groups of data are close: this hypothesis is well rejected (at the 5% significance level) and we can consider that the change between the two climate scenarios remains statistically significant.

This intensification is more pronounced between 2000 and 2080-2100:

- The intensification of the low-order percentiles remains fairly small (the median of *U* changing by around 5 km/h between the 2000 and 2080-2100 climates and that of *SLP* by 2hPa);
- It is in the higher values above the 75% percentile (upper limit of the box) that the intensification is more pronounced; the 90% and 95% percentiles of *U* change by around 10 km/h and those of *SLP* by 5 to 7hPa.

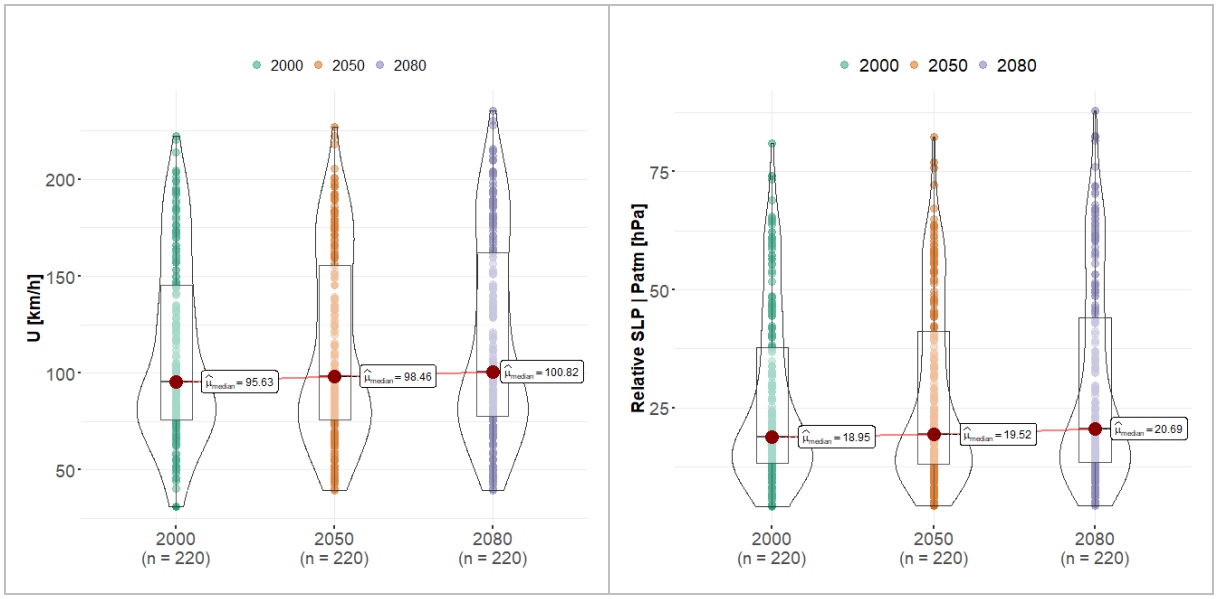


*Figure 16 : Evolution of statistical quantities (represented in the form of a boxplot and a violin diagram) of the maximum values reached in the zone defined at +/- 2° around Mauritius. Left: wind speed noted U; right: relative atmospheric pressure noted SLP (compared with the reference pressure 1011hPa) for different climates (2000, 2050 and 2080-2100).*

In order to analyse the effect on extreme values, we fit a GPD model. The thresholds identified for the fit are 110 km/h for U and 25 hPa for SLP. This model enables us to describe the extreme values in the form of a return level plot (Figure 10 for *U* and Figure 11 for *SLP*).

Several observations can be made:

- The comparison between the 2000 and 2050 climates (Figure 17 and Figure 18 on the left) shows the same trend as the comparison of empirical percentiles: the two curves are very close and the uncertainties of adjustment (indicated by the dotted lines) do not make it possible to discriminate between extreme levels;
- The influence of intensification is much clearer between the 2000 and 2080-2100 climates (Figure 17 and Figure 18 on the right), with the 100-year return levels of *U* and *SLP* increasing by around 14km/h and 8hPa respectively;
- For return periods greater than 100 years, the intensification is of the same order of magnitude, i.e. an increase of 5% for *U* and 10% for *SLP*.

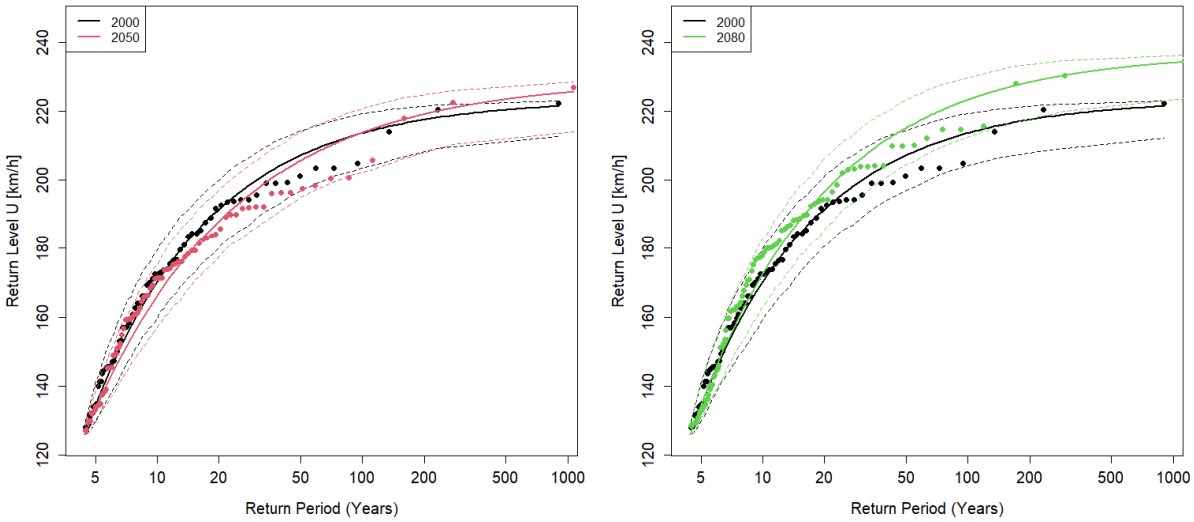


*Figure 17 : Evolution of return level plot for maximum wind speed values U reached in the zone defined at +/- 2° around Mauritius for different climates 2000 and 2050 (left) and 2000 and 2080-2100 (right).*

*The points represent the return levels calculated empirically from the data. The curve shows the fit of the statistical model (solid line: best estimate, dashed line: uncertainty envelope at the 95% level estimated by the bootstrap method).*

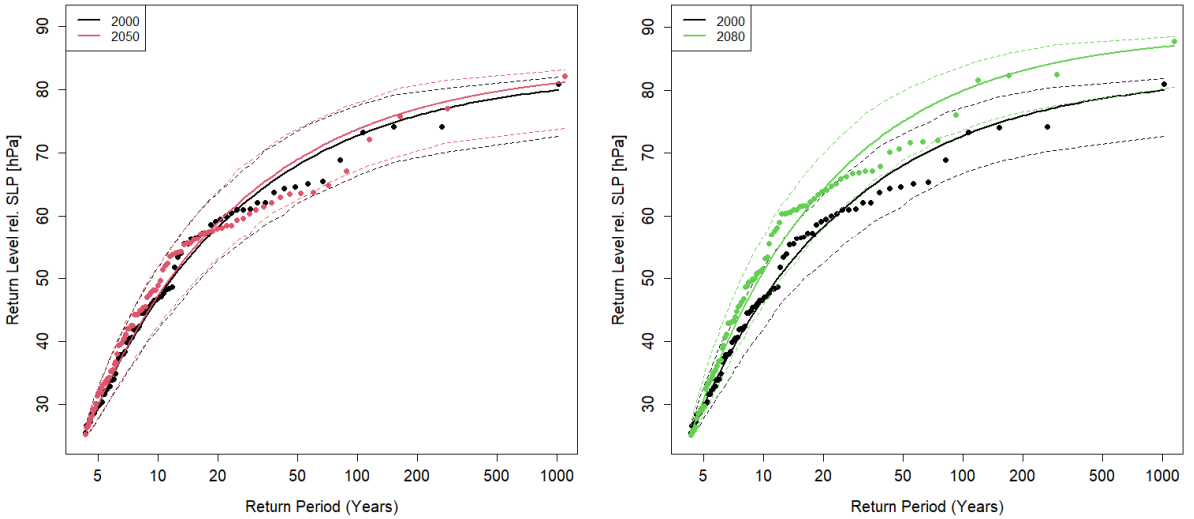


*Figure 18 : Evolution of return level plot for maximum relative atmospheric pressure values SLP reached in the zone defined at +/- 2° around Mauritius for different climates 2000 and 2050 (left) and 2000 and 2080-2100 (right).*

*The points represent the return levels calculated empirically from the data. The curve shows the fit of the statistical model (solid line: best estimate, dashed line: uncertainty envelope at the 95% level estimated by the bootstrap method).*

#### *3.3.3.2.2 Analysis at Rodrigues*

Figure 19 illustrates for one cyclone (the 164th) the evolution of the wind speed and atmospheric pressure field for different climates. In this example, as in the case of Mauritius, we see an

intensification of the order of 10 to 20% for *U* between 2000 and 2080-2100, and of the order of 10% for *SLP*. This tendency is observed for each of the 164 cyclones.

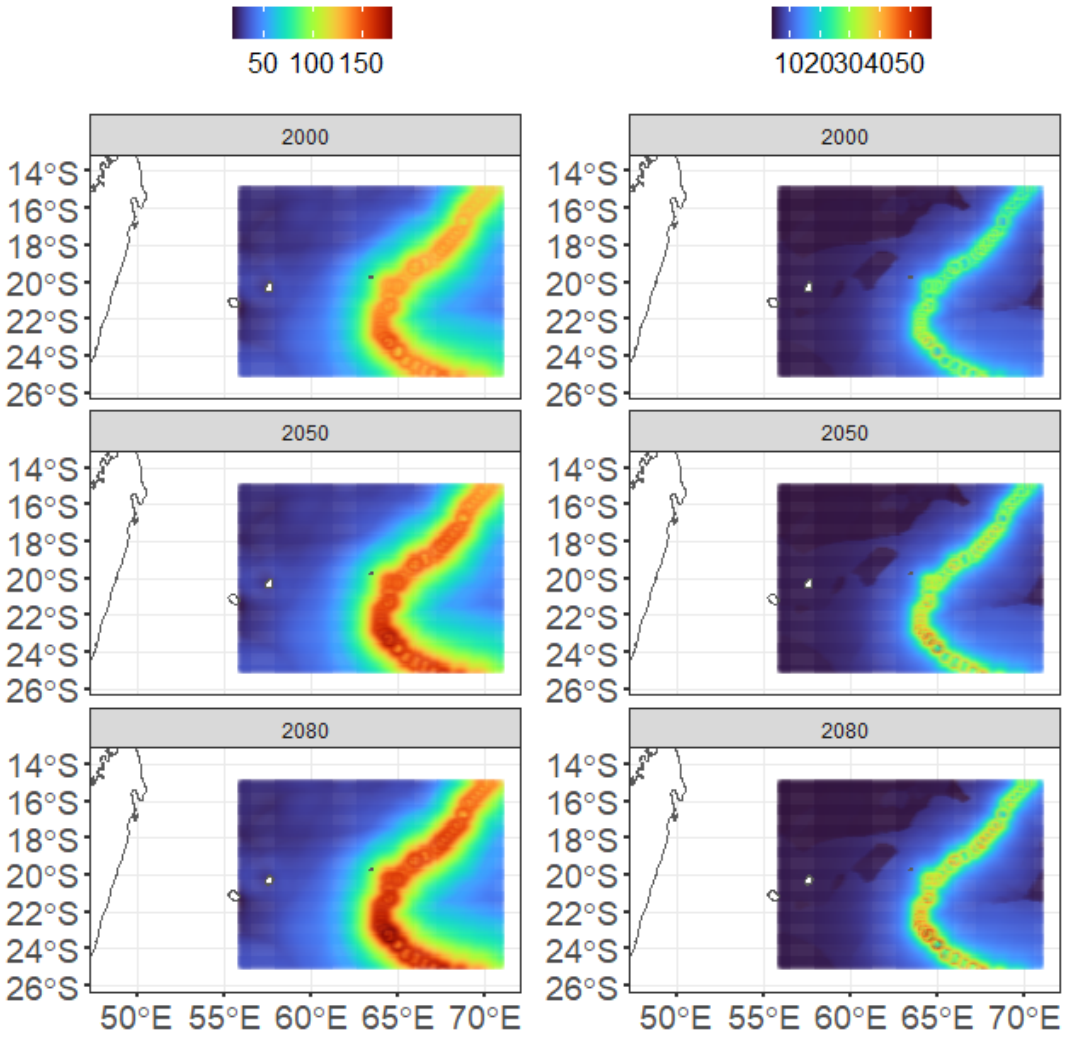


*Figure 19 : Example of the evolution of the wind speed field (left), expressed in km/h, and relative atmospheric pressure (right) expressed in hPa (compared with the reference pressure 1011 hPa) for the 18th cyclone in 2000, 2050, 2080-2100 in Rodrigues.*

Figure 20 shows the evolution of the statistical quantities of the maximum values reached in the zone defined at +/- 2° around Rodrigues. We can see here the relatively moderate effect of intensification of statistical magnitudes between the "2000" and "2050" climates. In contrast to Mauritius, the application of the Durbin-Conover test here shows that the small change between the two climates is not statistically significant (p-value of the test respectively 39% and 48%, i.e. well above the 5% significance level). This reflects the small magnitude of these differences. However, in order to reach a definitive conclusion on the possible impact of these differences in terms of hazards (erosion/submergence), further analysis is required.

As in Mauritius, this intensification is more pronounced between 2000 and 2080-2100:

- The intensification of low-order percentiles remains fairly low (the median of U changing by around 6 km/h between the "2000" and "2080-2100" climates and that of *SLP* by 2hPa);
- It is on the higher values above the 75% percentile (upper limit of the box) that the intensification is more pronounced; the 90% and 95% percentiles of *U* changing by more than 10km/h and those of SLP by just under 10hPa.

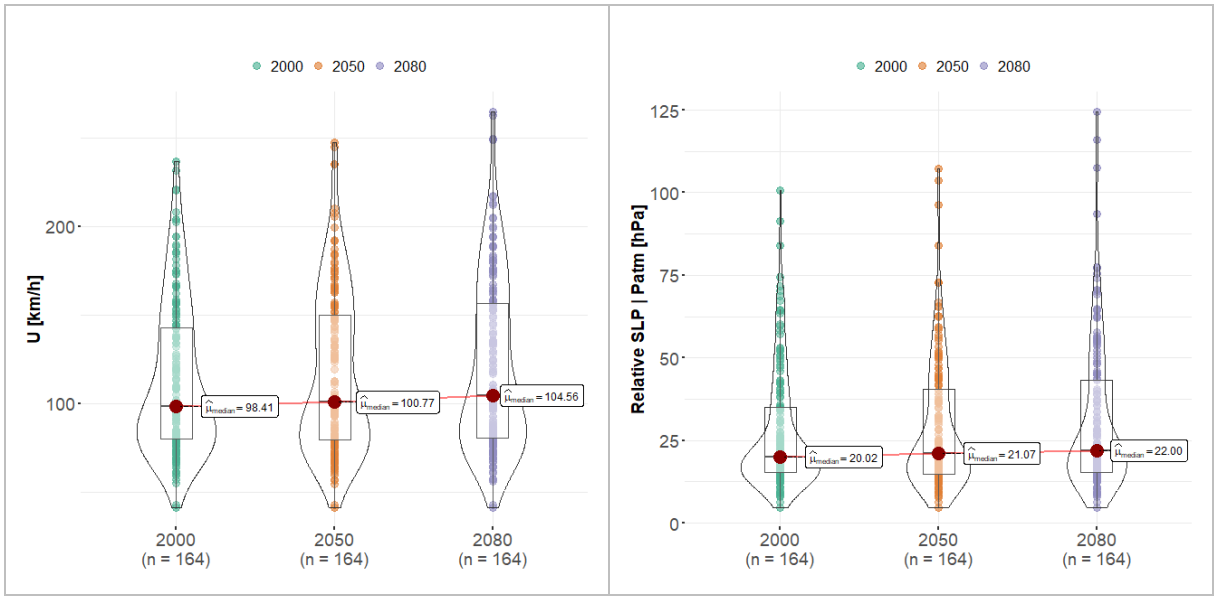


*Figure 20 : Evolution of statistical quantities (represented in the form of a boxplot and a violin diagram) of the maximum values reached in the zone defined at +/- 2° around Rodrigues. Left: wind speed noted U; right: relative atmospheric pressure noted SLP (compared with the reference pressure 1011hPa) for different climates (2000, 2050 and 2080-2100).*

In order to analyse the effect on extreme values, we fit a GPD model. The thresholds identified for the fit are 110 km/h for U and 25 hPa for SLP. This model enables us to describe the extreme values in the form of a level-return period curve (Figure 14 for U and Figure 15 for SLP). Several observations can be made:

- The comparison between the 2000 and 2050 climates (Figure 21 and Figure 22 on the left) is along the same lines as the analysis of empirical percentiles: the uncertainties of adjustment (indicated by the dotted lines) make it difficult to discriminate between extreme levels (although a slight difference can be noted);
- The influence of intensification is much clearer between the 2000 and 2080-2100 climates (Figure 21 and Figure 22 on the right), with the 100-year return levels of *U* and *SLP* increasing by around 20 km/h and 15 hPa respectively;
- For return periods greater than 100 years, the intensification is of the same order of magnitude, i.e. ~10% and 15-20% for *U* and *SLP*.

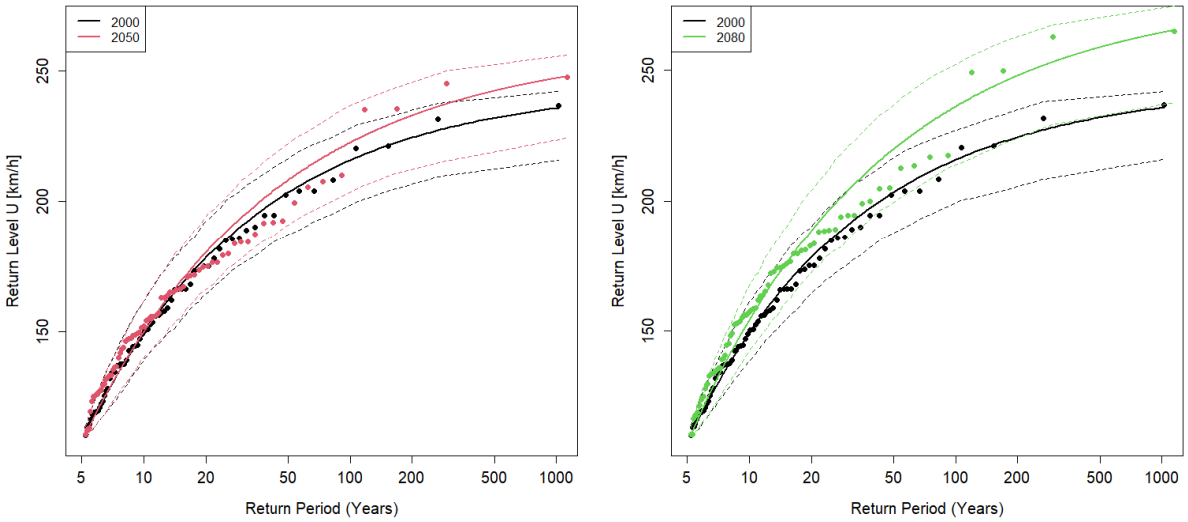


*Figure 21 : Evolution of return level plot for maximum wind speed values U reached in the zone defined at +/- 2° around Rodrigues for different climates 2000 and 2050 (left) and 2000 and 2080-2100 (right).*

*The points represent the return levels calculated empirically from the data. The curve shows the fit of the statistical model (solid line: best estimate, dashed line: uncertainty envelope at the 95% level estimated by the bootstrap method).*

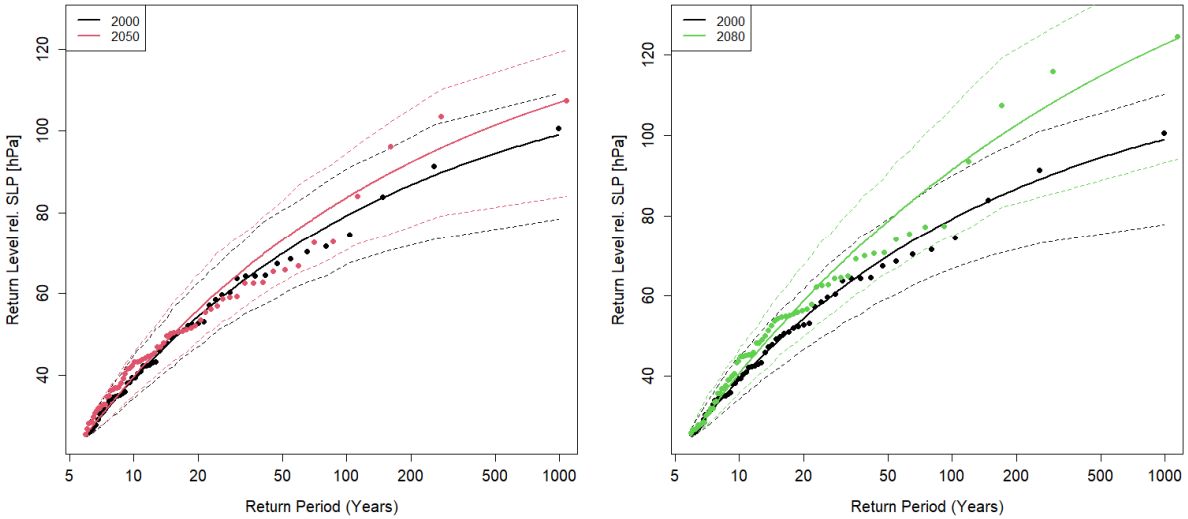


*Figure 22 : Evolution of return level plot for maximum relative atmospheric pressure values SLP reached in the zone defined at +/- 2° around Rodrigues for different climates 2000 and 2050 (left) and 2000 and 2080-2100 (right).*

*The points represent the return levels calculated empirically from the data. The curve shows the fit of the statistical model (solid line: best estimate, dashed line: uncertainty envelope at the 95% level estimated by the bootstrap method).*

#### 3.3.3.3 In summary

Analysis of the changes in wind speed and atmospheric pressure induced by future cyclones (2050 and 2080-2100) compared with the current climate shows an intensification of these two variables in Mauritius and Rodrigues, especially for the 2080-2100 climate. Analysis of the extreme values shows an increase of between 5% and 10% in wind speed and up to 20% in atmospheric pressure reduction. This intensification appears to be greater in Rodrigues than in Mauritius.

These results will serve as a basis for further study, aimed at translating the evolution of these variables into a response in terms of coastal hazards (marine flooding and erosion).

## 3.4 ANALYSIS OF THE CYCLONE-INDUCED EXTREME METEOCEANIC FORCING CONDITIONS (PRESENT DAY AND FUTURE)

In this section, we assess the extreme meteo-oceanic conditions that are induced by the cyclones offshore of Mauritius and Rodrigues for present day and future climate conditions. This analysis provides the offshore forcing conditions that constrain the boundary conditions for the high resolution hydrodynamic numerical models used to simulate the coastal flooding (see Sect.4.2.1.2).

In the following, we first describe the data and methods used to carry out the analysis. Then, we analyse and compare the results for both sites, Mauritius and Rodrigues, and for present day and future climate conditions.

### 3.4.1 Data

The analysis is based on the dataset of 220 and 164 storm systems (cyclones and tropical storms) provided by *Météo-France La Réunion*, within a radius of 200 km around Mauritius and Rodrigues (information on these datasets is provided in Sect. 3.3). The atmospheric wind and pressure fields of each of these systems are used to calculate wave fields with the WW3 code (Tolman et al.2009, model described in Sect. 4.2.1.2) and sea surface heights induced by the inverse barometer.

Two computing grids have been set up, centred on Mauritius and Rodrigues respectively (Figure 23). These are unstructured grids constructed from the regional DTMs for the Indian Ocean described in Sect 4.2.1.2.2. The mesh size varies from ~8km offshore to 500m near the islands.

The implementation of these WW3 configurations was validated by comparing the simulation results with satellite Hs observations for significant historical cyclones. These wave altimetry data are global in scope and cover the period from 1991 to 2018 (Piollé et al. 2020). They come from several satellite missions (Envisat, CryoSat-2, Jason-1, Jason-2, Jason-3, SARAL, Sentinel-3A) and are available at https://catalogue.ceda.ac.uk/uuid/3ef6a5a66e9947d39b356251909dc12b.

Cyclonic wind fields were constructed using best-tracks from IBTrACS database (Knapp, et al. 2010) and the parametric method described in Lecacheux et al. 2012.

Figure 24, Figure 25 and Figure 26 show, for example, the comparison of simulated values with those observed for cyclone the intense tropical cyclone DINA on 3 different dates. We note that the Hs fields of cyclonic waves are well reproduced, particularly near the eye. Hs may be underestimated far from the eye of the cyclone (Figure 24). This is probably linked to the propagation of non-cyclonic waves over these sectors, which are not taken into account here.

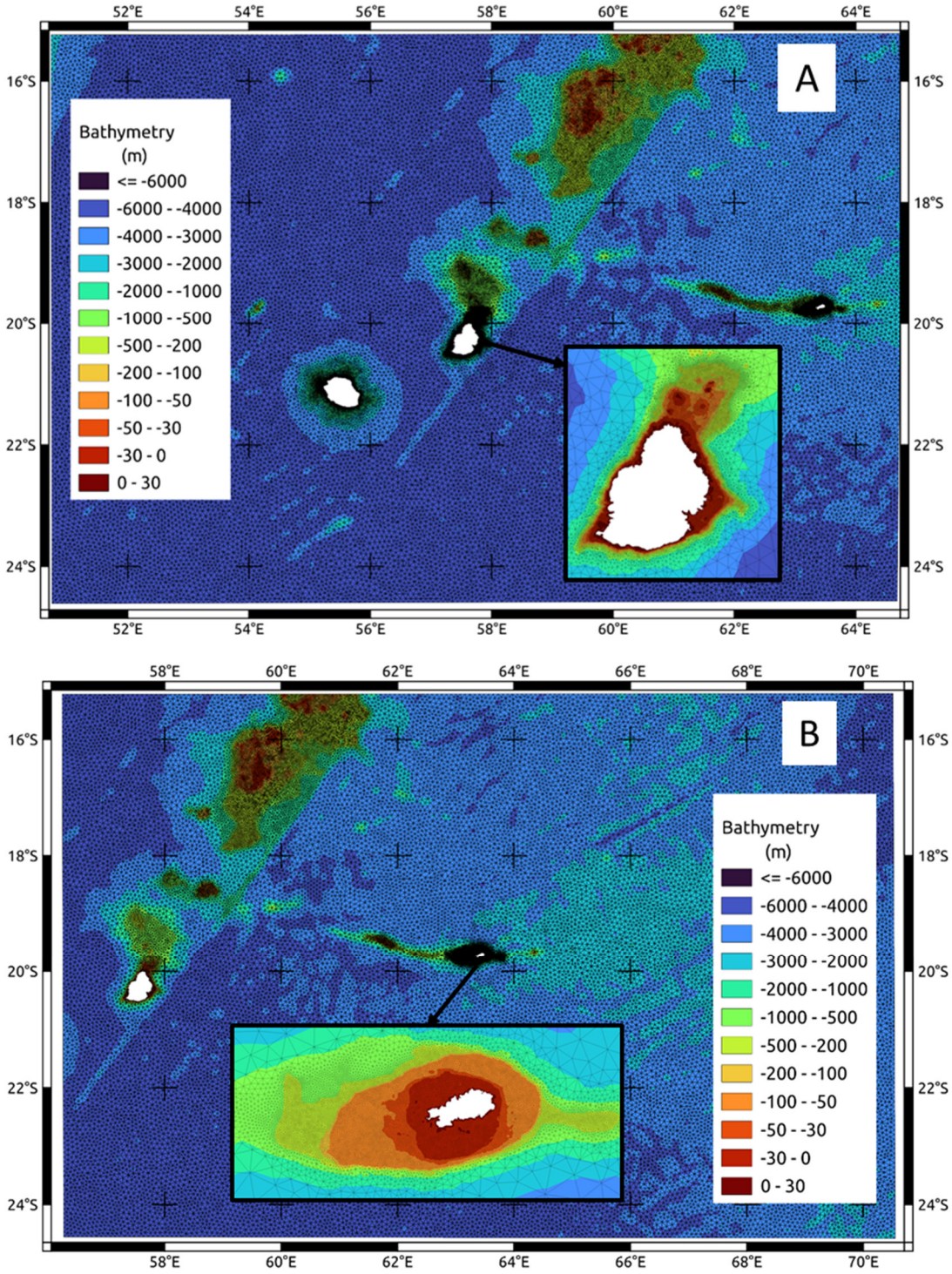


*Figure 23 : Meshes used to calculate waves on Mauritius (A) and Rodrigues (B).*

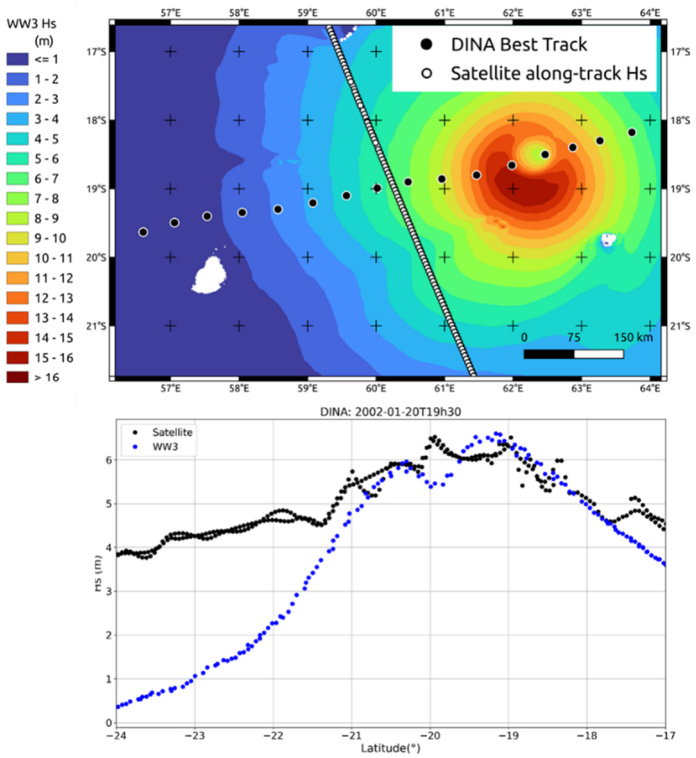


*Figure 24 : Comparison of waves from WW3 and satellites for ITC DINA on 20/01/2002 at 19:30 UTC.*

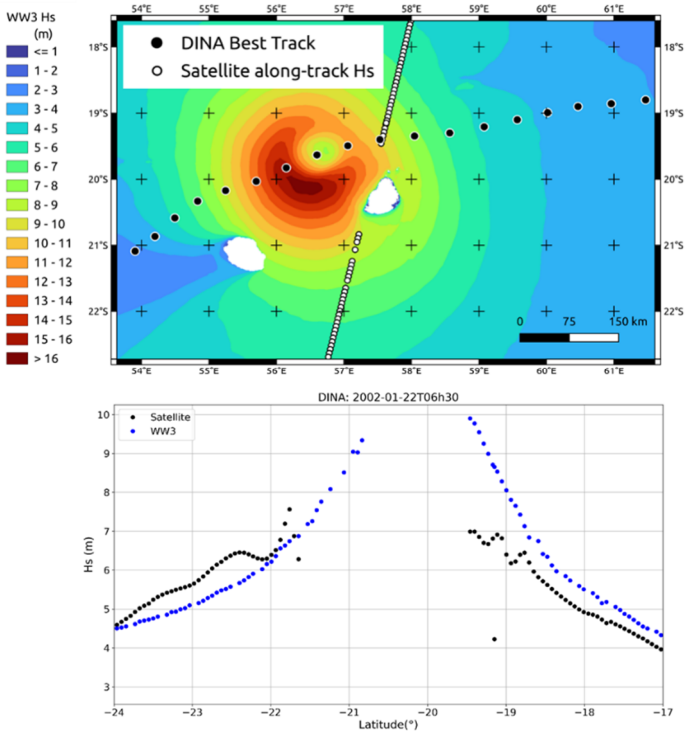


*Figure 25 : Comparison of waves from WW3 and satellites for ITC DINA on 22/01/2002 at 06:30 UTC.*

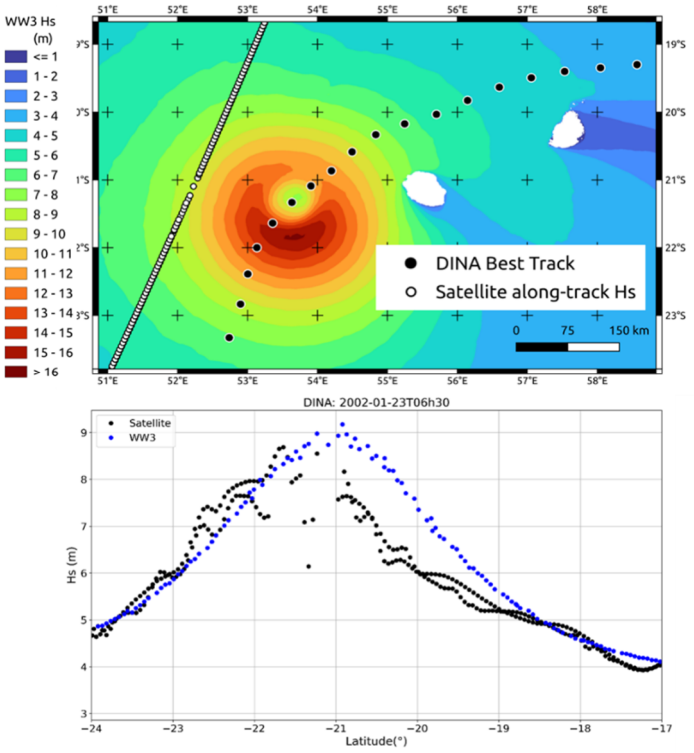


*Figure 26 : Comparison of waves from WW3 and satellites for ITC DINA on 23/01/2002 at 06:30 UTC.*

For analysis, we extract the maximum values over the time evolution of each cyclone for:

- the significant wave height Hs, and the peak period Tp and direction Dp (taken at the same instant of the maximum value);
- the wind speed U and the direction Du (taken at the same instant of the maximum value);
- the sea surface height SSH that account for the cyclone-induced surge.

A phenomenological analysis of the processes was performed to select the most critical points offshore Rodrigues and Mauritius (see Figure 27). The sixplets (*Hs; SSH*; *U; Tp; Dp; Du*) used to fit the statistical models (described below) are extracted at these specific spatial locations.

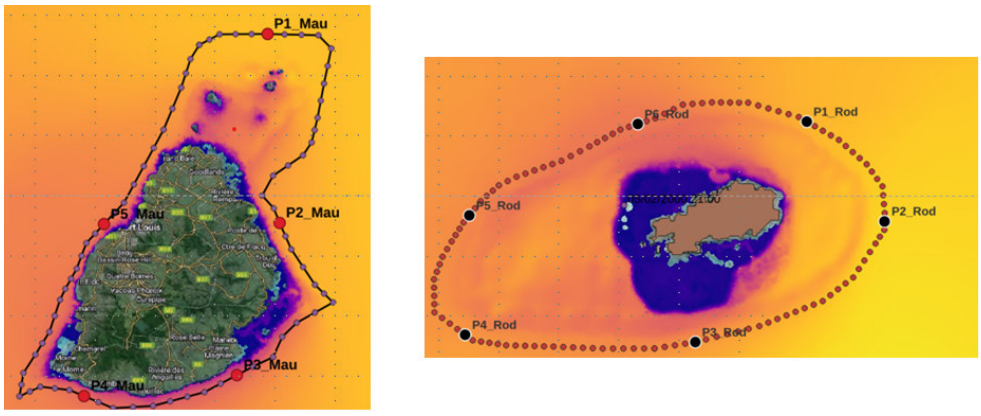


*Figure 27: Localisation of the points where the local high resolution hydrodynamic models are forced for both sites of interest (left: Mauritius, right: Rodrigues).*

*The most critical points with respect to flood risk occurrence were identified as P1_Mau and P1_Rod for both sites.*

Statistical analysis of the regional wind and atmospheric pressure fields has shown us that these conditions change at the limit of significance between the current climate and that of 2050. In what follows, we therefore concentrate on analysing the extreme values in a current climate and the one involving the most significant changes, i.e. that of 2080-2100. The latter scenario is denoted in the following “future climate condition”.

## 3.4.2 Methods

The phenomenon of coastal flooding is the result of the combination of multiple drivers that may be partly correlated with each other (e.g. Louisor et al., 2021). This means that the return period of a single driver is not representative and a joint analysis of the extreme values that the combined drivers can take simultaneously is necessary. In this study, we consider the joint effect of cyclone-induced waves, winds and sea surface height (surge). The extreme values are analysed within the framework of multivariate extreme value theory (Coles et al., 2001).

Our objective is to determine the probability that the three variables, *Hs*, *SSH* and *U* jointly exceed a given threshold. This determines a set of triplets (*Hs* ; *SSH* ; *U*) associated to a given level of probability. This probability level is here interpreted in terms of return period (here chosen as 100 years) by assuming that the average number of cyclone occurrences is respectively of 0.65 and 0.53 for Mauritius and Rodrigues. These values were determined using 400 years as the representative number of years associated to each set of storm systems and after applying a debiasing correction for the number of cyclones identified in the climate simulations.

The different steps of the procedure hold as follows:

**i. Fitting of the probability laws** (named ‘marginal’) for each variable *H*s, *SSH* et U taken separately; To do so, we follow a peaks-over-threshold approach (Coles et al., 2001) by fitting a combination of the Generalized Pareto Distribution GPD (to model the tail distribution) and of the empirical cumulative distribution $\tilde{F}$ as follows:

$$F(x) = \begin{cases} \tilde{F}(x) & x \leq u \\ 1 - \left(1 - \tilde{F}(u)\right)\left[1 + \xi \frac{(x-u)}{\sigma}\right]_+^{-\frac{1}{\xi}} & x > u \end{cases}$$

where

- *x=Hs* or *U* or *SSH*;
- The threshold *u* is chosen high enough by application of several analysis (Coles et al. (2001)): mean residual life plots and analysis of quantitative values resulting from statistical tests Chi-squared, Kolmogorov-Smirnov, or quantile-quantile graphs (not shown);
- $\sigma$ and $\xi$ are the GPD parameters to be evaluated using the observations. Three methods for estimating the parameters of the GPD have been tested (Hosking and Wallis, 1987): the method of moments, the weighted method of moments, and the maximum likelihood method; the estimation method leading to the largest return level is selected.

**ii. Modelling of the dependence between the three variables *H*s, *SSH et U*** using the conditional extreme model of Heffernan and Tawn (2004).
To do so, the three variables (*Hs*; *SSH*; *U*) are transformed onto the Gumbel scales using the standard probability integral transformation. Let us note the transformed variables $Y_i$ where i=Hs, U, or SSH, and $Y_{-i}$ a vector for all variables excluding $Y_i$. A multivariate non-linear regression model is then applied to $Y_{-i}\,|Y_i > v$:

$$Y_{-i} = aY_i + Y_i^b W \qquad \text{for } Y_i > v \text{ and } Y_i > Y_{-i}$$

where $a$ and $b$ are vectors of parameters, v a threshold, and *W* is a vector of residuals. Each fitted model describes the dependence between the variables (except $Y_i$). The models were adjusted using the maximum likelihood estimation method and assuming that the residuals *W* are normally distributed. Using the diagnostic tools described by Heffernan and Tawn (2004):Sect. 4.4, we have selected the threshold value for v (expressed as a probability of non- exceeding this threshold).

**iii. Simulation by means of a Monte-Carlo-based approach of a large number of** (*H*s ; *SSH* ; *U* ) combinations using the marginals and the dependence model. Once the parameters of the dependence model are estimated, we randomly generate a set of combinations (*Hs*; *U*; *SSH*) that are representative of a given number of years. The latter is chosen as 100 times the reference number of years of the original cyclone datasets, i.e. 400x100 = 40,000.

**iv. Identification of** (*H*s ; *SSH ; U*) scenarios on the joint exceedance contour (Hawkes et al., 2002); the latter is defined as the set (*x* ; *y* ; *z*) so that the joint exceedance probability Pr(*SSH* > x, Hs > y, U > z) is constant (and equal to the probability associated to the return period of interest; here chosen at 100 years) at every point around the contour.

**v. Estimates of the peak period**
Once the (*Hs; SSH ; U*) combinations are identified, each *Hs* is associated to its peak period *Tp*. The peak period *Tp* was simulated following the approach described by Gouldby et al. (2014). In this approach, a regression model of steepness $S_t$, conditional on *Hs* is used:

$$S_t = \frac{2\pi\, Hs}{g T_p^2}$$

where *g* is gravitational constant.

This model was used to simulate the steepness (and *Tp*) from Monte-Carlo simulations of Hs (generated at step iii, see previous section). In order to associate *Tp* to *Hs*, we take values around the median of the simulated periods for each of the *Hs* considered.

**vi. Selection of Dp, Du values**.

For the peak directions Dp associated to waves, and wind directions Du, we base the selection on the identification of the dominant direction leading to extreme *Hs* and *U* using wave and wind rose analysis and as well as the identification of most critical configurations with respect to flood risk.

**vii. Selection of the scenarios of forcing conditions.**

Based the results of steps iv-vi, a limited number (a few tens) of (*H*s ; *SSH ; T*p ; *D*p ; *U ; Du*) offshore forcing conditions (associated to the joint return period of 100 years) are defined and passed to the hydrodynamic models to select the most critical ones with respect to the occurrence of flood risk (4.2.1.2).

## 3.4.3 Results at Mauritius forcing point

We provide in this section the detailed implementation of the afore-described procedure in Mauritius for present day and future climate conditions.

### 3.4.3.1 Marginals

The Figure 28, Figure 29, Figure 30 depict the fitting results in the form a return level plot (return period versus the considered variable level). Uncertainty in the estimates is assessed by applying the delta method (Coles et al., 2001). Table1 summarises the return levels at 100 years for both

climate conditions. From present day to future climate conditions, we note an increase of the return levels of the order of 5-10% with a larger difference outlined for *U* and *SSH*. These differences are consistent which the increase of these climate variables analysed at regional scale see previous section. Interestingly, the increase does not necessarily correspond to a constant shift of the whole return level plot but by a change of shape, which indicates a change in extreme regimes.

*Table1 : 100-year return levels for each driver using the marginal for Mauritius (present day and future climate scenario). Numbers in brackets correspond to the 95% confidence interval.*

| Climate conditions | *Hs* (m) | *U* (m/s) | *SSH* (m) |
|---|---|---|---|
| Present day | 17.9<br>[16.35 ; 19.5] | 53.2<br>[49.7 ; 56.8] | 0.58<br>[0.47 ; 0.69] |
| Future climate | 18.3<br>[17.2 ; 19.4] | 56.4<br>[52.5 ; 60.3] | 0.66<br>[0.59 ; 0.72] |

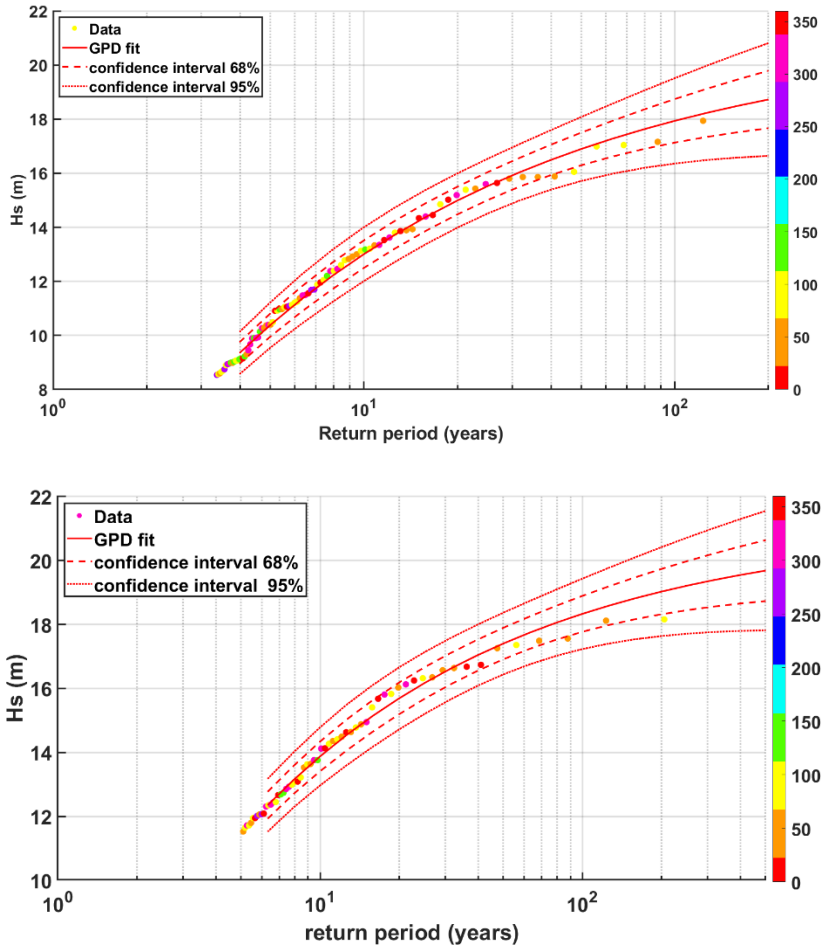


*Figure 28: Return level plot for significant wave height Hs at Mauritius forcing point for present day (top) and future (bottom) climate scenario.*

*The points represent the return levels calculated empirically from the data. The curve shows the fit of the statistical model (solid line: best estimate, dashed line: uncertainty envelope at the 95% level estimated by the Delta method). The coloured dots represent the peak direction Dp.*

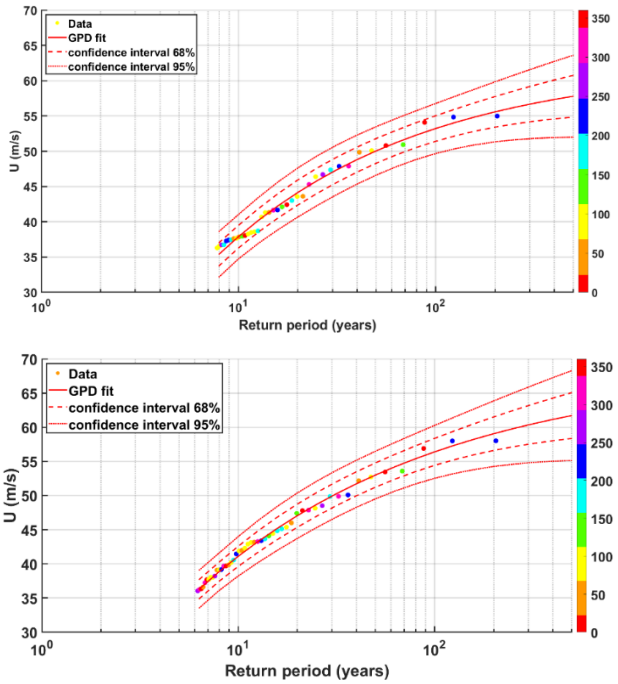


*Figure 29: Return level plot for wind speed U at Mauritius forcing point for present day (top) and future climate scenario (bottom). The points represent the return levels calculated empirically from the data.*

*The curve shows the fit of the statistical model (solid line: best estimate, dashed line: uncertainty envelope at the 95% level estimated by the Delta method). The coloured dots represent the wind direction Du.*

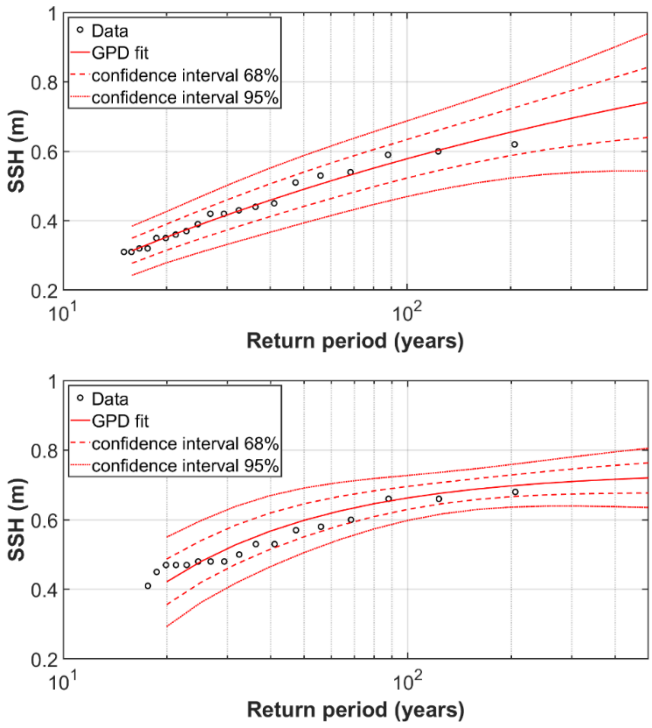


*Figure 30: Return level plot for sea surface height SSH at Mauritius forcing point for present day (top) and future climate scenario (bottom). The points represent the return levels calculated empirically from the data.*

*The curve shows the fit of the statistical model (solid line: best estimate, dashed line: uncertainty envelope at the 95% level estimated by the Delta method).*

### 3.4.3.2 Multivariate extreme value analysis

Using the diagnostic tools described by Heffernan and Tawn (2004):Sect. 4.4, we have selected v = 0.75 for both climate scenarios. Once the parameters of the dependence model have been estimated, we randomly generate a set of combinations (Hs; U; SSH)) that are representative of 40,000 years. To illustrate how the observations (outlined in black) are extrapolated using the approach, Figure 31 depicts the distribution of the generated samples (outlined in blue) in 2D diagrams for the present-day climate scenario.

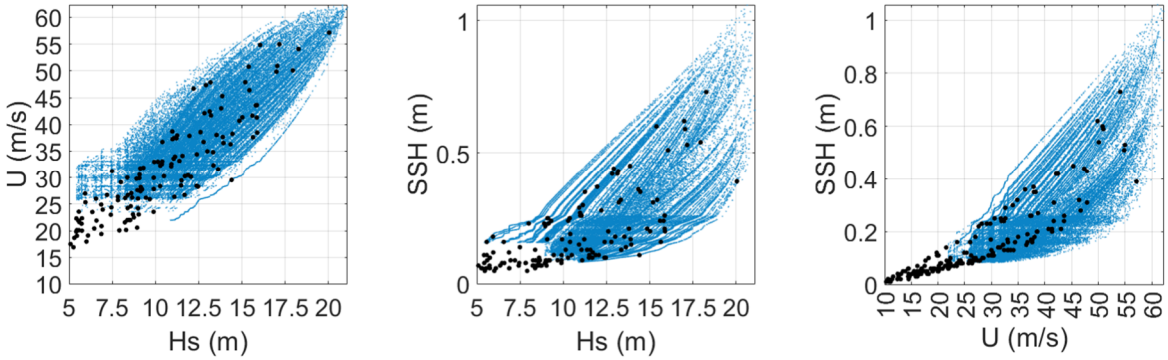


*Figure 31: Observations (black) and Monte-Carlo-based randomly generated (blue) combinations (Hs; U; SSH) in Mauritius for present day climate conditions depicted in 2D diagrams Hs versus U; Hs versus SSH and U versus SSH at Mauritius forcing point (present day climate scenario).*

The 100-year joint exceedance contours are constructed for present day and future climate conditions (Figure 32). This takes the form of a set of 2D joint exceedance iso-contours within the space (*SSH ;* Hs); each of these 2D iso-contours varies with *U* values (as indicated by the colour scale in (Figure 32). From present day to future scenario, a change in the form and shape of the iso-contours indicates a change in the magnitude of the extremes (see in particular the shift in the leftmost part of along the *SSH* axis) but also a change in the dependence structure (see in particular the rightmost part of (Figure 32), hence indicating a change of the co-occurrence between the extreme drivers in the future.

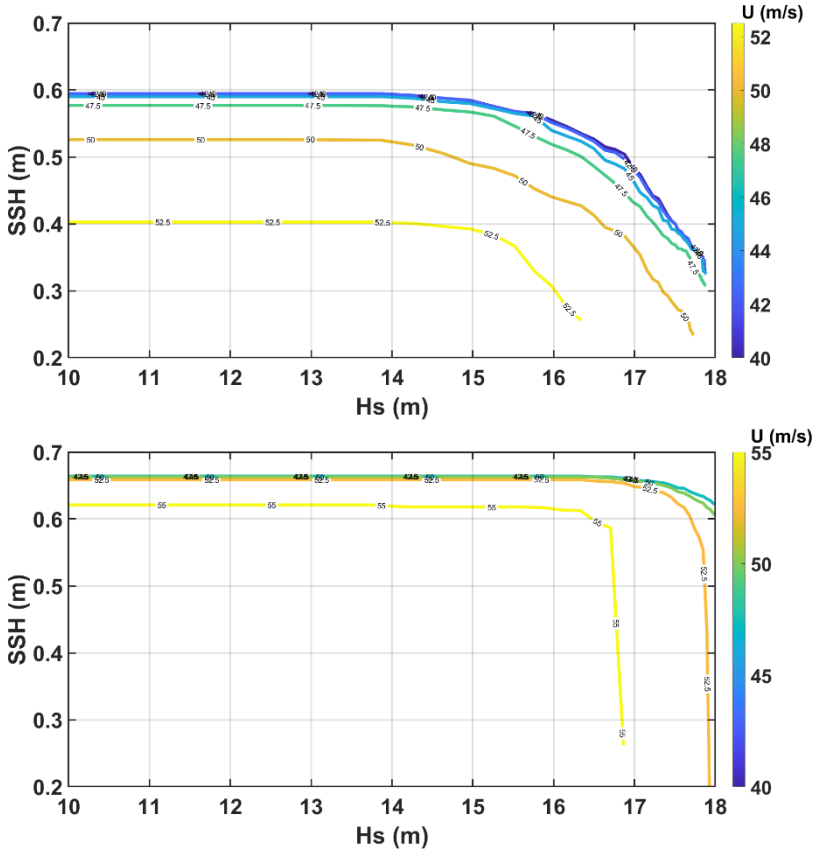


*Figure 32: Joint exceedance iso-contours for return period of 100 years within the space (SSH ; Hs) with the colour indicating the U values in Mauritius forcing point for present day (top) and future (bottom) climate scenario.*

*Note the change in the colorscale between both cases.*

### 3.4.3.3 Covariate estimates

Figure 33 depicts the relation between Tp and Hs for both climate scenarios.

Finally, for the remaining covariates, namely peak directions *Dp* associated to waves, and wind directions *Du*, we base the selection on the identification of the dominant direction leading to extreme Hs and U using the wave (Figure 34) and wind rose analysis (Figure 35).

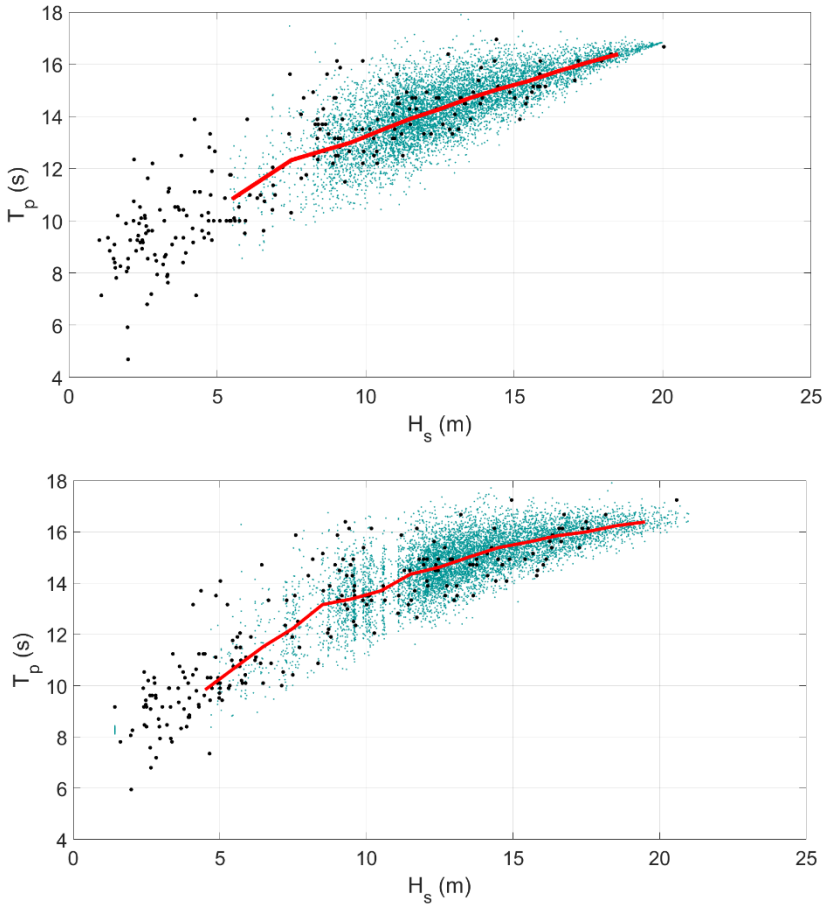


*Figure 33: Relation between peak period Tp and significant wave height Hs at Mauritius forcing point for present day (top) and future (bottom) climate scenario.*

*The black dots are the observations; the green dots are the randomly simulated ones, and the red curve is the statistical model (median value) established using Gouldby et al. (2014)'s approach.*

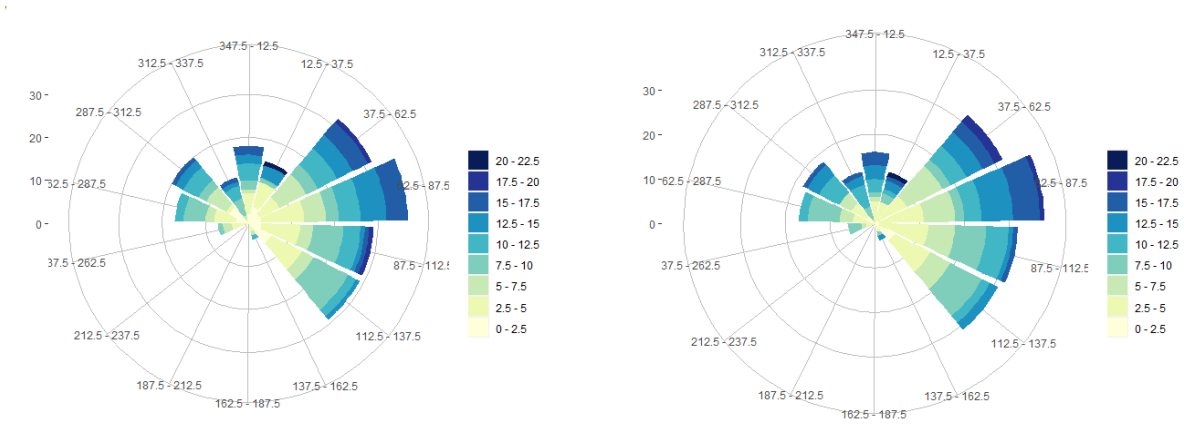


*Figure 34: Wave rose in Mauritius forcing point for present day (left) and future climate scenario (right).*

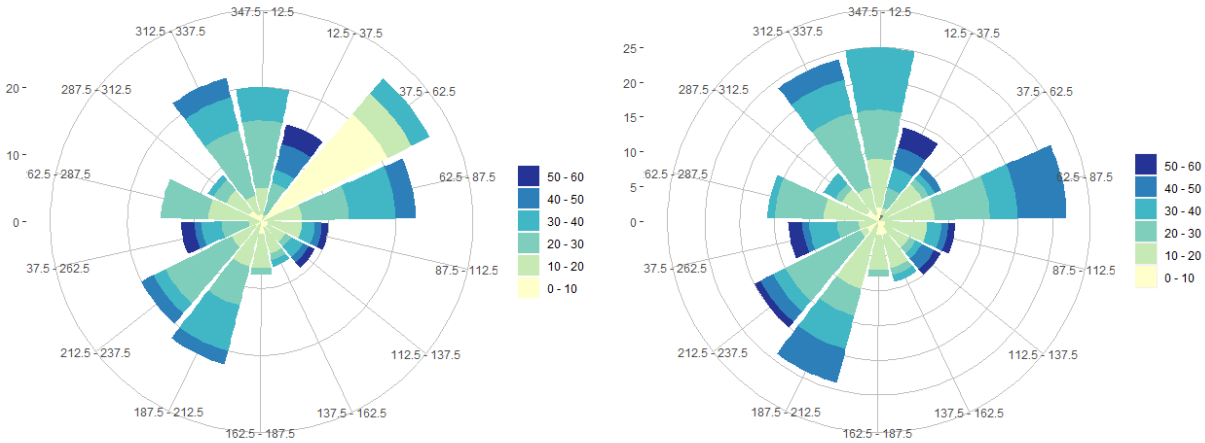


*Figure 35 : Wind rose in Mauritius forcing point for present day (left) and future climate scenario (right).*

## 3.4.4 Results at Rodrigues forcing point

We provide in this section the detailed implementation of the afore-described procedure at Rodrigues for present day and future climate conditions.

### 3.4.4.1 Marginals

The Figure 36, Figure 37 and Figure 38 depict the fitting results in the form a return level plot (return period versus the considered variable level). Uncertainty in the estimates is assessed by applying the delta method (Coles et al., 2001). Table 2 summarises the return levels at 100 years for both climate conditions. From present day to future climate conditions, we note an increase of the return levels of the same order than the one at Mauritius for *U* and *SSH*. The changes in Hs remain however relatively minor.

*Table 2. 100-year return levels for each driver using the marginal for Rodrigues (present day and future climate scenario). Numbers in brackets correspond to the 95% confidence interval.*

| **Climate conditions** | ***Hs* (m)** | ***U* (m/s)** | ***SSH* (m)** |
|---|---|---|---|
| Present day | 17.0<br>[16.15 ; 17.9] | 55.7<br>[47.8 ; 63.6] | 0.66<br>[0.54 ; 0.79] |
| Future climate | 17.2<br>[16.4 ; 18.0] | 58.5<br>[53.0 ; 63.8] | 0.78<br>[0.63 ; 0.94] |

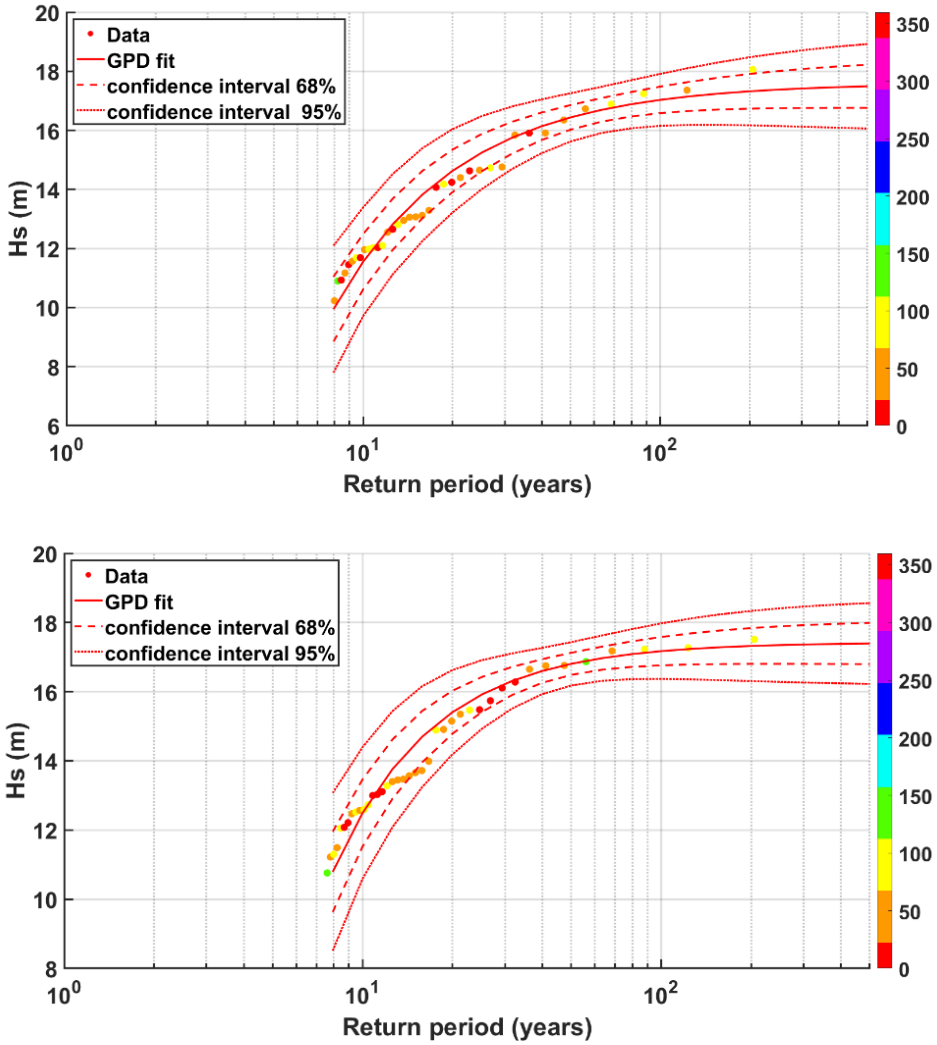


*Figure 36: Return level plot for significant wave height Hs at Rodrigues forcing point for present day (top) and future (bottom) climate scenario.*

*The points represent the return levels calculated empirically from the data. The curve shows the fit of the statistical model (solid line: best estimate, dashed line: uncertainty envelope at the 95% level estimated by the Delta method). The coloured dots represent the peak direction Dp.*

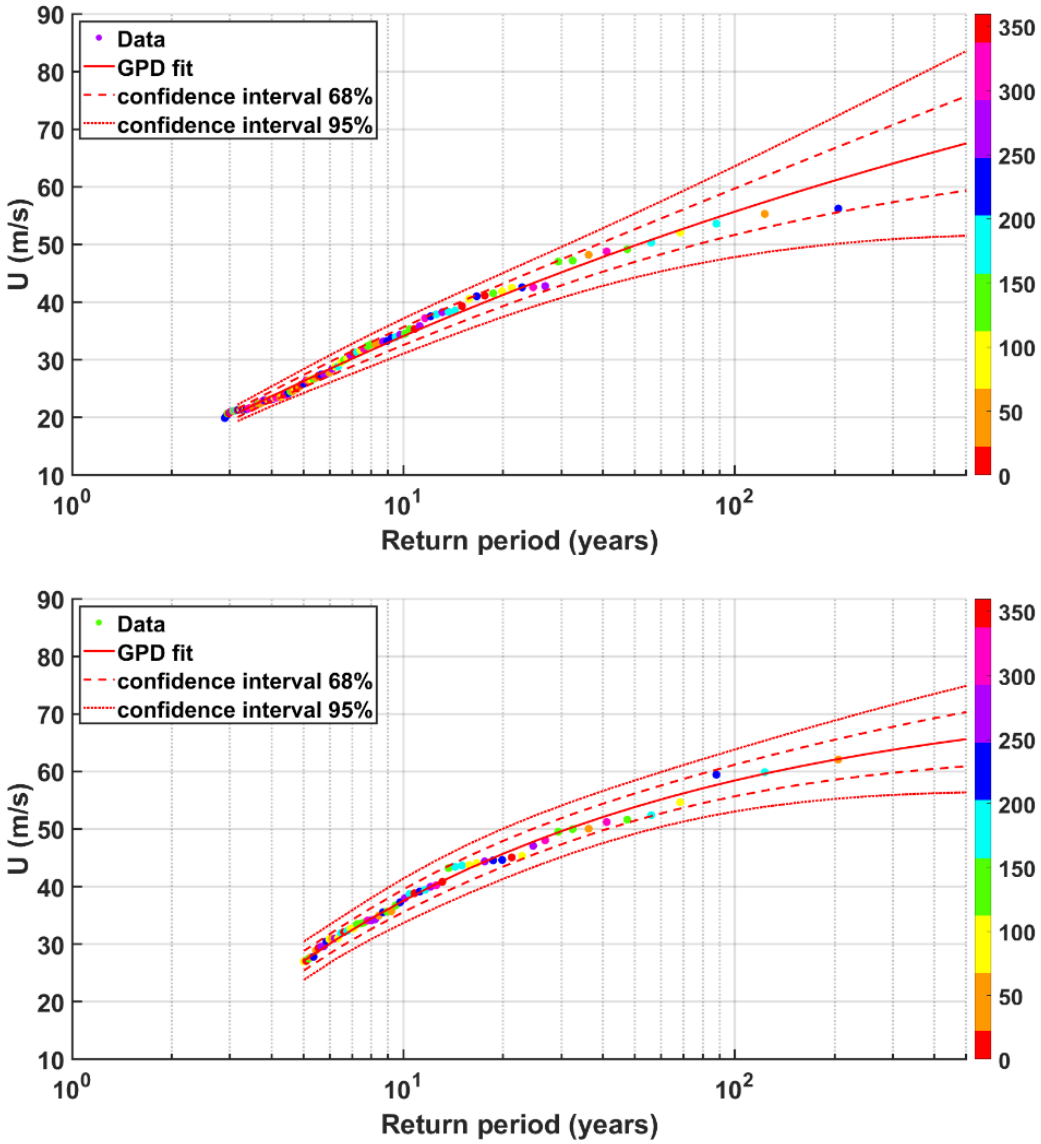


*Figure 37: Return level plot for wind speed U at Rodrigues forcing point for present day (top) and future climate scenario (bottom).*

*The points represent the return levels calculated empirically from the data. The curve shows the fit of the statistical model (solid line: best estimate, dashed line: uncertainty envelope at the 95% level estimated by the Delta method). The coloured dots represent the wind direction Du.*

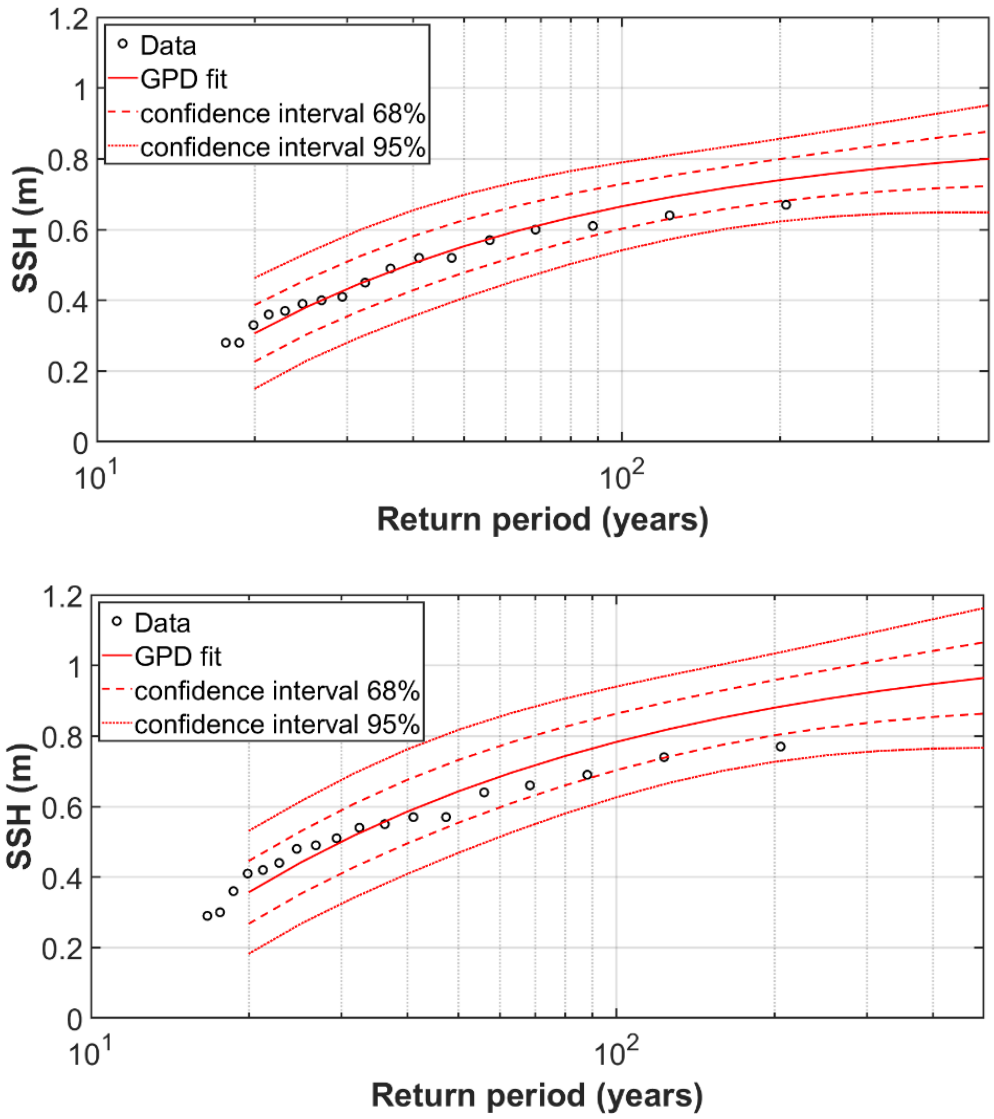


*Figure 38: Return level plot for sea surface height SSH at Rodrigues forcing point for present day (top) and future climate scenario (bottom).*

*The points represent the return levels calculated empirically from the data. The curve shows the fit of the statistical model (solid line: best estimate, dashed line: uncertainty envelope at the 95% level estimated by the Delta method).*

### 3.4.4.2 Multivariate extreme value analysis

Using the diagnostic tools described by Heffernan and Tawn (2004): Sect. 4.4, we have selected v = 0.65 and 0.675 for each respective climate scenario. Once the parameters of the dependence model have been estimated, we randomly generate a set of combinations (Hs; U; SSH)) that are representative of a given number of 40,000 years.

The 100-year joint exceedance contours are constructed for present day and future climate conditions (Figure 39). Between the two climate scenarios, a change in the form and shapes of the iso-contours is less marked than for Mauritius. Between both climate scenarios, we note a change in the magnitude of the extremes especially for *SSH* and *U* as also indicated by the analysis of the marginals (see in particular the shift in the leftmost part of Figure 39 along the *SSH* axis).

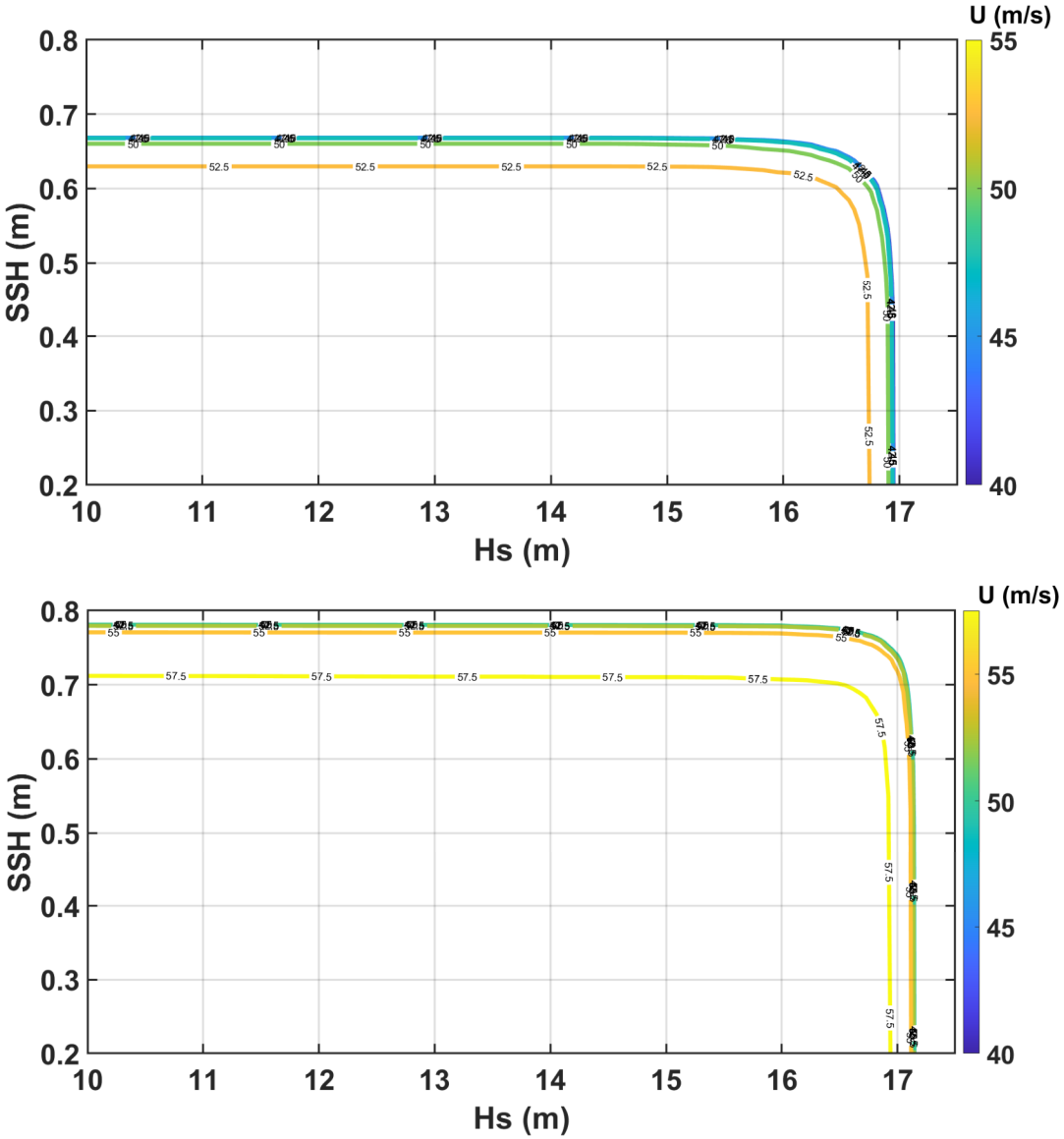


*Figure 39: Joint exceedance iso-contours for return period of 100 years within the space (SSH ; Hs) with the colour indicating the U values at Rodrigues forcing point for present day (top) and future (bottom) climate scenario.*

*Note the change in the colorscale between both cases.*

### 3.4.4.3 Covariate estimates

The Figure 40 depicts the relation between *Tp* and *Hs* for both climate scenarios.

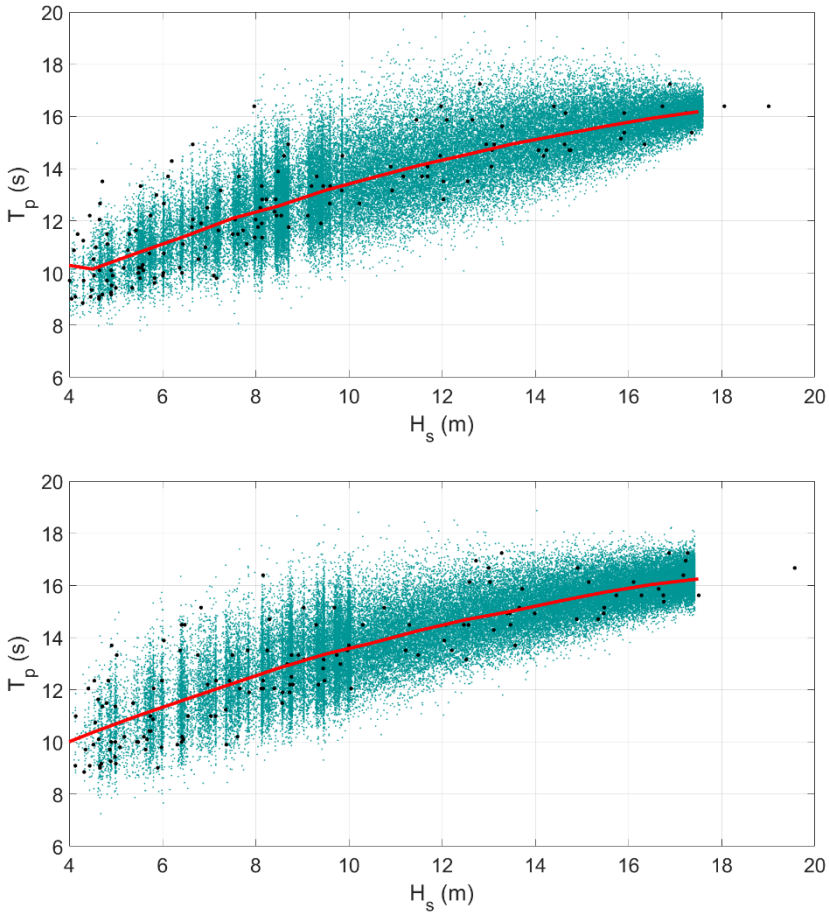


*Figure 40: Relation between peak period Tp and significant wave height Hs at Rodrigues forcing point for present day (top) and future (bottom) climate scenario.*

*The black dots are the observations; the green dots are the randomly simulated ones, and the red curve is the statistical model (median value) established using Gouldby et al. (2014)'s approach.*

Finally, for the remaining covariates, namely peak directions *Dp* associated to waves, and wind directions *Du*, we base the selection based on the identification of the dominant directions leading to extreme *Hs* and *U* using the wave (*Figure 41*) and wind rose analysis (Figure 42).

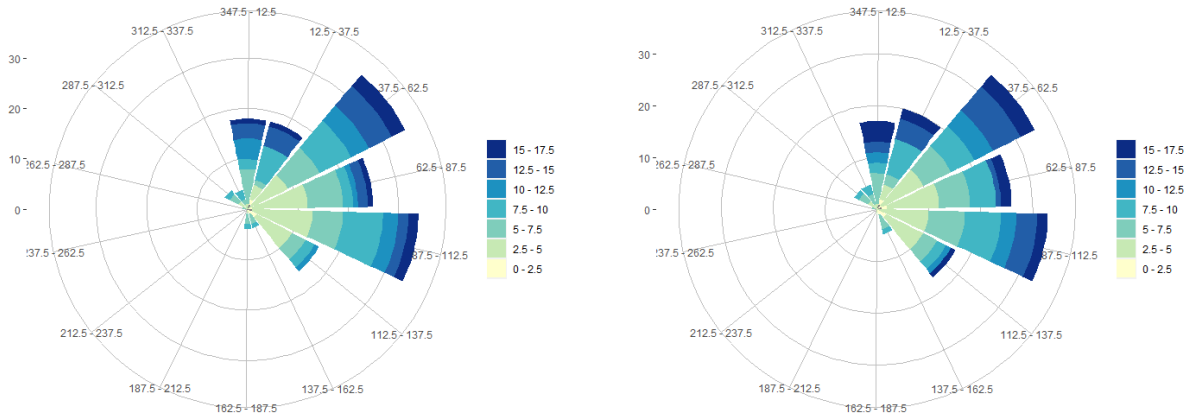


*Figure 41: Wave rose at Rodrigues forcing point for present day (left) and future climate scenario (right).*

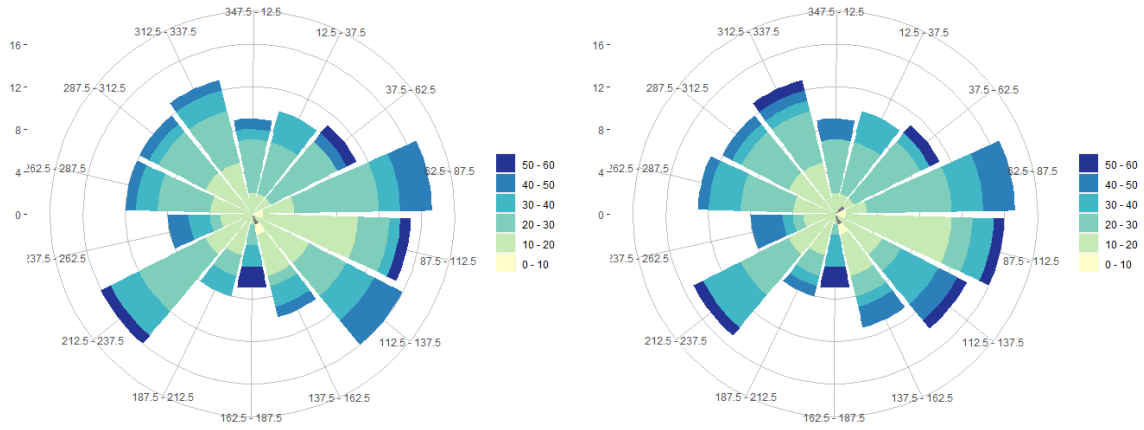


*Figure 42: Wind rose at Rodrigues forcing point for present day (left) and future climate scenario (right)*

# 3.5 ANALYSIS OF SEA LEVELS IN MAURITIUS AND RODRIGUES

## 3.5.1 Introduction

The global mean sea level rose at an average rate of 1.4 mm/year (+/-0.6 mm/year) between 1900 and 1990. This rise accelerated progressively over the 20th century, reaching a rate of 3.4 mm/year (+/- 0.4 mm/year) over the period 1993-2018 (Frederikse *et al*., 2020; IPCC, 2021). Over this last period, around 60% of the global mean sea level rise can be attributed to the melting of glaciers and land ice caps, and around 40% to the thermal expansion of the ocean. However, in the vast majority of cases, global estimates do not correspond to what is observed locally; additional processes influencing relative sea level must therefore be taken into account, such as vertical ground movements, regional climate variability and terrestrial gravitational and rotational changes. This analysis constitutes the first part of this chapter.

The second part describes the relative sea-level (RSL) projections that have been developed. RSL projections have been designed for the entire 21st century and are used as boundary conditions for flood modelling and shoreline changes.

## 3.5.2 Analysis of recent sea levels in Mauritius and Rodrigues

### 3.5.2.1 Data

The characterisation of sea levels in Mauritius and Rodrigues is based on tide gauge records, altimetric observations, data from permanent Global Positioning System (GPS) stations and the results of climate models.

#### *3.5.2.1.1 Tide gauges*

Tide gauge measures the relative sea level, i.e. in a local terrestrial reference frame. The sea level measured by tide gauges therefore incorporates both the climatic and dynamic components of sea level, as well as local ground movements. Mauritius and Rodrigues each have usable data for at least one operational tide gauge, the observational characteristics of which are described in Table 3.

Mauritius has two tide gauge records at Port-Louis (noted 103b and 103c on the GESLA portal - https://gesla787883612.wordpress.com/) and one at Grand Port (PSMSL portal - https://psmsl.org/data/obtaining/map.html#plotTab). The sea level record for Grand Port was not analysed however because only partial monthly data are available for the period 1958-1960. The Port-Louis 103b record was not considered either because hourly data are only available for a period of less than 2 years (1964-1965). The Port Louis 103c record supplied by GESLA was the only tide gauge record selected and analysed because it has hourly data for the recent period and because it covers more than three decades (33 years).

On the GESLA and PSMSL portals, the island of Rodrigues only has a single tide gauge record at Port Mathurin. In what follows, we analyse the hourly tide gauge record provided by GESLA for the period 1986-2017.

| Name of tide gauge | Port Louis (Maurice) - 103c | Rodrigues - 105a |
|---|---|---|
| Coordinates | 57.495°E/-20.155°N | 63.418°E/-19.668°N |
| Number of years | 33 | 32 |
| Start date | 1986/08/01 00:00:00 | 1986/11/08 14:00:00 |
| End date | 2018/12/31 23:00:00 | 2017/09/04 23:00:00 |
| Resolution | Hourly | Hourly |
| Source | GESLA | GESLA |

*Table 3: Characteristics of tide gauge observations*

#### *3.5.2.1.2 Satellite altimetry*

Satellite measurements are used to obtain the absolute sea level, i.e. in a terrestrial reference frame. The mathematical relationship between absolute and relative sea level trends is as follows:

$$N = U + S \text{ (Eq. 1)}$$

With $N$ the absolute sea level trend, $S$ the relative sea level trend and $U$ the vertical ground motion velocity. The difference between absolute sea level and relative sea level therefore enables a local estimate of vertical ground movements.

In the following analysis, we use daily sea-level-anomaly altimetry data. This dataset is produced by the Copernicus Marine Environmental Monitoring Service (CMEMS) and is available for downloading from the Copernicus Climate Change Service (C3S; https://cds.climate.copernicus.eu). The data are interpolated on a regular 0.25°x0.25° grid (longitude x latitude) and have been supplied since 1 January 1993. Our analysis is based on the DT2018 version, which ran up to 2020.

#### *3.5.2.1.3 GPS stations*

Measurements from permanent GPS stations are used to characterise vertical ground motion velocity (term $U$ in Equation 1). However, the temporal coverage of GPS measurements on the islands of Mauritius and Rodrigues is discontinuous. On the SONEL platform (https://www.sonel.org/), results from a single GPS station are available in Mauritius for 3 GPS solutions (ULR, NGL and JPL); this is the VACS station (57.49703615°E/-20.29707590°N, Vacoas), which has been producing estimates since July 2008, i.e. for almost 13 years. The VACS station is located inland, around ten kilometres from the Port-Louis tide gauge. The SONEL platform does not have any data for Rodrigues. On the NGL platform (http://geodesy.unr.edu), estimates of vertical ground movements are provided for 4 GPS stations in Mauritius (including VACS) and 1 GPS station in Rodrigues (RDRG). Apart from VACS, the results from the GPS stations supplied by NGL cover short periods of time (less than 4 years). Finally, it should be noted that the results for the NGL platform are only provided for one GPS solution: the NGL solution.

#### *3.5.2.1.4 Climate modelling*

In addition to tide gauge, altimeter and GPS observation data, the following analysis is supplemented by the results of climate model simulations. These simulations are from the Coupled Model Intercomparison Project (CMIP5). These simulation results have been used to construct the global and regional mean sea level projections in the IPCC AR5 (2013) and SROCC (2019) reports. They are available at: https://www.cen.uni-hamburg.de/icdc.

Output from climate models (coupled ocean-atmosphere models) can be used to estimate the sterodynamic component, which includes thermal expansion and dynamic variations in sea level. Changes in ocean mass due to the melting of continental glaciers, the melting of ice caps, or the transfer of liquid water from continents to the ocean, on the other hand, are not estimated by the climate models. They are therefore estimated indirectly by imposing the results of CMIP5 climate

simulations (precipitation, temperature, etc.) as boundary conditions for glaciology models and hydrological models. Sea level projections are then obtained by summing all the components linearly. The results are distributed annually at a spatial resolution of 1°x1° (longitude x latitude).

Historical simulations, also known as 'hindcasts', are constrained by boundary conditions observed over the period 1850-2006, such as greenhouse gas concentrations, solar irradiance and volcanic eruptions. For the historical simulations (before 2006), we use the simulation dataset of Slangen et al. (2017) and Meyssignac et al. (2017). The projections are constrained by projected greenhouse gas emission scenarios that depend on global socio-economic pathways over the period 2007-2100. For the CMIP5 projections, RCP scenarios were used.

### 3.5.2.2 Results

This section presents recent changes in sea level observed in Mauritius and Rodrigues. The results of the observations are then compared with the results of climate models.

#### ***3.5.2.2.1*** *Observations*

The annual means of relative sea level in Mauritius and Rodrigues measured by the tide gauges are shown in Figure 43. The tide gauges recorded a mean rise in relative sea level of 4.0 (+/-0.7) mm/year in Mauritius and 5.4 (+/- 0.9) mm/year in Rodrigues over the entire period observed. It is therefore significantly higher in Rodrigues than in Mauritius. Moreover, these two estimates are higher than the trend in global mean sea level rise, which has averaged around 3.5 mm/year since 1993.

The tide gauge recordings (Figure 43) also show a high degree of interannual to near-decadal variability, which differs from the linear trend. Interannual variability shows fluctuations of around 5 cm. Although there are similarities, the inter-annual variations between the two tide gauges are not identical: for example, the order of the height of the 2010 and 2014 peaks is reversed between Mauritius and Rodrigues. This suggests that, despite their geographical proximity, the two islands are subject to different variations in sea level on a regional scale. On a near-decadal scale, the change in relative sea level is very similar between the two tide gauges: there was a slight fall between 1987 and the end of the 1990s, followed by a very sharp rise in the 2000s of more than 10 cm over 10 years, and finally an attenuated rise from 2010 onwards.

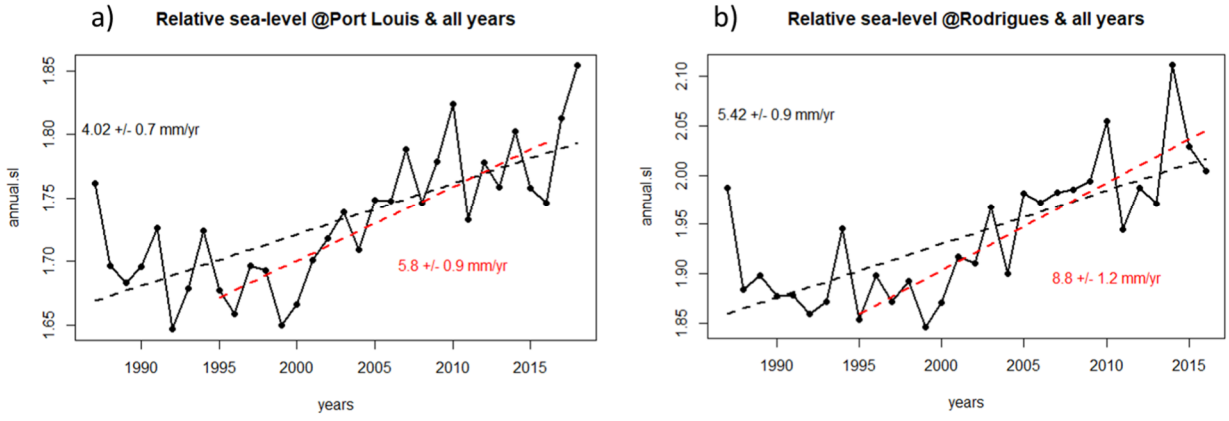


*Figure 43: Annual relative sea level measured by tide gauges in (a) Mauritius and (b) Rodrigues between 1987 and 2016-2017. The sea level trend and its uncertainty, derived from a linear regression, is calculated either over the entire observed period (black dashed line) or over the period 1995-2017 (red dashed line).*

To improve our understanding of the changes in relative sea level recorded in Mauritius and Rodrigues, as well as the differences between the two tide gauges, we continued the analysis

using altimetry data. The comparison between tide gauge observations (relative sea level) and altimetry observations (absolute sea level) is shown in Figure 44. Here, the altimeter grid point that is closest to the tide gauge has been selected.

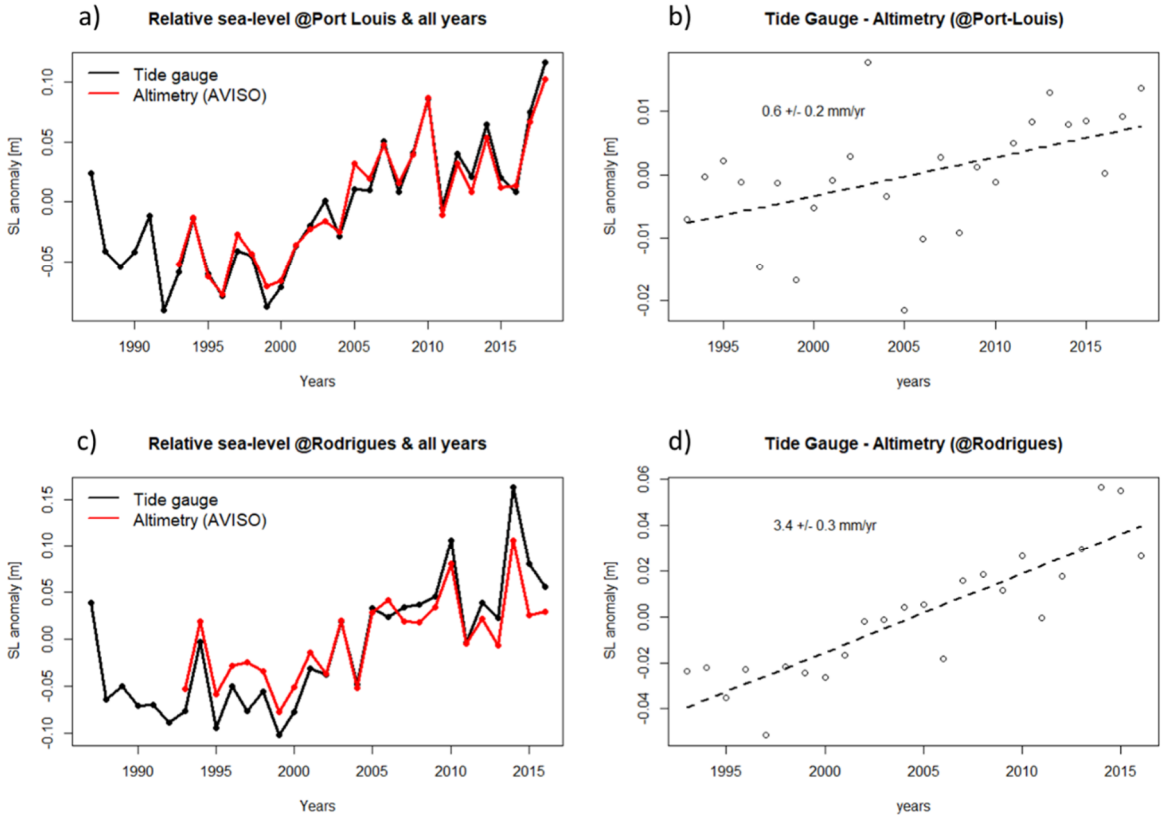


*Figure 44: Superposition of annual time series of relative sea level (black) and absolute sea level (red) in Mauritius (a) and Rodrigues (c) compared with the reference period 1995-2016. Differences between absolute and relative sea levels in (b) Mauritius and (d) Rodrigues.*

First of all, we can see that over the common observation period (from 1993), the interannual to near-decadal variations in relative and absolute sea levels are very similar for the two tide gauges. In Rodrigues, however, over the whole of the common period, the trend for absolute sea level rise (red curve) is lower than that for relative sea level rise (black curve). This observation becomes clearer when we calculate the difference between relative and absolute sea levels (Figure 44). In Mauritius (Figure 44b), the relative sea level is 0.6 (+/- 0.2) mm/year higher than the absolute sea level, while in Rodrigues (Figure 44d), the relative sea level is 3.4 (+/- 0.3) mm/year higher than the absolute sea level. This last result suggests a context of weak, strong, subsidence at the respective tide gauge location for Mauritius and Rodrigues. Estimates of vertical velocities deduced from permanent GPS on the two islands also suggest subsidence contexts of the order of 1 mm/year where permanent GPSs are located. However, the GPS results do not show any significant differences between Mauritius and Rodrigues.

| Solution / Station | ULR | NGL | JPL | GFZ |
|---|---|---|---|---|
| ***VACS (Mauritius)*** | -1.00 +/- 0.16 | -0.88 +/- 0.72 | -0.93 +/- 0.36 | x |
| ***FG06 (Mauritius)*** | x | -1.60 +/- 1.42 | x | x |
| ***RDGR (Rodrigues)*** | x | -0.84 +/- 0.83 | x | x |

*Table 4: Ground movement vertical velocity (in mm/year) estimated by different solutions at the permanent GPS stations available in Mauritius and Rodrigues.*

To better understand the origin of the near-decadal variations recorded by tide gauges and altimetry measurements, we analysed separately the sea level trends measured by altimetry over the periods 1993-2000, 1999-2010 and 2009-2018 at the scale of the Indian Ocean basin (Figure 45). They reveal sea level trend patterns that vary greatly in time and space. The southern boundary of the Indian Ocean, between Australia and Africa, is marked by alternating positive and negative fine quasi-circular structures indicative of ocean eddies. This eddy pattern can be seen in all three periods, although the amplitude is more pronounced between 1993 and 2000. Off Madagascar, sea level trends reveal very extensive and distinct geometrical shapes:

- over the period 1993-2000, the trends show a fall in sea level of more than 10 mm/year, which describes a tongue-shaped area stretching from north-west Madagascar to southern Indonesia, combined with a rise in sea level of more than 10 mm/year concentrated on the Indo-Pacific boundary. This spatial pattern is very similar to the main mode of decadal sea level variability in the Indian Ocean (Nidheesh et al., 2019; Sajidh and Chatterjee, 2023) and is consistent with the identification of a prolonged sea level decline in Rodrigues and Mauritius between 1993 and 2000 (Figure 44);
- over the period 1999-2010, a tongue-shaped area similar to that of the period 1993-2000 but of opposite sign (rise of more than 10 mm/year) was observed off Madagascar. In contrast to the geometrical shape obtained over the 1993-2000 period, the positive tongue-shaped area in 1999-2010 is spread out more along the north-south axis;
- over the period 2009-2018, there is no broad, consistent spatial pattern in the sea level trend.

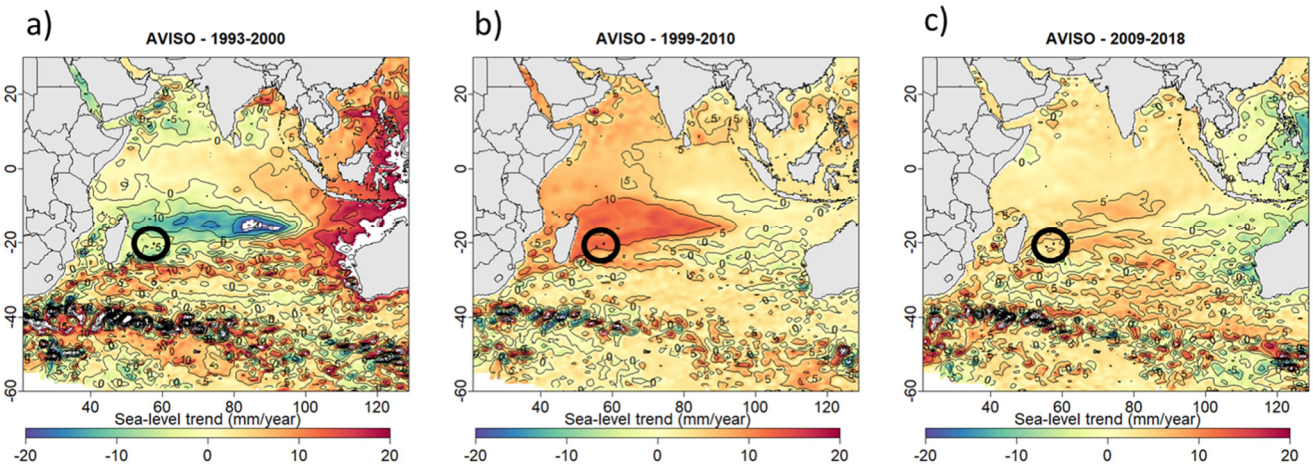


*Figure 45: Trends in sea level rise in the Indian Ocean calculated from altimetry data over the periods (a) 1993-2000, (b) 1999-2010 and (c) 2009-2018. Mauritius and Rodrigues are in the black circle.*

In summary, this comparative analysis of tide gauge records and altimetry observations reveals that relative sea levels in Mauritius and Rodrigues are subject to a long-term rise that is consistent with the increase in global sea level due to global warming. This rise in relative sea level seems to be amplified locally due to local subsidence, particularly in Rodrigues. Finally, the rise in relative sea level is strongly modulated by natural interannual to decadal climate variability. The results

of altimetry observations show that Mauritius and Rodrigues are located in a region of the Indian Ocean where decadal variations in sea level are particularly pronounced.

#### *3.5.2.2.2 Comparison between observations and models*

In this section, we compare the observed sea level with the sea level simulated by historical simulations (up to 2006) and projections (from 2006 onwards) from climate models that were used in the CMIP5 exercise. The aim is to assess the relevance of climate models for regional sea level projections in Mauritius and Rodrigues. To carry out our hindcast reconstruction and projections of sea level based on the results of climate models, we use an ensemble approach. The latter, used by the IPCC, consists in considering a set of simulations of the same climate scenario using different models. The mean of the ensemble then corresponds to the central estimate (or best estimate) while the dispersion around the mean of the ensemble quantifies the uncertainty.

The results for the Mauritius tide gauge are shown in Figure 46. Note that the possible contribution of subsidence, which is small at this tide gauge (~0.5 mm/year), has not been added to the results of the climate simulations. The results of the climate simulations show a gradual rise in sea level which accelerates over time and which, until 2030, is independent of the climate scenario considered. The range of uncertainty in the sea level simulated by the models is of the same order of magnitude as the interannual variations observed by the tide gauge (~5 cm): this result suggests that the CMIP5 models are capable of reproducing dynamic variations in sea level on an interannual scale. On the other hand, at near-decadal scales, the values of relative sea level observed before 1990 and after 2007 are very different from the range of uncertainty obtained in the simulations. This last result suggests that the sea level obtained in the simulations does not represent the magnitude and phase of the near-decadal variations associated with the natural variability of the coupled ocean-atmosphere system. This result is not surprising given that:

- the reduced spatial resolution of global models often leads to an underestimation of intrinsic variations in the climate system;
- the ensemble approach, which consists in averaging a maximum number of results, tends to smooth out random variations. In other words, the phases of internal variations in the observed climate cannot be reproduced due to the intrinsic nature of the ensemble approach;
- finally, the ensemble approach also assigns equal weighting to each model regardless of its performance.

Without more analysis, it is not possible to push this comparison between tide gauge observations and simulation results any further.

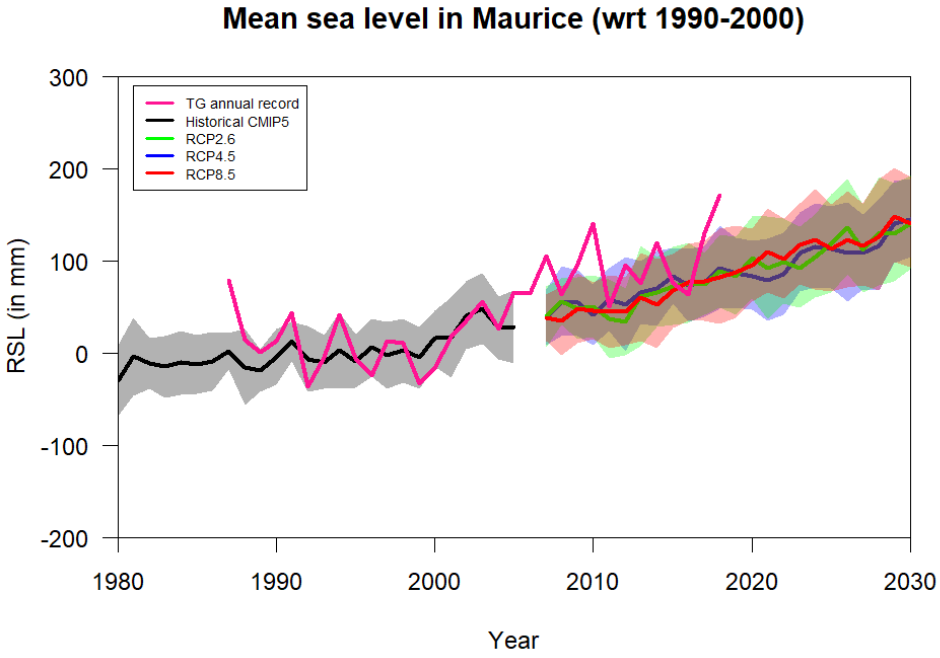


*Figure 46: Comparison between the annual mean relative sea level observed at the Mauritius tide gauge (pink curve) and the regional level simulated by the historical simulations (black curve, before 2006) and the projections (tinted curves, after 2007) of the CMIP5 climate models.*

*The RCP2.6 (green), 4.5 (blue) and 8.5 (red) scenarios are shown. The envelopes show the 5-95% uncertainty bounds. All the time series show the anomaly in relation to the common reference period of 1990-2000.*

### 3.5.2.3 Summary

This work presents an analysis of the changes in sea level observed in Mauritius and Rodrigues and compares these observation results with the regional sea level reconstruction resulting from climate simulations. Our results highlight the importance of considering the regional and local processes that contribute to the rise in relative sea level. In Mauritius and Rodrigues, our analysis clearly shows a local increase in relative sea level over the period observed, which is consistent with the global rise in sea level in response to climate change.

However, our results show that **the rise in relative sea level is accentuated by subsidence**, and that the **sea level exhibits multi-annual fluctuations due to natural climatic variability**.

In line with observations, the reconstruction of sea level using numerical simulations makes it possible to represent the rise caused by the climate and to take account of interannual fluctuations linked to local dynamic variations. However, a comparison between observations and the results produced by the models suggests that the near-decadal variability of sea level is underestimated in the reconstructions.

## 3.5.3 Future relative sea levels in Mauritius and Rodrigues

### 3.5.3.1 Method

Our RSL projections are designed using the same approach than that used in §2.5.2.2.2 for comparing climate model results and observations over the historical period, but also used by the IPCC (Oppenheimer et al., 2019). More details on the approach are provided hereafter. Basically, it consists in combining the different contributors of sea-level rise following the equation:

$$\boldsymbol{\Delta RSLC = \Delta Z + \Delta R_{barystatic-GRD} + \Delta VLM} \text{ (Eq. 1)}$$

where $\boldsymbol{\Delta RSLC}$ defines the temporal relative sea-level change, $\boldsymbol{\Delta Z}$ is the sterodynamic temporal sea-level change, $\boldsymbol{\Delta R_{barystatic-GRD}}$ is the barystatic (i.e. mass) component change and $\boldsymbol{\Delta VLM}$ accounts for changes in vertical land motions. All components are regionalized as described hereinafter.

#### *3.5.3.1.1 The sterodynamic component ($\Delta Z$)*

Results of the simulations of the coupled ocean-atmosphere climate models that participated in the international exercises CMIP5 (Taylor et al., 2012) and CMIP6 (Eyring et al., 2016) allow obtaining directly the sterodynamic component: i.e. the thermal expansion of the ocean, the changes in ocean circulation and the inverse barometer effect (the latter has a modest effect). An example of the sterodynamic contribution projection is shown on Figure 36. It shows very strong regional variations. The resolution of this component depends on the resolution of the climate models, and is typically of the order of 1°x1° in longitude/latitude (i.e. a grid of around 150 km resolution).

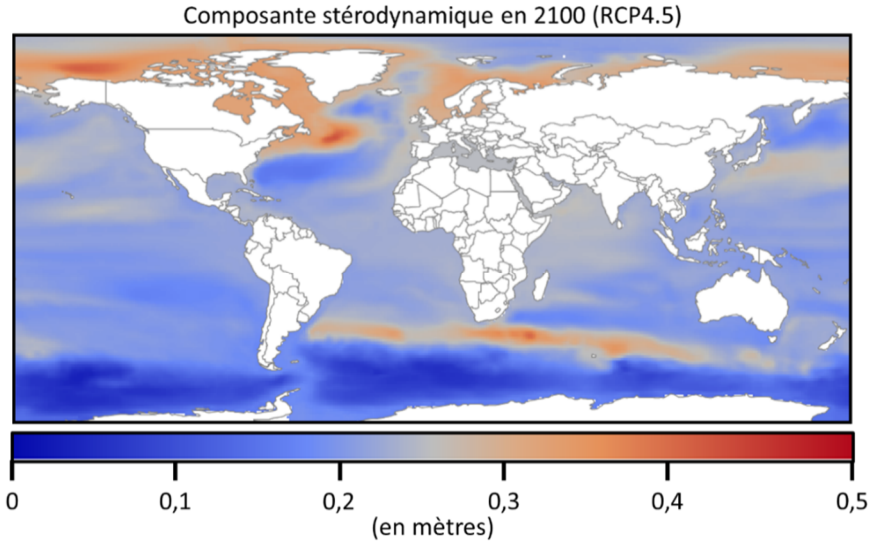


*Figure 47 : Example of the average sterodynamic component (in m) simulated by the CMIP5 models ensemble in 2100 (relative to the 1986-2005 reference period) according to the RCP4.5 climate scenario. This map is produced with the climate service https://sealevelrise.brgm.fr. The spatial resolution is 1° x 1° longitude x latitude.*

#### *3.5.3.1.2 The barystatic (mass) component ($\Delta R_{barystatic-GRD}$)*

In their current design, climate models do not include glaciers and ice-sheets module to estimate the melting of land glaciers or ice caps in response to climate change. Instead, cryosphere

modelling groups climate model outputs (typically temperature and precipitation) as boundary conditions for their glaciers and ice-sheets models. As the spatial resolution of global climate models is too coarse to represent meteorological processes in the ice caps, temperature and precipitation projections are generally refined locally using dynamical downscaling (i.e. from high-resolution regional climate models) and/or statistical downscaling methods.

The results from glacier and ice-sheet models allows estimating changes in surface mass balance, localized by region and translated into global sea-level equivalents. To obtain the regionalization of the sea-level change associated with these regionalized melts, it is necessary to take into account changes in gravity and the Earth's rotation (also known as GRD effects), which are deduced from the resolution of the sea-level equation (see, for example, Spada et al., 2019). The sum of the contributions to relative sea level of the mass losses of all terrestrial ice regions *i* is then expressed as follows:

$$\Delta \boldsymbol{R}_{\boldsymbol{barystatic-GRD}} = \sum_{\boldsymbol{i}} \boldsymbol{\delta M_i \phi_i} \text{ (Eq. 2)}$$

where $\boldsymbol{\delta M_i}$ is the global sea-level equivalent associated with mass loss of region *i* and $\boldsymbol{\phi_i}$ is the corresponding spatial fingerprint of GRD effects with mass loss of region *i.*

Figure 48 shows an example of spatial fingerprints associated with the mass balance change of the Greenland Ice Sheet (GrIS) and major continental glaciers. It is clear that the rise in sea level resulting from these localized ice melts is not uniformly distributed around the globe. A drop in sea level (negative values) is observed within a radius of around 2,000 km around the source regions, followed by a gradual rise as one moves away from them.

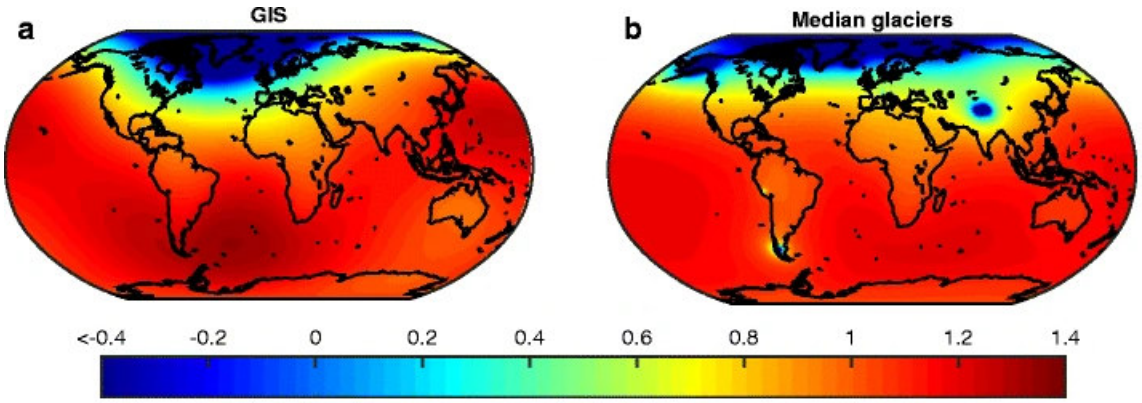


*Figure 48 : Spatial fingerprint of relative sea level associated with mass balances of (a) the Greenland ice sheet and (b) continental glaciers. Values are unitless coefficients corresponding to the ratio between local and global elevation. From Kopp et al. (2015).*

### *3.5.3.1.3 Vertical land motions ($\Delta VLM$)*

The last term in equation 1 corresponds to the contribution of local vertical land motions, which are measured locally, either by GPS or other techniques. As changes in relative sea level due to contemporary mass transfer and isostatic adjustment are already included in the $\Delta \boldsymbol{R}_{\boldsymbol{barystatic-GRD}}$ term, the local solid-earth deformation signal must be subtracted from the estimates of local vertical land motions in order not to double-count their contribution. These two terms are also estimated from spatial fingerprints derived from the resolution of the sea-level equation (Frederikse et al., 2019). It should be noted, however, that deformations of the solid Earth due to contemporary mass transfers and glacial isostatic adjustment are modest for the islands of Mauritius and Rodrigues. All the vertical land motions measured in these regions are therefore caused by local processes.

#### 3.5.3.2 Data

The projections are based on the results of models and data published by the IPCC in the SROCC report (Oppenheimer et al., 2019). Uncertainties are also taken into account using the SROCC method. However, our approach slightly deviates from the initial SROCC dataset. We recall that the simulation results used for historical reconstructions (see §2.5.2) and projections are consistent. The most significant elements of the data description are detailed below.

##### *3.5.3.2.1 The contribution of land and groundwater, Greenland icesheet, and continental glaciers to sea-level changes.*

The sea-level projections from the IPCC SROCC special report (Oppenheimer et al., 2019) were developed based on the results of climate model simulations from the CMIP5 exercise and expert judgements based on the most exhaustive recent scientific literature available. Due to the absence of a new climate model intercomparison exercise (CMIP) between AR5 (2013) and SROCC (2019), the additional studies of projections of the various sea-level components were found to be consistent with the initial AR5 (2013) projections. The synthesis work carried out by the SROCC has thus led to future estimates (including uncertainties) of glacier, Arctic ice cap and groundwater contributions identical to the AR5. These projections, regionalized using the spatial fingerprints calculated by Slangen et al (2014), are available for the three RCP scenarios and the whole of the 21st century via the ICDC server in Hamburg (https://www.cen.uni-hamburg.de/icdc/data/ocean/ar5-slr.html).

##### *3.5.3.2.2 The sterodynamic component*

In AR5 and SROCC, the projections of the sterodynamic component (see also §3.1.2.1) and the estimation of related uncertainties result from the ensemble average of 21 CMIP5 models for the RCP4.5 and RCP8.5 climate scenarios. The work of Le Cozannet et al. (2019) has shown that 2 models (MIROC-ESM and MIROC-ESM-CHEM) project a thermal expansion that is abnormally high compared to the remaining models of the ensemble (and unrealistic). MIROC-ESM and MIROC-ESM-CHEM are therefore excluded from our model selection. As a consequence, this modification of the original IPCC model sample results in sterodynamic component projections that become normally distributed around the mean and the estimate of the mean sea-level rise by 2100 is reduced by ~2 cm compared to the SROCC estimate.

##### *3.5.3.2.3 The contribution of Antarctica*

Since the release of AR5 in 2013, the Antarctic contribution to sea level has been highly debated. Studies (DeConto and Pollard, 2016; Bamber et al., 2019) have alerted to the possibility of an Antarctic ice sheet collapse that could significantly worsen its contribution to sea-level rise from the mid-21st century and beyond. This hypothesis is based on the possibility of MISI (Marine Ice Sheet Instability) and MICI (Marine Ice Cliff Instability) mechanical instabilities, which could explain West Antarctic collapses during the last interglacial period (Vaughan, 2008). MISI is a self-sustaining retreat of the grounding line (where continental ice begins to float on the ocean) in areas where bedrock is sinking inland. Studies based on satellite observations and modelling results (Joughin et al., 2014; Rignot et al., 2014) suggest that MISI instability may be already happening because of the warm waters of the deep circumpolar circulation. The MICI theory proposes a self-sustained retreat of the ice front in areas where it is 100 m or more above the ocean surface. This requires the total disappearance of the floating ice shelf beforehand. MICI is still debated, however, as it has not been observed in the modern era, and it is not yet clear whether this mechanism is really needed to reproduce sea level variations deduced from paleoclimate records (Edwards et al., 2019).

The SROCC projections have revised the Antarctic component upwards for the RCP8.5 scenario compared with AR5. This updated estimate, which combines the Levermann et al. (2014), Golledge et al. (2015 & 2019), Ritz et al. (2015) and Bulthuis et al. (2019) studies, leads to an

Antarctic contribution to sea-level rise in 2100 increased by almost 10 cm compared with AR5 for the RCP8.5 scenario.

#### *3.5.3.2.4 Subsidence*

The analysis of tide gauge, altimeter and GPS data revealed possible subsidence contexts, identified in particular in Rodrigues (§3.5.2.2.1). The possibility of a subsidence scenario of the order of 2mm/year is therefore considered.

### 3.5.3.3 Design of a "*high-end*" scenario

In addition to the IPCC RCP2.6, 4.5 and 8.5 scenarios, we have defined a so-called "high-end" scenario. This type of scenario has been conceptualized in decision-making contexts where tolerance to uncertainty is low (e.g. for the design of a coastal nuclear power plant; Stammer et al., 2019), and the 2021 IPCC report reiterates that this type of scenario cannot be ruled out in the current state of knowledge (IPCC, 2021). To design this scenario, we have followed the approach of van de Wal et al. (2022), which we have regionalized, considering a high warming scenario (+5°C in 2100) and which is consistent with the RCP8.5 scenario. Their overall estimate leads to a global sea-level rise of 1.6 meters by 2100 with respect to the reference period (1986-2005).

Among the critical processes that could lead to a runaway contribution from glacial components in the 21st century, estimates by van de Wal et al. (2022) include:

- for Greenland, strong positive feedback through a reduction in albedo and correction of underestimates of the effect of atmospheric circulation in climate models (Delhasse et al., 2020),

- for Antarctica, all the processes leading to rapid destabilization and collapse of the ice-sheet. These include accelerated surface and basal melting, hydro-fracturing and ice calving.

Source data and details by cryospheric component for the definition of the high-end scenario are given in Table 5. For the groundwater component, we use the values given by van de Wal et al. (2022). For the sterodynamic component, we use the method of Thiéblemont et al. (2019), which involves considering the CMIP5 climate model with the highest thermal expansion according to the RCP8.5 scenario.

*Table 5 : Data sources and estimates for the Glaciers, Greenland and Antarctica components in 2050 and 2100 use to design the high-end scenario.*

*Contributions are expressed in sea-level equivalent (in m)*

| Component | References | 2050 | 2100 |
|---|---|---|---|
| ***Glaciers*** | Marzeion et al., (2020) | 0.08 | 0.27 |
| ***Greenland*** | Delhasse et al. (2020) et Goelzer et al. (2020) | 0.06 | 0.29 |
| ***Antarctica*** | Levermann et al. (2020) 66% en 2050 & Levermann et al. (2020), Bulthuis et al. (2019) & Golledge et al. (2019) en 2100 | 0.10 | 0.59 |

### 3.5.3.4 Results

#### *3.5.3.4.1 Mauritius*

All projections for Mauritius indicate a rise in relative sea level, which increases with increasing climate warming (Figure 49). A median rise of almost 50 cm for the RCP2.6 scenario is projected by 2100, while a median rise of more than 85 cm is obtained for the RCP8.5 scenario (). However, uncertainties are substantial, and a sea-level rise of more than 1.2 m in 2100 cannot be ruled out. For the "High-End" scenario, a sea-level rise of over 1.8 m is projected for 2100. Although the

probability of such a rise is very low, it cannot be ruled out in case of a strong warming and an ice-sheets collapse. It should be noted that sea-level projections for 2050 are not very sensitive to the climate change scenario.

The historical reconstruction and the projections from early 21st century (i.e. before 2020) are compared with tide gauge observations over the overlapping period. As discussed in the 3.5.2, the observed global trend is relatively well reproduced by the models, but decadal variations, notably the sharp rise between 2000 and 2010, are not reproduced by the models (see Phase 1 report for related discussion). As a result, high relative sea levels around 2010 are underestimated by the models when we consider the uncertainty range of the projections and reconstructions. An additional uncertainty of approximately ten centimetres could therefore be added to compensate for this underestimation of the models' internal variability representation (note that this additional uncertainty is not quantified in Table 6).

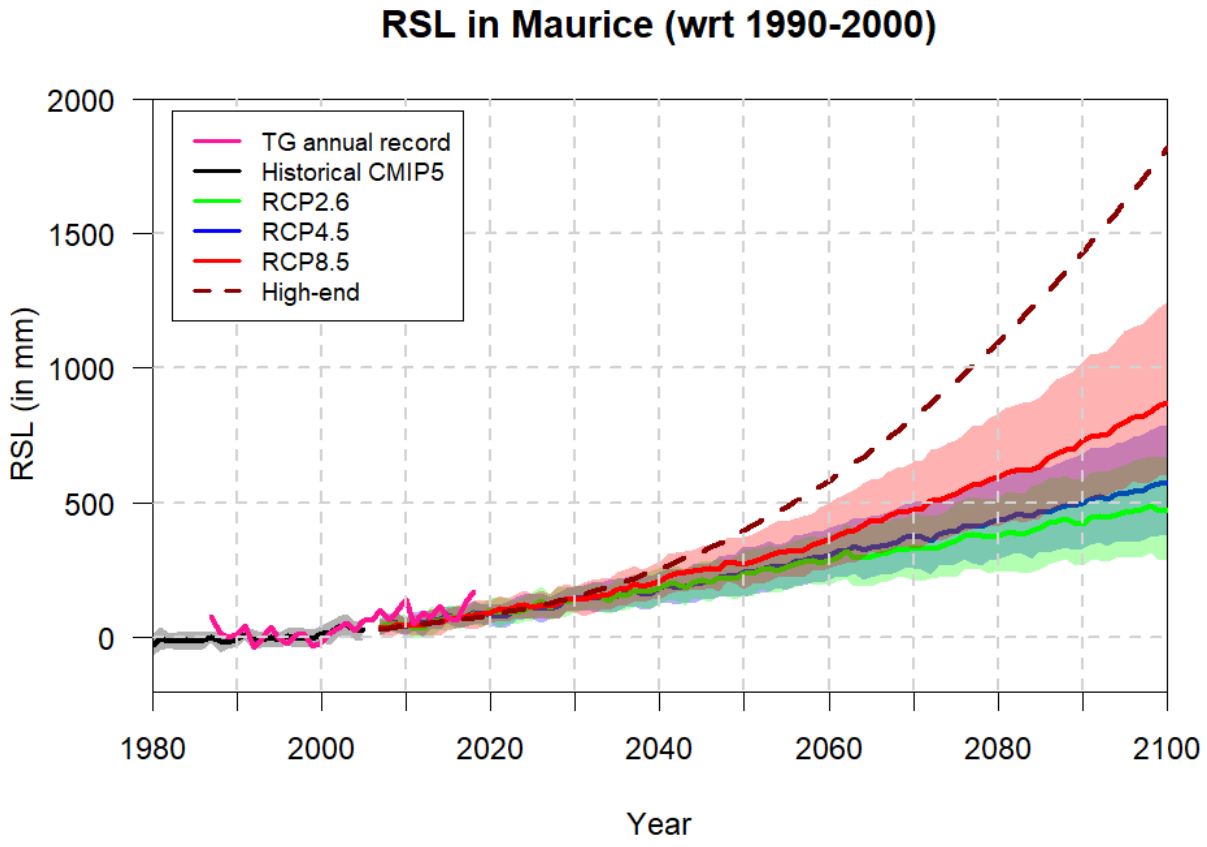


*Figure 49 : Results of sea-level projections for Mauritius relative to the reference period (1990-2000) for historical reconstruction (black), RCPs 2.6 (green), 4.5 (blue), 8.5 (red) and the high-end scenario (dark red dash). The envelope indicates the likely range (66%-100% probability in IPCC terminology). The pink curve shows the annual average of tide gauge observations.*

*Table 6: Values of relative sea level projections corresponding to Figure 49 for Mauritius in 2050 and 2100 with respect to the reference period. The median is shown in bold and the likely range is in brackets.*

| | **2050** | **2100** |
|---|---|---|
| **RCP2.6** | 0.24 *(0.16-0.33)* | 0.48 *(0.29-0.67)* |
| **RCP4.5** | 0.24 *(0.15-0.34)* | 0.57 *(0.38-0.79)* |
| **RCP8.5** | 0.27 *(0.18-0.37)* | 0.87 *(0.61-1.24)* |
| **High-end** | 0.40 | 1.82 |

### *3.5.3.4.2 Rodrigues*

Without considering land subsidence, relative sea-level projections for Rodrigues (Figure 50, Table 7) are very close to those of Mauritius. On the other hand, the agreement of model results with local tide gauge observations is poor: models underestimate sea-level rise values relative to local tide gauge measurements over the period 1986-2017. This underestimation is particularly noticeable after 2010.

This underestimation could be linked to Rodrigues Island subsidence. We have therefore reiterated the projections but we added a land subsiding velocity of 2 mm/year. Such a scenario results in an additional 20 cm rise in relative sea level by 2100 (Table 7). By including subsidence (Figure 51), we can see that the overall trend over the observed period is in better agreement between tide gauge data and modelling results. Including such a scenario in long-term projections should be considered with caution, however, as subsidence observations in Rodrigues are local (in line with the tide gauge) and based on a quite short period of observations. A linear extrapolation of such a trend over 100 years is therefore a very strong assumption.

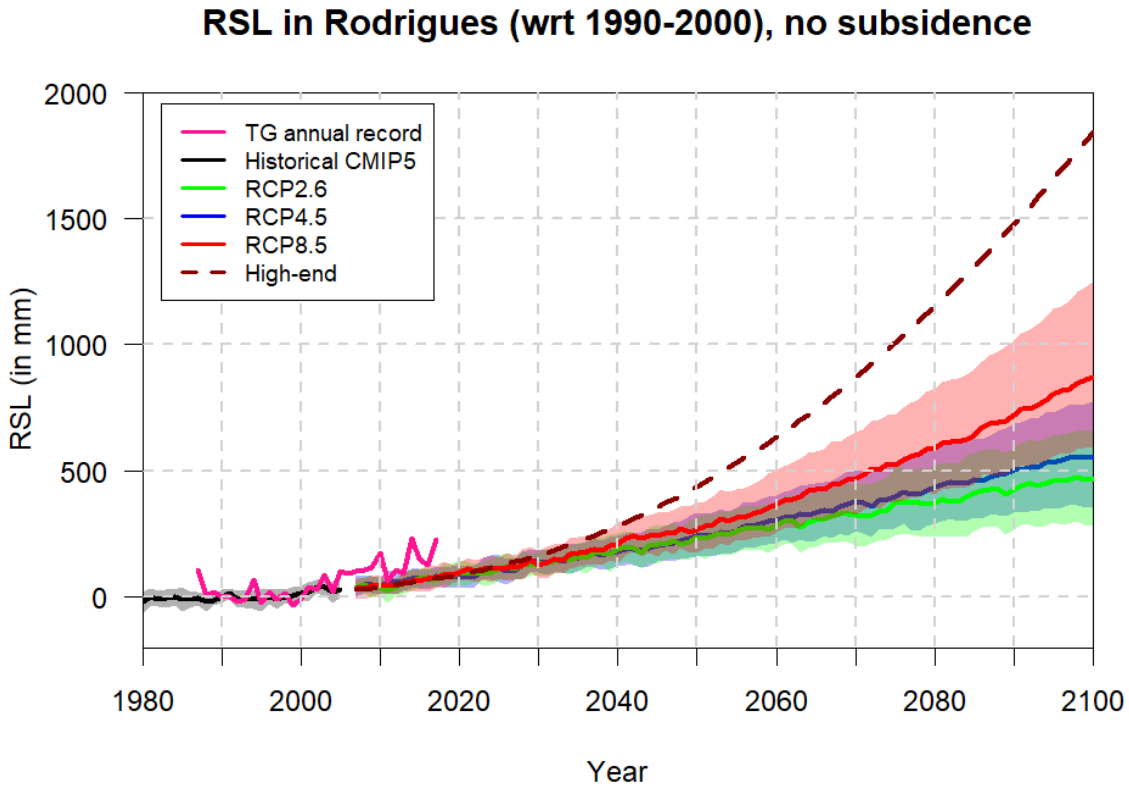


*Figure 50 : Results of sea-level projections for Rodrigues relative to the reference period (1990-2000) for historical reconstruction (black), RCPs 2.6 (green), 4.5 (blue), 8.5 (red) and the high-end scenario (dark red dash). The envelope indicates the likely range (66%-100% probability in IPCC terminology). The pink curve shows the annual average of tide gauge observations.*

*Table 7 : Values of relative sea level projections corresponding to Figure 50 for Rodrigues in 2050 and 2100 with respect to the reference period. The median is shown in bold and the likely range is in brackets.*

| | **2050** | **2100** |
|---|---|---|
| **RCP2.6** | 0.24 *(0.16-0.31)* | 0.47 *(0.28-0.66)* |
| **RCP4.5** | 0.24 *(0.16-0.33)* | 0.56 *(0.36-0.77)* |
| **RCP8.5** | 0.26 *(0.17-0.37)* | 0.87 *(0.60-1.25)* |
| **High-end** | 0.44 | 1.84 |
| **VLM (subsidence 2mm/yr)** | +0.11 | +0.21 |

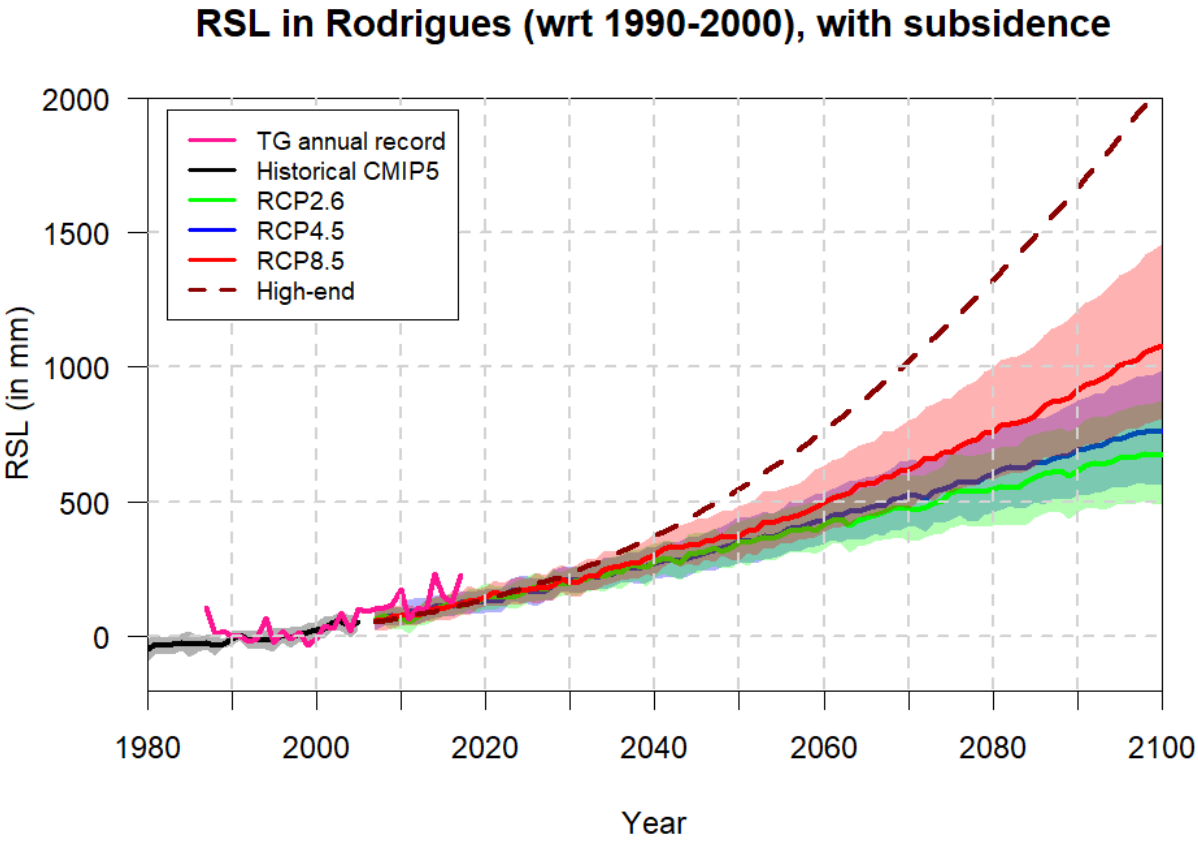


*Figure 51 : As Figure 50 but considering an additional land subsidence of 2 mm/year*

## 3.6 SOUTHERN SWELLS

Assessing and mapping of coastal flooding today and in the future requires a thorough understanding and quantification of environmental conditions and forcings leading to flooding. In this context, a dedicated study has been carried out to assess how austral swells affect Mauritius and Rodrigues and how they could be influenced by climate change. This work covers both the current period and the future, particularly focusing on the years 2050 and 2100, where coastal flooding is assessed (Appendix 2).

The islands of Mauritius and Rodrigues, located 600 km apart, are exposed to three main types of swells: Trade Wind swells, Cyclonic swells, and Southern swells.

The trade wind swells, which are present throughout the year in the south-west Indian Ocean basin, come predominantly from the south-east. They generally have a significant wave height (Hs) of less than 2 m and periods of between 5 and 10 s on the eastern coasts (Pedreros *et al.,* 2009). During winter in the southern hemisphere, the trade wind swells become stronger, reaching heights of around 5 m (Doorga *et al,* 2017).

Cyclone swells are highly energetic episodes that concentrate over a few days a year (48 to 72 hours), mainly between November and March. Depending on the trajectory of the cyclones, these swells generally impact the northern shores of the islands. They can reach maximum heights of around 10 metres and Hs of between 5 and 7 m.

Southern swells, the ones we focus on in the rest of this section, have relatively long periods of between 12 s and 20 s (Doorga et al., 2018), and average Hs[5] of around 4 m. They can reach up to 15 m Hs in their generation zone, with little energy loss along the way, and are generated by winter lows in the temperate zones of the Southern Hemisphere (Samiksha et al., 2012). They travel long distances, since they form in a zone 3,000 km from the coasts we are studying (Pedreros, et al. 2009). Furthermore, these swells are particularly erosive and can cause coastal flooding (Cazes-Duvat and Paskoff, 2004).

It should be noted that the presence of Réunion Island to the south-west of Mauritius creates a shadow zone that reduces the energy potential of the waves along the coast of Mauritius. Rodrigues, which is further away and less influenced by the nearest islands, is potentially more exposed to different types of swells. However, cyclone trajectories have a statistically less frequent impact on Rodrigues. The eastern and southern coasts are subject to trade winds and southern swells.

Kamranzad *et al*. (2022) show that the dominant wave direction is from the south-south-east, and the presence of the islands reduces wave power on the northern flank due to the shelter effect. The wave power is reduced by around 60% on the northern flank compared with the southern flank of the islands. The results also indicate that the spatial change in wave power depends rather on the swell climate than on the waves generated locally by the wind. The seasonality of the wave climate shows that wave power is highest during the southern winter and lowest during the southern spring on the northern flanks of the islands. The monthly variability of resources was also studied, revealing almost stable conditions for the wave period.

In order to study the wave climate change in the area, we use *in-situ* wave measurements, satellite altimetry measurements and re-analysed wave hindcast databases and climate model-driven wind wave projections (see appendix 2 of this report BRGM/RC-73987-FR).

Overall, the literature review and the analysis performed on a selection of CMIP6-driven wind-wave projections models revealed only modest changes in future wave climate, event under a strong climate change scenario (i.e. SSP5-8.5 or RCP8.5). A detailed analysis of the southern

[5] Hs: significant height

swell characteristics (Hs and Tp, average and extremes) similarly suggest small changes that are mostly not significant statistically and not robust among models in the vicinity of both Mauritius and Rodrigues Islands.

The details the analysis of southern swells around Mauritius and Rodrigues for the three dates are presented in the second appendix of the BRGM report (BRGM/RC-73987-FR).

# 4. ASSESSMENT AND MAPPING OF THE SHORELINE RETREAT AND COASTAL FLOODING HAZARDS IN THE MAURITIUS AND RODRIGUES ISLANDS

## 4.1 INTRODUCTION

### 4.1.1 Coastal erosion and coastal retreat hazard

#### 4.1.1.1 Concepts

The coastline is a concept which makes it possible to delimit what is considered to be part of the marine domain from what is part of the continental domain. The continental zone is considered to be the area that will remain emerged during normal periods, even during high tides with the highest coefficients. The marine area will either be permanently submerged (even during the lowest astronomical tides) or submerged more or less frequently depending on tidal conditions (coefficient, time of tide). The foreshore will therefore be considered to be part of the marine environment even though it is periodically submerged. Depending on the altimeter position on the foreshore, the immersion phases will be more or less long, known as hydroperiodicity. The continental shelf may be temporarily flooded by the sea during storms, which lead to a surge (a temporary rise in sea level; for example during the passage of cyclone Freddy in 2023) and generate waves (which may also contribute to temporary submersion, for example during the passage of cyclone Bellal 2024 in Port-Louis), during episodes of strong southerly swells or during tsunamis (for example in 2004 at Port Mathurin). These aspects (except tsunamis) are dealt with in the chapter dealing with the risk of coastal flooding (cf. 4.1.2).

The coastline can be represented by various indicators (upper beach, lower beach, limit of vegetation, top of cliff, limit of structure, etc.) depending on the nature and morphology of the coastline, but also on the type of issue in question (natural risks, navigation, urban planning and development, etc.).

With regard to coastal risks and the coastline hazard, the objective is to determine whether an area or issues are or will be exposed to a retreat of the coastline, which would lead to a loss of land use (loss of agricultural or urban land, natural areas of interest, etc.) and damage or even destruction of built assets (roads, bridges, buildings, industrial structures, etc.). The most relevant coastline indicator for this type of problem is that of the limit of the upper beach or of the permanent vegetation. This indicator does not exist on the scale of the islands of Mauritius and Rodrigues, so it was necessary to create one using the information available to us (orthophotographs).

#### 4.1.1.2 Coastline mobility factor

The mobility of the coastline (apart from human intervention such as the creation of embankments, reclamation, etc.) is linked to two factors: the sea level and the processes of erosion and accretion of the coastline.

Variations in relative sea level (chapter 3.5) will, depending on the topography of the coastline, have a direct impact on the position of the coastline. In the case of a rise in sea level, the lower and flatter the backshore topography, the more extensive and rapid the migration of the coastline towards the land. Conversely, if the back-coast has a pronounced, sloping topography, coastline

migration will be slower (Figure 52). This "geometric" effect makes it possible to assess the future position of the coastline, based on an assumption of the value of the rise in sea level for a given timeframe. However, during the time between the current period and the target date, the coastline will potentially undergo morphological changes as a result of erosion and accretion. In fact, depending on the nature of the coast (lithology), its morphology, its context (sediment balance and input, presence of a reef, etc.), its location and its exposure to meteorological and marine factors (waves, swells, currents, etc.), coasts undergo erosion and accretion, which in turn also change the position of the coastline. Thus, even in the absence of variations in sea level, depending on the site, the coastline may retreat or advance.

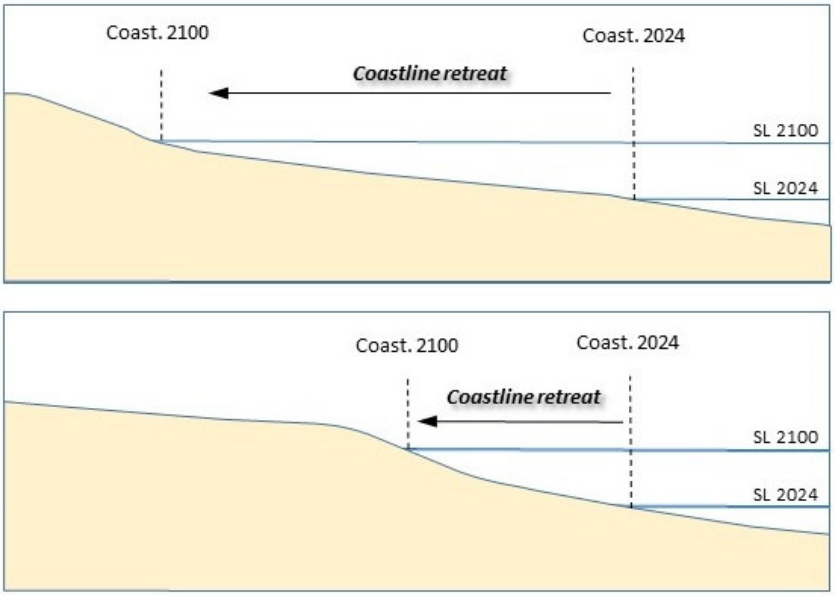


*Figure 52 : Impact of morphology and topography of the backshore on the coastal retreat linked to the sea level rise (SL: sea level; Coast.: coastline)*

In our case, these processes (erosion/sedimentation and variations in relative sea level) occur at the same time. These two phenomena are not independent in the sense that a higher sea level will induce, for example, higher wave action on the cross-shore morphological profile and therefore have an effect on the intensity of erosion and coastline migration. However, given the complexity of the phenomena involved and the absence of suitable and operational modelling tools, the effects of these two phenomena will be treated independently and their respective effects added together.

The choice of climate scenarios used to assess future hazards makes it possible to take into account the uncertainties about the future development of the application by states of GHG reduction protocols. This choice determines the climatic parameters and induced effects (sea level, wind regimes, wave climates, cyclogenesis, etc.) that will influence the evolution of the coastline. Our choice is based on the analyses presented in chapter 3.2. Our two scenarios are based on a moderate to optimistic climate trajectory (RCP 4.5) and a pessimistic trajectory (RCP 8.5, chapter 3.2. These scenarios will enable us to generate maps of the coastline retreat hazard for three time periods: the present, 2050 and 2100. By mapping the position of the coastline for each timeframe and for the two scenarios, we can generate envelopes of uncertainty for the position of the coastline in the future. These envelopes will form the coastline retreat hazard map.

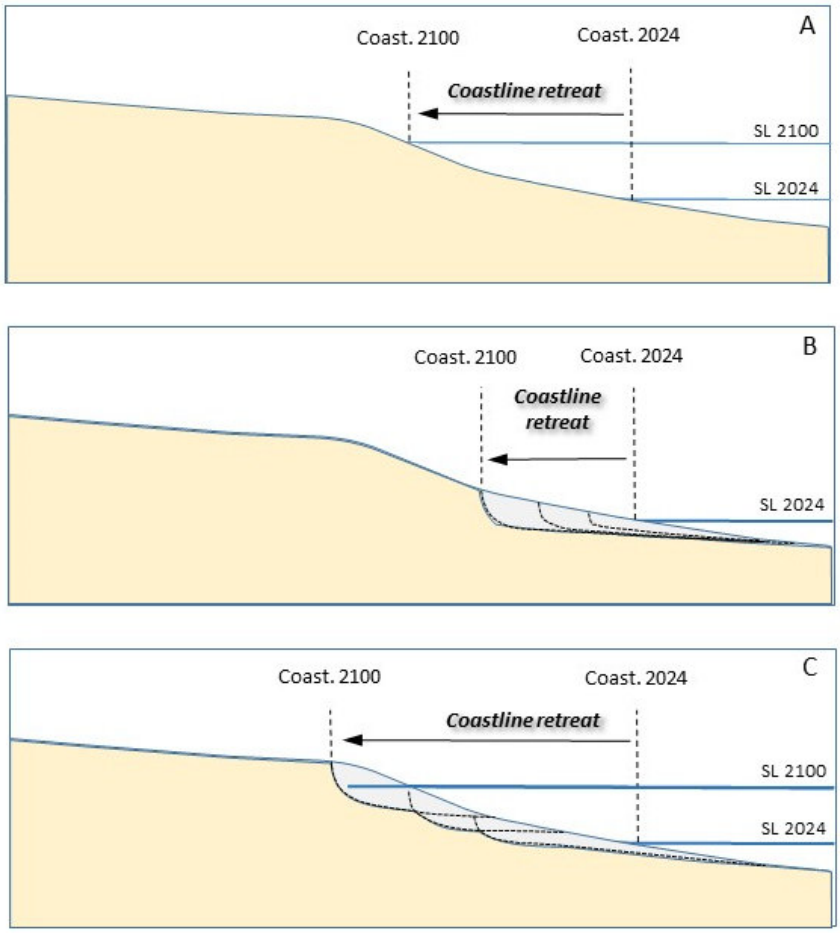


*Figure 53 : Effect on the coastal retreat of A) sea level rise, B) coastal erosion, C) both (SL: sea level, Coast: coastline)*

#### 4.1.1.3 Definition of the coastal retreat hazard

The coastline retreat hazard is a sector of coastline exposed to a retreat of the coastline in a given timeframe and according to assumed hypotheses (climate scenarios).

### 4.1.2 Coastal flooding

The islands of the Republic of Mauritius are exposed to coastal flooding, particularly as a result of the passage of cyclones close to the Mascarene archipelago, but also due to specific conditions that may occur without cyclones (cf. 3.6).

#### 4.1.2.1 Physical processes causing coastal flooding

"Coastal *flooding is the temporary inundation of coastal areas by the sea during unfavourable meteorological and oceanic conditions (low atmospheric pressure and strong inflow winds acting, for tidal seas, during high tide); it can last from a few hours to a few days*" (*Guide méthodologique PPRL, MEDDE*, mai 2014). Flooding is most often associated with temporary rises in sea level during storms or cyclones, or even tsunamis.

Apart from tsunamis, marine surges are controlled by two main processes (Figure 54):

- **atmospheric surge**: the passage of a major low-pressure system (cyclone, storm) is characterised by variations in sea level based on two mechanisms:

  - the drop in atmospheric pressure causes the water level to rise. This is the inverse barometer phenomenon: a decrease of one hPa is equivalent to a rise of one centimetre in the water level (values for a theoretical situation of an infinite water level and uniform atmospheric pressure);
  - To this must be added the effect of the wind, which, depending on its intensity and direction, is likely to cause accumulations of water on the coastal strip.

The rise in the water level caused by the drop in pressure and the action of the wind corresponds to the atmospheric (or meteorological) surge. The combination of the tide and this atmospheric surge generates the "resting" sea level (Figure 23). For convenience, this level is hereafter referred to as SWL ("still water level").

- **wave setup**: as it approaches the coast, the waves generated offshore break and transfer their energy to the water column, some of which causes a rise in the mean water level (wave setup) of up to several tens of centimetres.

The **mean water level** (or static level) during a storm or cyclone is the result of the contribution of the atmospheric surge, the wave surge and the tide (Figure 54).

Finally, the instantaneous water level will depend on the swash, i.e. the ebb and flow of waves on the foreshore. The maximum height reached by the sea above a reference level is called the runup.

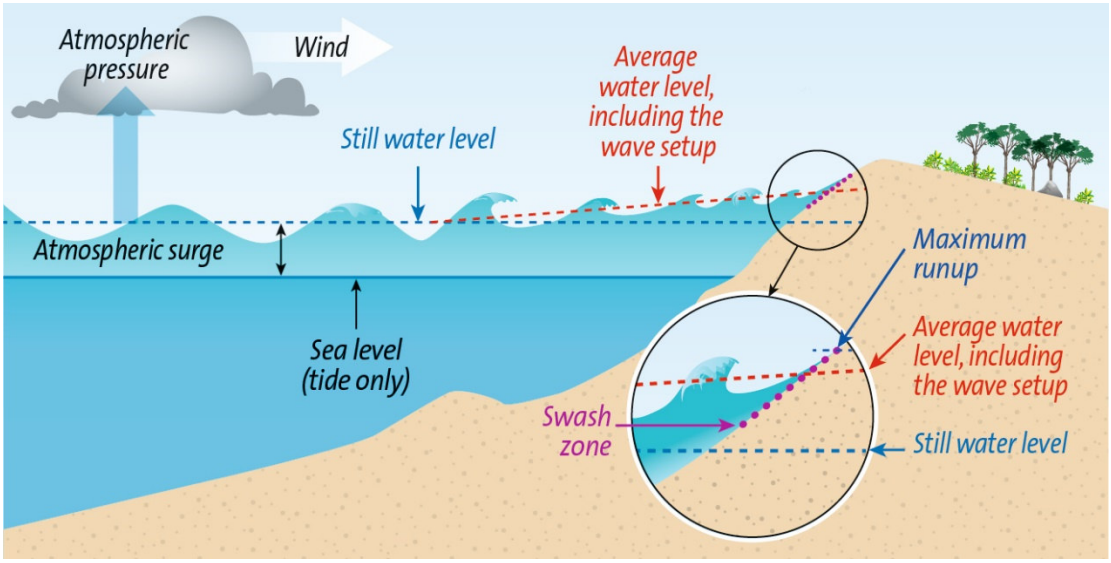


*Figure 54 : Diagram of the different contributions to the water level during a storm (surges) as far as the shore (source BRGM)*

### 4.1.2.2 Coastal flooding types

Coastal flooding can take three different forms:

- **wave overtopping**, which corresponds to the passage of waves over coastal defences (natural or artificial); the resulting accumulation of water can be significant, depending on the extent of overtopping, its duration and the length of the coastline concerned; overtopping is essentially determined by the position of the water level (static level) in

relation to the maximum elevation of the natural terrain or protective structures, and by the local characteristics of the waves (heights and periods);

- **Overflowing**, which corresponds to a rise in the static water level above the maximum elevation of the natural terrain or protective structures; this leads to the direct discharge of large quantities of water on land; the volumes of water involved depend on the difference between the water level and the maximum elevation of the natural terrain or protective structures, the duration of the overtopping and the speed of the flow;

- **the failure** of protective structures, which can be caused by repeated wave action and/or overtopping. Protective structures may then be damaged progressively or suddenly, and breaches or generalised failure may occur, causing a transition to an overflow regime. The discharge of water behind the structures is also likely to damage them further.

A flooding event may result from the succession of these different processes (Figure 55), or even from their simultaneous occurrence in different places. During storms, there is generally a gradual rise in the static level and an increase in wave intensity. Above a certain level of intensity, waves may break through in packets, but the associated flooding generally remains limited (time 1). If the static level continues to rise and exceeds the maximum elevation of the coastal defences, the flooding becomes overflowing (time 2). When the static level decreases as a result of the tide and/or the fall in the surcharge, depending on the configuration, there may be a partial "emptying" of the water accumulated on land towards the sea or new crossings until the sea conditions diminish in intensity. In the event of the failure of a protective structure, there may be flooding by overtopping even though the static level does not exceed the maximum elevation of the structure before failure (time 3).

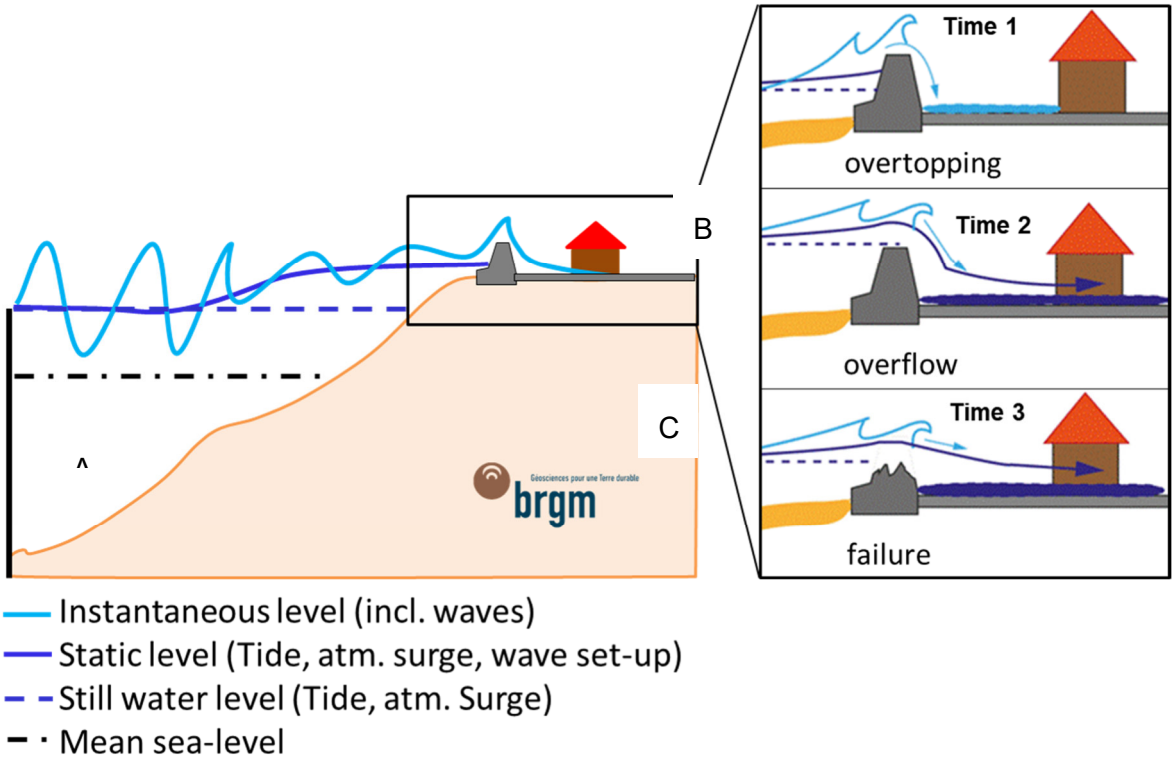


*Figure 55 : Example of possible chronologies in the event of marine submersion (overtopping / overflow / failure, ©BRGM)*

The numerical simulation of flooding water heights and currents velocities during an extreme event, allows to provide the coastal flooding hazard map of an area. The hazard is classified in four levels by means of the matrix shown in Figure 56. Remark that the results are obtained crossing simultaneous values of H and V and not with the maximum values during the whole simulation.

| | | Speed of currents (m/s) | | |
|---|---|---|---|---|
| | | V <= 0.2 | 0.2 < V <= 0.5 | V >= 0.5 |
| Water Heights (m) | H <= 0.5 | Low | Medium | High |
| | 0.5 < H <= 1 | Medium | Medium | High |
| | 1 < H <= 2 | High | High | Very High |
| | H > 2 | Very High | Very High | Very High |

*Figure 56 : Matrix for determining coastal flooding hazard.*

## 4.2 THE WHOLE COAST OF MAURITIUS AND RODRIGUES (1:20,000 SCALE)

### 4.2.1 Methods

#### 4.2.1.1 Method for assessment of coastal erosion and coastal retreat hazard at 1:20,000

##### *4.2.1.1.1 Introduction*

The aim of this study is to estimate the **possible retreat** of the coastline for the current period and for two time periods. The next step will be to map the risk of coastline retreat for the current period (2025), in 2050 and 2100. **Due to the complexity of the hydro-sedimentary processes involved, the results are not definitive predictions of future coastline positions. The results and maps are estimates of areas that could be affected by shoreline retreat in the medium and long term**. This study on the estimation of coastal retreat hazard zones is essentially based on existing and available data, supplied by the Republic of Mauritius.

##### *4.2.1.1.2 Method*

*4.2.1.1.2.1 Segmentation of the territory into homogeneous coastal zones (HCZ)*

The first phase of the work is a segmentation of the territory into homogeneous coastal zones. A homogeneous coastal zone is a part of the coastline whose coastal erosion phenomena are considered to be similar and of the same intensity. Two types of data are used to establish the segmentation of the coastline of the Republic of Mauritius:

- the work of JICA (2015) carried out on 14 sites in Mauritius, each site is segmented into a coastal sub-cell, equivalent to a homogeneous coastal zone,
- Data of « Coastline Nature and sensitive to erosion shapefile » which segment the coastline according to its rocky or sedimentary nature and the presence or absence of lagoons and coral reefs (report BRGM/RC-72793).

Figure 57 illustrates the mapping of the homogeneous coastal zones of Flic-en-Flac (FF). The zones based on the JICA segmentation are referred to as FF_SC11-1 (SubCell n°11-1 of the JICA study, 2015). In addition, the homogeneous zones determined from Erosion Index data (BRGM, 2023) are referred to as FF_CHZ01 (homogeneous zone n°1 of Flic-en-Flac).

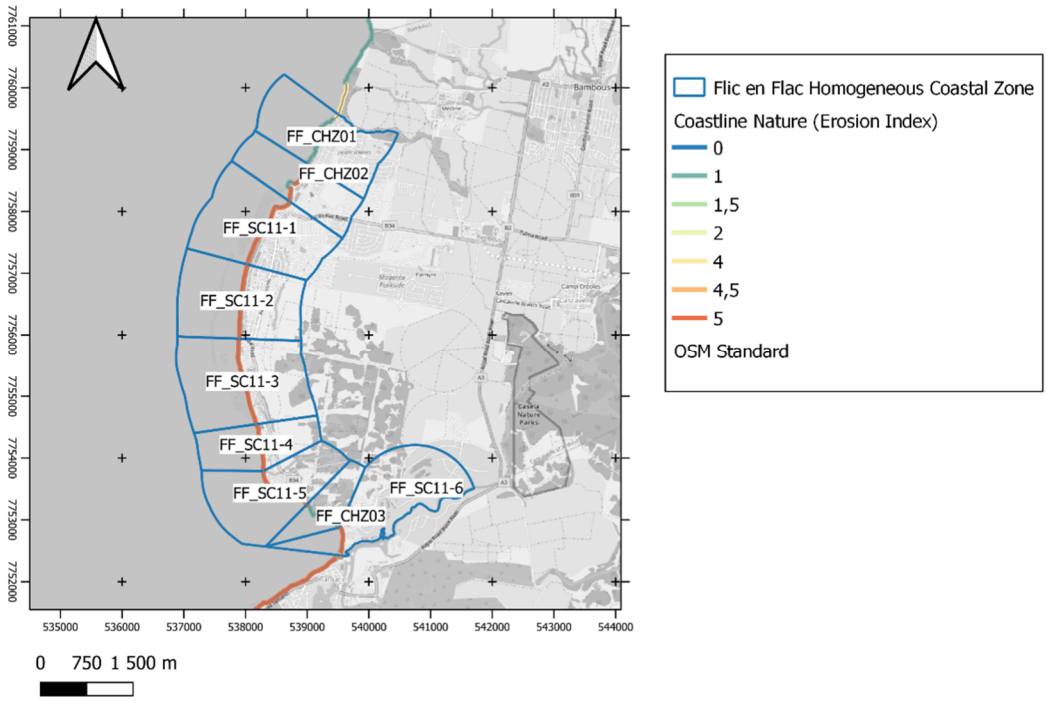


*Figure 57 : Homogeneous coastal zones of Flic-en-Flac*

#### *4.2.1.1.2.2 Analysis of sandy coastline change data*

The processes of coastline evolution have been treated by JICA (2015) on the basis of a diachronic analysis of orthophotographs, aerial photographs and georeferenced satellite images (6 sets of images between 1967, 1975, 1991, 1997-99, 2008 and 2012). This analysis is carried out by homogeneous evolution sector and provides quantified trends in the evolution of the coastline. The zones of homogeneous evolution are established at the scale of sedimentary sub-cells, delimited by inflections of the coastline associated with the presence of rocky zones, estuaries or developments. These data are the only available data on the evolution of the coastline for this study. In the absence of any other more recent or complete dataset, it was not possible to perform a critical analysis. The results of Jica's (2015) diachronic analyses form the basis of the quantified data used to assess the retreat of the Mauritian coastline.

The coastline evolution database, compiled by JICA (2015) on behalf of the Republic of Mauritius, is used to calculate several indicators. The aforementioned indicators will be employed to ascertain the extent of the hazard zones.

- Median rate of coastline change in the homogeneous zone ($Tx_{med\text{-}hz}$)

For each homogeneous zone, JICA (2015) estimated the average coastline change between the oldest georeferenced aerial image (1967) and the most recent image (2012). This rate was calculated over the longest possible period (45 years) and is defined for the purposes of this study as the median rate of coastline change in the homogeneous zone (Txmed). In the context of hazard mapping, the phenomenon of coastal accretion will not be considered, and the median rate of change will be regarded as zero.

The median rate of retreat for the homogeneous zone SC11-2 at Flic-en-Flac is -0.29 m/year, as indicated by the observed data for the coastline. In the case of homogeneous zone SC11-3 at Flic-en-Flac, the coastline demonstrates a median rate of advancement of +0.13 m/year, transformed into 0 m/year for coastline retreat projection calculations.

*Table 8 : Coastline change rates for Flic-en-Flac coastal sub-cells, according to JICA (2015)*

| | **Tx** (m/y) source : JICA (2015) | | | | |
|---|---|---|---|---|---|
| period (y) | 1967-1975 | 1975-1991 | 1991-1997 | 1997-2008 | 2008-2012 |
| | *8* | *16* | *6* | *11* | *4* |
| FF_HCZ01 | rock | | | | |
| FF_HCZ02 | no data | | | | |
| **FF_SC11-1** | 0.58 | 0.78 | -0.91 | 0.94 | -0.40 |
| **FF_SC11-2** | 0.79 | -0.73 | -1.59 | 0.26 | -0.25 |
| **FF_SC11-3** | -0.39 | 0.26 | 0.35 | 0.17 | 0.21 |
| **FF_SC11-4** | -1.33 | 0.70 | -0.34 | 0.06 | -0.15 |
| **FF_SC11-5** | -2.85 | 0.75 | 0.40 | 0.11 | -0.67 |
| FF_HCZ03 | rock | | | | |
| **FF_SC11-6** | -0.07 | 1.41 | -0.04 | 0.42 | -0.40 |

*Table 9 : Sandy coastline retreat settings for Flic-en-Flac coastal sub-cells*

| | **$Tx_{med}$** | **$Tx_{med-hz}$** | **$Tx_{hzd-hz}$** | **$Tx_{max-hz}$** |
|---|---|---|---|---|
| FF_HCZ01 | **rock** | | | |
| FF_HCZ02 | **No data** | | | |
| **FF_SC11-1** | **0.46** | 0.00 | -0.70 | -0.91 |
| **FF_SC11-2** | **-0.29** | -0.29 | -0.86 | -1.59 |
| **FF_SC11-3** | **0.13** | 0.00 | -0.39 | -0.39 |
| **FF_SC11-4** | **-0.03** | -0.03 | -0.74 | -1.33 |
| **FF_SC11-5** | **-0.22** | -0.22 | -2.12 | -2.85 |
| FF_HCZ03 | **rock** | | | |
| **FF_SC11-6** | **0.55** | 0.00 | -0.13 | -0.40 |

- Coastline retreat rate of the homogeneous zone ($Tx_{hzd-hz}$)

JICA (2015) also estimated the average change in the coastline between each georeferenced aerial image. These estimates generally show variations in evolution depending on the period. For example, for homogeneous zone SC11-2 at Flic-en-Flac, JICA (2015) estimates show that the coastline advanced by an average of +0.79 m/year between 1967 and 1975 (8 years). It retreated by -0.73 m/year between 1975 and 1991 (16 years) and by -1.59 m/year between 1991 and 1997 (6 years). It rose again by +0.26 m/year between 1997 and 2008 (11 years), then fell by -0.25 m/year between 2008 and 2012 (4 years). The coastline retreat rate for the homogeneous zone ($Tx_{hzd}$) is an average of observed retreats. For each period, each estimated retreat value is weighted by the length of observation period. For homogeneous zone SC11-2 at Flic-en-Flac, the rate of retreat is -0.86 m/year, estimated from 3 periods of observed retreat over a total period of 26 years. For homogeneous zone SC11-3, the retreat rate is -0.39 m/year, estimated on the basis of a single retreat period of 6 years.

- Maximum coastline retreat rate of the homogeneous zone ($Tx_{max-hz}$)

This indicator corresponds to the maximum coastal retreat value documented in the JICA study (2015) for a specified time frame. For example, $Tx_{max}$ reached -0.4 m/year for the period 2008-

2012 in zone SC11-6; -1.59 m/year for the period 1991-1997 in zone SC11-2 and even -0.85 m/year for the period 1967-1975 in zone SC11-5.

- Median rate of shoreline change for a coastal cell ($Tx_{med\text{-}cell}$)

Homogeneous coastal zones constitute sub-parts of larger units, designated as coastal hydrosedimentary cells. The JICA (2015) database is employed to calculate indicators of coastline change at the scale of coastal cells.

The median rate of shoreline change for the coastal cell is calculated as the mean of the median rates of change for the different homogeneous zones within the cell ($Tx_{med\text{-}hz}$). In the case of stable or accreting homogeneous zones, the $Tx_{med\text{-}hz}$ value is deemed to be zero. In the case of negative values, the weighting is determined by the length of the coastline within each homogeneous zone.

For the Flic-en-Flac coastal cell, the median rates of change for homogeneous zones SC11-2, SC11-4 and SC11-5 are -0.29 m/year, -0.03 m/year and -0.22 m/year respectively. These homogeneous zones are characterised by a coastline whose length is 1212 m, 781 m and 972 m respectively (based on the ESA coastline, 2013, with local correction by BRGM). The median rate of change in the coastline of the Flic-en-Flac coastal cell is therefore calculated as -0.09 m/year.

- Coastline retreat rate for the coastal cell ($Tx_{hzd\text{-}cell}$)

The coastline retreat rate for a given coastal cell is a weighted average of the retreat rates observed over a specified period for the various homogeneous zones within the cell. The weighting of the coastline retreat values (negative values from the JICA database, 2015) is calculated by multiplying the length of the affected coastline by the duration of the erosion period.

To illustrate, the rate of retreat of the Flic-en-Flac coastal cell, as determined from the JICA database (2015), is -0.85 meters per year. This rate of retreat is notable, particularly in relation to the high retreats estimated for homogeneous zones SC11-4 and SC11-5 between 1967 and 1975 at -1.33 m/yr and -2.85 m/yr, respectively) and between 1991 and 1997 for homogeneous zones SC11-1 and SC11-2 (at -0.91 m/yr and -1.59 m/yr, respectively).

- Evolution parameters of the sandy coastline of Rodrigues

For Rodrigues, there were no data on the evolution of the coastline before this study. Specific work has been carried out on several sensitive sectors (Report BRGM/RC-73987-FR Appendix 1) on the basis of satellite data used via Google Earth. The analysis period extends between 2005 and 2022, 5 to 7 images were studied to estimate values of the evolution of the coastline on 8 different sites (Report BRGM/RC-73987-FR Appendix 1).

As the frequency and duration of observation is different from that of Mauritius, the calculation of the analysis parameters has been adapted.

  - For Rodrigues, the parameter "Median rate of coastline change in the homogeneous zone" ($Tx_{med\text{-}hz}$) is estimated in the same way as for Mauritius.
  - The parameter "Maximum coastline retreat rate of the homogeneous zone ($Tx_{max\text{-}hz}$)" is calculated in the same way as the parameter "Coastline retreat rate of the homogeneous zone ($Tx_{hzd\text{-}hz}$)" of Mauritius.
  - The parameter "Coastline retreat rate of the homogeneous zone ($Tx_{hzd\text{-}hz}$)" corresponds to the Rodrigue "Maximum coastline retreat rate of the homogeneous zone ($Tx_{max\text{-}hz}$)", weighted by the ratio of the duration of retreat over the entire observation period.
  - The parameter "Median rate of shoreline change for a coastal cell ($Tx_{med\text{-}cell}$)" is the same of $Tx_{med\text{-}hz}$. For most of coastal cells, it is considered to be equal to zero, because the few sectors studied do not show recurrent erosion at the scale of an entire homogeneous zone or a coastal cell.

- The parameter "Coastline retreat rate for the coastal cell ($Tx_{hzd\text{-}cell}$) is set at -0.36m/y, corresponding to the median retreat value observed in the 2 sectors in medium regular retreat of Rodrigues (Petite Butte and Mourouk).

- Coastline evolution parameters for sectors with no observation data

In the absence of observed changes to the coastline, the calculation of coastline change parameters is not feasible. These parameters are delineated by experts, employing various criteria of similarity with homogeneous zones whose evolution is well-documented. The aforementioned criteria encompass the following: exposure to swell conditions, the presence and width of the lagoon, the orientation of the coast, and proximity to well-documented cells or sub-cells.

In the case of Flic-en-Flac, the sandy sector of homogeneous zone FF-HCZ02 has not been observed (Figure 57). Consequently, the evolution values for this zone are derived from expert opinion.

- Median rate of coastline change in the homogeneous zone ($Tx_{med\text{-}hz)}$ = Median rate of shoreline change for a coastal cell ($Tx_{med\text{-}cell}$), Cell 11 of JICA's study
- Coastline retreat rate of the homogeneous zone ($Tx_{hzd\text{-}hz}$) = Coastline retreat rate for the coastal cell ($Tx_{hzd\text{-}cell}$), Cell 11 of JICA's study
- Maximum coastline retreat rate of the homogeneous zone ($Tx_{max\text{-}hz}$) = $Tx_{max\text{-}hz}$ (FF_SC11-1), value of the adjacent homogeneous zone, measured in the JICA study (2015).

For entire coastal cells where no coastline evolution has been studied, the selection of homogeneous zone change values is made on a case-by-case basis by experts, according to similarity criteria and known values in neighbouring or similar coastal cells.

*4.2.1.1.2.3 Estimated impact of extreme events (Lmax)*

In accordance with the methodology employed by JICA (2015) for estimating potential coastline retreats for comparison with local « setback » (safety widths), BRGM recommends estimating an extreme event-driven coastline retreat value adapted to soft coastlines potentially subject to the effects of cyclones.

- Extreme event retreat value for sandy coast protected by a coral reef and a lagoon

In coastal areas protected by a coral reef and a lagoon, the work of Baird (2003) has enabled the development of two erosion models. These models are based on the maximum retreat data observed by MacIntire and Walker (1964) following the passage of cyclone Carol (1960). The initial model was developed for the Flic-en-Flac site. The resulting data will be used to determine the « Lmax » values for the lagoon beaches situated in the western region of Mauritius. The second model was constructed for the Bellemare site. The findings will be employed to determine the Lmax values of the lagoon beaches situated in the eastern region of Mauritius. The results of the Baird (2003) models were employed to delineate the anticipated retreats for the different study period (present - Lmax0, 2050 - Lmax25, and 2100 - Lmax75; Table 10).

*Table 10 : Instantaneous retreat values (Lmax) for present, 2050 and 2100*

| | **$Lmax_0$** | **$Lmax_{25}$** | **$Lmax_{75}$** |
|---|---|---|---|
| Lagoon, West | 8.5-11 | 11-13 | 14 |
| Lagoon, East | 3.5-5 | 5-10 | 14-20 |

- Extreme event retreat value for open sandy coast

For sandy Mauritius coasts open to the ocean, there is no dedicated model for estimating extreme retreats of the coastline. The Lmax retreat values were estimated by adapting the American 540 SF method (FEMA) to the Mauritian context. In the United States, the Federal Emergency Management Agency (FEMA) has proposed the implementation of a straightforward rule applicable to the Atlantic and Gulf of Mexico coasts.

This rule is based on the analysis of observational data series of dune retreat under effects of storms. This rule establishes the volume of dune eroded as a function of the return period event ("T" in years). For a profile perpendicular to the coastline, the dune is eroded by an area "A" (in m² or ft²) according to the following formula: $A = 8 \times T^{0.4}$.

For a centennial storm or cyclone, the erosion corresponds to 540 square feet (540 SF) and gives its name to the rule. The sedimentary dune reservoir is calculated by determining the surface area between the "centennial static water level" and the vertical at the highest point of dune (Figure 58). If the area in question exceeds 50 m² (or 540 square feet), the dune is deemed to have the capacity to withstand the storm.

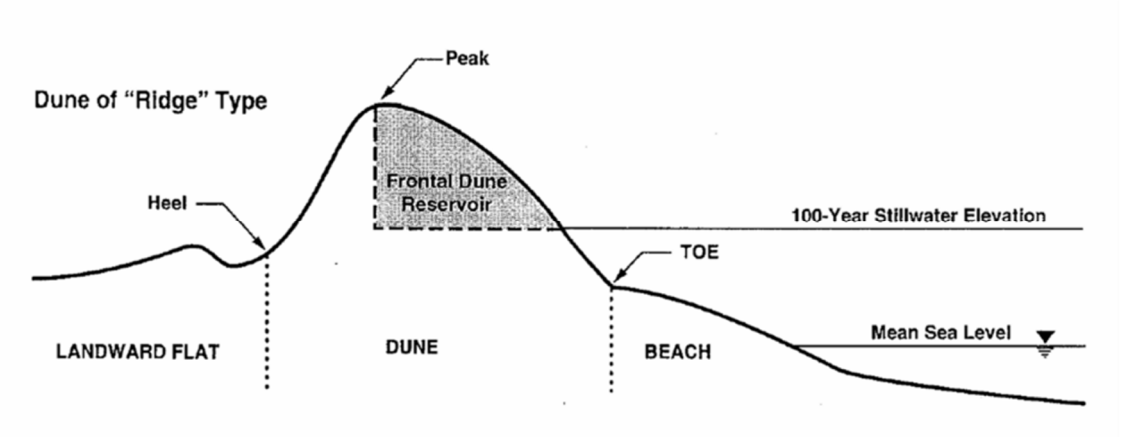


*Figure 58 : Calculation of the sedimentary dune reservoir used to assess the extreme retreat of an open sandy coastline (FEMA)*

This rule is also useful for obtaining a value for the maximum setback for an event with a return period of one hundred years, which removes a volume equal to 50 m². Subsequently, Lmax100 is derived for a specified beach profile, whereby the erodible surface is equal to 50 m².

Given the empirical nature of this rule and its adaptation to a territory in the Indian Ocean, it was necessary to ensure the consistency of the results obtained with the data available for Mauritius. As illustrated in then Table 11, the extreme event-related erosions estimated by the FEMA method are found to be higher than those modelled by Baird (2003). The differences range from +10 to +25% for the 10-year return period to +50 to 100% for the 50- to 100-year return periods. These order of magnitude estimates are consistent for the erosion of sandy beaches that are open to the ocean and do not benefit from the protection of the coral reef.

*Table 11 : Comparison of Lmax values from different sources*

| | **Erosion (A) m²/m** | Cosmos (Baird, 2003) | |
|---|---|---|---|
| **Return Period (T) years** | FEMA (1995) | Flic-en-Flac | Bellemare |
| **10** | 20.1 | 13-19 | 14-22 |
| **25** | 29.0 | 16-23 | 18-29 |
| **50** | 38.3 | 17-24 | 20-30 |
| **100** | 50.5 | 20-27 | 25.5-36 |

These erosion values associated with cyclones lead to variable retreats which depend on the sediment stock of the beach. This study considers three types of beaches:

- very low-lying sandy beaches, i.e. no more than 2m above sea level,
- low-lying sandy beaches, i.e. between 2 m and 2.5 m above sea level,
- (median) sandy beaches, where the elevation is greater than 2.5 m.

The results of the FEMA 540SF approach, adapted for the three types of beaches of Indian Ocean, allow for the definition of the setbacks for the different study timeframes (current - Lmax0, 2050 - Lmax25 and 2100 - Lmax75).

In the absence of a numerical storm erosion model implemented for Rodrigues, the FEMA method adapted for the Indian Ocean was used for Rodrigues.

*Table 12 : Instantaneous retreat values (Lmax) using FEMA 540SF approach for present, 2050 and 2100*

| | **$Lmax_0$** | **$Lmax_{25}$** | **$Lmax_{75}$** |
|---|---|---|---|
| Open Coast, very low | 10-15 | 15-20 | 25-30 |
| Open Coast, low | 8-12 | 12-20 | 20-25 |
| Open Coast, medium | 7-12 | 10-15 | 17-20 |

#### *4.2.1.1.2.4 Estimating the effect of climate change*

The estimation of the impact of climate change on the coastlines of the Republic of Mauritius employs the methodological framework outlined by JICA (2015). These elements are updated and detailed in order to propose a coherent approach for the entire coastline of the country, at the scale of homogeneous coastal zones.

Among the adverse effects of climate change on coastal zones is the anticipated rise in sea level, which is likely to exacerbate erosion of sandy coastlines and promote flooding of low-lying areas adjacent to the sea.

These two phenomena will have an impact on the retreat of the coastline.

- Sea level rise and flooding of low-lying areas

The retreat of the coastline caused by the flooding of low-lying areas can be mapped with relative simplicity using GIS, based on a number of assumptions. In this approach, the coastline under consideration is taken to correspond to an altitude between the high spring tide and the altitude

of the highest astronomical tides. This altitude is between 0.163 m and 0.456 m above mean level for Mauritius and between 0.447 and 0.926 above mean level for Rodrigues. It can be posited that altitudes below the level of the highest astronomical tides (HAT) can be considered as part of the marine domain. Such areas may be submerged by the sea on several occasions each year, even in the absence of waves and specific meteorological conditions. In the context of the prevailing circumstances, the oscillation of tides on beaches and low-lying areas is regarded as a typical phenomenon. However, as sea levels continue to rise, the foreshore (tidal zone) will retreat steadily over areas that are currently land, resulting in a net retreat of the coastline without further erosion.

For the purposes of this study, in the absence of a precise reference datum for the 2020 DTM, the elevation origin is considered to lie between the mean sea level at Port Louis and Port Mathurin and the Lowest Astronomical Tide level (-0.495 m below the mean sea level for Mauritius and -0.896 for Rodrigues). The "low limit" of the coastline retreat hazard zone is located above the Highest Astronomical Tide, between +0.456m and +0.951 m for the 2020 DTM in Mauritius and +0.926 and +1.822 m in Rodrigues. It should be noted that Chapter 2.1.2 has reservations about the accuracy of this Lidar dataset in the coastal zone of Mauritius. The "high limit » of the hazard zone corresponds to the sea level projected for the desired timeframe. Chapter 3.5.3.4 deals specifically with these SLR projections. For this study, the rise in sea level leading to the flooding of low-lying areas and a retreat of the coastline without additional erosion is estimated for the year 2100. In this timeframe, this effect of a retreat of the coastline without additional erosion can be mapped in a relevant manner at the scale used for the study (1:20,000).

- Additional erosion caused by sea level rise

The quantification of these effects is a challenging endeavour, with numerous research projects currently underway to develop estimation solutions. In the context of operational projects, the hypothesis proposed by Bruun (1983) is frequently employed to assess the impact of sea level rise on sandy coastlines. Despite considerable criticism in the scientific literature, this approach was selected by JICA (2015) for the global estimation of coastal erosion risk and the estimation of setback. This assumption will not be challenged in this study.

  - Empirical formula

The Bruun erosion rule deals with the long-term littoral sediment budget and exchanges of materials between the shore and the nearshore (Figure 59) in the context of sandy coastlines. The hypothesis is that the rise in sea level results in the nearshore deposition of sediment taken from the upper part of the beach. This equilibrium of the beach profile ultimately results in the erosion of the shore and a retreat of the coastline. It is important to note that this rule, which is based on the cross-shore transport of sediment towards the open sea, is a simplified representation of the long-term effects of coastal processes.

The Bruun rule is also based on another hypothesis for quantifying the sediment budget. It considers that the balance of the profile is restored when the deposits on the nearshore sector have compensated in height for the rise in sea level, as illustrated in Figure 59 and the corresponding parameter "a." This figure demonstrates that the sediments utilized to restore equilibrium to the pre-littoral zone come from the beach, which inevitably results in a retreat of the coastline, as indicated by parameter "s" in the Figure 59.

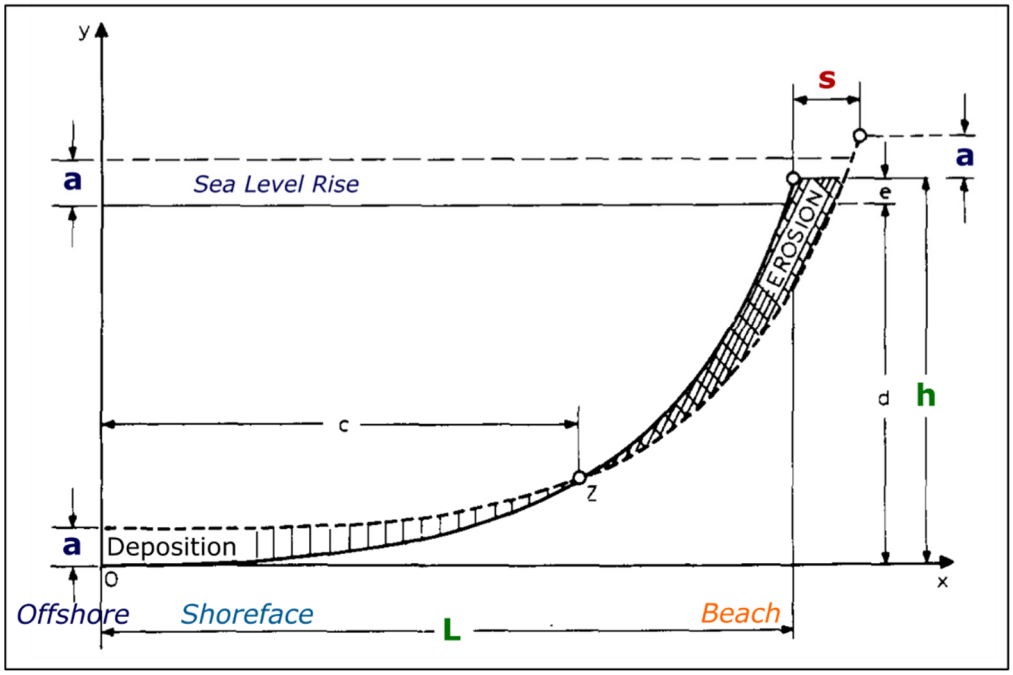


*Figure 59 : Bruun erosion rule. Assumed evolution of the beach profile and main descriptive parameters: a, rise in sea level; L, length of beach profile subject to wave influence; h, height between the coastline and the bottom of the pre-littoral domain. From Bruun 1983.*

In his study of theoretical beach profiles, Bruun (1983) demonstrates that the evolution of the entire beach profile is not a prerequisite for determining the retreat of the coastline. This is true provided that the ratio between the retreat rate, "s," and the length of the shore and nearshore domain, "L," (assumed to be of the order of one kilometre), is much less than 1 (s/L <<1). This is typically the case. Bruun's rule can thus be simplified by the following formula:

$$s.h = a.L$$

And :

$$s = \frac{a.L}{h} = \frac{a}{\tan(\alpha)}$$

In this context, the term "tan (α)" refers to the beach slope, which is also known as the "Bruun slope." Additionally, the value of "a" represents the sea level rise.

This simplified approach, which was adopted for the JICA (2015), differs from the one used in this study. The methodology developed for the present project also involves simplifying the shape of the beach profile in order to estimate the volumes of potential shoreface accumulations (sediment sink) as a function of the beach sediment source (Figure 60). In this case, the quantity of erodible sediment on the beach is not directly correlated with an estimation of the depth of wave action, but rather with a local estimation of the width of the beach (Lb). The width of the deposition zone designated as "C" is estimated to extend between the lower limits of the beach and the offshore extent of sedimentary deposits. The simplified “Bruun rule”, as applied to the coast of Mauritius, is expressed by the following formula:

$$s.Lb = a.C \quad \text{and } s = \frac{a.C}{Lb}$$

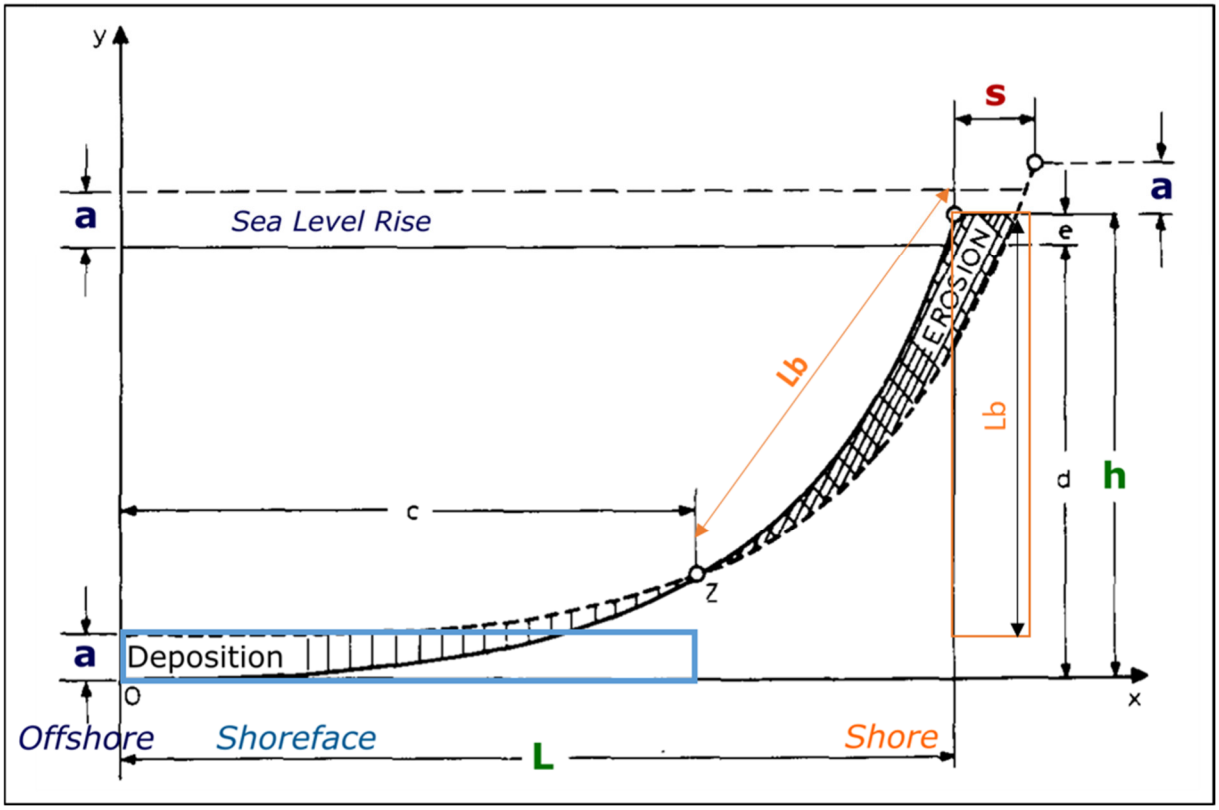


*Figure 60 : Modified Bruun rule used within the project*

- Defining sediment sinks

The coasts of Mauritius exhibit a variety of geomorphological features, including coral reefs and well-formed lagoons, extensive lagoons with channels, and open coastlines.

- In the case of a coral lagoon, the limit of the deposition zone is defined by the presence of the reef, which forms a barrier to the offshore transport of sediments. The average width of the lagoon is estimated on the basis of the homogeneous coastal zone.
- In the case of a large protected lagoon, the presence of morphological structures, such as channels, banks, and islets, can act as a barrier, preventing the transport of sediments towards the open sea. These structures are investigated to estimate the lagoon's potential depositional width. This width remains theoretical due to the fact that the preferential transport of sediments in lagoons over the long term is not typically cross-shore.
- The case of a large protected lagoon with uniform bathymetry is analogous to that of an open coastline, in the absence of a bathymetric structure. In order to quantify the width of the deposition zone, Bruun (1983) recommends estimating the depth of closure (Dc).

The depth of closure ($D_C$) is calculated based on the analysis of repeated measurements of a topographic and bathymetric profile. This depth represents the point at which no significant morphological variations are observed in the data. In the absence of regular bathymetric measurements, an empirical formula must be employed to estimate this depth. The most significant theoretical study on this subject was conducted by Hallermeier (1981). He defined two distinct closure depths, namely internal and external closure depths, as observed on a bathymetric profile. The internal closure depth ($d_i$) defines the extent of the active shoreface zone, where the sandy bottom is subject to frequent remobilization due to the action of breaking waves

and induced currents. The external closure depth ($d_i$) delineates the transition between the shoreface and the offshore marine zone, where wave interactions are minimal.

The following formula is used to estimate the internal closure depth ($d_l$), such that:

$$d_l = a_0 H_s + a_2 * {H_s^2}/{gT_s^2} \qquad (1)$$

The Hs and Ts terms correspond, respectively, to the significant wave heights and periods. The gravitational constant (9.81 m/s²) is represented by g, and the coefficients $a_0$ = 2.28 and $a_2$ = -68.5 are derived from a theoretical relationship for the suspension of quartz grains.

In the context of coastal engineering, Hallermeier (1981) specifies the interest in using this formula to estimate an annual closure depth. This value is based on the detection of the highest wave height exceeded during 12 consecutive hours during the year. This is done in order to establish the values Hsx and Tsx, which are then introduced into formula (1) for estimating the internal closure depth $d_l$.

In estimating the offshore limit of the Bruun slope, the annual closure depth is open to question. It may be beneficial to test the decadal values. In the case of Mauritius, the wave values are derived from the JICA (2015) study and the PRDW (2017) study for the purpose of analysing the Roches Noires wave buoy data and lagoon agitation data and model. The specific values for waves and estimates for closure depth are detailed in Table 13.

It is estimated that annual waves offshore reach a height of between 4 and 5 meters under the influence of a cyclone, with a duration of approximately 12 seconds. In lagoons of considerable width, such as that located on the east coast at Deux Frères, annual swells are estimated at 0.4 m and 3 sec, while ten-year swells are estimated at 0.8 m.

The internal closure depth for an open coast of Mauritius is equivalent to the 10-meter isobath. The internal closure depth for a wide lagoon is around the 1-meter isobath. The width of the deposition zone is estimated using bathymetric data or available nautical charts.

*Table 13 : Different closure depths in relation with wave characteristics and the type of coast*

| | $H_s$ (m) | $T_s$ (s) | **$D_l$ (m)** |
|---|---|---|---|
| Open coast | 5 | 12 | **10.19** |
| Large lagoon (annual wave) | 0.4 | 3 | **0.79** |
| Large lagoon (decadal wave) | 0.8 | 3 | **1.33** |

- Sediment Source

Beaches are sources of sediment which, according to Bruun's hypothesis, will be eroded and transported towards the shoreface under the effect of rising sea levels. In this simplified approach, the beach is an inclined plane and its retreat is a uniform translation. The average width of the beach is estimated for each homogeneous zone, from the top of the barrier beach or dune to the break in slope that forms the foot of the beach. This estimate is made by expert opinion, based on orthophotographs from 2020 or satellite images that allow the shallow waters to be observed by transparency.

- Impact of climate change on coasts with coral reefs

The Phase 1 report (Report BRGM/RC-72793-UK, 2023), which synthesises the work of Baird (2003), highlighted the importance of coral reef ecosystems in the sedimentary dynamics of the coastal zones of Mauritius. The studies by Baird (2003) and JICA (2015) have emphasised the

need to preserve these ecosystems in order to maintain the balance of Mauritius' coastal areas in the face of erosion.

Several phenomena related to the functioning of coral reefs are considered additional erosion factors. The rise in sea level will reduce the reef's ability to absorb wave energy from the open ocean or from cyclone-generated waves. If the reef's growth rate is slower than the rate of sea-level rise, this phenomenon could lead to an increase in the energy affecting the beaches, and thus to increased erosion. However, this point corresponds to a phenomenon that is theoretically included in the simplifications of the Bruun hypothesis presented in the previous paragraph.

In contrast, the increase in water temperature is likely to enhance coral bleaching events and may even contribute to the mortality of certain reefs. Furthermore, ocean acidification, resulting from the massive absorption of atmospheric $CO_2$, may hinder the proper calcification of organisms' skeletons and accelerate the degradation of calcareous sediments derived from the reef or from internal lagoon production.

The assessment of these effects on the ecosystems of the Republic of Mauritius lies outside the scope of this study and is a subject for future research. Nevertheless, the work of Baird (2003) has enabled the estimation of the production of sands and silts in coral lagoons at 5 kg/m²/year. This annual production of carbonate sediments contributes to the coastal sediment budget and serves as a mitigating factor for erosion, estimated at $E_m$ = 3 mm/year on the scale of the lagoon. For this study, it is therefore proposed to take into account the active production of coral sediments in the lagoon and to develop scenarios for the degradation of this mitigating factor over time.

Thus, the local sediment production, specific to relatively healthy coral reef sectors, may be incorporated into the local adaptation of the Bruun formula (1), as follows:

$$s.Lb = a.C - Lb.Em \quad (2)$$

With "s": retreat of the beach profile (and thus of the shoreline), « $L_b$ »: beach width (considered as an inclined plane), « a »: sea-level rise, « C »: width of the lagoon area, and « $E_m$ »: erosion mitigation through coral sediment production.

*4.2.1.1.2.5 Description of Shoreline Retreat Projection Scenarios*

The intricacies inherent in hydrosedimentary processes preclude the development of a comprehensive numerical model capable of replicating coastal morphodynamics over extended temporal periods and anticipating long-term shifts in coastline position over au large spatial scale. Presently, these tools lack operational capacity for the purpose of coastline retreat hazard mapping on a national scale over extended timeframes. Consequently, the coastline retreat projections produced for this study are based on data available for Mauritius and Rodrigues, as well as the various parameters collected and calculated as part of the study. The coastline retreat is estimated for three timeframes (present, 2050, and 2100) on the basis of predefined evolution scenarios. These scenarios articulate the underlying assumptions and parameters employed to estimate the exposed areas to shoreline retreat. The implementation of the scenarios requires the use of different calculation formulas presented in the previous part or detailed in the rest of this part, but also tools included in the GIS.

GIS tools (QGIS) was used to map the estimated retreat values for each scenario, at various time horizons. It allows the creation of a synthetic geographic database containing the estimated retreat values for each scenario, each time horizon, and each homogeneous coastal zone of Mauritius and Rodrigues.

The GIS is also employed to project these retreat values from a reference coastline and to produce hazard maps. The reference coastline used in this study is derived from the ESA coastline, corrected using the 2020 orthophotographs. Due to the lack of more recent data and updates, it is considered valid for the period 2020-2025, at the study scale of 1:20,000.

Buffering, clipping, merging, filtering, and smoothing tools are used to perform these projections and to address certain complex retreat scenarios, such as those involving mixed coastlines (sandy and rocky, see section 4.2.1.1.2.5.3) or to map the effect of sea level rise on low-lying areas (see section 4.2.1.1.2.5.4).

The following parameters have been taken into account to formulate the different scenarios for the evolution of the coastline:

- Tx, rate of retreat of the coastline
- Lmax, potential retreat caused by a cyclone at the end of the projection period.
- Sea level rise and flooding of low-lying areas
- Additional erosion caused by sea level rise (SLR-R)
- Decrease in coral sediment production (Em)
- Lithology of the coast (sand, basalt, limestone, mixed coast),
- Projection values rounded up to the nearest 5m.

#### *4.2.1.1.2.5.1 Main scenario for sandy and sedimentary coasts*

For sandy and sedimentary coastal areas, the scenario is based on coastline retreat data derived from an analysis of available data (JICA, 2015 and Report BRGM/RC-73987 – Appendix 1). These analyses have enabled the establishment of different parameters and rates of change by homogeneous zone or coastal hydrosedimentary cell. The parameters used to formulate the scenarios for projecting the retreat of the sandy coastline are:

- $Tx_{med\text{-}hz}$, median rate of shoreline change in the homogeneous zone
- $Tx_{hzd\text{-}hz}$, rate of retreat of the coastline in the homogeneous zone
- $Tx_{max\text{-}hz}$, maximum rate of coastline retreat in the homogeneous zone
- $Tx_{med\text{-}cell}$, median rate of shoreline change for the coastal cell
- SLR-R, the effects of climate change that could lead to additional erosion due to rising sea levels
- Lmax, the effects of a cyclonic event occurring at the end of the term.

- For the current period (2025)

The main scenario for coastline retreat (CLR) corresponds to:

$$\mathbf{CLR_{5y} = 5.Tx + Lmax_{5y}}$$

**5.Tx:** average potential retreat over a 5-year period.

**$Lmax_{5y}$**: potential retreat generated by a cyclone at the end of the projection period. The return period of the cyclone forcings taken into account is estimated at between 5 and 10 years.

- For the 2050 timeframe, the main scenario used to project coastline retreat (CLR) is as follows:

$$\mathbf{CLR_{25y} = 10.Tx_{median} + 15.Tx_{hzd} + SLR\text{-}R_{25y} + Lmax_{25y}}$$

**$10.Tx_{median}$**: Median annual retreat rate of the homogeneous zone studied. The main scenario considers that the zone studied will be subject to a median (low to moderate) retreat for 10 years during the projection period.

**$15.Tx_{hzd}$**: Annual retreat rate of the homogeneous zone. the main scenario considers that the homogeneous zone studied will be subject to moderate to strong retreat for 15 years during the projection period.

**SLR-$R_{25y}$** : the scenario considers additional erosion of the area due to rising sea levels. This parameter, based on an adaptation of Bruun's law to the lagoon and reef context, incorporates potential damping of this effect through sediment production within the coral reef and lagoon ecosystems.

**$Lmax_{25y}$**: potential retreat generated by a cyclone at the end of the projection period. The return period of the cyclone forcing taken into account is estimated at 25 years.

- For the 2100 timeframe, the main scenario for projecting coastline retreat (CLR) is as follows :

$$\mathbf{CLR_{25y} = [10.Tx_{median\text{-}hz} + 15.Tx_{hzd\text{-}hz} + SLR\text{-}R_{25y}] + 20.Tx_{median\text{-}hz} + 30.Tx_{hzd\text{-}cell} + SLR\text{-}R_{75y} + Lmax_{75y}}$$

**$[10.Tx_{median\text{-}hz} + 15.Tx_{hzd} + SLR\text{-}R_{25y}]$**: corresponds to the coastline retreat scenario for 2050

**$20.Tx_{median\text{-}hz}$**: Median annual retreat rate for the homogeneous zone studied. The scenario assumes that the median retreat established for the study zone (based on JICA data, 2015) can be expected to continue until 2070. The projection period based on this very local data is roughly the same as the period used to study past changes in the coastline (JICA, 2015).

**$30.Tx_{hzd\text{-}cell}$**: Median rate of shoreline change for the coastal cell. Beyond 2070, the values of possible local retreats become very uncertain. The main scenario considers that the significant coastal retreat phases that can be envisaged at this time may correspond to the retreat values observed at the scale of the coastal cell, grouping together several homogeneous zones.

**SLR-$R_{75y}$** : this parameter corresponds to the additional erosion of the area as a result of rising sea levels between 2050 and 2100.

**$Lmax_{75y}$** : potential retreat caused by a cyclone at the end of the projection period. The return period of the cyclone forcing taken into account is estimated at 100 years.

#### *4.2.1.1.2.5.2 Variants of scenario for sandy and sedimentary coasts*

For each designated timeframe, three variants of the primary scenario are delineated. These variants facilitate the consideration of variability in the available data and its subsequent effects on the extent of the zone potentially exposed to shoreline retreat.

A distinction is made between the median scenario, which employs the mean values of each of the parameters studied, and the safe scenario, which exploits the high margins (likely-range) of the calculated parameters, in order to propose a cautious projection that seeks to guard against unforeseen events and negative feedback.

The intermediate scenario, which is situated between these two variants, proposes the use of values and parameters which provide a balanced proposition between a classic approach and a safety vision of the retreat of the coastline.

- Coastline retreat rate (Tx)

The following table details the parameters used as "annual retreat rates" for the different timeframes in each scenario.

*Table 14: Coastline retreat rate parameters for the 3 variants of scenario and different study timeframes*

| *Coastline retreat rate parameters* | **Current** | **2050** | | **2100** | |
|---|---|---|---|---|---|
| *scenario* | 2020-2025 | 2025-2035 | 2035-2050 | 2050-2070 | 2070-2100 |
| **median** | $Tx_{med-hz}$ | $Tx_{med-hz}$ | $Tx_{med-hz}$ | $Tx_{med-hz}$ | $Tx_{hzd-cell}$ |
| **intermediate** | $Tx_{hzd-hz}$ | | $Tx_{hzd-hz}$ | | |
| **safe** | $Tx_{max-hz}$ | | $Tx_{max-hz}$ | | |

- Lmax

Table 15 and Table 16 detail the estimated maximum coastline retreat values of extreme event (Lmax) retained for the three scenarios, at the different projection timescales for the lagoon sectors of the west and east coasts of Mauritius. These values are derived from specific numerical models, calibrated for the environments of Mauritius (see section 4.2.1.1.2.3).

*Table 15: Lmax parameters for coral lagoons of the west coast of Mauritius, based on Baird study (2003) for Flic-en-Flac.*

| *West coast of Mauritius* | **$Lmax_{5y}$** | **$Lmax_{25y}$** | **$Lmax_{75y}$** |
|---|---|---|---|
| **Median** | 8.5 | 11 | 14 |
| **intermediate** | 10 | 12 | 14 |
| **Safe** | 11 | 13 | 14 |

*Table 16 : Lmax parameters for coral lagoons of the Est coast of Mauritius, based on Baird study (2003) for Bellemare.*

| *Est coast of Mauritius* | **$Lmax_{5y}$** | **$Lmax_{25y}$** | **$Lmax_{75y}$** |
|---|---|---|---|
| **median** | 3.5 | 5 | 14 |
| **intermediate** | 4 | 6 | 20 |
| **safe** | 5 | 10 | 20 |

Table 17 details the Lmax values adopted for the open coast scenarios in Mauritius and for all the coasts of Rodrigues.

*Table 17 : Lmax parameters for Mauritius (open sandy coast) and Rodrigues. Adaptation of the Fema 540SF method.*

| *Very low-lying sandy coast* | **$Lmax_{5y}$** | **$Lmax_{25y}$** | **$Lmax_{75y}$** |
|---|---|---|---|
| **median** | 10 | 15 | 25 |
| **intermediate** | 12 | 20 | 30 |
| **safe** | 15 | 20 | 30 |

| *Low-lying sandy coast* | **$Lmax_{5y}$** | **$Lmax_{25y}$** | **$Lmax_{75y}$** |
|---|---|---|---|
| **median** | 8 | 12 | 20 |
| **intermediate** | 10 | 15 | 25 |
| **safe** | 12 | 20 | 25 |

| *Sandy coast* | **$Lmax_{5y}$** | **$Lmax_{25y}$** | **$Lmax_{75y}$** |
|---|---|---|---|
| **median** | 7 | 10 | 17 |
| **intermediate** | 8 | 12 | 20 |
| **safe** | 12 | 15 | 20 |

- SLR-R

Table 18 and Table 19 detail the sea level values projected for the different timeframes, for the 3 study scenarios. Note that Rodrigue's safe scenario takes into account the local subsidence hypothesis (Vertical Land Motion 2050 = 0.055 m ; VLM 2100: 0.21m see section 4.2.1.1.2.4).

*Table 18: Sea-level rise parameters for coastline retreat study, Mauritius.*

| *SLR Mauritius (m)* | IPCC scenario | **2025-2050** | **2050-2100** |
|---|---|---|---|
| **median** | RCP4.5 | 0.12 | 0.45 |
| **intermediate** | RCP8.5 | 0.13 | 0.73 |
| **safe** | RCP8.5 (likely-range) | 0.18 | 1.05 |

*Table 19: Sea-level rise parameters for coastline retreat study, Rodrigues.*

| *SLR Rodrigues (m)* | IPCC scenario | **2025-2050** | **2050-2100** |
|---|---|---|---|
| **median** | RCP4.5 | 0.12 | 0.44 |
| **intermediate** | RCP8.5 | 0.13 | 0.74 |
| **safe** | RCP8.5 (likely-range+VLM) | 0.24 | 1.22 |

Table 20 proposes coefficients for the reduction in coral sediment production ($E_m$) for each scenario. Part 4.2.1.1.2.4 presents the coral production value adopted for this study. The uncertainty surrounding this value is very high, and the reduction coefficients chosen for this study are not based on observations or validated impact models.

*Table 20: Assumptions used to reduce the estimate of coral sediment production ($E_m$)*

| Sandy production in coral lagoons | $E_m$ | 5 kg/m²/y |
|---|---|---|
| *Global change effect hypothesis* | **2025-2050** | **2050-2100** |
| **median** | $E_m$ | 0.75 $E_m$ |
| **intermediate** | $E_m$ | 0.5 $E_m$ |
| **safe** | 0.5 $E_m$ | 0.33 $E_m$ |

#### *4.2.1.1.2.5.3 Scenarios for rocky, anthropogenic embankment and mixed coasts*

- Basaltic rocky coasts

In the context of basaltic rocky coasts, shoreline retreat has been observed to be generally low. However, this phenomenon is contingent upon the specific geological and morphological characteristics of the site, including but not limited to fracturing, weathering, undercutting, slope, and other related factors. Additionally, local forcing conditions, such as sea-state (waves and swell) and underground circulation in soil, play a significant role in rocky shoreline retreat. The consideration of these elements necessitates local approaches, which do not align with the scale of this study. To adequately address the potential retreat in the hard rock and basalt sectors, two fixed values (5m and 10m) have been employed to propose distinct retreat scenarios.

*Table 21: Coastline retreat scenarios (m) for basaltic rocky coast*

| *Basaltic rocky coast* | **CLR $_{5y}$** | **CLR $_{25y}$** | **CLR $_{75y}$** |
|---|---|---|---|
| **median** | 0 | 5 | 10 |
| **intermediate** | 5 | 5 | 10 |
| **safe** | 5 | 10 | 10 |

For unaltered rocky slopes, these overall fixed values may appear to be overestimated for the timeframes covered by the study. It should be borne in mind that possible rocky coasts retreat are diffuse in time and space. The entirety of the hazard band is likely to remain unaffected by these estimated hazards; the precise timing and location of their occurrence remains uncertain at present. However, it is crucial to note that, in contrast to sedimentary sectors, rock retreat is an irreversible phenomenon. Furthermore, the repercussions of extreme events, such as cyclones, on rocky coastline, must not be disregarded. The characteristics of these events, such as the exceptional wave action and block projections, have the potential to inflict damage to soil, property, and infrastructure.

- Limestone coasts of Rodrigues

For the sectors of limestone sandstone of aeolian origin encountered in Rodrigues, a specific study was carried out, based on an analysis of the size of the notches to determine the possible retreats (Report BRGM/RC-73987- Appendix 1, Chapter 2.3.1). The findings of this particular study were then employed to propose a range of coastline retreats scenarios.

*Table 22: Coastline retreat scenarios (m) for limestone coast of Rodrigues*

| *Limestone rocky coast* | **CLR $_{5y}$** | **CLR $_{25y}$** | **CLR $_{75y}$** |
|---|---|---|---|
| **median** | 5 | 10 | 20 |
| **intermediate** | 5 | 10 | 20 |
| **safe** | 10 | 20 | 20 |

- Man-made embankments

In Mauritius, the homogeneous coastal zones of Port Louis and Mahebourg are wholly or partly made up of embankments, which are protected by coastline retaining structures. For this particular type of coastline, the retreat scenarios selected are analogous to those employed for basaltic rocky coasts.

Port Mathurin in Rodrigues represents a distinctive case in this study. Similar to Port Louis, the town's entire homogenous zone is characterized by an embankment reinforced by riprap or walls. However, field surveys have revealed that the riprap has experienced substantial damage. Consequently, the efficacy of this riprap in impeding the coastline's retreat during a cyclone event is dubious. Consequently, the retreat scenarios assigned to Port Mathurin correspond to the values of the Lmax parameter for the sector, across the three scenario variants and the three study timeframes.

- Mixed coast (sand and rock)

In the context of mixed coasts, characterized by a sand layer overlying a rocky substrate, the scenarios developed for sedimentary coasts may, in certain locales, result in an overestimation of the retreat of the coastline. In instances where the retreat of the sandy coastline exceeds the width of the barrier beach, then sedimentary retreat is limited by the presence of hard bedrock, and a simplified scenario of rocky retreat is added.

The width of the barrier beach is determined using coastal geological maps that have been updated during the course of this study (BRGM/RC-72793-UK).

*Table 23: Simplified scenario for additional retreat of the rocky coastline, in the event of erosion of the barrier beach*

| *mixed coast (sand&rock)* | **CLR $_{5y}$** | **CLR $_{25y}$** | **CLR $_{75y}$** |
|---|---|---|---|
| **Basaltic rocky coast** | 0 | 5 | 10 |
| **Limestone rocky coast** | 5 | 10 | 20 |

#### *4.2.1.1.2.5.4 Scenarios of sea-level rise on low-lying areas*

For this study, the rise in sea level leading to the flooding of low-lying areas and a retreat of the coastline without additional erosion is estimated for the year 2100.

This approach enables the delineation of an altitude limit that can be attained by the sea in the absence of an extreme energy event (SLR-R parameter). Consequently, this altitude can be regarded as a surrogate for the coastline. The observed retreat is not attributable to the erosive action of the sea; rather, it is a consequence of the flooding of low-lying areas, whether temporary, chronic, or permanent in nature.

The scenarios established to deal with this subject consider that the origins of the DTMs used for Mauritius and Rodrigues are at the altitude of the LAT (Lowest Astronomical Tide) and that the coastline indicator corresponds to the altitude of the HAT (Highest Astronomical Tide). The values are rounded in 0.25 m increments to facilitate mapping. The intermediate scenario for Rodrigues is rounded up to the next 0.25 m in order to incorporate (in part) the uncertainty associated with local subsidence.

The safe scenarios are contingent upon the parameters delineated for Mauritius and Rodrigues in section 3.5.3. These scenarios are regarded as maximizing. For Rodrigues, this choice is linked to the possible effect of subsidence. For Mauritius, this choice is linked to the non-quantifiable uncertainties present in the DTM data.

*Table 24 : Scenarios for estimating the SLR-R parameter, this altitude corresponds to the possible rise in sea level over low-lying areas of Mauritius.*

| *SLR Mauritius (m)* | IPCC scenario | **2025-2100** | HAT-LAT | Altitude SLR | **SLR-R** |
|---|---|---|---|---|---|
| **median** | RCP4.5 | 0.45 | 0.951 | 1.40 | **1.5** |
| **intermediate** | RCP8.5 (likely-range) | 1.06 | | 2.01 | **2** |
| **safe** | High-end | 1.62 | | 2.57 | **2.5** |

*Table 25: Scenarios for estimating the SLR-R parameter, This altitude corresponds to the possible rise in sea level over low-lying areas of Rodrigues.*

| *SLR Rodrigues (m)* | IPCC scenario | **2025-2100** | HAT-LAT | Altitude SLR | **SLR-R** |
|---|---|---|---|---|---|
| **median** | RCP4.5 | 0.44 | 1.822 | 2.26 | **2.25** |
| **intermediate** | RCP8.5 | 0.74 | | 2.56 | **2.75** |
| **safe** | RCP8.5 (likely-range+VLM) | 1.22 | | 3.04 | **3** |

### 4.2.1.2 Method for assessment of coastal flooding hazard at 1:20 000

Our numerical strategy to assess coastal flooding hazard is based upon the usage of 3 numerical tools: the UHAINA hydrodynamic model (Filippini et al. 2024) for water level simulation, the spectral model WAVEWATCH3 (WW3) (Tolman 2009) and the phase-resolved model SWASH

(Zijlema et al. 2011) for waves propagation. The modelling strategy is based on a three-steps chaining WW3 and UHAINA to simulate coastal flooding by overflowing. Step 1 consist in a first UHAINA simulation, accounting only for tidal signal and meteorological forcing, used to compute the spatial variability of mean water level and currents for WW3 needs. Step 2 is performed running WW3, propagating wave spectra from the boundary into the computational domain, forcing the mean water levels and currents computed in the previous step. In the final Step 3, UHAINA is run accounting for wave-setup and wave-induced currents to compute the overflowing scenarios. In areas submitted to overtopping, waves propagation and runup is computing with the SWASH model on transects perpendicular to the coast. When overtopping water can spread ashore and flood low-lying coastal areas, these water volumes are injected into the UHAINA simulation, providing a complete representation (overtopping + overflowing) of the flooding event.

#### *4.2.1.2.1 Description of numerical modelling tools*

**UHAINA**:

This hydrodynamic model is used for water level propagation and the simulation of flooding by overflowing. UHAINA (Filippini et al. 2024) is a new-generation hydrodynamic code co-developed by a consortium of French institutes (including INRIA, EPOC, IMB, IMAG and BRGM). It implements the shallow water system of equations and uses numerical schemes based on arbitrarily high-order finite elements on unstructured meshes. Due to a specific treatment of the shoreline, UHAINA guarantees the respect of the topographic heights during flooding and good numerical properties in terms of stability, mass conservation and preservation of the equilibrium state, also in presence of complex topo-bathymetries.

For the purposes of this work, UHAINA will account for:

- the predicted tide, determined from the FES2014 harmonic component database;
- the atmospheric surge generated by the action of wind and atmospheric pressure on the water surface;
- the surge generated by breaking waves (wave setup) and wave-induced currents, through chaining with the WW3 spectral model;
- overtopping water volumes, through chaining with the SWASH Boussinesq model;
- topo-bathymetric features (dykes, channels, roads, etc) that drives the flow in land, integrated into the mesh using constraint lines;
- spatially varying friction coefficient for representing the seabed and land coverage;
- hydraulic structures (nozzles, hydraulic weirs, locks) and culverts via hydraulic laws integrated into the model.

The model provides a map of the evolution of water level, water height and currents every 10 minutes. It also calculates the maximum water level and velocity, as well as the hazard, every 5 minutes.

**WAVEWATCH3 (WW3)**:

The WW3 model (Tolman 2009) solves the wave action density conservation equation using structured (finite difference) or unstructured (finite element) calculation grids. It is capable of reproducing the various processes linked to waves from the open sea to the shore, such as wind generation, propagation in space (refraction, interactions with currents, etc.) and dissipation (bottom friction, breaking, etc.).

The main constraint for this model is to correctly reproduce the characteristics of the waves in the breaking zone in order to ensure the correct calculation of the wave setup (carried out in a second

step in UHAINA). This implies the use of a fine mesh (10 to 20 m spatial resolution) in this breaking zone. Because of the extent of the study areas, it was decided to use WW3 with an unstructured mesh and, for simplicity, the same numerical grids have been used for WW3 and UHAINA, having care of satisfying the needs of both models in terms of resolution. This choice has also made the WW3-UHAINA chaining more robust and efficient by refraining from spatial interpolation of wave parameters.

WW3 was parameterised as described in Ardhuin et al (2010), with the wave spectrum discretised into 36 directions (10° steps) and 32 frequencies (corresponding to wave periods ranging from ~1.4 to ~27 seconds). Bottom friction and wave breaking were activated.

Each run of the model requires:

- the wave spectra at the domain boundaries from the large scale scenarios computations;

- the unsteady water level and currents, resulting from the tide and the atmospheric surge. These variable are in general not homogeneous on the studied area and are computed in by a UHAINA run in Step 1] of the chaining strategy;

- the directional wave spectra at the domain boundaries from large scale scenarios computations: constructed from wave characteristics (significant height, period, peak direction and directional spread). These variables are calculated using the WAFO toolbox (Brodtkorb, et al. 2000);

- the unsteady wind intensity and direction, which may or may not be homogeneous depending on the studied area and scenario.

WW3 provides UHAINA and SWASH with wave data information (Hs, Tp, Dp) every 10 minutes.

**SWASH**:

SWASH (Zijlema et al. 2011) is a phase-resolved code adapted to simulate marine submersion by overtopping and crossing of waves in natural to heavily urbanised areas over small spatial areas (a few km²), providing a detailed description of onshore flows. The model takes into account the phenomena of refraction, diffraction, reflection, swelling, breaking, interactions (waves-waves, waves-currents), generation of wave-induced currents and treatment of exposed banks.

In this work we use SWASH to simulate the propagation of waves on short one-dimensional transects perpendicular to the coast, in order to characterise possible flooding by overtopping and, in this eventuality, to simulate wave runup and overtopping water volumes. These volumes can be taken into account into the UHAINA run, in the final Step 3] of the modelling strategy. It should be noted that SWASH has not been used in 2DH mode because the extent of the coastline to be covered and the duration of the simulations (1 to several days) made the computational effort required simply out of reach.

SWASH uses as input the spectral wave and water level conditions derived from coupled level-current-wave modelling (Step 1] and Step 2]). The 1D profiles on which SWASH has been deployed have a spatial resolution of 1 m for a correct propagation of waves and takes into account the topo-bathymetry data and bottom friction.

#### *4.2.1.2.2 Production of the topo-bathymetric DTMs*

For the purposes of modelling coastal flooding, a regional DTM (Digital Terrain Model) has been realized at the scale of the Indian Ocean. The resolution of this DTM is 0,004° (mesh size around 400 to 500 m). It has been used to generate the meshes of the 2 modelled areas for Mauritius and Rodrigues (see chapter 4.2.1.2.4).

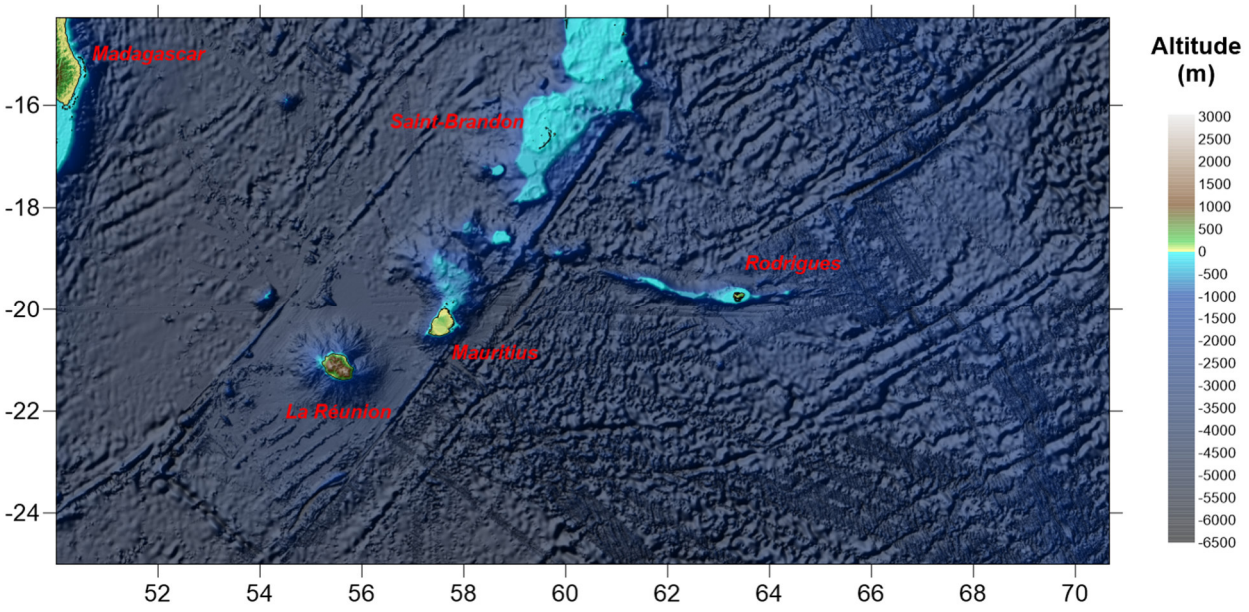


*Figure 61 : Overview of the DTM at the regional DTM (note that the inland part of Mauritius is not integrated)*

For the downscaling at the scale of the islands of Mauritius and Rodrigues, the topographic and bathymetric data provided by Mauritian authorities (chapter 2.1) have been used to generate coastal DTMs for both Mauritius and Rodrigues islands. These data have completed with others publicly available data and/or corrected (see 2.1).

For Mauritius, the coastal DTM has a 30 m resolution (Figure 62), and for Rodrigues the resolution is 4 m (Figure 63). This difference is explained by the limited area of Rodrigues, which allows to anticipate the local high-resolution simulations.

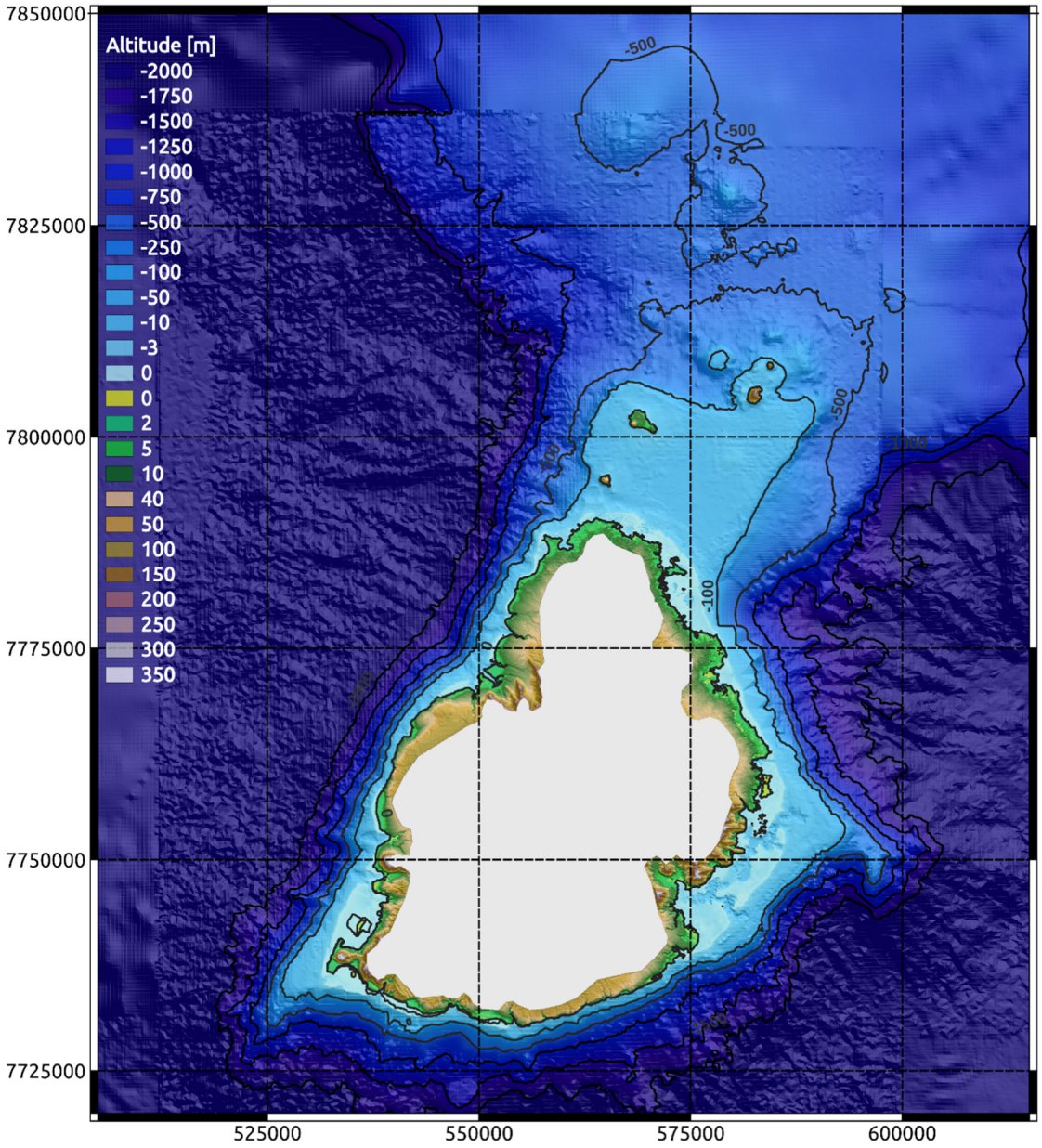


*Figure 62 : Overview of the coastal DTM of Mauritius Island (note that the inland part is not integrated and the corresponding DTM corresponds to an interpolation of the coastal data)*

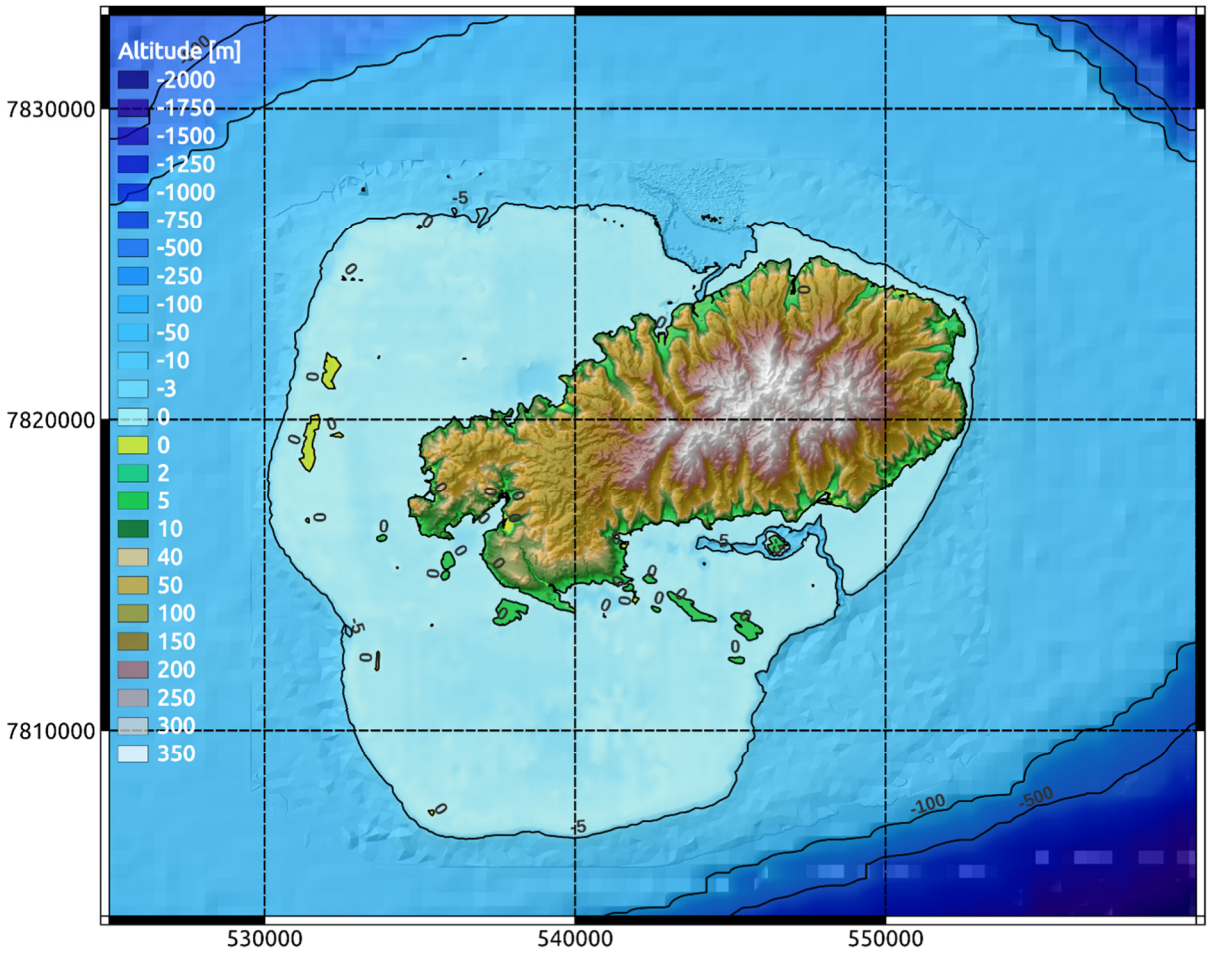


*Figure 63 : Overview of the coastal DTM of Rodrigues Island*

#### *4.2.1.2.3 Identification of hydraulic features*

Realistic simulation of coastal flooding requires consideration of culverts in low-lying areas, such as lines of constraint (such as canals, drains, reefs, dykes and other structures that can slow or facilitate flows) and hydraulic connections (pipes and nozzles that allow flood propagation despite obstacles). Particular attention has been paid to hotspots, so that the data can be reused directly for high-resolution local simulations.

***Constraint lines***

The identification of stress lines is essential in order to adapt the mesh for a correct representation of these elements. The stress lines were identified on the basis of topographic data and field visits to the entire coastal zone of the 2 islands. It should be noted that only the main structures have been treated, and that small obstacles, such as small private boundary walls for example, have not been taken into account due to their low resistance and the uncertainty about their persistence. Two categories of stress lines can be distinguished:

- "*high constraint lines*" which block flows, such as dykes, dunes, embankments, walls, etc.
- "*low constraint lines*" which facilitate flows, like channels, drains, estuaries…



*Figure 64 : Examples of « high constraint lines » (obstacles to the flow): dike in Trou d'Eau Douce (left) and raised seafront in Grand-Baie (right)*



*Figure 65 : Examples of « low constraint lines » (preferential passage for the flow): stream outlet in Rivière du Rempart (left) and channel between the mainland and an island near Rivière des Galets (right)*

The following Figure 66 and Figure 67 show the extensive use of constraint lines that has been made to build up the large scale numerical models. Similar pictures, with a specific focus on the local sites of Flic-en-Flac and Anse La Raie can be found in section 4.3.2.

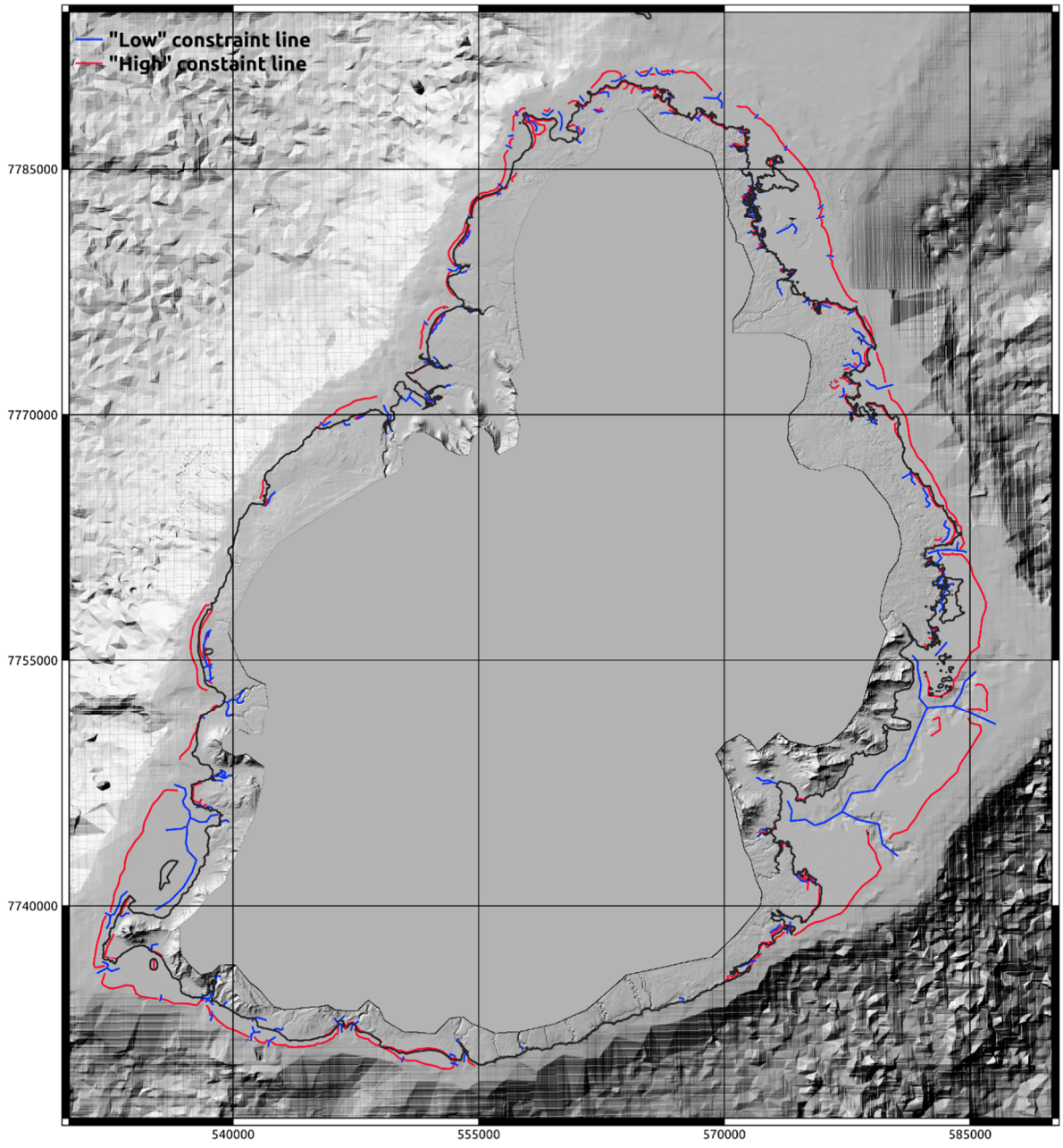


*Figure 66 : Use of constraint lines in the Maurice island model (DTM in the background). Black line represents the coastline.*

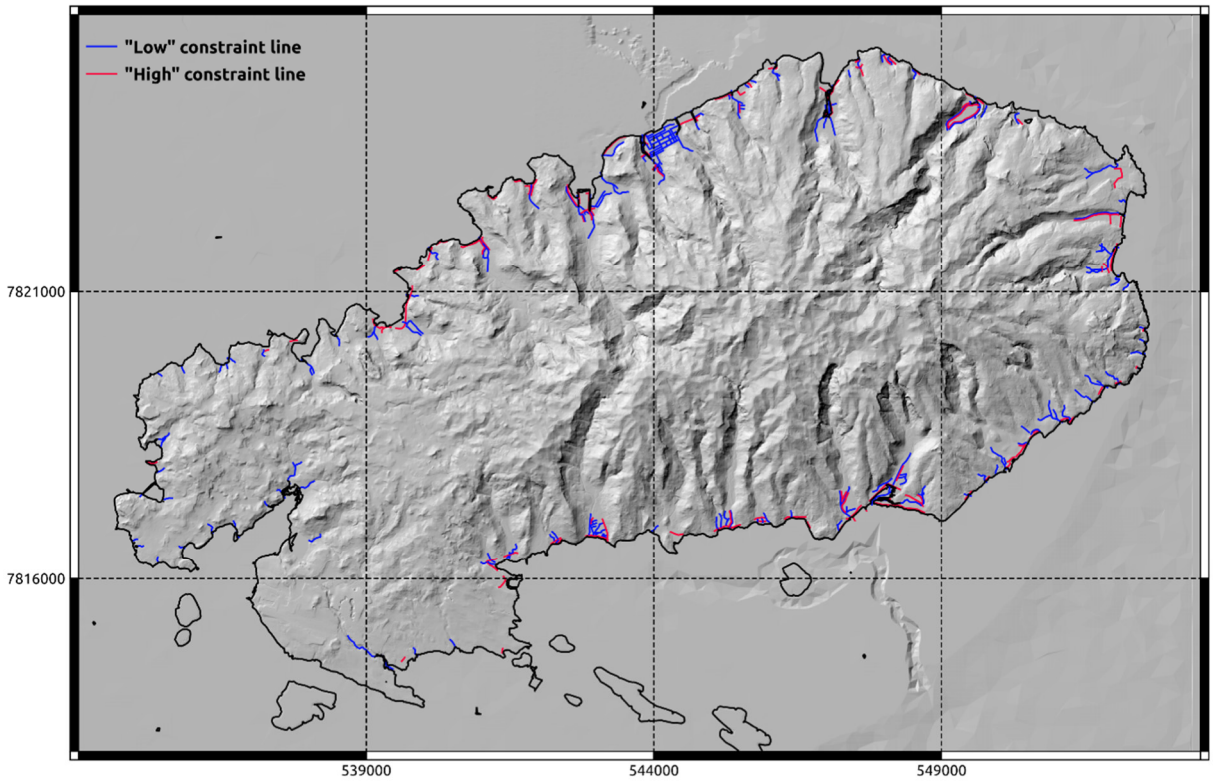


*Figure 67 : Use of constraint lines in the Rodrigues Island model (DTM in the background). Black line represents the coastline.*

### *Culverts*

Culverts can be implemented in the simulations through hydraulic formulas to assure that the model can transmit water across obstacles and constraint lines. It should be noted that for large hydraulic connections, insofar as the mesh resolution allowed, a “low constraint line” have been preferred to avoid hydraulic formulas.



*Figure 68 : Examples of hydraulic connections in Port-Louis (left) and Trou d’Eau Douce (right)*

Figure 69 and Figure 70 show some of the identified culverts on both islands that have been taken into account in our coastal flooding models.

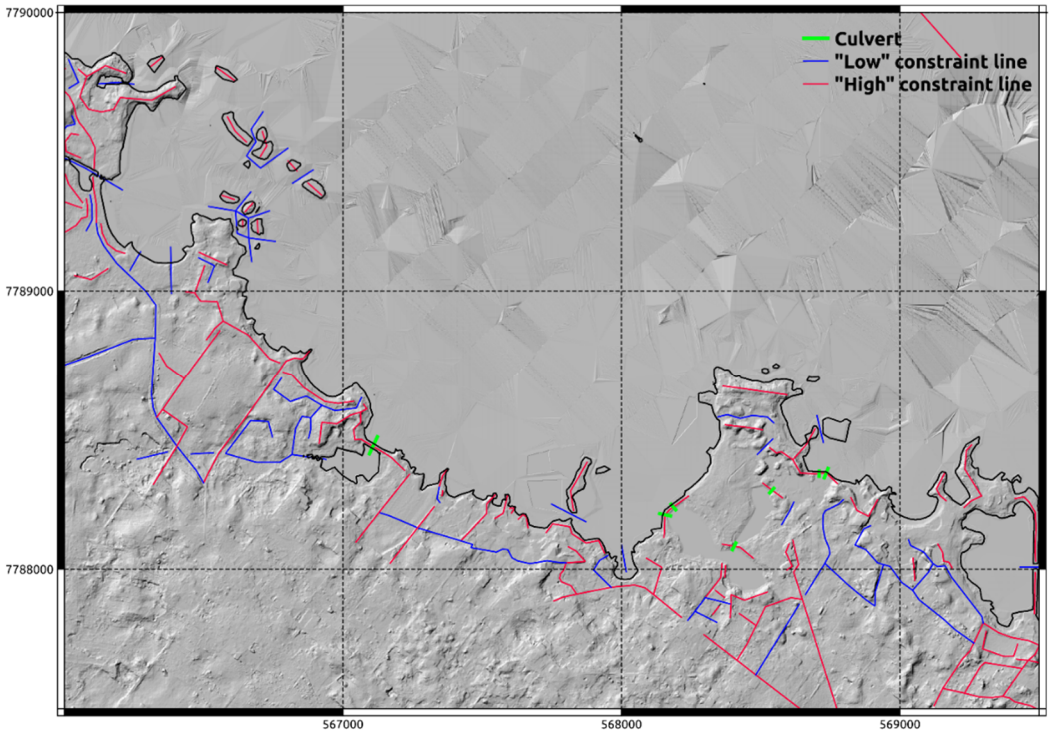


*Figure 69 : zoom on some culverts in the Calodyne and Butte à l'herbe beach area that are taken into account in the Anse la Raie model (DTM in the background). Black line represents the coastline.*

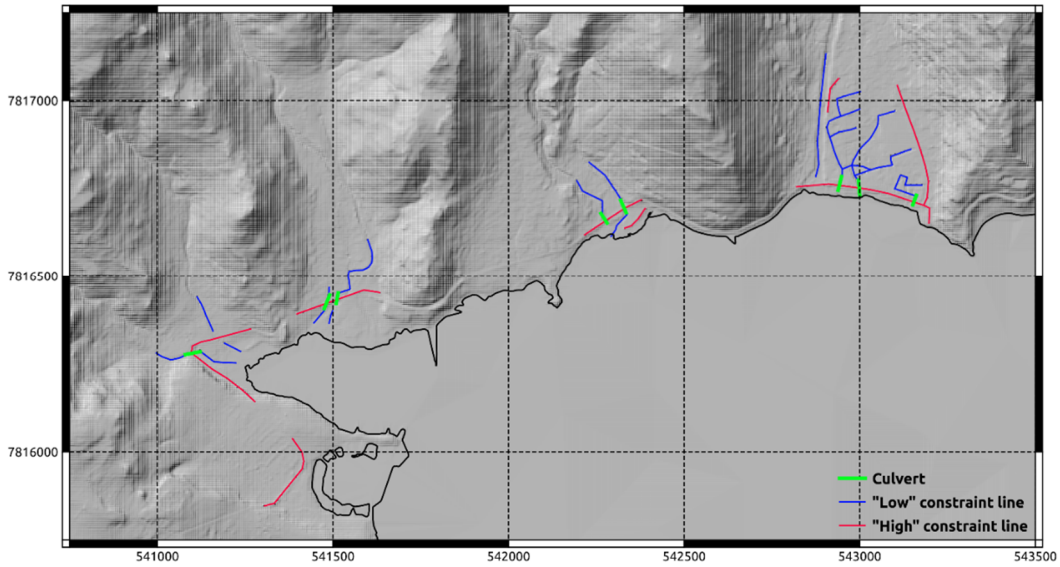


*Figure 70 : zoom on some culverts in the Anse Grande Var area that are taken into account in the Rodrigues model (DTM in the background). Black line represents the coastline.*

#### *4.2.1.2.4 Meshing*

In order to study the coastal flooding hazards on the Mauritius and Rodrigues islands, two different meshes were constructed. In general, they cover extensive sea areas: wide enough to account for the presence and shape of the island shelf and reefs; while on land, the boundary limit is located between the +10 m and +20m level lines of the topography. The mesh size is variable, adapted to the water depth and more refined on land and around abrupt changes of the sea bathymetry (shelf, reefs, etc). The two meshes are represented in Figure 71 and Figure 72 for Mauritius and Rodrigues respectively. The mesh size varies from 500m offshore to 40m on land for Mauritius, limited by the resolution of the topographic data, and 15m for Rodrigues, where finer data were available.

The dimensions of the computational domains are such that it is not possible to assume spatially homogeneous atmospheric forcing. Wind and atmospheric pressure have to be described by spatio-temporal fields, and their effects on water level are calculated by the respective source terms, directly implemented in the model. In addition, the particular configuration of the computational domain, with a circular sea external boundary in deep waters, means that only the contribution of the tide to the total water level mist be imposed and propagate from the boundary. However, imposing a single uniform boundary signal would be unrealistic. For this reason, the sea boundary has been partitioned in multiple segments with homogeneous tidal values, computed from the FES2014 database at chosen forcing points. The number and position of these points has been chosen depending on tide variability around the two islands and it is shown in Figure 71 and Figure 72 respectively.

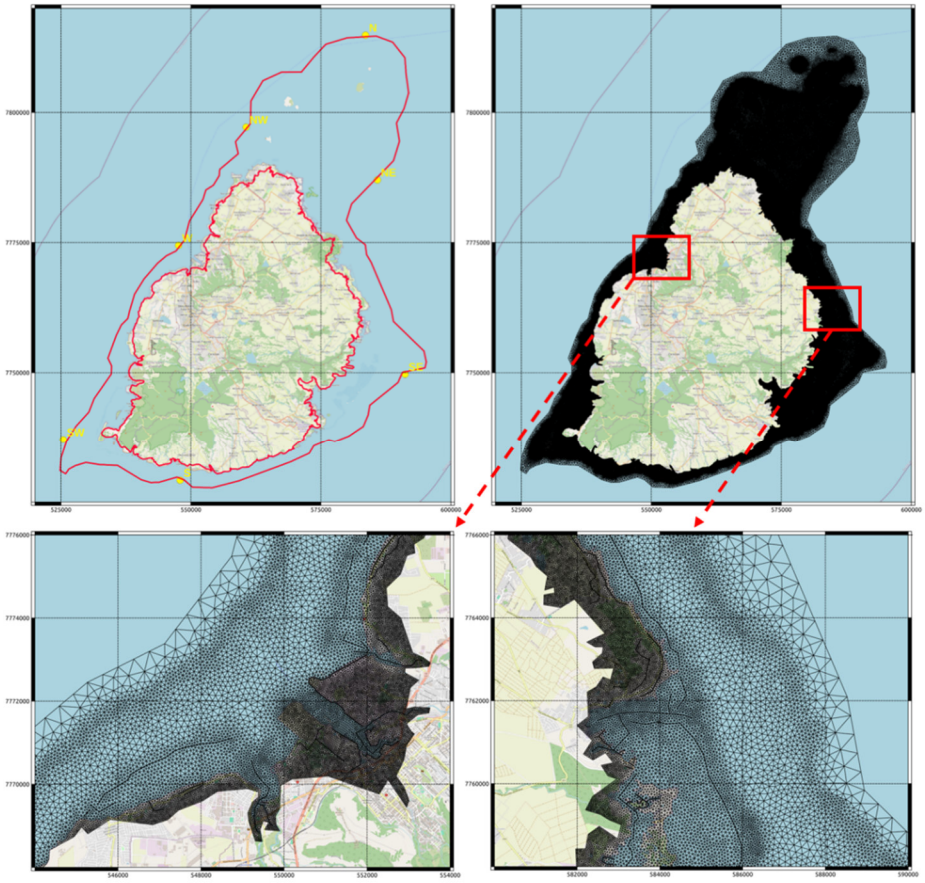

*Figure 71 : Extension of the computational mesh on the Mauritius Island, including the location of the forcing points; grid overview with two zooms on the Port Louis (bottom left) and Trou d'Eau Douce (bottom right) areas.*

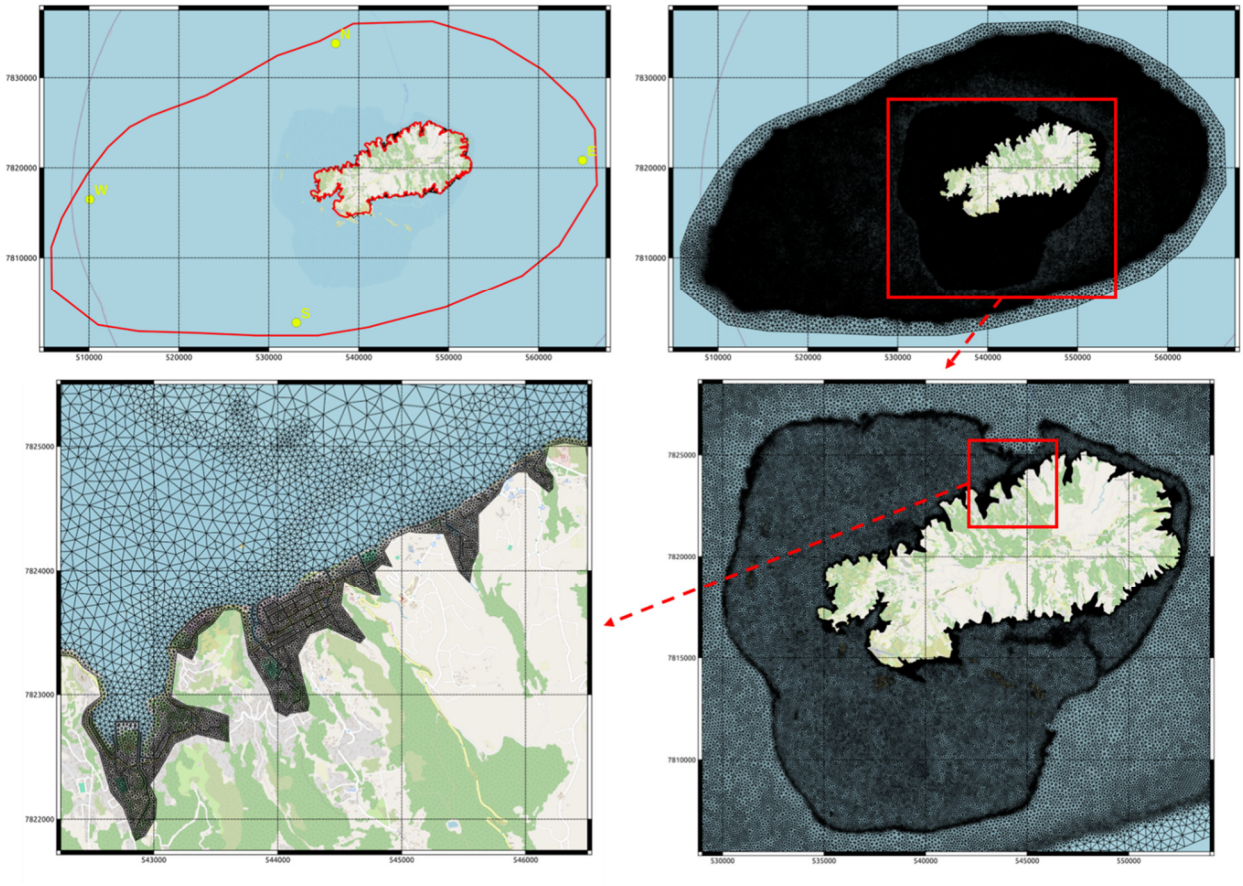

*Figure 72 : Extension of the computational mesh on the Rodrigues Island, including the location of the forcing points; grid overview with two subsequent zooms on the lagoon (bottom right) and on the Port Mathurin (bottom left) area.*

#### *4.2.1.2.5 Land use and bottom friction*

In the model UHAINA, the bottom friction is included via the classic Manning approach (Filippini et al. 2024). The Manning coefficient must be heterogeneous, in order to represent the great variability of land coverage. Moreover, since the mesh resolution is not fine enough to represent the presence of buildings and structures on the ground, the cumulative slow down effect of urbanized areas on the flow is represented via a high value of the roughness coefficient.

A sufficiently accurate database of the land coverage on the two islands was not available. Therefore, it has been produced during this project based mainly upon field visits and satellite images (see Appendix 3, BRGM/RC-73987). The results are sketched in Figure 73 Figure 74 for Mauritius and Rodrigues respectively.

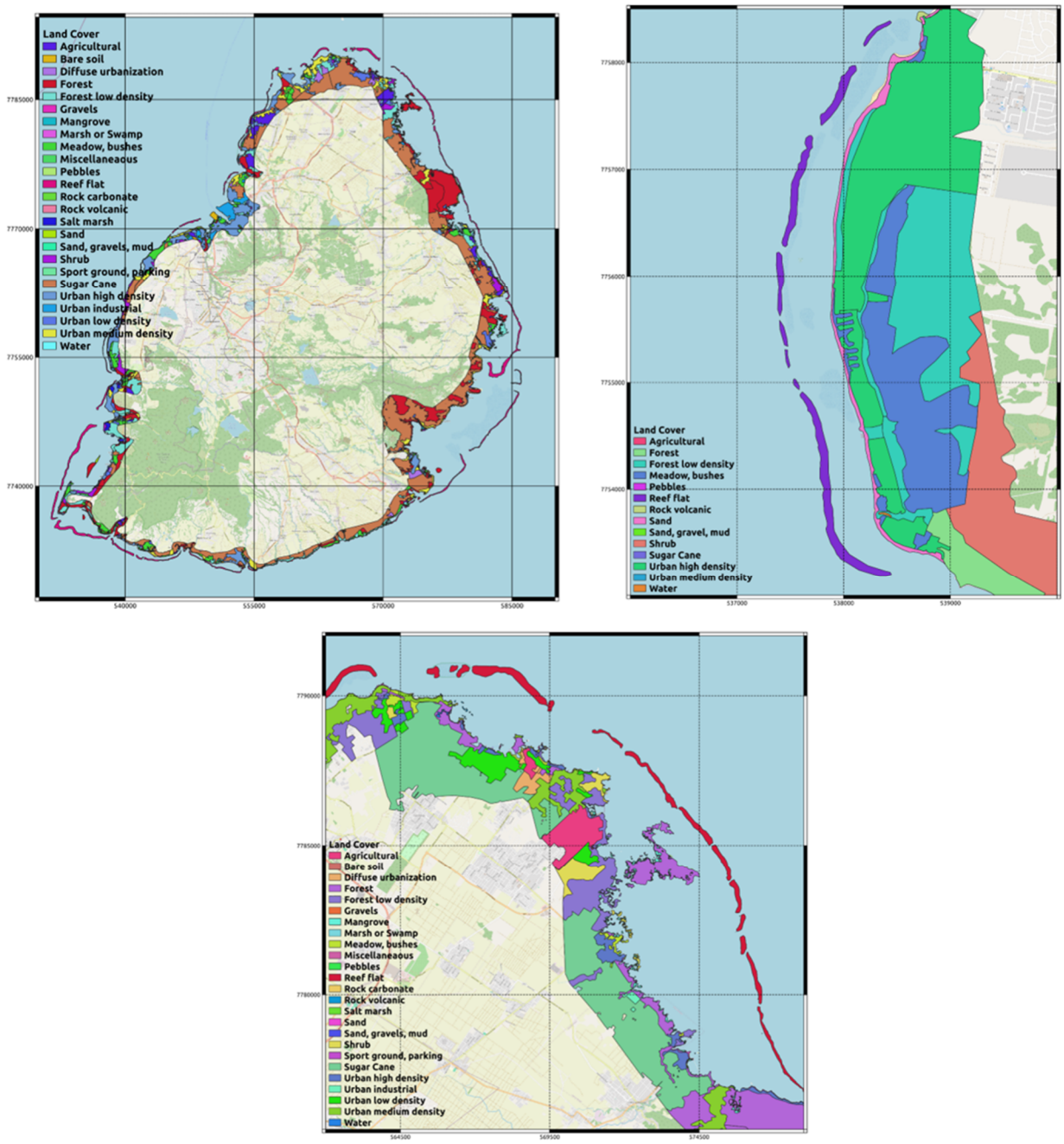


*Figure 73 : Land cover in Mauritius; close-up views on the Flic-en-Flac (top-right) and Maurice-north areas.*

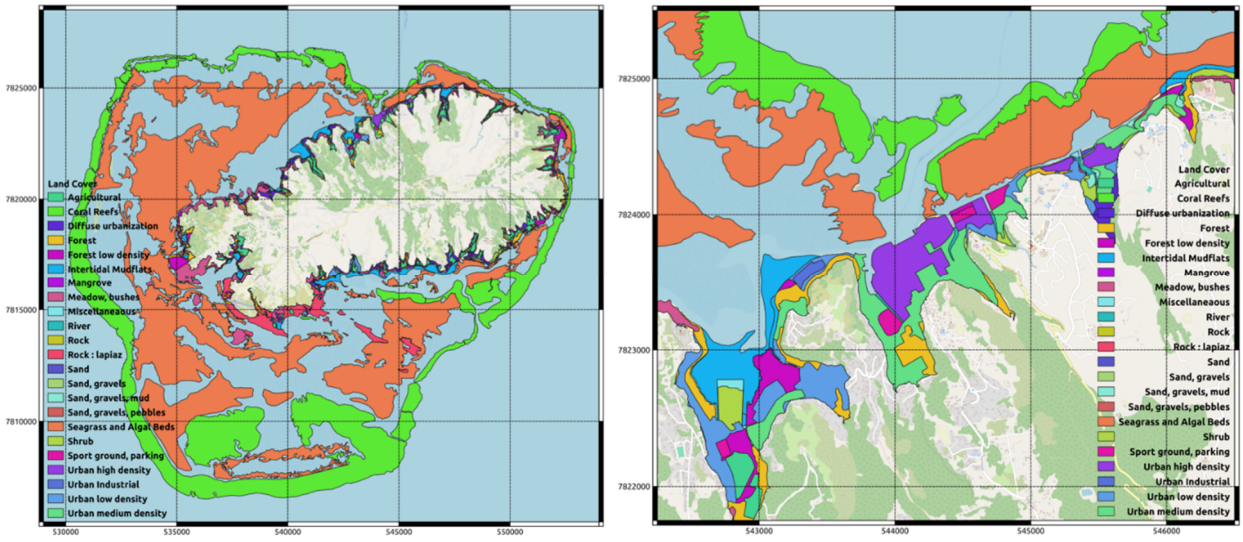


*Figure 74 : Land cover in Rodrigues and close-up view on the Port Mathurin area (right).*

In the literature, there exist some databases, such as HEC-RAS (USACE), providing Manning's coefficient values for various classes of land use to be used in hydrodynamic software. Based on these data, a table of correspondence between the identified classes of land coverage and the friction coefficient was drawn up, which ranges from 0.022s/m$^{1/3}$ on asphalted roads to 0.33s/m$^{1/3}$ on high density urbanized areas.

## 4.2.2 Results

### 4.2.2.1 Mauritius

#### *4.2.2.1.1 Coastal retreat hazard*

The projected shoreline retreat scenarios were applied to the entire coastline of Mauritius and Rodrigues. For Mauritius, 267 homogeneous zones were studied, and 36 homogeneous zones for Rodrigues.

For each homogeneous zone, the three projection scenarios (median, safe, or intermediate) were employed, contingent on the nature of the coastline (sandy or rocky). These scenarios were utilized to estimate the possible retreat for the three study timeframes: 5 years for the current hazard, 25 years for the hazard in 2050, and 75 years for the retreat hazard in 2100.

The various parameters employed and the methodology for implementing these projection scenarios are delineated in 3.2.1. The projected shoreline retreat values obtained for each homogeneous zone facilitate the description of the hazard of shoreline retreat due to erosion at the scale of the Republic of Mauritius as a whole. This description is the subject of this section of the report.

In accordance with the projection scenarios presented in 3.2.1, the work involved in estimating the coastline retreat hazard is also reflected in cartographic representations of the coastline projection. These representations are based on analyses and operations carried out using GIS. These operations include the following:

- Drawing coastline projections for three scenarios and three timeframes,
- Adjusting projections for sectors with mixed, sandy, and rocky coasts,

- Taking into account the projected rise in sea level by the year 2100.

The following chapter provides illustrative maps for informational purposes. A more comprehensive presentation of these maps is reserved for the chapter dedicated to the three « hot spots » (see section 4.3.2, report BRGM/RC-73988-FR).

*4.2.2.1.1.1 Current timeframe*

By the current deadline of 2025, the areas susceptible to coastal retreat along the Mauritius coastline are projected to range between 5 and 20 meters, contingent upon the intermediate scenario (Figure 75). Occasional retreats of 5 meters may occur on rocky coasts in the event of boulder falls on a cliff or extreme events impacting the surface of certain rocky slopes.

The highest-risk areas are low-lying sandy sectors that may be open to the ocean (passes or sectors without a coral lagoon). The intermediate scenario delineates three sectors where the current hazard zone is estimated at 20 meters. These coastal zones are characterized by a relatively elevated risk of erosion during a cyclone event, even in instances where the impact is limited in scope.

Figure 76 and Figure 77 illustrate the differences between the three scenarios for the current timeframe. The median scenario posits that the rocky coasts will not be eroded in the very short term, implying that approximately 25% of the homogeneous areas of Mauritius have a zero hazard. The remaining sedimentary coastline, however, is susceptible to retreat of 5 to 10 meters, contingent upon chronic erosion trends and the sensitivity of the coastline to cyclones.

The approach selected for the safe scenario diverges from the previous one: all coasts, including rocky coasts, may retreat, akin to the intermediate scenario. The retreat values are distributed between 5 and 25 meters, evenly allocating the values across the various retreat classes. In this scenario, the effect of chronic retreat, and more notably, the impact of cyclonic events is slightly greater, with 25% of the cells exhibiting retreats exceeding 20 meters.

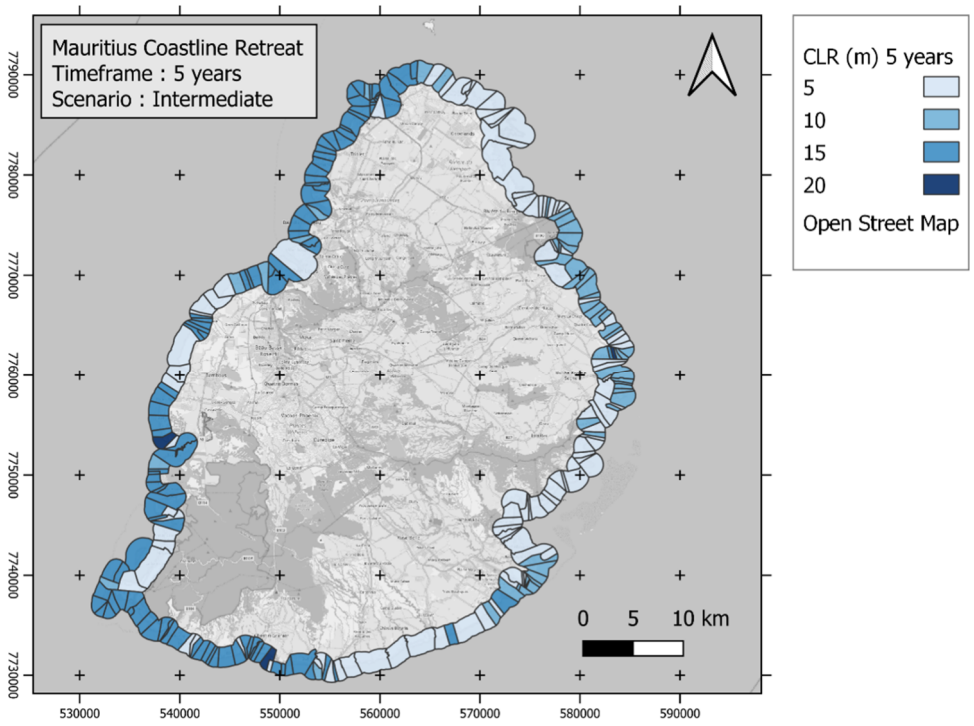


*Figure 75 : Map of potential coastline retreat (CLR) by sediment cell and homogeneous coastal zone in Mauritius for the current period and intermediate scenario.*

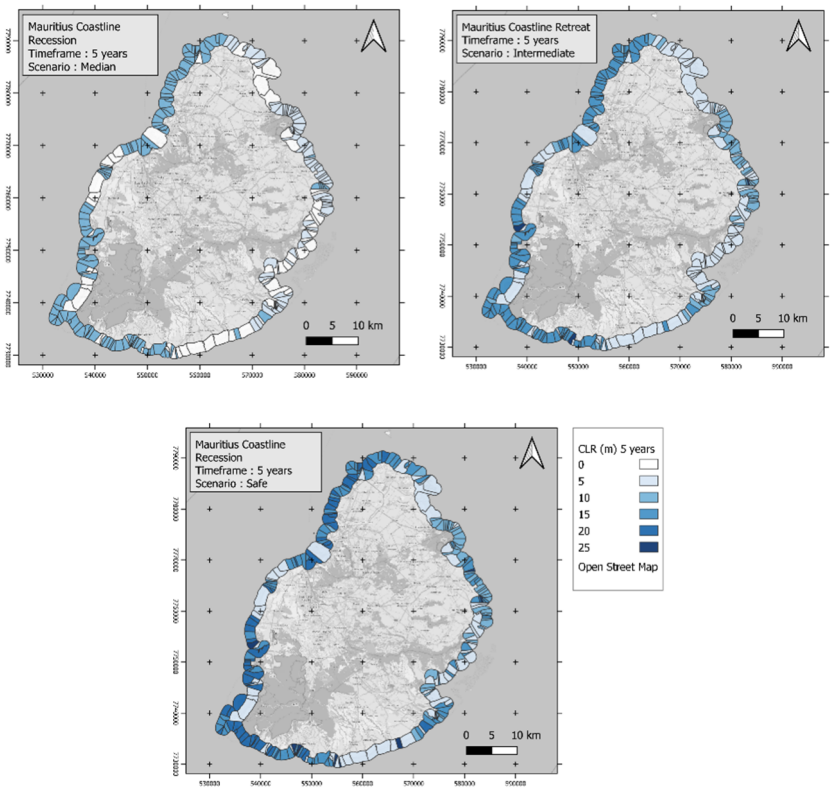


*Figure 76 : Maps of potential coastline retreat (CLR) by sediment cell and homogeneous coastal zones in Mauritius for the current period and the three studied scenarios.*

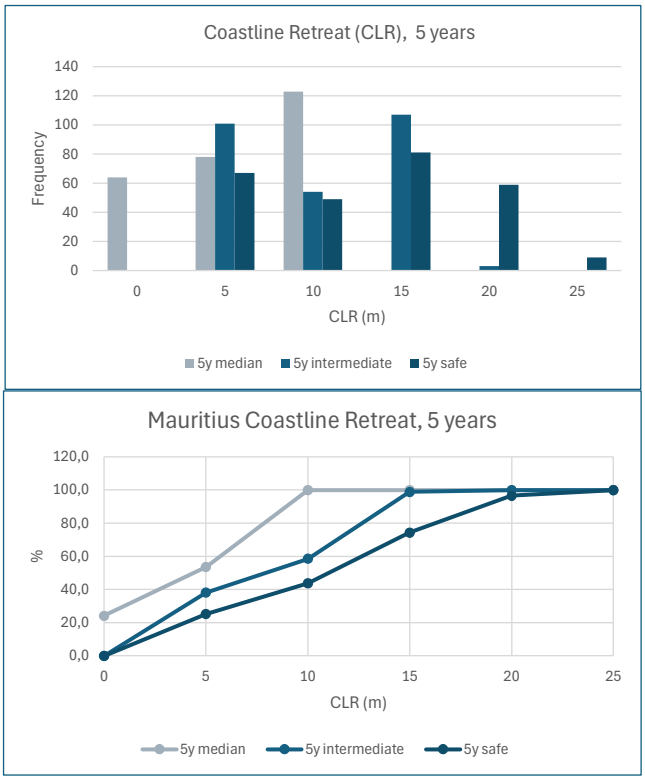


*Figure 77 : Assessment of potential coastline retreats (CLR) assessed by sedimentary cells and homogeneous zones for the current period in Mauritius. Frequency histogram and cumulative percentage graph.*

#### *4.2.2.1.1.2 Timeframe 2050*

At the 2050 timeframe, a period of 25 years henceforth, the areas susceptible to the retreat of the Maurice coastline are estimated to range between 5 and 50 meters, contingent upon the intermediate scenario (Figure 78). Punctual retreats of 5 meters may occur on rocky coasts, similar to current patterns. The 15, 20, and 25-meter retreat classes are the most prevalent, constituting 55% of the hazard values.

This intermediate scenario identifies 44 homogeneous areas where the risk of shoreline retreat in 2050 is between 30 and 50 meters. By this date, the effects of climate change and the impact of a cyclone on the coastline could be felt more acutely in these 44 sensitive areas of Mauritius.

Figure 79 and Figure 80 illustrate the possible differences depending on the scenario chosen to estimate the coastline retreat hazard zone in 2050.

The median scenario posits that approximately 80% of the homogeneous regions of Mauritius are susceptible to a coastline retreat hazard of less than or equal to 15 meters by the year 2050. The remaining 50 affected areas could undergo a retreat of between 20 and 30 meters.

In the context of the safe scenario, the rocky coastlines, constituting 25% of the homogeneous zones, are projected to recede by 10 meters. For sedimentary coasts, the setbacks extend between 25 and 40 meters for 50% of homogeneous coastal zones in Mauritius. The most precipitous retreats, which correspond to 15 to 20% of more sensitive coastal areas, are situated between 45 and 65m.

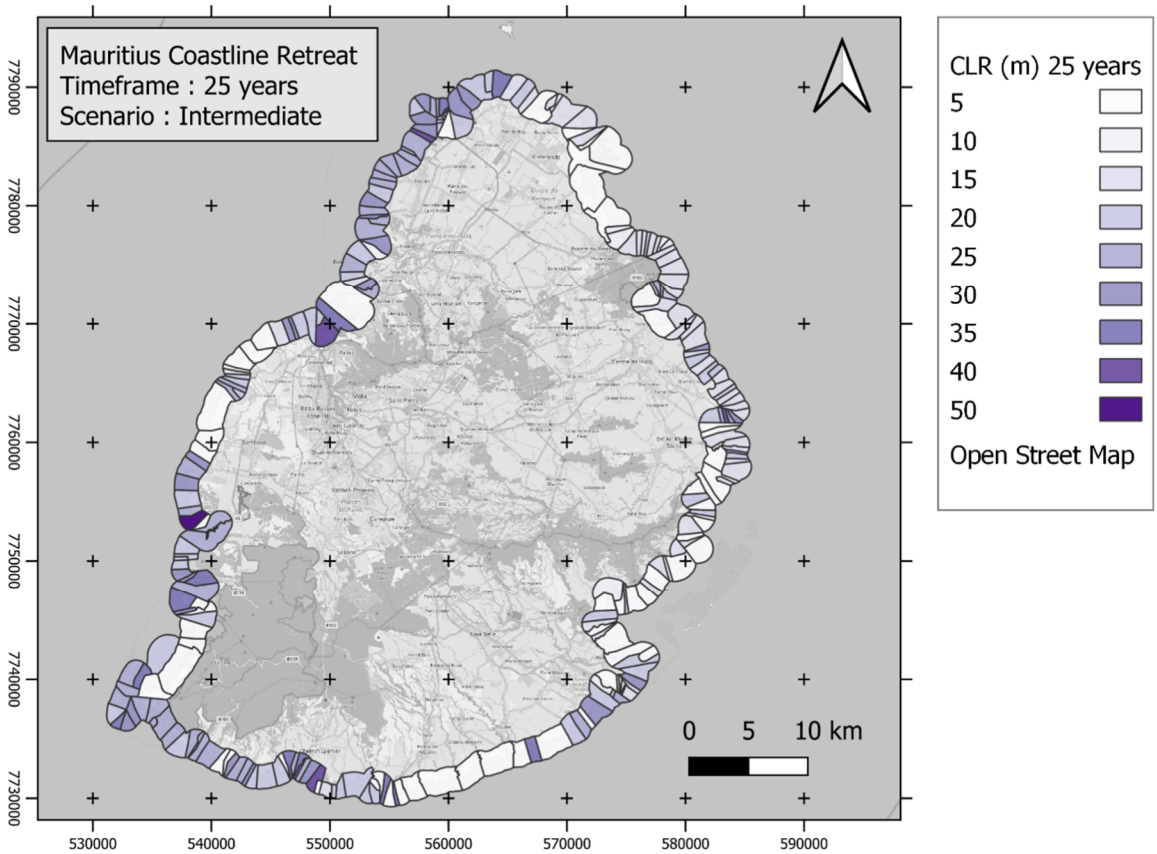


*Figure 78 : Map of potential coastline retreat (CLR) by sediment cell and homogeneous coastal zone in Mauritius for the 2050 period and intermediate scenario.*

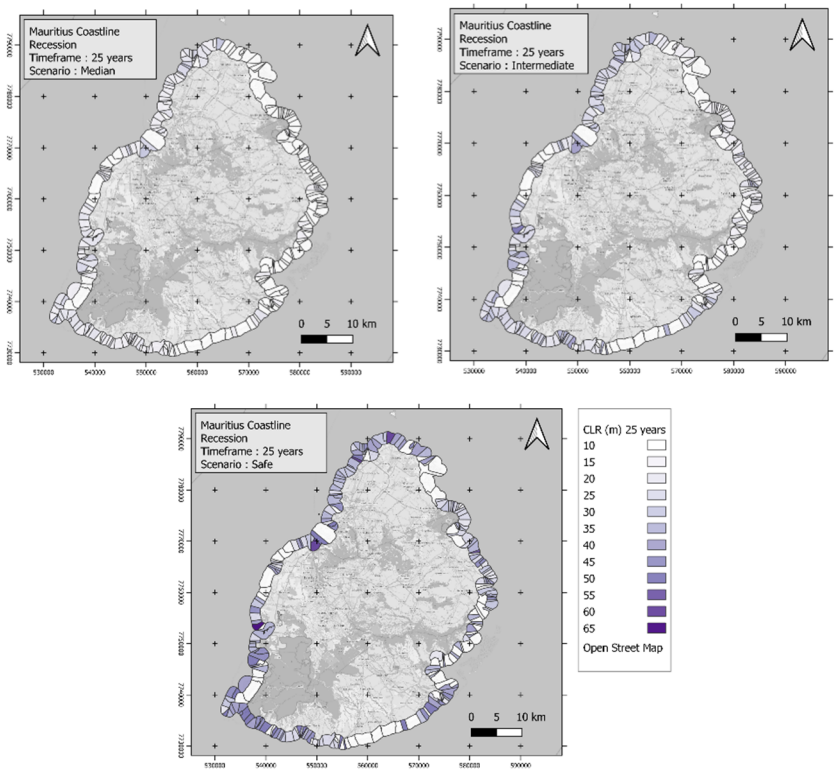


*Figure 79 : Maps of potential coastline retreat (CLR) by sediment cell and homogeneous coastal zones in Mauritius for the 2050 period and the three studied scenarios*

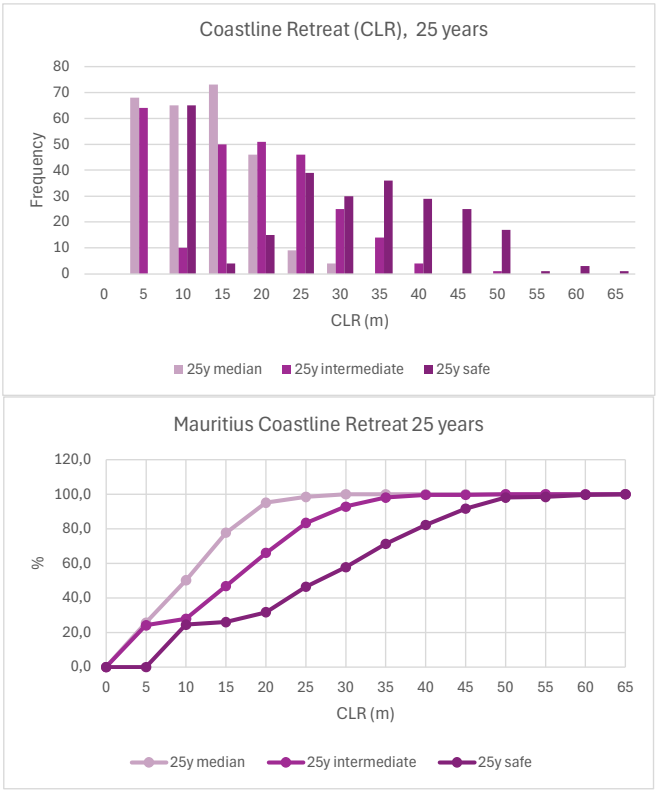


*Figure 80 : Assessment of potential coastline retreats (CLR) assessed by sedimentary cells and homogeneous zones for the 2050 period in Mauritius. Frequency histogram and cumulative percentage graph.*

#### *4.2.2.1.1.1 Timeframe 2100*

For a 75-year time horizon, by the year 2100, the areas at risk of coastal retreat in Mauritius are estimated to range from 10 to 160 meters, depending on the intermediate scenario (Figure 81). Occasional retreats of 10 meters may occur along rocky coastlines.

For sedimentary coastlines, the most frequent retreat ranges from 55 to 75 meters, representing slightly more than 35% of the homogeneous zones. The most sensitive homogeneous zones, which account for about 25% of the total, should be set back between 80 and 160 meters. Within this group, approximately 5% of homogeneous areas are expected to undergo retreats exceeding 100 meters, making them particularly vulnerable to the long-term effects of coastline retreat. These areas are likely to be significantly affected by climate change, depending on the additional erosion factors incorporated into the given scenario.

Figure 82 and Figure 83 illustrate the potential variations in the projected coastline retreat hazard zone for 2100, depending on the chosen scenario. By this time, uncertainties regarding the retreat of sandy coastlines become more pronounced, particularly with respect to sea level rise projections and the possible retreat values that may impact the coastal cells. These uncertainties lead to substantial differences between the various scenarios considered.

For homogeneous sedimentary zones under the median scenario, 45% of the zones are expected to retreat by 25 to 50 meters by 2100. These retreats are significantly lower than those projected under the intermediate scenario (55 to 75 meters). More sensitive homogeneous zones, which represent 30% of the sectors, are expected to face potential retreats between 55 and 110 meters.

In the safe scenario, the estimated range of retreats is particularly wide, spanning from 40 meters to 220 meters. The "majority" class accounts for 40% of homogeneous zones, with projected retreat hazard zones ranging between 60 and 95 meters. This class appears to be broader than in the intermediate scenario and exhibits slightly higher retreats. The differences between the intermediate and safe scenarios become particularly evident when examining the most sensitive homogeneous areas (30% of sectors in the safe scenario). Significant setbacks, ranging from 100 to 220 meters, are anticipated for these sectors, likely due to their high sensitivity to additional erosion induced by rising sea levels. The considerable discrepancies of several tens of meters between the intermediate and safe scenarios can be attributed to the substantial uncertainties associated with sea level rise projections, the erosion models employed, and the parameters considered in these long-term retreat estimates.

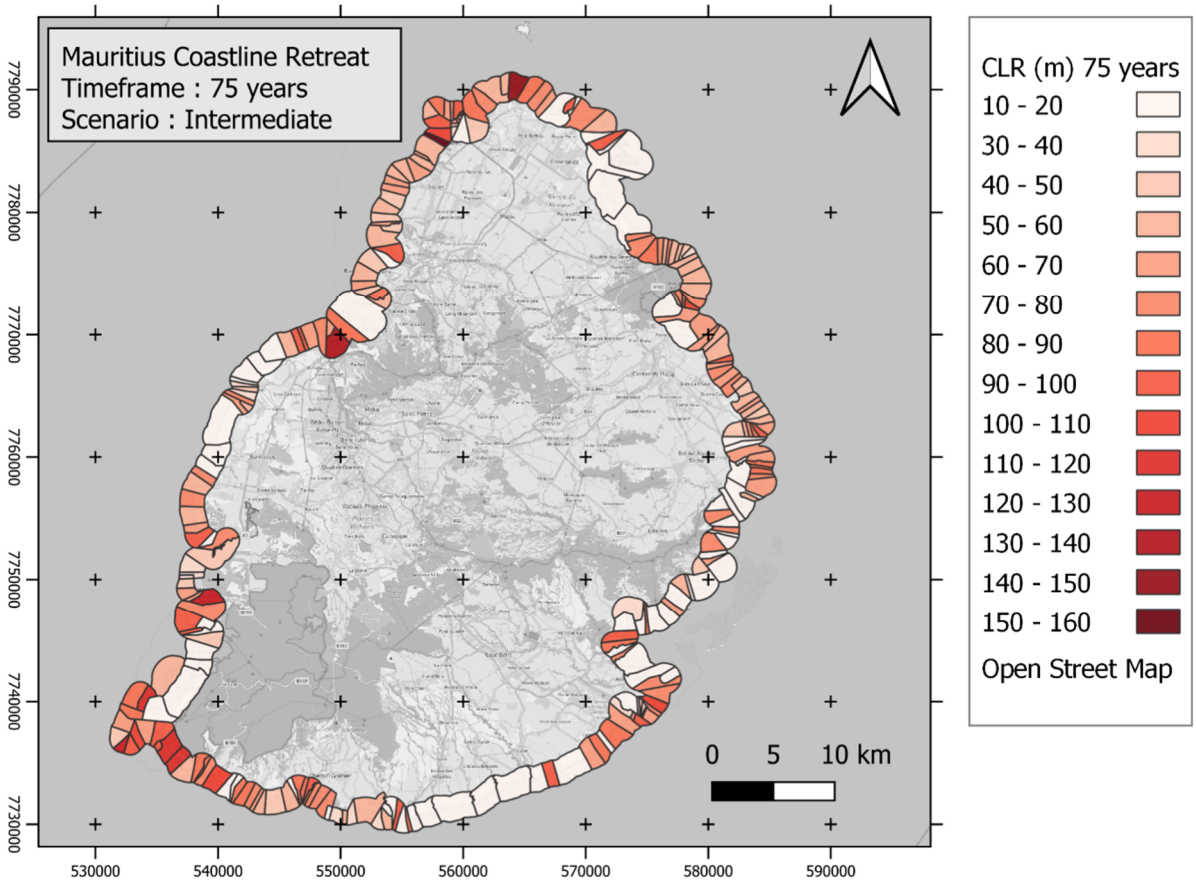


*Figure 81 : Map of potential shoreline retreat (CLR) by sediment cell and homogeneous coastal zone in Mauritius for the 2100 period and intermediate scenario.*

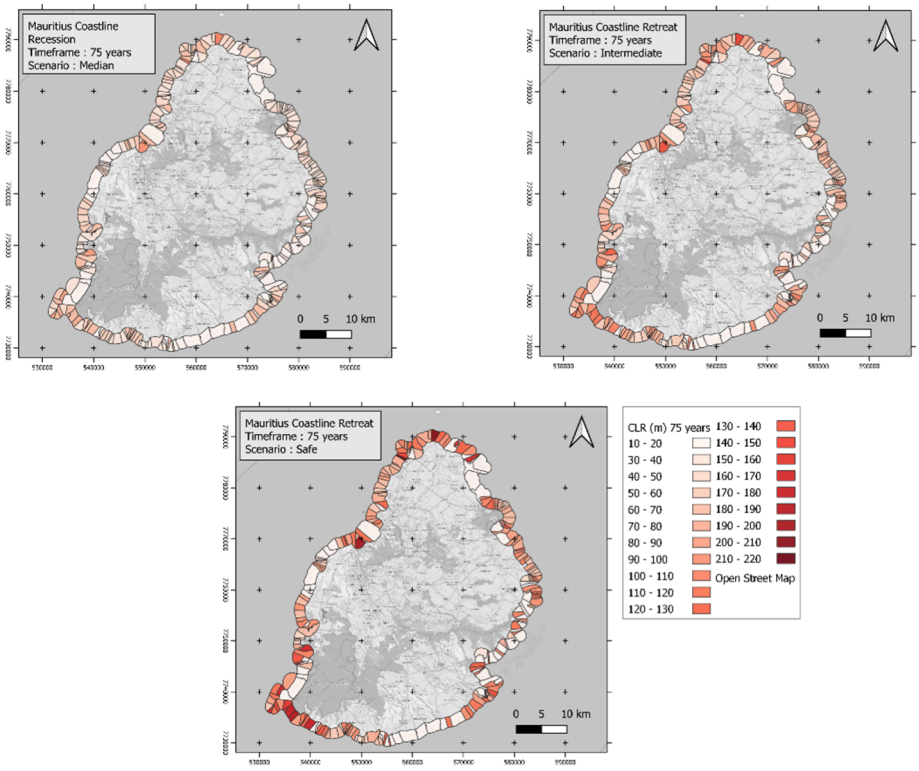


*Figure 82 : Maps of potential coastline retreat (CLR) by sediment cell and homogeneous coastal zones in Mauritius in 2100 (Mauritius) and the three studied scenarios*

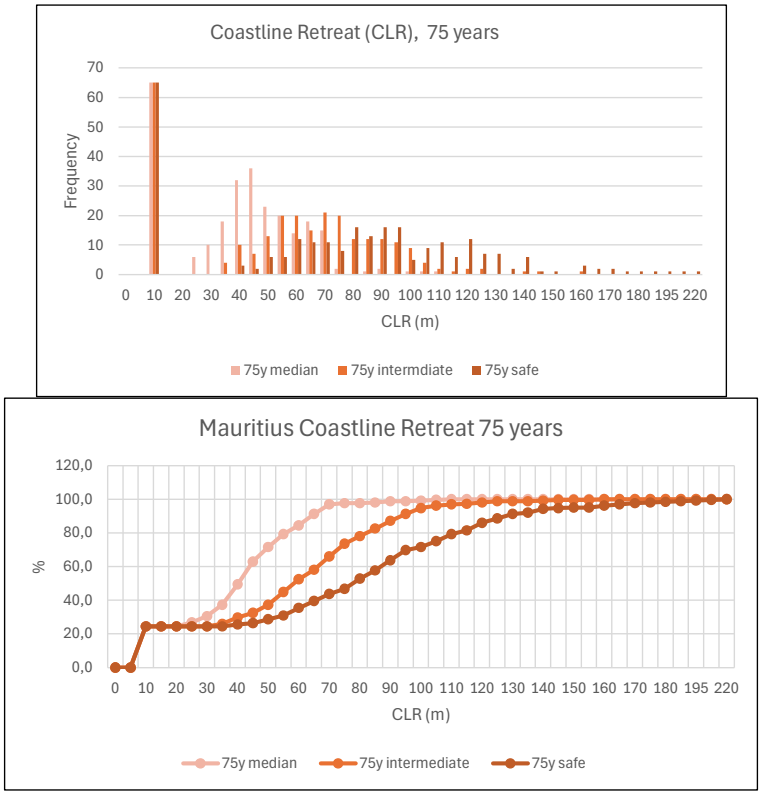


*Figure 83 : Assessment of potential coastline retreats (CLR) assessed by sedimentary cells and homogeneous coastal zones in 2100 (Mauritius). Frequency histogram and cumulative percentage graph.*

#### *4.2.2.1.2 Coastal flooding hazard*

##### *4.2.2.1.2.1 Model Validation on historical event*

The modelling approach described in the previous section was validated on the tropical cyclone Berguitta (2018). To this purpose we used data from the IBTrACS database (Knapp, et al. 2010, see Figure 84) to reconstruct wind and pressure fields using the parametric method described in Lecacheux et al 2012.

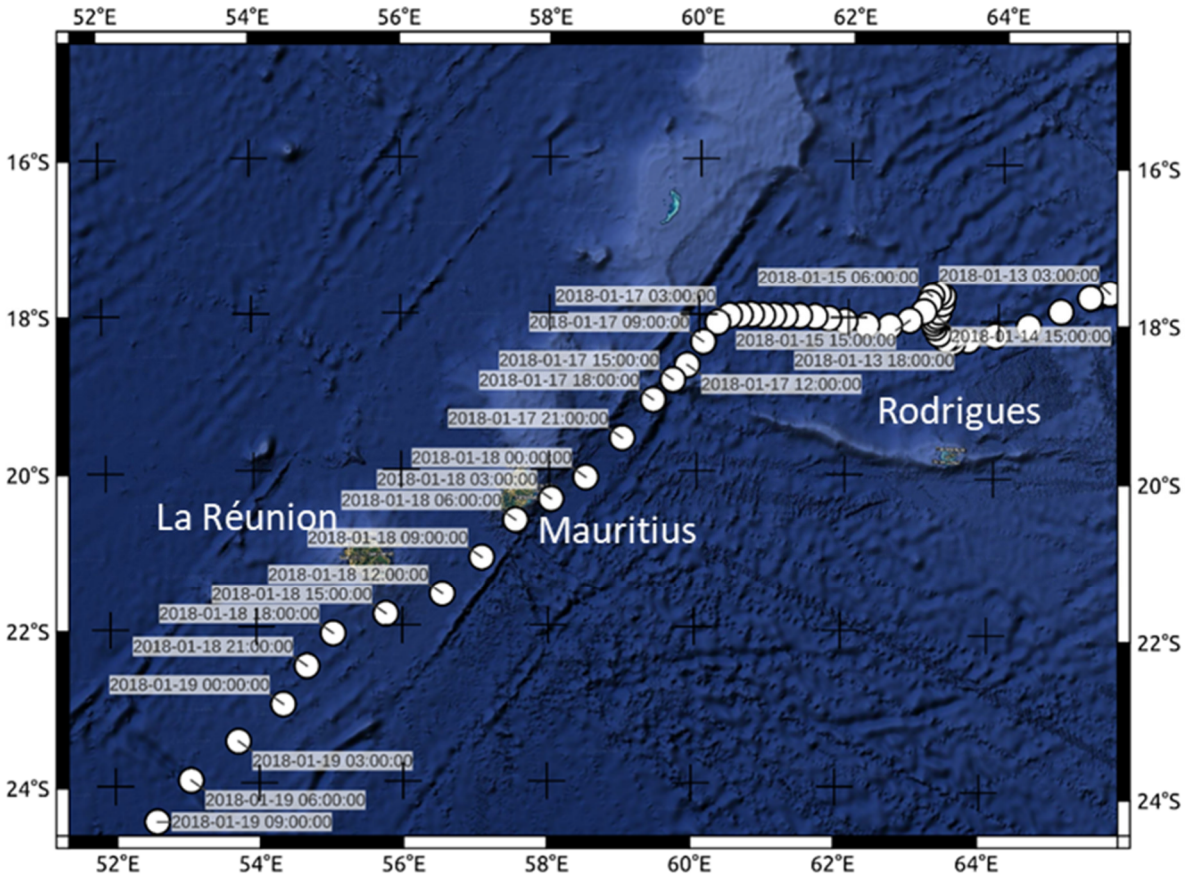


*Figure 84 : Cyclone Berguitta 2018 best track form the IBTrACS database.*

Figure 85 shows good agreement between the Hs from WW3 and the values observed by satellite (Piollé et al. 2020) with good reproduction of the maximum values close to 8m.

The modelling results show:

- Strong exposure of the eastern side of the island to waves propagating head-on to the coast with Hs exceeding 6m and Tp of 12 to 13s offshore (Figure 86);

- Maximum water levels of around ~1m on the north, east and south sides and ~0.7m on the west side (Figure 87);

- An excellent agreement between water levels calculated and measured on the Port-Louis tide gauge (Figure 88).

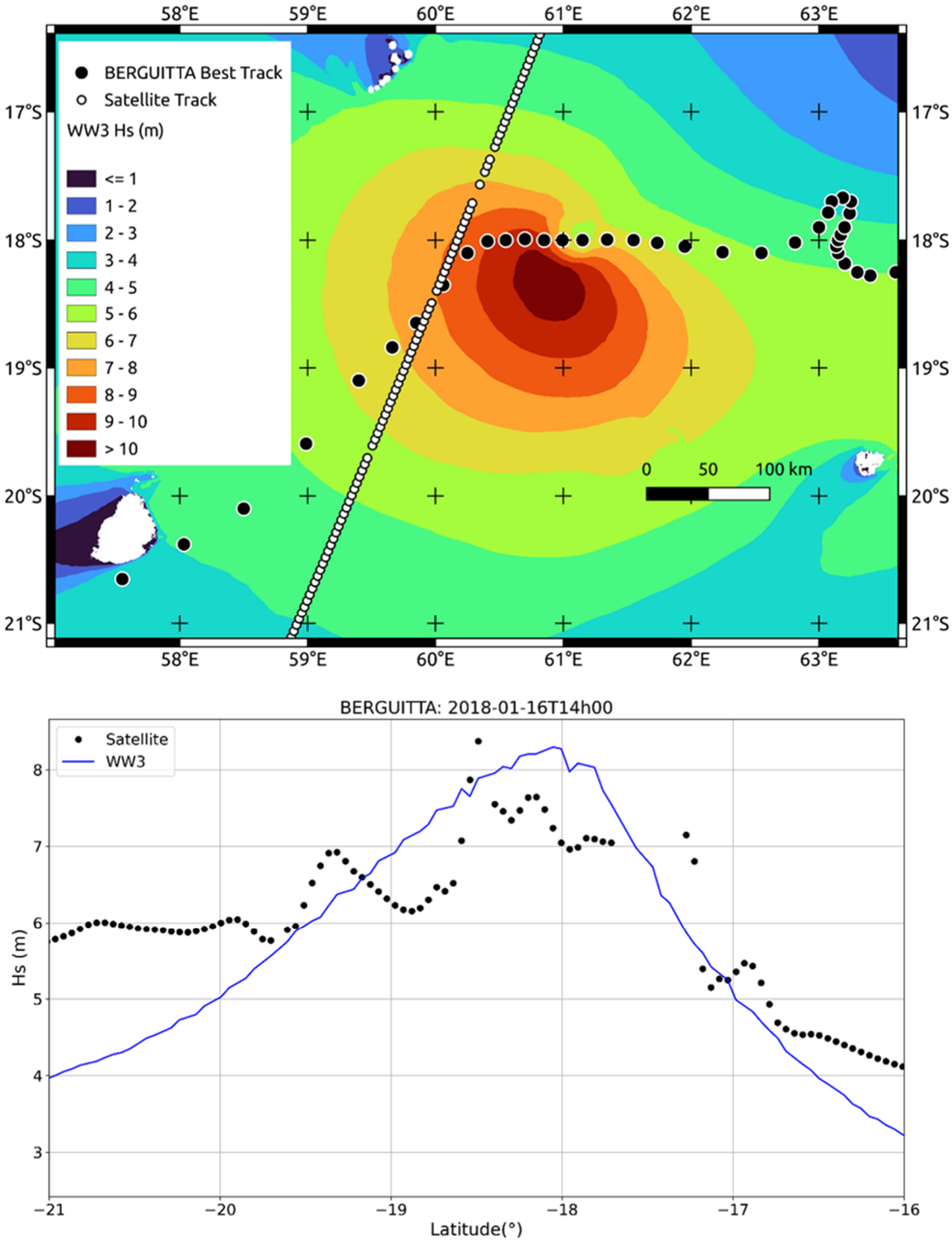


*Figure 85 : Comparison of waves from WW3 and satellites for TC Berguitta on 16/01/2018 at 14:00 UTC*

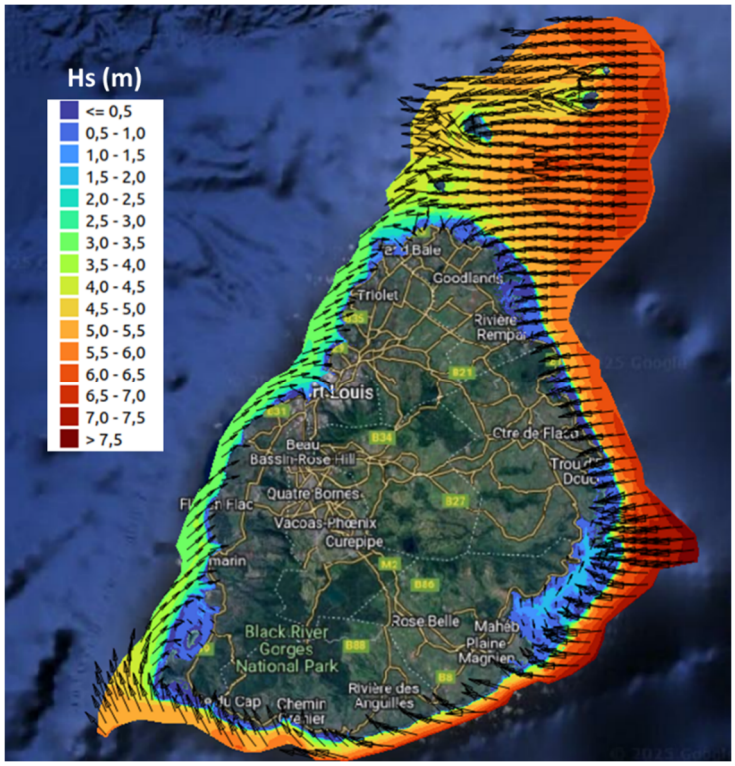


*Figure 86 : Simulation of maximum Hs and wave peak directions generated by Berguitta (2018) in Mauritius.*

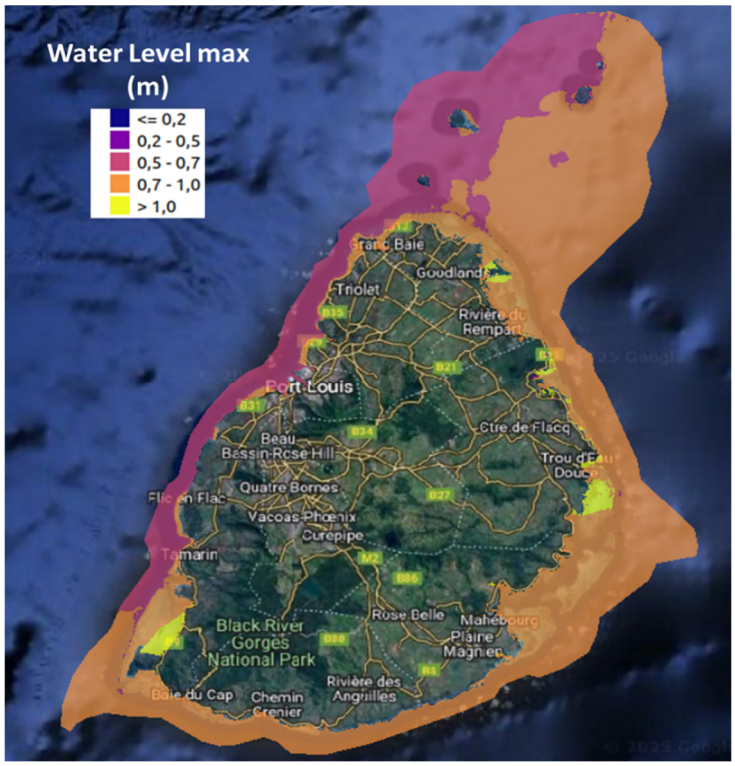


*Figure 87 : Simulation of maximum water levels generated by Berguitta (2018) in Mauritius.*

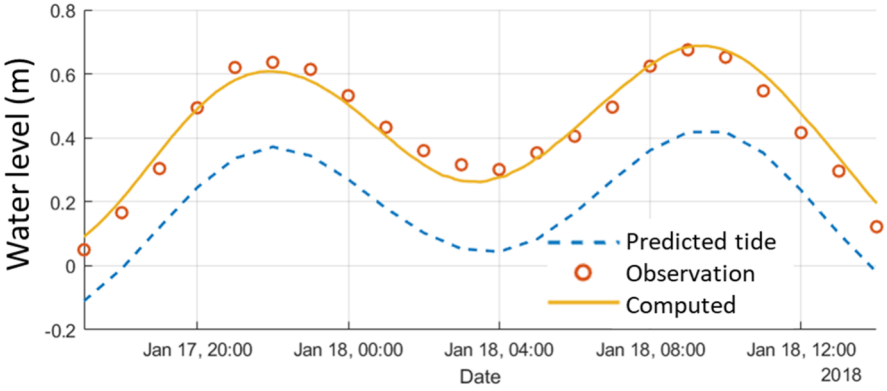


*Figure 88 : Validation of the computed water level against tidal gauge data at Port-Louis.*

A Defimedia video also shows overflows at the public beach of Poste Lafayette (Figure 89). This coastal flooding is also well reproduced by numerical simulation in the area, as shown in Figure 83. Water height less than 20cm have been calculated for much of the flooded area.



*Figure 89 : Extract from the video showing the coastal flooding on the public beach at Poste Lafayette during Berguitta (source, https://www.facebook.com/www.defimedia.info/videos/cyclone-berguitta-le-niveau-de-la-mer-monte-%C3%A0-poste-lafayette-dans-lest-de-l%C3%AEle/1717829278280088/).*

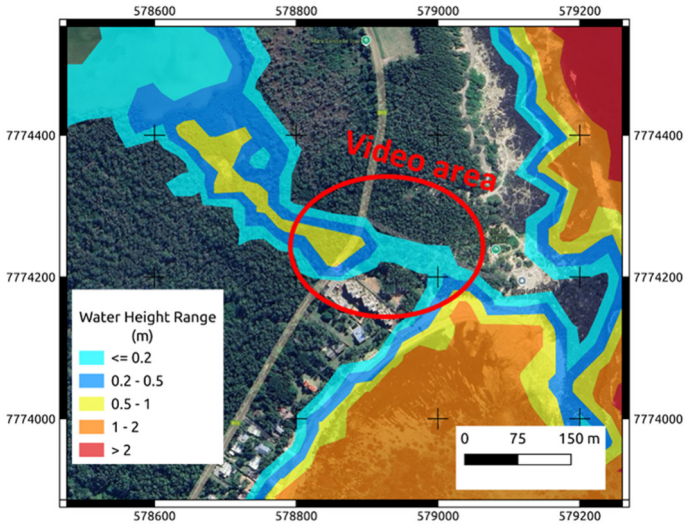


*Figure 90 : Simulated water heights on Poste Lafayette beach during Berguitta.*

#### *4.2.2.1.2.2 Determining actual, 2050 and 2100 climate reference scenarios*

As far as cyclones are concerned, it is very difficult to generate a realistic time series of meteo-oceanic forcing based solely on the parameters studied in the joint statistical analyses. It is also important to take into account the trajectory, chronology and variations in wind and wave direction.

One method of getting around this problem is to find, among the simulated scenarios, those whose wave, storm surge and wind speed parameters are closest to the joint centennial curves calculated ((§ 3.4.3) and to use them as reference scenarios (Pedreros et al. 2023, Bouvier et al. 2024).

We also need to take into account cyclone tracks and, in the case of Mauritius, consider cyclones that pass through the western and eastern seaboards.

Based on these criteria, the scenarios selected to represent one hundred years return period conditions are:

- on actual and 2050 climate: 1498 and 357 Intense Tropical Cyclone (ITC);
- on 2100 climate: 1498 (ITC) and 2423 Very Intense Tropical Cyclone.

Figure 91 and Figure 92 show the position of these scenarios in the joint exceedance iso-contours for return period of 100 years for the different climate horizons.

The tracks of these scenarios cover the east and west sides of Mauritius (Figure 93).

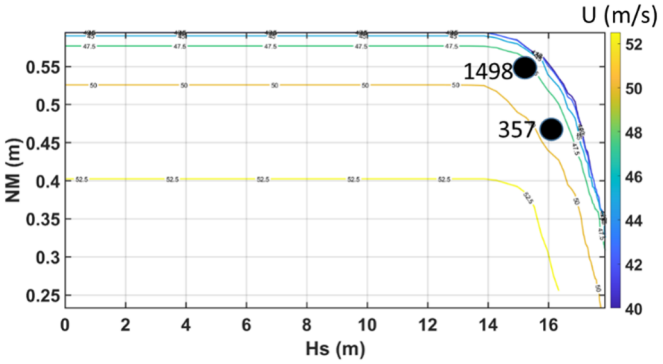


*Figure 91 : Positioning of scenarios 1498 and 357 in the joint exceedance iso-contours for return period of 100 years within the space (NM ; Hs) with the colour indicating the U values in Mauritius forcing point for actual and 2050 climate scenario.*

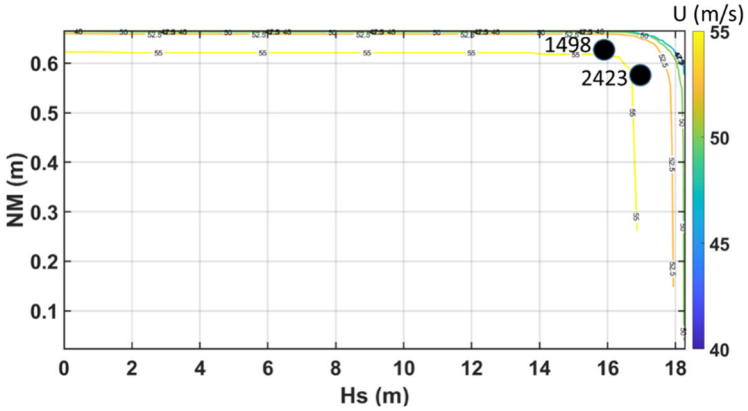


*Figure 92 : Positioning of scenarios 1498 and 2423 in the joint exceedance iso-contours for return period of 100 years within the space (SSH ; Hs) with the colour indicating the U values in Mauritius forcing point for 2100 climate scenario.*

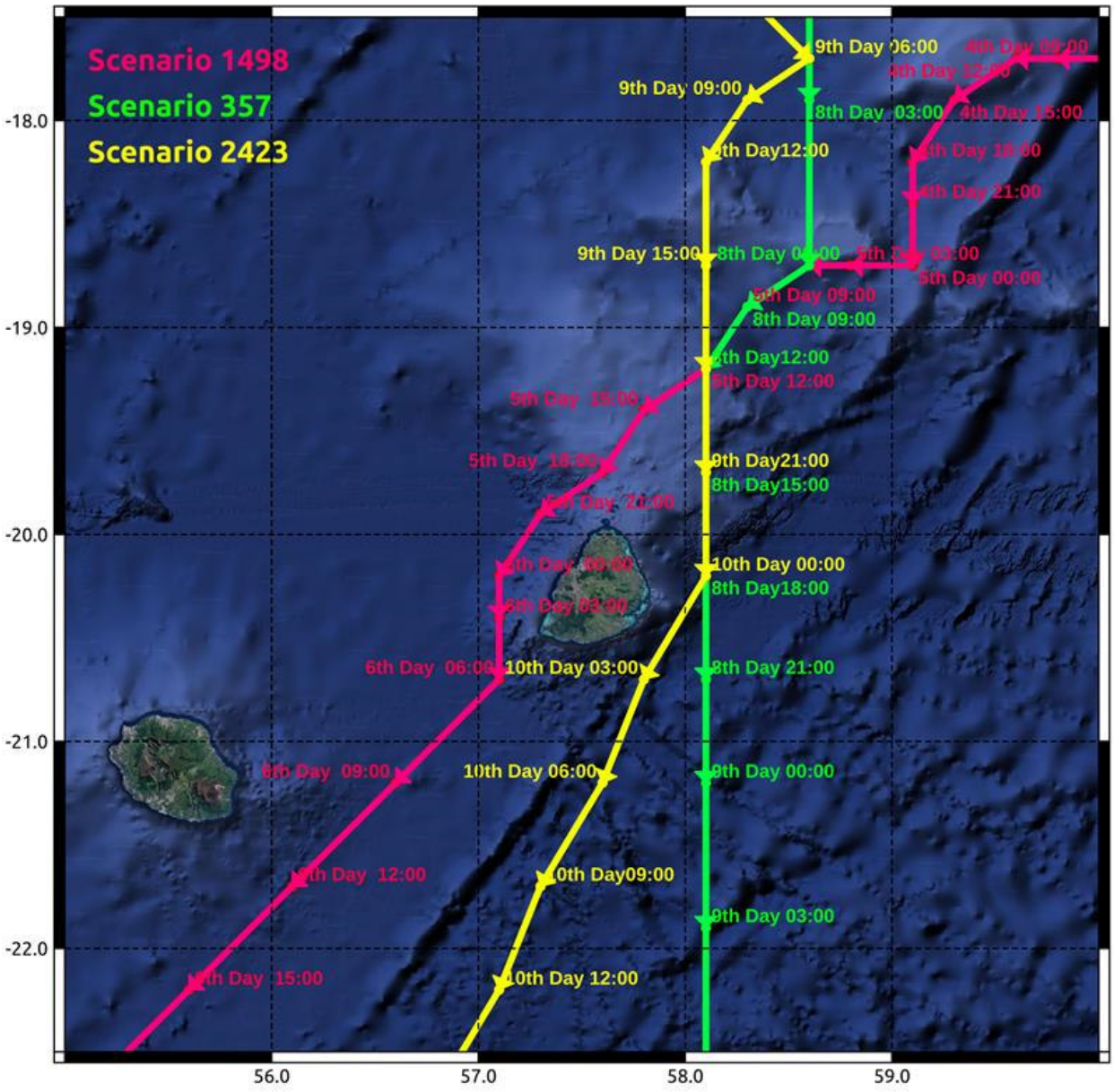


*Figure 93 : Cyclones' tracks for the three chosen scenarios 357, 1498, and 2423 of the Météo-France database.*

In the following, we will show the pressure and wind fields of the selected scenarios, directly on the computational grid. Moreover, we also report the tidal signal imposed as boundary condition to our numerical simulations, provided by FES2014 on the forcing points of the boundary. The taken tidal signals are representative of a Mean High Water Springs conditions in the area, and we have phased the signals so that the considered scenarios will strike under similar tidal conditions.

Some offsets are applied to account for different contributions and to account for the sea level rise on different climate conditions. In particular, the offsets used in this study are composed as follows:

- **+ 0.25 m of security margin**: the study by Barroso et al. 2024 reveals annual and monthly anomalies in mean sea levels (MSL) at 798 tide gauges around the world, with amplitudes that can exceed 18cm. These anomalies are generally attributed to steric effects of water

levels associated with heat fluxes and water exchange with the atmosphere, ocean circulation, precipitation, and river discharge (Qu et al., 2022) and the influence of gyres (Wu et al. 2020). What about Mauritius? The analysis of de-trended monthly variations of the mean sea level (MSL) at the Port-Louis tide gauge between 1986 and 2024 (Figure 94) shows higher MSL values during the cyclone period (December to March), with mean/maximum values of up to ~10cm and over 30cm respectively. It is therefore important to allow a security margin to take into account these anomalies. The value used for this type of study is 0.25 m (Laigre et al. 2024, Bouvier et al. 2024).

- **+ 0.27 m**: sea level rise at horizon 2050 (§ 3.5.3.4.1);
- **+ 0.87 m**: sea level rise at horizon 2100 (§ 3.5.3.4.1).

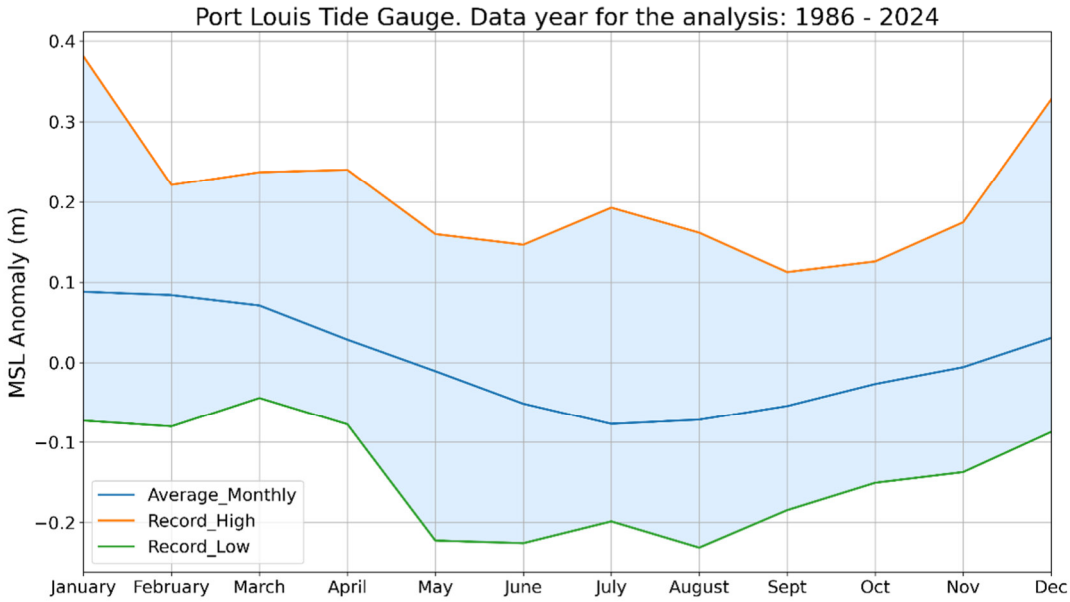


*Figure 94 : De-trended monthly MSL (mean sea level) plotted for each month of the year for the length of the respective tide gauge record of Port-Louis (1986-2024).*

**The scenario 357:**

The track of this cyclone passes to the east of the Maurice's island (green line on Figure 93). The same atmospheric forcing has been used for both the actual and 2050 climate events, since the differences on the pressure (Figure 95) and wind intensity fields (Figure 96) are negligible.

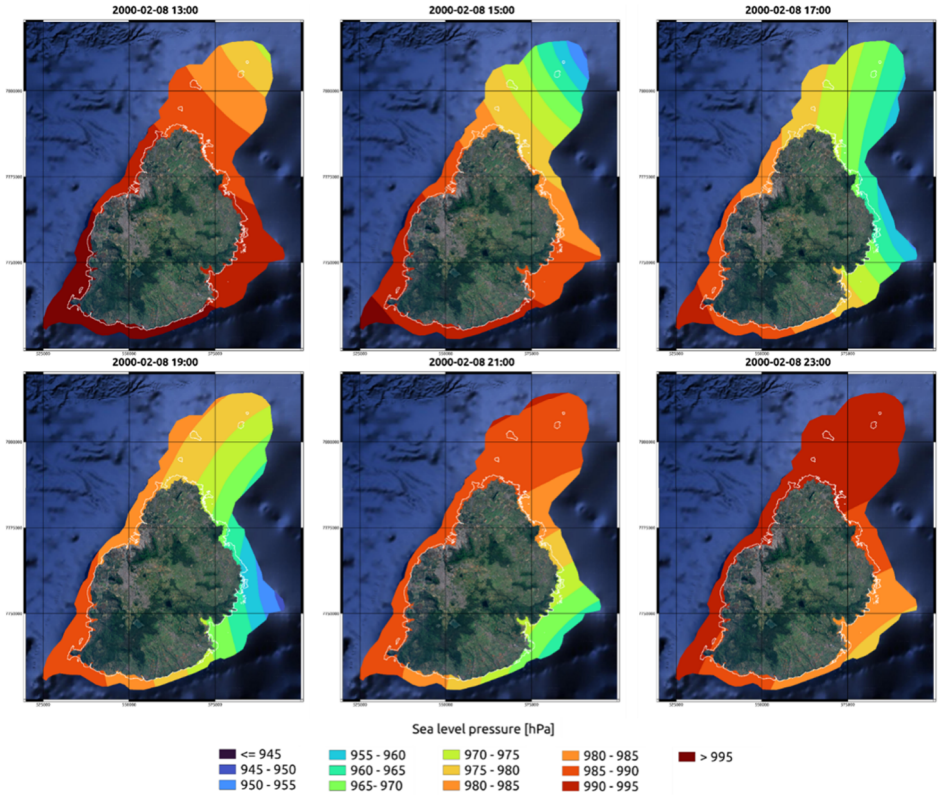


*Figure 95 : Time evolution of the pressure field over the Mauritius computational domain during the 357 scenario on actual and 2050 climate.*

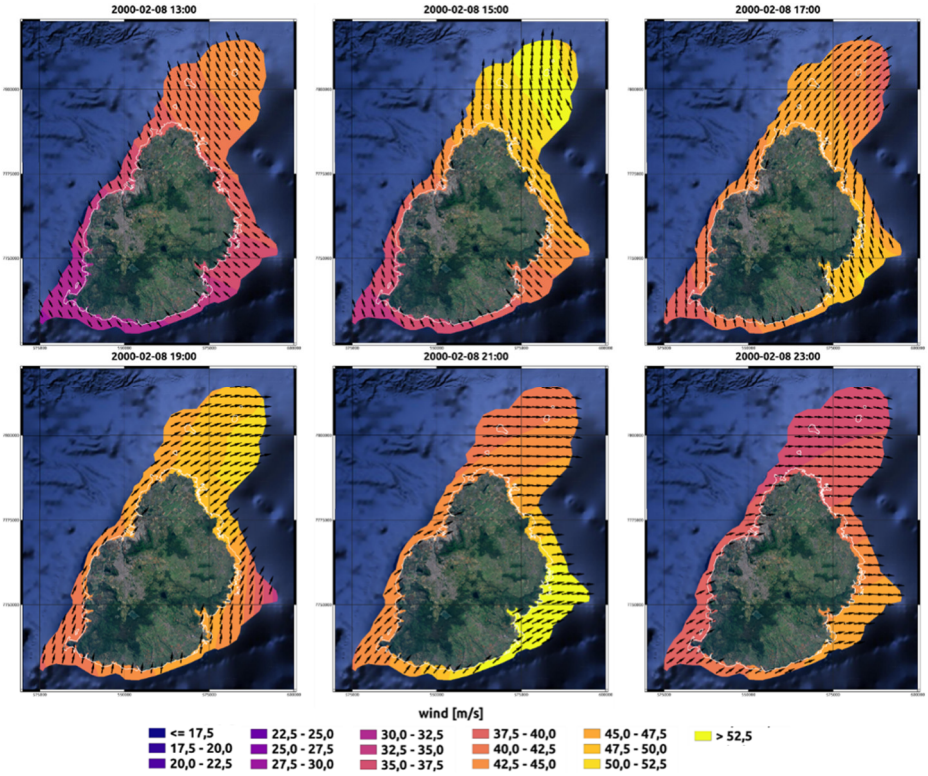


*Figure 96 : Time evolution of the wind field over the Mauritius computational domain during the 357 scenario on actual and 2050 climate.*

The sea level boundary signals for this scenario are displayed on Figure 97. It can be noticed that the cyclone approaches the island the most at around 18:00 on the 08/02, in correspondence of the second peak of the tide.

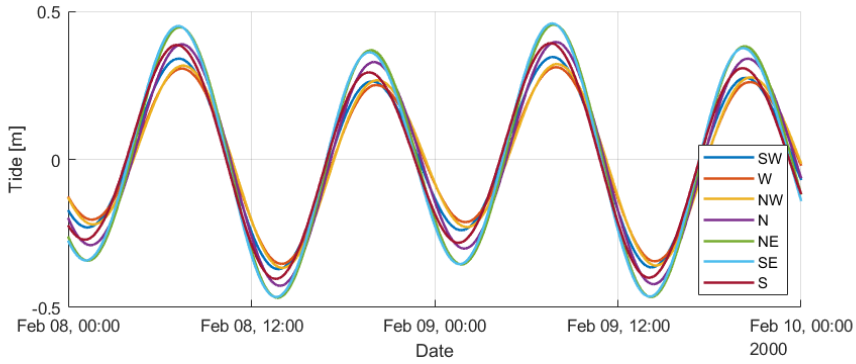


*Figure 97 : Tidal signal during the 357 scenarios, provided by the FES2014 database on the seven forcing locations of the Mauritius model.*

**The scenario 1498:**

The track of this cyclone passes to the west of the Maurice's island (pink line on Figure 93). As it was the case for the previous scenario, also here little difference exist between the actual and 2050 climate scenarios. Therefore, the same atmospheric forcing has been used for both the events. The pressure and wind fields are displayed in Figures Figure 98 and Figure 99 respectively. A significant increase in intensity can be appreciated, instead, on 2080-2100 climate in both depression and wind intensities (Figures Figure 100 and Figure 101 respectively).

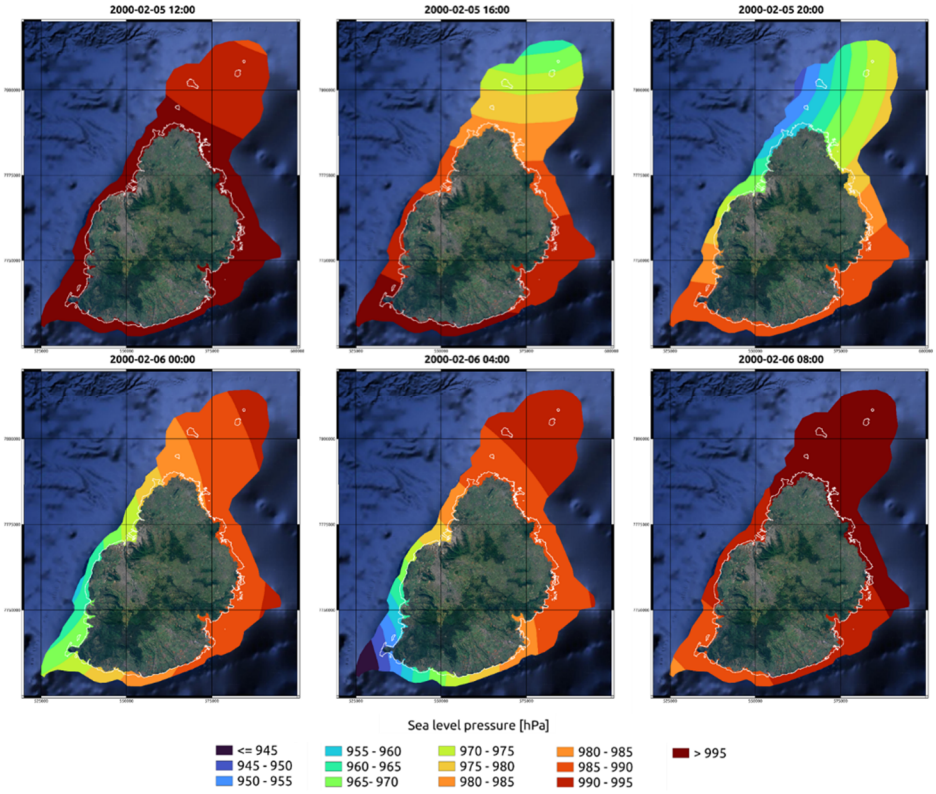


*Figure 98 : Time evolution of the pressure field over the Mauritius computational domain during the 1498 scenario on actual and 2050 climate.*

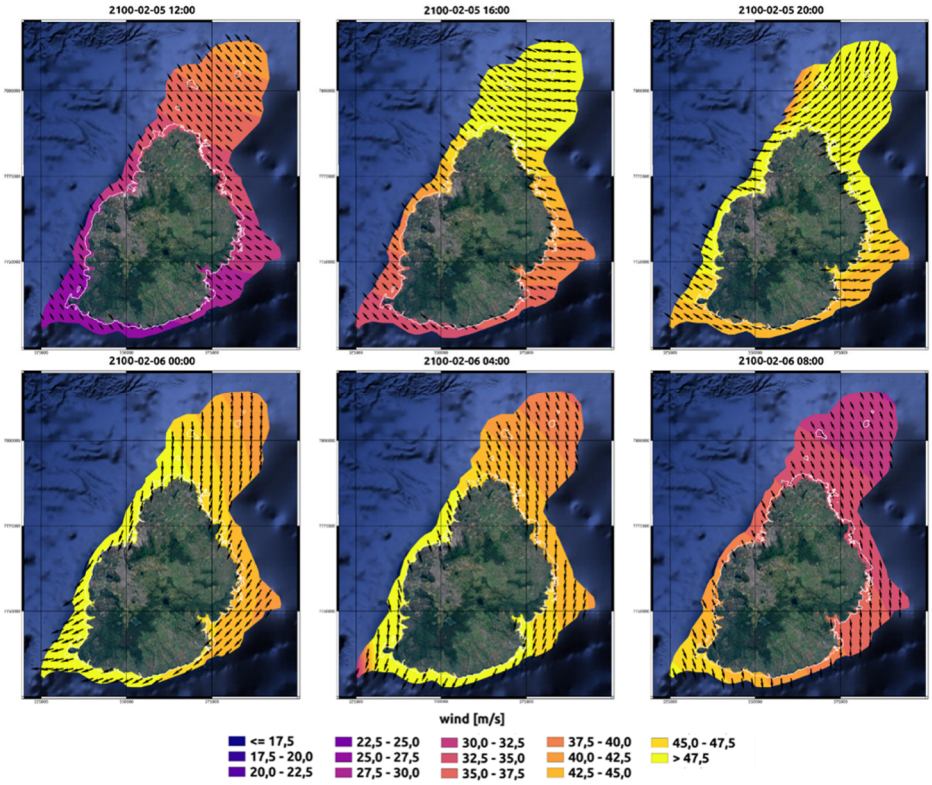


*Figure 99 : Time evolution of the wind field over the Mauritius computational domain during the 1498 scenario on actual and 2050 climate.*

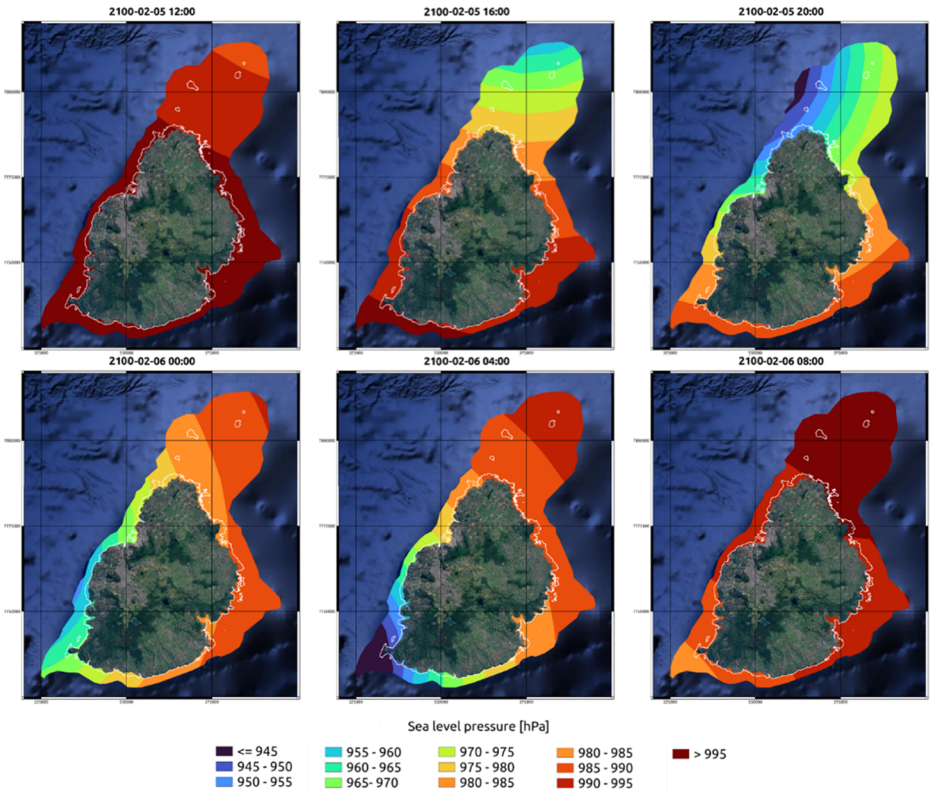


*Figure 100 : Time evolution of the pressure field over the Mauritius computational domain during the 1498 scenario on 2080-2100 climate.*

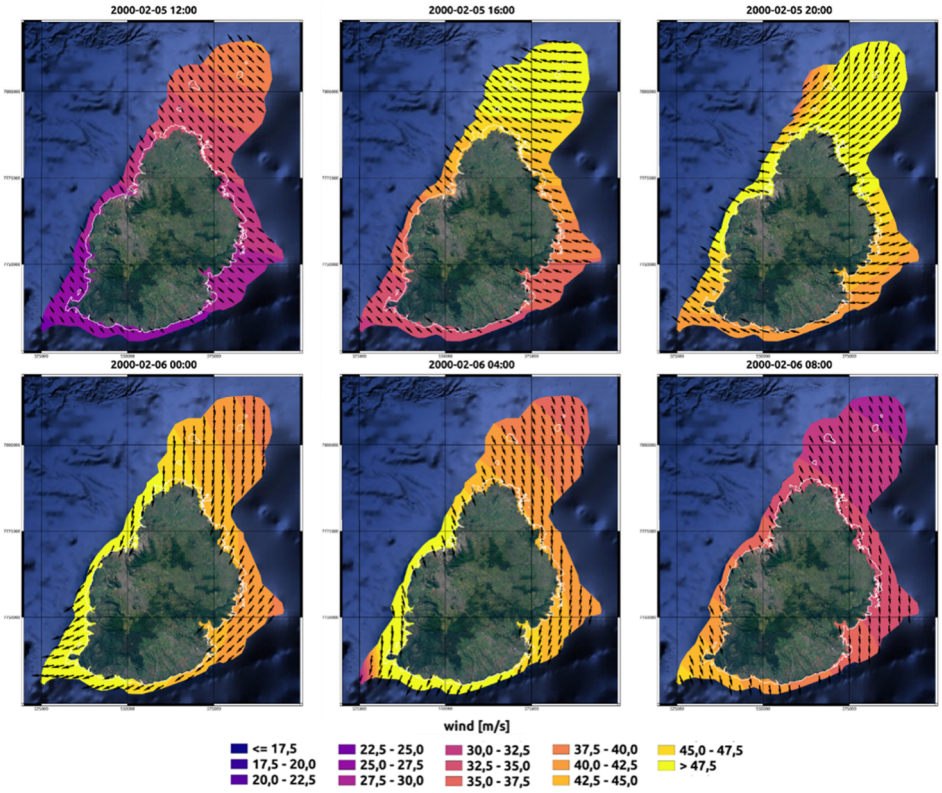


*Figure 101 : Time evolution of the wind field over the Mauritius computational domain during the 1498 scenario on 2080-2100 climate.*

The sea level boundary signals for this scenario are displayed on Figure 102. It can be noticed that the cyclone approaches the island from north at around 20:00 on the 05/02, in correspondence of the third peak of the tide, thus, in comparable tidal conditions to the previous scenario 357. Almost five tidal period are simulated in this scenario, in contrast to the four of the previous case. This is due to the different (slower) travelling speed of the cyclone and to its particular track that strictly follows the west coast of the island before leaving to the south-west.

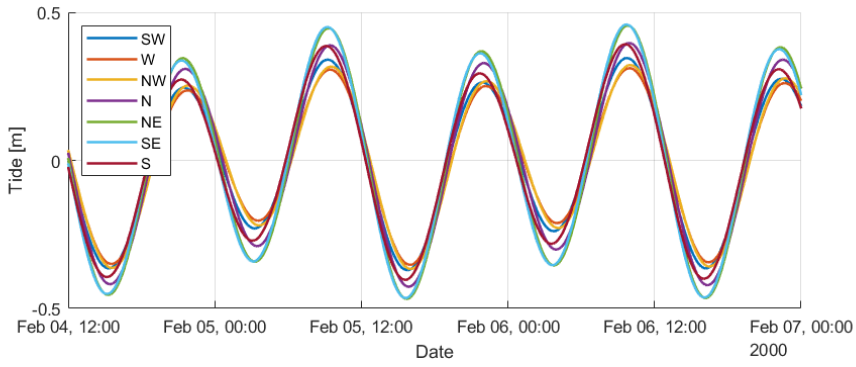


*Figure 102: Tidal signal during the 1498 scenario, provided by the FES2014 database on the seven forcing locations of the Mauritius model.*

**The scenario 2423:**

The track of this cyclone is close to the 357's one, passing to the east of the Maurice's island (yellow line on Figure 93). However, as far as scenario 357 was the majoring one (on the east side of the island) on actual and 2050 climate, the scenario 2423 becomes more relevant on 2100 climate. His pressure and wind fields are represented in Figure 103 and Figure 104 respectively.

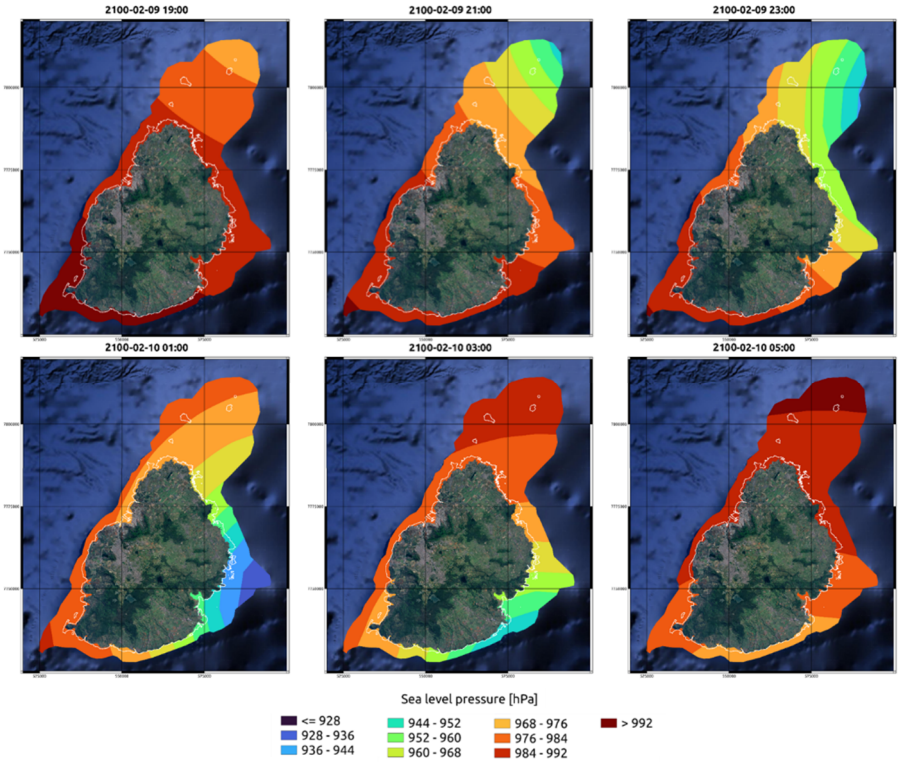


*Figure 103 : Time evolution of the pressure field over the Mauritius computational domain during the 2423 scenario on 2100 climate.*

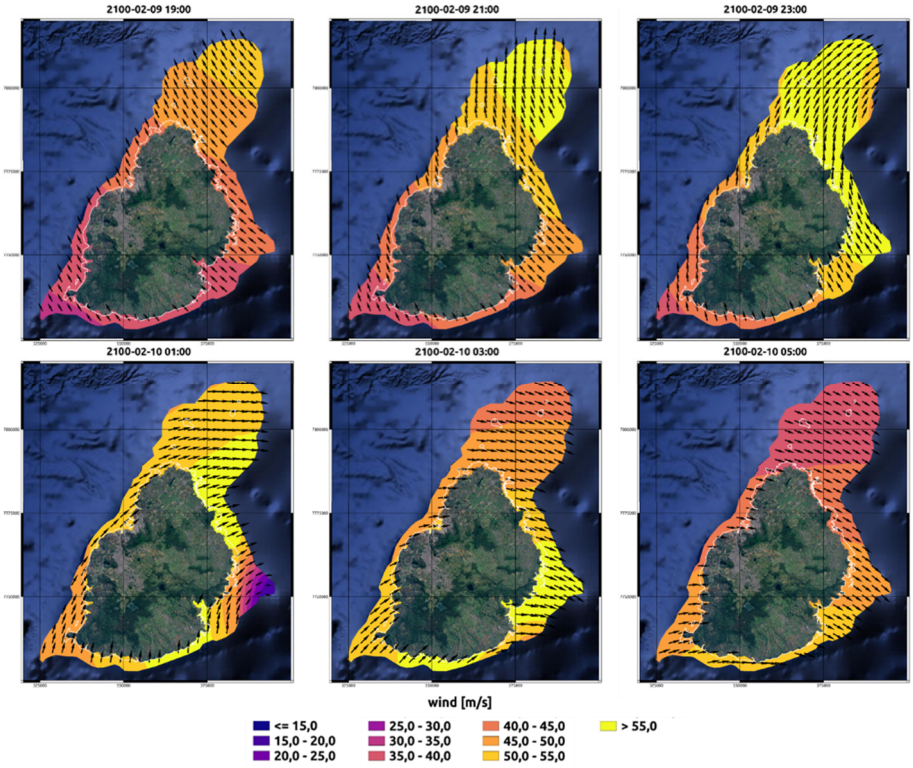


*Figure 104 : Time evolution of the wind field over the Mauritius computational domain during the 2423 scenario on 2100 climate.*

As for the previous scenarios, we report in Figure 105 the sea level signals imposed at the boundaries of the computational domain. The cyclone approaches the island at around 23:00 on the 09/02, in comparable tidal conditions to the two previous scenarios. Almost five tidal periods are simulated also in this case.

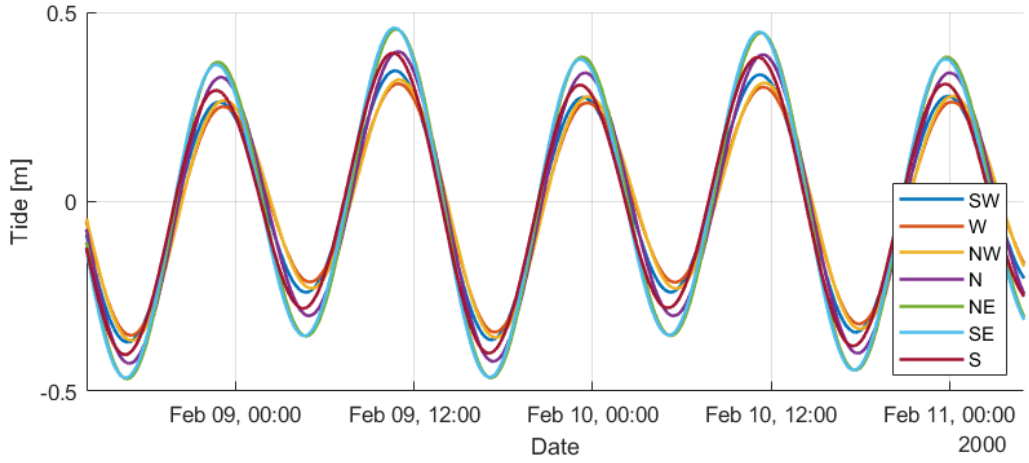


*Figure 105 : Tidal signal during the 2423 scenario, provided by the FES2014 database on the seven forcing locations of the Mauritius model.*

#### *4.2.2.1.2.3 Simulation results*

The simulated scenarios generate the wave fields described by the following Figure 106, Figure 107 and Figure 108. The scenario 1498 is characterized by extreme values of the maximum significant wave height (Hs_max) investing all sides of the island, except of the south coast which appear to be screened and protected by the presence of the island itself. The values of Hs_max that we observe are around 14m on the west side of island, while surpassing 15m on the north and east sides (these values augment of about 0.5m everywhere under 2100 climate conditions). The northern island shelf plays an important role in reducing Hs to about 12m before the waves reach the lagoon reef. Where the reef is present (North-Est, south-east and south-west coasts) waves break outside of it and we find very low values of Hs inside the lagoons (<1,5m). Slightly higher values can be seen inside the south-east lagoon, where the large channels allow waves to penetrate with larger amplitudes, ~2,5m and attending 3m in some zones. The west coast is particularly exposed to wave's action. This can induce flooding by overtopping, as we will discuss in the specific section devoted to the Flic-en-Flac site (§ 4.3.4.1.2).

The waves pattern produces by cyclones 357 and 2423 is, in some sort, complementary to the previous one. There are still strong values of Hs investing the island from east (~14,5m for the 357 and attending 17,5m on the scenario 2423), but the south coast is also experiencing 14m of Hs while the west is fully protected by the island itself. Waves cross the northern insular shelf predominantly in the east-west direction and Hs is much more reduced than in the previous 1497 scenario, when they finally approach the reef (Hs = ~10m). Again, the reefs play a fundamental role in breaking the incoming waves, but the south-east lagoon is penetrated with (on average) higher Hs values than in the previous 1497 case. However, the main different in here is given by the waves orientation, which is directed south-west on the 1497 scenario and north-west on the 357 and 2423 ones.

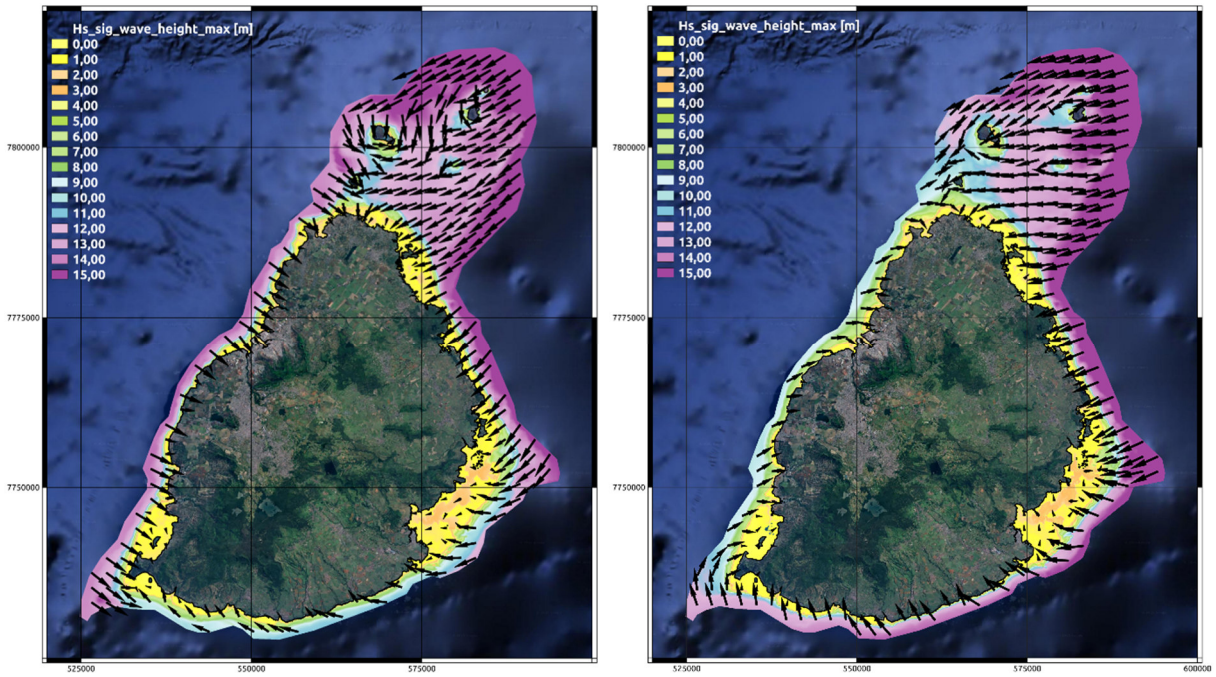


*Figure 106 : Overall map of the computed maximum significant wave height with actual climate on scenarios 1498 (left) and 357 (right).*

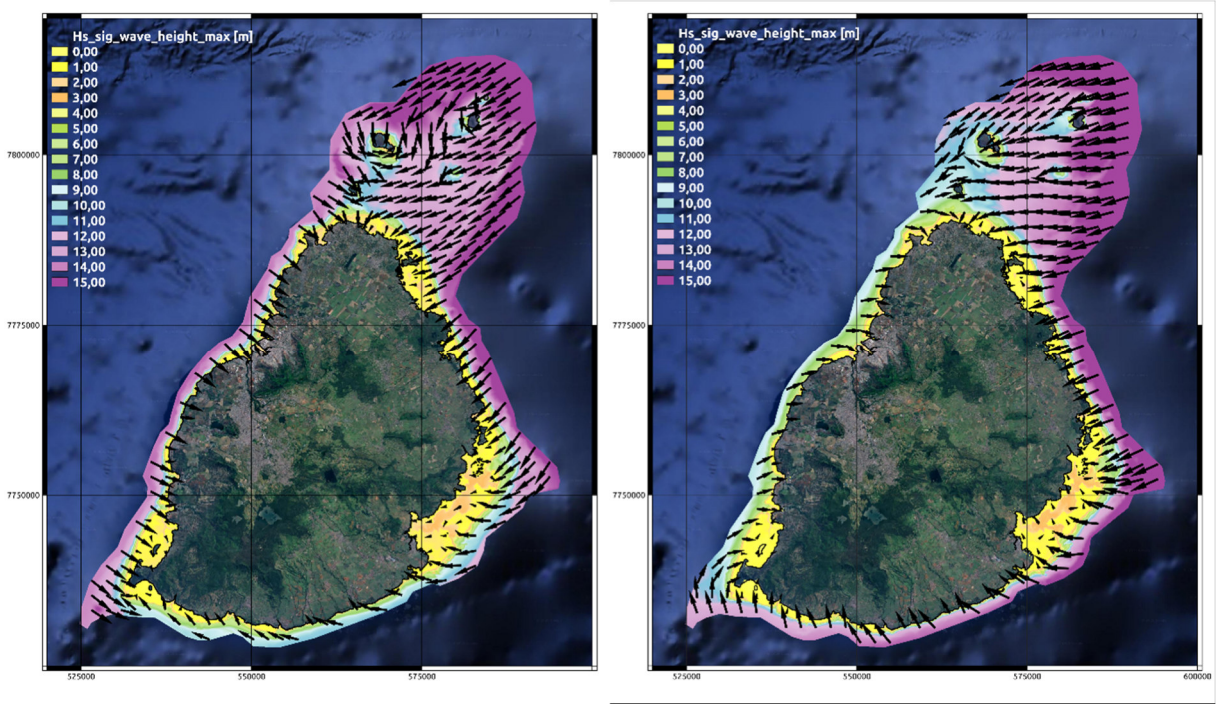


*Figure 107 : Overall map of the computed maximum significant wave height with 2050 climate on scenarios 1498 (left) and 357 (right).*

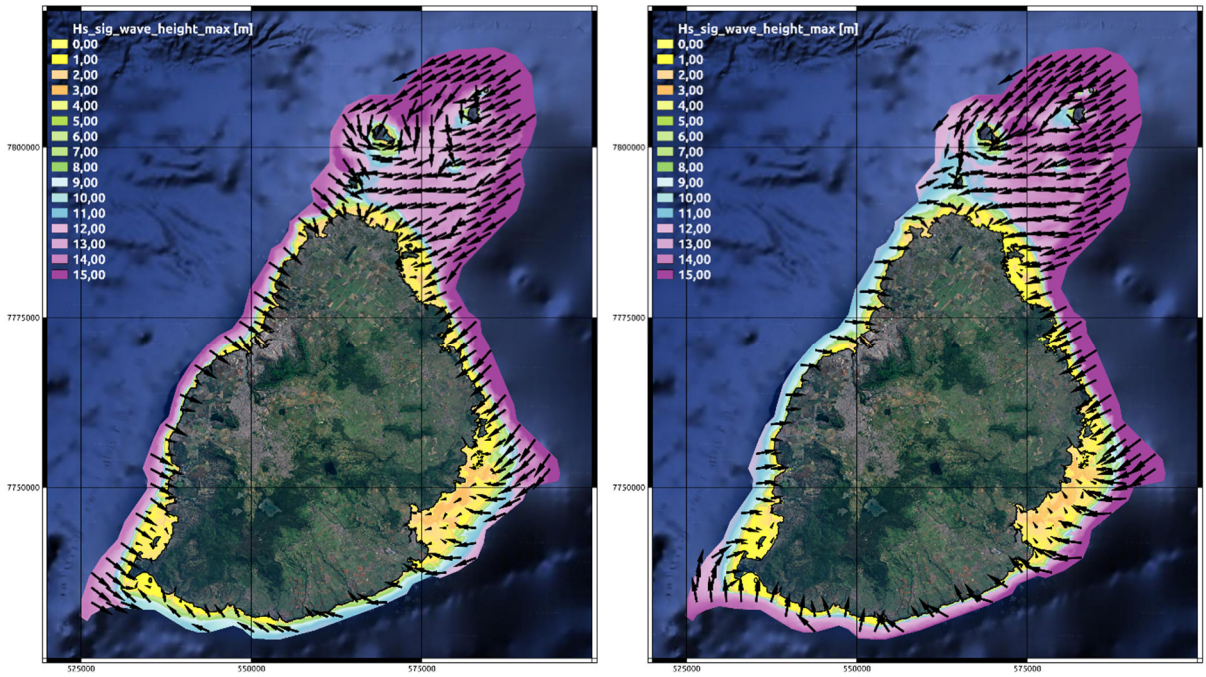


*Figure 108 : Overall map of the computed maximum significant wave height with 2080-2100 climate on scenarios 1498 (left) and 2423 (right).*

Figure 109, Figure 110 and Figure 111 represent the maximum computed currents velocities on the several simulated scenarios. Currents intensities are strongly related to the wave dynamics described above. Indeed, the highest velocities are concentrated in the wave breaking region beyond the reef and on the northern insular shelf (around the Gabriel and Flat islands in particular). In these regions values surpass 2.5m/s and often attend 3m/s in all scenarios. Intense currents can be also found inside the lagoons, where the maximum values can achieve 1.5m/s. In this case the scenarios are complementary: the strongest currents are induced by the cyclone 1498 on the north and south-west lagoons, and by the cyclones 357 and 2423 on the east and south-east ones.

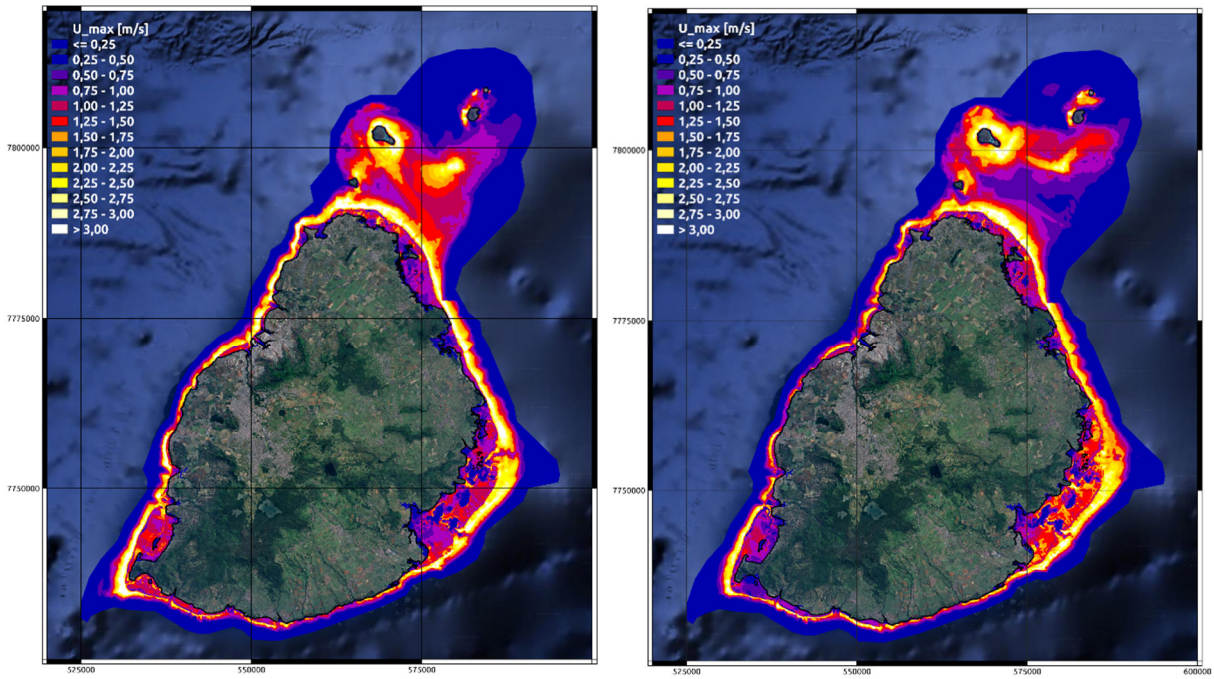


*Figure 109 : Overall map of the computed maximum sea currents velocity with actual climate on scenarios 1498 (left) and 357 (right).*

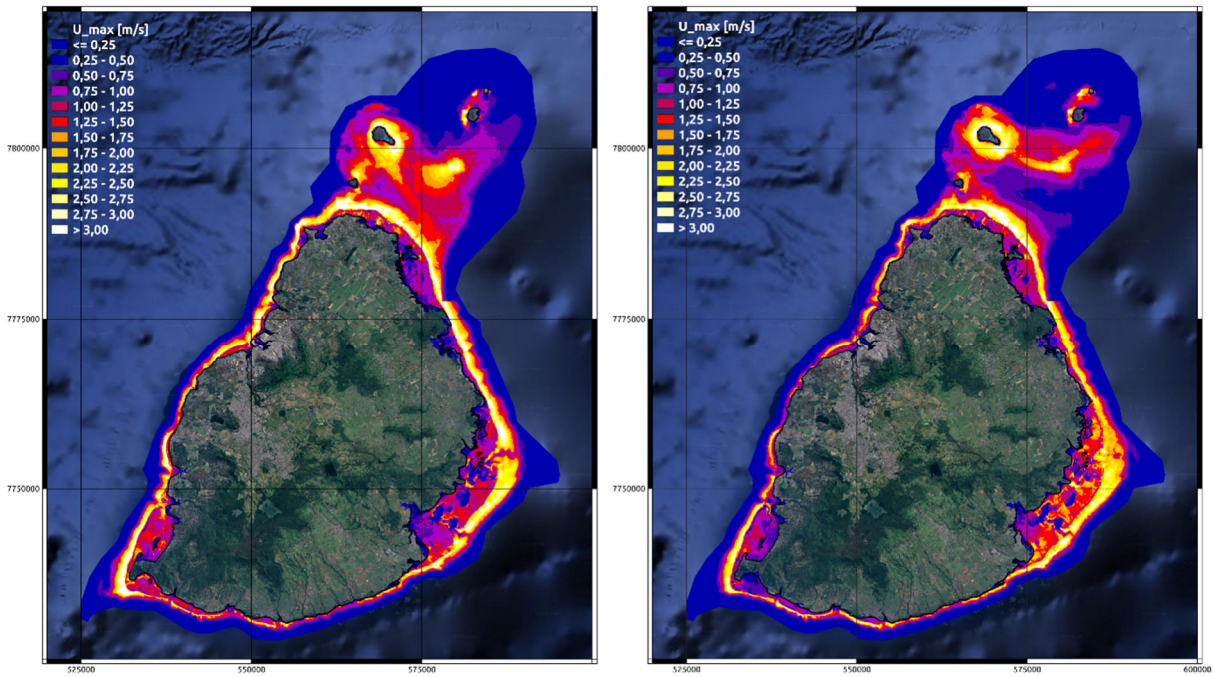


*Figure 110 : Overall map of the computed maximum sea currents velocity with 2050 climate on scenarios 1498 (left) and 357 (right).*

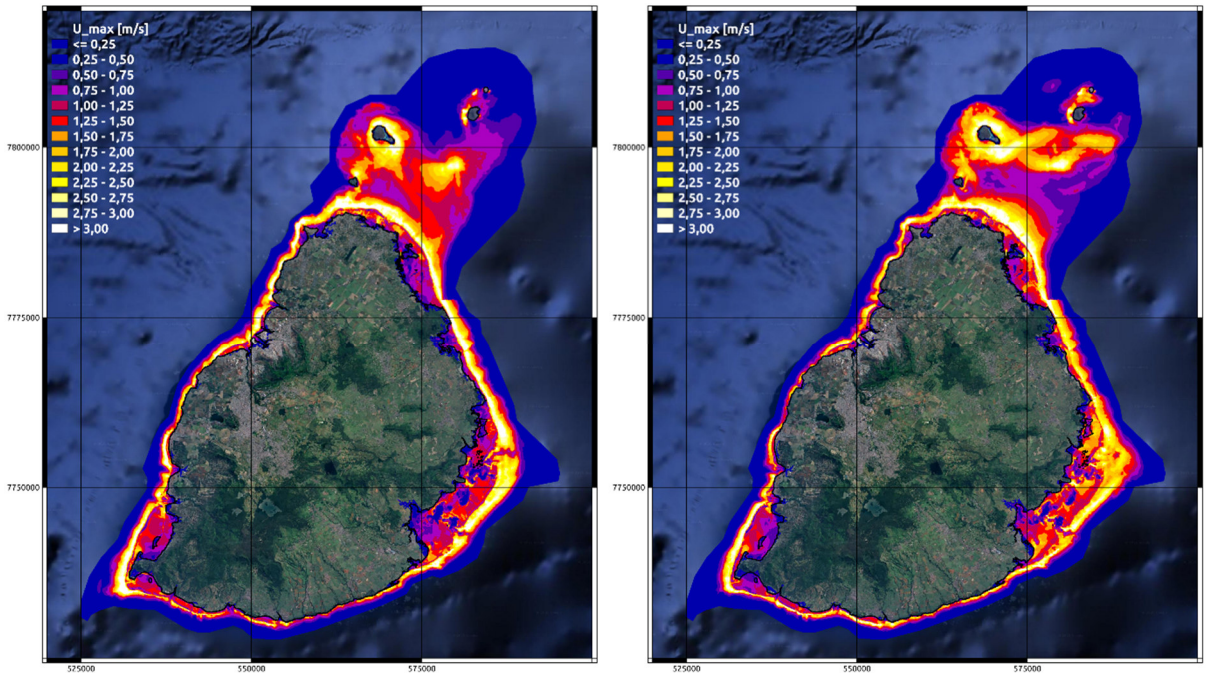


*Figure 111 : Overall map of the computed maximum sea currents velocity with 2080-2100 climate on scenarios 1498 (left) and 2423 (right).*

The resulting maximum sea surface heights for all the simulated scenarios are displayed in Figure 112, Figure 113 and Figure 114. In all climate configurations, cyclone 1498 appears to be the majoring scenario on the West and North coasts of the island, but also on the North-Est lagoon and Poste Lafayette bay. On the other side, cyclones 357 and 2423 are more impactful on the South and South-Est coasts of Mauritius, excluding the Port Mahébourg area. Here, in fact, the maximum water levels are reached under the cyclone 1498, mainly due to the particular direction of the waves, previously highlighted, that in this scenario pump water to the south-west side of the lagoon. Maximum water levels at the coast surpass 2.5m already on actual climate, in particular with cyclone 1498, attending maximum values of 3.5m with on 2100 climate.

On present-day climate conditions the flooded area is mostly restricted to river estuaries and eastern coastal low lands covered by marshes and forests (especially in the sectors of Pointe d'Esny, Vieux Grand Port, Poste Lafayette, Poste de Flacq, Roches Noires and Poudre d'O), but the seafront of a few urbanized area is also affected the flooding (Roches Noires, Mahébourg, Elisabethville and a few docks of the port area in Port Louis). This same picture is found with little differences with 2050 climate. At horizon 2100, however, new large sectors are flooded by water, including larger urbanized areas (please refer to Figure 115 and Figure 118 for a close-up view on Grand Baie; Figure 116 and Figure 119 for Mahébourg; Figure 117 and Figure 120 for Port Louis).

We have to mention that the computed flooding area on some sites of the west coast (including Port Louis) is probably underestimated at this level. Indeed, the absence of a wide lagoon exposes the coast to waves overtopping. This aspect has been taken into account only in the simulations for the Flic-en-Flac site (see § 4.3.4.1.2).

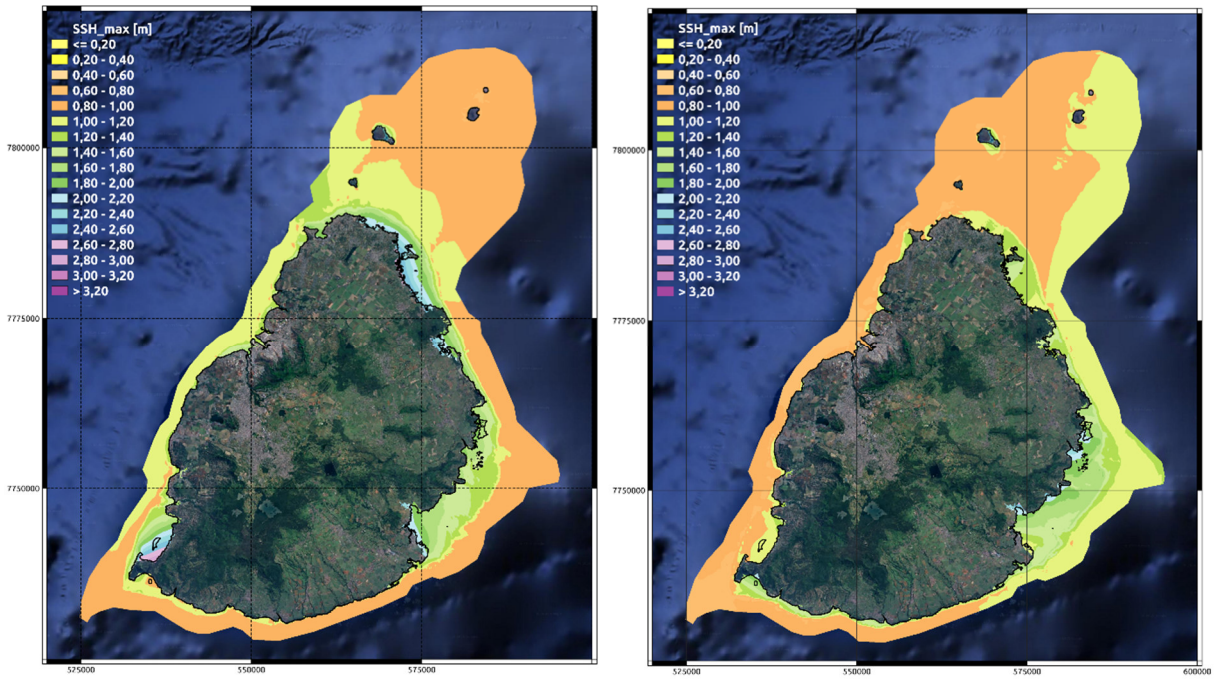


*Figure 112 : Overall map of the computed maximum sea surface height with actual climate on scenarios 1498 (left) and 357 (right).*

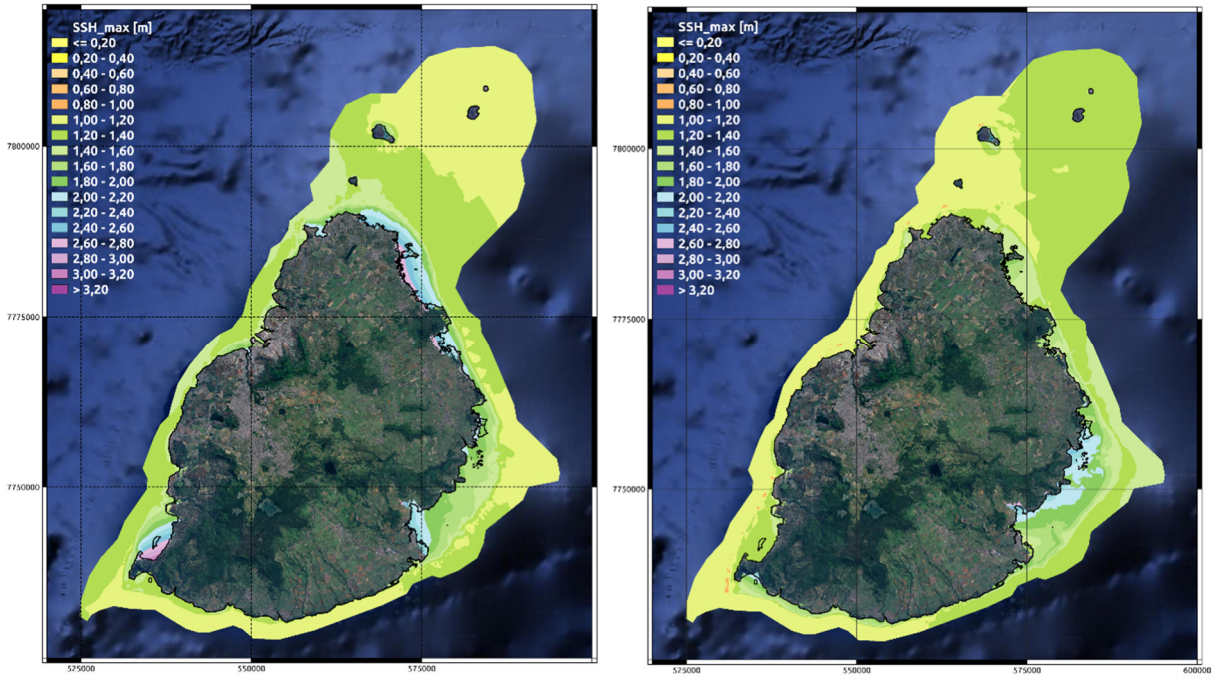


*Figure 113 : Overall map of the computed maximum sea surface height with 2050 climate on scenarios 1498 (left) and 357 (right).*

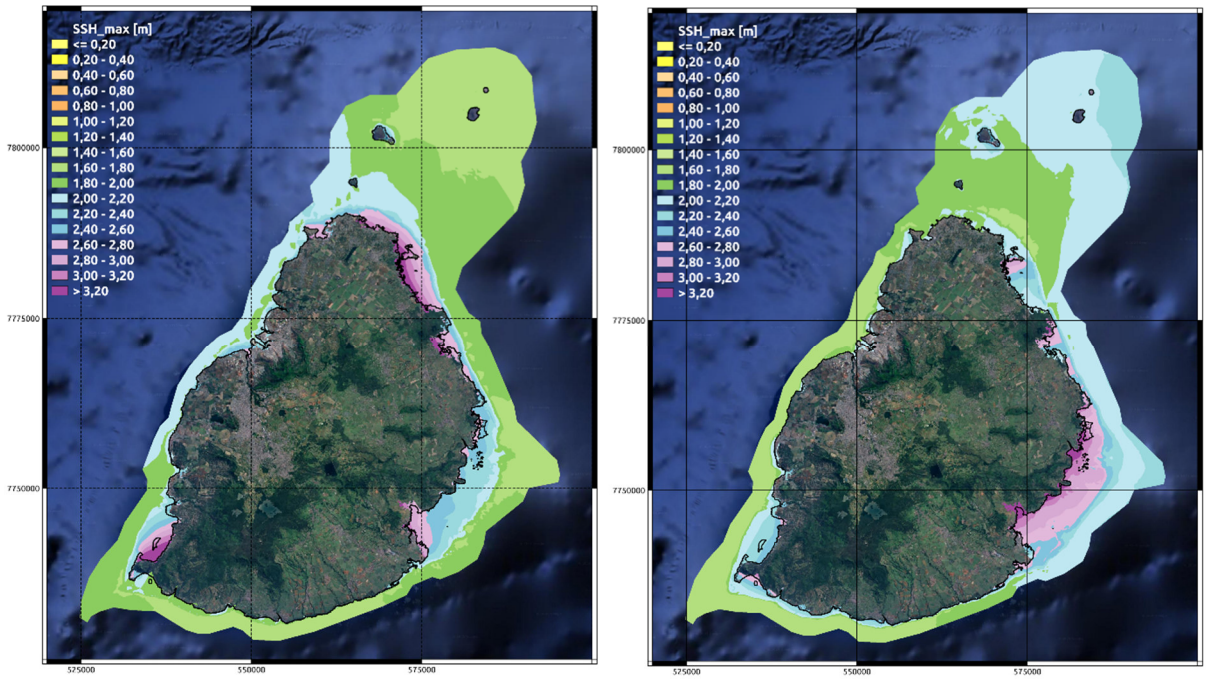


*Figure 114 : Overall map of the computed maximum sea surface height with 2080-2100 climate on scenarios 1498 (left) and 2423 (right).*

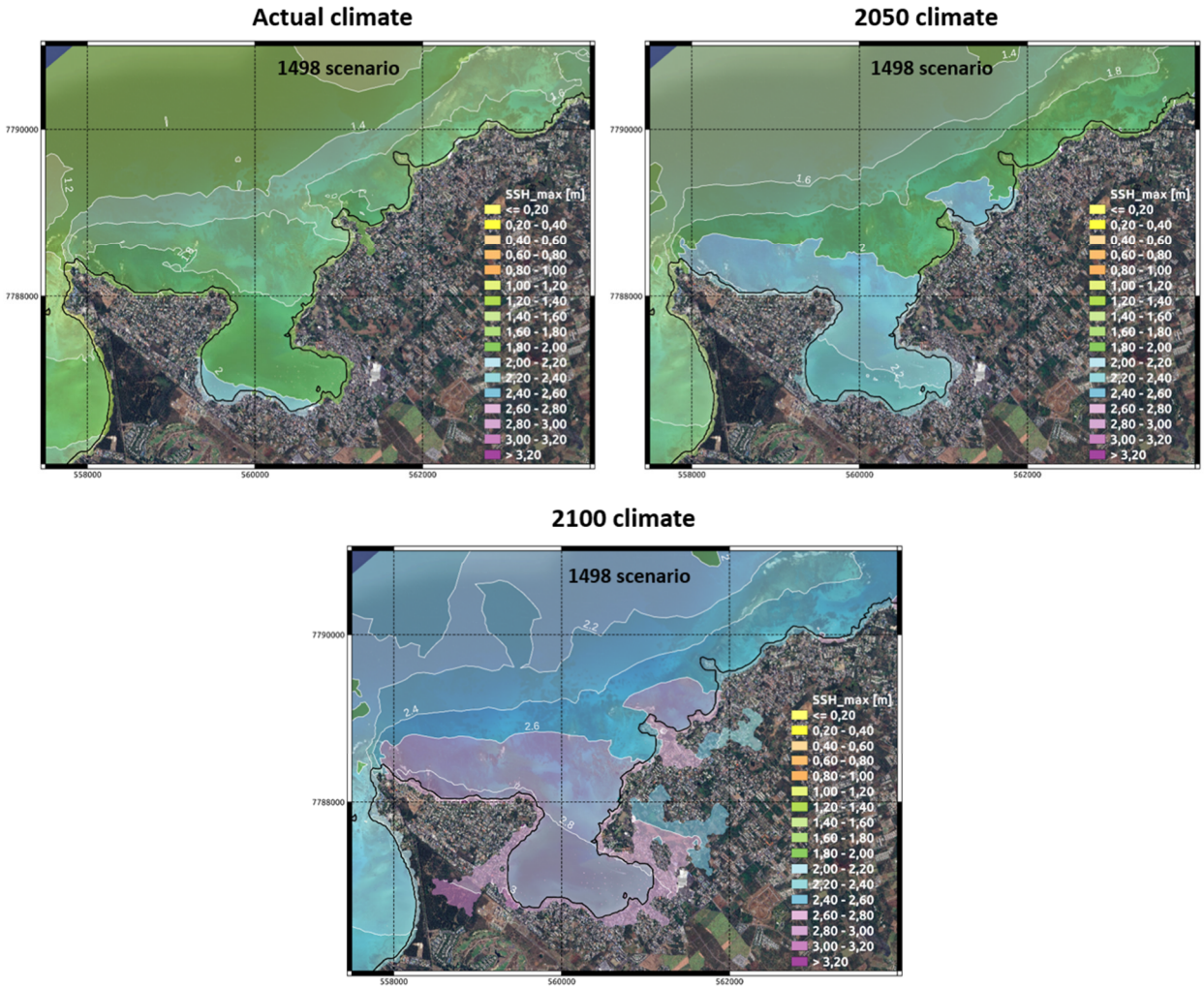


*Figure 115 : A close-up comparison of the computed maximum sea surface height on the Grand Baie area for the most impactful scenarios.*

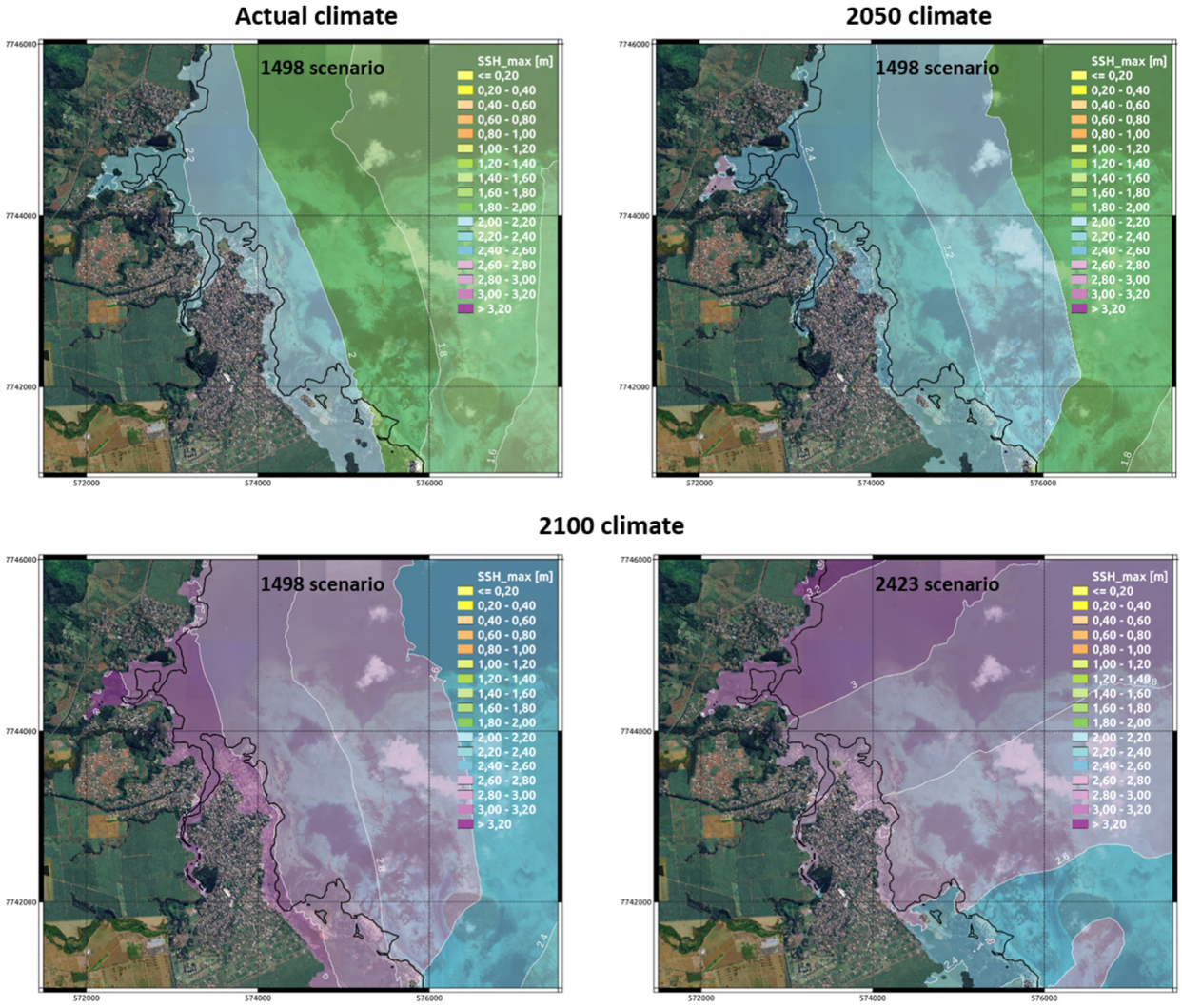


*Figure 116 : A close-up comparison of the computed maximum sea surface height on the Mahébourg area for the most impactful scenarios.*

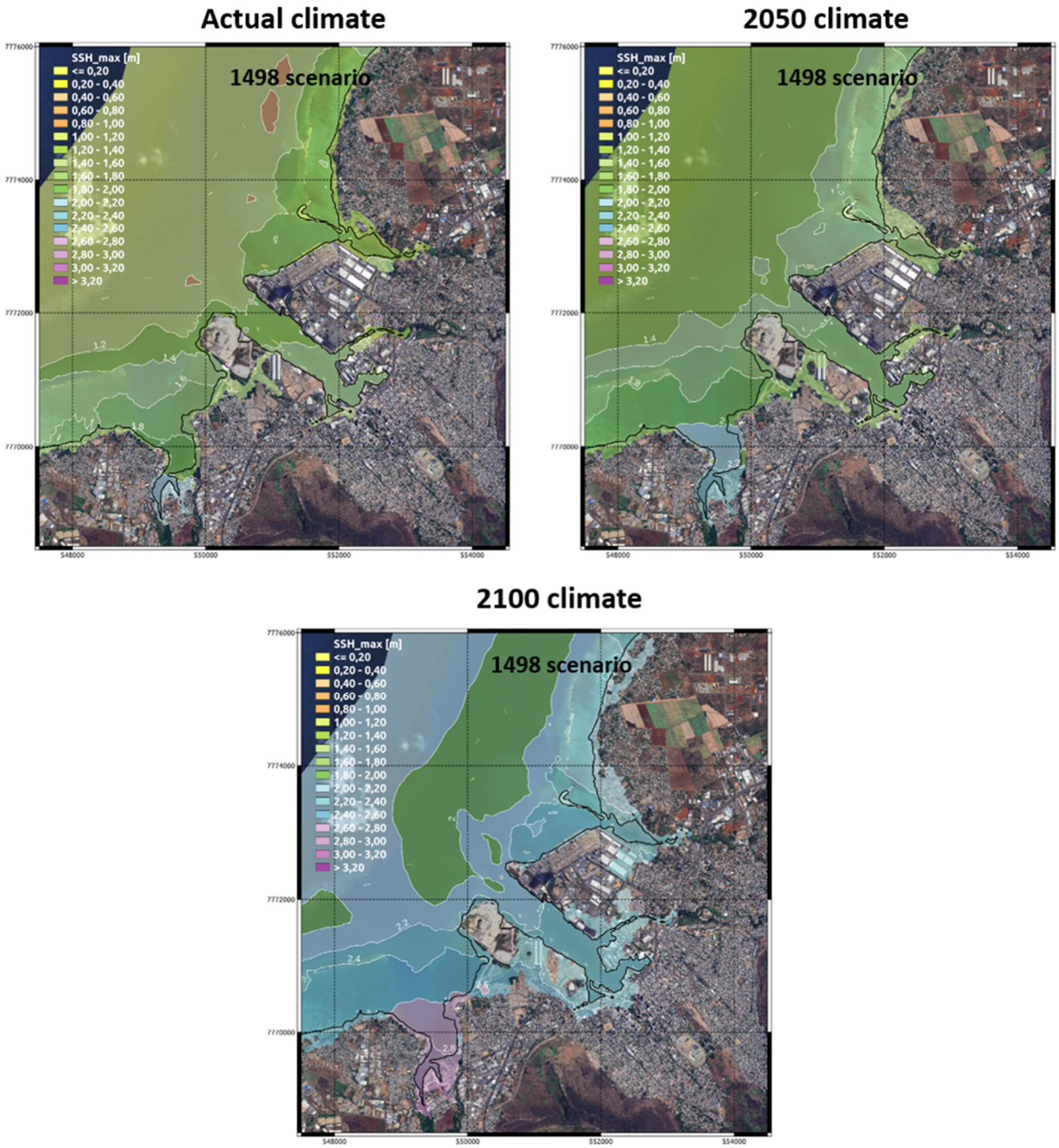


*Figure 117 : A close-up comparison of the computed maximum sea surface height on the Port Louis area for the most impactful scenarios.*

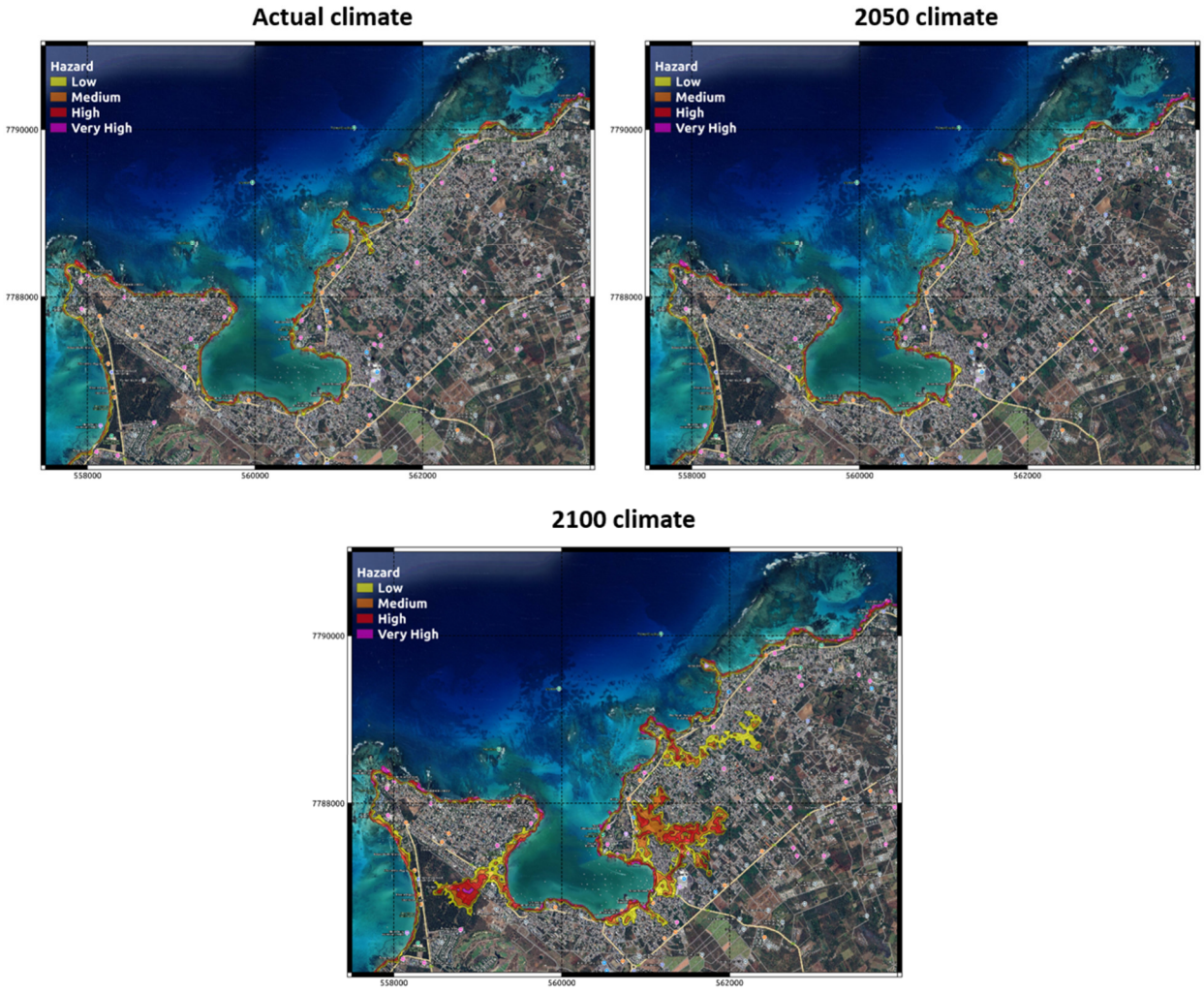


*Figure 118 : Flooding hazard maps on the Grand Baie area for present-day climate conditions (top), 2050 climate (centre) and 2080-2100 climate (bottom).*

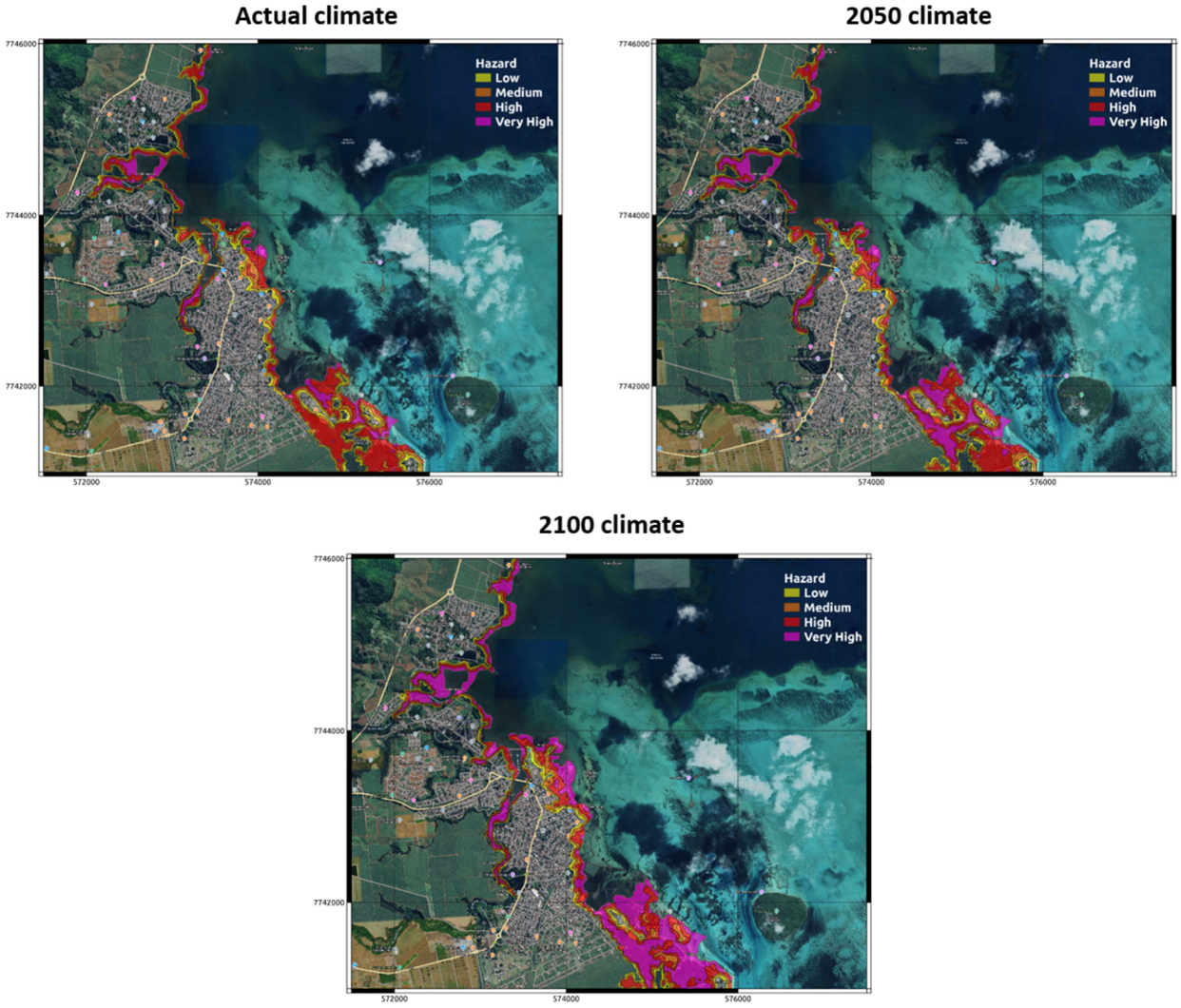


*Figure 119 : Flooding hazard maps on the Mahébourg area for present-day climate conditions (top), 2050 climate (centre) and 2080-2100 climate (bottom).*

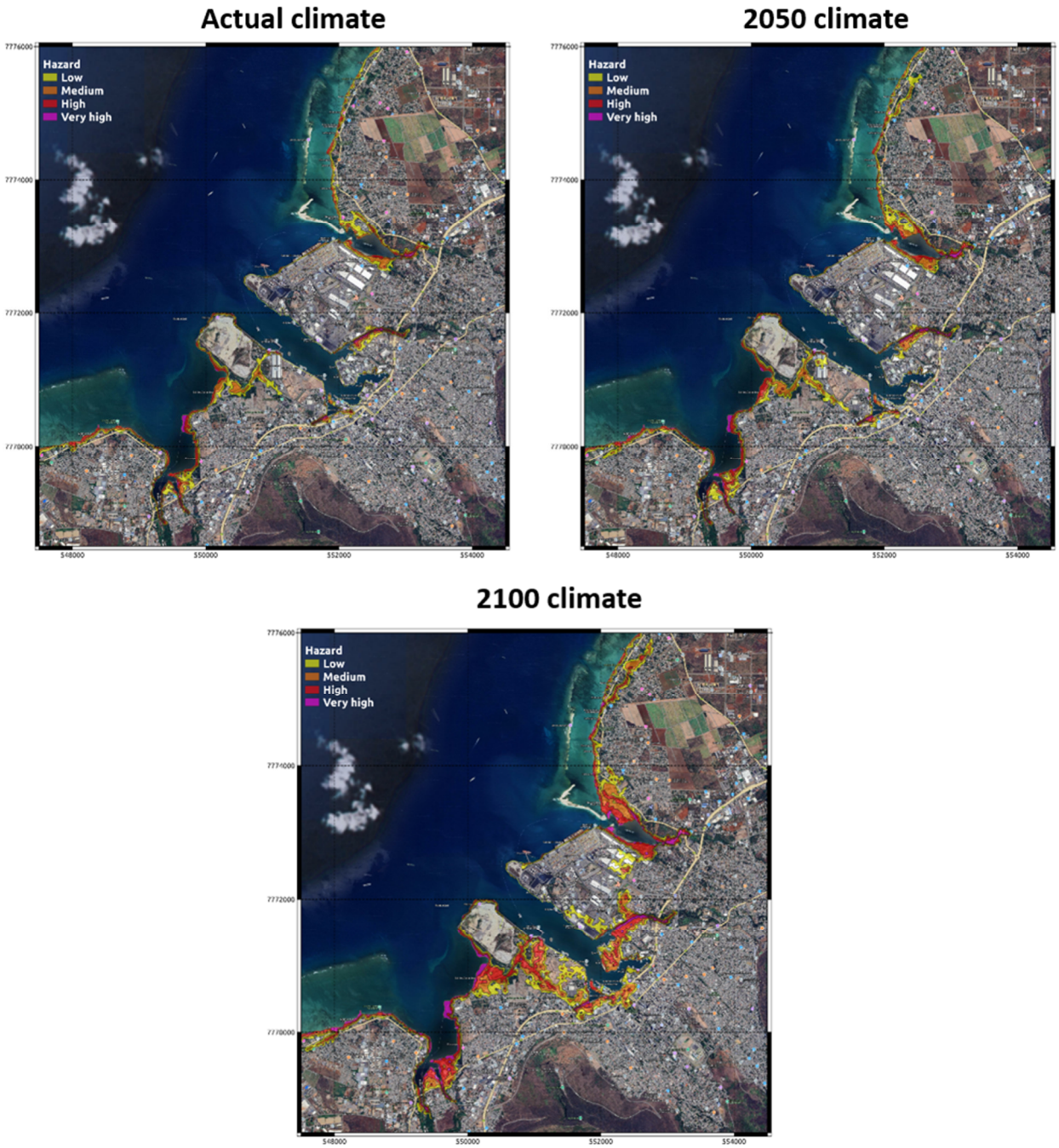


*Figure 120 : Flooding hazard maps on the Port Louis area for present-day climate conditions (top), 2050 climate (centre) and 2080-2100 climate (bottom).*

## 4.2.2.2 Rodrigues

### *4.2.2.2.1 Coastal retreat hazard*

For Rodrigues, coastline retreat projections have been conducted for the 36 homogeneous zones using the defined scenarios.

Six of Rodrigues' coastal zones are distinguished by a predominantly rocky coastline, interspersed with sedimentary sectors, bays and modest beaches of limited size (Figure 121). Additional retreat estimates have been conducted for these regions, with the aim of assessing the potential retreat of the sedimentary sectors. These supplementary retreat values were utilized in the context of the mixed coastline scenario, with the objective of enhancing the precision of the projected shoreline retreat mapping. It should be noted that these highly localised retreat values are not taken into account in the general presentation of the Rodrigues hereafter.

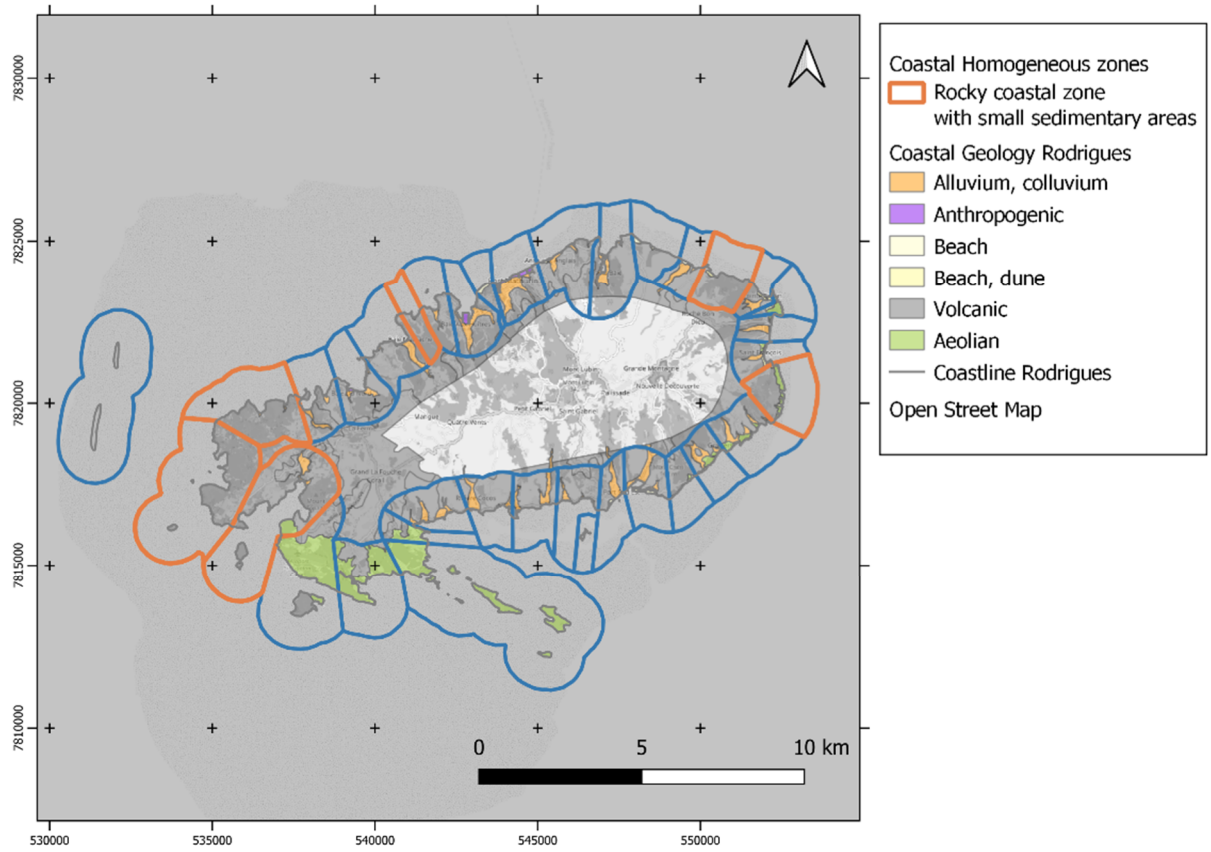


*Figure 121 : Coastal zones of Rodrigues and geology. Six rocky areas with small sedimentary areas whose potential retreat has been assessed.*

#### *4.2.2.2.1.1 Current timeframe*

By the projected deadline of 2025, the areas susceptible to the retreat of the Rodrigues coastline are estimated to range between 5 and 15 meters, contingent upon the intermediate scenario (Figure 122). Occasional retreats of 5 meters may occur along rocky coastlines mainly in the western and eastern sides of the island.

The highest-hazard areas are on the north and south coasts, characterized by sandier, lower-altitude coastal sectors which may be open to the ocean through reef passes.

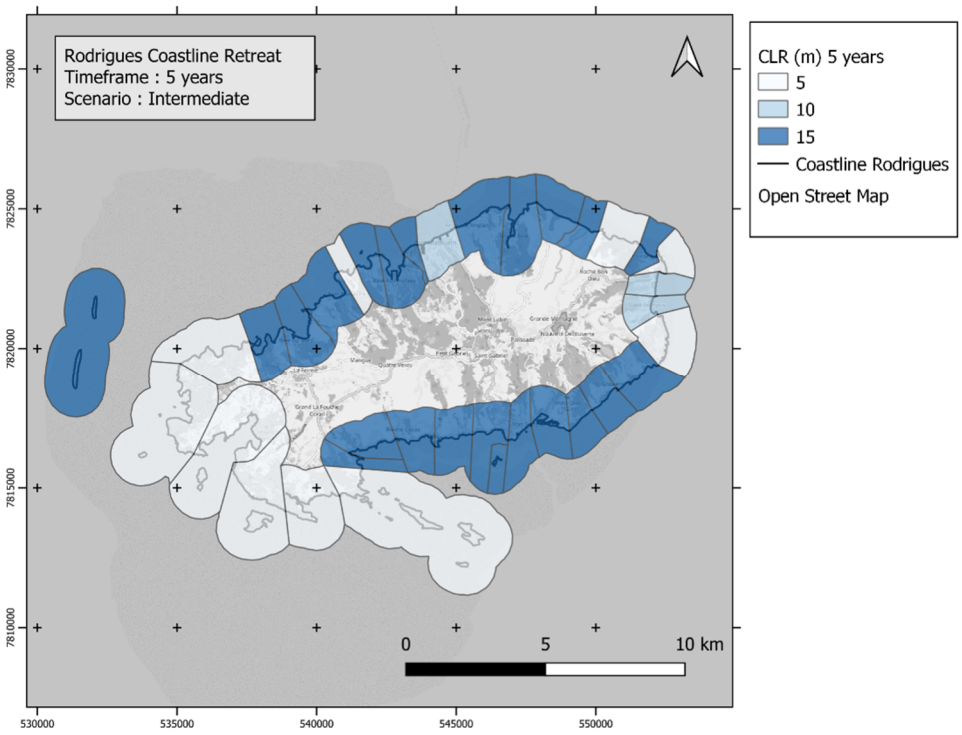


*Figure 122 : Map of potential shoreline retreat (CLR) by sediment cell and homogeneous coastal zone in Rodrigues for the current period and intermediate scenario.*

Figure 123 and Figure 124 illustrate the differences between the three scenarios for the current timeframe. The median scenario posits that the basaltic rocky coasts will not be eroded in the very short term, implying that five homogeneous zones of Rodrigues are at zero hazard level. For the limestone rocky coasts, the median scenario anticipates a potential retreat of 5 meters in five additional homogeneous regions of Rodrigues. The remaining 70% of homogeneous zones are characterized by a current hazard zone of 10 meters. The Mourouk sediment cell is distinguished by a hazard zone of 15 metres, a distinction attributable to its low altitude and its alignment with a reef channel, which makes it more exposed to cyclonic swells.

The approach adopted for the safe scenario diverges from the previous one. In this scenario, all coasts, including basaltic rocky coasts, are capable of retreating. The predominantly rocky coasts (basalt or limestone) constitute approximately 30% of the homogeneous zones of Rodrigues. For sedimentary and sandy areas, the retreat values range from 15 to 25 meters. Furthermore, more than 55% of the homogeneous zones exhibit a current potential retreat of 20m, according to this scenario. Five zones have been identified as being particularly vulnerable to erosion: two sectors in Port Mathurin, Grand Baie, and two additional sectors between Gravier and Var Brûlé beach.

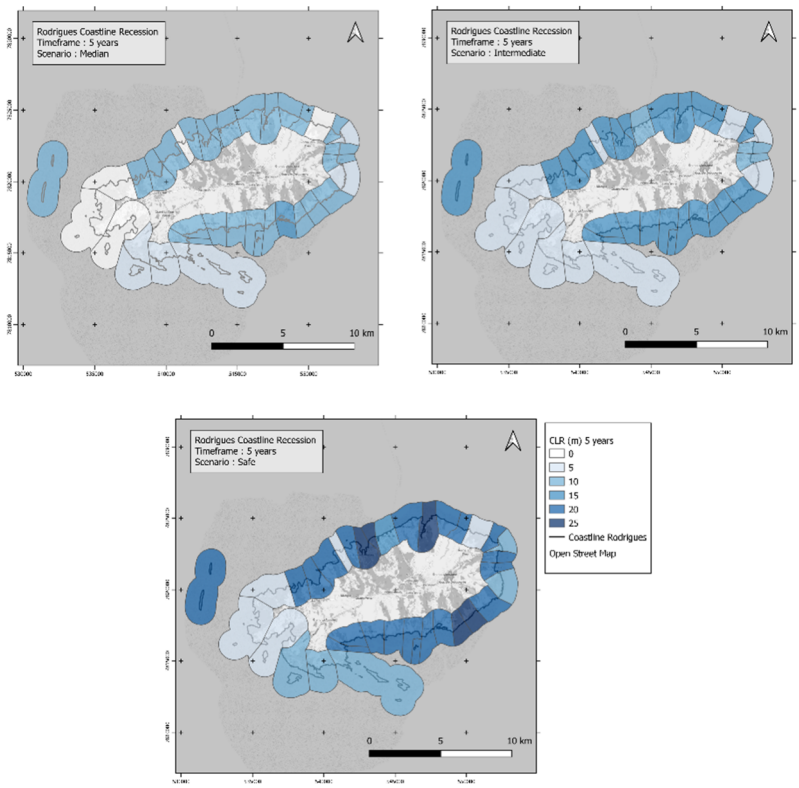


*Figure 123 : Maps of potential coastline retreat (CLR) by sediment cell and homogeneous zones in Rodrigues for the current period and the three studied scenarios*

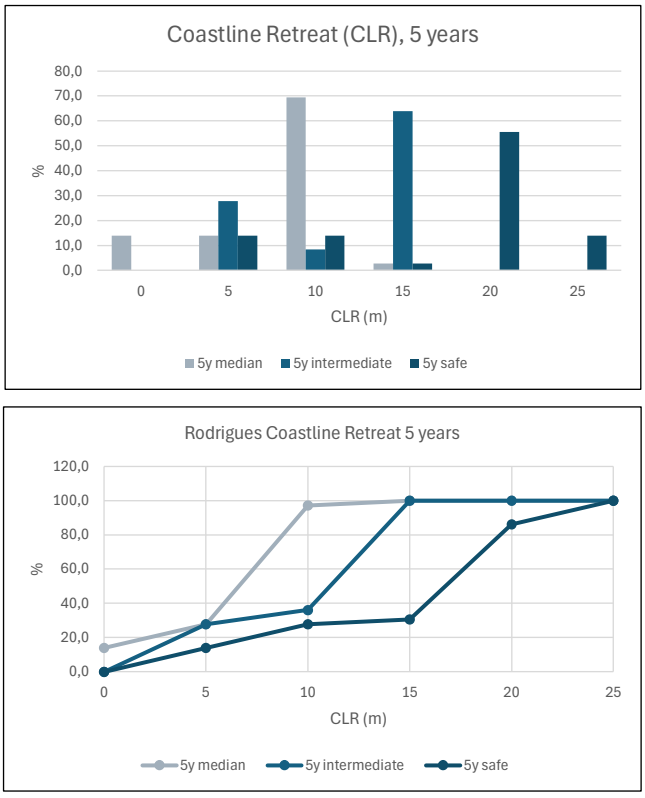


*Figure 124 : Assessment of potential coastline retreats (CLR) assessed by sedimentary cells and homogeneous coastal zones for the current period in Rodrigues. Frequency histogram (%) and cumulative percentage graph.*

#### *4.2.2.2.1.2 Timeframe 2050*

At 2050 timeframe, the areas at risk of coastal retreat along the Rodrigues coastline are estimated to range from 5 to 40 meters, depending on the intermediate scenario (Figure 125). Occasional retreats of 5 meters and 10 meters may occur along rocky coasts. The retreat classes of 25 meters, 30 meters, and 35 meters are the most frequent, accounting for over 60% of the hazard values. This intermediate scenario identifies five homogeneous areas where the shoreline retreat hazard in 2050 exceeds 30 meters: Port Mathurin, between Pointe L'Herbe and Pointe Monnier, Baie aux Huîtres, Baie Diamant, Baie du Nord, and Anse Mourouk. By this time, the effects of climate change and the impact of cyclonic activity on the coastline may be more pronounced than at present in these five sensitive areas of Rodrigues.

Figure 126 and Figure 127 illustrate the potential variations depending on the scenario selected to estimate the coastline retreat hazard zone for 2050. The median scenario assumes that 75% of the homogeneous areas of Rodrigues are subject to a shoreline retreat hazard of 20 meters or less by this date. Under this scenario, two additional sensitive areas are projected to experience retreats exceeding 20 meters (Anse Mourouk and Petite Butte).

In the safe scenario, the projected retreat of sedimentary coasts appears significantly greater than in the previous scenarios. Retreat values are estimated to range from 45 to 55 meters for nearly 65% of the homogeneous coastal zones of Rodrigues. The higher setbacks predicted in this scenario are primarily attributable to the inclusion of the parameter $Tx_{max\text{-}hz}$ (maximum rate of coastline retreat in the homogeneous zone) in the projections. Despite the application of a weighting factor to these values (see 4.2.1.1.2.2), this parameter may be slightly overestimated due to the lack of observational data on coastline dynamics in the area, the method used to estimate retreats in this study, and the relatively short observation period, which is notably shorter than the projected time horizon.

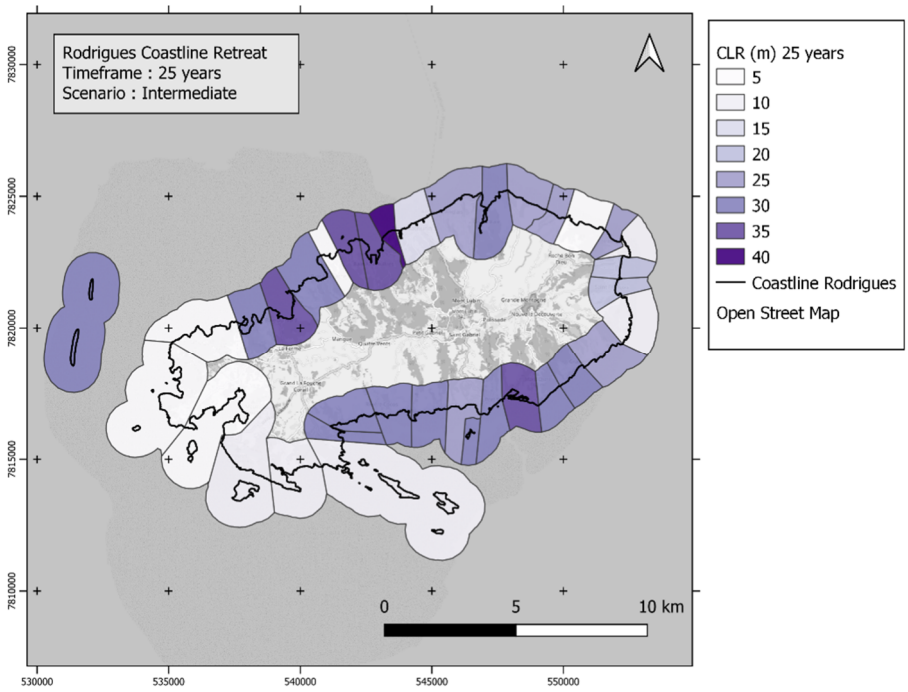


*Figure 125 : Map of potential coastline retreat (CLR) by sediment cell and homogeneous coastal zone in Rodrigues for the 2050 period and intermediate scenario.*

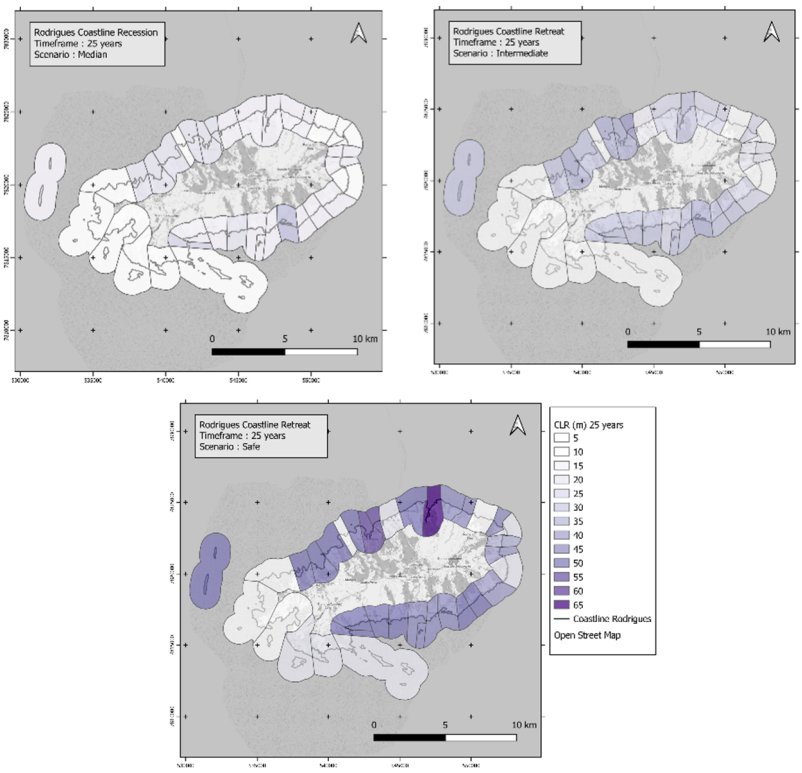


*Figure 126 : Maps of potential coastline retreat (CLR) by sediment cell and homogeneous coastal zones in Rodrigues for the 2050 period and the three studied scenarios*

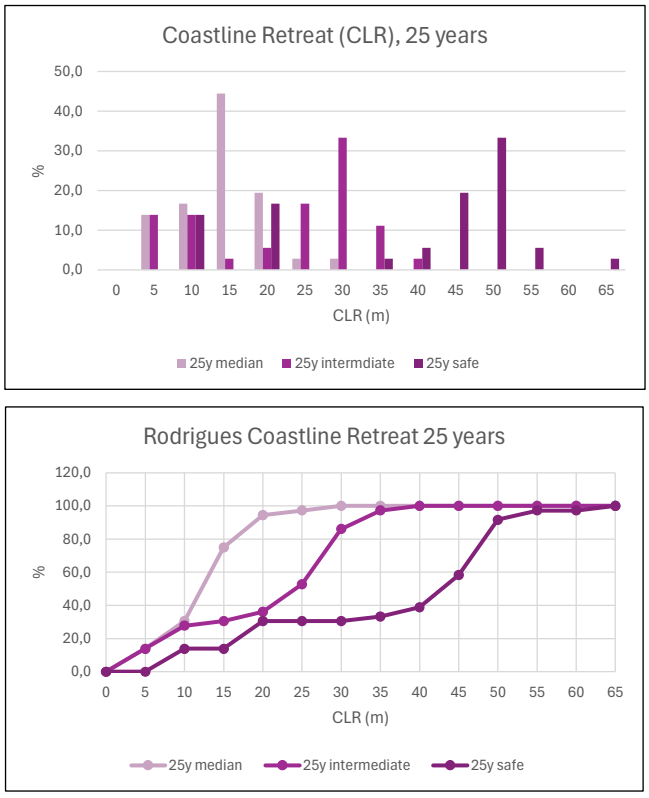


*Figure 127 : Assessment of potential coastline retreats (CLR) assessed by sedimentary cells and homogeneous coastal zones for the 2050 period in Rodrigues. Frequency histogram (%) and cumulative percentage graph.*

#### *4.2.2.2.1.3 Timeframe 2100*

In 2100, the hazard of coastal retreat along the Rodrigues coastline is estimated to range from 10 to 95 meters, depending on the intermediate scenario (Figure 128). Occasional retreats of 10 meters and 20 meters may occur along rocky coasts. For sedimentary coastlines, the most frequent retreat classes are between 60 and 85 meters, representing 55% of the homogeneous zones. The most sensitive homogeneous zones for this timeframe, approximately 10% of the total, may experience retreats ranging from 85 meters to 95 meters.

Figure 129 and Figure 130 illustrate the potential differences depending on the scenario selected to estimate the coastline retreat hazard zone for 2100. By this time, uncertainties regarding the retreat of sandy coastlines become more pronounced, particularly with respect to sea level rise scenarios and the possible retreat values that could affect the coastal cells. These uncertainties lead to significant variations between the scenarios considered.

For homogeneous sedimentary zones in the median scenario, 55% of the zones are projected to experience a retreat of between 40 and 55 meters by 2100. These retreats are considerably less than those projected in the intermediate scenario (60 to 85 meters). The more sensitive homogeneous zones, which account for 10% of the sectors, are projected to face potential retreats ranging from 60 to 70 meters.

In the safe scenario, the estimated range of retreat for sedimentary sectors is broader, spanning from 75 meters to 130 meters. The "majority" class represents more than 50% of homogeneous zones, with estimated retreat hazard zones ranging from 80 meters to 115 meters. This class appears more extensive than in the intermediate scenario and presents significantly higher retreat values.

Compared to the results obtained for Mauritius, the safe scenario for Rodrigues shows higher retreat values, which is reflected in the differing shapes of the "cumulative %" curves (Figure 130). This difference can be partly attributed to the high level of uncertainty in the Rodrigues projections, stemming from the absence of a long-term coastline evolution dataset.

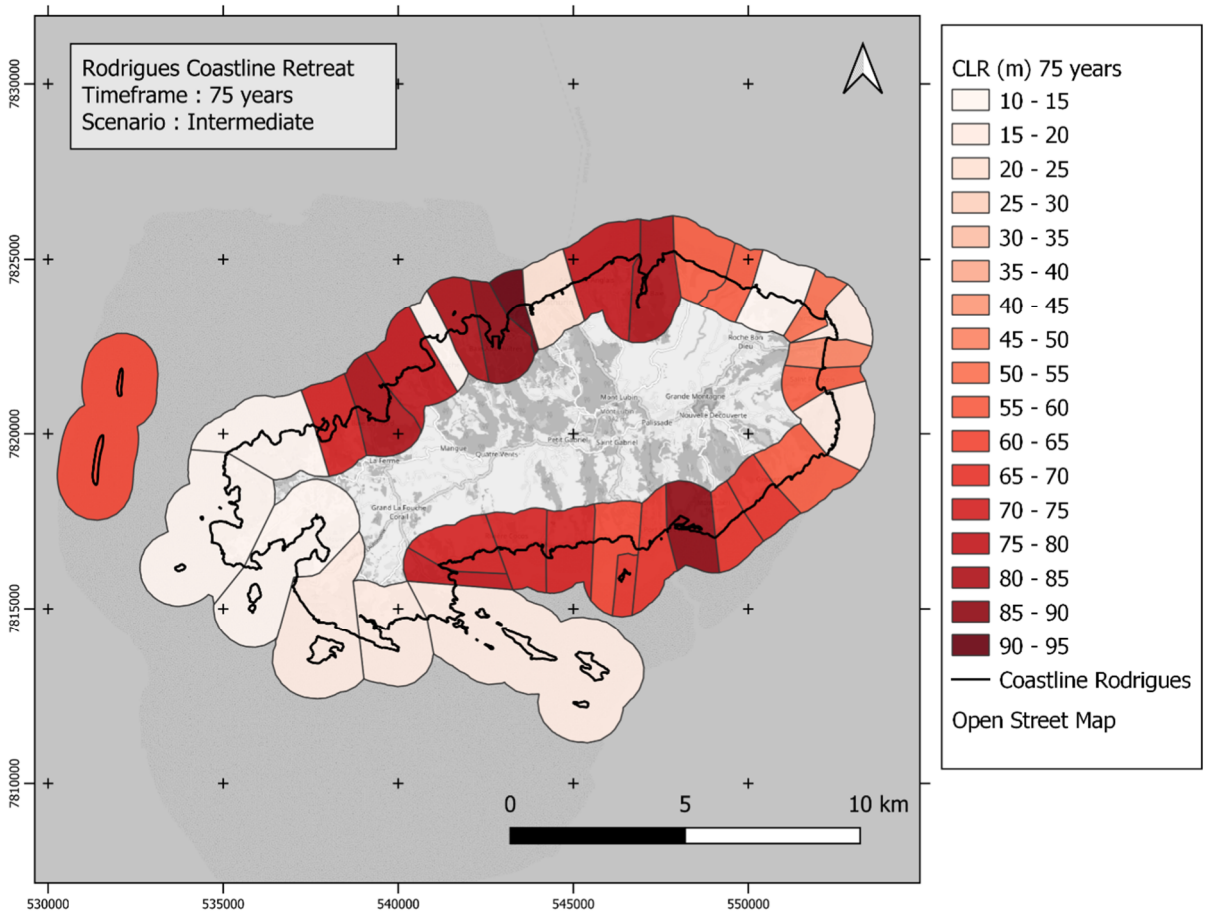


*Figure 128 : Map of potential shoreline retreat (CLR) by sediment cell and homogeneous coastal zone in Rodrigues for the 2100 period and intermediate scenario.*

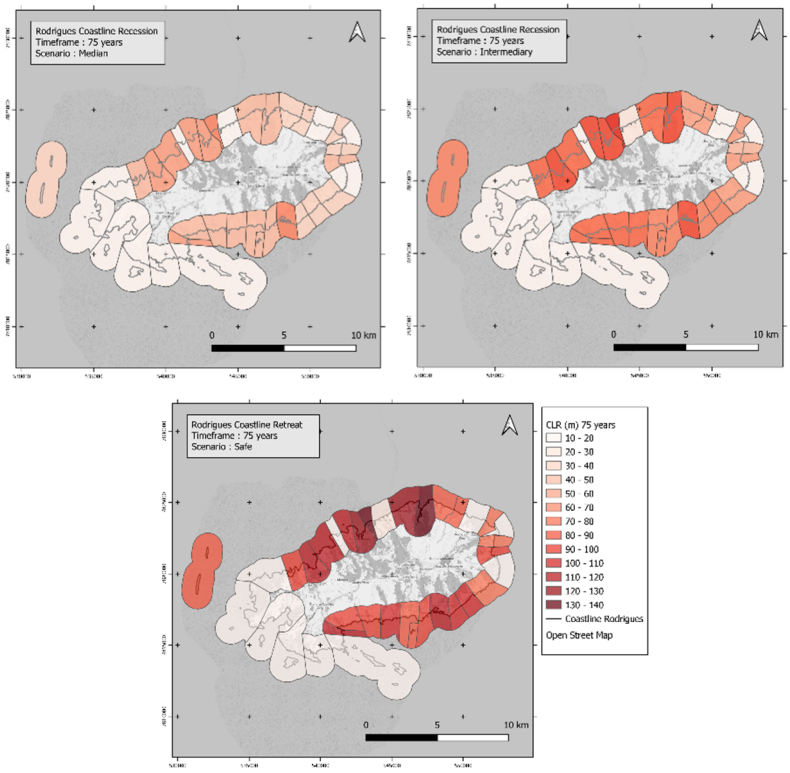


*Figure 129 : Maps of potential coastline retreat (CLR) by sediment cell and homogeneous coastal zones in Rodrigues for the 2100 period and the three studied scenarios*

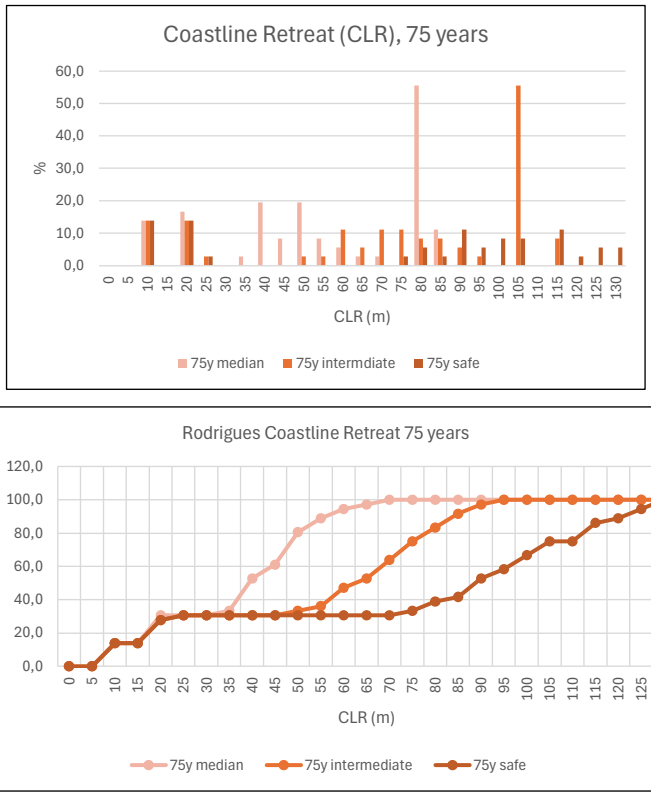


*Figure 130 : Assessment of potential coastline retreats (CLR) assessed by sedimentary cells and homogeneous coastal zones for the 2100 period in Rodrigues. Frequency histogram (%) and cumulative percentage graph.*

#### *4.2.2.2.2 Coastal flooding hazard*

##### *4.2.2.2.2.1 Model Validation on historical event*

The modelling approach described in the previous section was validated on the historical cyclone Bella (January 1991) whose track is illustrated in Figure 131. This is a major event for the island, where coastal flooding have been observed in the north coast and at Port-Mathurin (Donguy 1992), and where tide gauge measurements exist at this site.

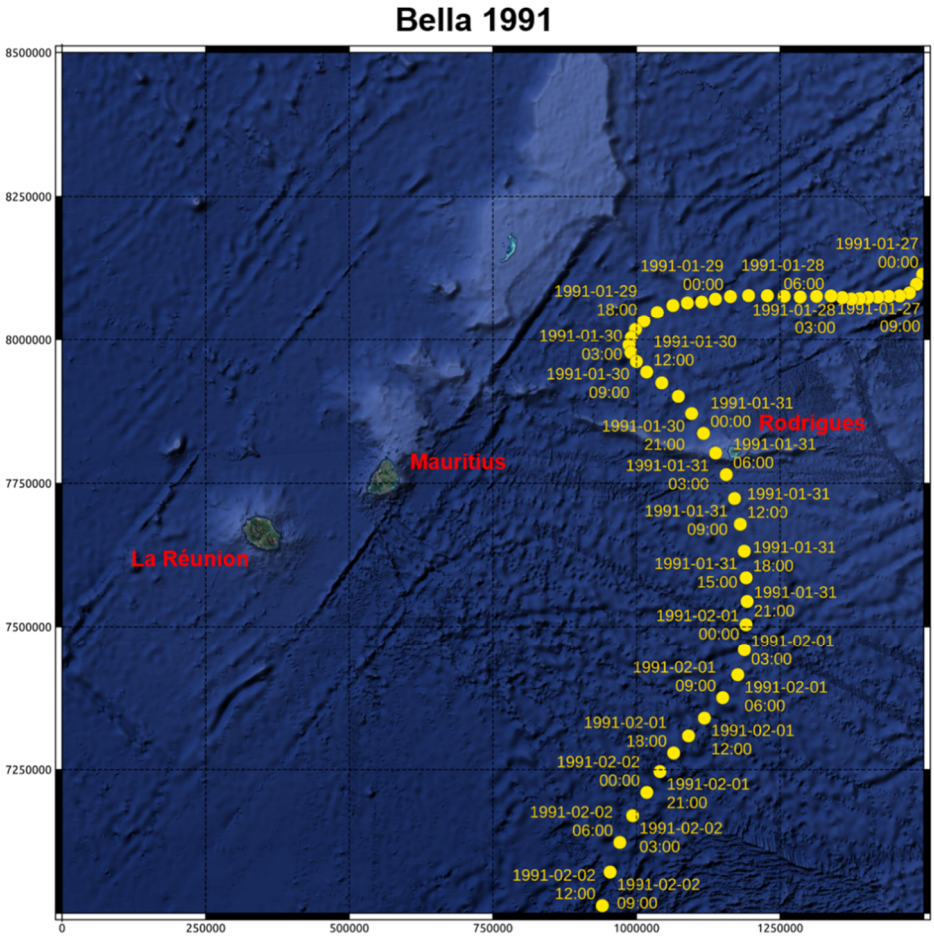


*Figure 131 : Cyclone Bella 1991 best track from the IBTrACS database.*

Simulation results show:

- Strong exposure of the north of the island with Hs and Tp close to 12m and 14s respectively. In the lagoon these values reach 1m and 3.5s;

- Maximum water levels of around 1.2-1.4 m on the NE, E and SW of the island (Figure 133);

- A good agreement between water levels calculated and measured on the Port-Mathurin tide gauge, in particular at the peak (Figure 134);

- the flooding of Port-Mathurin as reported by Donguy (1992) with water height between 0.25m-0.5m in the street of the city.

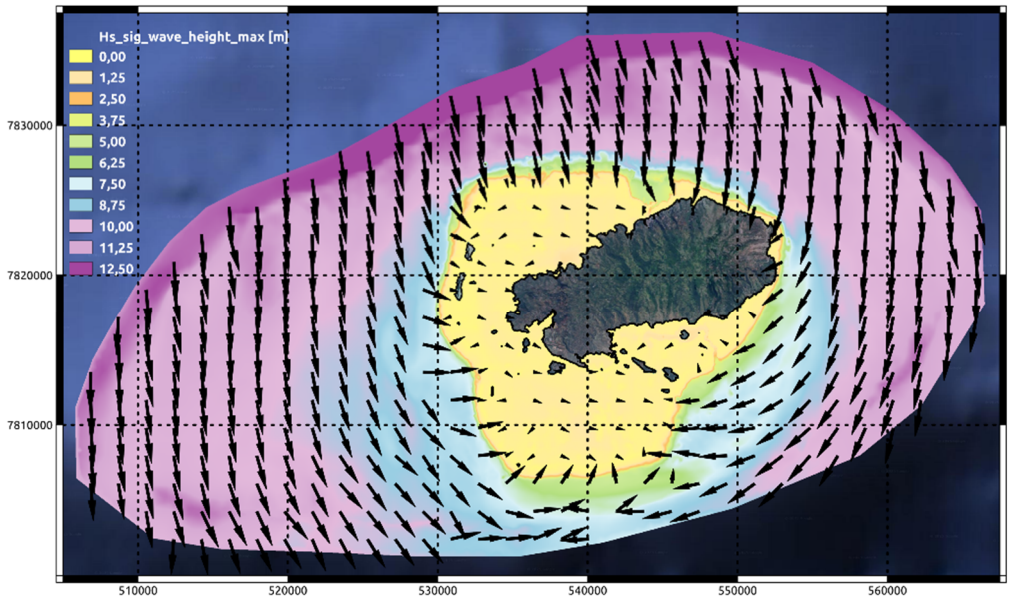


*Figure 132 : Computed maximum significant wave height and the wave propagation peak direction generated by Bella (1991) on the whole computational domain.*

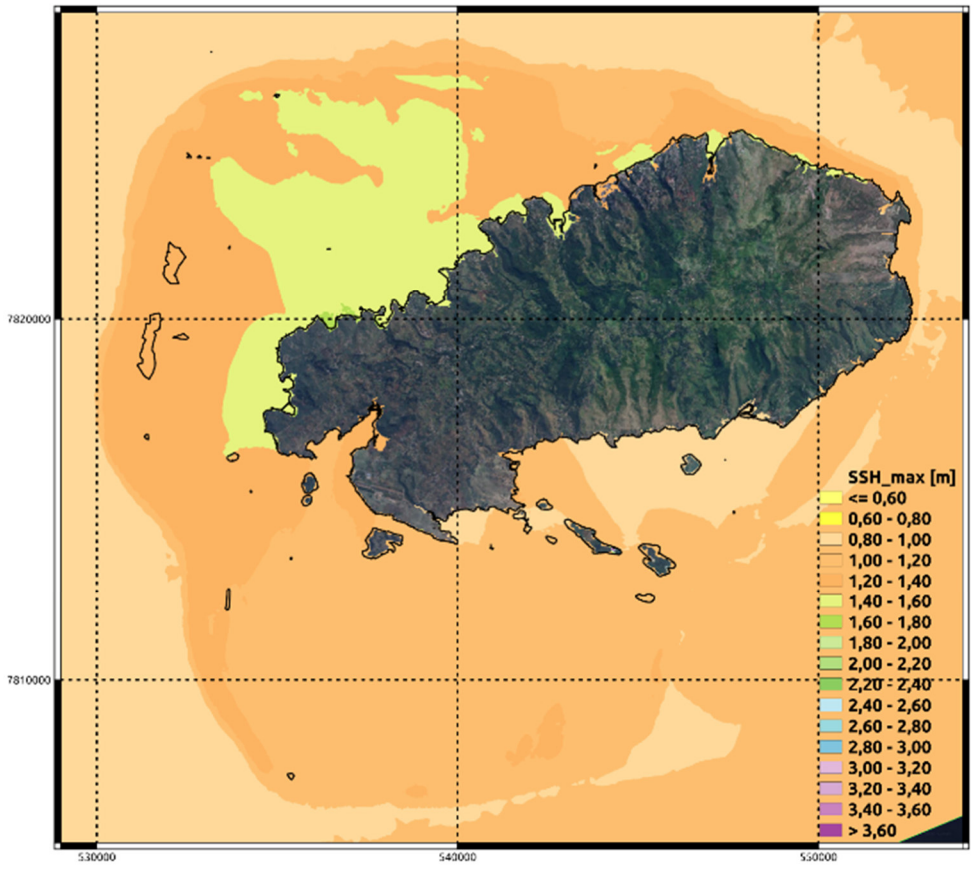


*Figure 133 : Computed maximum water levels (SSH_max) on the cyclone Bella (1991).*

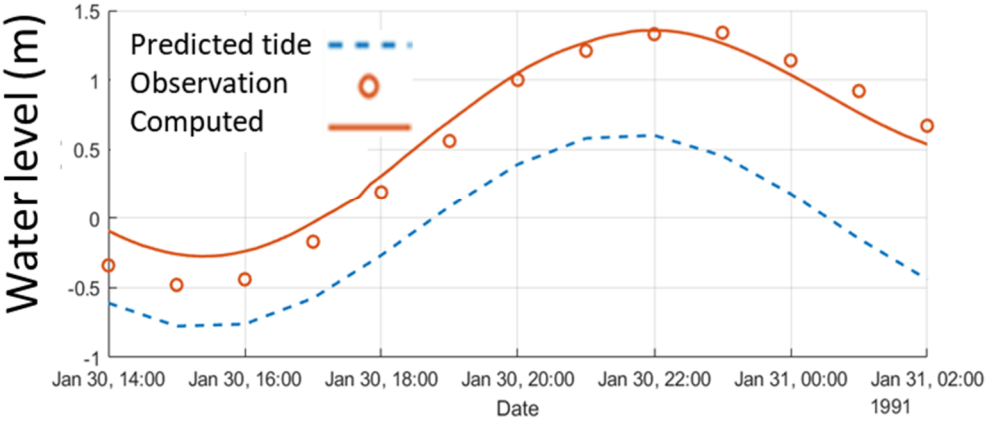


*Figure 134 : Validation of the computed water level against tidal gauge data at Port-Mathurin.*

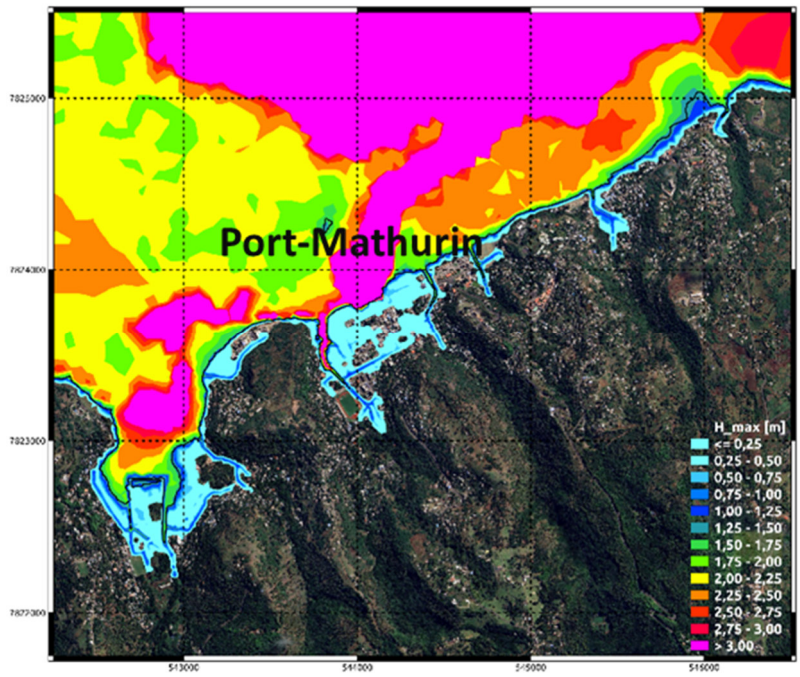


*Figure 135 : Computed and water height on the cyclone Bella (1991)– zoom on the Port Mathurin area.*

#### *4.2.2.2.2.2 Determining actual climate, 2050 and 2100 climate reference scenarios*

By applying the same criteria as those indicated in 4.2.2.1.2.2, two scenarios of the database of Météo-France were selected as reference events with a return period of one hundred years under actual, 2050 and 2100 climate conditions: scenarios 63 and 591 (Intense Tropical Cyclone (ITC).

Figure 136 and Figure 137 show the position of these scenarios in the joint exceedance iso-contours for return period of 100 years for the different climate horizons around Rodrigues (§ 3.4.4).

Figure 138 shows the tracks of the cyclones, which passes to the north and west of the island,

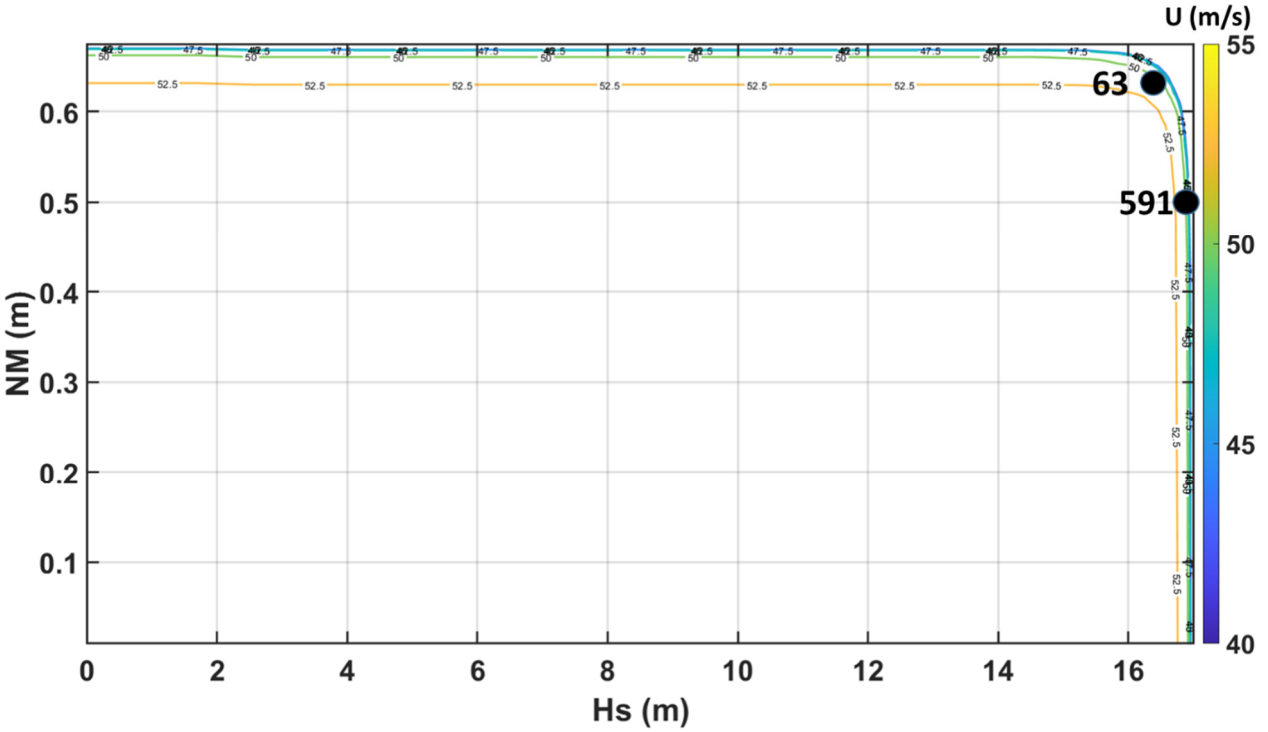


*Figure 136 : Positioning of scenarios 63 and 591 in the joint exceedance iso-contours for return period of 100 years within the space (NM; Hs) with the colour indicating the U values at Rodrigues forcing point for actual and 2050 climate scenario.*

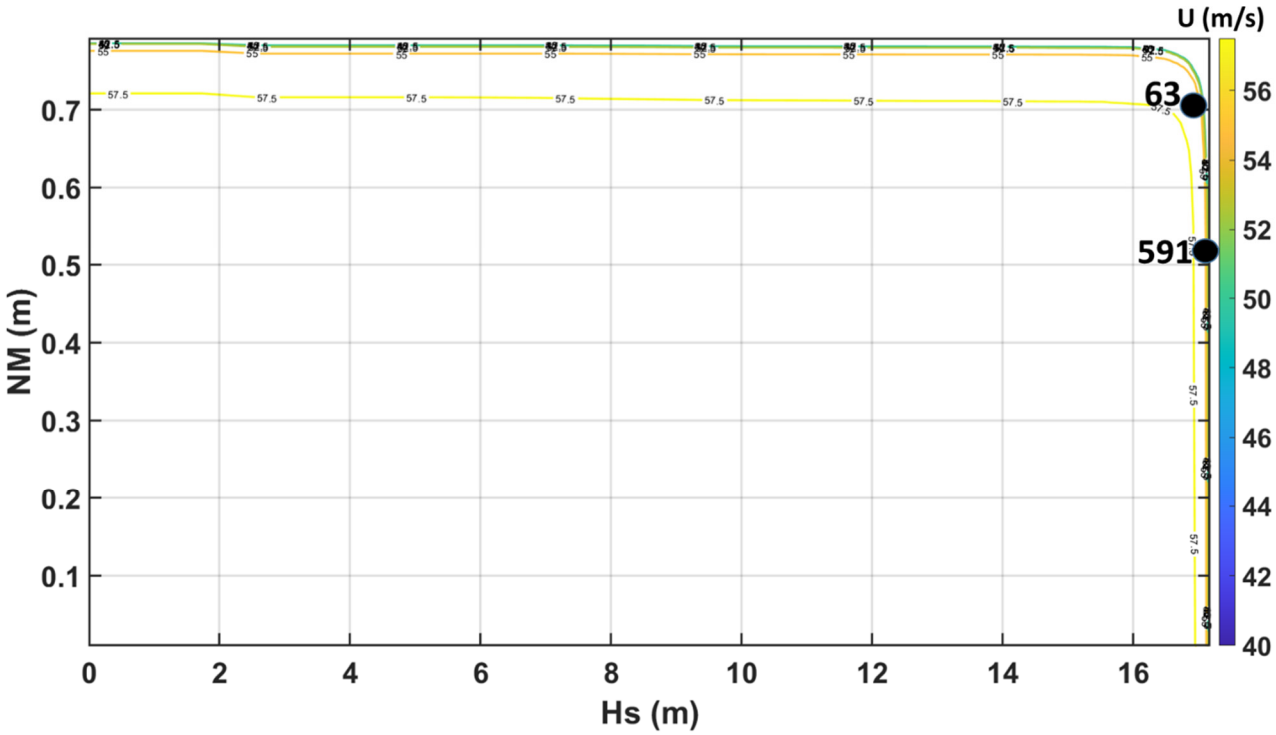


*Figure 137 : Positioning of scenarios 63 and 591 in the joint exceedance iso-contours for return period of 100 years within the space (NM; Hs) with the colour indicating the U values at Rodrigues forcing point for 2100 climate scenario.*

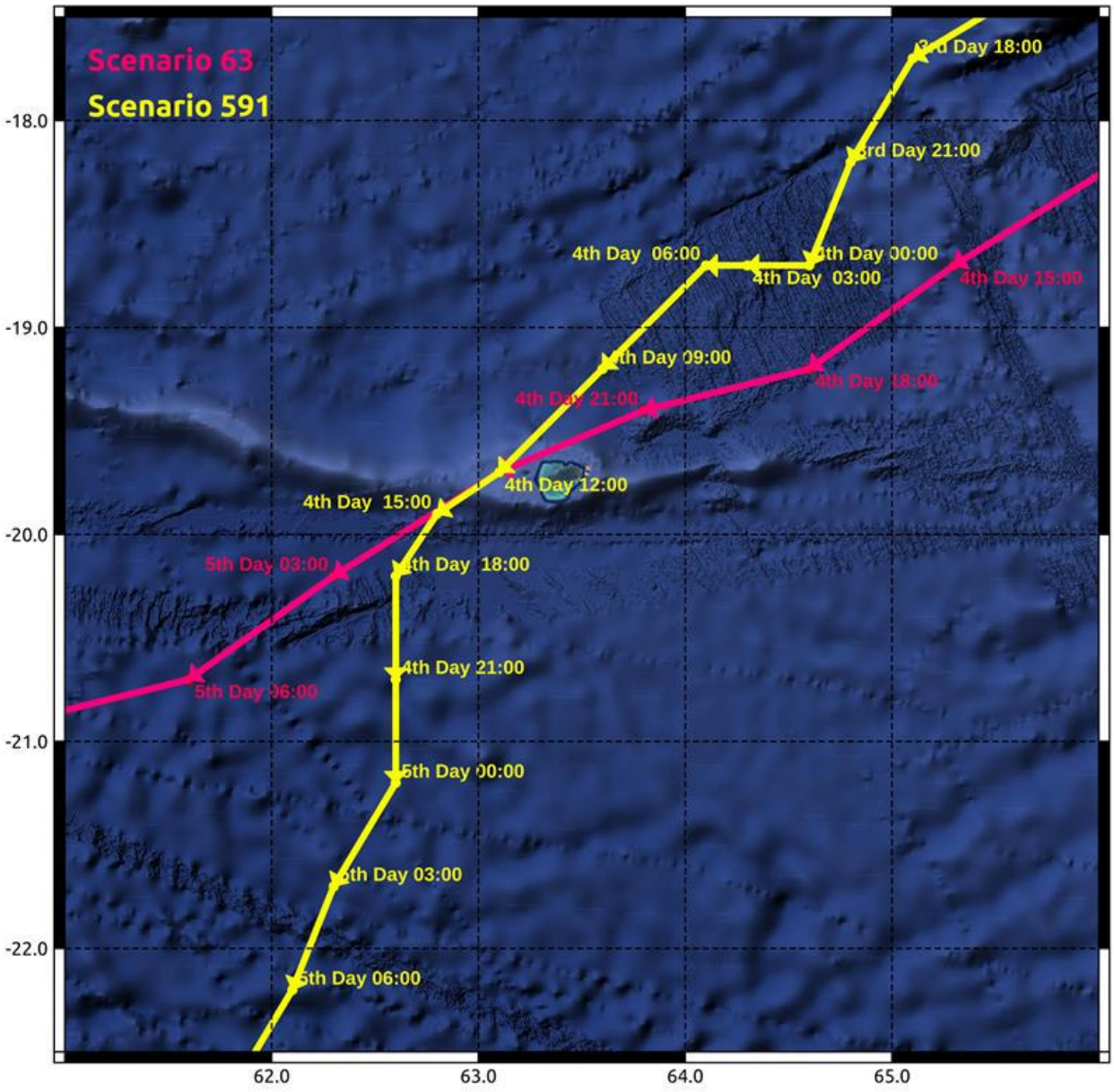


*Figure 138 : Cyclones' tracks for the scenario ITC 63 and ITC 591of the Météo-France database.*

The simulations also take into account the influence of tide representative of a Mean High Water Springs conditions in the area. These signals are provided by the database FES2014. The considered scenarios will strike under similar tidal conditions.

Different offsets are added in order to account for different contributions and for sea level rise. In particular, the offsets are composed as follows:

- **+ 0.25 m of security margin**: In order to take into account monthly anomalies in mean sea levels (MSL) due to steric effects and the gyre circulation (§ 4.2.2.1.2.2). These anomalies are illustrated on the recordings from the Port-Mathurin tide gauge (Figure 139) with higher MSL values during the cyclone period (December to March), with mean/maximum values of up to ~10cm and over 25cm respectively;
- **+ 0.26 m**: sea level rise at horizon 2050 (§ 3.5.3.4.2);

- **+ 0.11 m**: island subsidence at horizon 2050 (§ 3.5.3.2.4);
- **+ 0.87 m**: sea level rise at horizon 2080-2100 (§ 3.5.3.4.2);
- **+ 0.21 m**: island subsidence at horizon 2080-2100 (§ 3.5.3.4.2).

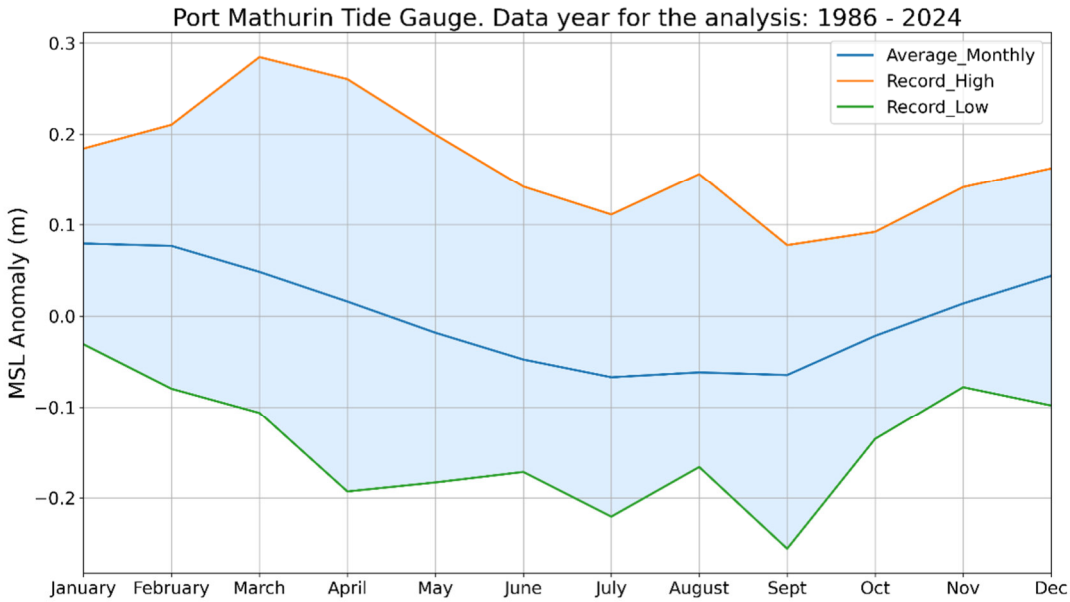


*Figure 139 : De-trended monthly MSL (mean sea level) plotted for each month of the year for the length of the respective tide gauge record of Port-Mathurin (1986-2024).*

For the sake of clarity, in the following (Figure 140 to Figure 143), we will only show the pressure and wind fields of scenario 63 as this is the scenario with the greatest impact on the Rodrigues coastline. The atmospheric forcing on the actual climate has been also employed on 2050 climate due to negligible differences.

Moreover, we also report the tidal signal (Figure 144) imposed as boundary condition to our numerical simulations, provided by FES2014 on the forcing points of the boundary.

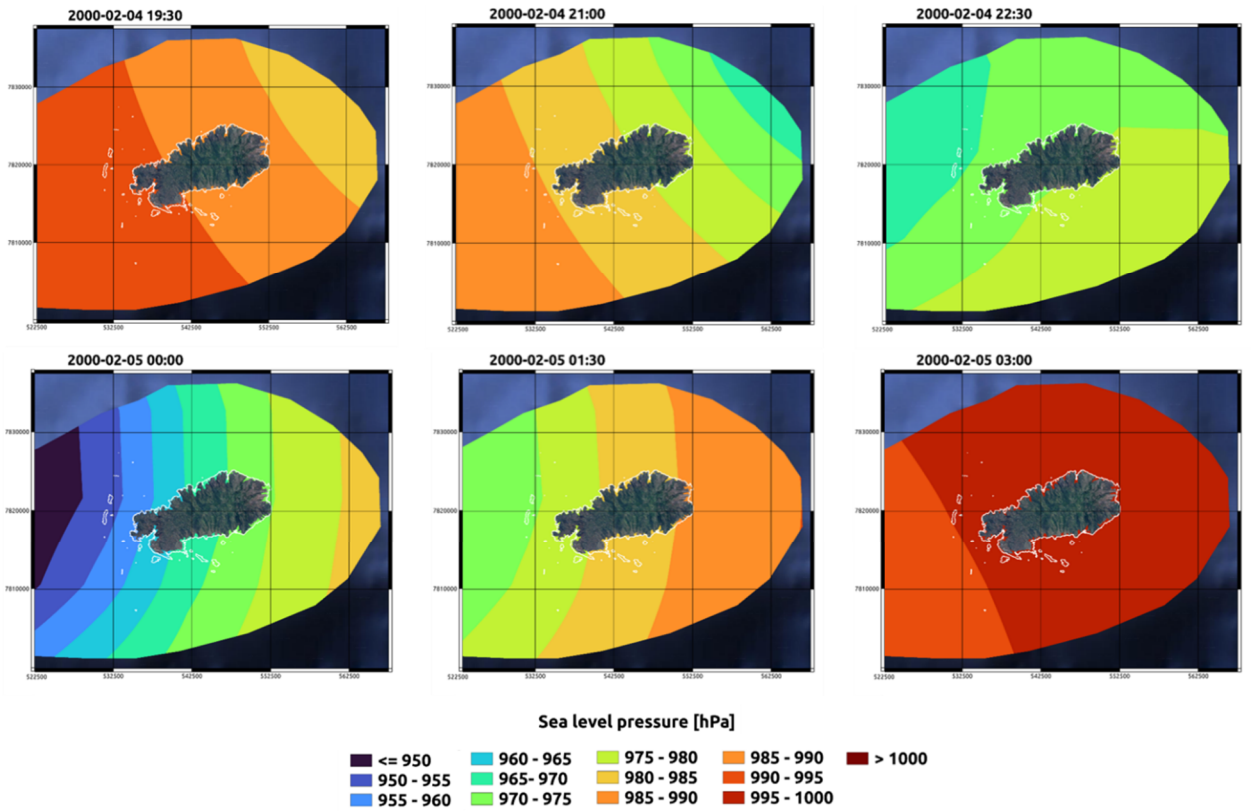


*Figure 140 : Time evolution of the pressure field over the Rodrigues computational domain during the 63 scenario on actual and 2050 climate.*

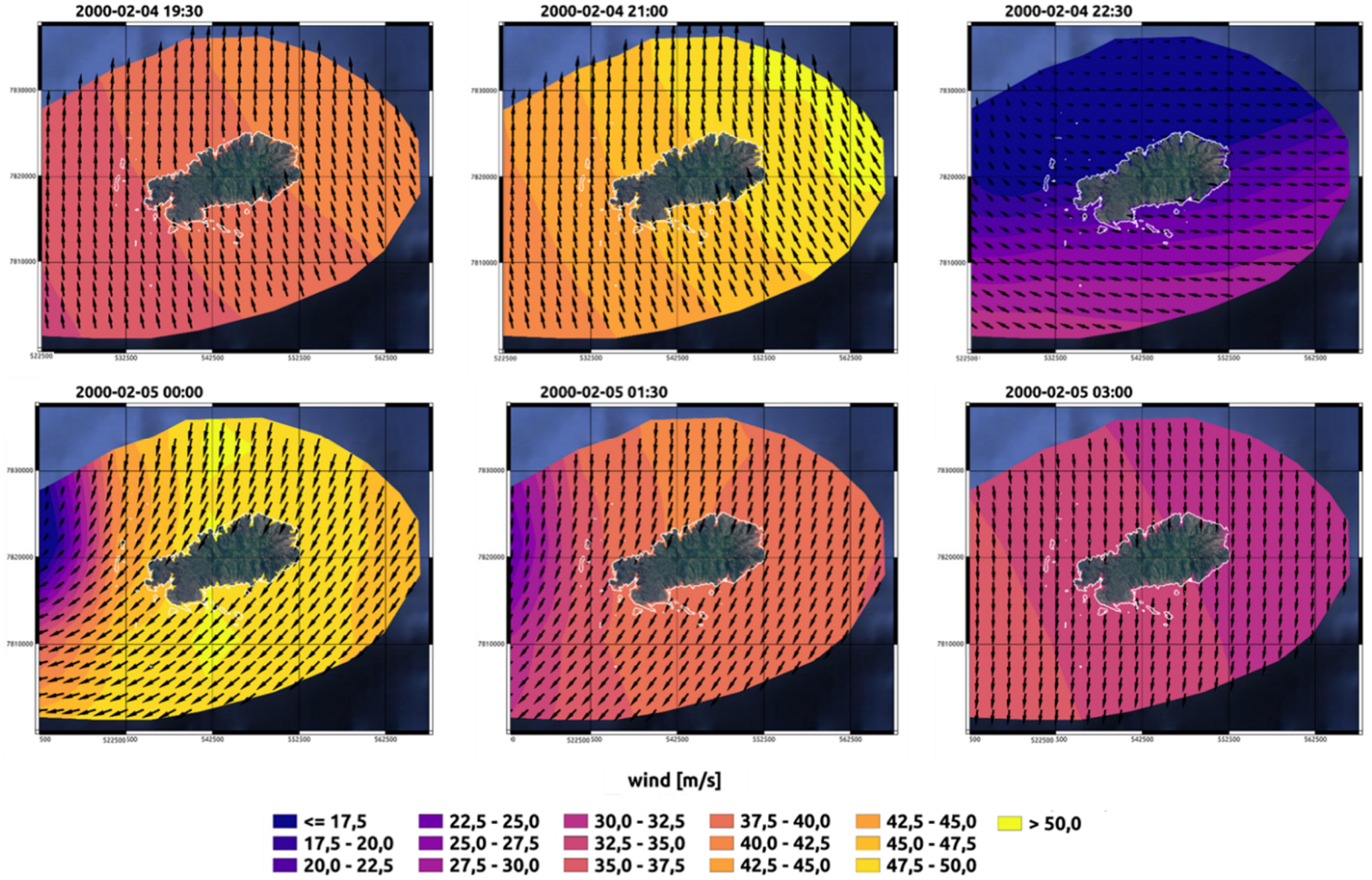


*Figure 141 : Time evolution of the wind field over the Rodrigues computational domain during the 63 scenario on actual and 2050 climate.*

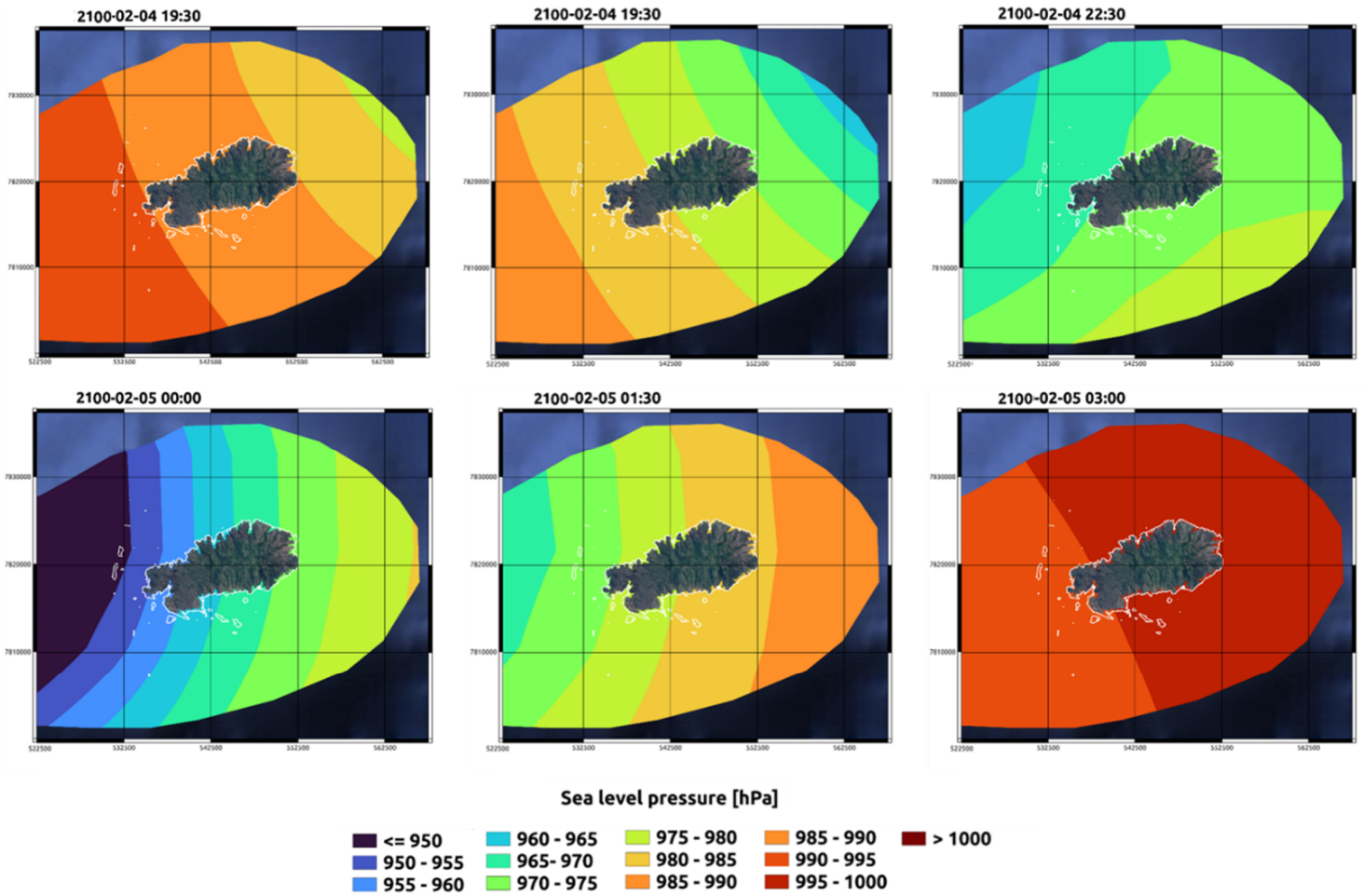


*Figure 142 : Time evolution of the pressure field over the Rodrigues computational domain during the 63 scenario on 2080-2100 climate.*

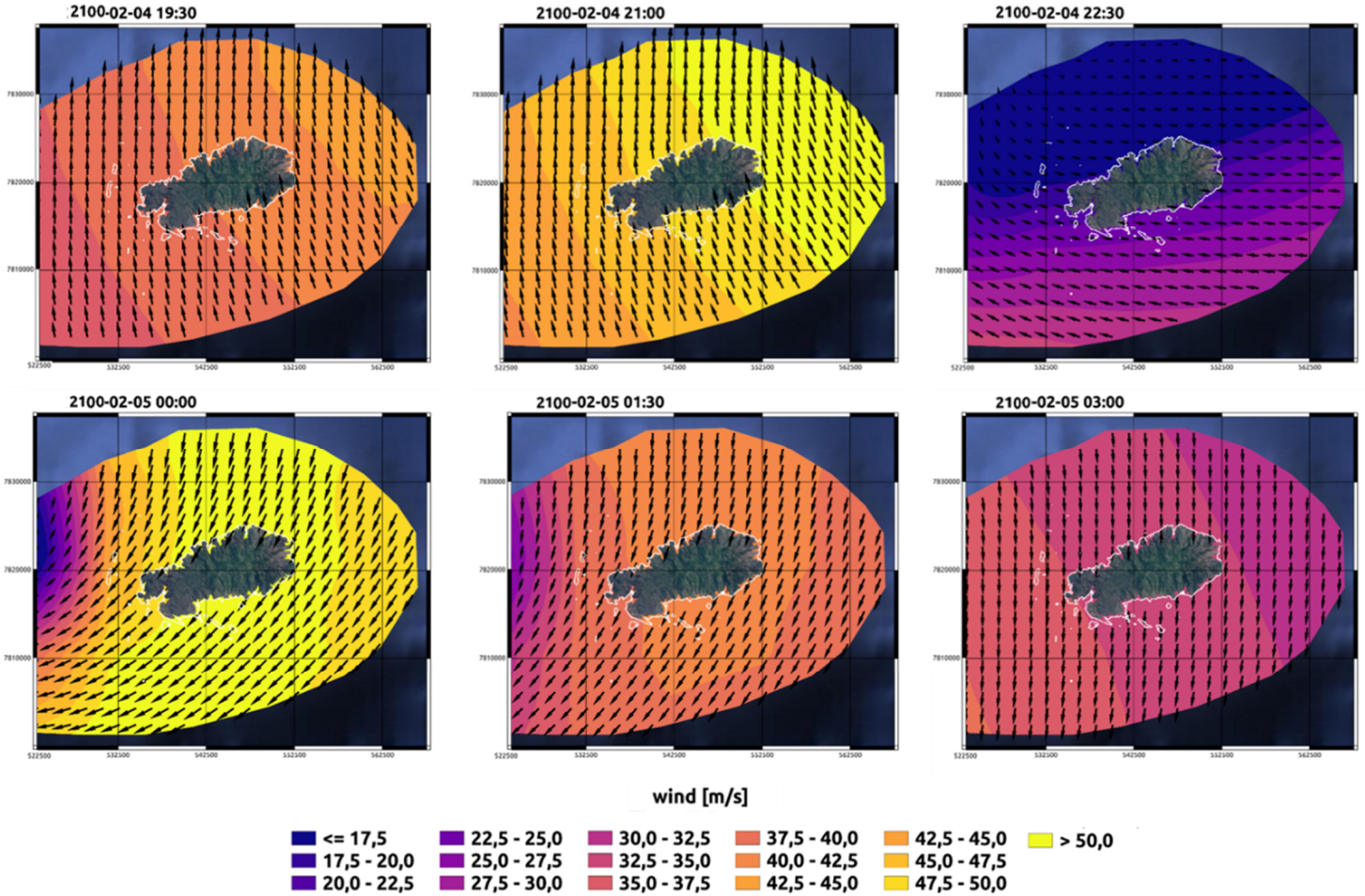


*Figure 143 : Time evolution of the wind field over the Rodrigues computational domain during the 63 scenario on 2100 climate.*

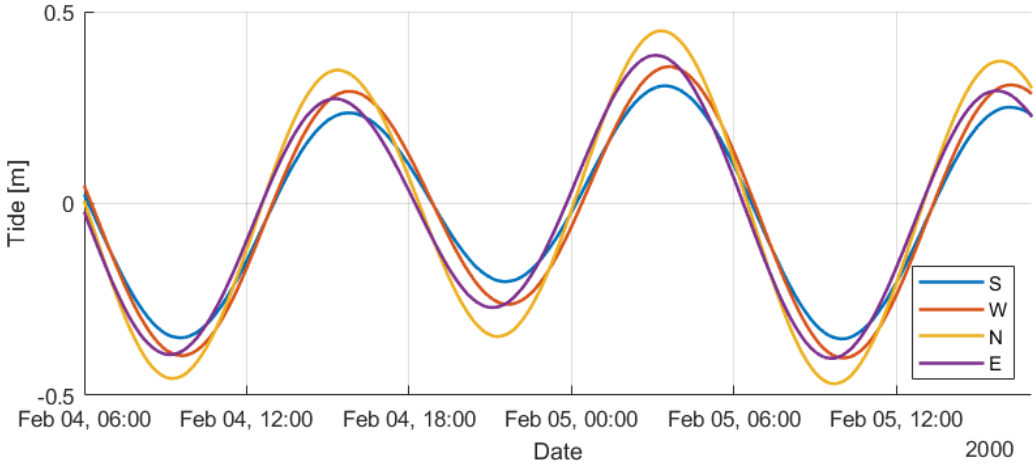


*Figure 144 : Tidal signal during the 63 scenario, provided by the FES2014 database on the four forcing locations of the Rodrigues model.*

#### *4.2.2.2.2.3 Simulation results*

Here again, we are only presenting the results of scenario 63 as this is the scenario with the greatest impact on the Rodrigues coastline.

The scenario 63 generates waves with 15m of maximum significant wave height (Hs) wrapping the island from all the sides (Figure 146). Waves break as they approach the lagoon reef. The value of Hs falls very rapidly from above 12-15m offshore to only approximately 1m inside the lagoon, with the only exception of the two channels that give access to the lagoon: in the north (Figure 147 left) and in the south (Figure 147 right). Sea currents are mainly driven by waves, that strongly break approaching the lagoon reef. By consequence currents are very intense offshore all around the reef, achieving 3m/s in some spots, while rarely reach 1m/s inside the lagoon, with the only exception being the narrow passage between the Paille and Queue island and the Gombrani island. On the flooded areas on land, the currents intensity are usually below 0.25m/s, expect on the Anse Mourouk, Rivière du Sel and Rivière Cocos sites, where they can exceed 2m/s along the coast, and at Port Mathurin (please refer to section § 4.3.2.3).

Both wave fields and sea currents velocities are very little affected by the different configurations played (climate conditions or island subsidence), as evidenced by Figure 145 and Figure 146 respectively, which compare the results on the two extreme cases on actual climate and on 2080-2100 climate with subsidence.

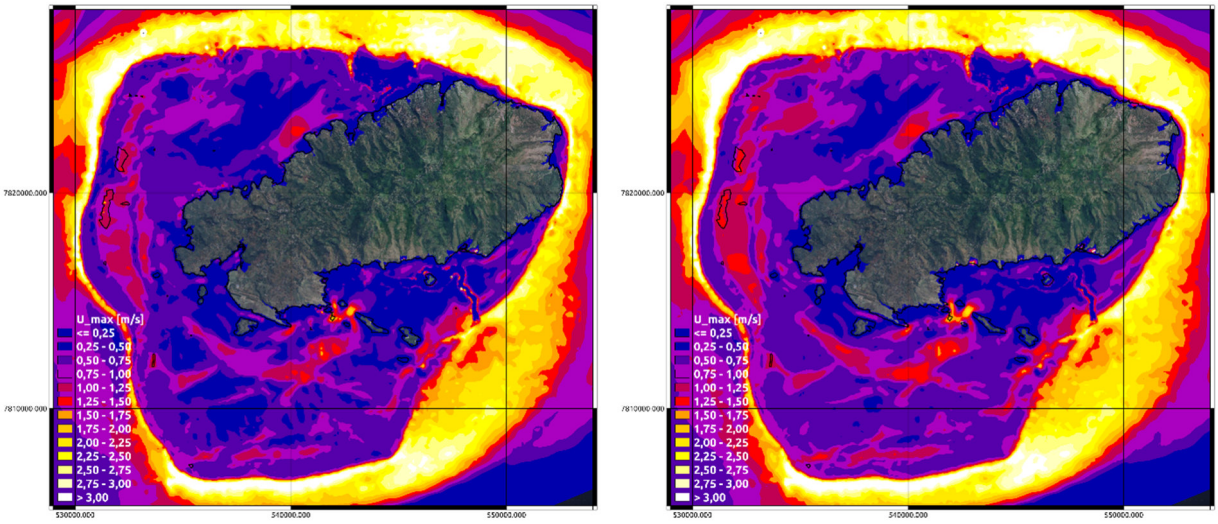


*Figure 145 : Overall map of the computed maximum sea currents velocity on the scenario 63 with actual climate (left) and with 2080-2100 climate and island subsidence (right).*

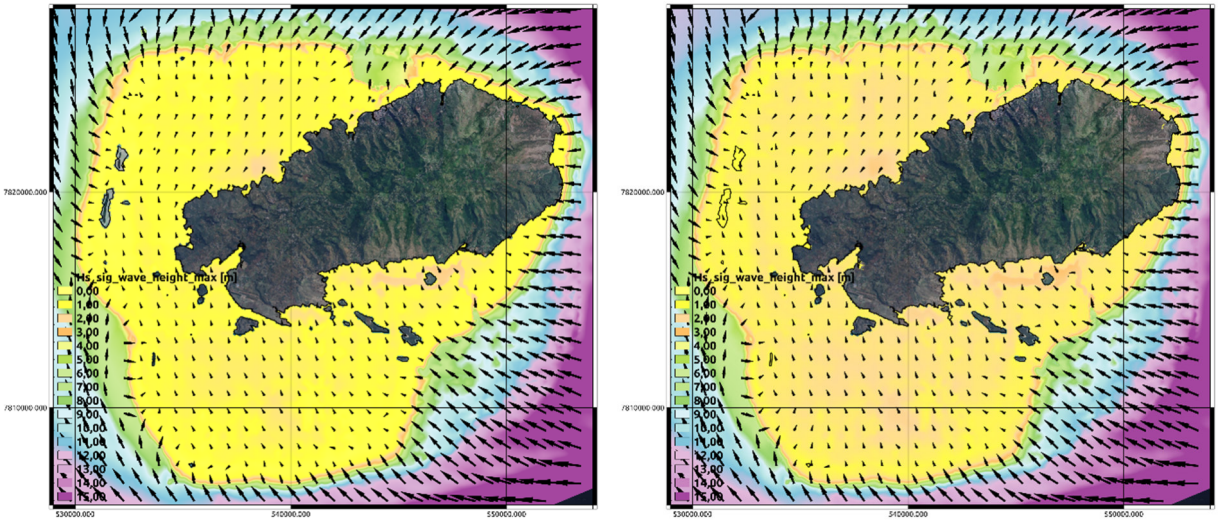


*Figure 146 : Overall map of the computed maximum significant wave height on the scenario 63 with actual climate (left) and with 2080-2100 climate and island subsidence (right).*

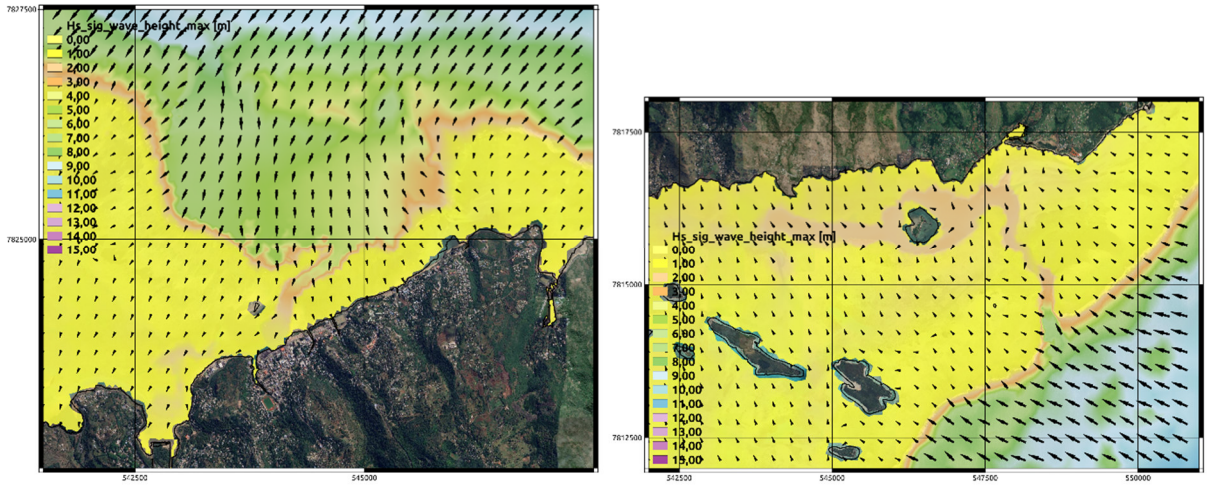


*Figure 147 : Close-up view on the north (right) and south lagoon channels for the computed maximum significant wave height on the scenario 63 with actual climate.*

Figure 148 shows the simulated maximum sea surface height on the overall domain around the island and on the lagoon for the different climate conditions. In general, the scenario produces greater water levels on the south coast of the island that can achieve 2,60m on actual climate, 3m in 2050 and exceed 3m60 in 2080. The largest flooded sectors are on Anse Mourouk, Grand Baie and on urban area of Port Mathurin, but a special focus on this latter is provided in the further section § 4.3.2.3. Despite this, the extension of the flooded region is controlled by the topography and do not increase considerably, but flooded areas suffer greater water heights with future climate conditions. This is visible on the close-up comparison shown in Figure 149 and Figure 150 on the Anse Mourouk area and in Figure 152 and Figure 153 on the Grand Baie area. Mainly due to the extreme sea water levels generated on the south coast of the island, the flooding hazard in Anse Mourouk is from “very high” to “high” already in present-day climate conditions (Figure 151). In Grand Baie, instead, the hazard rises progressively from actual to 2100 climate (Figure 154).

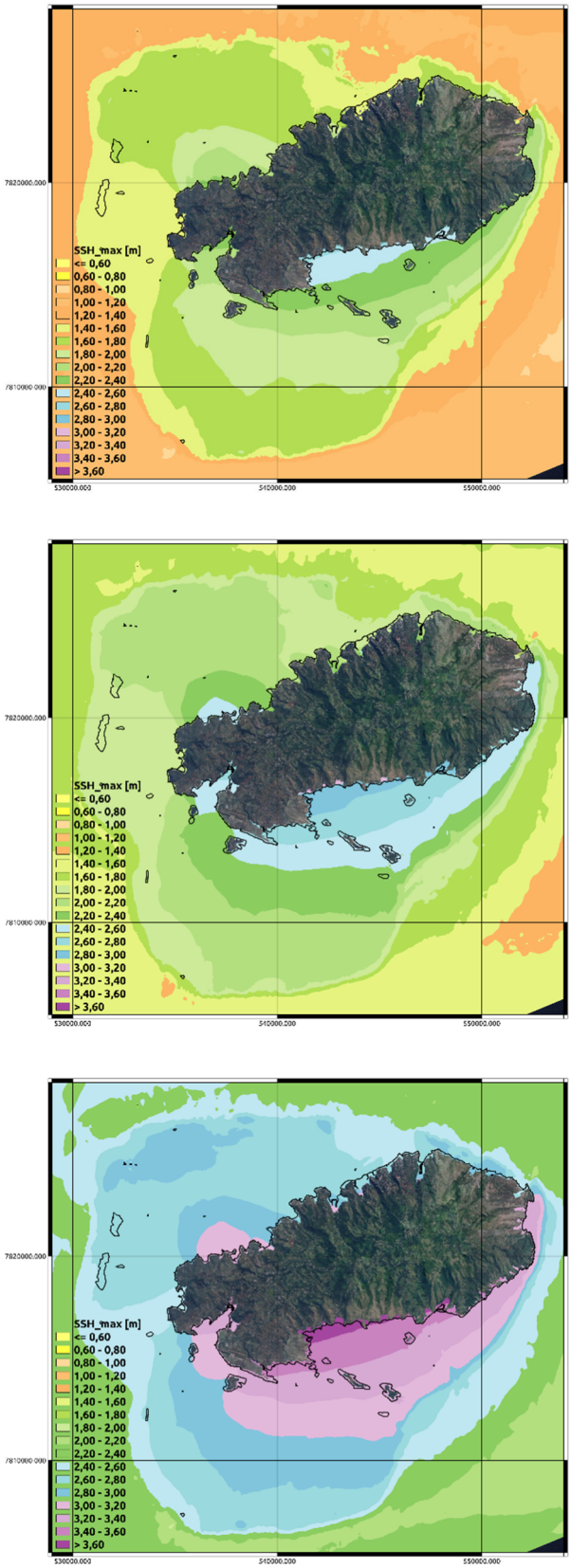


*Figure 148 : Overall map of the computed maximum sea surface height (SSH_max) on the scenario 63 with present-day climate conditions (top), 2050 climate (centre) and 2100 climate (bottom).*

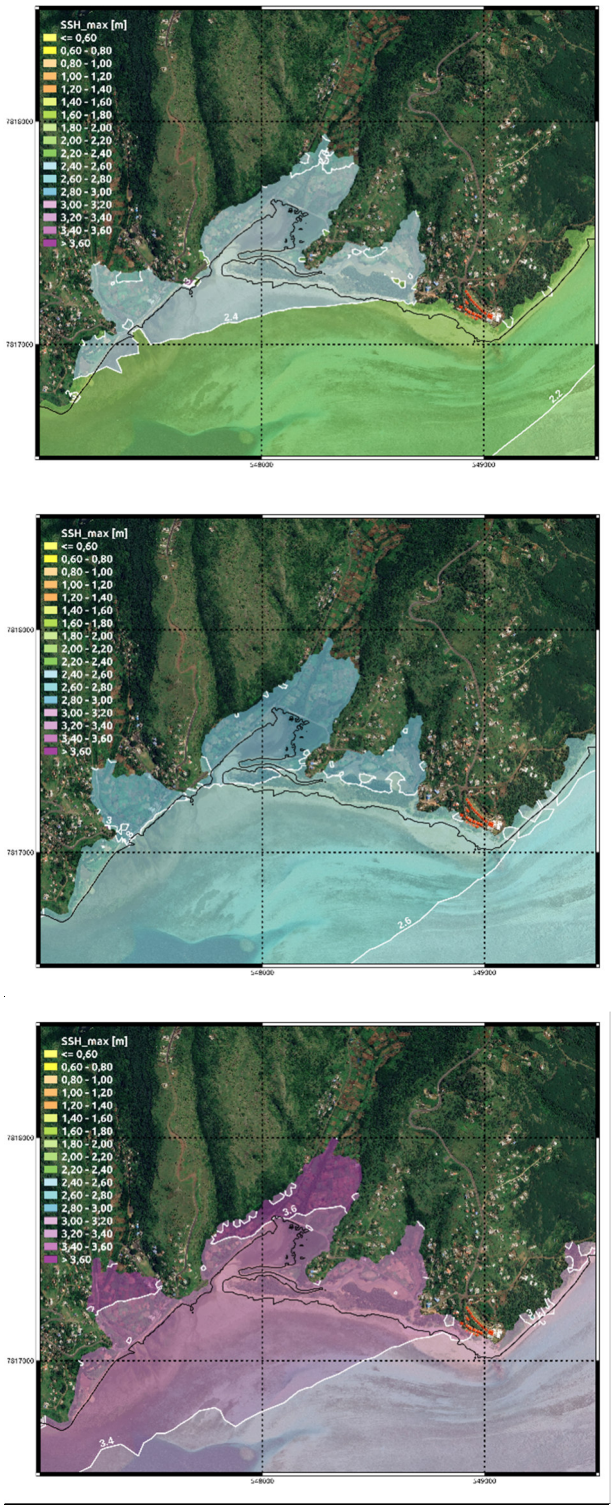


*Figure 149 : A close-up comparison on the Anse Mourouk area of the computed maximum sea surface height (SSH_max) on the scenario 63 with present-day climate conditions (top), 2050 climate (centre) and 2100 climate (bottom).*

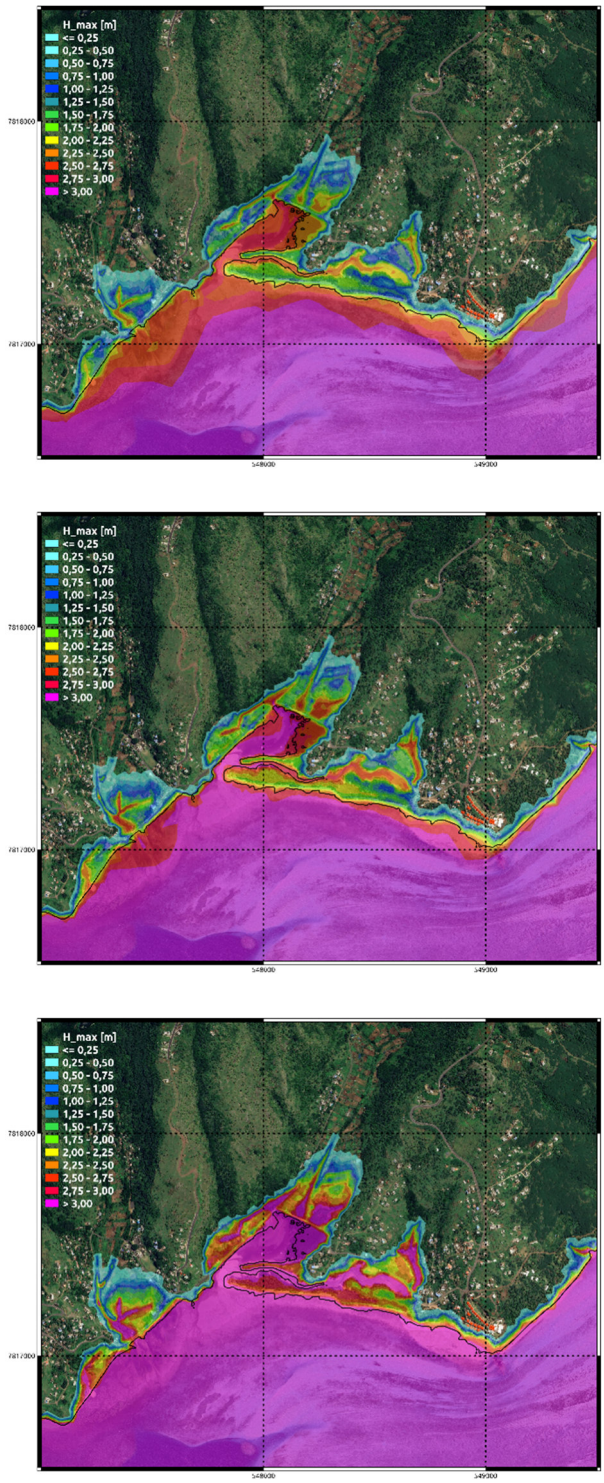


*Figure 150 : A close-up comparison on the Anse Mourouk area of the computed maximum water height (H_max) on the scenario 63 with present-day climate conditions (top), 2050 climate (centre) and 2100 climate (bottom).*

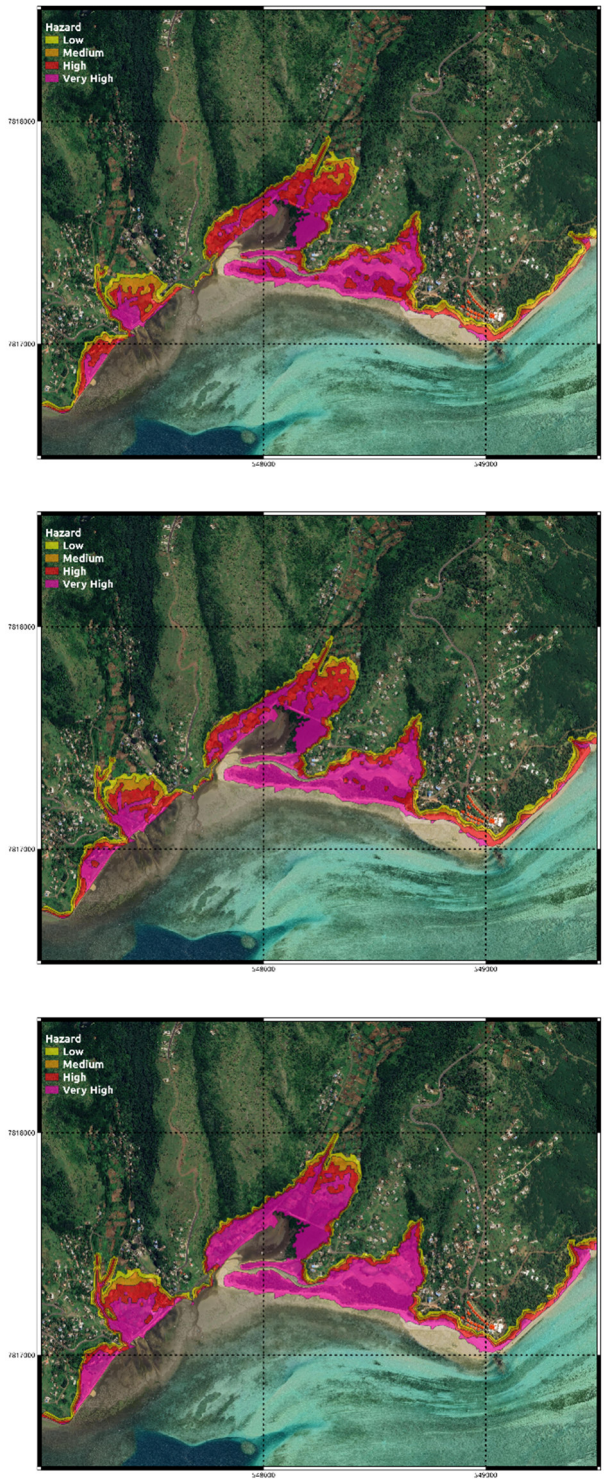


*Figure 151 : Flooding hazard maps on the Anse Mourouk area for present-day climate conditions (top), 2050 climate (centre) and 2100 climate (bottom).*

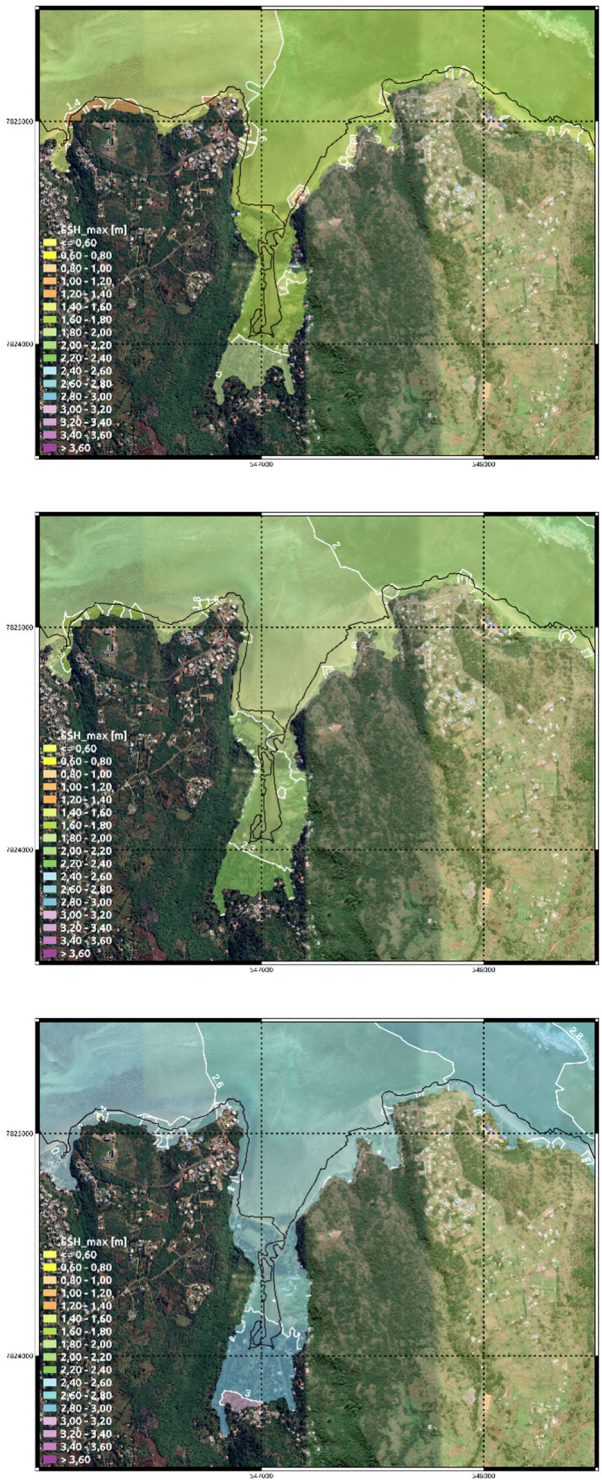


*Figure 152 : A close-up comparison on the Grand Baie area of the computed maximum sea surface height (SSH_max) on the scenario 63 with present-day climate conditions (top), 2050 climate (centre) and 2100 climate (bottom).*

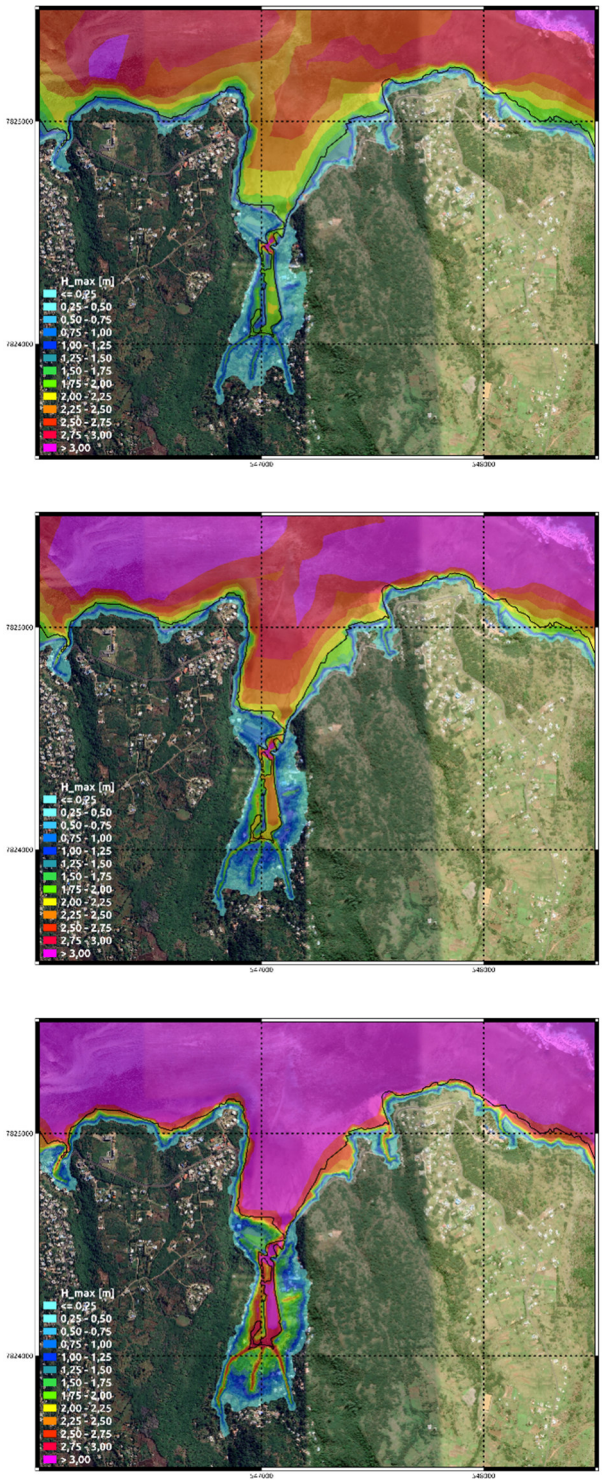


*Figure 153 : A close-up comparison on the Grand Baie area of the computed maximum water height (H_max) on the scenario 63 with present-day climate conditions (top), 2050 climate (centre) and 2100 climate (bottom).*

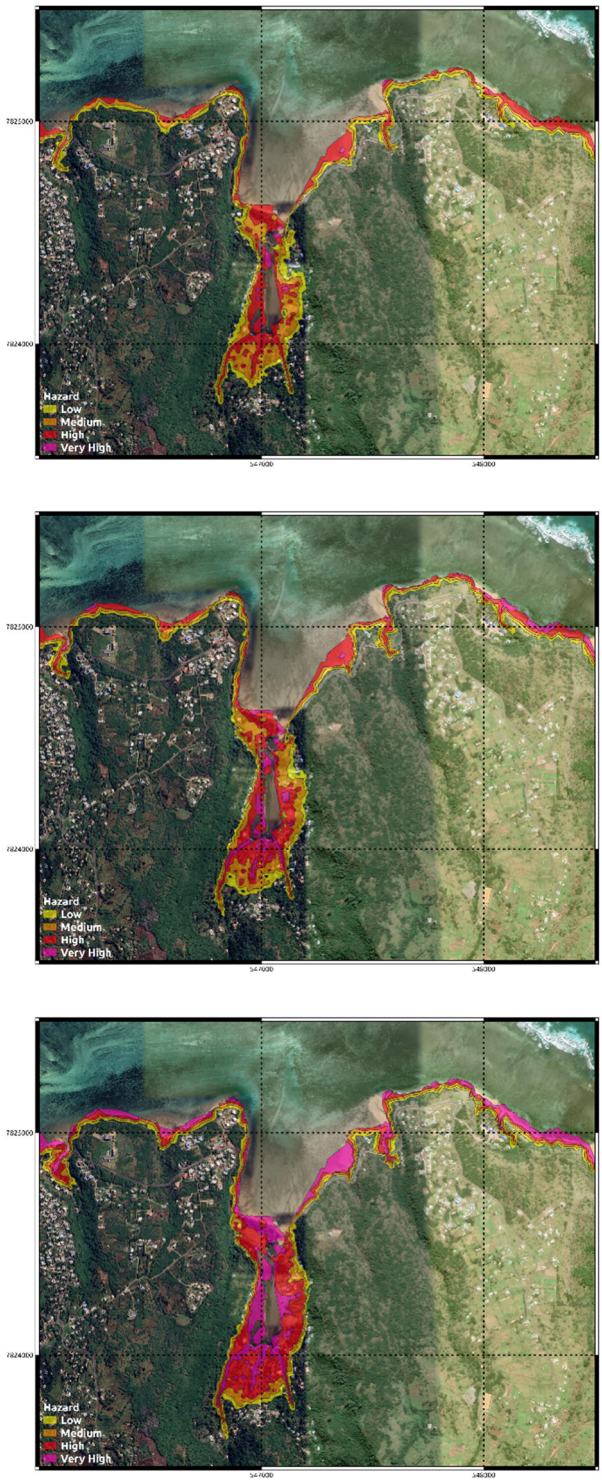


*Figure 154 : Flooding hazard maps on the Grand Baie area for present-day climate conditions (top), 2050 climate (centre) and 2100 climate (bottom).*

The peak of surge does not happen everywhere at the same time. Figure 155 shows how the peak of sea level comes first on the south side of the island and only a few hours later on the north side. This is mainly the result of the effect of the wind that pushes great amount of water across the wide lagoon firstly northward and, only after the cyclone passage, southward. Therefore, all the south coast of the island (Baie Topaze and Port Sud-Est in Figure 155) experiences big positive surges at the beginning of the event, followed by great negative surges (compared to the tidal signal) in the second phase of the simulation. The peak coincides with the peak of tide. The north side (Baie du Nord in Figure 155) experiences the opposite dynamics, but the area is closer to the cyclone track and, by consequence, the role played by the depression is more important, generating the double peak visible on Baie du Nord and Port Mathurin time-series in Figure 155. Identical considerations can be done in 2050 and 2080-2100 climate conditions, whose time series are very analogous and are not shown here.

Waves breaking on the reef generate a strong setup inside the lagoon, especially on the first phase of the event. In Figure 156 we show the time-series of the setup generated by waves on several locations in the case of present-day climate conditions. The setup has been computed by subtracting to the total water level the level computed running a simulation with only the atmospheric forcing (dashed lines in Figure 156). In general the setup contributes to ~0.3m in to determine the resulting total water level, but this contribution increases in correspondence of the high tide phase with peaks that often achieve ~0.5m (Port Mathurin, Baie Topaze, Port Sud-Est) and, in some cases (Baie du Nord, Trou d'Argent) can achieve or surpass 1m. Baie of Topaze experiences a double peak of setup, when the bay is submerged again after being drained at low tide. Analogous considerations are valid also for the simulations with other climate conditions.

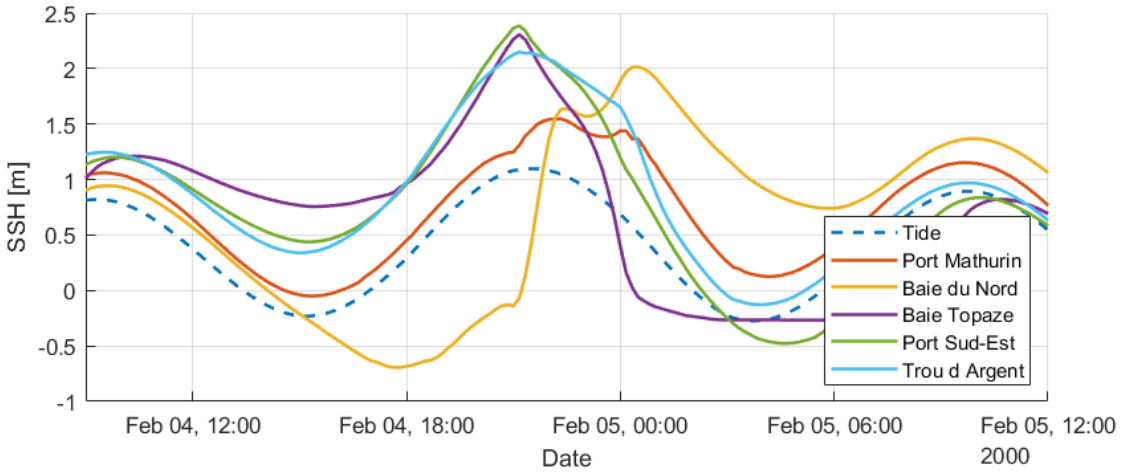


*Figure 155 : Time series of the sea surface level on different locations around the island for the actual climate scenario.*

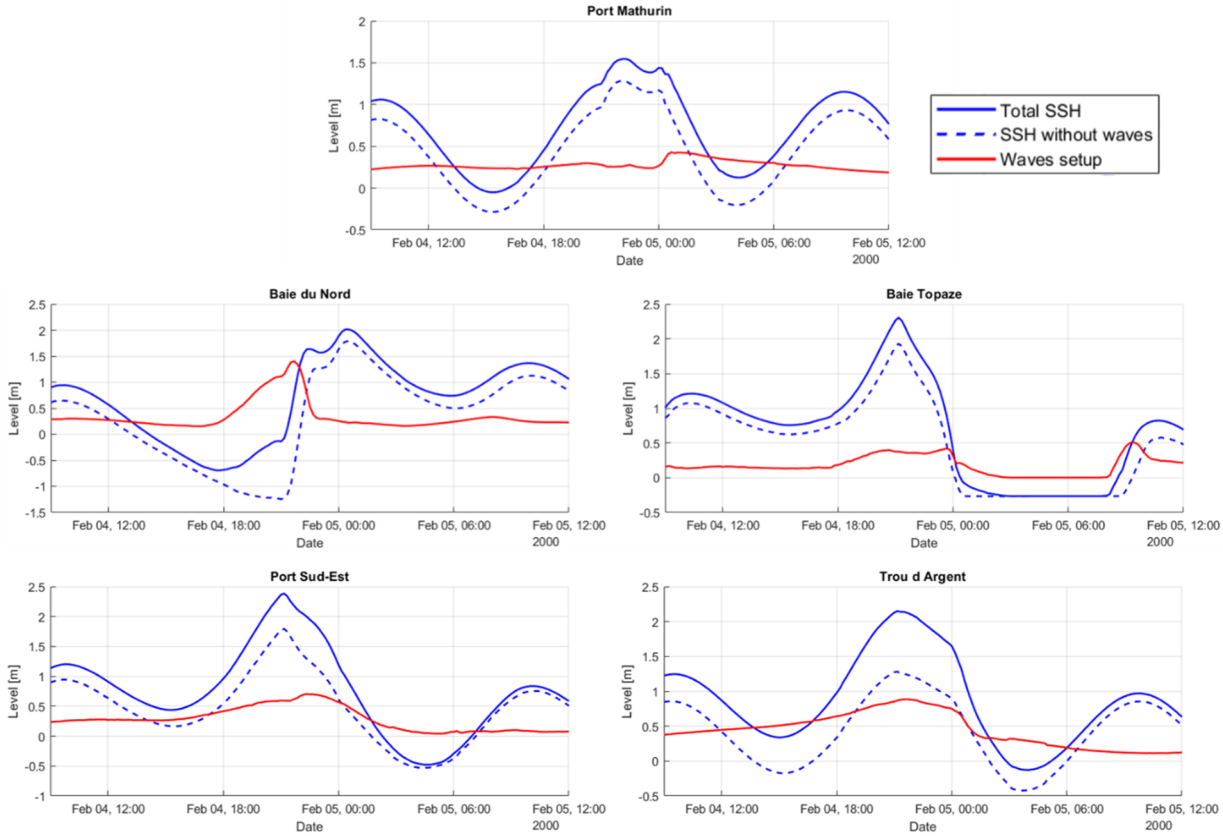


*Figure 156 : Wave setup time history for some locations of the Rodrigues island on the scenario 63 with actual climate conditions.*

Scenarios without accounting for the island subsidence at horizon 2050 and 2100 have also been computed, but for sake of clarity they are not presented in here.

## 4.3 FLIC-EN-FLAC, ANSE LA RAIE (MAURITIUS) AND PORT-MATHURIN (RODRIGUES) SITES AT 1:5,000 SCALE

### 4.3.1 Introduction

The choice of sites for a more detailed assessment (hotspots) was proposed by the project team and then validated by the project steering committee.

Two sites are located in Mauritius:

- the first (Flic-en-Flac) is representative of Mauritius' sandy coasts, behind which there are many issues (habitat, network, tourist infrastructures),

- The second is relatively undeveloped, with landscape, environmental and recreational issues at stake (this site will potentially be the focus of tourism development in the coming years).

The third site, Port-Mathurin, is located in Rodrigues. It is a highly urbanized site with numerous urban, port, residential, logistics, administrative and energy (power station) issues.

The first two sites are exposed to the two hazards of coastline erosion/retreat and coastal flooding, while the third (Port-Mathurin) is mainly exposed to the hazard of coastal flooding and to a lesser extent to coastline retreat. The coastline here is highly developed, with numerous coastal structures and facilities. In some areas, man-made embankments have been built on top of which people's livelihoods are at risk. The structures and facilities along the Port-Mathurin coastline are exposed to wave impacts during storms and hurricanes, as they have been built on embankments protruding above the natural terrain, causing deterioration and damage to structures.

### 4.3.2 Sites presentation (*hotspots*)

#### 4.3.2.1 Flic-en-Flac (Mauritius)

Flic-en-Flac is located on the west coast of Mauritius. Running generally north-south, the sandy beach extends for around 6.4 km and is bordered to the north by basalt formations forming a rocky coastline and then cliffs, and to the south by the Tamarin estuary.

The beach is protected by a reef and the lagoon, which is relatively shallow, is between 300 m and 500 m wide. Bioclastic sands produced by the reef are the main source of sediment for the beach. In the northern half of the beach, the longshore drift is oriented towards the north, whereas in the southern half it is southwards. Some channels export bioclastic sands produced by the reef towards the open sea (sediment sinks), excluding them from the beach sediment balance.

The beach rests on a sandy dune ridge that varies in width from around sixty metres to almost 250 metres. The height of the dune is fairly low, around 4 to 5 metres (Figure 157, uncorrected DTM). Behind this barrier, parallel to the coast, there is a long, low-lying area occupied by two rivers flowing from north to south. At their estuaries, in the southern part of the Flic-en-Flac beach, these two rivers break through the sandy barrier. Around these mouths, there are low-lying areas.

The Flic-en-Flac sector is an area with multiple assets, with the old village to the north, a residential area with private housing in the centre and large hotel complexes to the south. Some parts of Flic-en-Flac are public beaches and are very popular.

This sector has been the subject of several studies in the past (Baird 2003, JICA 2015, Duvat Magnan et al., etc.). For example, Baird (2003) carried out modelling of the effect of cyclones on

the retreat of the coastline, which was estimated at between 11 and 14m. Independently of this retreat during an extreme events, some sectors of Flic-en-Flac are subject to chronic erosion.

This sector is monitored by the Public Authority and the ICZM Division of the Ministry of the Environment and has been the subject of several development and erosion prevention projects:

- Revegetation test plots with endemic trees in place of filaos to increase the beach's resilience to erosion,

- The gabion walls that had been installed to protect the beach against erosion were recently removed as they were not very effective and were having harmful effects on both sides of the structures,

In areas occupied by private property or hotels, structures, walls, etc. have been installed to prevent the coastline from retreating.

The sandy dune presents a risk of breach with a potential increase in the risk of flooding in the future (sea level rise and increase in the intensity of cyclones in the future (2050, 2100). It is also potentially crossed by the sea during the occurrence of extreme events.

The Flic-en-Flac sector is therefore exposed to the two hazards of erosion and coastline retreat and to coastal flooding.

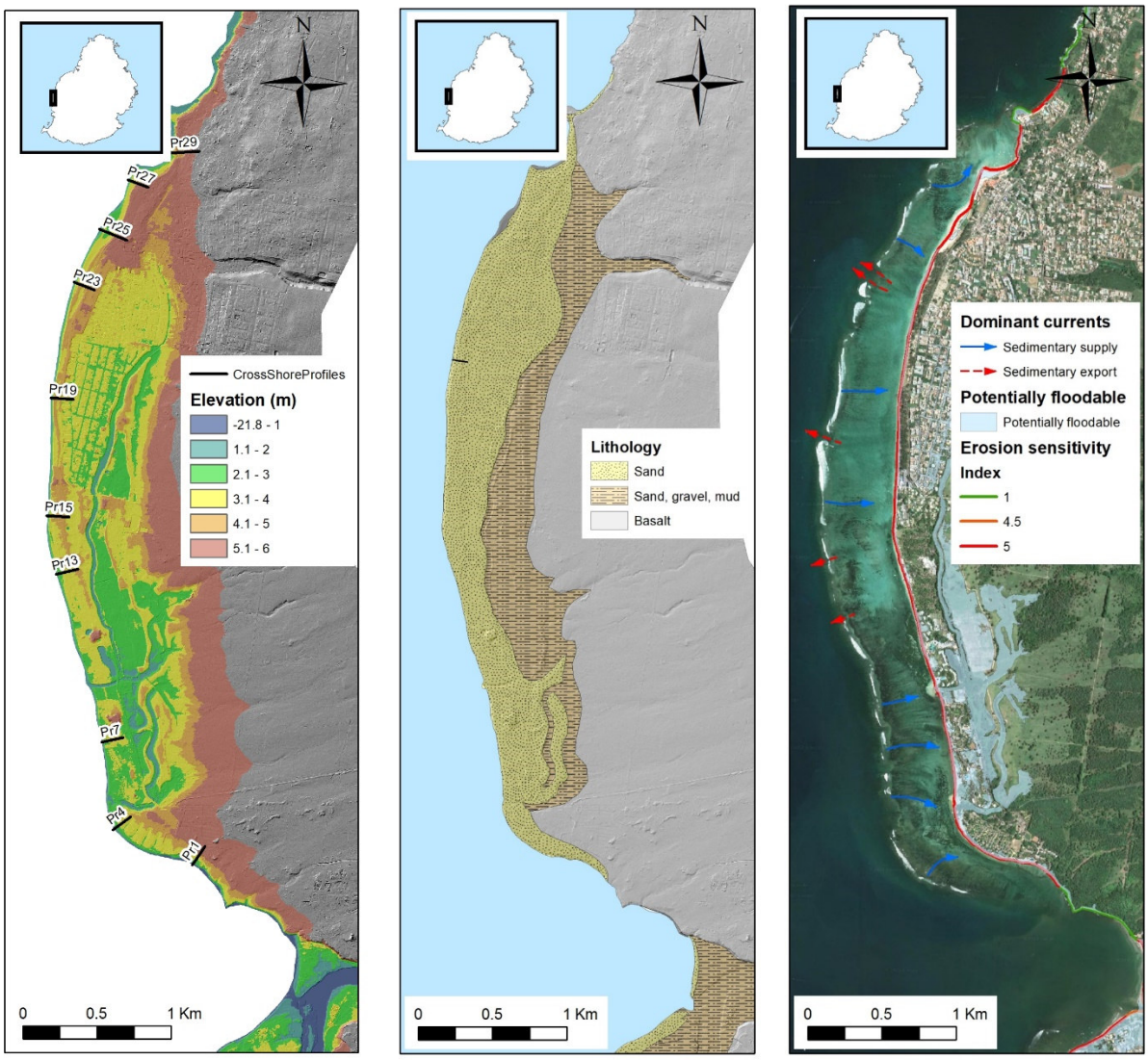


*Figure 157 : Left: topography and location of profiles at the Flic-en-Flac site; centre: lithology of the coastline; right: potential hazards and flow of sediments.*





*Figure 158 : Erosion scarp of the upper beach (Flic-en-Flac, northern third of the beach, 2022)*

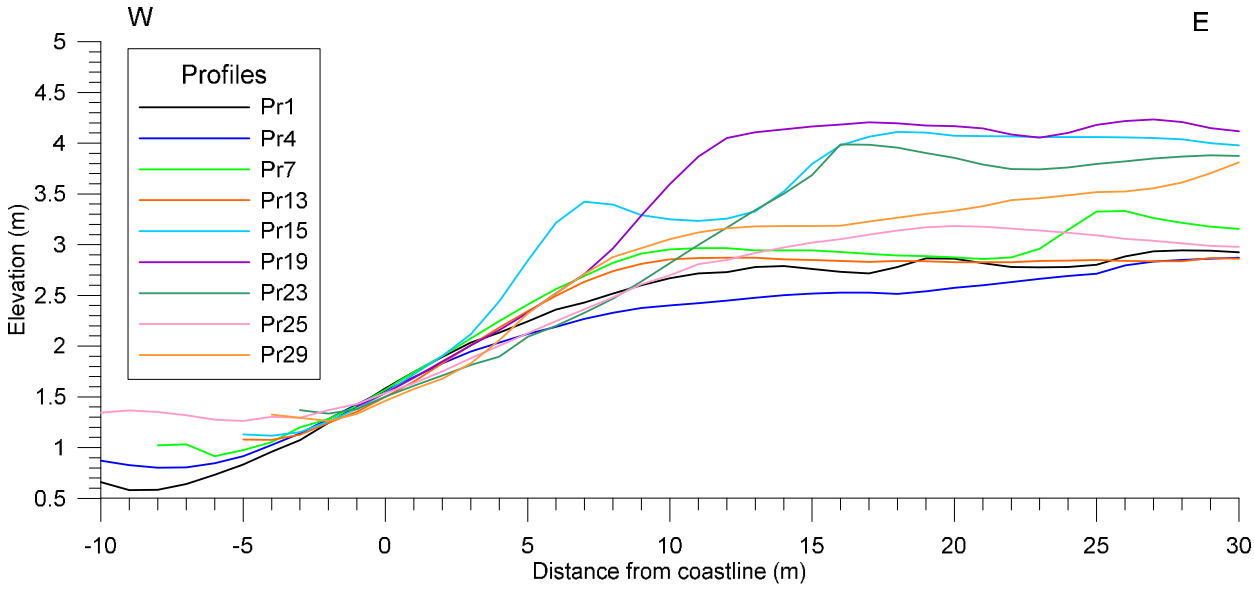


*Figure 159 : Variability of the topographic sections of the dune (Flic-en-Flac, profiles location in the Figure 157)*

### 4.3.2.2 Anse la Raie (Mauritius)

Anse la Raie is located in the north of Mauritius. Its coastline runs broadly from NNW to SSW and is therefore exposed to NNE swells and waves. There is a reef offshore at a distance of between 2,000 m and 2,700 m. It is a cove in front of which the bathymetry is low and which is protected by the presence of numerous basaltic rocky islets located at the entrance to the cove.

Anse la Raie is a sandy beach extending for around 800m. The north-facing shoreline in the northern part gradually bends to the west in the southern part. The bay is therefore exposed to waves and swells from the north-east to the east. The two rocky headlands that delimit Anse la Raie are formed by basaltic peaks that also form the shallow rocky islets and plateaux located opposite the anse (Figure 160). The sandy beach rests on a low vegetated sandy spit (herbaceous plants and *Filaos*) (around 2.6 m on the DTM before calibration) which rests on a basaltic basement. This sandy spit varies in width, up to a maximum of 260 m. This sandy spit isolates a large lagoon area behind it, which is connected to the ocean by a mouth. Around this mouth, the elevation of the land is very low (Figure 160 and Figure 162); like the coastal road that rests on it, it is subject to frequent flooding during storms and cyclones. Behind the lagoon formations and the sandy spit, the basaltic rock formations form small headlands whose altitude is higher and generally greater than 6m.

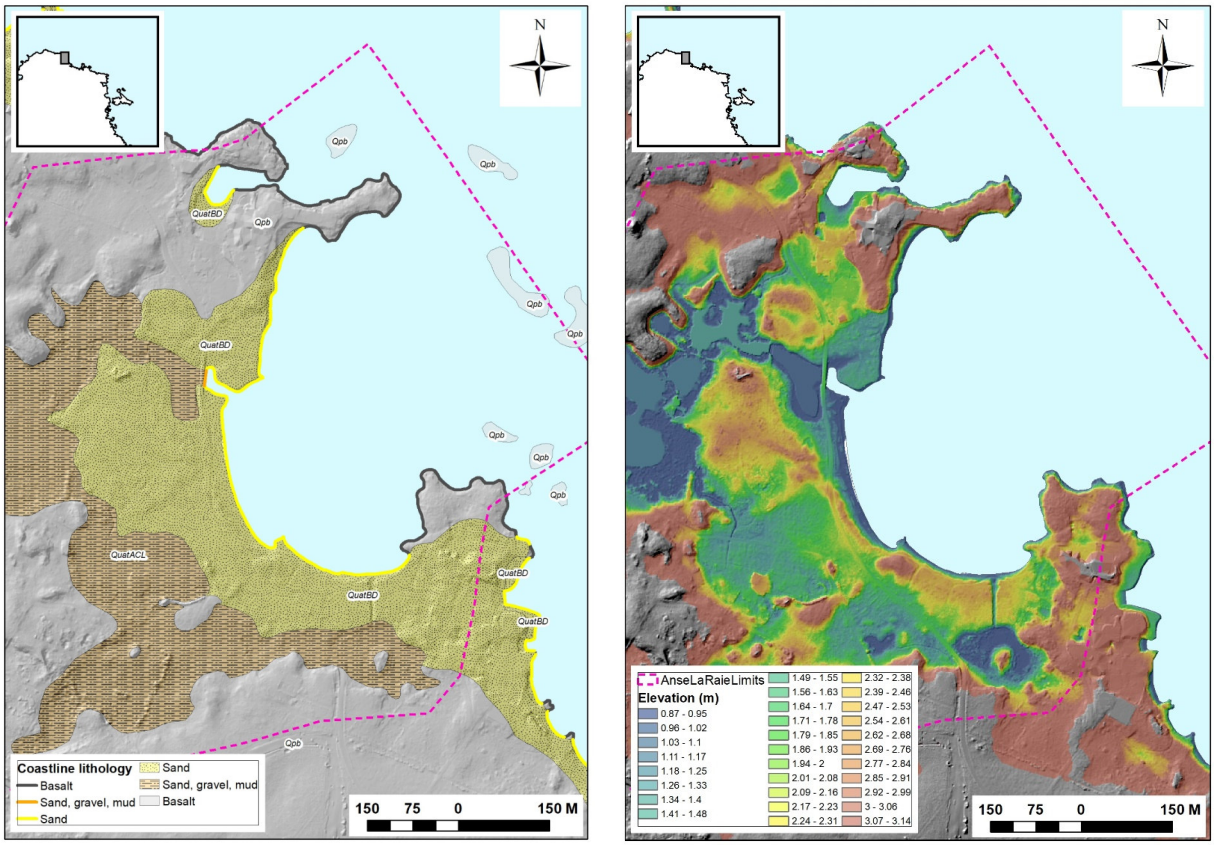


*Figure 160 : Left: lithology of the coastline at Anse la Raie, right: topography behind Anse la Raie*

The input of bioclastic sands from the reef is probably very limited because the dominant currents and sediment flows are not directed towards the coast but curve westwards towards a pass that constitutes a sedimentary sink (Figure 161). In addition, the presence of shallows and numerous islets in front of the Anse tends to form a discontinuous barrier that isolates the Anse from the reef. Bioclastic sediment inputs from the reef to the beach therefore appear to be rather limited and make little contribution to the sediment budget.

The beach at Anse la Raie, apart from the two basaltic points bordering it, has been considered to be very sensitive to erosion (Figure 161, Rapport BRGM-RC-72793-FR, 2023).

The bathymetry of Anse la Raie is low (§ 4.3.3.2.1) and, due to the presence of the shallows and islets, is very well protected from incoming swells.

There are few human or economic assets at Anse la Raie apart from the road and a few buildings. The other assets in the vicinity are hotel facilities located on the basalt outcrops that border the north and south of the anse.

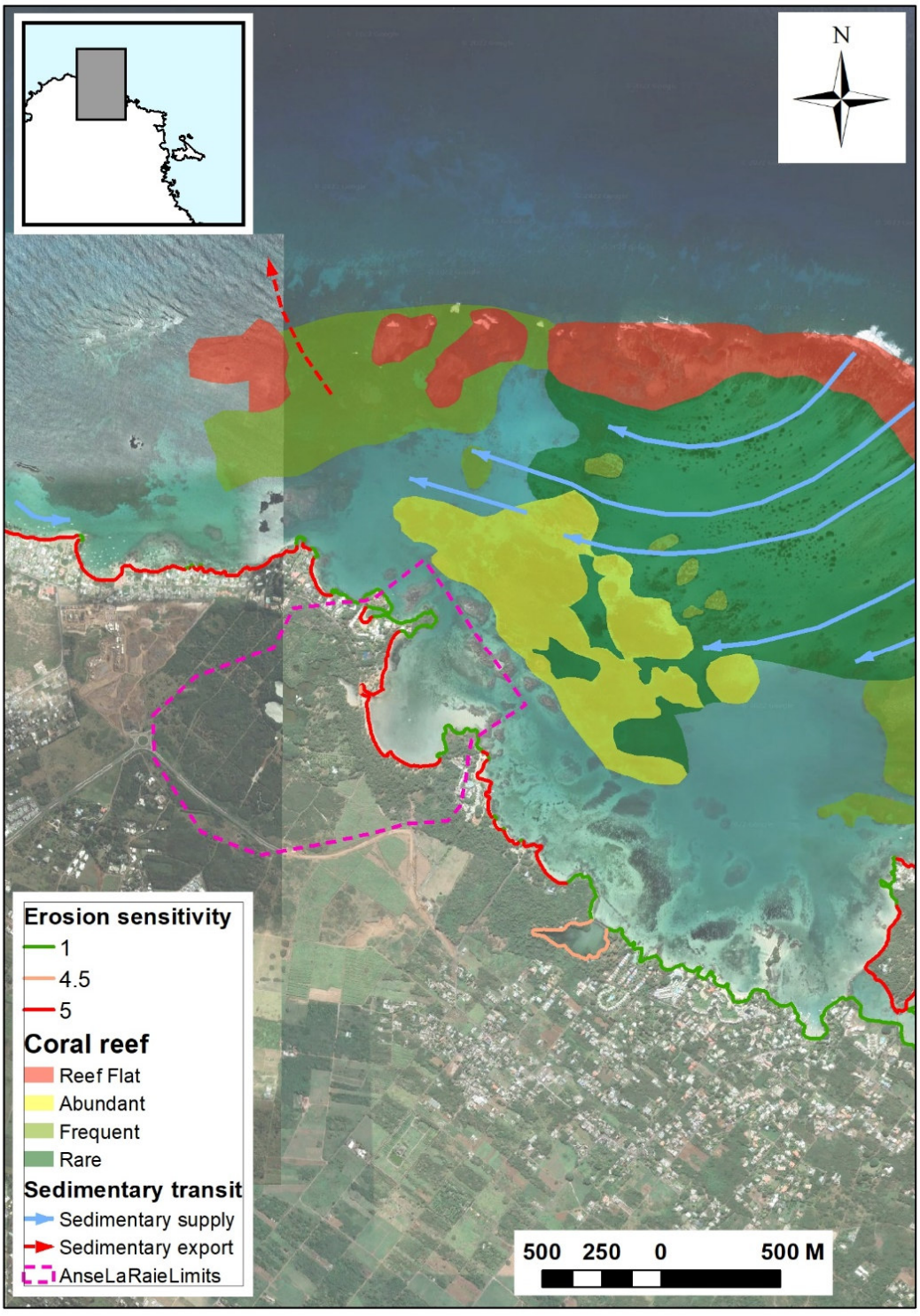


*Figure 161 : The relationship between Anse la Raie and the reef complex and the input of bioclastic sand*




*Figure 162 : Very low-lying area of Anse la Raie - Note the high vulnerability of the road to coastal flooding*

#### 4.3.2.3 Port-Mathurin (Rodrigues)

The Port-Mathurin site is located on the north-west coast of Rodrigues in a sector where the reef front is relatively close to the coast (between 500 and 900 m approximately) compared with other sectors of Rodrigues. The coastline is around two kilometres long and runs SW-NE. The reef flat has been dug out and cut into to form a harbour access channel 155 m wide and around 1,200 m long. Starting from the open sea, this channel has a NE-SW orientation and then bends in a NNE SSW direction before widening to form the outer harbour basin (Figure 163).

The Port-Mathurin area is urbanised and its coastline has been heavily artificialized by the creation of large embankments to gain land on the sea or by the presence of various structures: walls, riprap, concrete quays, etc. (Figure 164). Only the Pointe Monnier sector is less artificial, although there are walls at the top of the beach. Most of the coastline at Port-Mathurin is therefore artificial, with only the Pointe Monnier sector consisting of more or less gravelly sand mixed with man-made elements at the top of the beach. The sector to the east of the harbour basin is located behind a shallow flat. The Pointe Monnier sector is bordered by a channel, while the further west you go, the wider the flat becomes (Figure 163).

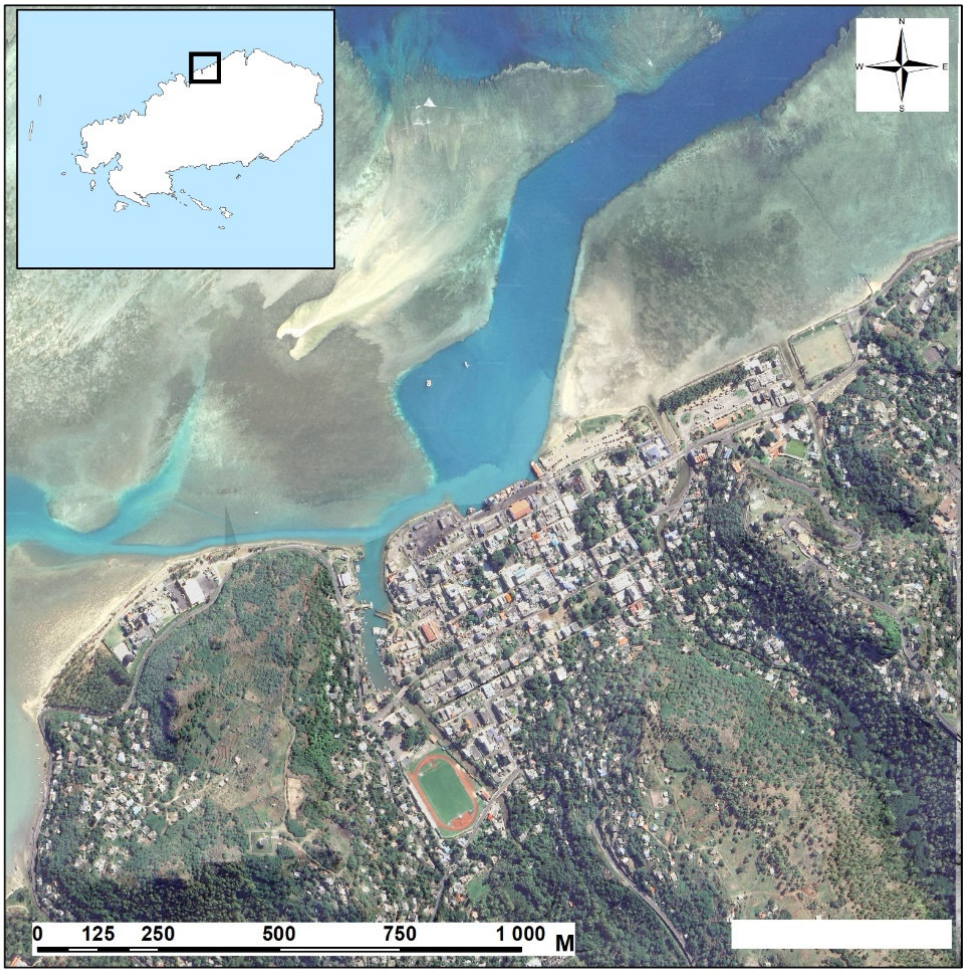


*Figure 163 : The Port-Mathurin site*

*Note the channel cut into the reef platform*

Port-Mathurin is an urban area with housing, shops, administration, transport and energy infrastructure (power station) which has been established in a low-lying area (altitude between 2.5 m and 3 m above mean sea level) crossed by several rivers whose mouths are in the urban area (Figure 165 and Figure 166). The hinterland is made up of steep slopes bordering the low-lying area; the distance between the coast and these slopes varies between a hundred and a few hundred metres. Only the Pointe Monnier, on which the electric power station is located, is narrower and only about a hundred metres wide. The Port-Mathurin site appears to be exposed to both coastal flooding and river flooding during cyclones or strong tropical depressions, due to its proximity to landforms and the presence of rivers.

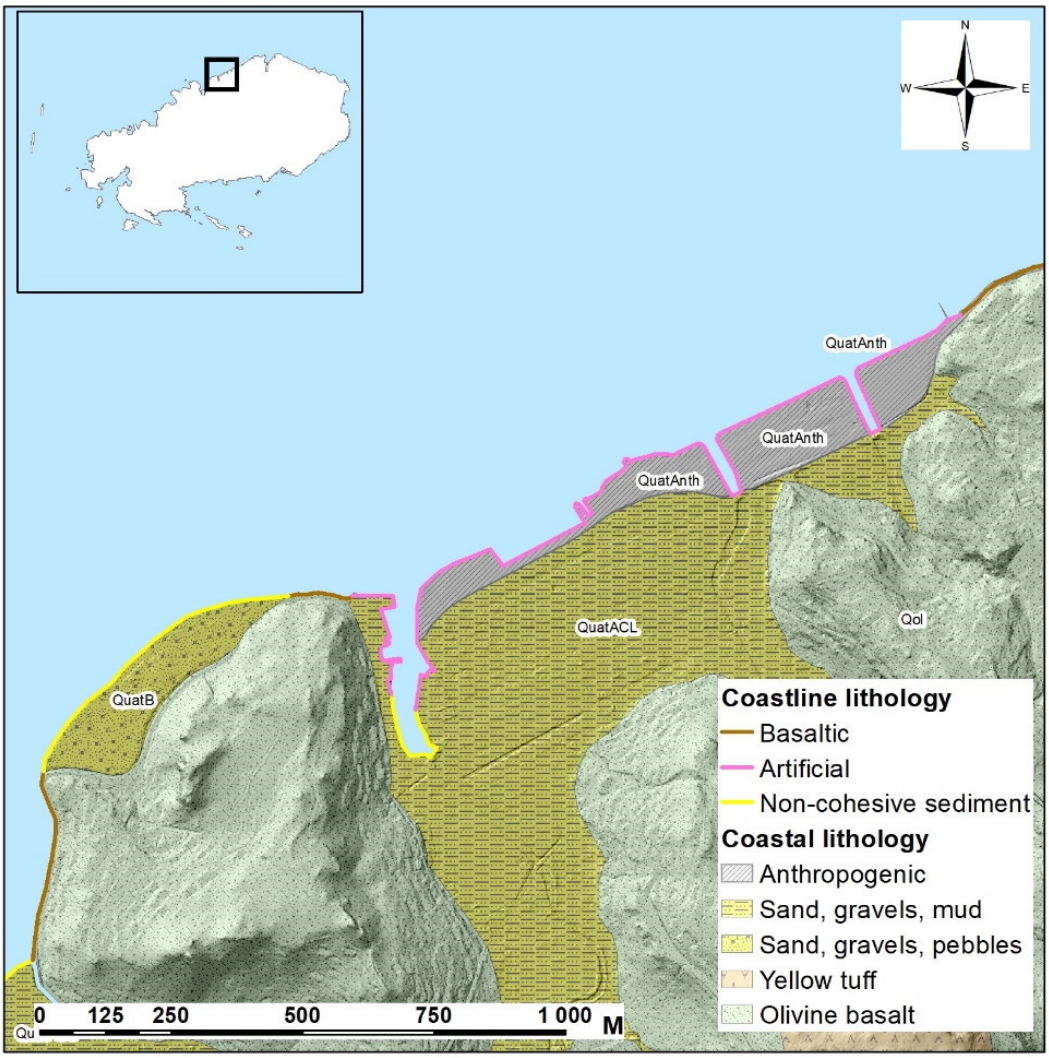


*Figure 164 : Lithology and topography of the Port-Mathurin site*



*Figure 165 : Left: concrete quay at the Port-Mathurin harbour; right: low-lying urban area immediately behind the Port-Mathurin coastline*



*Figure 166 : low-lying urban area on either side of a river mouth (Port-Mathurin); right: low-lying area on the seafront made up of embankments and protected by revetments (Port-Mathurin)*

## 4.3.3 Methods

### 4.3.3.1 Assessment method of the coastal erosion and coastline retreat at local scale (1:5,000)

The method for assessment of coastal erosion and coastline retreat at local scale is the same as at the regional scale, see 4.2.1.1.

### 4.3.3.2 Assessment method of the coastal flooding hazard at local scale (1:5,000)

#### *4.3.3.2.1 Elaboration of the high-resolution topo-bathymetric DTMs*

In order to simulate flooding at a local scale, local high-resolution coastal DTM (Digital Terrain Model) are built for each site.

**Flic-en-Flac**

As evoked in chapter 2.1.2 and illustrated in Figure 7, some defaults have been identified in the provided LiDAR DTM in the area of Flic-en-Flac.

Consequently, a correction has been arbitrarily applied to the topography of Flic-en-Flac, supposing a linear bias (following a linear correction with latitude, the north part of the area has been lowered, whereas the south part of the area has been slightly raised). On the beach, this correction appears to be satisfactory (better consistency of the DTM with geomorphological considerations and field observations). Nevertheless, in absence of other wedging elements, the uncertainty remains important inland, especially because we have no clue about an eventual bias of the LiDAR DTM with the longitude in this area.

After this correction, a new topo-bathymetric coastal DTM has been generated for Flic-en-Flac, with a 4m-resolution (Figure 167).

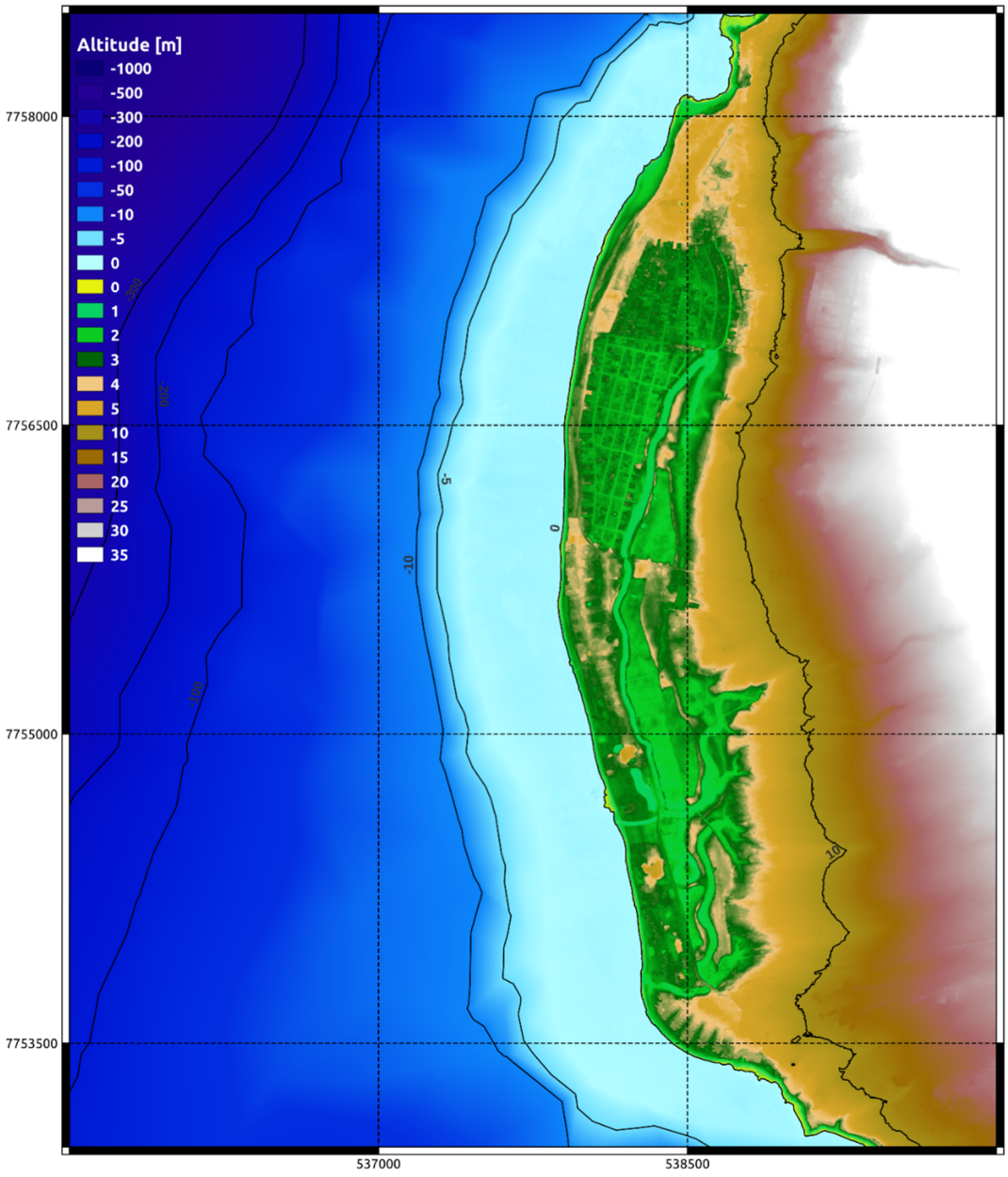


*Figure 167 : Overview of the local DTM of the Flic-en-Flac site on the Mauritius Island (2m resolution)*

## Anse La Raie

The bias seems to be very small in the north part of Mauritius. Consequently, the LiDAR DTM has been directly used to generate a topo-bathymetric coastal DTM with a 1m-resolution (Figure 168).

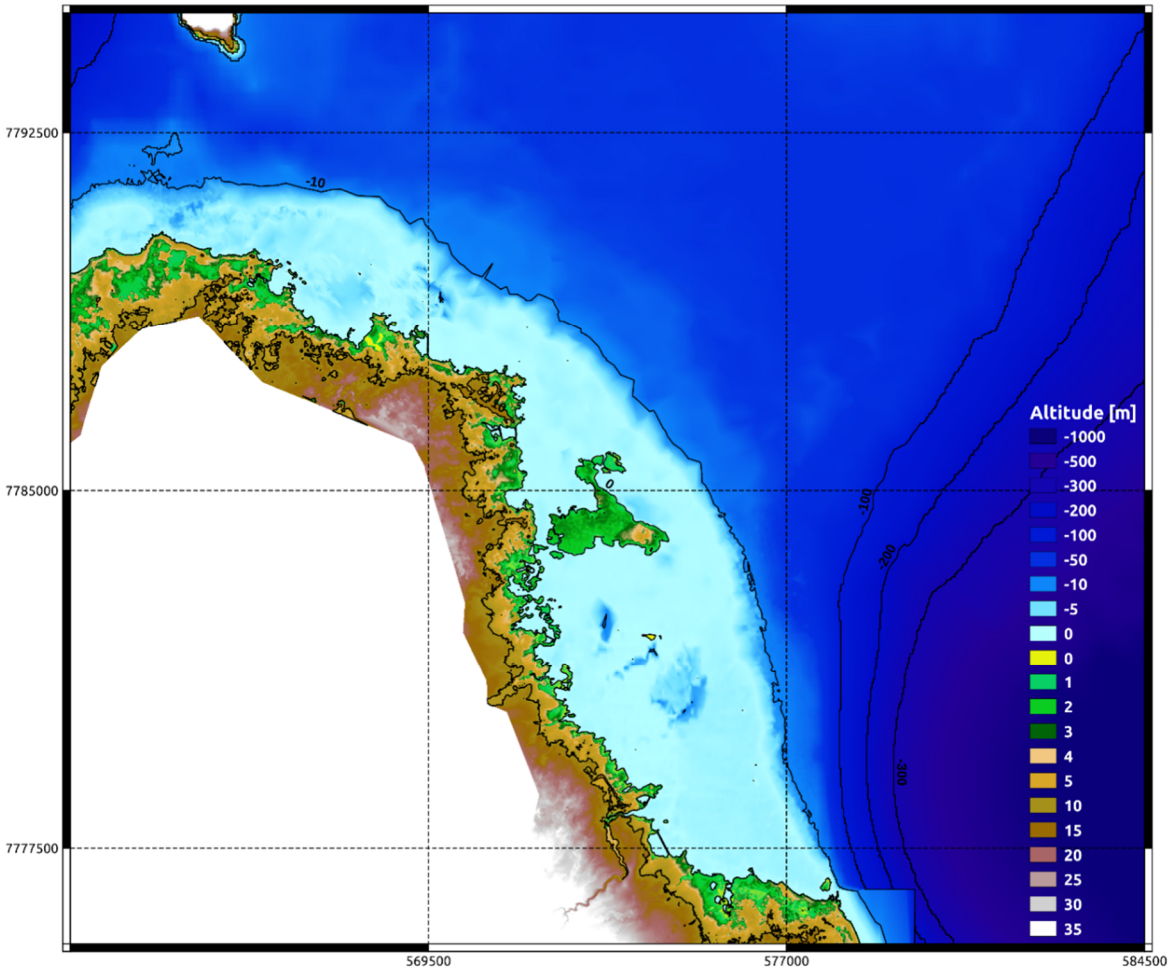


*Figure 168 : Overview of the local DTM of the Anse la Raie site on the Mauritius Island (2m resolution).*

**Port-Mathurin**

The local simulations for Port-Mathurin are directly based on the topo-bathymetric DTM realized for Rodrigues island, at a 4m-resolution (Figure 3).

#### *4.3.3.2.2 Culverts identification*

The need of a detailed representation of the main topo-bathymetric features in our models to precisely describe the flooding has already been expressed in section 4.2.1.2.3. High resolution data allow to identify many more of these features so that they will be taken into account in the model representation of the site. The following Figure 169 and Figure 170 show all the constraint lines that have been used to generate the local meshes on Anse La Raie and Flic-en-Flac respectively.

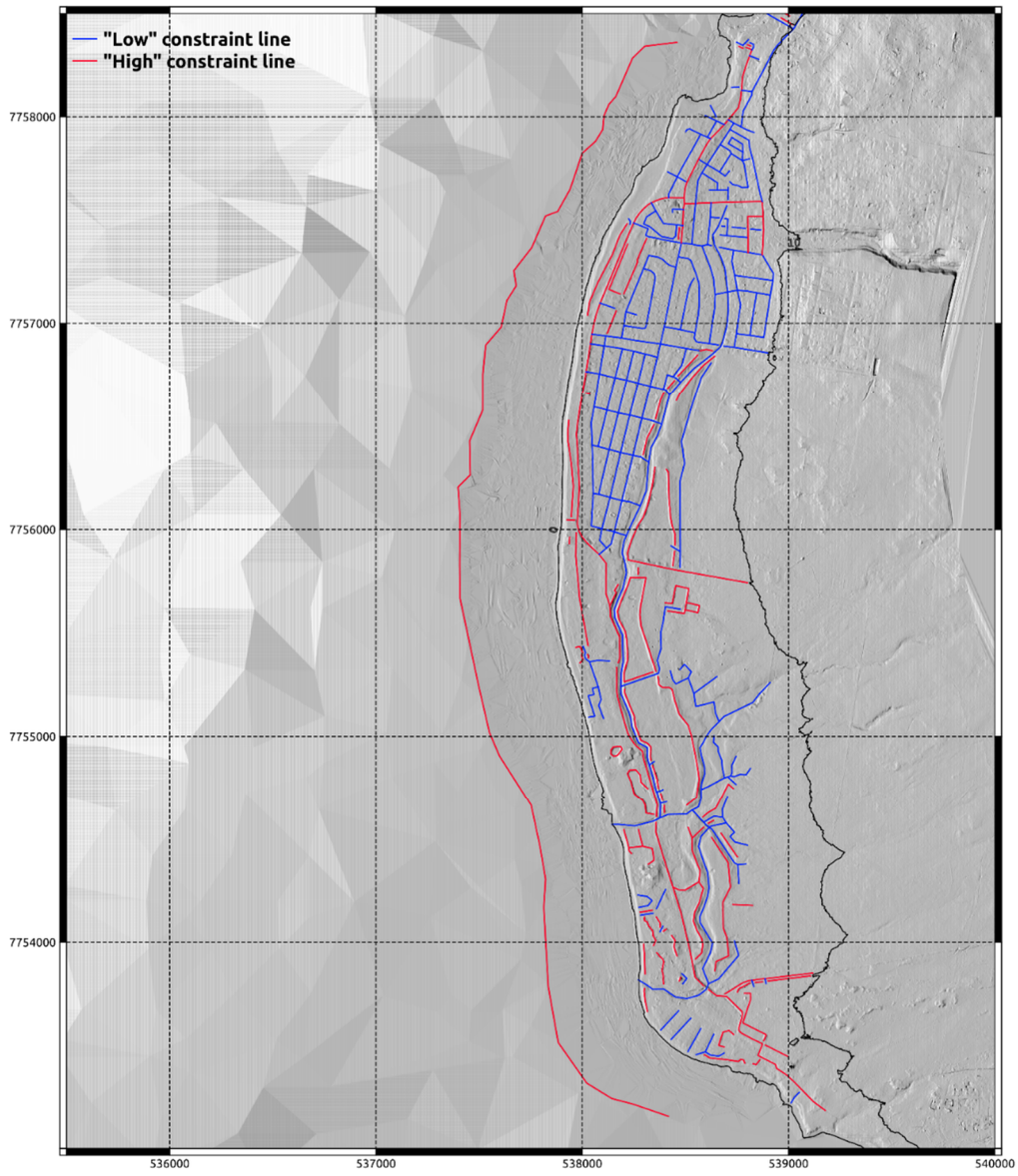


*Figure 169 : Use of constraint lines in the Flic-en-Flac model (DTM in the background).*

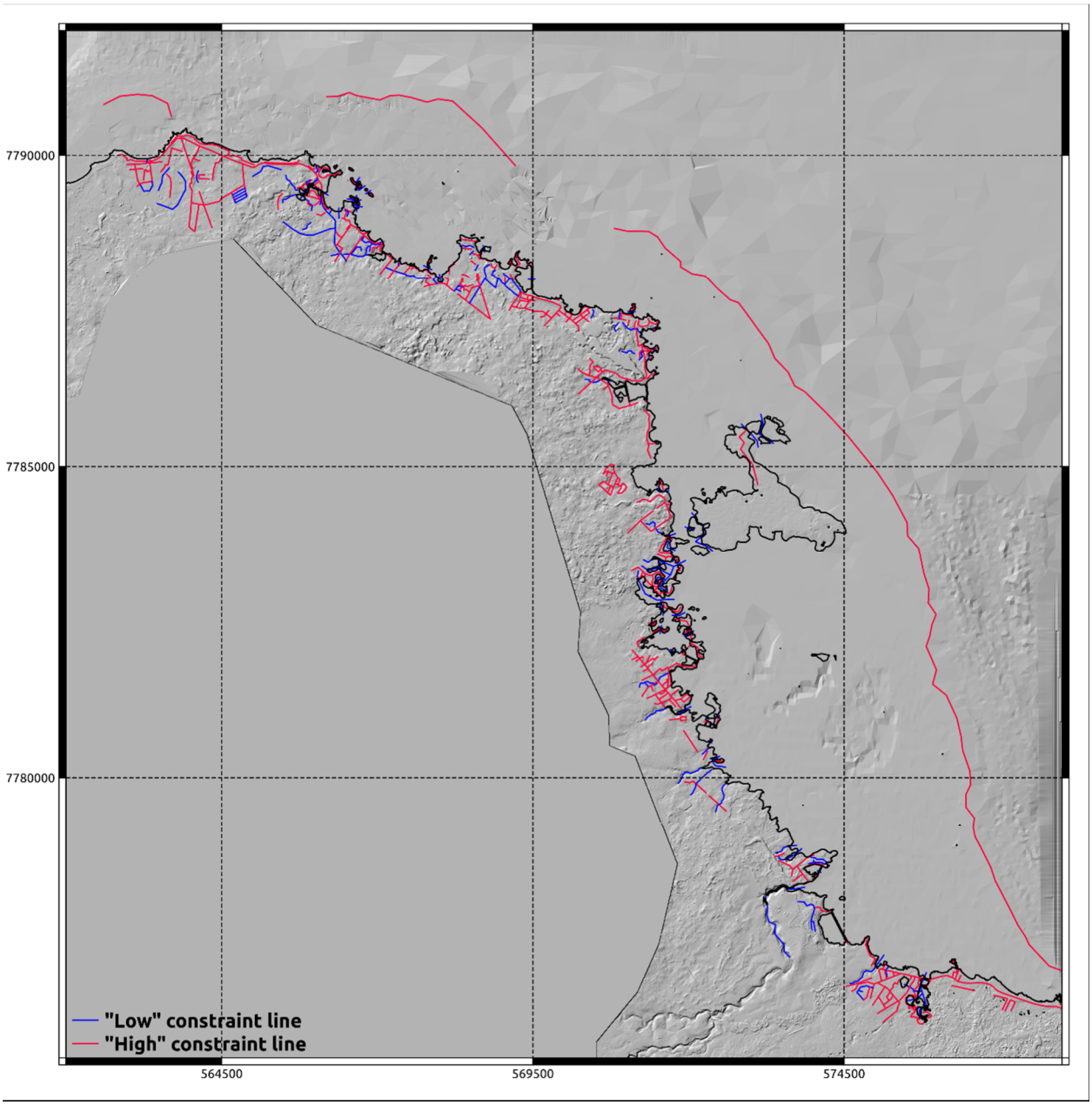


*Figure 170 : Use of constraint lines in the Anse la Raie model (DTM in the background).*

#### *4.3.3.2.3 Meshing*

In order to study the coastal flooding hazards on the Flic-en-Flac and Anse La Raie areas, two different meshes were constructed. In general, they cover extensive sea areas in front of the site of interest: wide enough to account for the presence and shape of the island shelf and reefs; while on land, the boundary limit is located between the +10 m and +20m level lines of the topography. The mesh size is variable, adapted to the water depth and more refined on land and around abrupt changes of the sea bathymetry (shelf, reefs, etc).

The Flic-en-Flac mesh is represented in Figure 171. The mesh size varies from 350m offshore to 15m on land. The relatively small dimensions of the computational domain allow to consider a

homogeneous tide signal propagating from the sea boundary and computed thank to the FES2014 database on the yellow forcing point visible in the same figure.

On the other site, Figure 172, Anse la Raie face a wide northward shelf and its lagoon stretches far in the southeast following the Mauritius coastline. Wind and waves can generate important surges in these areas that can propagate towards the Anse la Raie Bay. It is thus important to include all these areas in the local computational domain, which results in a quite big one, covering a large portion of Mauritius north-east. The mesh size varies between 500m offshore to 15m on land. The sea boundary of the domain is partitioned in three parts for a heterogeneous tide representation and the forcing points, where tidal signals are calculated, are shown in yellow in the same picture.

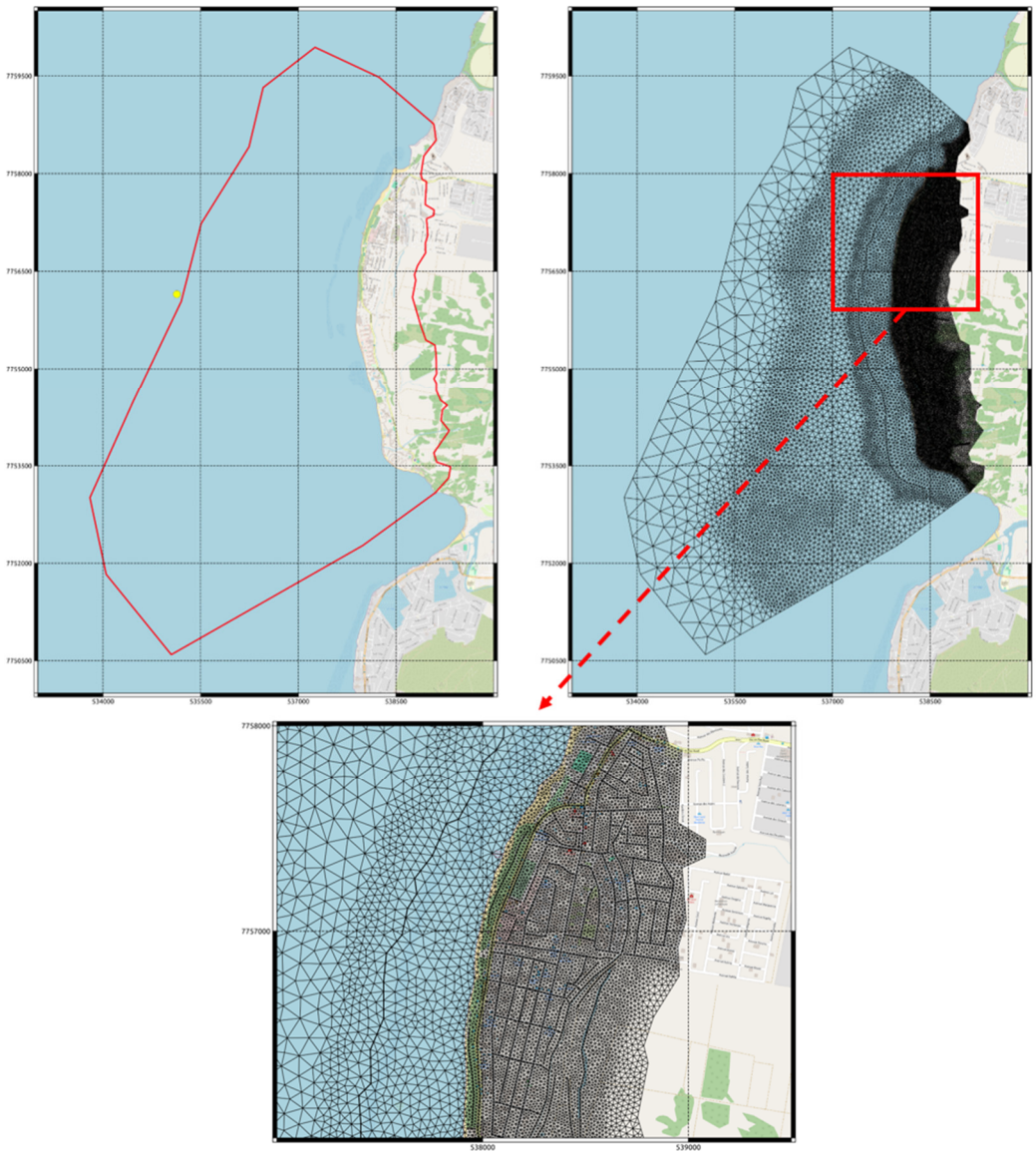

*Figure 171 : Extension of the computational mesh and grid overview on the Flic-en-Flac area, including the location of the forcing point.*

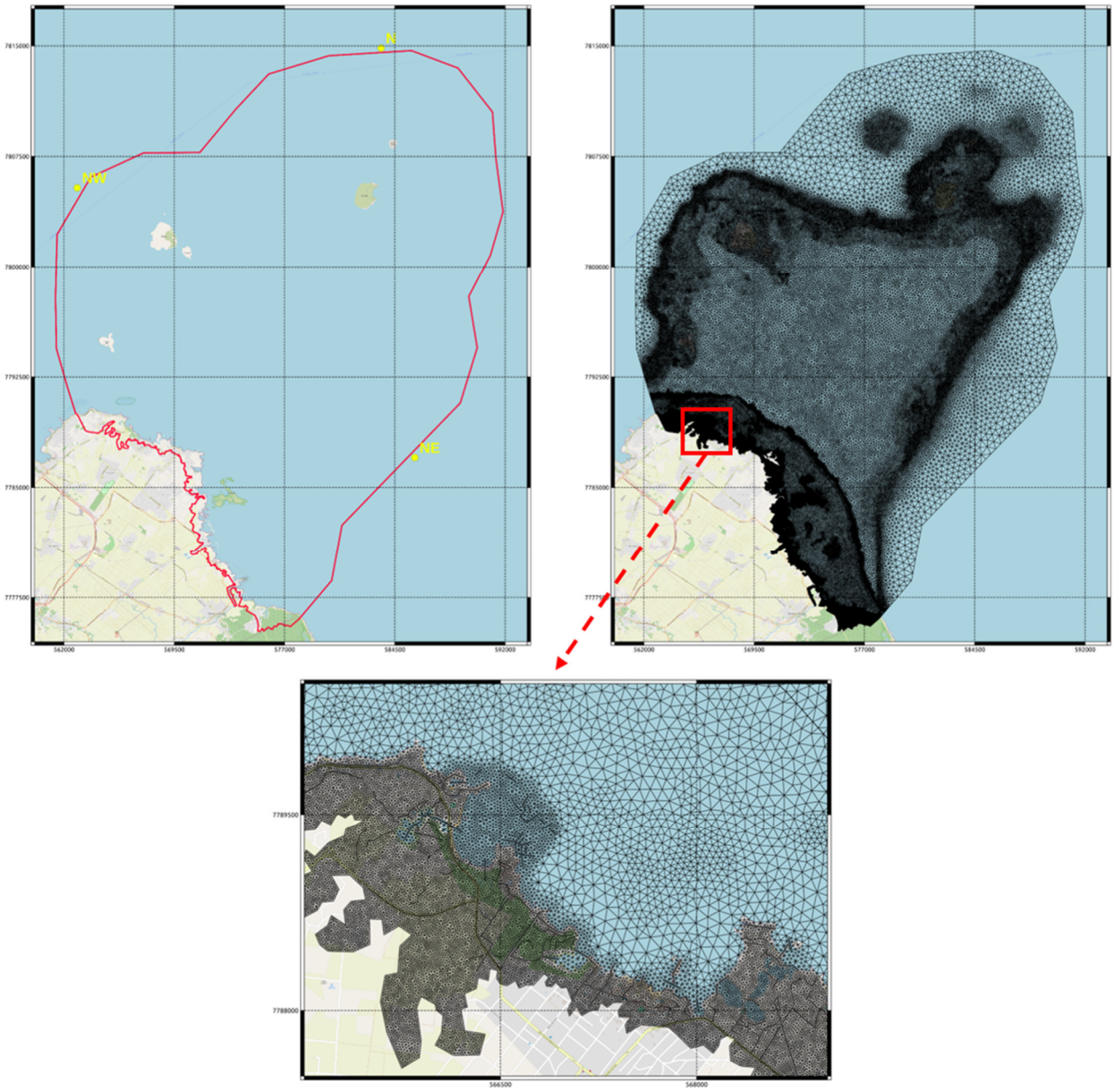

*Figure 172 : Extension of the computational mesh and grid overview on the Anse la Raie area, including the location of the forcing points.*

#### *4.3.3.2.4 Land use and bottom friction*

Description on how the land use has been taken into account to generate a heterogeneous bottom friction coefficient can be found in section §4.2.1.2.5.

# 4.3.4 Results

## 4.3.4.1 Flic-en-Flac (Mauritius)

### *4.3.4.1.1 Coastal retreat hazard*

#### *4.3.4.1.1.1 Coastal homogeneous zones and sedimentary sub-cells*

As illustrated in Figure 57 and § 4.2.1.1.2.1, the Flic-en-Flac area is made up of 9 homogeneous zones or sub-cells (Figure 173). Six sandy sub-cells were delineated and studied by Jica (2015), named FF_SC11-1 to FF_SC11-6, 3 homogeneous zones were delineated for this study (2 rocky zones, FF_HCZ01 and 03 and 1 mixed zone FF_HCZ02).

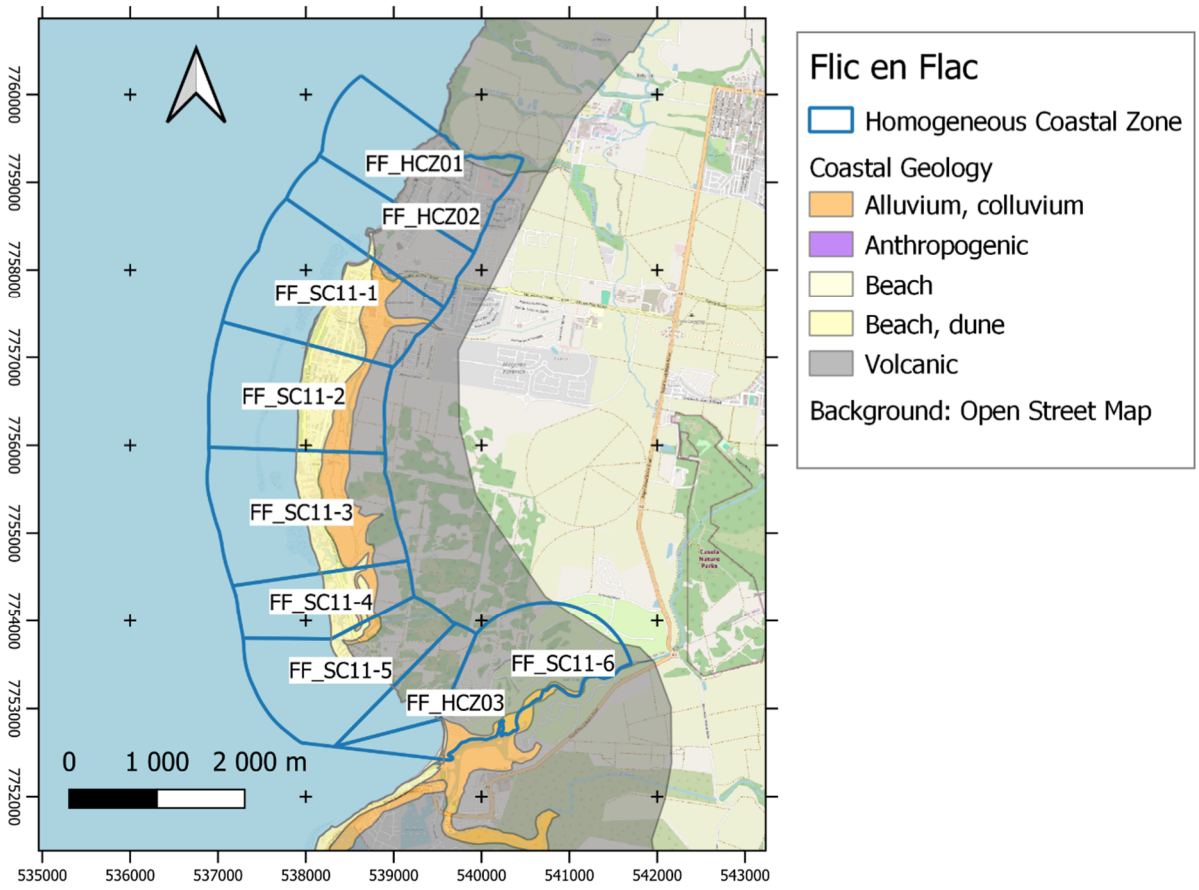


*Figure 173 : Homogeneous coastal zones, sub-cells (JICA, 2015) and coastal geology of Flic-en-Flac.*

#### *4.3.4.1.1.2 Analysis of coastline evolution*

The analysis of coastline evolution data from the JICA study (2015) enabled the calculation or attribution of the various coastline retreat parameters for each sub-cell and for the territory as a whole (Table 26). The calculation method and the example of Flic-en-Flac have been described in detail in part 4.2.1.1.2.2 of this report. For the mixed zone FF_HCZ02, which was not previously studied by JICA (2015), the parameters $Tx_{med\text{-}hz}$, $Tx_{hzd\text{-}hz}$ and $Tx_{max\text{-}hz}$ were assigned based of expert opinion. These parameters correspond respectively to $Tx_{med\text{-}cell}$ and $Tx_{hzd\text{-}cell}$, values of

retreat calculated at the scale of the littoral cell studied by JICA (2015), and to $Tx_{max\text{-}hz\text{-}SC11\text{-}1}$ , which corresponds to the maximum retreat observed in the adjacent sub-cell.

*Table 26 : Coastline retreat parameters for each sub-cell, HCZ and coastal cell of Flic-en-Flac territory*

| Tx (m/y) | *Shoreline nature* | $Tx_{med\text{-}hz}$ | $Tx_{hzd\text{-}hz}$ | $Tx_{max\text{-}hz}$ |
|---|---|---|---|---|
| FF_HCZ01 | rock | | | |
| **FF_HCZ02** | sand | -0.09 | -0.85 | -0.91 |
| **FF_SC11-1** | sand | 0.00 | -0.70 | -0.91 |
| **FF_SC11-2** | sand | -0.29 | -0.86 | -1.59 |
| **FF_SC11-3** | sand | 0.00 | -0.39 | -0.39 |
| **FF_SC11-4** | sand | -0.03 | -0.74 | -1.33 |
| **FF_SC11-5** | sand | -0.22 | -2.12 | -2.85 |
| FF_HCZ03 | rock | | | |
| **FF_SC11-6** | sand | 0.00 | -0.13 | -0.40 |
| **$Tx_{med\text{-}cell}$** | | **-0.09** | | |
| **$Tx_{hzd\text{-}cell}$** | | **-0.85** | | |

For the parameter (Lmax) used to estimate the eventual retreat in the event of a major cyclone, the analysis of the Flic-en-Flac area shows 2 configurations of the coast: the coral lagoon protects the majority of the coastal sectors and one or two cells appear open towards the open sea, without protection from the reef (Table 27a). For the different types of coastline encountered, a suitable estimation method has been proposed in part 4.2.1.1.2.3. For the coastline protected by the lagoon, the parameter Lmax is established for each scenario and each timeframe on the basis of the modelling results of Baird (2003) for the Flic-en-Flac sector (Table 27b). To estimate the impact of a cyclone, the sandy sector of zone FF_HCZ02 was considered to be relatively protected by the lagoon. For the open side (FF_HCZ03), the adapted Fema540SQ method was used. The local elevation of the barrier beach is considered to be low, which makes it possible to determine the retreat values associated with the scenarios (Table 27c). It should also be noted that the Lmax5y-median value of the Fema approach (8m) has been adjusted to that of Baird (8.5m) by making the values consistent on a local scale. For the 5-year and 25-year timeframes, the retreat values between the open coast and the lagoon are comparable. However, for the safe 25-year scenario and the 75-year timeframe, the instantaneous retreats envisaged for the open coast zone exceed 20m, while they remain below 15m in the lagoon.

*Table 27 : Estimated impact of extreme events (Lmax) -Flic-en-Flac*

(a)

| | *Shoreface exposition* | **Lmax (method)** |
|---|---|---|
| FF_HCZ01 | open | |
| **FF_HCZ02** | lagoon(&open) | *Lagoon, Mauritius west coast* |
| **FF_SC11-1** | lagoon | |
| **FF_SC11-2** | lagoon | |
| **FF_SC11-3** | lagoon | |
| **FF_SC11-4** | lagoon | |
| **FF_SC11-5** | lagoon | |
| FF_HCZ03 | open | |
| **FF_SC11-6** | open | *Open & Low-lying sandy coast* |

(b)

| *Lagoon, Mauritius west coast* | **$Lmax_{5y}$** | **$Lmax_{25y}$** | **$Lmax_{75y}$** |
|---|---|---|---|
| **median** | 8,5 | 11 | 14 |
| **intermediate** | 10 | 12 | 14 |
| **safe** | 11 | 13 | 14 |

c)

| *Open & Low-lying sandy coast* | **$Lmax_{5y}$** | **$Lmax_{25y}$** | **$Lmax_{75y}$** |
|---|---|---|---|
| **median** | 8,5 | 12 | 20 |
| **intermediate** | 10 | 15 | 25 |
| **safe** | 12 | 20 | 25 |

#### *4.3.4.1.1.3 Additional erosion caused by sea level rise (SLR-R)*

The methodology for estimating the additional erosion associated with sea level rise (SLR-R) is outlined in section 4.2.1.1.2.4. The SLR-R parameter is calculated for the timeframes of 2050 and 2100, considering various scenarios for each homogeneous zone or sedimentary sub-cell. The extent of potential additional erosion is contingent on the type of shoreface and its exposure to wave action. The resulting coastal retreat is influenced by the availability of sediment, which is assessed by estimating the width of the beach. The parameters considered in the impact model are estimated at the scale of homogeneous zones, as a global phenomenon such as sea level rise can lead to different outcomes depending on the affected environments

Thus, while it is possible to calculate average values at the scale of coastal sediment cells, this study opts to retain estimates at the level of sub-cells and homogeneous zones in order to provide a more detailed understanding of the sensitivity of the environment to erosion at a local scale. Table 28 illustrates that, for the 2050 timeframe, the estimated values of additional coastal retreat are generally low, with most zones and scenarios predicting less than 3m of retreat (equating to an additional retreat of 0.12m/year). Only the two sectors exposed to the open sea (FF_HCZ02 and FF_HCZ03) show potential retreats exceeding 3m, with up to 5m of retreat observed in HCZ03. These additional retreats, though modest, may still affect the overall stability of certain sub-cells, such as FF_SC11-3, which has a median rate $Tx_{med}$ of +0.13m/y.

For this timeframe and under the coral sediment production scenarios presented in this study (refer to section 4.2.1.1.2.5.2), estimates suggest that coral production could mitigate 60% of the additional retreat in both the median and intermediate scenarios, and 20% in the safe scenario. This mitigation is a contributing factor to the relatively low estimated declines for the median and intermediate scenarios.

By 2100, the impact of sea level rise could become significantly more pronounced for Flic-en-Flac, depending on the scenarios considered. For sub-cells protected by the lagoon, additional retreats remain relatively moderate, ranging from 4m to 14m according to the median and intermediate scenarios. These retreats correspond to additional annual retreat rates of between 0.08m/year and 0.28m/year, nearly doubling the average retreat rate observed in sub-cell SC11-2, the sub-cell exhibiting the highest median retreat rate along the Flic-en-Flac coastline.

For this timeframe and under the coral sediment production scenarios used in this study (see section 4.2.1.1.2.5.2), estimates suggest that coral production could mitigate 25% of the retreat in the median scenario, 10% in the intermediate scenario, and 5% in the safe scenario. The safe scenario is based on the likely-range trajectory of the IPCC 8.5 scenario for sea level rise projection and assumes that coral sediment production is reduced by a factor of three. The estimated additional retreats for this scenario range from 12m to 21m (0.24m/year to 0.42m/year), resulting in a shift from a locally stable or moderately eroding system to a sedimentary cell undergoing widespread chronic retreat.

For the sub-cells and homogeneous zones exposed to the open sea, the additional retreats are even more significant, ranging from 10m to 12m (0.20m/year to 0.24m/year) under the median scenario, 17m to 21m under the intermediate scenario, and 25m to 30m (0.5m/year to 0.59m/year) under the safe scenario.

*Table 28 : Estimated values of additional coastal retreat for Flic-en-Flac coastline*

| *Sub-cell & HCZ* | *Shoreface exposition* | **SLR-R 2025-2050 (m)** | | | **SLR-R 2050-2100 (m)** | | |
|---|---|---|---|---|---|---|---|
| | | median | intermediate | safe | median | intermediate | safe |
| FF_HCZ01 | open | rock | | | rock | | |
| **FF_HCZ02** | open(&lagoon) | 2.8 | 3.2 | 4.3 | 10.5 | 17.2 | 24.6 |
| **FF_SC11-1** | lagoon | 0.5 | 0.7 | 1.7 | 3.9 | 7.7 | 11.7 |
| **FF_SC11-2** | lagoon | 0.8 | 1.1 | 2.7 | 6.1 | 11.9 | 18.1 |
| **FF_SC11-3** | lagoon | 0.8 | 1.1 | 2.7 | 6.1 | 11.9 | 18.1 |
| **FF_SC11-4** | lagoon | 1.0 | 1.3 | 3.1 | 7.2 | 14.0 | 21.4 |
| **FF_SC11-5** | lagoon | 1.0 | 1.2 | 2.7 | 6.2 | 11.7 | 17.7 |
| FF_HCZ03 | open | rock | | | rock | | |
| **FF_SC11-6** | open | 3.4 | 3.8 | 5.2 | 12.6 | 20.6 | 29.5 |

#### *4.3.4.1.1.4 Coastline retreat hazard at the sub-cells scale*

The determination of various projection parameters allows for the calculation of the potential retreat of the sandy coastline over different timescales and for the three scenarios, according to the methods outlined in section 4.2.1.1.2. The estimated retreat values, rounded to the nearest 5m, are presented for the sandy sub-cells of Flic-en-Flac. For rocky areas, the setback values have been defined based on expert opinion, as detailed in section 4.2.1.1.2.5.3. The estimated

coastline retreat values for all homogeneous zones and sub-cells of Flic-en-Flac are presented in Table 29.

*Table 29 : Coastline retreat estimations for homogeneous zones and sub-cells of Flic-en-Flac, 2025, 2050 and 2100 timeframes*

| | **2025** | | | **2050** | | | **2100** | | |
|---|---|---|---|---|---|---|---|---|---|
| Flic-en-Flac | median | intermediate | safe | median | intermediate | safe | median | intermediate | safe |
| **FF_CHZ01** | 0 | **5** | 5 | 5 | **5** | 10 | 10 | **10** | 10 |
| **FF_CHZ02** | 10 | **15** | 20 | 20 | **30** | 35 | 60 | **75** | 85 |
| **FF_SC11-1** | 10 | **15** | 20 | 15 | **25** | 30 | 45 | **60** | 70 |
| **FF_SC11-2** | 10 | **15** | 20 | 20 | **30** | 45 | 60 | **75** | 95 |
| **FF_SC11-3** | 10 | **15** | 15 | 15 | **20** | 25 | 50 | **60** | 70 |
| **FF_SC11-4** | 10 | **15** | 20 | 15 | **25** | 40 | 50 | **70** | 85 |
| **FF_SC11-5** | 10 | **20** | 25 | 20 | **50** | 65 | 60 | **95** | 110 |
| **FF_CHZ03** | 0 | **5** | 5 | 5 | **5** | 10 | 10 | **10** | 10 |
| **FF_SC11-6** | 10 | **15** | 15 | 15 | **25** | 35 | 65 | **80** | 95 |

The results of the intermediate scenario for the 3 timeframes of the study are presented in the maps of the homogeneous areas of Flic-en-Flac (Figure 174, Figure 175, Figure 176).

By 2050 (Figure 175), the situation for zone SC11-5 is even clearer, with a potential retreat of 50m, the highest in Mauritius.

For the rest of the Flic-en-Flac beach, the estimated potential retreats range from 20m to 30m. Sub-cell SC11-2 has the highest coastline retreat potential (30m), which corresponds to the public beach, bounded to the south by the Pearl Beach hotel. To the south of this area, sub-cell SC11-6 is characterised by the presence of a sandy mouth spit. These coastal environments exhibit strong morphological dynamics and phases of erosion that can sometimes be critical. However, long-term observations by JICA (2015) do not reflect this trend at the scale of the sub-cell. The estimated retreat value for 2050 in this sub-cell is 25m. On the scale of Mauritius, this falls within the majority retreat class for this scenario (55% of potential retreats between 15m and 25m), while still exceeding the median (Figure 80).

The two rocky sectors, located to the north and south, are logically the least affected by erosion. Currently (Figure 174), the retreat hazard values are similar across the sandy sub-cells, estimated at 15m, mainly influenced by the Lmax parameter and the potential impact of a cyclone. On the scale of Mauritius, this retreat value of "15m" represents the majority class, accounting for 40% of the island's homogeneous coastal zones.

In contrast, the SC11-5 sub-cell represents an outlier on the island scale, as only three sub-cells are estimated to have a retreat of 20m for this scenario. The unique nature of this sub-cell is linked to a retreat rate of 2.85m/y recorded by JICA (2015) over the period 1967-1975. This exceptional retreat value for the island significantly influences the calculation of all the Tx parameters.

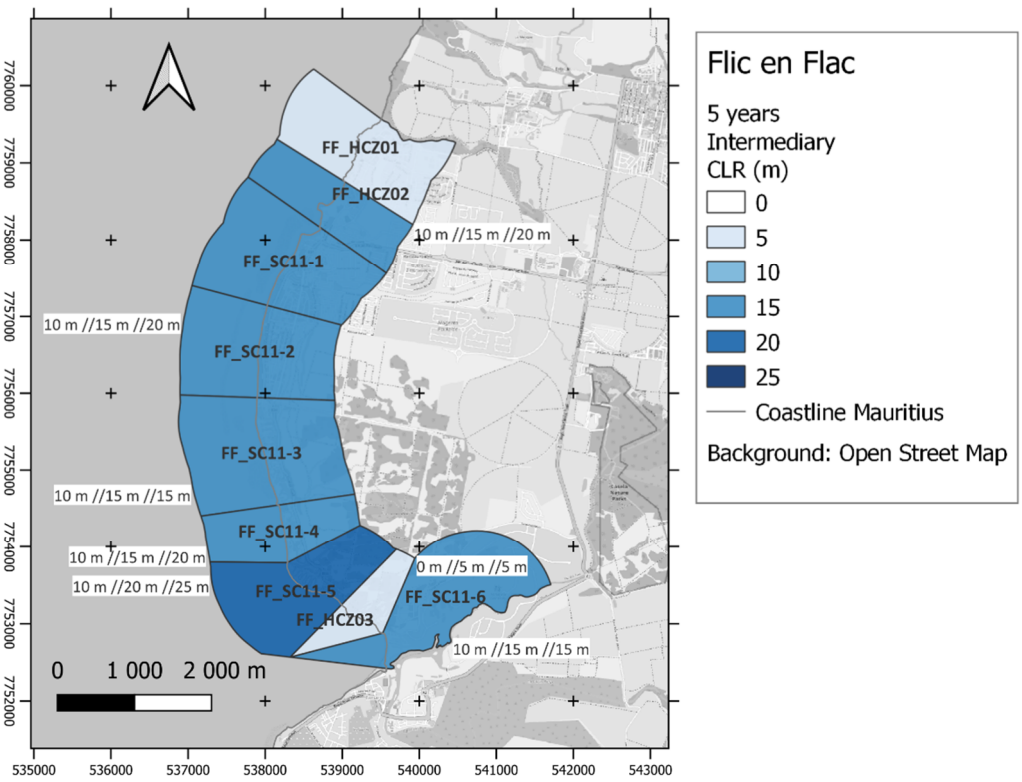


*Figure 174 : Map of coastline retreat estimations (CLR) for 2025 timeframe, at the scale of homogeneous coastal zones and sub-cells of Flic-en-Flac.*

By 2050 (Figure 175), the situation for zone SC11-5 is even clearer, with a potential retreat of 50m, the highest in Mauritius.

For the rest of the Flic-en-Flac beach, the estimated potential retreats range from 20m to 30m. Sub-cell SC11-2 has the highest coastline retreat potential (30m), which corresponds to the public beach, bounded to the south by the Pearl Beach hotel. To the south of this area, sub-cell SC11-6 is characterised by the presence of a sandy mouth spit. These coastal environments exhibit strong morphological dynamics and phases of erosion that can sometimes be critical. However, long-term observations by JICA (2015) do not reflect this trend at the scale of the sub-cell. The estimated retreat value for 2050 in this sub-cell is 25m. On the scale of Mauritius, this falls within the majority retreat class for this scenario (55% of potential retreats between 15m and 25m), while still exceeding the median (Figure 80).

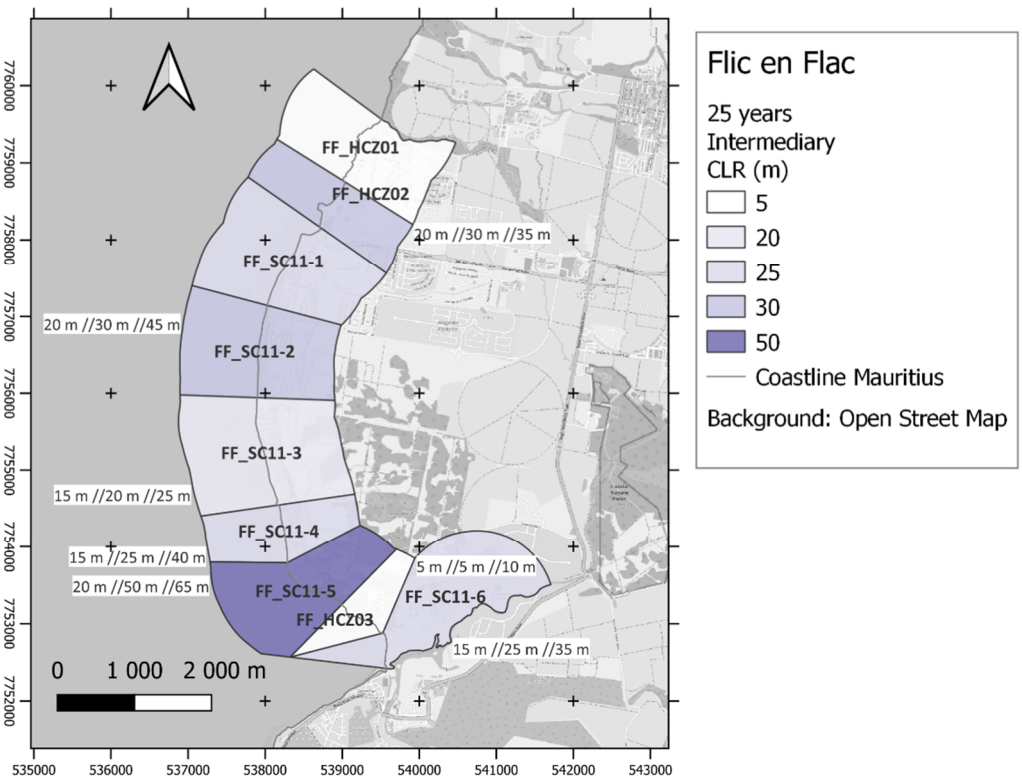


*Figure 175 : Map of coastline retreat estimations (CLR) for 2050 timeframe, at the scale of homogeneous coastal zones and sub-cells of Flic-en-Flac.*

By 2100 (Figure 176), the estimated retreat values for sandy shores under the intermediate scenario become more varied, ranging from 60m for sub-cells SC11-1 and SC11-3 to 95m for sub-cell SC11-5. The potential retreat of sub-cell FF_SC11-6 is relatively high, estimated at 80m, due to the absence of coral reefs in this river mouth area. These coastline recession values, which are higher than the median, are relatively high for Mauritius as a whole (Figure 83). The high projected retreat values for 2100 (rate of -0.85m/y) can be explained by the high retreat rate observed in the Flic-en-Flac by JICA (2015) through diachronic studies of historical orthophotography and satellite imagery between 1967 and 2012.

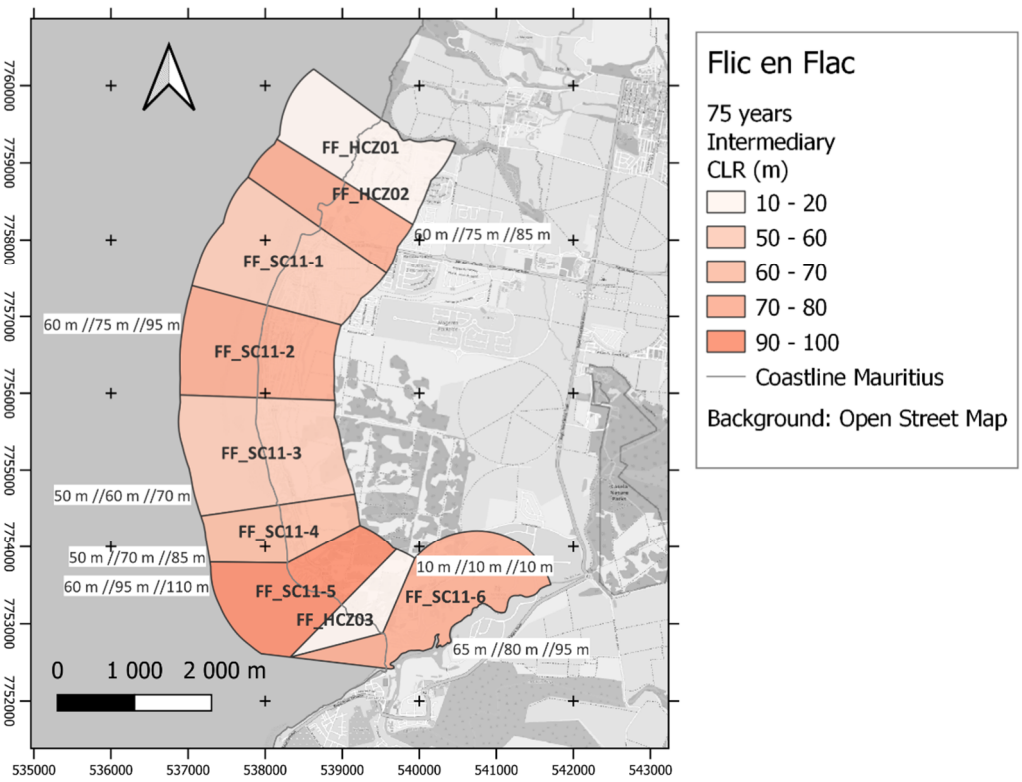


*Figure 176 : Map of coastline retreat estimations (CLR) for 2100 timeframe, at the scale of homogeneous coastal zones and sub-cells of Flic-en-Flac.*

#### *4.3.4.1.1.5 Maps of coastline retreat hazard at local scale*

Maps of exposure to shoreline retreat hazard on a local scale (1:10,000 to 1:5,000) have been drawn up using estimates of possible retreat values for homogeneous zones over the three time horizons of the study. The special cases of mixed coasts (sediment and rock) and low-lying areas are included in the shoreline retreat projection scenarios (see section 4.2.1.1.2.5) and implemented for Flic-en-Flac.

The GIS data provided in the deliverables of the project are of course compatible at the scale of 1:5,000 useful for local and detailed mapping.

Figure 177, Figure 178, and Figure 179 illustrate the projected retreat of the coastline at various timeframes.

Figure 180, Figure 181 and Figure 182 depict the projected shoreline retreat by timeframe for the various scenarios.

These figures offer detailed zooms at a scale of 1:10,000 of four various hazard-sensitive areas for Flic-en-Flac within sub-cells SC11-2, 3, 4, 5, and 6.

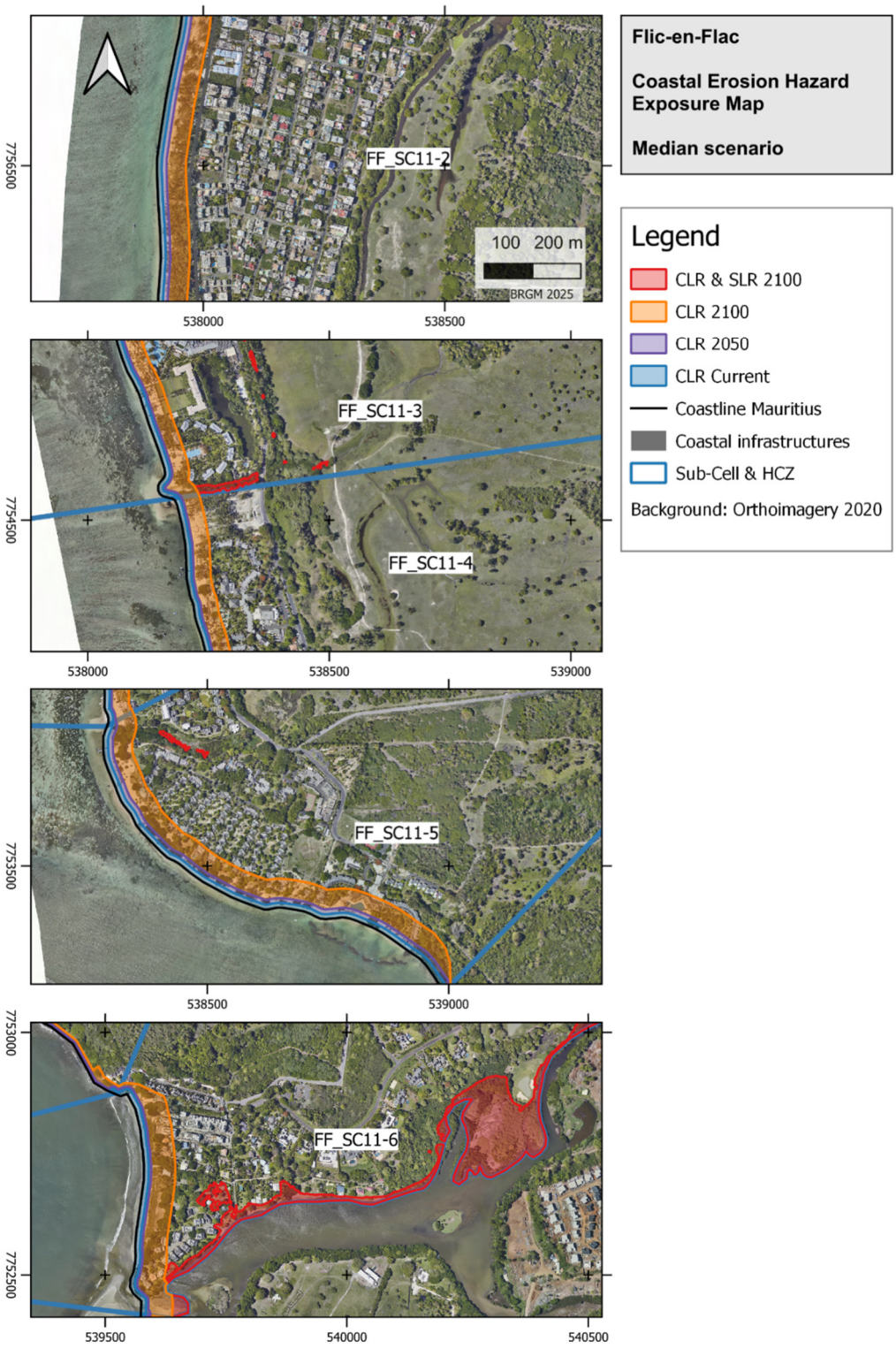


*Figure 177 : Maps of coastline retreat hazard for 2025, 2050 and 2100, median scenario. Zoom of 4 hazard-sensitive areas for Flic-en-Flac.*

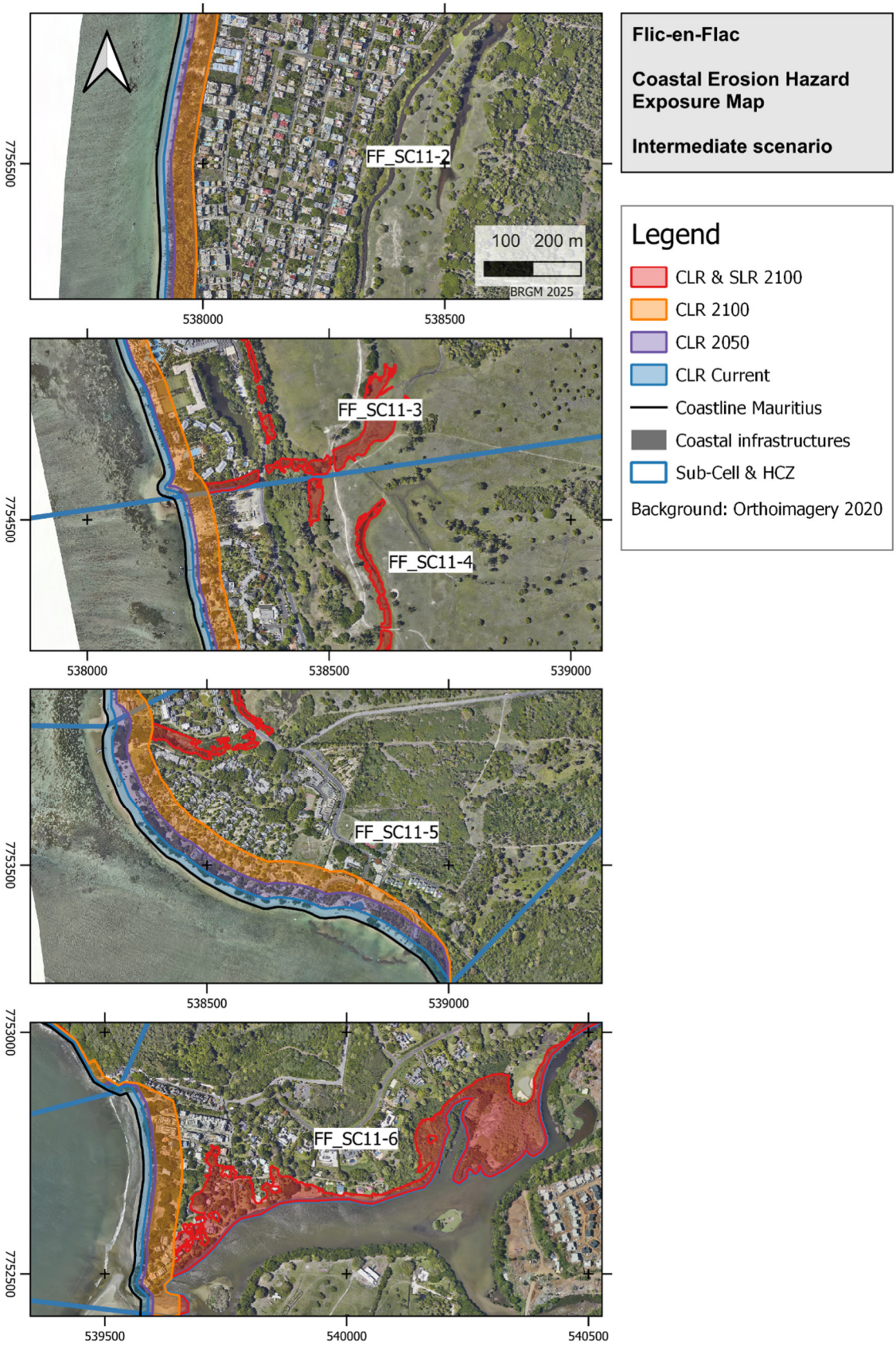


*Figure 178 : Maps of coastline retreat hazard for 2025, 2050 and 2100, intermediate scenario. Zoom of 4 hazard-sensitive areas for Flic-en-Flac*

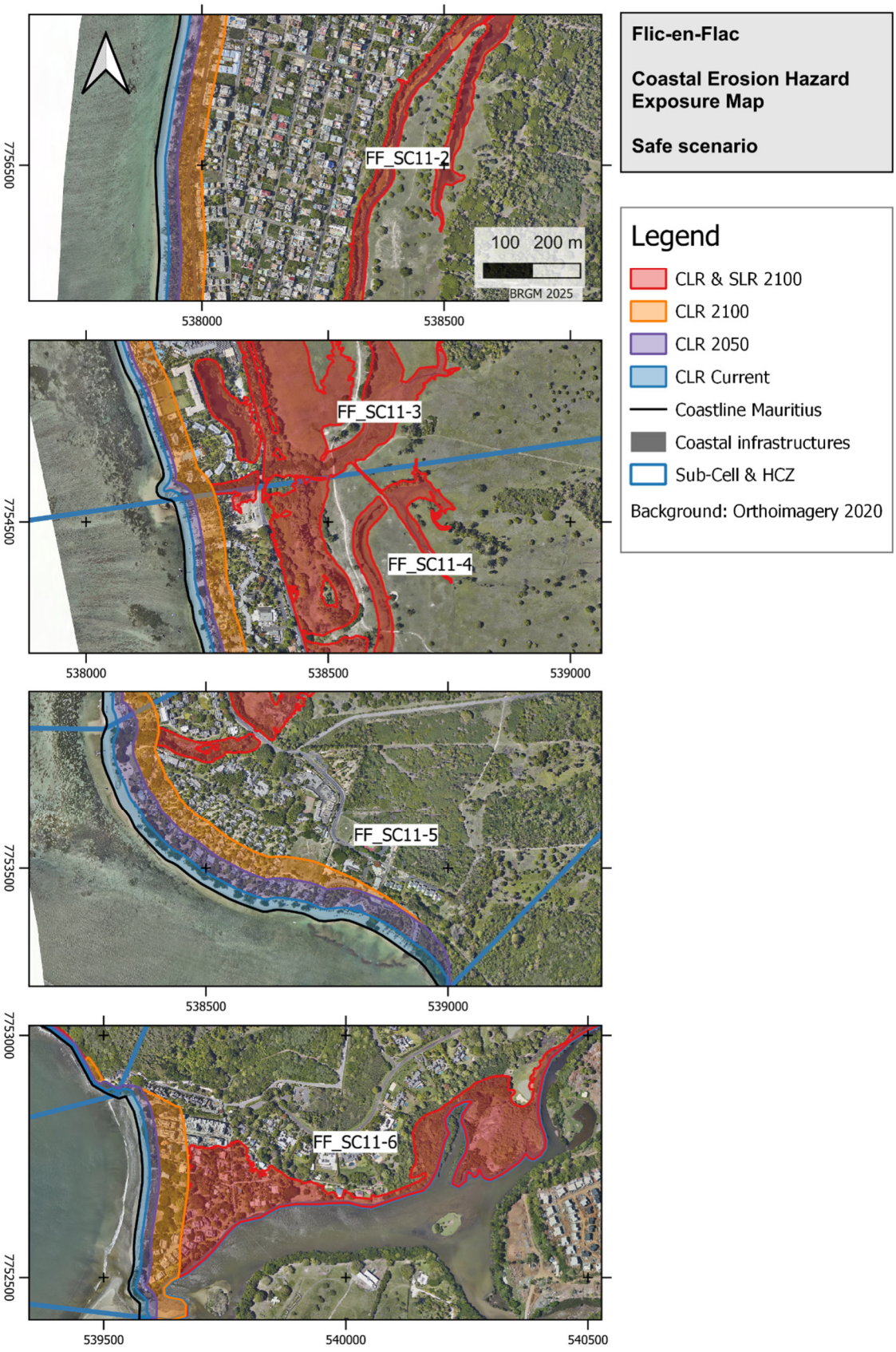


*Figure 179 : Maps of coastline retreat hazard for 2025, 2050 and 2100, safe scenario. Zoom of 4 hazard-sensitive areas for Flic-en-Flac.*

At present (2025, Figure 180), the potential hazard zone for shoreline retreat concerns the beach and may affect certain hotel facilities (Pearl Beach, to the south of SC11-2, see appendix) or private homes (CHZ02, see appendix) located on the upper beach or in the immediate vicinity.

The beach at Flic-en-Flac is subject to sand nourishment measures, but we did not have access to any quantified data on nourishment volumes. In the short term, as a result of these periodic replenishments and in the absence of major cyclones, we consider that the position of the coastline will remain relatively stable at the scale of the sedimentary sub-cells.

By the year 2050 (Figure 181), the retreat scenarios adopted do not show any major changes in trend. The Flic-en-Flac coastline may experience phases of gradual retreat or more severe during cyclonic events. These changes are potentially reinforced by the still limited effects of rising sea levels. In the context of a productive reef system and preserved backshore area, as is the case at the Public Beach (SC11-2 for example), the effects of the natural dynamics on the coastline retreat remain limited. Nevertheless, the safe scenario estimates that the retreat could exceed the current regulatory setback (30m), which could cause problems in hotel sectors where tourist facilities are close to the beach. At this time, the projections made for the SC11-5 sub-cell estimate significant retreat of the coastline, well beyond the regulatory setback. These significant retreats obtained, higher to others observed in Mauritius, are explained by the erosion values documented in the JICA study (2015). The projections illustrate the particular sensitivity of this sector to coastal erosion and retreat of the coastline.

Projections indicate that by 2100, the Flic-en-Flac region will undergo profound changes (Figure 182). The mapping of low-lying areas potentially impacted by rising sea levels transforms the distribution of hazard zones. For the scenario maps (Figure 177, Figure 178, Figure 179), the 2100 projection of potential low-lying flooding (SLR) is shown separately from the estimated effect of coastal erosion in order to illustrate the expected phenomena. It is noteworthy that the selection of the highest astronomical tide elevation (HAT) signifies that not all the mapped areas are entirely and permanently inundated by the sea.

The median scenario posits the occurrence of marine water ingress at the two river mouths of sub-cells SC11-3 and SC11-5, as well as along the banks of the Rivière du Rempart (SC11-6). The safe scenario indicates a potential significant coastline retreat within sub-cells SC11-3 and SC11-4, which are occupied by major hotel establishments. On the one hand, the retreat of the coastline significantly affects beach and backshore areas up to the main hotels buildings. On the other, the low-lying areas surrounding the river are susceptible to regular inundation from the sea. In sub-cell SC11-6, projections for the year 2100 identify the possibility of a virtual disappearance of the sandy spit that currently occupies the river's mouth. This is a result of a combination of marine erosion of the beach and invasion by the sea of the low-lying areas bordering the river.

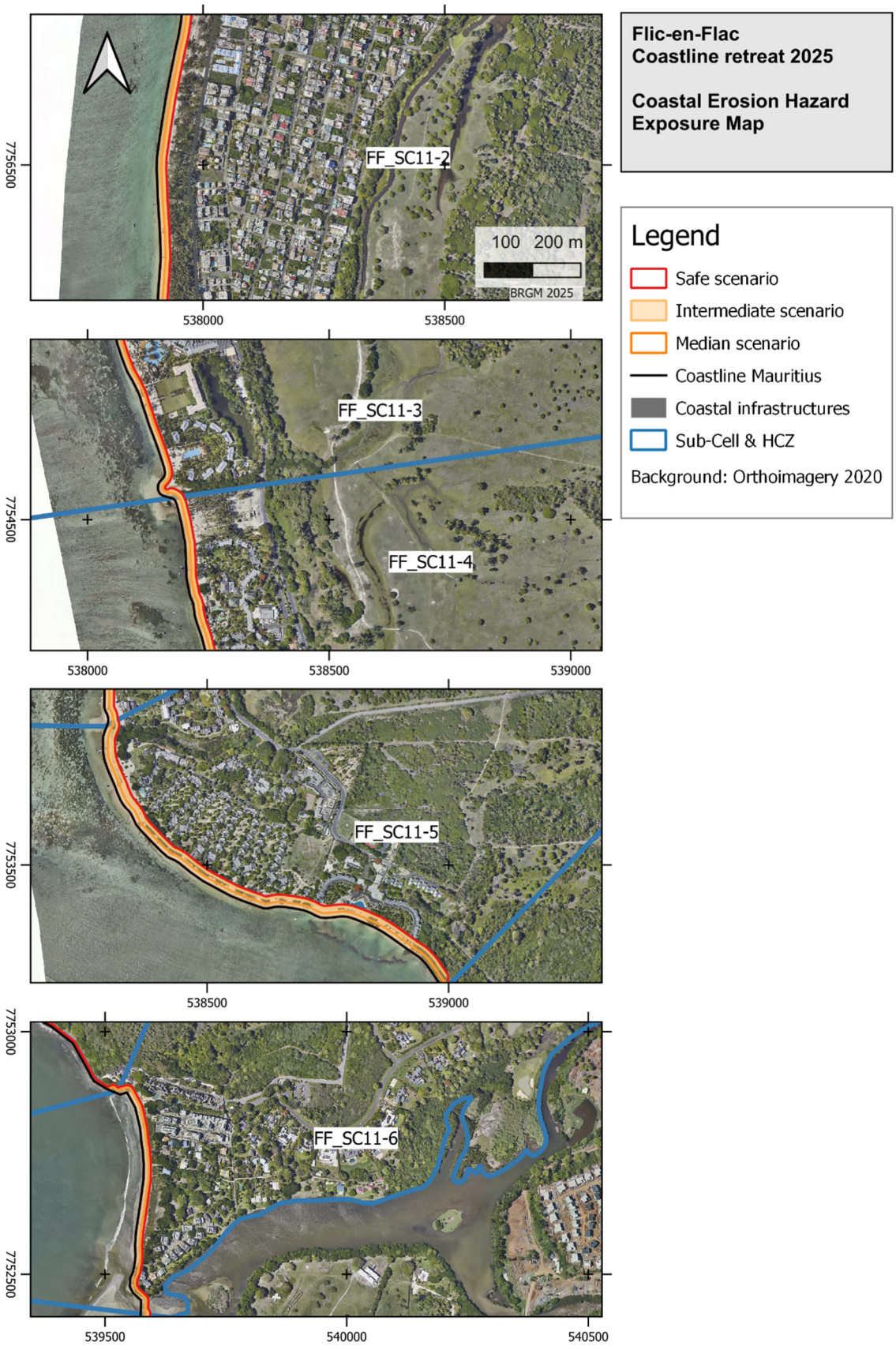


*Figure 180 : Maps of coastline retreat hazard for 2025, median, intermediate and safe scenarios. Zoom of 4 hazard-sensitive areas for Flic-en-Flac.*

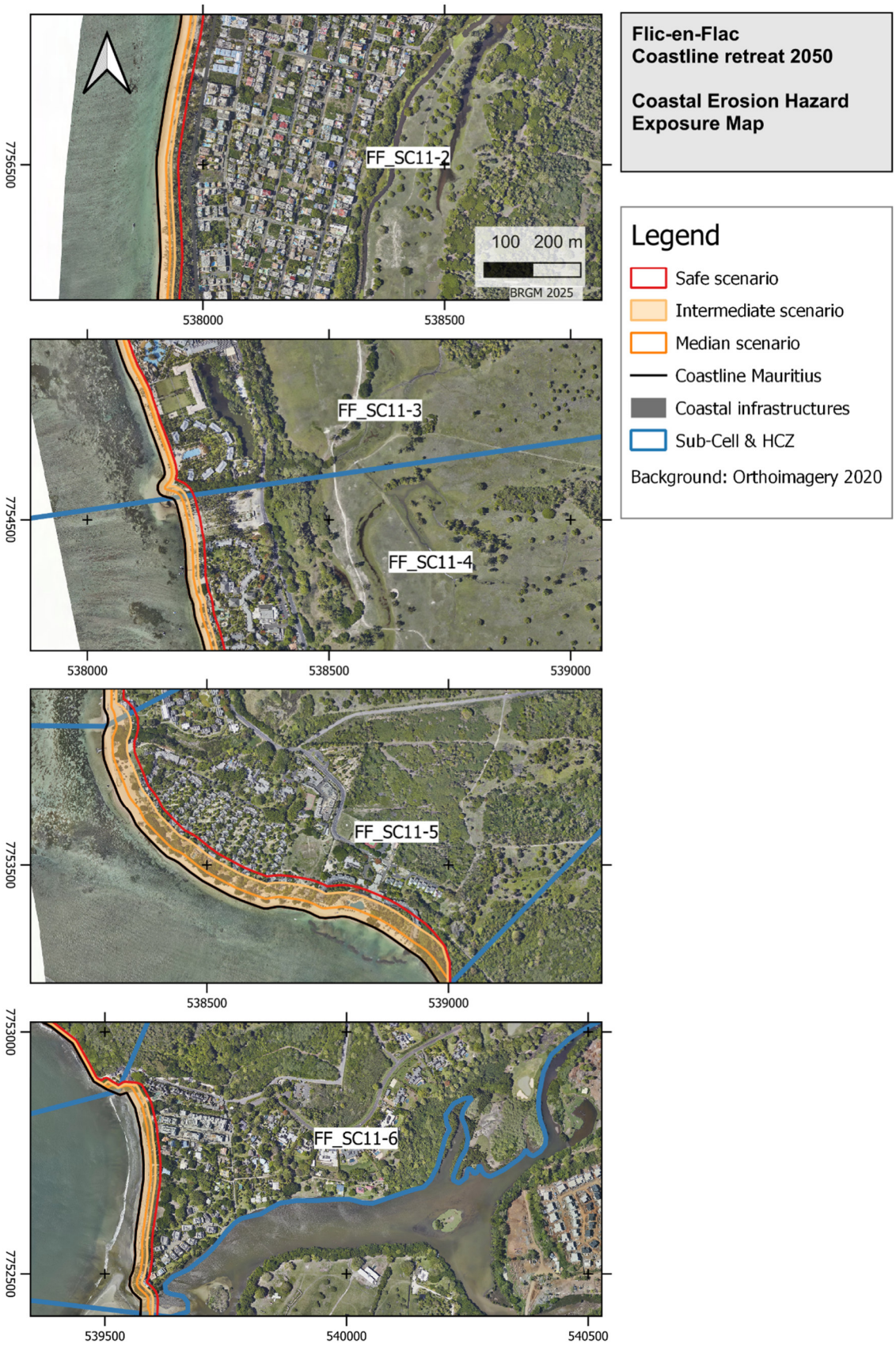


*Figure 181 : Maps of coastline retreat hazard for 2050, median, intermediate and safe scenarios. Zoom of 4 hazard-sensitive areas for Flic-en-Flac*

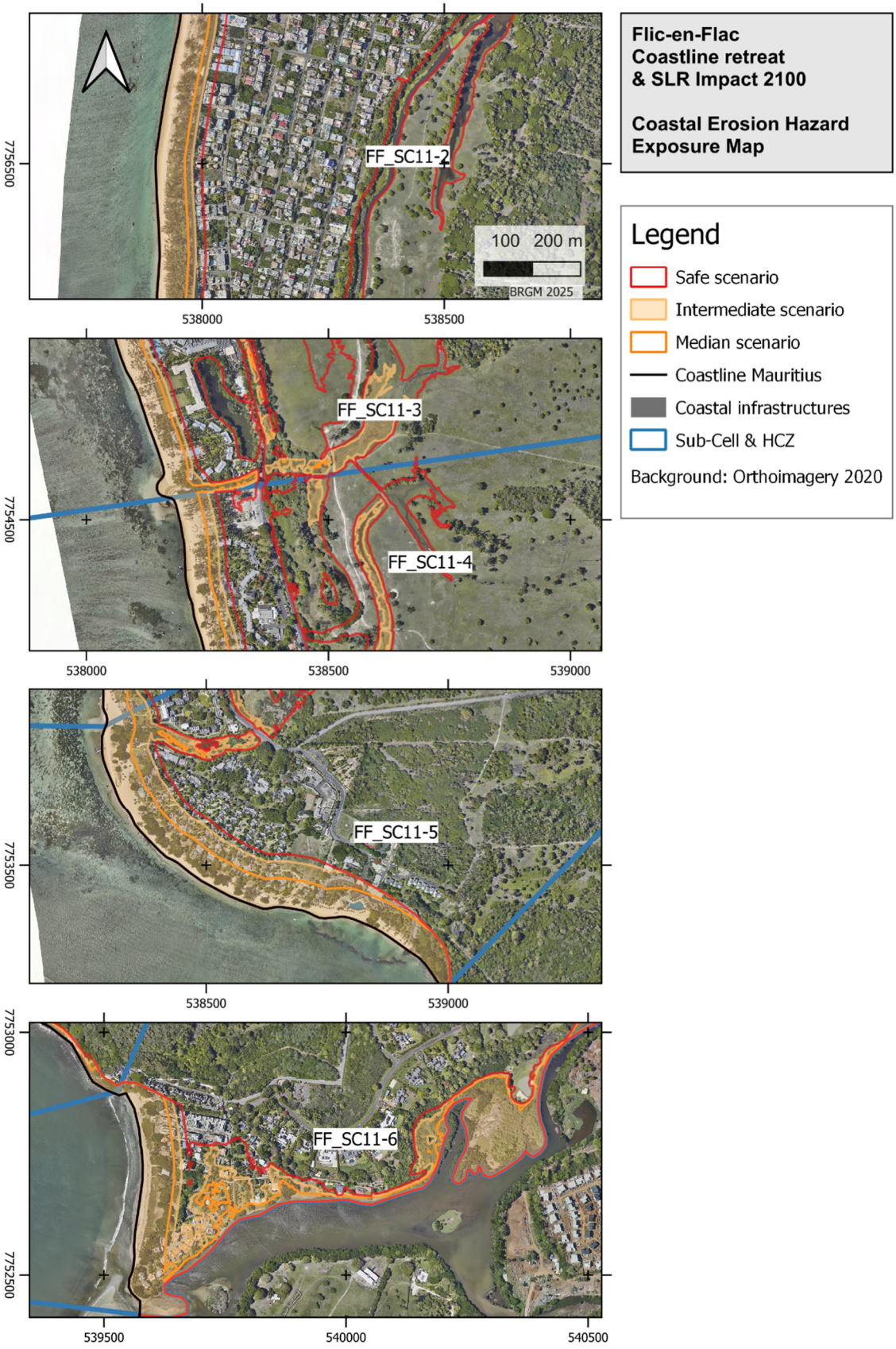


*Figure 182 : Maps of coastline retreat hazard and sea level rise impacts for 2100, median, intermediate and safe scenarios. Zoom of 4 hazard-sensitive areas for Flic-en-Flac.*

The database of coastal structures and infrastructures produced for the present study is also shown on the figures (see appendix 1 of report BRGM/RC-73989). At a scale of 1:10,000, it can be seen that most of the shoreline protection structures and infrastructures are barely discernible on the maps of Flic-en-Flac.

The road behind the public beach in sub-cell SC11-2 or the breakwaters opposite the Sand Hotel in sub-cell SC11-5 have been identified but not taken into account for two reasons:

- Firstly, there is an absence of data that would allow for the incorporation of the observed effects of coastal structures and infrastructures,
- The scale of the effects is very local and not very significant within homogeneous zones.

For example, the less extensive erosion observed to the east of the Sands Hotel (SC11-5) is not a result of the protective measures implemented, but rather a consequence of the presence of bedrock behind the coastal sand barrier.

The field observations confirm the vulnerability estimated at the scale of the study. They show that major modifications to the structures have been carried out since the 2020 ortho-photograph used as a reference for this study. The major reinforcement of the structures, which seems to have taken place in 2023, is a sign that the hotel is highly sensitive to the retreat of the coastline. In addition, in the immediate vicinity of the breakwaters, the sensitivity to erosion may be locally amplified, as indicated by the presence of trees about to be uprooted by the retreat of the coastline.

Similarly, the issue of sand nourishment and others soft engineering is not directly addressed in the scenarios of coastline retreat due to the lack of data available for this study. To incorporate this variable into projection scenarios, comprehensive data regarding the methodologies employed in beach nourishment operations is imperative. It is imperative to observe and quantify the effects of these sand nourishments on the coastline in a local and systematic manner prior to their incorporation into short- and medium-term projections.

#### *4.3.4.1.2 Coastal flooding hazard*

In order to reproduce the flooding by overtopping to which Flic-en-Flac is subjected, a 3rd model had to be implemented. This was the SWASH model, which was coupled to UHAINA and WW3 according to the strategy described in § 4.2.1.2.1.

The Figure 183 shows the position of the 57 SWASH profiles on Flic-en-Flac and the injection points in UHAINA.

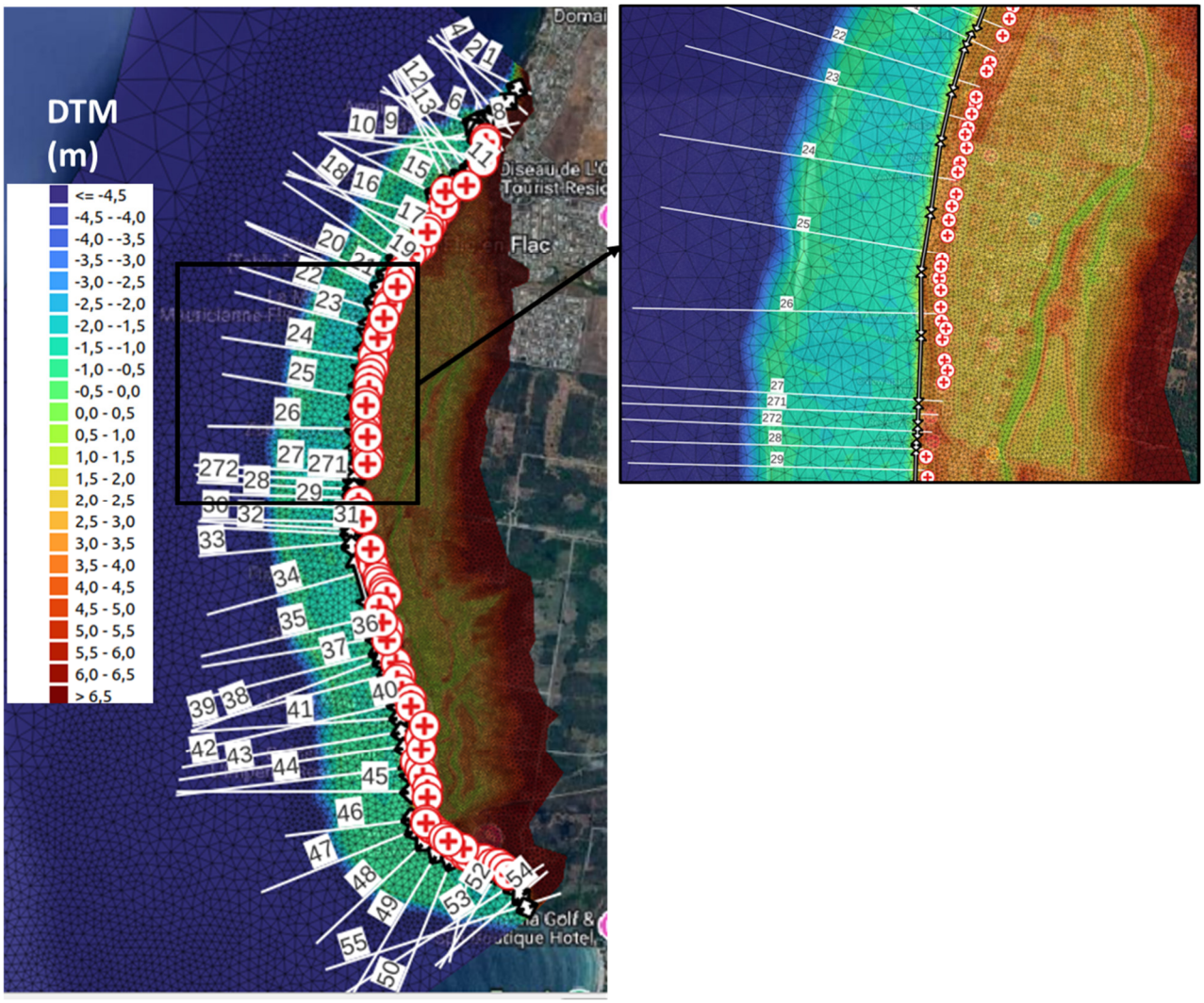


*Figure 183 : Layout of SWASH profiles on Flic-en-Flac and Uhaina injection points (red crosses). Right panel: zoom between the profiles 22 and 29.*

#### *4.3.4.1.2.1 Model Validation on historical event*

The model has been validated on the recent event of the cyclone Belal (2024). This cyclone passed close to the east coast of Réunion (Figure 184), generating high waves in Mauritius. Simulation results (Figure 185) indicate maximum Hs of 5.5- 6m offshore, which is in line with observations of 5 to 7m[6], and Tp of 10s.

[6] *https://www.francetvinfo.fr/monde/afrique/maurice/cyclone-belal-de-nombreux-degats-a-l-ile-maurice_6307206.html*

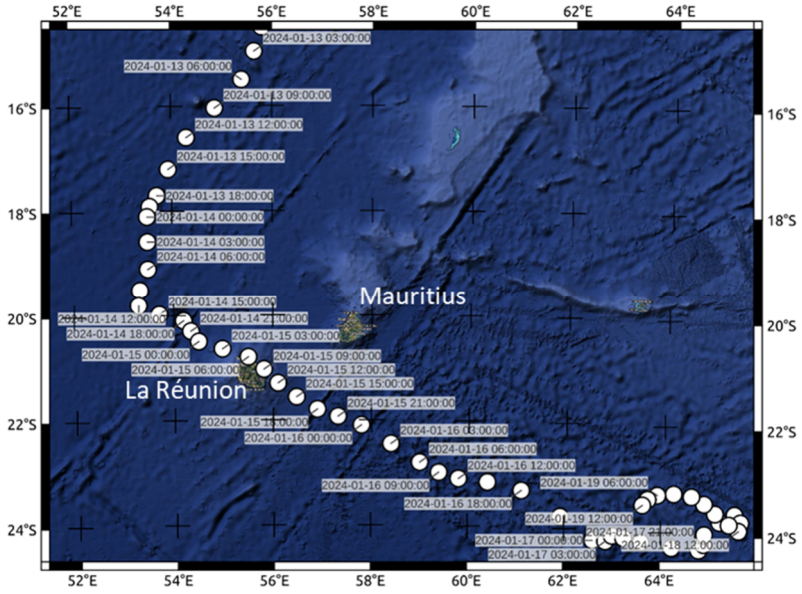


*Figure 184 : Cyclone Belal 2024 best track from the IBTrACS database.*

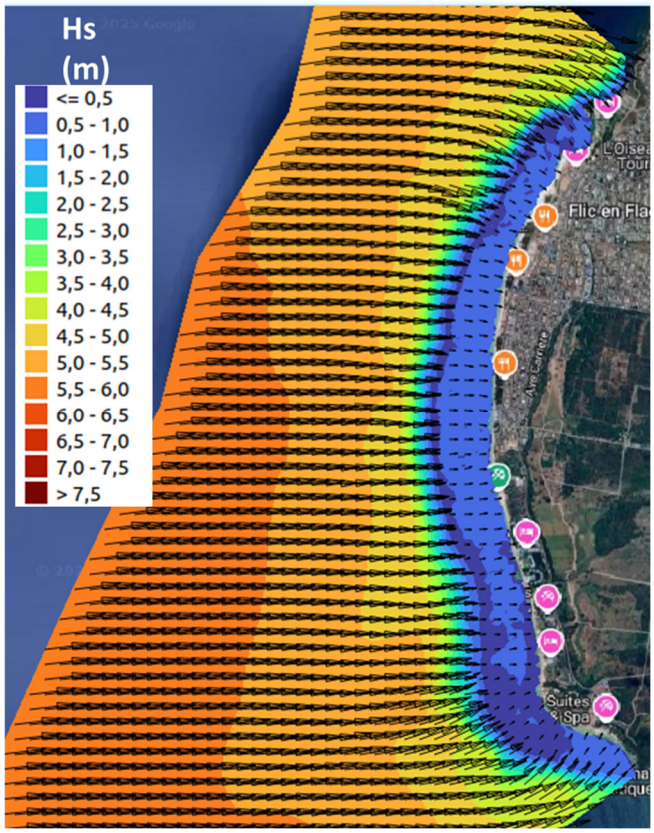


*Figure 185 : Simulation of maximum Hs and wave peak directions generated by Belal (2024) on Flic-en-Flac.*

The simulations show that the overtopping are limited to the back shore under the Filaos (Figure 186). This is in line with videos taken in the area during the event (Figure 187).

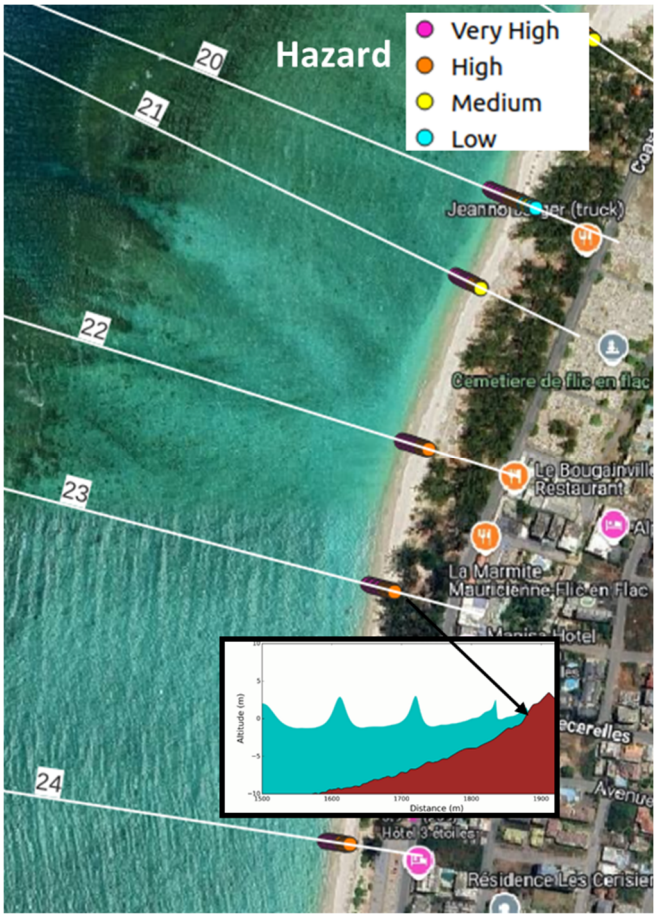


*Figure 186 : Simulated overtopping for Belal at Flic-en-Flac between profiles 20 and 24.*



*Figure 187 : Extract from the video showing the coastal flooding on Flic-en-Flac during Belal (source: https://www.tiktok.com/@radiomoris/video/7324249532991032608).*

#### *4.3.4.1.2.2 Simulation results*

The climate reference scenario (actual, 2050 and 2100) for Flic-en-Flac is the number 1498 (see 4.2.2.1.2.2 for details).

The waves simulated for the 3 climate horizons are comparable offshore, with Hs that can exceed 14m and Tp of ~13s. On the other hand, waves will be higher in the lagoon by 2100 (Hs ~1.5m) because of the higher sea level.

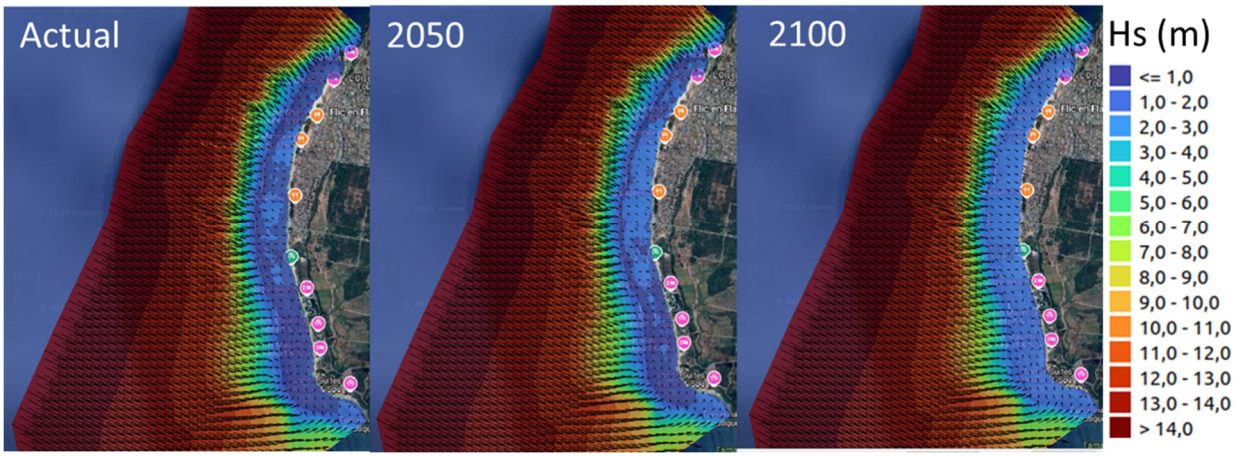


*Figure 188 : Simulation of maximum Hs and wave peak directions generated by the scenario 1498 on the three climate horizons at Flic-en-Flac.*

Figure 189 shows that flooding at Flic-en-Flac occurs in 4 main stages:

- Penetration of the overtopping preferentially via the streets in the central part of the town up to the channel (T0+1h);
- Central part of the town completely flooding (T0+6h);
- flooding spreads to the north and south of this sector and via the channel (T0+9);
- Maximum extent of the coastal flooding 14 hours after the start of the flooding (T0+15).

This sequence occurs in a comparable way for the actual, 2050 and 2100 timeframes.

With regard to the hazard (matrix defined in Figure 56), we can see that it is comparable in the northern part of the town with high values. The differences are apparent in the southern sector, where the hazard increases from the actual to 2100 climate scenario (Figure 190).

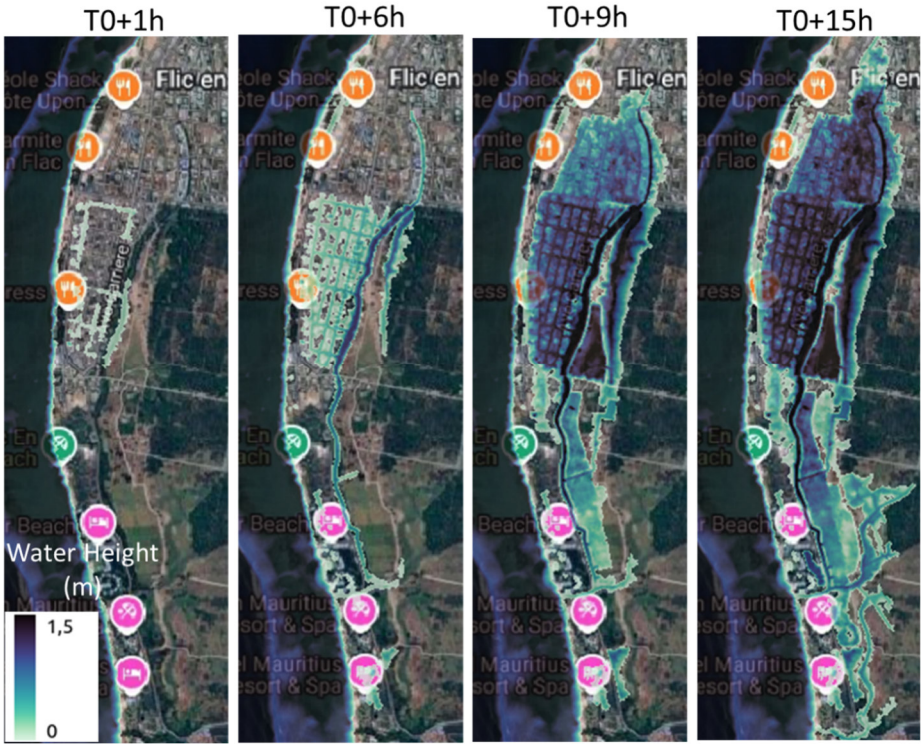


*Figure 189 : Main stages of the coastal flooding at Flic-en-Flac (actual climate scenario; T0: beginning of the simulation).*

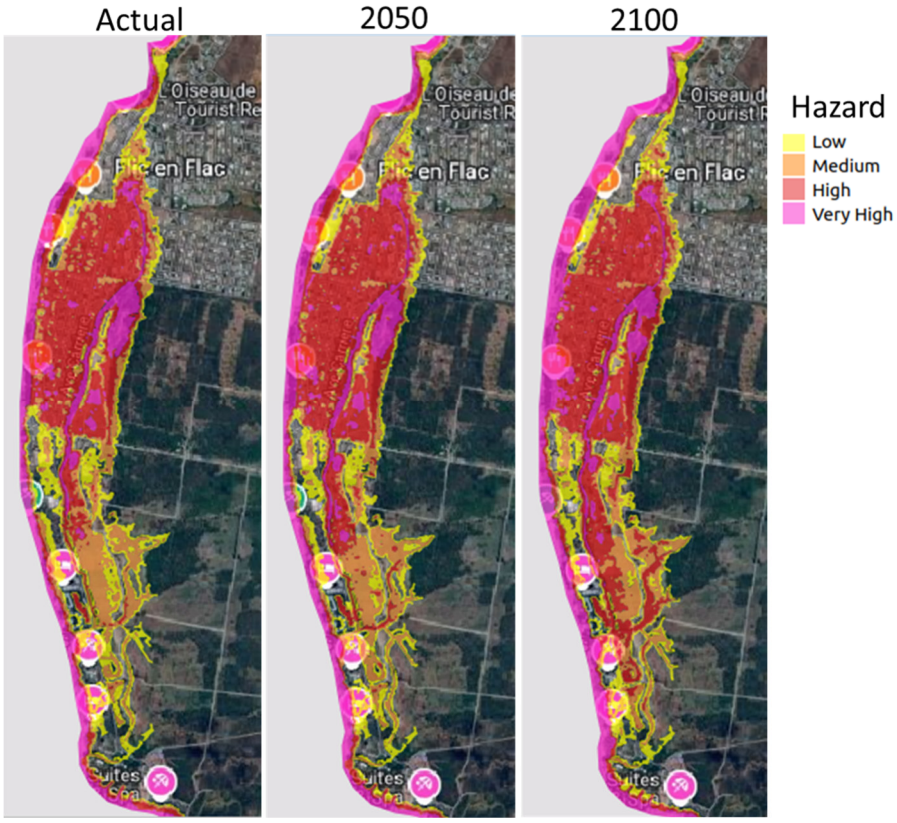


*Figure 190 : Coastal flooding hazard generated by the scenario 1498 on the three climate horizons at Flic-en-Flac.*

## 4.3.4.2 Anse la Raie (Mauritius)

### *4.3.4.2.1 Coastal retreat hazard*

Due to the lack of data about Anse la Raie shoreline changes, a specific analysis was carried out as part of this project and is presented in Appendix 1 of this report BRGM/RC-73987-FR). These data are used to assess the risk of shoreline recession at Anse la Raie.

#### *4.3.4.2.1.1 Coastal homogeneous zones and sedimentary sub-cells*

Anse la Raie is a coastal sector in the municipality of Cap Malheureux. According to the segmentation method used in Mauritius (see 4.2.1.1.2.1), the Anse la Raie study area corresponds to a single homogeneous zone (CaM_CHZ04), clearly delimited by two rocky headlands (Figure 191).

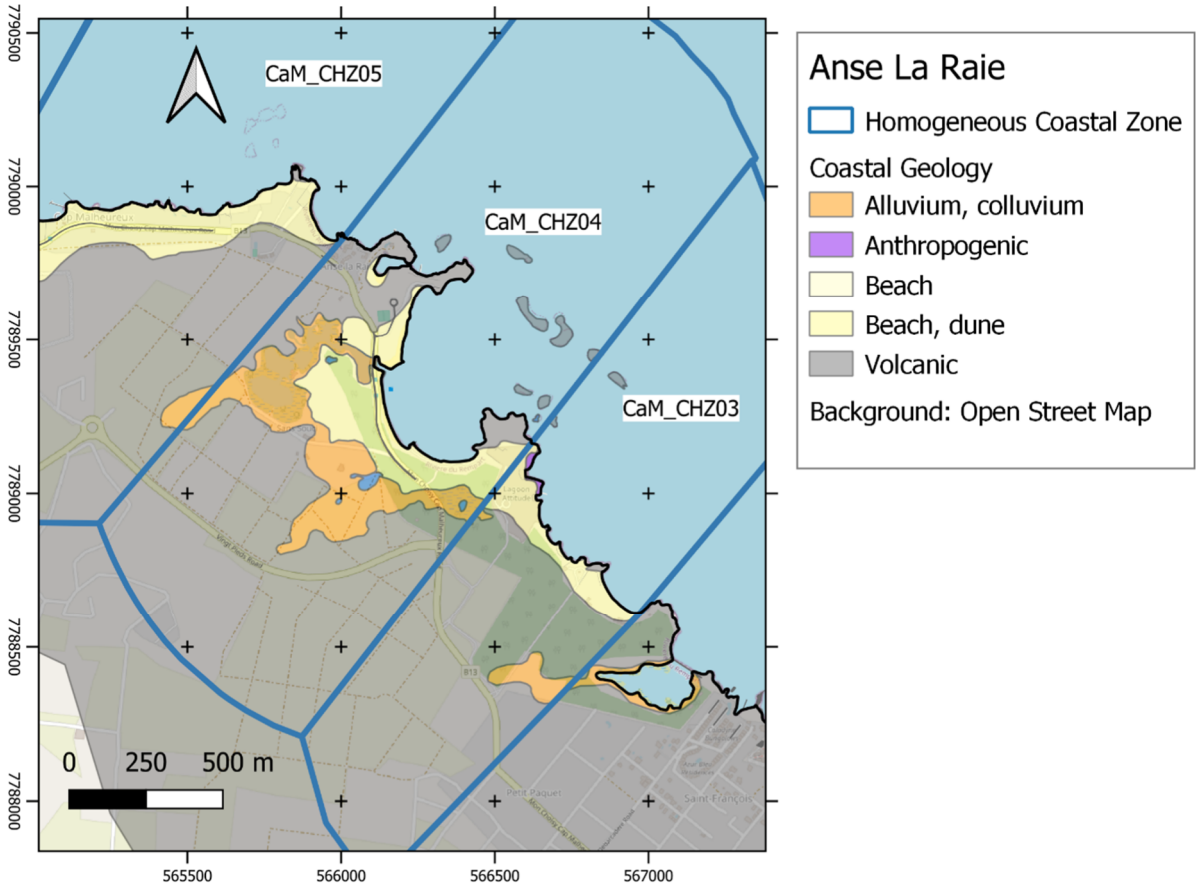


*Figure 191 : Homogeneous coastal zones and coastal geology of Anse la Raie, Cap Malheureux.*

#### *4.3.4.2.1.2 Analysis of coastline evolution*

This site was not monitored as part of the JICA study (2015). It was the subject of an initial analysis of satellite images in order to initiate the characterisation of local coastline dynamics (Appendix 1 of this report BRGM/RC-73987-FR and Figure 192). These observations were used to validate the method chosen to establish scenarios for projecting shoreline retreat in areas without prior observations (See part 4.2.1.1.2.2). The solution is to define the various parameters of coastline change on the basis of expert opinion.

These parameters are delineated by experts, employing various criteria of similarity with homogeneous zones whose evolution is well-documented. The aforementioned criteria encompass the following: exposure to swell conditions, the presence and width of the lagoon, the orientation of the coast, and proximity to well-documented cells or sub-cells.

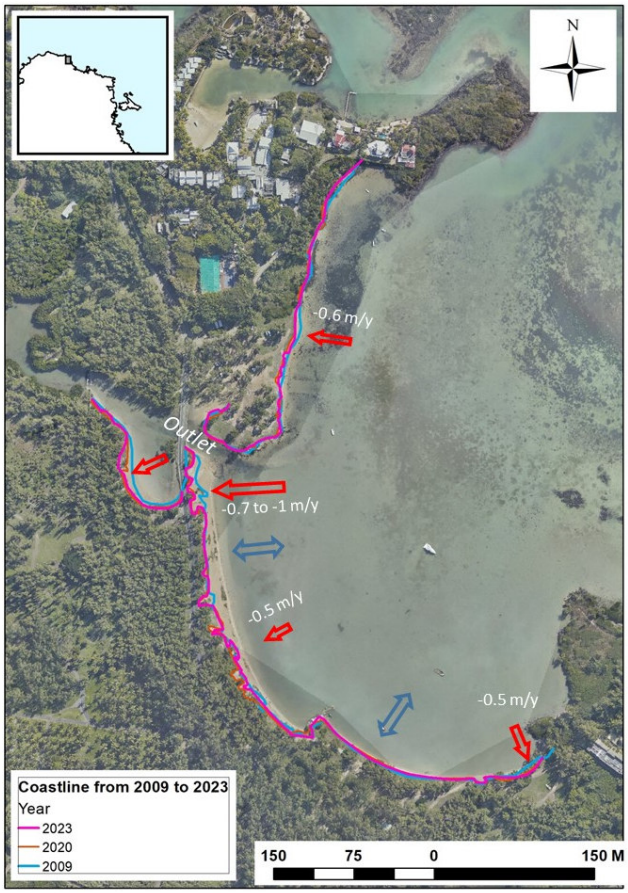


*Figure 192 : Coastline change at Anse la Raie from 2009 to 2023 (appendix 1)*

In the case of Cap Malheureux and Anse la Raie, the closest and most similar JICA (2015) monitoring areas are located to the west, at Grand Baie and Pointe aux Canonniers, and to the south-east at Roches Noires. The median rate of change ($Tx_{med}$) in these areas is low, identical for Pointe aux Canonniers and Roches Noire (0.04m/yr) or similar (0.07m/yr) for Grand Baie (Table 30).

Grand Baie is a well-sheltered sandy bay with morphological similarities to Anse la Raie. However, the mean retreat ($Tx_{hzd\text{-}cell}$) and maximum retreat ($Tx_{max\text{-}cell}$) values for Grand Baie (Table 30) are significantly lower than the values observed locally at Anse La Raie from recent satellite images (Figure 192). In the Cap Malheureux area, there is also the cemetery sector (CaM_HCZ06) which appears to be particularly sensitive to erosion. This means that the values for the Grand Baie cell cannot be used, as the average and maximum retreat rates appear to be too low locally to take into account the sensitivity of the area.

The Pointe aux Canonniers cell is a sector whose coastal geomorphology is fairly similar to that of the Cap Malheureux area. However, this coastal cell is not protected by coral reefs neither large lagoons. The sector would therefore appear to be potentially more vulnerable than most of

the homogeneous areas of Cap Malheureux. The mean retreat values are the highest of the three coastal cells analysed (0.31m/year, Table 30). The maximum rate of retreat for the cell (-0.74m/yr) is comparable to the retreat observations made for Anse La Raie (Figure 192). The sub-cell most sensitive to erosion at Pointe aux Canonniers (GrB_SC02-04) has a median rate of change of 0.16m/yr and a mean rate of retreat of 0.39m/yr.

The Roches Noires coastal cell is further away in distance, but has a similar orientation and geomorphology to Cap Malheureux. Unlike Pointe aux Canonniers, the JICA (2015) study area at Roches Noires corresponds to an area protected by a vast lagoon and reef system. The mean retreat values (0.27m/yr, Table 30) are slightly lower than for Pointe au Canonniers (0.31m/yr), but the maximum retreat value exceeds 1m/yr, which corresponds to a one-off retreat value observed at Anse La Raie.

*Table 30 : Coastline retreat parameters for neighbouring or similar coastal cells to Cap Malheureux, whose evolution is dealt with by JICA (2015).*

| Tx (m/y) | *Wave exposure* | $Tx_{med}$ | $Tx_{hzd}$ | $Tx_{max}$ |
|---|---|---|---|---|
| **Cell Pointe aux Canonniers** | open | -0.04 | -0.31 | -0.74 |
| Sub-Cell GrB_SC02b-04 | | -0.16 | -0.39 | -0.74 |
| **Cell Grand Baie** | protected | -0.07 | -0.20 | -0.26 |
| **Cell Roches Noires** | lagoon | -0.04 | -0.27 | -1.17 |

The decisions made to qualify the potential retreat of the coastline for the Cap Malheureux area are based on this analysis and the resulting working hypotheses. They are subjective and open to criticism and cannot replace the implementation of in situ measurements and observations and the local quantification of changes in the coastline. However, these working hypotheses make it possible to build scenarios of retreat and to establish projections.

The first assumption is that the Cap Malheureux area has similarities with the Roches Noires area. The coastline evolution values for the area will be based mainly on those for Roches Noires, particularly for zones CaM_CHZ01, CaM_CHZ03 and CaM_CHZ05 (Table 31).

The second hypothesis is that the Cap Malheureux area also has similarities with the neighbouring Pointe aux Canonniers sector. Certain coastline evolution values could be based on the Pointe au Canonniers parameters.

- CaM_CHZ07 is a homogeneous zone close in distance and characteristics to the Pointe aux Canonniers cell. The mean values of this cell are used to qualify the dynamics of this homogeneous zone (Table 31).
- The CaM_CHZ06 homogeneous zone corresponds to the Cap Malheureux cemetery sector. It is an area not protected by a reef and lagoon system. The median rate and the retreat rate chosen are those of the most sensitive sub-cell of Pointe aux Canonniers (SC02-04). The maximum retreat rate is that of Roches Noires.
- The homogeneous zone CaM_CHZ04 corresponds to the Anse La Raie study area. The median rate and maximum retreat rate parameters are those of Roches Noires (Table 31). The retreat rate parameter corresponds to that of the most sensitive cell at Pointe aux Canonniers (SC02-04) in order to propose a retreat value that is consistent with the quantifications made from satellite images used for around ten years (Figure 192) and the values adopted for the Cap Malheureux territory.

*Table 31 : Coastline retreat parameters for each homogeneous zone of Cap Malheureux territory, on the basis of expert opinion. The Anse la Raie site corresponds to the CaM_CHZ04 zone.*

| Tx (m/y) | *Shoreline nature* | $Tx_{med-hz}$ | $Tx_{hzd-hz}$ | $Tx_{max-hz}$ |
|---|---|---|---|---|
| **CaM_CHZ01** | sand | -0.04 | -0.27 | -1.17 |
| CaM_CHZ02 | rock | | | |
| **CaM_CHZ03** | sand | -0.04 | -0.27 | -1.17 |
| **CaM_CHZ04** | sand&rock | **-0.04** | **-0.39** | **-1.17** |
| **CaM_CHZ05** | sand | -0.04 | -0.27 | -1.17 |
| **CaM_CHZ06** | sand | -0.16 | -0.39 | -1.17 |
| **CaM_CHZ07** | sand | -0.04 | -0.31 | -0.74 |

The parameter Lmax, which is employed to evaluate the impact of a major cyclone on shoreline retreat at the end of the period, was selected based on expert consensus. Baird (2003) proposed two impact models for lagoon sectors that are protected from the direct effect of offshore waves:

- one for the Flic-en-Flac site, which was used in this study for all the lagoon coasts of the west coast (see 4.3.4.1.1.2 and Table 27);
- and the other for the Belle Mare site, which was used in this study for all the lagoon and reef areas on the east coast of Mauritius (Table 32).

Anse La Raie is a coastal area protected by a lagoon and a group of rocky islets, but it is located on the north coast of Mauritius. However, it should be noted that the characteristics of Anse La Raie, particularly with regard to wave exposure and coastal morphology, bear certain differences to those observed in the two models developed for Mauritius. Notwithstanding these discrepancies, the Bellemare model was selected to determine the Lmax values used in the shoreline projection scenarios for Anse la Raie. Two arguments were presented in support of this decision:

- The estimated retreat values at Bellemare for cyclones with a return period of between 5 and 25 years are lower than those at Flic-en-Flac. Anse la Raie, a sector characterized by its protection from the waves of the open sea, is estimated to be less sensitive to certain cyclones.
- However, the local morphology of the site is characterized by its flatness, and the sediment stock on the beach is limited. In the event that a particularly intense cyclone has the capacity to exert a negative effect on the coastline, the consequences could be substantial, potentially resulting in considerable retreat. The Bellemare model is distinguished by its notably higher setbacks in comparison to those observed at Flic-en-Flac for the most intense cyclones.

*Table 32 : Estimated impact of extreme events (Lmax) for Anse La Raie, based on Baird model (2003) for Bellemare*

**Baird model (2003)**

| *Lagoon, Mauritius Est coast* | $Lmax_{5y}$ | $Lmax_{25y}$ | $Lmax_{75y}$ |
|---|---|---|---|
| **median** | 3.5 | 5 | 14 |
| **intermediate** | 4 | 6 | 20 |
| **safe** | 5 | 10 | 20 |

#### *4.3.4.2.1.3 Additional erosion caused by sea level rise (SLR-R)*

The methodology for estimating the additional erosion associated with sea level rise (SLR-R) is outlined in section 4.2.1.1.2.4.

The extent of potential additional erosion is contingent on the type of shoreface and its exposure to wave action. The resulting coastal retreat is influenced by the availability of sediment, which is assessed by estimating the width of the beach.

Anse la Raie is a sandy bay that extends approximately 500 meters. The area is nearly encircled by rocky islets and a coral reef that forms a 300-meter-wide belt in front of the site and could contribute in a limited way to feeding the site with bioclastic sediments (Figure 193).

This particular configuration appears to be relatively favourable for the conservation of coastal sedimentary stocks in the face of rising sea levels. However, it should be noted that sediment stocks on the beach appear to be limited, with the beach width estimated to be approximately 12 meters for the specified sector. The parameters of bay size, reef width, and beach width are used to calculate the parameters of additional shoreline retreat associated with sea level rise and the potential for mitigation through coral sediment production.

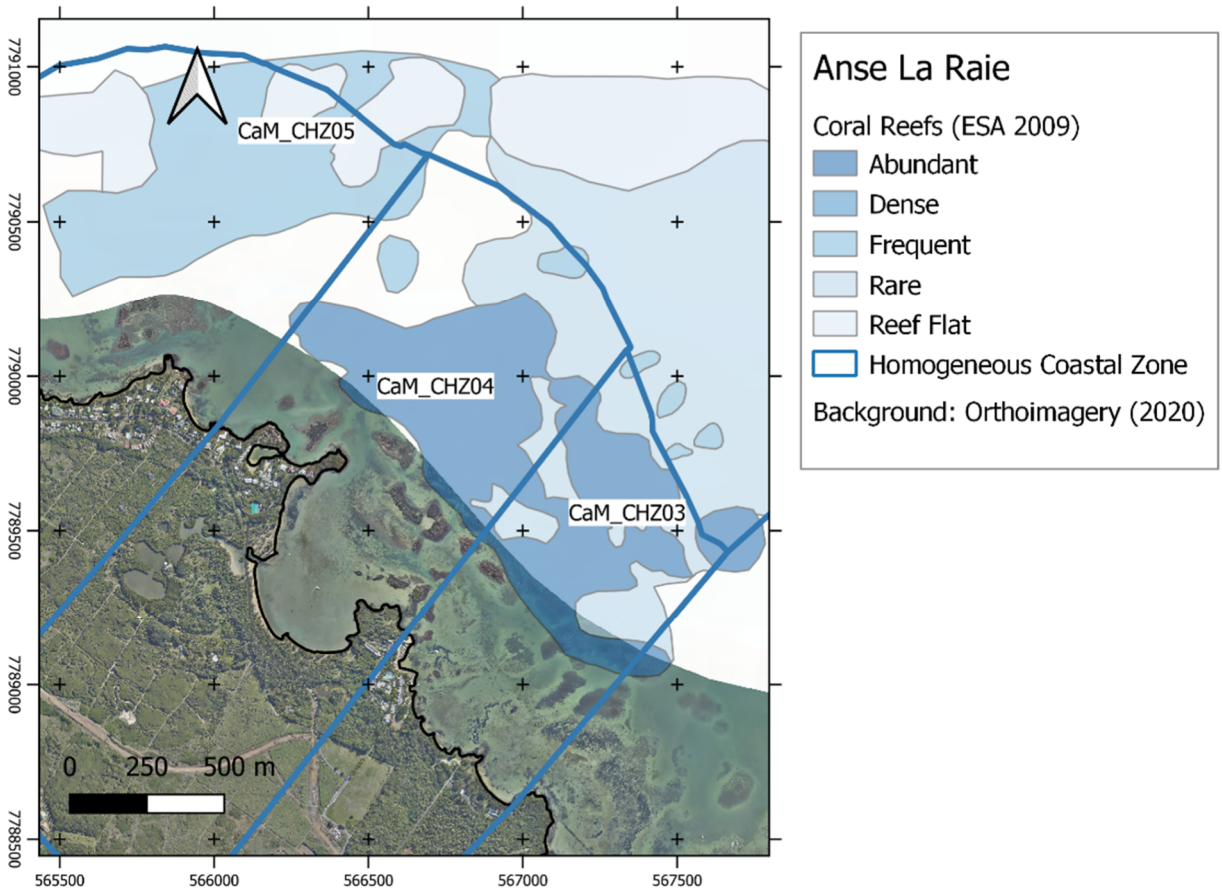


*Figure 193 : Position and condition of the coral reefs in front of Anse la Raie (according to ESA, 2009)*

For Anse la Raie, the estimated additional retreat (SLR-R) is between 3.1m and 6.7m in 2050 (3.75m for the intermediate scenario) and 16 to 42.7m in 2100 (28.75m for the intermediate scenario).

*Table 33 : Estimated values of additional coastal retreat for Anse la Raie coastline*

| *Cap Malheureux* | *Shoreface exposition* | **SLR-R 2025-2050 (m)** | | | **SLR-R 2050-2100 (m)** | | |
|---|---|---|---|---|---|---|---|
| | | median | intermediate | safe | median | intermediate | safe |
| **Anse La Raie** | Lagoon | 3.13 | 3.75 | 6.77 | 15.94 | 28.75 | 42.71 |

#### *4.3.4.2.1.4 Coastline retreat hazard at the sub-cells scale*

The determination of projection parameters allows for the calculation of the potential retreat of the sandy coastline over three timescales (current, 2050, 2100) and for the three scenarios (safe, intermediate, median), according to the methods outlined in section 4.2.1.1.2. The estimated retreat values, rounded to the nearest 5m, are presented for the homogeneous coastal zone of Anse la Raie. The estimated coastline retreat values for Anse la Raie are presented in Table 34. The results of the intermediate scenario for the 3 timeframes of the study are presented in the maps of Anse la Raie and the neighbouring homogeneous zones of Cap Malheureux (Figure 194, Figure 195 and Figure 196).

*Table 34 : Coastline retreat estimations (m) for homogeneous zone of Anse la Raie (Cap Malheureux), 2025, 2050 and 2100 timeframes*

| | **2025** | | | **2050** | | | **2100** | | |
|---|---|---|---|---|---|---|---|---|---|
| **Anse la Raie** | median | interme diate | safe | median | interme diate | safe | median | interme diate | safe |
| CaM_HCZ04 | 5 | **10** | 15 | 10 | **20** | 35 | 50 | **75** | 100 |

The current zone of exposure to shoreline retreat in Anse la Raie is estimated to range between 5 and 15 meters, depending on the scenario. The intermediate scenario proposes a value of 10 meters, which aligns with the median class of potential retreat in Mauritius. However, this value is lower than that observed in the majority of sedimentary shoreline, which are inherently more sensitive than rocky coasts. In comparison to the homogeneous zones around Cap Malheureux, the current median scenario for Anse la Raie is more pronounced due to the selection of a higher median retreat rate ($Tx_{hzd}$). This choice is justified by local observations derived from satellite imagery.

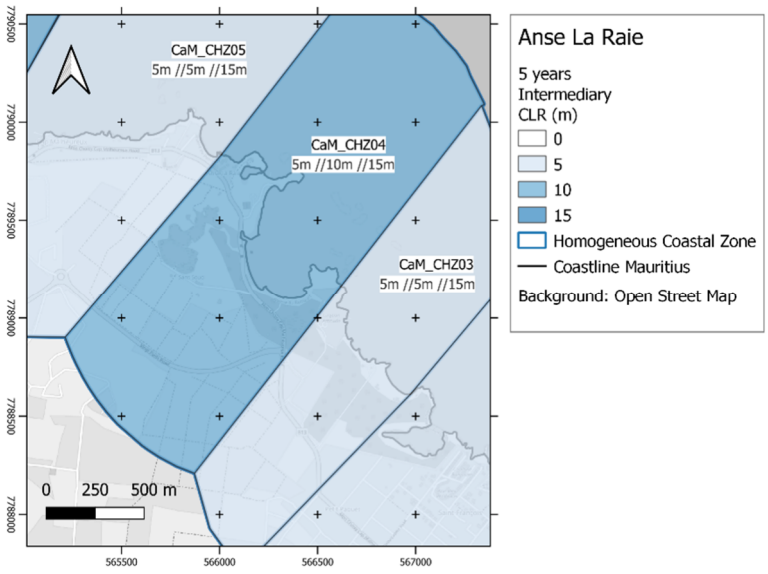


*Figure 194 : Map of coastline retreat estimations (CLR) for 2025 timeframe, at the scale of Anse la Raie and neighbouring sub-cells of Cap Malheureux.*

The potential retreat of the coastline by 2050 for Anse la Raie is projected to be between 10 and 35 meters, depending on the scenario. The intermediate scenario suggests a retreat value of 20 meters, slightly above the median of estimated retreats for all homogeneous zones in Mauritius, including rocky coasts. The safe scenario places Anse la Raie in the upper quartile, indicating a sector potentially more exposed to hazards than others. This projection of the safe scenario may appear slightly pessimistic, as the choice of the maximum retreat value ($Tx_{hzd\text{-}max}$) is based on JICA (2015) observations at Roches Noires. This value, exceeding 1 meter per year, may seem maximizing given the limited number of available observations and the lack of in situ measurements. The safe scenario for the homogeneous areas adjacent to Anse la Raie indicates even higher values for coastline retreat by 2050, due to their potentially greater local sensitivity to sea-level rise.

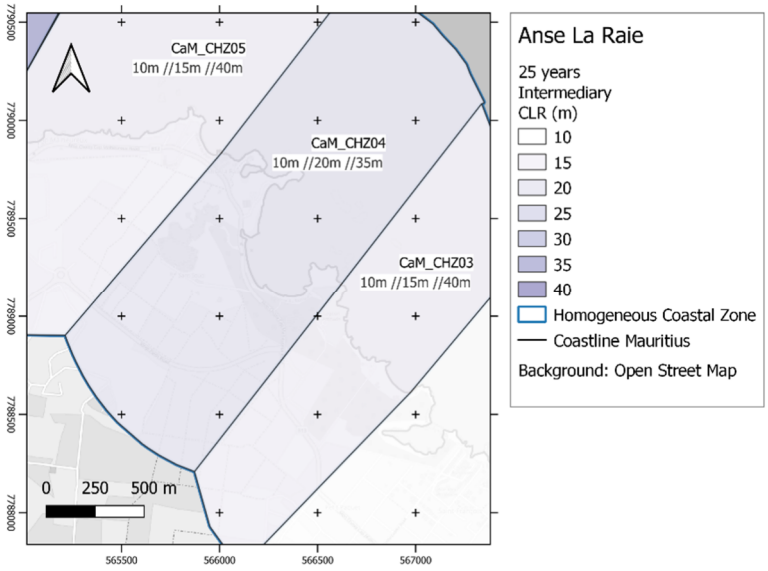


*Figure 195 : Map of coastline retreat estimations (CLR) for 2050 timeframe, at the scale of Anse la Raie and neighbouring sub-cells of Cap Malheureux.*

The estimated zone of exposure to shoreline retreat in 2100 for Anse la Raie ranges between 50 and 100 meters, depending on the scenario. The intermediate scenario proposes a value of 75 meters, which corresponds to the upper quartile of potential retreats in Mauritius. This significant retreat, greater than that of the majority of homogeneous zones in Mauritius, is attributed to the low sediment stocks estimated on the beaches of Anse la Raie, which appear insufficient to mitigate the erosive effects of sea-level rise. The homogeneous zones neighbouring Anse la Raie exhibit comparable or higher retreat values by 2100, due to their even greater local sensitivity to sea-level rise.

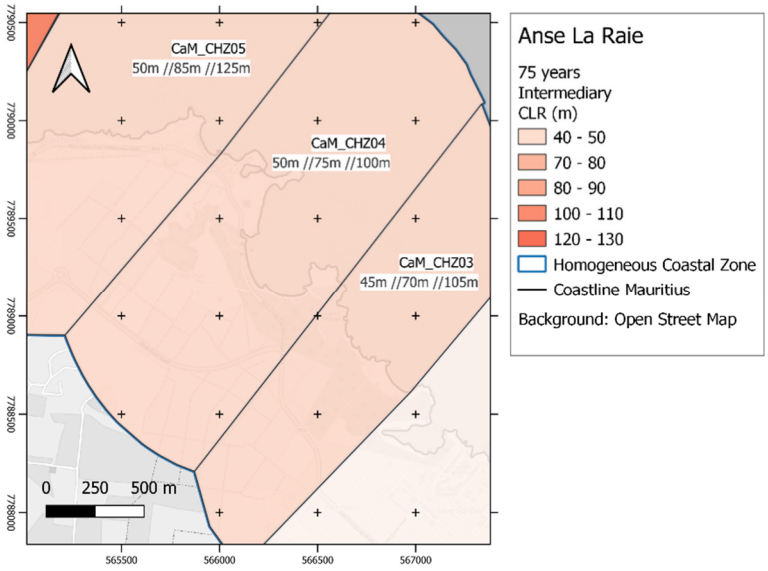


*Figure 196 : Map of coastline retreat estimations (CLR) for 2100 timeframe, at the scale of Anse la Raie and neighbouring sub-cells of Cap Malheureux.*

#### *4.3.4.2.1.5 Maps of coastline retreat hazard at local scale*

Maps of exposure to shoreline retreat hazard on a local scale (1:10,000) can be drawn up using estimates of possible retreat values for homogeneous zones over the three timeframes of the study.

The GIS data provided in the deliverables of the Mauriscot project are of course compatible at the scale of 1:5,000, useful for local and detailed mapping.

The special cases of mixed coasts (sediment and rock) and low-lying areas are included in the shoreline retreat projection scenarios (see section 4.2.1.1.2.5) and implemented for Anse la Raie.

Figure 197, Figure 198 and Figure 199 depict the projected shoreline retreat by timeframe for the various scenarios.

Figure 200, Figure 201, and Figure 202 illustrate the projected retreat of the coastline at various timeframes for each scenario.

The estimated potential retreats for the current period (Figure 197) and for the year 2050 (Figure 198) appear relatively limited and remain below the regulatory 30-metres setback, except under the safe scenario for 2050.

Erosional processes can affect the upper beach and backshore, leading to the retreat of the intertidal zone and beaches of the bay. These processes may also impact human infrastructure and developments located in close proximity to the shoreline, including areas composed of rocky substrates. In this regard, the northern part of the study area shows a lower level of hazard over the rocky zones, though artificialized areas around the Paradise Cove Hotel may be affected.

In rocky sectors, an extreme event does not necessarily result in the full retreat of the coastline but may instead cause soil erosion, displacement of boulders, or damage to build infrastructure. Moreover, it is conceivable that an extreme event could affect the structural integrity of the bridge in the current time frame. By 2050, chronic erosion or an extreme event could also locally impact the coastal road, depending on the safe scenario.

By 2100, Figure 199 suggests that erosion and sea-level rise may significantly alter the landscape of Anse la Raie. Low-lying areas adjacent to rivers and ponds could experience regular marine inundation. Chronic erosion may affect the sandy shoreline of the bay, including the small dune systems currently observed to the south of Anse la Raie. Rocky headlands on either side of the bay may evolve into small islands, resembling those presently enclosing the bay's entrance.

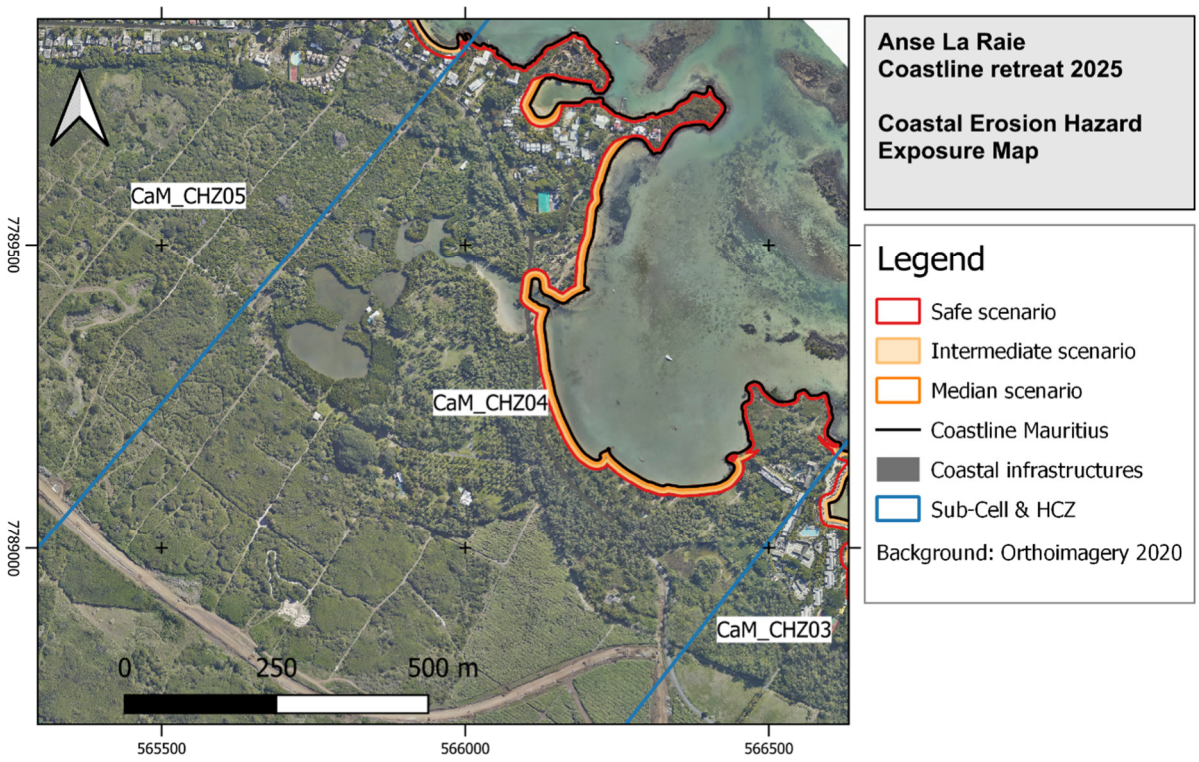


*Figure 197 : Coastline retreat hazard for 2025, median, intermediate and safe scenarios for Anse la Raie.*

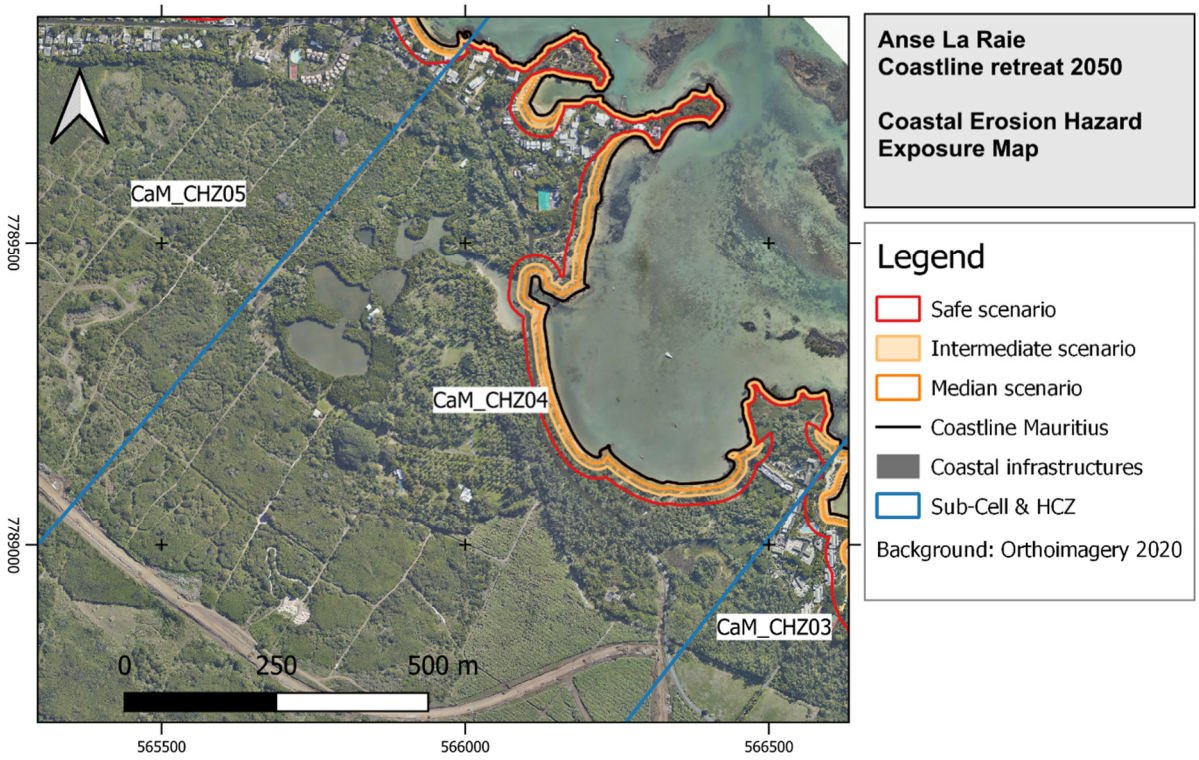


*Figure 198 : Coastline retreat hazard for 2050, median, intermediate and safe scenarios for Anse la Raie.*

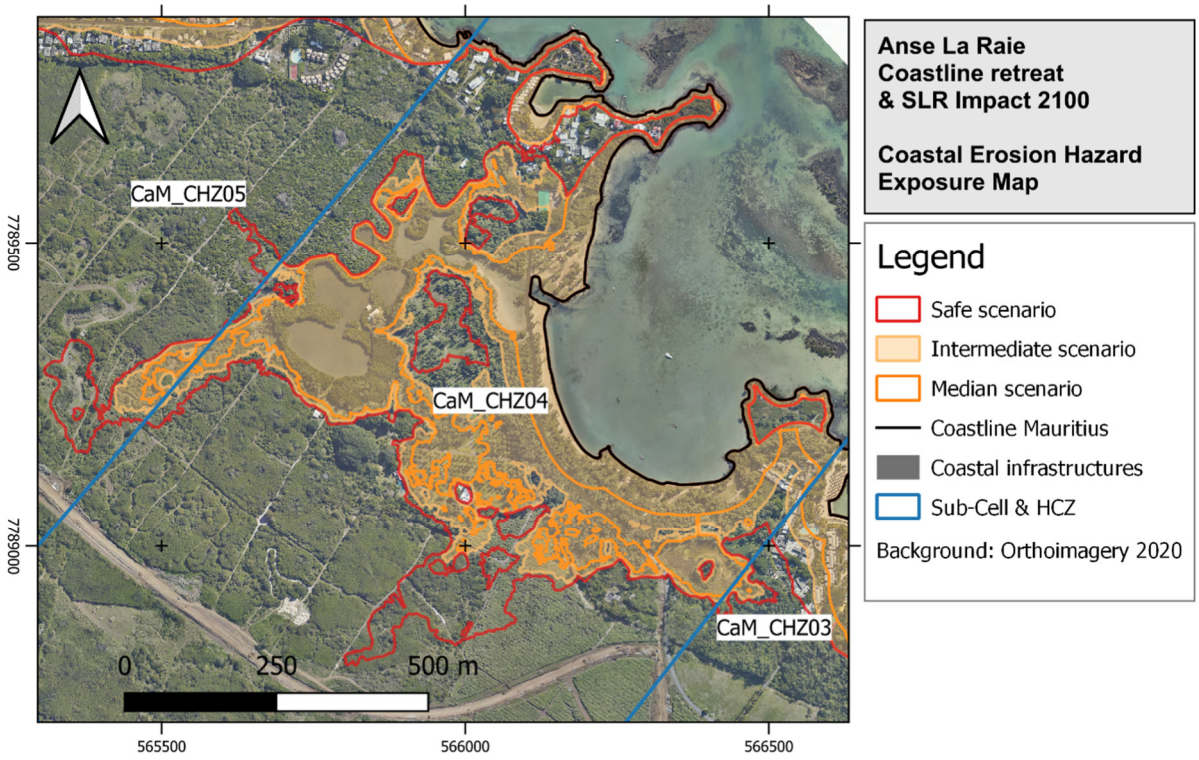


*Figure 199 : Coastline retreat hazard and sea-level rise impacts for 2100, median, intermediate and safe scenarios for Anse la Raie.*

Figure 200, Figure 201, and Figure 202 illustrate the degree of uncertainty surrounding the future of low-lying coastal zones susceptible to erosion. In the case of Anse la Raie, these uncertainties primarily relate to the acceleration of sea-level rise towards the end of the century. The different possible trajectories of sea-level rise are integrated into the scenarios developed for the projections.

The median scenario projects a trajectory that, while involving significant shoreline retreat and a more increased marine inundation of existing marshlands, does not radically alter the landscape. Conversely, the intermediate and safe scenarios foresee a merging of eroded beach zones with low-lying areas that may become submerged at the back of the bay. Under such conditions, the coastline could retreat by 300 to 500 metres in the lowest-lying areas relative to its current position.

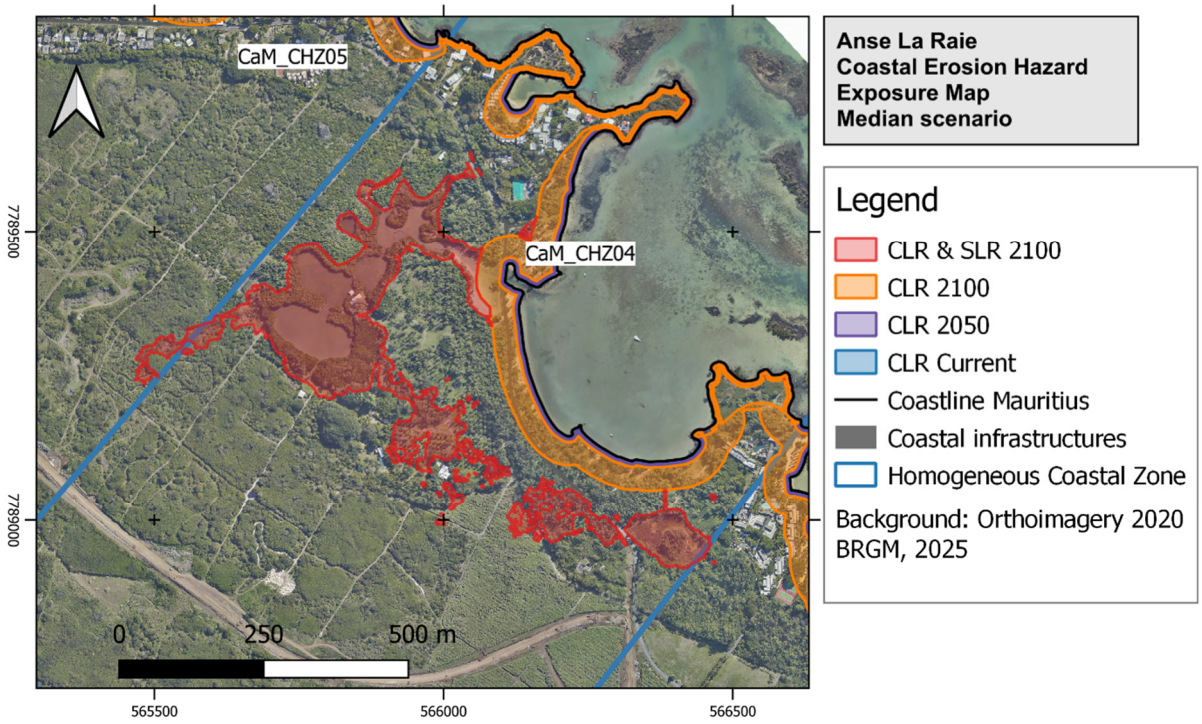


*Figure 200 : Maps of coastline retreat hazard for 2025, 2050 and 2100, median scenario for Anse la Raie.*

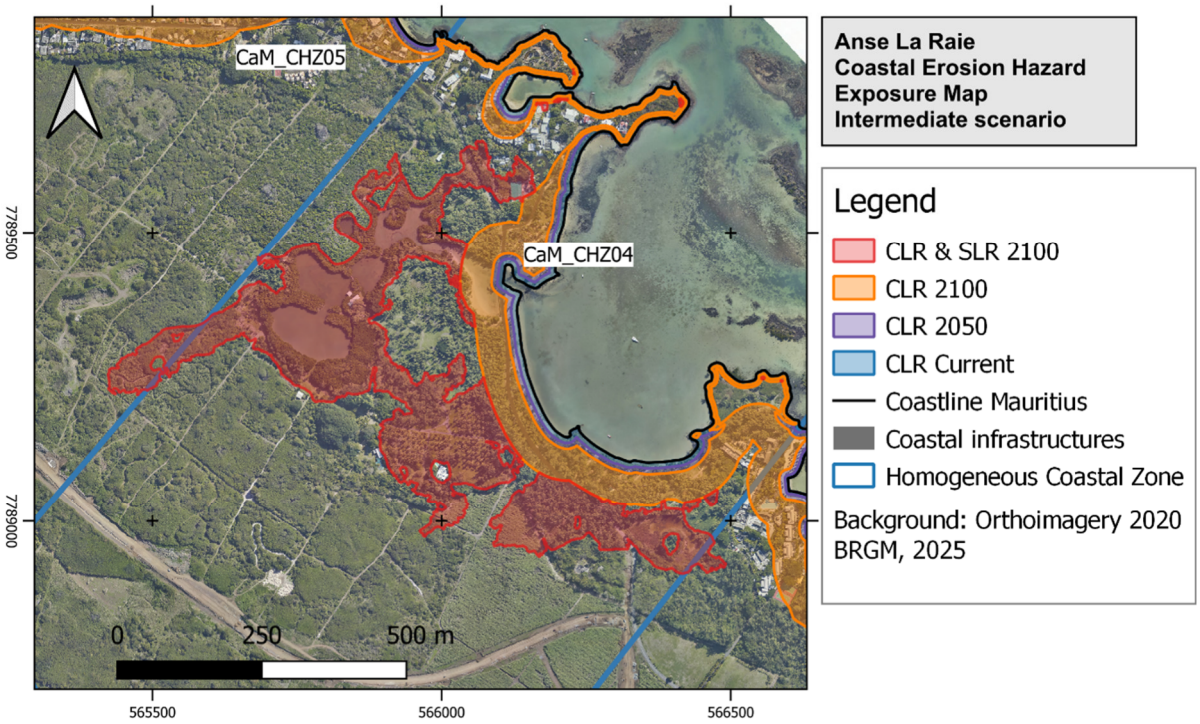


*Figure 201 : Maps of coastline retreat hazard for 2025, 2050 and 2100, intermediate scenario for Anse la Raie.*

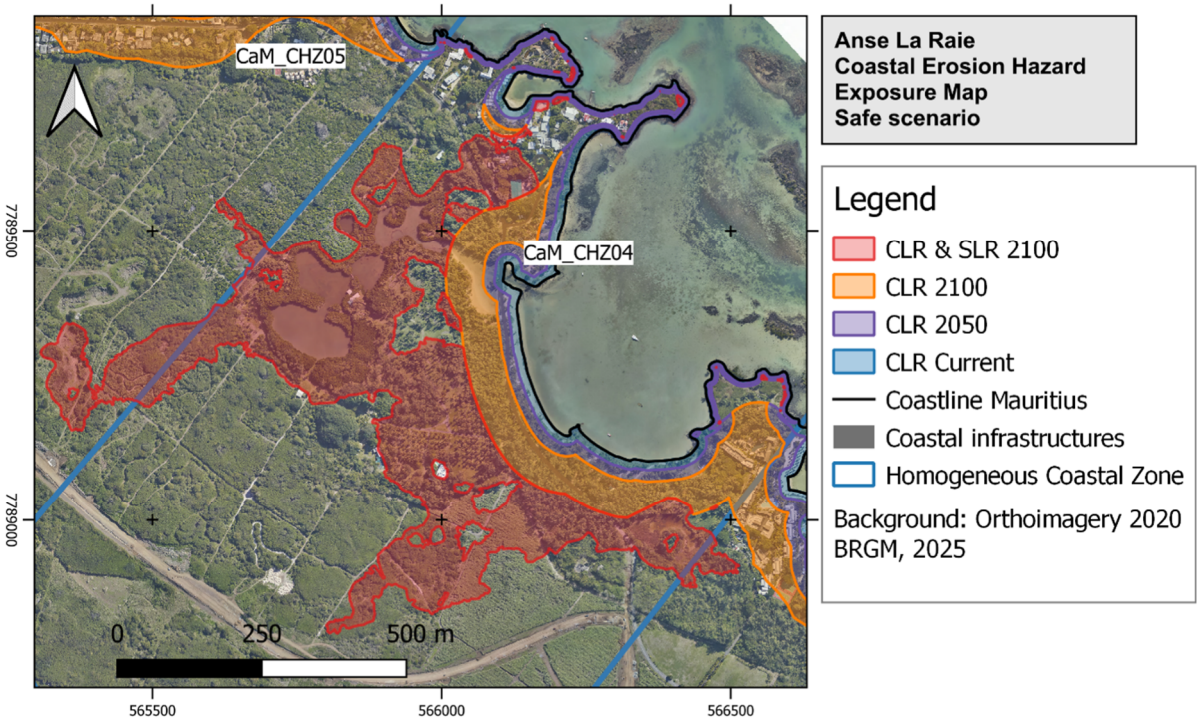


*Figure 202 : Maps of coastline retreat hazard for 2025, 2050 and 2100, safe scenario for Anse la Raie.*

#### *4.3.4.2.2 Coastal flooding hazard*

##### *4.3.4.2.2.1 Model Validation on historical event*

The cyclone Berguitta (see details in §4.2.2.1.2.1) also caused minor flooding at Anse La Raie, as shown in Figure 203.

This was well reproduced by the model with simulated water heights <0.2m (Figure 204).



*Figure 203 : Extract from the video showing the coastal flooding in Anse La Raie during Berguitta (source:https://www.facebook.com/www.defimedia.info/videos/cyclone-berguitta-en-direct-danse-la-raie-dans-le-nord-de-l%C3%AEle/1717750718287944/)*

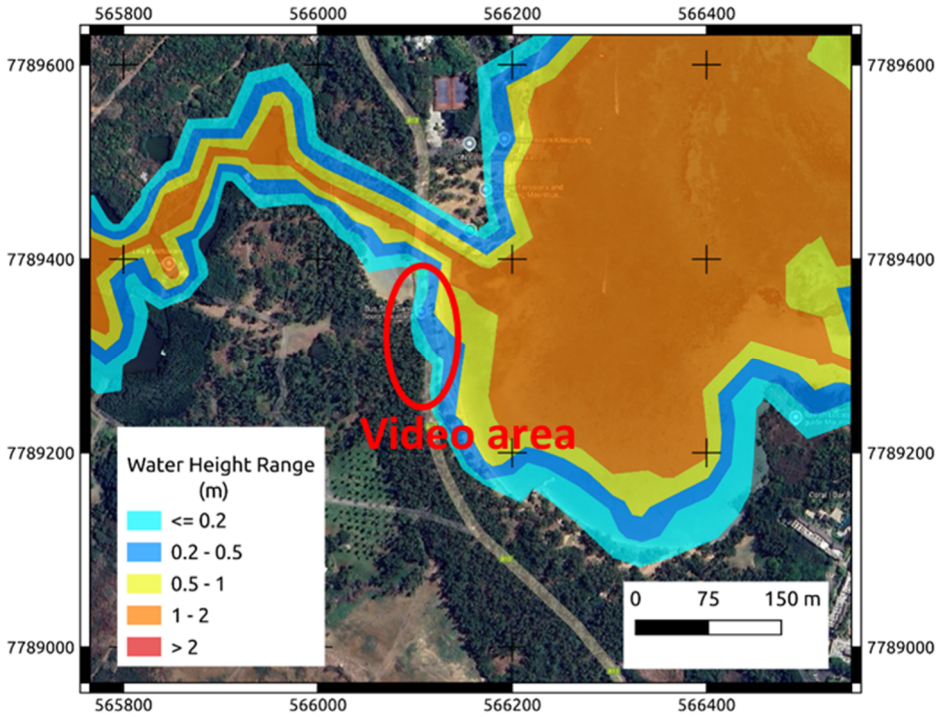


*Figure 204 : Simulated water heights at Anse La Raie beach during Berguitta.*

#### *4.3.4.2.2.2 Simulation results*

Previous results on section §4.2.2.1.2.3 have shown that the reference scenario for the Anse la Raie site is represented by cyclone 1498 for all climate conditions. Therefore, the scenario has been simulated again on the computational domain described by Figure 172 in order to obtain a finer description of the flooding on the desired area. Figure 205 and Figure 207 show the obtained results in terms of maximum significant wave height (Figure 205 left), maximum velocities (Figure 205 right) and maximum sea surface heights Figure 207. We can appreciate that a great accordance exists between the new results and those displayed in section §4.2.2.1.2.3. However, when differences appear and in the flooded region in particular, these latter results should be trusted more, since they are generated with a finer grid resolution, by making an extensive use of constraint lines in the mesh generation and by taking into account the presence of culverts on the terrain.

In this sector of the island the northern insular shelf and the reefs offer a full coastal protection against the incoming waves. Indeed, the former reduces the maximum Hs of about 3m in all climate scenarios, while the latter triggers wave breaking outside the lagoon. As a result of this, typical maximum Hs values inside the lagoon never surpass 2.5m. Locally on the Anse la Raie site, an additional protection element against waves is given by the presence of a chain of islets at the bay entrance. Thus, maximum Hs never attend 1.5m inside the bay, almost 1m less than in the value in the outer lagoon, as displayed by Figure 205 top-right. Sea current velocities are strongly correlated to the wave forcing. High intensities (>2m/s) are achieved in the breaking region but also on the insular shelf all around the Flat island and in the areas of reduced water depth (Figure 205 bottom). Maximum values in the lagoon are in general <1m/s with the exception of areas in the vicinity of access channels.

Wave breaking on the reef produces a wave setup, whose contribution to determine the total water level is displaced in Figure 206 for the three climate conditions considered. The values of the setup vary between 0.2 and 0.5m in all the configurations, representing ~25% of the surge during the peak. The trace of the cyclone passage is very close in the three pictures, comforting the idea that the sea level rise is the major flooding driver induced by the climate change.

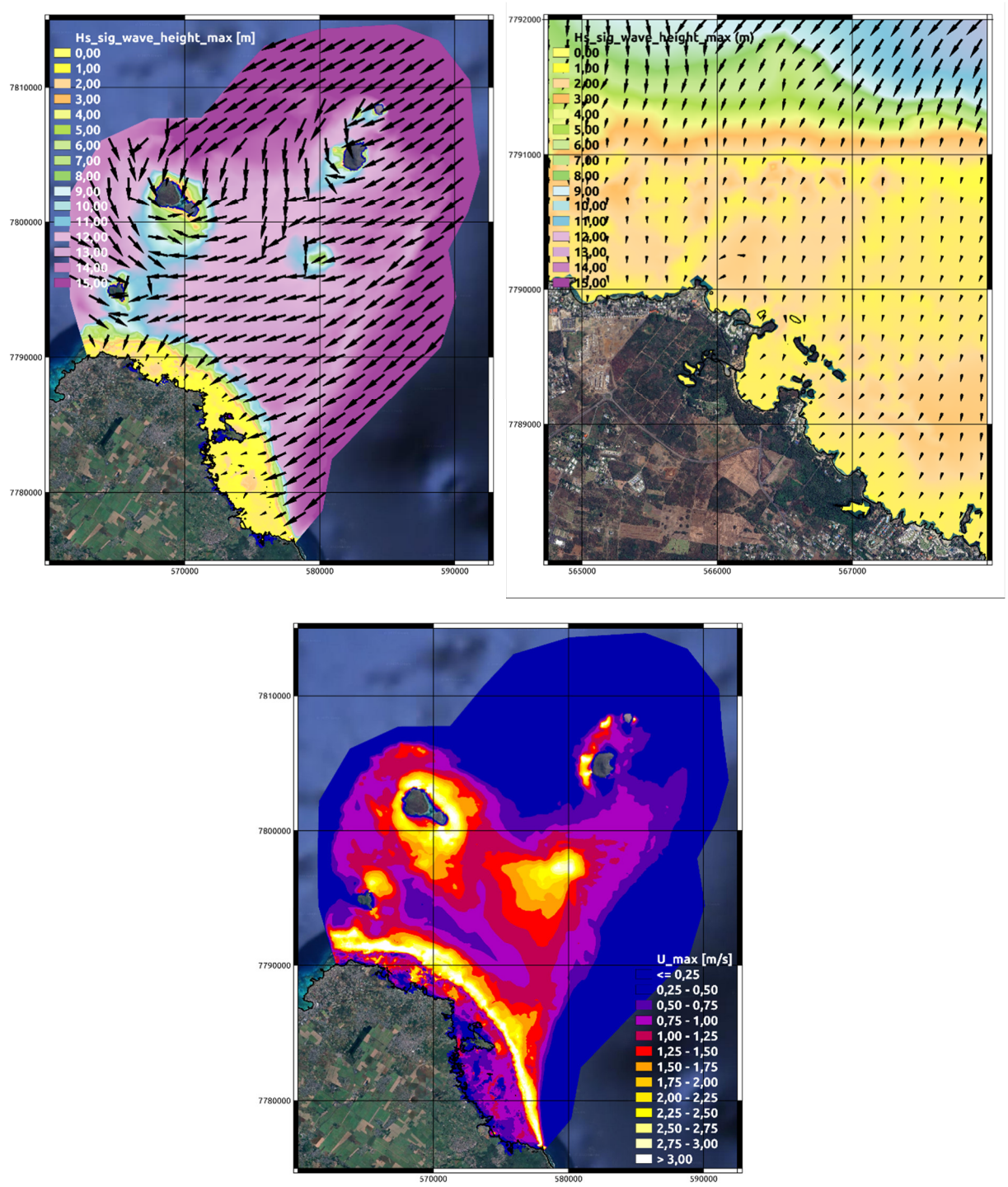


*Figure 205 : Computed maximum significant wave height (top) and sea current velocities (bottom) for the scenario 1498 with present-day climate conditions.*

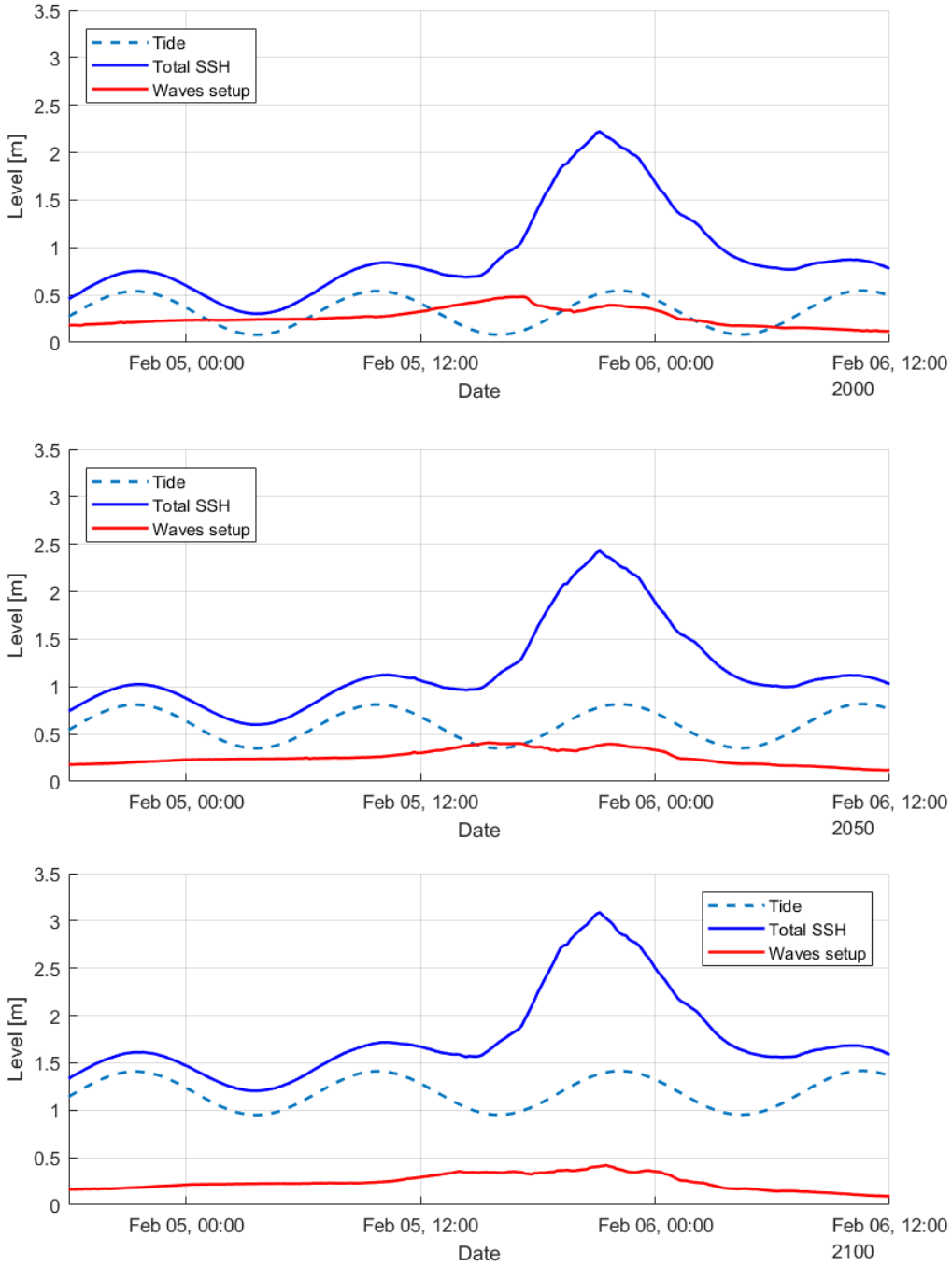


*Figure 206 : Time series of the total sea level (SSH) and wave setup contribution on Anse la Raie for actual climate (top), 2050 climate (centre) and 2080-2100 climate (bottom).*

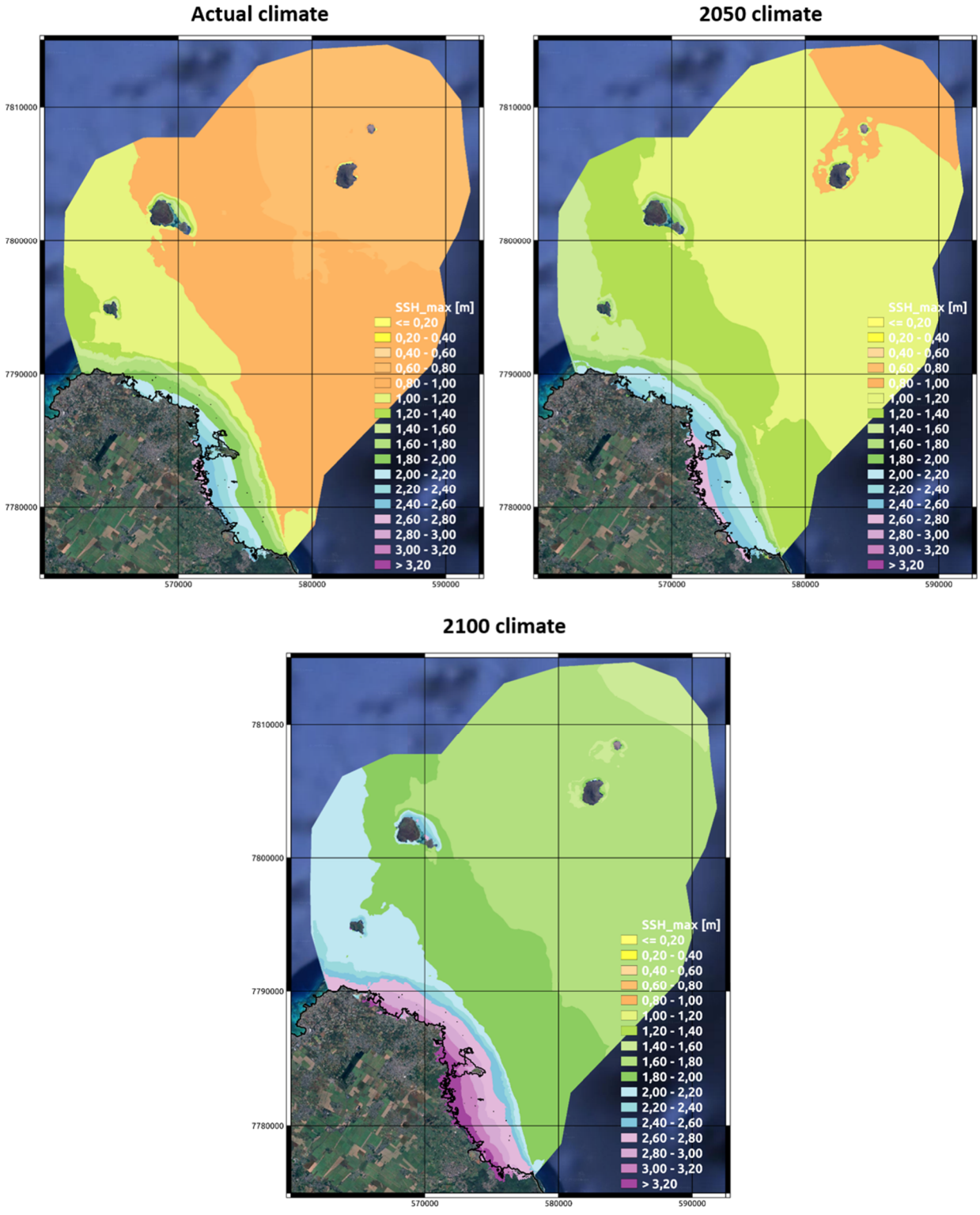


*Figure 207 : Computed maximum sea surface height (SSH_max) on the scenario 1498 with present-day climate conditions (top-left), 2050 climate (top-right) and 2100 climate (bottom).*

The resulting maps of the computed maximum sea-surface levels (Figure 207) show that the highest levels are reached on the east side of the island: i.e. Poudre d'Or suffers 0.5m of water more than Anse la Raie in present-day climate and 0.3m on 2100 climate. The extension of the

flooded area in Anse la Raie is better described in the following Figure 208, Figure 209, Figure 210 and Figure 211. Between present-day and 2050 climate, the limits of the flooded zone do not vary too much, but the maximum water height values on the east part of the bay increase (from 0.3 to 0.5m more) and hazard rises from “medium” to “high” there. The flooding occurs in two phases, firstly from the ponds and only in a second moment from the sea front. The computed hazard is high around the ponds and on some low areas on the east sector of the bay. Only a few stakes are affected, but the coastal road is already attended by water. On 2100, the flooded area widens considerably and the hazard in all the sector is classified from “high” to “very high”. Water propagates from Anse la Raie, reaching the suburbs of Cap Malheureux on the west, while on the south-est the sea-front of Calodyne is also inundated. However the water heights involved are relatively small and the currents not intense, therefor the hazard is predominantly “medium” or “low” in these areas.

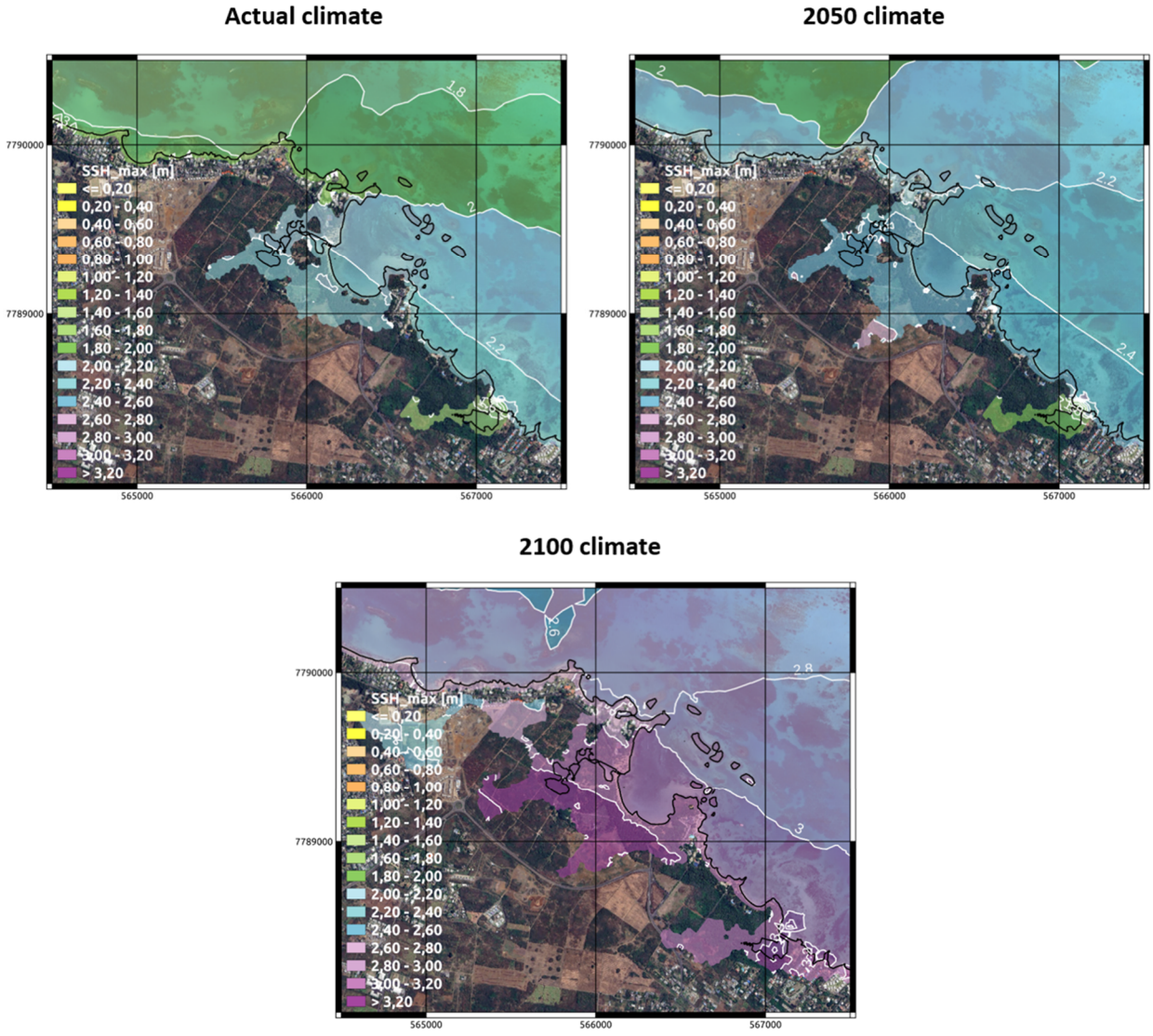


*Figure 208 : Close-up view of the computed maximum sea surface height (SSH_max) on the Anse la Raie area for the three climate scenarios.*

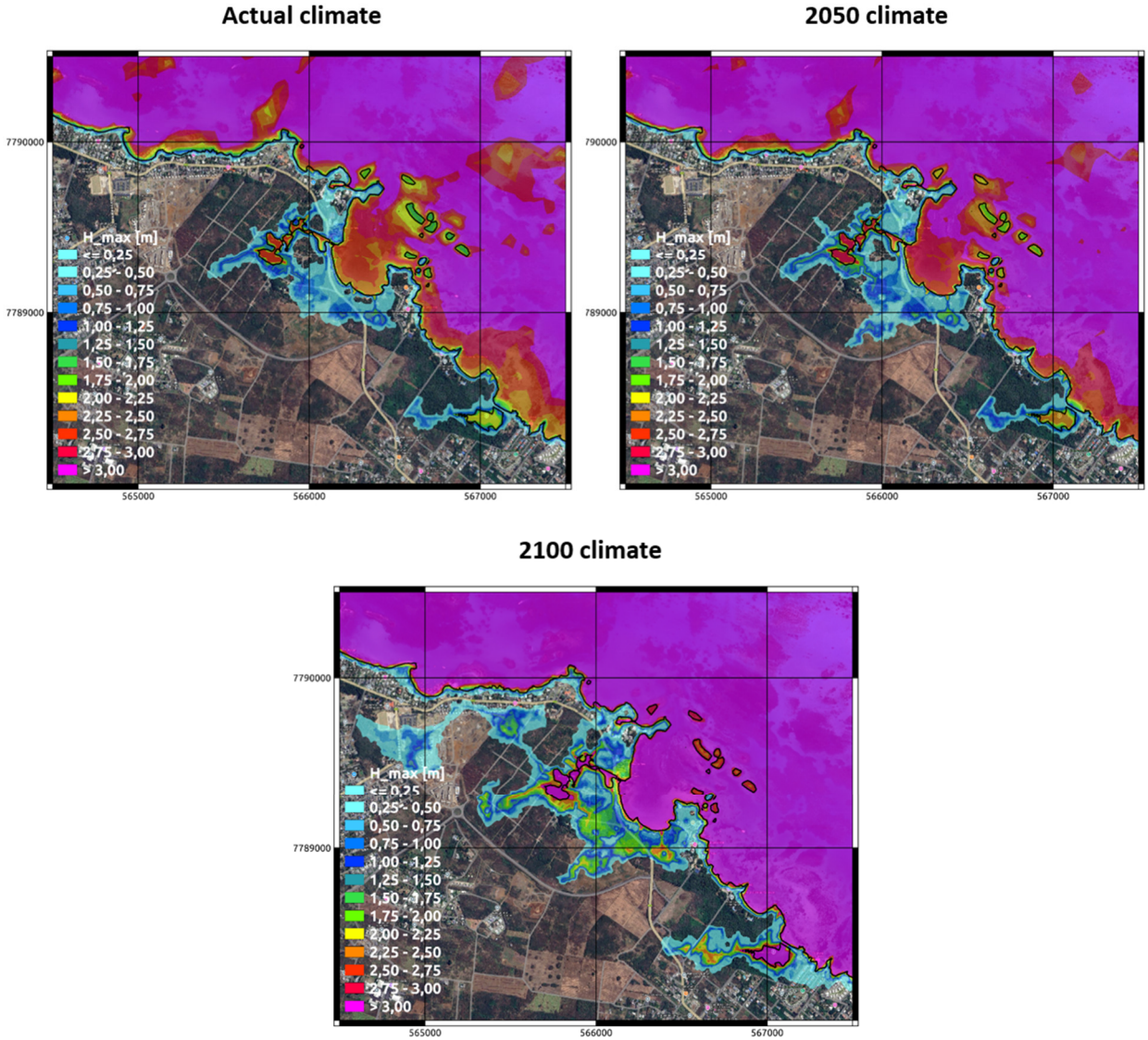


*Figure 209 : Close-up view of the computed maximum water height (H_max) on the Anse la Raie area for the three climate scenarios.*

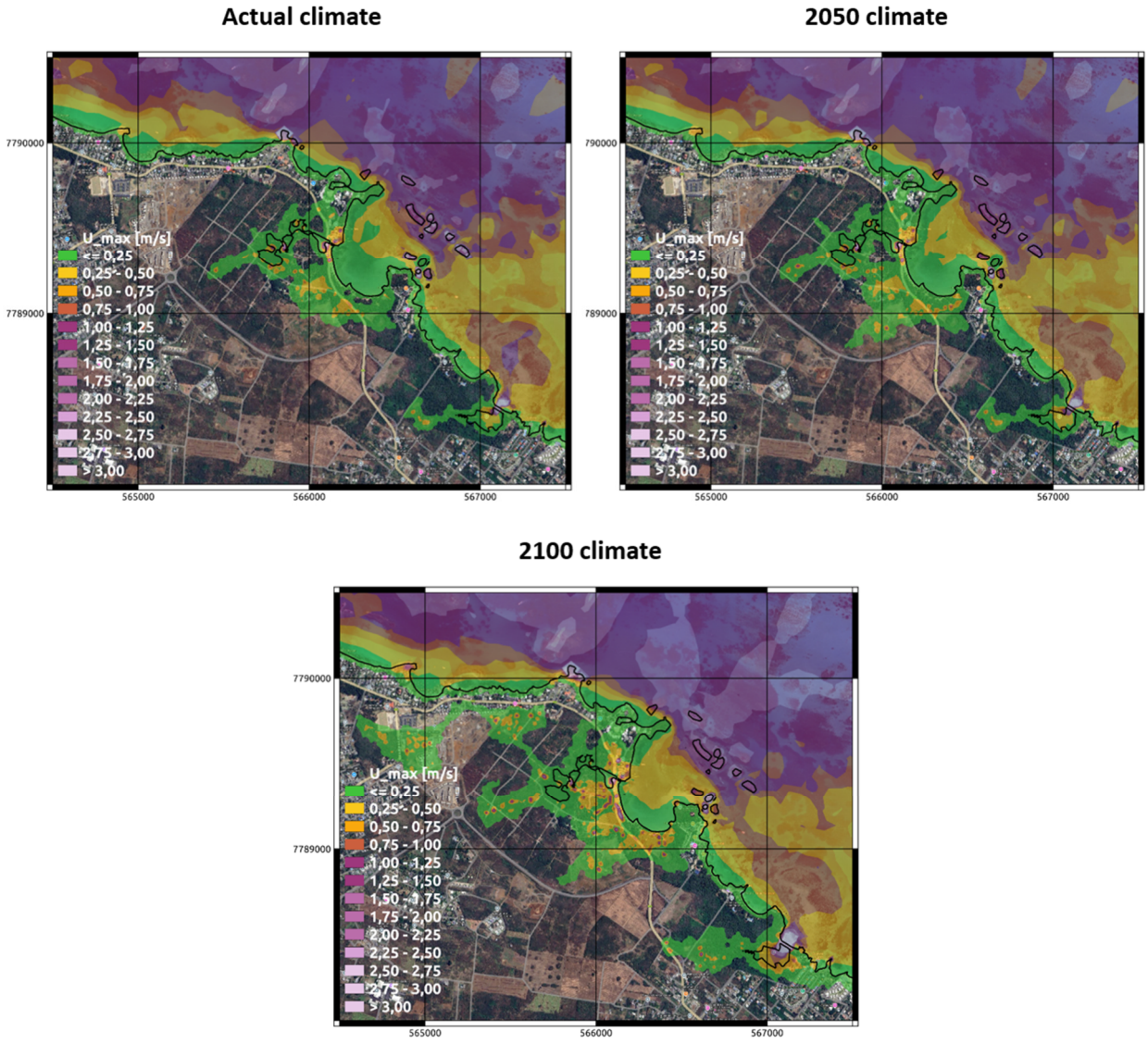


*Figure 210 : Close-up view of the computed maximum current velocities (U_max) on the Anse la Raie area for the three climate scenarios.*

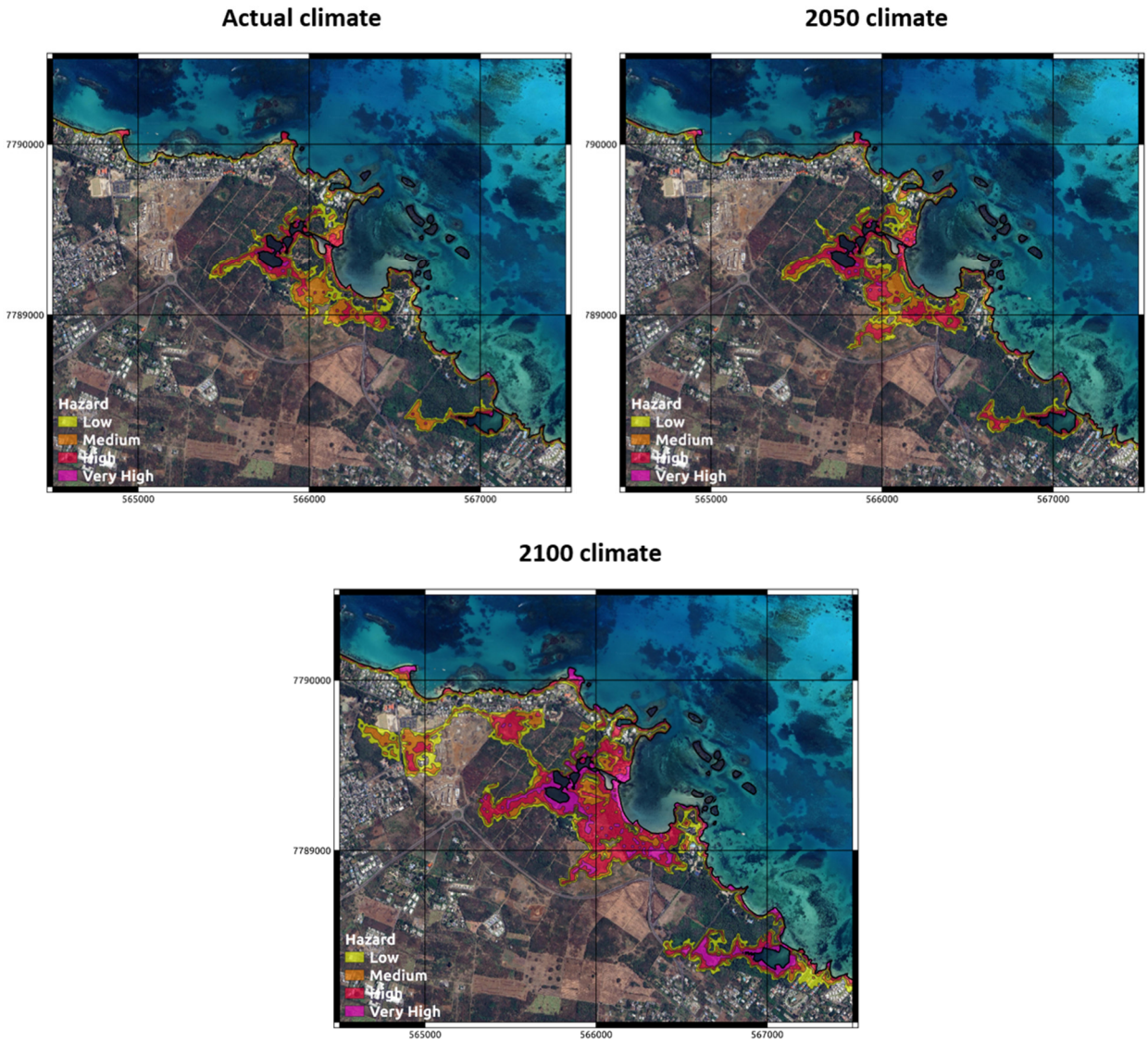


*Figure 211 : Computed hazard on the Anse la Raie area for the three climate scenarios.*

Compared to the previous computations carried out using the model covering the full Mauritius island, the computational grid used here for a zoom on Anse la Raie also provides to us a finer description of the flooding in other locations of the Mauritius north-east coast like: Calodyne, Grand Gaube, Poudre d'Or and Roches Noires. For example, Figure 212 shows the computed hazard map on the Roches Noires area, which is particularly affected by the flooding even in present-day climate. For this reason, the final results of the hazard at the Mauritius island scale has been obtained by merging the layers provided by the computations of section §4.2.2.1.2 and by these ones.

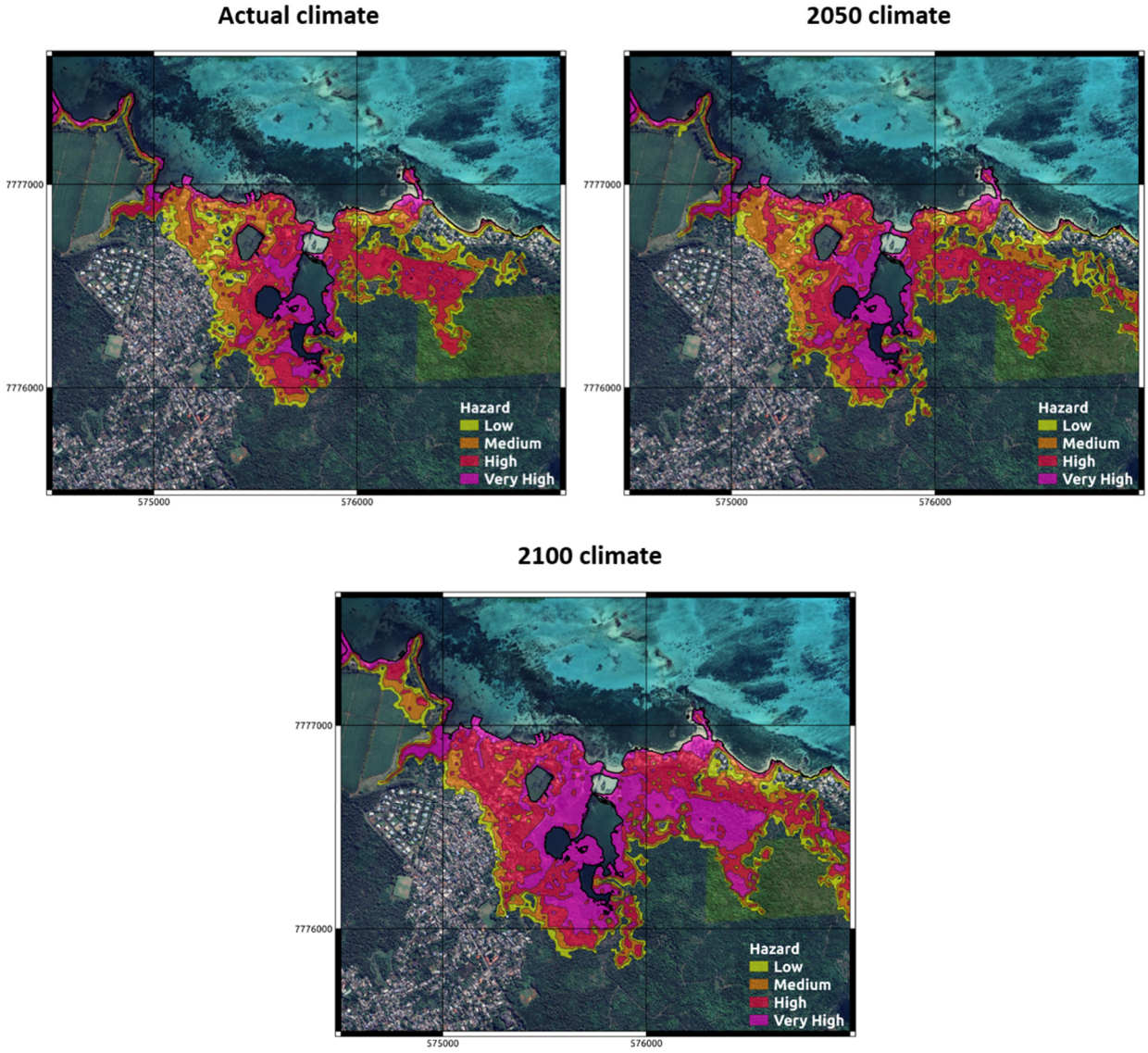


*Figure 212 : Computed hazard map on the Roches Noires area for the three climate scenarios.*

## 4.3.4.3 Port Mathurin (Rodrigues)

### *4.3.4.3.1 Coastal retreat hazard*

#### *4.3.4.3.1.1 Coastal homogeneous zones and sedimentary sub-cells*

The study area of Port Mathurin has been subdivided into two geomorphologically homogeneous units. To the west, zone RPoM_01 extends between Point l'Herbe and Pointe Monnier. It is characterised by a sandy beach environment situated at the foot of rocky escarpments. To the east, zone RPoM_02 spans from the Camp du Roi River to the Baie Lascars Cemetery. This unit corresponds to the urban sector of Port Mathurin, developed on a coastal plain composed of alluvial deposits and anthropogenic fill materials associated with port infrastructure and land reclamation works.

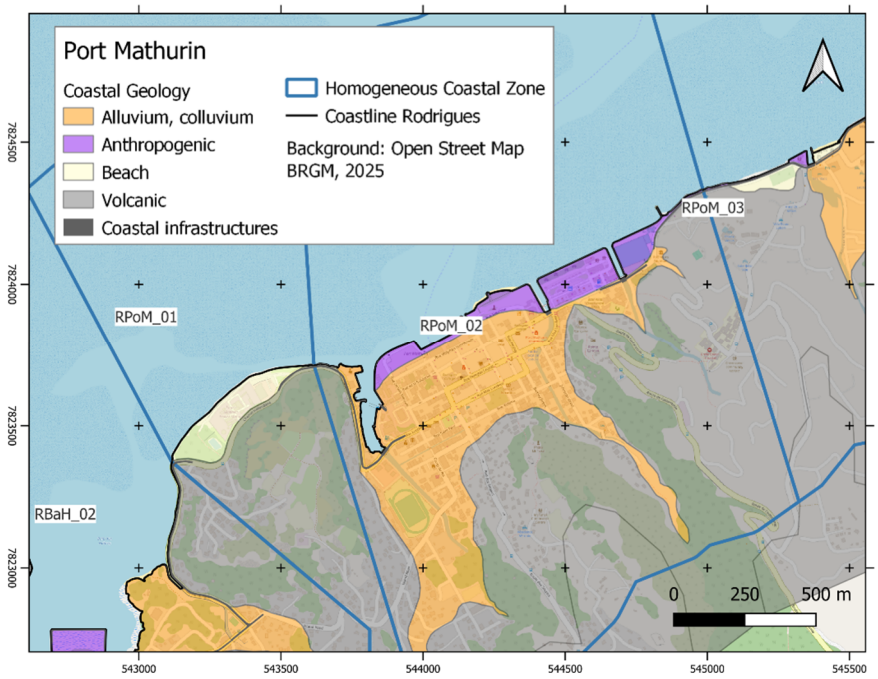


*Figure 213 : Homogeneous coastal zones and coastal geology of Port Mathurin, Rodrigues.*

#### *4.3.4.3.1.2 Analysis of coastline evolution*

- Port Mathurin, downtown

In Mauritius, the homogeneous coastal zones of Port Louis and Mahébourg are composed wholly or in part of embankments, which are protected by coastal retaining structures. For this specific coastal typology, the retreat scenarios adopted are analogous to those applied to basaltic rocky shorelines (See 4.2.1.1.2.5.3).

Port Mathurin, located on Rodrigues Island, constitutes a distinctive case within this study. Similar to Port Louis, the town's entire homogeneous coastal zone is characterised by an embankment reinforced with riprap or retaining walls. However, field surveys have identified significant degradation of the riprap. As a result, the effectiveness of this protection in mitigating coastline retreat during cyclone events is considered questionable. Accordingly, the retreat scenarios applied to Port Mathurin correspond to the maximum retreat parameter ($L_{max}$) for the sector, across all three scenario variants and study time horizons.

For the urbanised sector of Port Mathurin (RPoM_02), the selected Lmax values correspond to those established using the adapted FEMA 540 SQ method, for low-lying areas (see Table xx). Depending on the scenario and cyclone intensity, event-based retreat distances are estimated to range between 8 and 12 metres for the present period, 12 to 15 metres for the 2050 horizon, and 20 to 25 metres for the year 2100.

*Table 35 : Estimated impact of extreme events (Lmax) -Port Mathurin, downtown (RPoM_02).*

| *Low-lying sandy coast* | **$Lmax_{5y}$** | **$Lmax_{25y}$** | **$Lmax_{75y}$** |
|---|---|---|---|
| **median** | 8 | 12 | 20 |
| **intermediate** | 10 | 15 | 25 |
| **safe** | 12 | 20 | 25 |



*Figure 214 : Damages observed on the Port Mathurin riprap structures (December 2024).*

- Pointe Monnier

Prior to this study, no data on shoreline change were available for Rodrigues. A few highly localised areas of the island had been previously examined using satellite imagery to estimate shoreline evolution rates (see Appendix 1 and Table 36).
However, as with the majority of the island, the sector between Pointe l'Herbe and Pointe Monnier had not been subject to any shoreline retreat measurements or observations. The methodology employed to establish shoreline retreat scenarios is presented in section 4.2.1.1.2.2 and detailed for the Anse la Raie sector in Mauritius (see Section4.3.4.2.1.2).

The solution is to define the various parameters of coastline change on the basis of expert opinion. These parameters are delineated by experts, employing various criteria of similarity with homogeneous zones whose evolution is documented. The aforementioned criteria encompass the following: exposure to swell conditions, the presence and width of the lagoon, the orientation of the coast, and proximity to well-documented cells or sub-cells.

*Table 36 : Coastline retreat parameters for shoreline change sectors of Rodrigues based on satellite image analysis.*

| | | **$Tx_{med}$** | **$Tx_{hzd}$** | **$Tx_{hzd-max}$** |
|---|---|---|---|---|
| Homog. zone | *Name* | **North Coast** | | |
| **RRBD_01** | *Rivière Banane* | 0 | -0.68 | -1.45 |
| **RGrB_01** | *Grand Baie (A)* | 0 | -0.29 | -1.31 |
| | *Grand Baie (B)* | 0 | -0.94 | -2.11 |
| | | **South Coast** | | |
| **RGra_02** | *St françois (A)* | 0.00 | -0.16 | -0.93 |
| | *St françois (B)* | 0.00 | -0.01 | -0.03 |
| **RGra_05** | *Gravier* | 0.00 | -0.81 | -3.25 |
| **RPSE_01** | *Var Brulé (C )* | 0.00 | -0.24 | -0.42 |
| | *Var Brulé (B)* | -0.63 | -0.73 | -1.05 |
| | *Var Brulé (A)* | 0.00 | -1.04 | -1.85 |
| **RPSE_02** | *Mourouk* | -0.36 | -0.44 | -0.63 |
| **RPIC_02** | *Petite Butte* | -0.36 | -0.69 | -1.38 |

Along the northern coast of Rodrigues, two sites were selected to collect shoreline change data: Grand Baie and Rivière Banane. Grand Baie exhibits a distinctive geomorphology, consisting of an estuarine beach located within a sheltered bay. The observation point situated behind the artificial groyne is characterised by very high retreat rates, linked to sediment depletion (–0.94 m/year). Updrift of the groyne, more moderate retreat rates were recorded (–0.29 m/year).
Rivière Banane is a pocket beach located between rocky headlands. Over the observation period, a high retreat rate was measured (–0.68 m/year). The site's morphology and wave exposure appear more comparable to those of Pointe Monnier.

For the homogeneous zone RPoM_P1 at Pointe Monnier, the retreat rate used is that of Rivière Banane (Table 37). The median retreat rate ($Tx_{med}$) is considered null, as the site appears to be in a state of relative equilibrium. However, its proximity to the artificial channel of Port Mathurin could increase its vulnerability to wave exposure and episodic erosion. The retreat rate of –0.68 m/year is comparable to other chronically retreating sectors such as Petite Butte (–0.69 m/year), Var Brûlé (B, –0.73 m/year), and Graviers (–0.81 m/year).

The median retreat rate within the coastal cell ($Tx_{hzd-cell}$) was used in the projection scenario between 2070 and 2100. Sectors showing evidence of chronic retreat are located on the southern coast of Rodrigues (Table 36), including Var Brûlé (–0.63 m/year), Mourouk, and Petite Butte (–0.36 m/year). For the study area, a moderate retreat value was selected (–0.36 m/year). This rate of chronic retreat at the coastal cell scale is comparable to those observed in Mauritius within coral lagoon environments.

*Table 37 : Coastline retreat parameters for Pointe Monnier homogeneous zone (RPoM_01), Port Mathurin, Rodrigues.*

| Homog. zone | *Name* | **$Tx_{med}$** | **$Tx_{hzd}$** | **$Tx_{hzd-max}$** | **$Tx_{hzd-cell}$** |
|---|---|---|---|---|---|
| **RPoM_01** | *Pointe Monnier* | 0 | -0.68 | -1.45 | -0.36 |

For the Pointe Monnier sector, the selected $L_{max}$ values correspond to those established using the adapted FEMA 540 SQ method, for very low-lying areas (Table 38). Depending on the scenarios and cyclone intensity, event-based retreat distances are estimated at 10 to 15 metres

for the present period, 15 to 20 metres for the 2050 horizon, and 25 to 30 metres for the year 2100.

*Table 38 : Estimated impact of extreme events (Lmax) -Pointe Monnier, Port Mathurin, (RPoM_01).*

| *Very low-lying sandy coast* | **$Lmax_{5y}$** | **$Lmax_{25y}$** | **$Lmax_{75y}$** |
|---|---|---|---|
| **median** | 10 | 15 | 25 |
| **intermediate** | 12 | 20 | 30 |
| **safe** | 15 | 20 | 30 |

#### *4.3.4.3.1.3 Additional erosion caused by sea level rise (SLR-R)*

The methodology for estimating the additional erosion associated with sea level rise (SLR-R) is outlined in section 4.2.1.1.2.4. The extent of potential additional erosion is contingent on the type of shoreface and its exposure to wave action. The resulting coastal retreat is influenced by the availability of sediment, which is assessed by estimating the width of the beach.

For the Port Mathurin sector, the urban zone (RPoM_02) is heavily artificialized. The coastline is stabilised by riprap structures, and the method applied in this study does not allow for the evaluation of additional erosion effects. In this context, the potential flooding of low-lying areas due to sea level rise appears to be a much more significant hazard to the town. The sea level scenarios adopted for this study are presented in section 4.2.1.1.2.5.2 (see Table 19). The specific projections for Port Mathurin are discussed in the following section.

In the Pointe Monnier sector, the shoreface morphology is complex. It consists of a triangular-shaped intertidal flat bordered by a channel.

Under these conditions, the determination of impact parameters for the projection formulas remains somewhat subjective. The maximum width of the reef flat and the channel is approximately 400 m. For this zone, it is assumed that an adjacent area roughly 100 m wide may contribute to the production of coral-derived sediments. Finally, the beach width, which provides an estimate of the local sediment stock, is narrow, estimated at around 8 m.

For Pointe Monnier (Table 39), the estimated additional retreat (SLR-R) is between 5.1m and 11.5m in 2050 (5.6m for the intermediate scenario) and 20.6 to 60.4m in 2100 (36.1m for the intermediate scenario).

*Table 39 : Estimated values of additional coastal retreat for Pointe Monnier coastline (Port Mathurin)*

| *Port Mathurin* | *Shoreface exposition* | **SLR-R 2025-2050 (m)** | | | **SLR-R 2050-2100 (m)** | | |
|---|---|---|---|---|---|---|---|
| | | median | intermediate | safe | median | intermediate | safe |
| **Pointe Monnier (RPoM_01)** | Lagoon | 5.1 | 5. 6 | 11.5 | 20.6 | 36.1 | 60.4 |

#### *4.3.4.3.1.4 Coastline retreat hazard at the sub-cells scale*

The determination of projection parameters allows for the calculation of the potential retreat of the sandy coastline of Pointe Monnier over three timescales (current, 2050, 2100) and for the three scenarios (safe, intermediate, median), according to the methods outlined in section 4.2.1.1.2. The estimated retreat values, rounded to the nearest 5m, are presented for the homogeneous coastal zones of Port Mathurin. The estimated coastline retreat values for Port Mathurin are presented in Table 40. The results of the intermediate scenario for the 3 timeframes of the study

are presented in the maps of Port Mathurin and the neighbouring homogeneous zones of Rodrigues (Figure 215, Figure 216, Figure 217).

*Table 40 : Coastline retreat estimations (m) for homogeneous zone of Port Mathurin (Rodrigues), 2025, 2050 and 2100 timeframes.*

| | **2025** | | | **2050** | | | **2100** | | |
|---|---|---|---|---|---|---|---|---|---|
| **Port Mathurin** | median | **Inter mediate** | safe | median | **Inter mediate** | safe | median | **Inter mediate** | safe |
| RPoM_01 | 10 | **15** | 25 | 20 | **40** | 55 | 65 | **95** | 135 |
| RPoM_02 | 10 | **10** | 15 | 15 | **15** | 20 | 20 | **25** | 25 |

The current zone of exposure to shoreline retreat in Port Mathurin is estimated to range between 10 and 25 metres (Table 40), depending on the scenario and location (RPoM_01 or RPoM_02). Under the intermediate scenario, a value of 15 metres is assigned to Pointe Monnier (RPoM_01) and 10 metres to the Port Mathurin urban area (RPoM_02), corresponding to the dominant retreat class in Rodrigues.

Compared to the homogeneous zones surrounding Port Mathurin (Figure 215), scenario differences across the three timeframes are less pronounced in the urban sector, due to the presence of engineered coastal defences such as riprap and harbour infrastructure. Although partially degraded, these structures continue to constrain shoreline mobility and maintain the current coastline position.

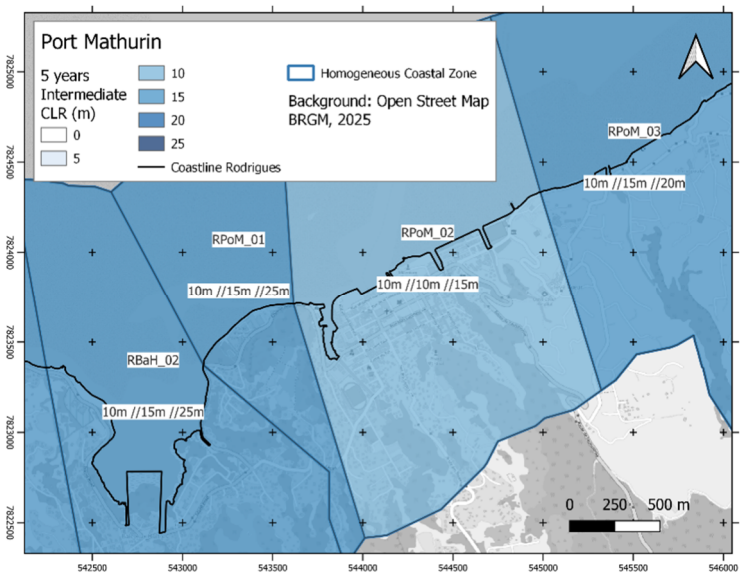


*Figure 215 : Map of coastline retreat estimations for 2025 timeframe, at the scale of Port Mathurin and neighbouring sub-cells in Rodrigues.*

The potential retreat of the coastline by 2050 in Port Mathurin is projected to be between 15 and 55 meters (Table 40), depending on the scenario and zones. The intermediate scenario suggests a retreat value of 40 meters in Pointe Monnier. This represents the highest erosion potential on the island for that timeframe. This potential is mainly explained by the higher Lmax value compared to neighbouring sites (Figure 216), due to a flat coastal morphology and a limited sediment stock.

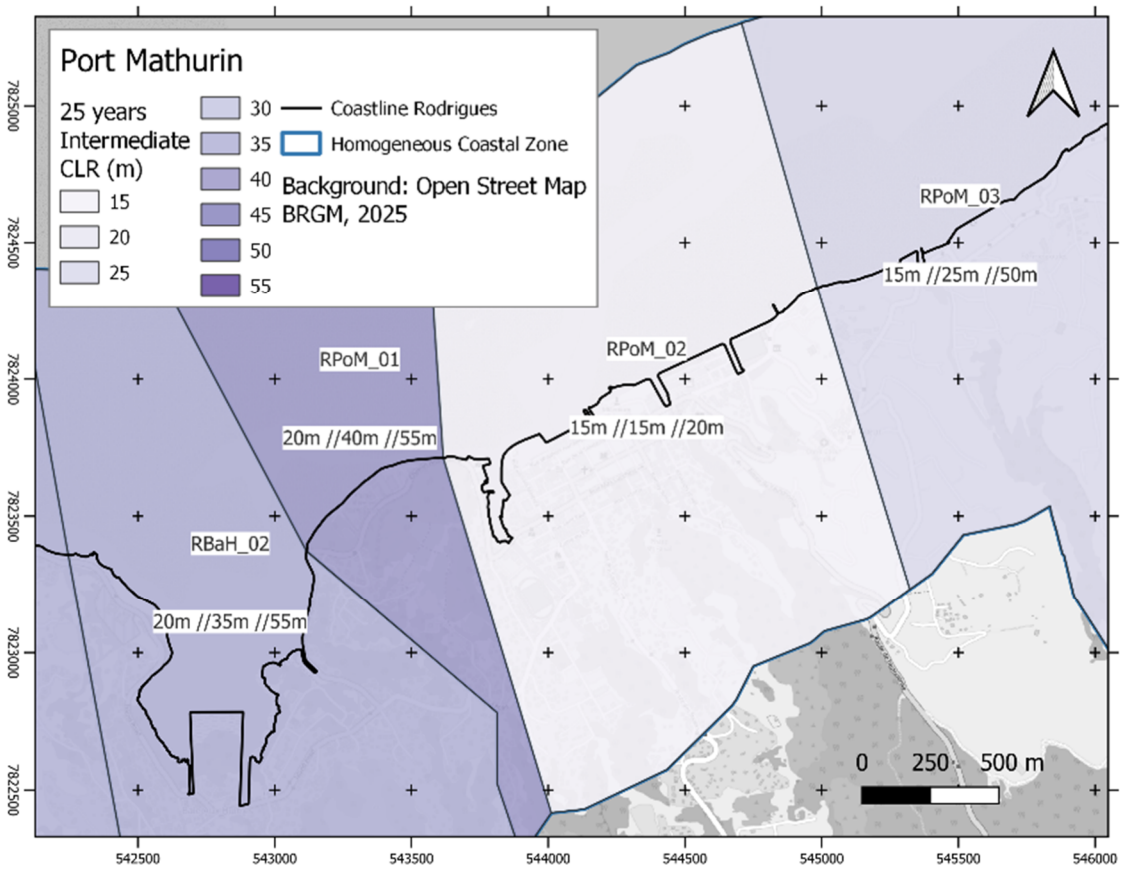


*Figure 216 : Map of coastline retreat estimations for 2050 timeframe, at the scale of Port Mathurin and neighbouring sub-cells in Rodrigues.*

By 2100, the erosion potential appears even more contrasted between the two homogeneous zones studied in Port Mathurin. Projected shoreline retreat in the Pointe Monnier area ranges from 65 to 135 metres under the median and high-risk scenarios, and 95 metres under the intermediate scenario (Table 40). This makes it one of the most sensitive sectors in Rodrigues, alongside Anse Mourouk on the southern coast and Grand Baie on the northern coast. The various bays along the island's northern coast (Baie aux Huîtres -Figure 217, RBaH_02, Baie Malgache, and Baie du Nord) are also identified as potentially sensitive to long-term shoreline retreat due to erosion. However, it should be noted that the morphology of these bays and their exposure to coastal forcing differ significantly from Pointe Monnier, and the potential mitigating role of the mangrove ecosystems present in these bays was not taken into account in this study.

As for the urban area of Port Mathurin, the scenario used assumes that the coastline remains largely unaffected by long-term erosion, although it may still be subject to episodic cyclone-induced impacts, with Lmax retreat values for this sector estimated between 20 and 25 metres.

However, the following section demonstrates that the coastline could be significantly affected by sea level rise in low-lying areas.

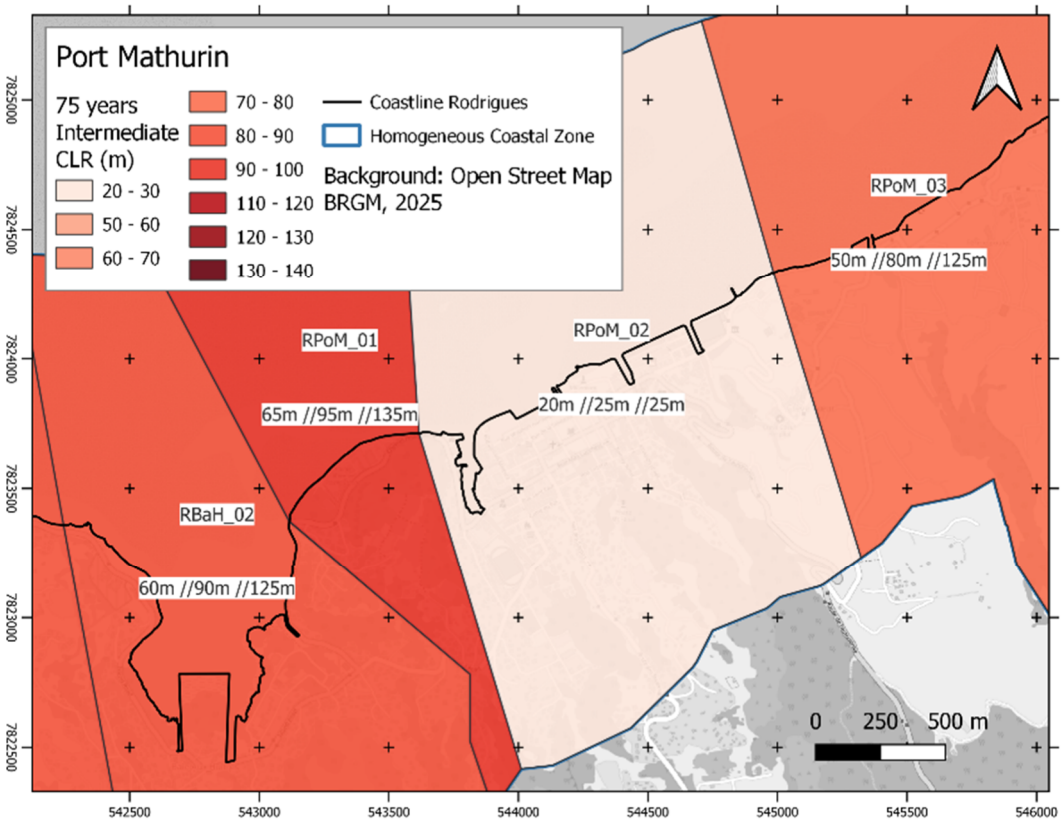


*Figure 217 : Map of coastline retreat estimations for 2100 timeframe, at the scale of Port Mathurin and neighbouring sub-cells in Rodrigues.*

#### *4.3.4.3.1.5 Maps of coastline retreat hazard at local scale*

Maps of exposure to shoreline retreat hazard on a local scale (1:10,000) can be drawn up using estimates of possible retreat values for homogeneous zones over the three time horizons of the study.

The GIS data provided in the deliverables of the Mauriscot project are of course compatible at the scale of 1:5000, useful for local and detailed mapping.

The special cases of mixed coasts (sediment and rock) and low-lying areas are included in the shoreline retreat projection scenarios (see section 4.2.1.1.2.5) and implemented for Port Mathurin.

Figure 218, Figure 219 and Figure 220 depict the projected shoreline retreat by timeframe for the various scenarios. Figure 221 illustrate the projected retreat of the coastline at various timeframes for each scenario.

The Port Mathurin study area is characterised by a high concentration of assets along the coastline. As a result, even relatively limited hazard zones may correspond to significant levels of risk. This aspect is addressed in greater detail in Volume 2 of this study.

In general, the maps of exposure to coastline retreat for the 5-year (Figure 218) and 25-year time horizons (Figure 219) clearly illustrate the specific vulnerability of urban coastal zones.

For Port Mathurin town centre (RPoM_02), the hazard zone was estimated using formulas for retreat affecting open sedimentary coasts under the influence of a cyclone event. This

assessment may be somewhat conservative for certain localised sectors that are more sheltered from hydrodynamic forcing, such as riverbanks or robust, well-maintained port structures. These would need to be assessed in a high-resolution, site-specific study. Nevertheless, field observations suggest that the method adopted to delineate the zone exposed to event-driven retreat provides a realistic representation for a large portion of the town's coastline.

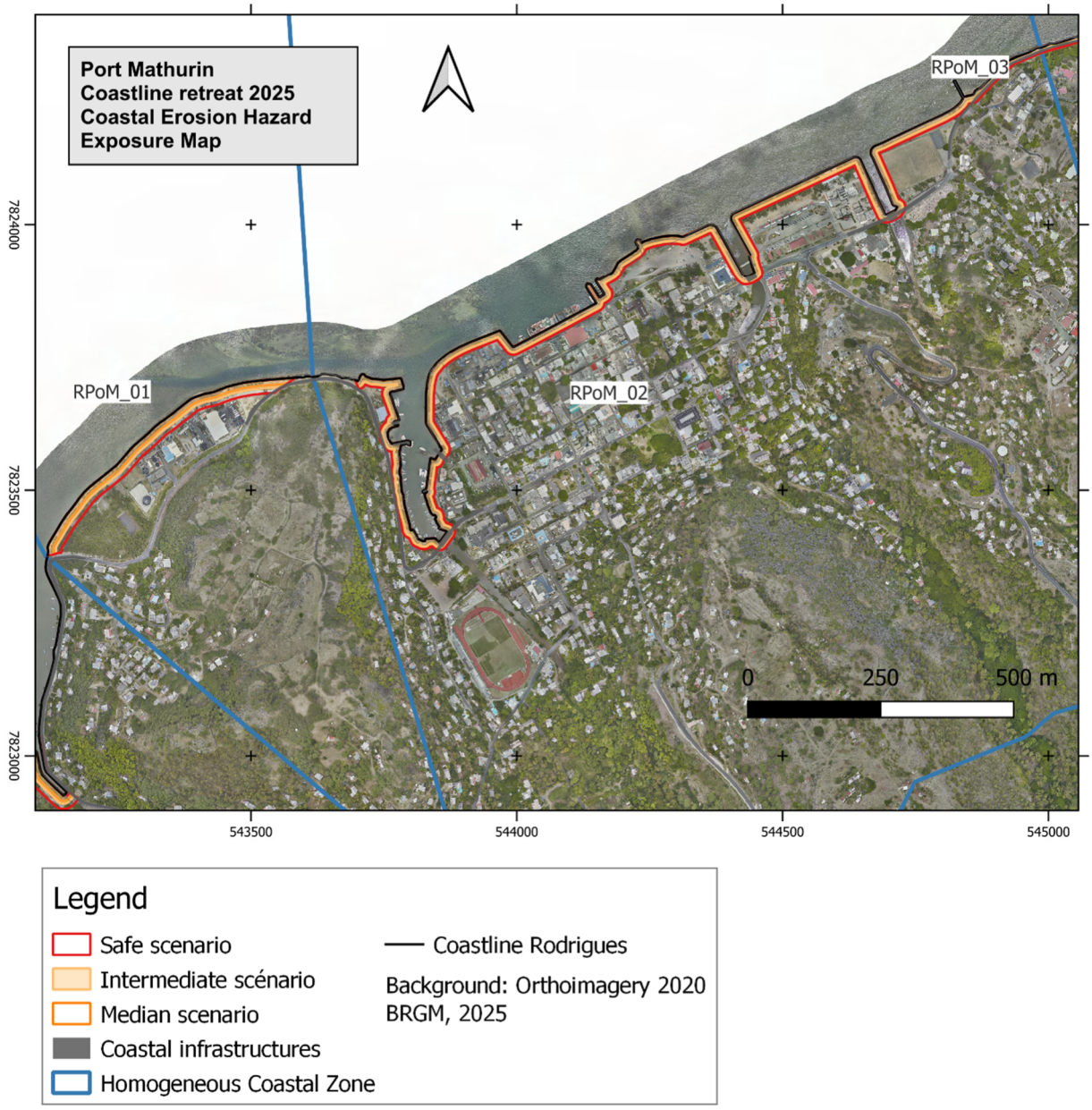


*Figure 218 : Coastline retreat hazard in Port Mathurin for 2025 under median, intermediate, and safe scenarios.*

At Pointe Monnier (RPoM_01), the presence of the island's power station adds particular significance to the potential sensitivity to coastline retreat. As early as the current timeframe, both intermediate and safe scenarios show potential impacts in the immediate vicinity of the power station. Field surveys, along with the new artificial structures database created for this project, reveal the presence of two small walls between the coastline and the installations. These

structures may offer some degree of protection from moderate-intensity cyclone-induced erosion, but further investigation at a fine spatial scale would be necessary to evaluate their actual and future performance under cyclone conditions.

By 2050, the intermediate and safe scenarios indicate potentially significant erosion impacts directly affecting infrastructure. The projected retreat distances in these scenarios largely exceed the regulatory setback value of 30 m, while the median scenario estimates a more limited retreat of around 20 m, with less severe consequences.

When critical infrastructure is potentially threatened by a mid-term hazard, the reliability of both the projections and the input data must be carefully considered. In the case of Rodrigues, data required for analysing coastal dynamics are extremely limited, and this study represents a first attempt to address this gap. At present, no local data exist describing sediment dynamics or shoreline evolution at Pointe Monnier. In the absence of such essential information, the retreat projections rely on expert judgment and remain open to discussion and refinement.

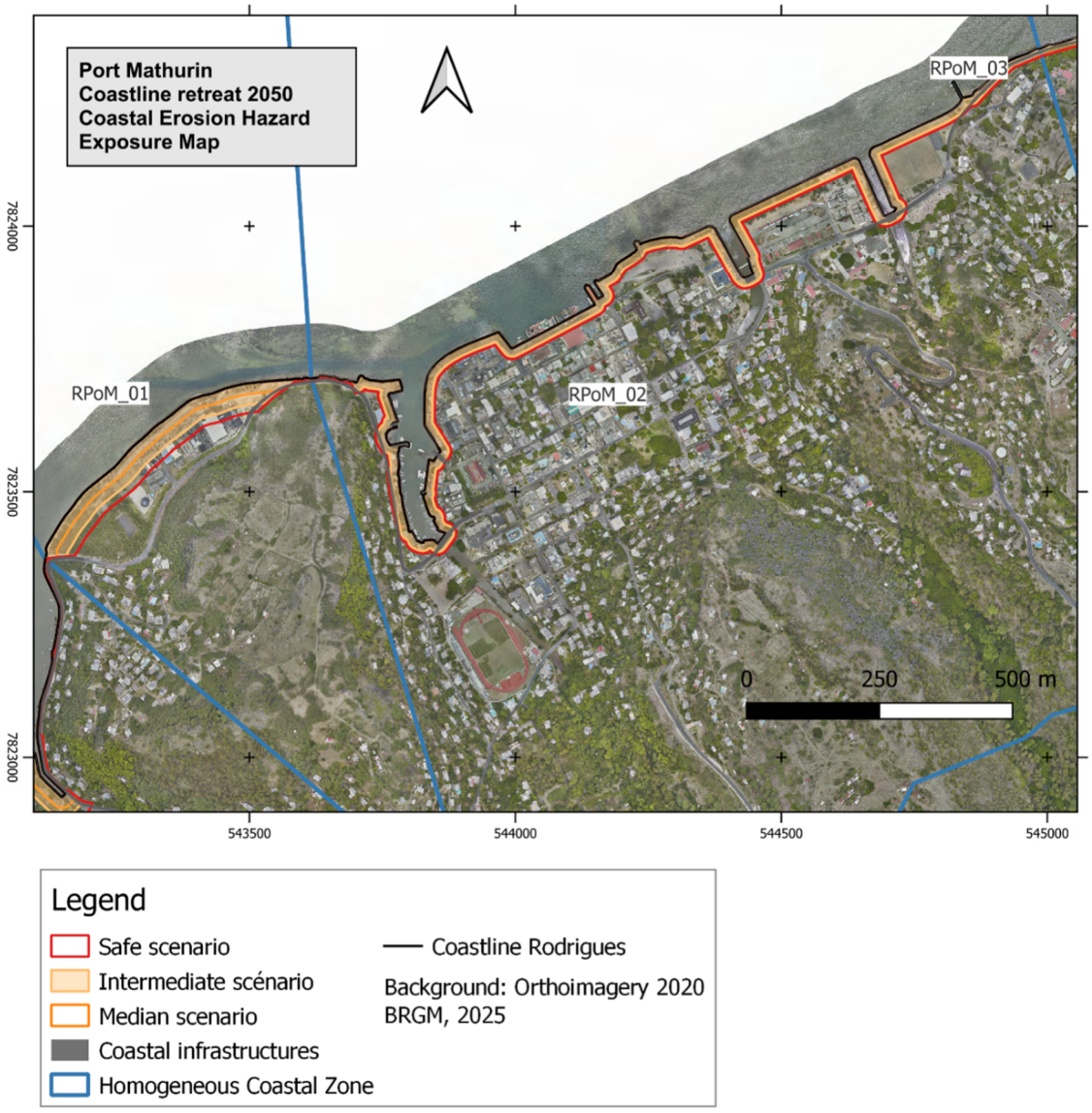


*Figure 219 : Coastline retreat hazard in Port Mathurin for 2050 under median, intermediate, and safe scenarios.*

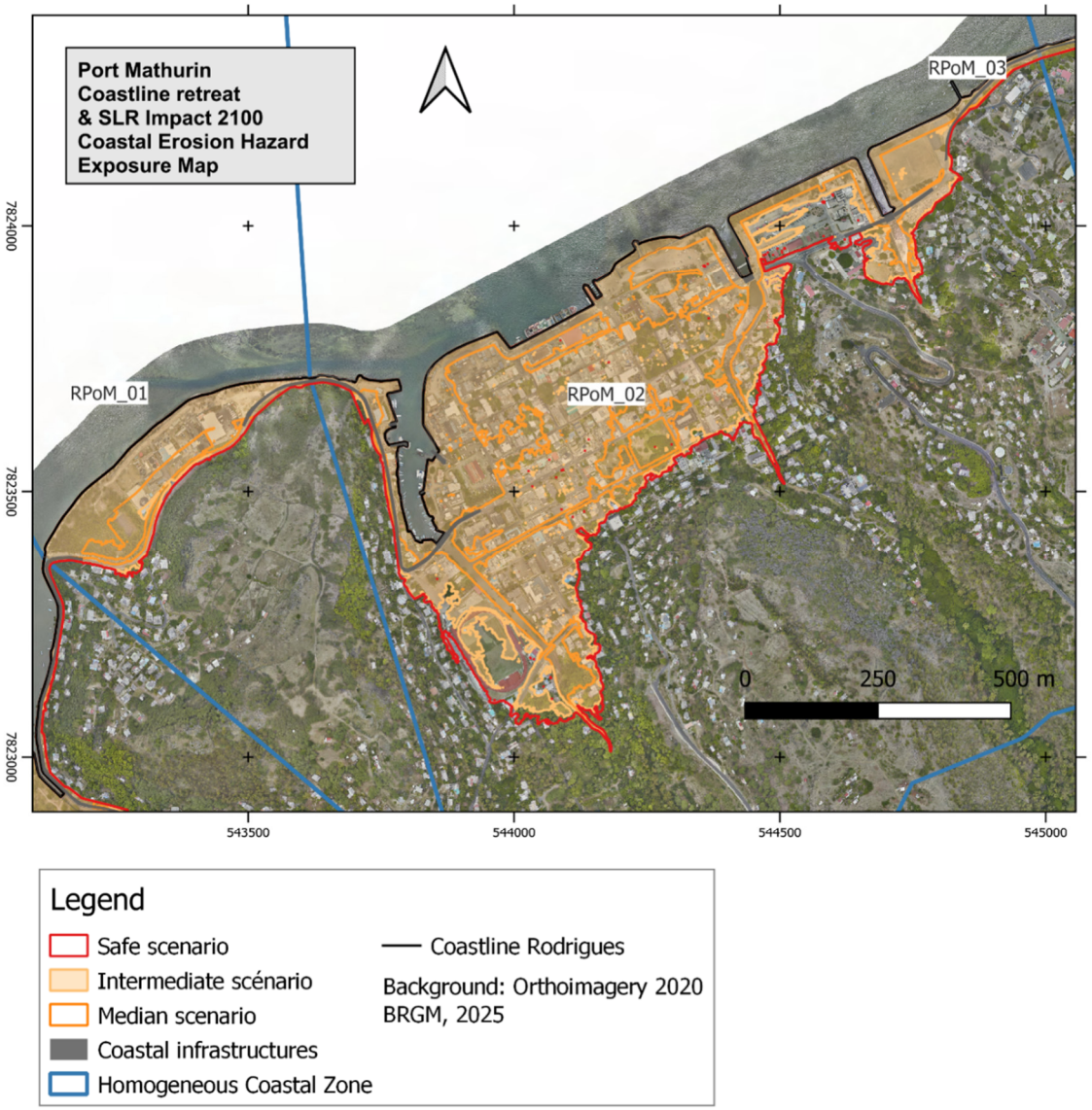


*Figure 220 : Coastline retreat hazard in Port Mathurin for 2100 under median, intermediate, and safe scenarios.*

In 2100 (Figure 220), Port Mathurin is much more exposed to the coastline retreat hazard than in 2050. In the intermediate scenario, the potentially impacted area becomes extensive, extending to nearly the entire town.

Figure 221 shows that this sharp increase in hazard levels is mainly driven by sea level rise and the progressive flooding of low-lying areas by the ocean.

The median scenario corresponds to the median projection under the IPCC's RCP4.5 pathway. It indicates a relatively limited extent of permanent marine flooding. Moreover, the selected indicator reflects the level of Highest Astronomical Tide (HAT), which is a conservative estimate and does not represent tidal levels reached on a daily basis.

In contrast, the intermediate and safe scenarios highlight a critical sensitivity threshold for the entire urban area of Port Mathurin. These scenarios incorporate projections based on the IPCC's RCP8.5 pathway and assume a HAT elevation greater than +2.5 m relative to the local vertical datumCa .

As previously mentioned with regard to the vulnerability of critical infrastructure at Pointe Monnier, the extent of the potential impacts raises questions. The reliability of both projections and input data must therefore be carefully examined. While the assumptions used for the intermediate and safe scenarios may appear somewhat pessimistic, they are counterbalanced by uncertainties related to the precise alignment of the digital elevation model (DEM) with the local vertical datum and tide gauge records—uncertainties which call for a precautionary approach. These concerns are legitimate for a territory like Rodrigues, where such hazard assessments are still new. They will likely require further investigation through more detailed, high-resolution studies.

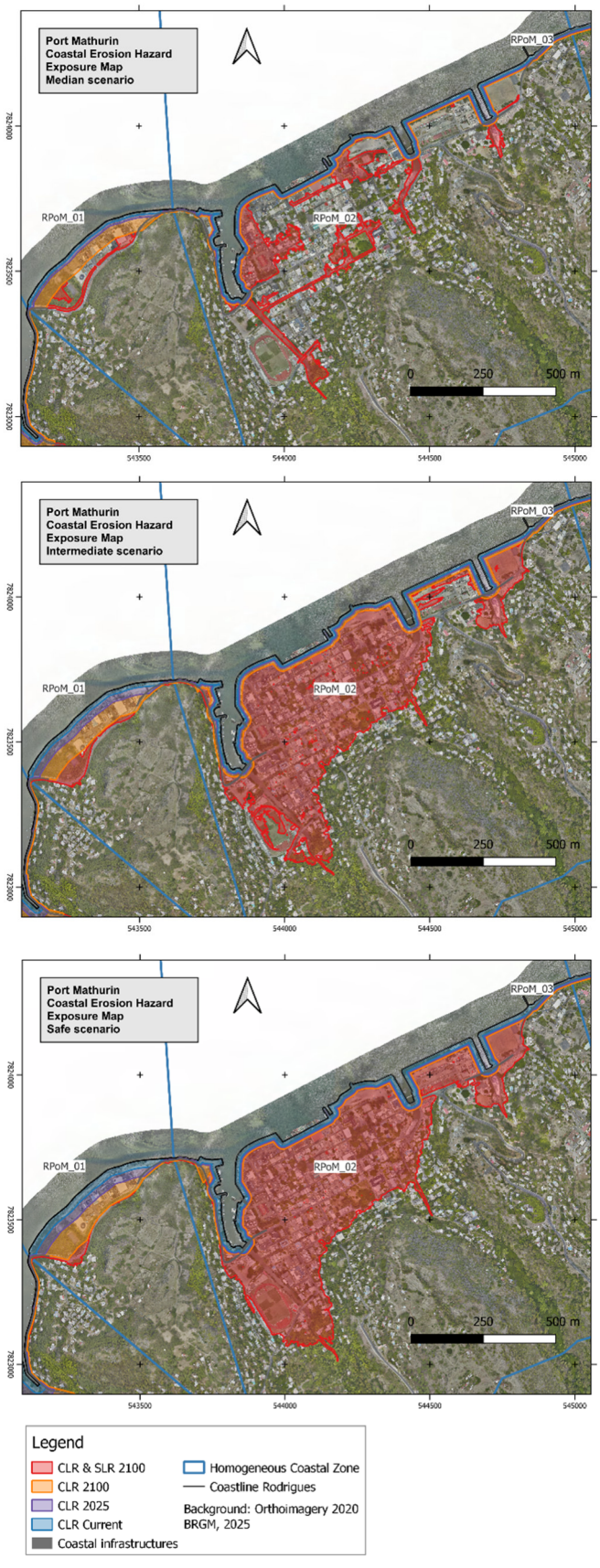


*Figure 221 : Coastline retreat hazard in Port Mathurin by 2025, 2050, and 2100 under the median (a), intermediate (b), and safe (c) scenarios.*

#### *4.3.4.3.2 Coastal flooding hazard*

Since one single numerical model has been built for the Rodrigues Island, the results that we present in this section are a close-up view of the simulations already discussed in section §4.2.2.2.2 on the Port Mathurin urban area.

The reference scenario for this site on all climate condition is represented by the cyclone 63 of the Météo-France database (please refer to §4.2.2.2.2.2). Figure 222 shows the time series of the sea surface level at the Port Mathurin tide gauge for the different climate scenarios. The cyclone signature on the water level is noticeably the same in all scenarios, comforting the conclusion that the determinant driver for the flooding is the sea level rise. In front of Port Mathurin the lagoon is absent in practice. This fact, together with the presence of the channel for accessing the harbour, reduce the wave setup contribution to the total water level with respect to other sectors of the island to only ~0.30m. This contribution is almost constant during the whole event, with only a small peak of value (~0.5m), but still represents ~70% of sea water level during the peak of surge.

Figure 223, Figure 224 and Figure 225 present the results of the simulations carried out on the Port Mathurin area in terms of maximum sea surface height, maximum water height and maximum sea currents velocities for the different climate scenarios. The map of the flooding hazard generated by crossing water height and current velocity values, according to the hazard matrix (Figure 56), is then shown in Figure 226.

Port Mathurin is strongly exposed to flooding by overflowing already on present-day climate conditions. Water floods in all the city centre and Camp du Roi quartier, coming from the sea front but also driven by the Rivière Camp du Roi. However, on actual climate, the maximum water heights rarely achieve 0.5m and currents have a limited intensity (<0.2m/s), therefore the hazard is predominantly “low”. The bus terminal quarter, the Camp du Roi quarter and the power plant of Pointe Monnier are not reached by the water on this scenario.

In 2050, the hazard is from “medium” to “high” in all the city centre. Water floods the Camp du Roi and bus terminal quarters. Maximum water heights in the city achieve 1m in some streets and maximum currents become intense (>0.5m/s) on the sea front (at the bus terminal and at the harbour docks and at Pointe Monnier) but also on the Camp du Roi quarter.

In 2100 the hazard is “high” or “very high” almost everywhere in the flooded area. Maximum water heights in the city surpass 1.5m and also the speed of currents is more important, attending 0.5m/s in the main streets and open spaces. Currents are also very intense at the sea front (>1m/s), especially at the bus terminal and at the harbour docks, potentially impacting the electric power plant installed there. Also the thermal power plant in Point Monnier is flooded by water on this scenario.

On the two sides of the main city, Anse aux Anglais and Baie aux Huitres are also affected by flooding. In particular, Baie aux Huitres suffers the greatest sea water levels in this sector. The flooded area does not vary much among the different simulations, limited by the topography, but the hazard is classified as “medium” or “high” already on present-day climate scenario. Maximum water height surpass 1.75m in some sectors in the 2100 scenario and currents can be strong already in present-day climate (>0.5m/s) especially in the east part of the bay.

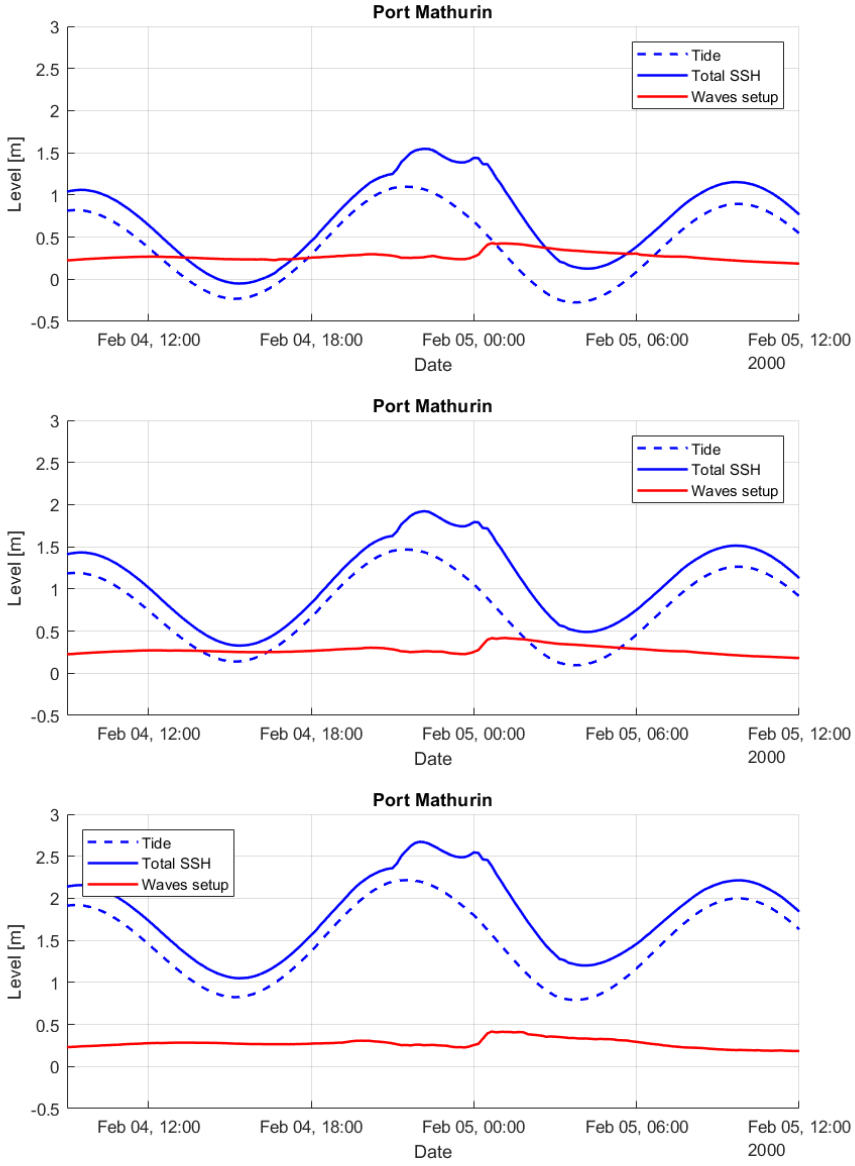


*Figure 222 : Time series of the total sea level (SSH) and wave setup contribution at the tide gauge position on Port Mathurin for the actual climate scenario (top), 2050 climate (centre) and 2100 climate (bottom).*

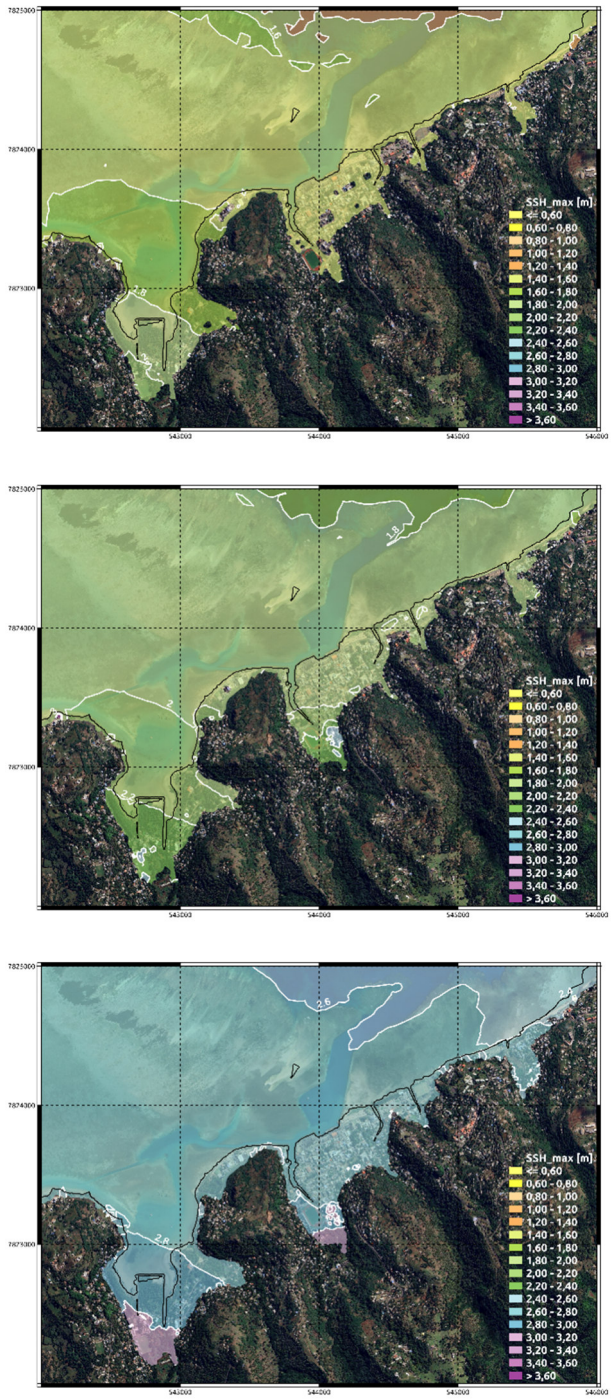


*Figure 223 : A close-up comparison on the Port Mathurin area of the computed maximum sea surface height (SSH_max) on the scenario 63 with present-day climate conditions (top), 2050 climate (centre) and 2100 climate (bottom).*

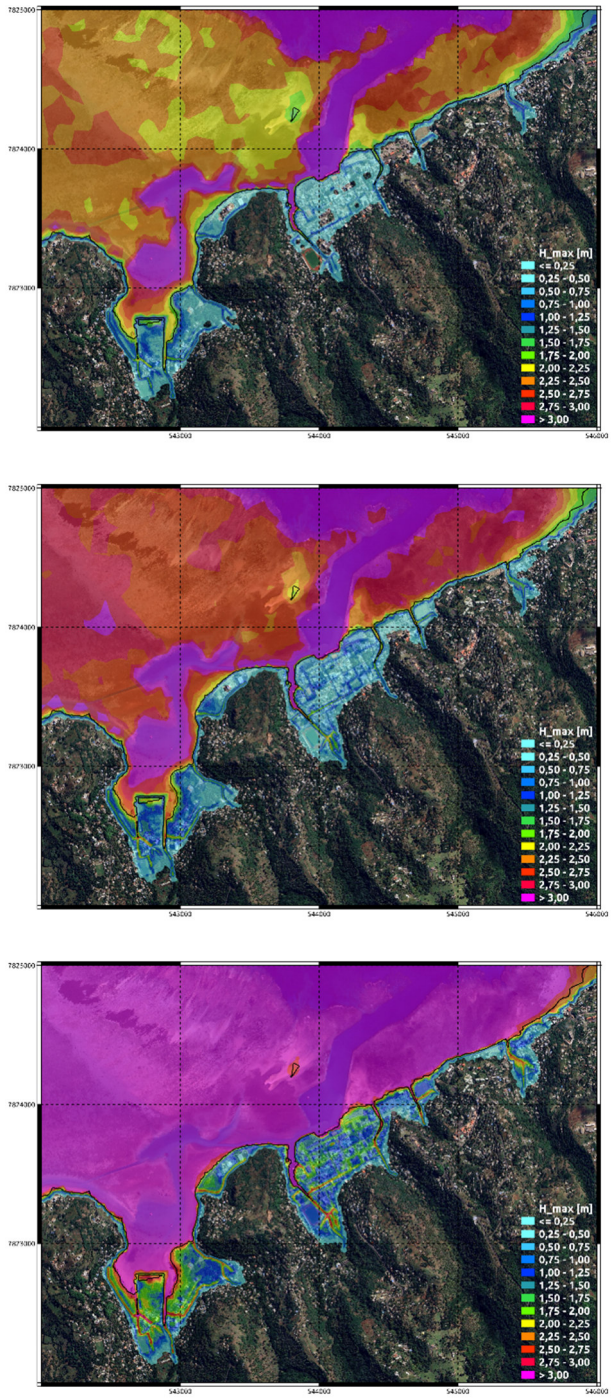


*Figure 224 : A close-up comparison on the Port Mathurin area of the computed maximum water height (H_max) on the scenario 63 with present-day climate conditions (top), 2050 climate (centre) and 2100 climate (bottom).*

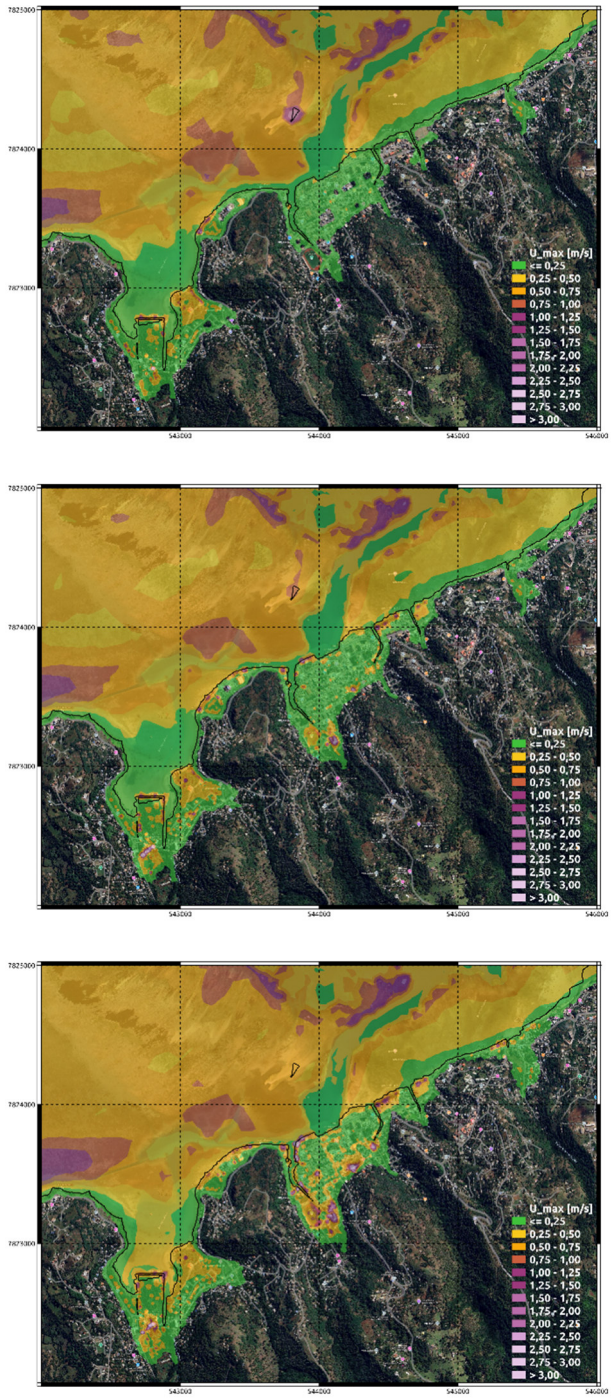


*Figure 225 : A close-up comparison on the Port Mathurin area of the computed maximum sea currents velocity (U_max) on the scenario 63 with present-day climate conditions (top), 2050 climate (centre) and 2100 climate (bottom).*

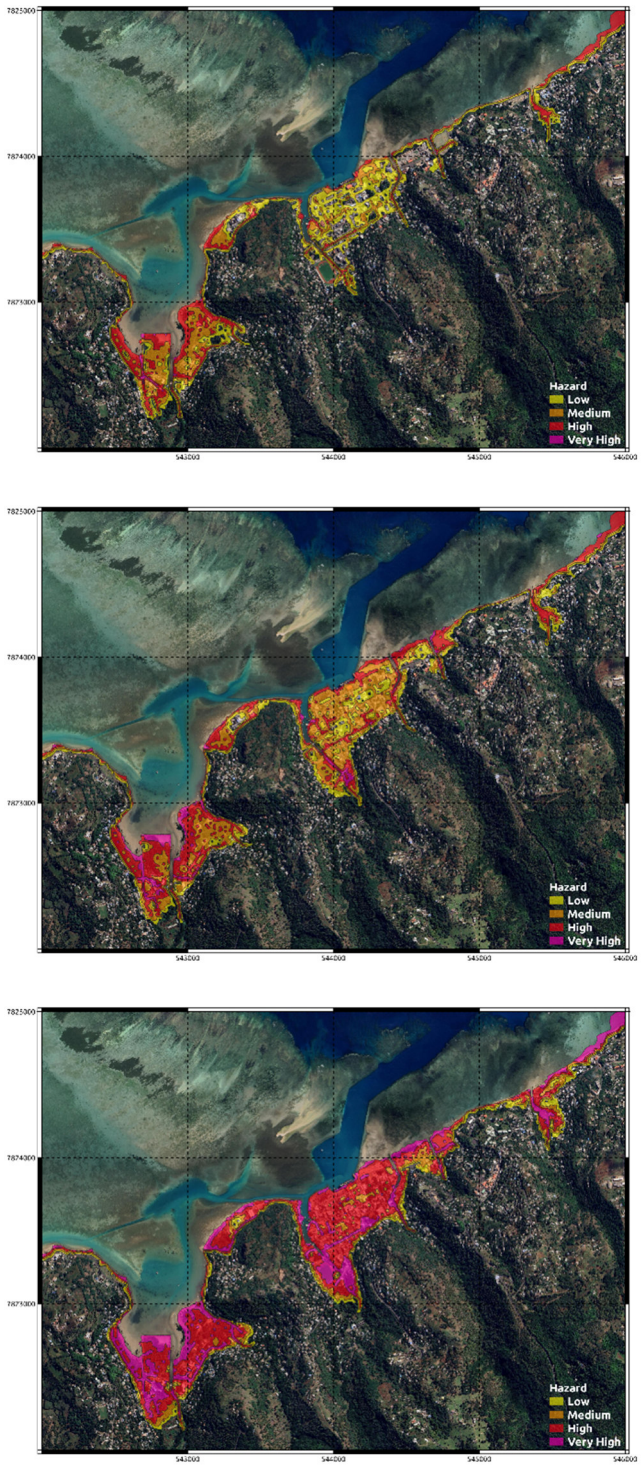


*Figure 226 : Flooding hazard maps on the Port Mathurin for present-day climate conditions (top), 2050 climate (centre) and 2100 climate (bottom).*

# 5. CONCLUSION

In this volume 1 of the phase 2 report, the various forcing factors for coastal flooding, erosion and coastline retreat hazards active on the islands of Mauritius and Rodrigues were identified and characterised (cyclones, variations in sea level, austral swells). Their current intensity was assessed and their future evolution in 2050 and 2100 was quantified. The nature of the coasts was characterised, and topo-bathymetric models were created from existing data for the two islands.

Using these forcing factors and characteristics of the coasts, physical modelling and empirical approaches based on several scenarios were carried out in order to assess the characteristics of present and future (2050, 2100) coastal flooding and the erosion processes leading to shoreline retreat.

Based on these characteristics, hazard levels were defined. Hazard maps and GIS layers were then produced for the entire coastline of the two islands, as well as higher resolution maps and assessments for 3 local sites (hotspots).

These hazard maps are then used to assess the risks by cross-referencing the hazards with the exposed stakes, which are the subject of the second volume of the report (BRGM/RC-73988-FR).

# 6. REFERENCES


Ardhuin, F., et al. (2010), Semi-empirical dissipation source functions for wind-wave models: Part I, definition, calibration and validation, J. Phys. Oceanogr., 40(9), 1917–1941.

Baird et al. (2003) - Study on coastal erosion in Mauritius – Final technical report 2nd edition). 447 p. W.F. Baird & associated coastal engineers LTD.

Barroso, A., Wahl, T., Li, S., Enriquez, A., Morim, J., Dangendorf, S., et al. (2024). Observed spatiotemporal variability in the annual sea level cycle along the global coast. Journal of Geophysical Research: Oceans, 129, e2023JC020300. https://doi. org/10.1029/2023JC020300

Cazes-Duvat V., Paskoff, R. (2004) - Les littoraux des Mascareignes entre nature et aménagement, L'Harmat'an, 186p.

Coles, S., Bawa, J., Trenner, L., & Dorazio, P. (2001). An introduction to statistical modeling of extreme values (Vol. 208). London: Springer.

Conover, W. J. (1999). Practical Nonparametric Statistics (Third ed.). Wiley. pp. 388–395.

Copernicus Climate Change Service, Climate Data Store, (2023) - ERA5 hourly data on single levels from 1940 to present. Copernicus Climate Change Service (C3S) Climate Data Store (CDS), 10.24381/cds.adbb2d47 (Accessed on 19-12-2022).

Delhasse, A., Kittel, C., Amory, C., Hofer, S., van As, D., S. Fausto, R., and Fettweis, X.: Brief communication: Evaluation of the near-surface climate in ERA5 over the Greenland Ice Sheet, The Cryosphere, 14, 957–965, https://doi.org/10.5194/tc-14-957-2020, 2020.

Donguy P., 1992. Cyclonic Phenomena in Indian Ocean Watched by Meteosat (Season 1990-1991). Météo-France report. p. 80 (https://horizon.documentation.ird.fr/exl-doc/pleins_textes/pleins_textes_6/b_fdi_49-50/010014451.pdf).

Doorga J.R.S., Chinta D., Gooroochurn O. *et al.* (2018) - Assessment of the wave potential at selected hydrology and coastal environments around a tropical island, case study: Mauritius. *Int J Energy Environ Eng* 9, 135–153 (2018). https://doi.org/10.1007/s40095-018-0259-7

Duvat V. K., Anisimov A., Magnan A. K. (2020) - Assessment of coastal risk reduction and adaptation-labelled responses in Mauritius Island (Indian Ocean). Regional Environmental Change. 20: 1-15.

Duvat, V.K., Anisimov, A. & Magnan, A.K. (2020). Assessment of coastal risk reduction and adaptation-labelled responses in Mauritius Island (Indian Ocean). *Reg Environ Change* 20, 110.

Efron, B. (1992). Bootstrap methods: another look at the jackknife. In Breakthroughs in Statistics (pp. 569-593). Springer New York.

ESA (2009) – Environmentally sensitive areas – Classification report. NWFS Consultancy. 198 p., 16 fig., 4 tab. June 2009

Eyring, V., Bony, S., Meehl, G.A. et al, (2016): Overview of the Coupled Model Intercomparison Project Phase 6 (CMIP6) experimental design and organization. *Geosci Model Dev* 9, 1937–1958. https://doi.org/10.5194/gmd-9-1937-2016.

Filippini A.G., L. Arpaia, V. Perrier, R. Pedreros, P. Bonneton, D. Lannes, F. Marche, S. De Brye, S. Delmas, S. Lecacheux, F. Boulahya, M. Ricchiuto, An operational discontinuous Galerkin shallow water model for coastal flood assessment, Ocean Modelling, Volume 192, 2024, 02447, ISSN 1463-5003, https://doi.org/10.1016/j.ocemod.2024.102447.

Frederikse T., Landerer F., Caron L. et al. (2020) - The causes of sea-level rise since 1900. *Nature* 584, 393–397, https://doi.org/10.1038/s41586-020-2591-3.

Frederikse, T., Landerer, F. W., and Caron, L. (2019): The imprints of contemporary mass redistribution on local sea level and vertical land motion observations, *Solid Earth*, 10, 1971–1987, https://doi.org/10.5194/se-10-1971-2019.

Garcin M., Nicolae-Lerma A., Pedreros R., Paris F. (2012) - Evaluation de la submersion marine maximale à l'échelle régionale. Rapport BRGM/RP-62259-FR, 97 p., 40 fig., 9 tab., 4 ann.

Garcin M., Vendé-Leclerc M. (2016) - Observatoire du littoral de Nouvelle-Calédonie – Bilan des activités 2015, Typologie, méthodes et suivi des sites pilotes. BRGM/RP-65637-FR, 169 p., 148 fig., 14 tabl., 2 ann..

GIBB (Mauritius) Ltd in association with PRDW AFRICA Ltd, DIOSPYROS Ltd and MOONEERAM ASSOCIATES Ltd (2017-2019) - Consultancy Services for Coastal Protection, Landscaping and Infrastructural Works in Mauritius – ENV/RFP/06/2016. Detailed design reports : Bois des Amourettes site, Bambous Virieux – Anse Jonchée site, Pointe aux Feuilles to Grand Sable site, Petit Sable to Bambous Virieux site, Providence site

Golledge, N. R. *et al.* (2019): Global environmental consequences of twenty-first-century ice-sheet melt. *Nature* 566, 65–72

Golledge, N.R.; Kowalewski, D.E.; Naish, T.R.; Levy, R.H.; Fogwill, C.J.; Gasson, E.G.W. (2015): The multi-millennial Antarctic commitment to future sea-level rise. *Nature*, 526, 421.

IPCC (2013): *Climate Change 2013: The Physical Science Basis. Contribution of Working Group I to the Fifth Assessment Report of the Intergovernmental Panel on Climate Change* [Stocker, T.F., D. Qin, G.-K. Plattner, M. Tignor, S.K. Allen, J. Boschung, A. Nauels, Y. Xia, V. Bex and P.M. Midgley (eds.)]. Cambridge University Press, Cambridge, United Kingdom and New York, NY, USA, 1535 pp.

IPCC (2023) - *Climate Change 2023: Synthesis Report.* A Report of the Intergovernmental Panel on Climate Change. Contribution of Working Groups I, II and III to the Sixth Assessment Report of the Intergovernmental Panel on Climate Change [Core Writing Team, H. Lee and J. Romero (eds.)]. IPCC, Geneva, Switzerland, (in press)

IPCC, (2021): *Climate Change 2021: The Physical Science Basis. Contribution of Working Group I to the Sixth Assessment Report of the Intergovernmental Panel on Climate Change* [Masson-Delmotte, V., Zhai, P., Pirani, A. et al (eds.)]. Cambridge University Press, Cambridge, United Kingdom and New York, NY, USA, in press. https://doi.org/10.1017/9781009157896

IPCC, (2022) - *Climate Change 2022: Impacts, Adaptation, and Vulnerability. Contribution of Working Group II to the Sixth Assesment Report of the Intergovernmental Panel on Climate Change*, Cambridge, (coll. « Cambridge University Press »).

Japan International Cooperation Agency (2015) - Capacity development on coastal protection and rehabilitation in the republic of Mauritius. Final report. Prepared for ministry of environment and ndu government of Mauritius.

Kamranzad B., Takara K., Louisor J., Guillou N. (2022) - Wave resource assessment and climate change impacts in Reunion and Mauritius. Coastal and offshore science and engineering, 2022.hal-03763276.

Knapp, K.R., Kruk, M.C., Levinson, D.H., Diamond, H.J., Neumann, C.J., 2010. The international best track archive for climate stewardship (IBTrACS) unifying tropical cyclone data. Bulletin of the American Meteorological Society 91, 363–376.

Le Cozannet, G.; Thiéblemont, R.; Rohmer, J.; Idier, D.; Manceau, J.-C.; Quique, R. Low-End Probabilistic Sea-Level Projections. Water 2019, 11, 1507. https://doi.org/10.3390/w11071507

Lecacheux, S., Pedreros, R., Le Cozannet, G., Thiébot, J., De La Torre, Y., and Bulteau, T. (2012): A method to characterize the different extreme waves for islands exposed to various wave regimes: a case study devoted to Reunion Island, Nat. Hazards Earth Syst. Sci., 12, 2425-2437, doi:10.5194/nhess-12-2425-2012, 2012.

Levermann, A., Winkelmann, R., Albrecht, T., Goelzer, H., Golledge, N. R., Greve, R., Huybrechts, P., Jordan, J., Leguy, G., Martin, D., Morlighem, M., Pattyn, F., Pollard, D., Quiquet, A., Rodehacke, C., Seroussi, H., Sutter, J., Zhang, T., Van Breedam, J., Calov, R., DeConto, R., Dumas, C., Garbe, J., Gudmundsson, G. H., Hoffman, M. J., Humbert, A., Kleiner, T., Lipscomb, W. H., Meinshausen, M., Ng, E., Nowicki, S. M. J., Perego, M., Price, S. F., Saito, F., Schlegel, N.-J., Sun, S., and van de Wal, R. S. W.: Projecting Antarctica's contribution to future sea level rise from basal ice shelf melt using linear response functions of 16 ice sheet models (LARMIP-2), Earth Syst. Dynam., 11, 35–76, https://doi.org/10.5194/esd-11-35-2020, 2020

Levermann, A., Winkelmann, R., Nowicki, S., Fastook, J. L., Frieler, K., Greve, R., Hellmer, H. H., Martin, M. A., Meinshausen, M., Mengel, M., Payne, A. J., Pollard, D., Sato, T., Timmermann, R., Wang, W. L., and Bindschadler, R. A. (2014) : Projecting Antarctic ice discharge using response functions from SeaRISE ice-sheet models*, Earth Syst. Dynam.*, 5, 271–293, https://doi.org/10.5194/esd-5-271-2014.

Marzeion, B. *et al.* (2020): Partitioning the uncertainty of ensemble projections of global glacier mass change. *Earths Future* https://doi.org/10.1029/2019EF001470.

Meinshausen M. et al. (2011) - The RCP greenhouse gas concentrations and their extensions from 1765 to 2300. *Clim. Change* 109, 213–241 (2011).

Meyssignac, B., Slangen, A.A., Melet, A., Church, J.A., Fettweis, X., Marzeion, B., Agosta, C., Ligtenberg, S.R.M., Spada, G., Richter, K. and Palmer, M.D., (2017). Evaluating model simulations of twentieth-century sea-level rise. Part II: regional sea-level changes. Journal of Climate, 30(21), pp.8565-8593

Ministère de l'Environnement, de la Gestion des Déchets et du Changement Climatique, (2019) - « Zones côtières et Environnement marin », Les Assises de l'Environnement, 16 – 17 décembre 2019, Caudan Art Centre, 5p.

Nidheesh AG, Lengaigne M, Vialard J, Izumo T, Unnikrishnan AS, Krishnan R (2019) - Natural decadal sea-level variability in the Indian Ocean: lessons from CMIP models. *Clim. Dyn.* 53:5653–5673. https://doi.org/10.1007/s00382-019-04885-z

NWFS Consultancy (2009) - Environmentally Sensitive Areas classificiation report. Final report. Prepared for the ministry of environment, sustainable development, disaster and beach management (MOESDDBM).

O'Neill B.C., et al. (2014) - A New scenario Framework for Climate Change Research: The Concept of Shared Socioeconomic Pathways. *Climatic Change* 122 (3): p. 387 400. DOI: 10.1007/s10584-013-0905-2.

Oppenheimer, M. *et al.* (2019): Sea Level Rise and Implications for Low-Lying Islands, Coasts and Communities. In IPCC Special Report on the Ocean and Cryosphere in a Changing Climate (eds Pörtner, H.-O. *et al.*) (IPCC, 2019).

Pedreros R., Lecacheux S., Le Cozannet G., Biangy A., De La Torre Y. (2009) - « HOULREU » Quantification de la houle centennale de référence sur les façades littorales de La Réunion. BRGM/RP-57829-FR, 119 p., 93 fig., 14 tab.

Pedreros, Rodrigo ; Filippini, Andrea Gilberto ; Coulet, Christophe ; Laigre, Thibault ; Louisor, Jessie ; Rohmer, Jérémy ; Moisan, Manuel ; Chêne, Frédéric ; Delahaye, Thibault (2023) - Cartographie de l'aléa submersion marine sur les 7 communes du Territoire à Risque d'Inondation de Guadeloupe. Rapport final . BRGM/RP-73076-FR, 266 p.

Piollé, J.-F.; Dodet, G.; Quilfen, Y. (2020): ESA Sea State Climate Change Initiative (Sea_State_cci) : Global remote sensing daily merged multi-mission along-track significant wave height, L3 product, version 1.1. Centre for Environmental Data Analysis, 30 January 2020. doi:10.5285/3ef6a5a66e9947d39b356251909dc12b.

Pomeroy. A. (2017) - Mauritius Wave Energy Resource Assessment. Report. The University of Western Australia.

PRDW (2017) – Mauritius Coastal Protection Woks – Hydrodynamic and Wave Modelling reports. Reports PRDW (in collaboration with GIBB ltd). S2050-RP-CE-001-R1, S2050-RP-CE-002-R1, S2050-RP-CE-003-R0, S2050-RP-CE-001-R0.

Qu, Y., Jevrejeva, S., Williams, J., & Moore, J. C. (2022). Drivers for seasonal variability in sea level around the China seas. Global and Planetary Change, 213, 103819. https://doi.org/10.1016/j.gloplacha.2022.103819.

Ritz, C.; Edwards, T.L.; Durand, G.; Payne, A.J.; Peyaud, V.; Hindmarsh, R.C.A. (2015): Potential sea-level rise from Antarctic ice-sheet instability constrained by observations. *Nature*, 528, 115.

Sajidh, C.K., Chatterjee, A. (2023) - Indian Ocean dynamic sea level, its variability and projections in CMIP6 models. *Clim Dyn* https://doi.org/10.1007/s00382-023-06676-z

Samiksha S. V., Vethamony P., Aboobacker V. M., Rashmi R. (2012) - Propagation of Atlantic Ocean swells in the north Indian Ocean: a case study. Nat. Haz. Ear. Sys. Sci. 12, 3605–3615 (2012)

Slangen ABA, Carson M, Katsman CA, van de Wal RSW, Köhl A, Vermeersen LLA, Stammer D (2014) Projecting twenty-first century regional sea-level changes. Clim Change 124:317–332. https://doi.org/10.1007/s10584-014-1080-9

Slangen, A. B. A., Church, J. A., Zhang, X. & Monselesan, S. P. (2015): The sea level response to external forcings in historical simulations of CMIP5 climate models. *J. Clim*. 28, 8521–8539.

Slangen, A. B. A., Meyssignac, B., Agosta, C., Champollion, N., Church, J. A., Fettweis, X., Ligtenberg, S. R. M., Marzeion, B., Melet, A., Palmer, M. D., Richter, K., Roberts, C. D., & Spada, G. (2017). Evaluating Model Simulations of Twentieth-Century Sea Level Rise. Part I: Global Mean Sea Level Change, *Journal of Climate*, 30(21), 8539-8563. Retrieved Sep 15, 2022, from https://journals.ametsoc.org/view/journals/clim/30/21/jcli-d-17-0110.1.xml

Spada, G. and Melini, D. (2019) : SELEN4 (SELEN version 4.0): a Fortran program for solving the gravitationally and topographically self-consistent sea-level equation in glacial isostatic adjustment modeling, Geosci. Model Dev., 12, 5055–5075, https://doi.org/10.5194/gmd-12-5055-2019.

Stammer, D., van de Wal, R. S. W., Nicholls, R. J., Church, J. A., Le Cozannet, G., Lowe, J. A., et al. (2019). Framework for high-end estimates of sea level rise for stakeholder applications. Earth's Future, 7, 923–938. https://doi.org/10.1029/2019EF001163

Taylor, K.E., Stouffer, J.R., and Meehl, G.A., (2012) An overview of CMIP5 and experiment design, *Bull. Am. Meteorol. Society*, 2012, vol. 93, iss. 4, pp. 485..

Thiéblemont, R.; Le Cozannet, G.; Toimil, A.; Meyssignac, B.; Losada, I.J. (2019): Likely and High-End Impacts of Regional Sea-Level Rise on the Shoreline Change of European Sandy Coasts Under a High Greenhouse Gas Emissions Scenario. *Water*, *11*, 2607. https://doi.org/10.3390/w1112260

Tolman, H. L., & al. (2009). User manual and system documentation of WAVEWATCH III TM version 3.14. Technical note, MMAB Contribution, 276, 220.

van de Wal, R. S. W., Nicholls, R. J., Behar, D., McInnes, K., Stammer, D., Lowe, J. A., et al. (2022). A high-end estimate of sea level rise for practitioners. Earth's Future, 10, e2022EF002751. https://doi.org/10.1029/2022EF002751

Williams D.S., Rosendo S., Sadasing O., Celliers L. (2020) - « Identifying local governance capacity needs for implementing climate change adaptation in Mauritius », *Climate Policy*, 27 mai 2020, vol. 20, nº 5, p. 548-562.

Wu, W., Du, Y., Qian, Y.-K., Cheng, X., Wang, T., Zhang, L., & Peng, S. (2020). Structure and seasonal variation of the Indian Ocean tropical gyre based on surface drifters. Journal of Geophysical Research: Oceans, 125, e2019JC015483. https://doi.org/10.1029/2019JC015483.

Young I.R., Sanina E., Babanin A.V. (2017) - Calibration and cross validation of a global wind and wave database of altimeter, radiometer, and scatterometer measurements. *J. Atmos. Ocean. Technol*. 2017, 34, 1285–1306.

Zijlema, M., Stelling, G., Smit, P., 2011. SWASH: An operational public domain code for simulating wave fields and rapidly varied flows in coastal waters. Coastal Engineering 58, 992–1012.

# 7. APPENDIX

The appendices to this report set out in detail the methods used, and the results obtained. Given the number of pages, each appendix constitutes an independent document.

The list of appendices is as follows:

Appendix 1: Additional data on coastal erosion

> Manuel GARCIN, Franck DESMAZES (2025) – Additional data on coastal erosion in Rodrigues (Appendix 1). final. BRGM/RC-73987-FR, 58 p., 51 fig., 17 tab.

Appendix 2: Southern swells (Mauritius and Rodrigues)

> Jessie LOUISOR, Rémi THIEBLEMONT, Jeremy ROHMER (2025) – Southern swells (Maurice and Rodrigues) – Appendix 2. Rapport Final. BRGM/RC-73987-FR, 42 p., 34 fig., 5 tab.

Appendix 3: Coastal land cover database

> GARCIN Manuel (2025) – Coastal land cover database (Appendix 3). Rapport Final. BRGM/RC-73987-FR, 14 p., 4 fig., 1 tab.

RÉPUBLIQUE
FRANÇAISE
*Liberté*
*Égalité*
*Fraternité*

Géosciences pour une Terre durable
brgm

**Centre scientifique et technique**
3, avenue Claude-Guillemin
BP 36009
45060 – Orléans Cedex 2 – France
Tél. : 02 38 64 34 34

**www.brgm.fr**